Determining the causes of recessive retinal dystrophy

By

Mohammed El-Sayed Mohammed El-Asrag

BSc (hons), MSc (hons) Genetics and Molecular Biology

Submitted in accordance with the requirements for the degree of

Doctor of Philosophy

The University of Leeds

School of Medicine

September 2016

Jointly authored publications statement

Chapter 3 (first results chapter) of this thesis is entirely the work of the author and appears in:

Watson CM*, **El-Asrag ME*,** Parry DA, Morgan JE, Logan CV, Carr IM, Sheridan E, Charlton R, Johnson CA, Taylor G, Toomes C, McKibbin M, Inglehearn CF and Ali M (**2014**). Mutation screening of retinal dystrophy patients by targeted capture from tagged pooled DNAs and next generation sequencing. **PLoS One** 9(8): e104281. *Equal first-authors.

Shevach E, Ali M, Mizrahi-Meissonnier L, McKibbin M, **El-Asrag ME**, Watson CM, Inglehearn CF, Ben-Yosef T, Blumenfeld A, Jalas C, Banin E and Sharon D (**2015**). Association between missense mutations in the *BBS2* gene and nonsyndromic retinitis pigmentosa. **JAMA Ophthalmology** 133(3): 312-318.

Chapter 4 (second results chapter) of this thesis is entirely the work of the author and appears in:

Ravesh Z, **El-Asrag ME***, Weisschuh N, McKibbin M, Reuter P, Watson CM, Baumann B, Poulter JA, Sajid S, Panagiotou ES, O'Sullivan J, Abdelhamed Z, Bonin M, Soltanifar M, Black GC, Amin-ud Din M, Toomes C, Ansar M, Inglehearn CF, Wissinger B and Ali M (**2015**). Novel *C8orf37* mutations cause retinitis pigmentosa in consanguineous families of Pakistani origin. **Molecular Vision** 21: 236-243. *Equal first-authors.

Bedoni N*, Haer-Wigman L*, Vaclavik V, Tran HV, Farinelli P, Balzano S, Royer-Bertrand B, **El-Asrag ME**, Bonny O, Ikonomidis C, Litzistorf Y, Nikopoulos K, Yioti G, Stefaniotou M, McKibbin M, Ellingford J, Booth AP, Black G, Toomes C, Inglehearn CF, Hoyng CB, Bax N, Klaver CCW, Thiadens AA, Murisier F, Schorderet DF, Ali M, Cremers FPM, Andréasson S, Munier FL and Rivolta C (**2016**). Mutations in the polyglutamylase gene *TTLL5*, expressed in photoreceptor cells and spermatozoa, are associated with cone-rod degeneration and reduced male fertility. **Human Molecular Genetics** doi:10.1093/hmg/ddw282. *Equal first-authors.

Khan KN*, **El-Asrag ME***, Ku CA, Holder GE, McKibbin M, Arno G, Poulter JA, Carss K, Bommireddy T, Bagheri S, NIHR BioResource-Rare Diseases, UK Inherited Retinal Disease Consortium, Bakall B, Scholl HP, Raymond FL, Toomes C, Inglehearn CF, Pennesi ME, Moore AT, Michaelides M, Ali M, and Webster AR **(2016)**. Recessive mutations in *MFSD8* are a cause of non-syndromic rod-cone dystrophy with severe macular involvement. **Submitted to Investigative Ophthalmology and Visual Science**. *Equal first-authors.

Chapter 5 (third results chapter) of this thesis is entirely the work of the author and appears in:

El-Asrag ME*, Sergouniotis PI*, McKibbin M, Plagnol V, Sheridan E, Waseem N, Abdelhamed Z, McKeefry D, Van Schil K, Poulter JA, Johnson CA, Carr IM, Leroy BP, De Baere E, Inglehearn CF, Webster AR, Toomes C and Ali M (**2015**). Biallelic mutations in the autophagy regulator *DRAM2* cause retinal dystrophy with early macular involvement. **American Journal of Human Genetics** 96(6): 948-954. *Equal first-authors

Sergouniotis PI*, McKibbin M*, Robson AG, Bolz HJ, De Baere E, Muller PL, Heller R, **El-Asrag ME**, Van Schil K, Plagnol V, Toomes C, Ali M, Holder GE, Charbel Issa P, Leroy BP, Inglehearn CF and Webster AR (**2015**). Disease expression in autosomal recessive retinal dystrophy associated with mutations in the *DRAM2* gene. **Investigative Ophthalmology and Visual Science** 56(13): 8083-8090. *Equal first-authors

Publication in preparation from this thesis

El-Asrag ME, McKibbin M, Poulter JA, Abdelmottaleb DI, Black GC, Toomes C, Inglehearn CF and Ali M. Whole exome sequencing identifies *LARGE* as novel gene candidate for autosomal recessive retinal dystrophy. **In preparation**.

Publications related to other work done during this study

Al-Amri A, Saegh AA, Al-Mamari W, **El-Asrag ME**, Ivorra JL, Cardno AG, Inglehearn CF, Clapcote SJ and Ali M **(2016)**. Homozygous single base deletion in *TUSC3* causes intellectual disability with developmental delay in an Omani family. **American Journal of Medical Genetics Part A** 170(7): 1826-1831.

El-Asrag ME, McKibbin M, Mohamed MD, Toomes C, Inglehearn CF and Ali M. Next generation sequencing identifies novel loss of function mutations in *NRL* cause autosomal recessive retinitis pigmentosa. **In preparation.**

Acknowledgements

First and above all, I praise God Almighty for providing me this opportunity, for without His blessings, guidance and assistance, this study would not have been possible. I also offer my immeasurable appreciation and deepest gratitude to Dr Manir Ali for his expert guidance, profound interest, support, assistance, valuable remarks and continuous encouragement. I also my grateful thanks to Prof. Chris Inglehearn for accepting me as a doctoral student at Leeds University, for his friendly advice, thoughtful guidance and for imparting his knowledge and bringing his expertise to this study. Also many thanks to Dr Carmel Toomes for her unfailing advice and constructive criticism; she did not spare any efforts in guiding me towards the best. Sincere appreciation also goes to my colleague Dr James Poulter for his valuable help and friendship throughout this study.

I would also like to thank all my laboratory colleagues, past and present, in Section of Ophthalmology and Neuroscience, Leeds Institute of Biomedical and Clinical Sciences (LIBACS) who in one way or another have contributed to the successful completion of this study, particularly Ahmed, Zakia, Kamron, Claire, Evi, Carla, Layal, Tom, Denisa, Emma, Ekram, Clare, Suba and Kasia. Many thanks also to Dr David Parry and Dr Ian Carr for their help with bioinformatics analysis and to Prof. Colin Johnson and Dr Jacquelyn Bond for their friendly advice. I would also like to thank Mr Martin McKibbin for providing the clinical data and images of the patients.

I would also like to acknowledge the financial support that I received from the Egyptian Ministry of Higher Education.

I would like to warmly thank my parents and my brother Ahmed for their spiritual support in all aspects of my life. To my dearest daughters, Maram and Maryam, as you grow older, I want you to know that just watching you smile makes me realize how beautiful my life is, and that I love you, and have done this for you. Hopefully, I have made you proud. Finally, my lovely wife, dear Dina, although I know that you did not want to be named, you put your own career on hold to come with me to the United Kingdom. Without your constant support and encouragement, I would never have finished this work. You became the bedrock of our family, and I know how difficult it was for you, so all I can say is: Thank you for everything and may Allah reward you for your generosity of spirit.

Abstract

Inherited retinal dystrophies (RDs) are a clinically heterogeneous group of eye diseases that result from mutations in more than 250 genes. Genetic diagnosis of these diseases has, until recently, been hampered by the lack of suitable technologies to perform high throughput screening. This thesis describes two different strategies for using next generation sequencing (NGS) in RD patients to find the pathogenic mutation(s) involved.

In the first results chapter, a customised capture reagent (called Retinome) designed against the known retinal dystrophy genes (RetNet, June 2010) was used in NGS analysis of 20 RD families. The disease-causing mutations were identified in 12 of 20 cases (60%). These included previously reported mutations in *ABCA4* (c.6088C>T, p.R2030*; c.5882G>A, p.G1961E), *RDH12* (c.601T>C, p.C201R; c.506G>A, p.R169Q), *PROM1* (c.1117C>T, p.R373C), *GUCY2D* (c.2512C>T, p.R838C), *RPGRIP1* (c.3565C>T, p.R1189*), *BBS2* (c.1895G>C, p.R632P) and *SPATA7* (c.253C>T, p.R85*) and new mutations in *CRB1* (c.2832_2842+23del), *USH2A* (c.12874A>G, p.N4292D), *RP2* (c.884-1G>T) and *ABCA4* (c.3328+1G>C). In eight cases the causative mutation could not be unambiguously identified.

In the second results chapter, whole-exome NGS was performed on five RD families that had been pre-screened with the Retinome reagent. This identified mutations in three known RD genes, *MFSD8* (c.1006G>C, p.E336Q; c.1394G>A, p.R465Q), *C8orf37* (c.555G>A, p.W185*) and *TTLL5* (c.1627G>A, p.E543K), and mutations in two potentially new RD genes, *LARGE* (c.2089G>T, p.V697L) and *FDFT1* (c.930C>G, p.F310L).

In the third results chapter, whole-exome NGS was performed, without pre-screening of known genes, in a family with atypical adult-onset RD with early macular involvement. NGS identified a mutation in a novel RD gene, *DRAM2* (c.140delG, p.G47Vfs*3). Further *DRAM2* screening in DNA panels identified a compound heterozygote case (c.494G>A, p.W165*; c.131G>A, p.S44N). DRAM2 was localised to the photoreceptor inner segment and retinal pigment epithelium.

The relative merits of each approach are discussed. Identifying the pathogenic mutation facilitates counselling, carrier testing and may lead to a clearer prognosis. It may also influence future prospects for these families as new treatments become available.

Table of contents

List of figures

List of tables

List of appendices

List of abbreviations

AAV	Adeno-associated virus
Ab	Antibody
ABCA4	ATP binding cassette subfamily A, member 4
ACHM	Achromatopsia
AD	Autosomal dominant
adRP	Autosomal dominant retinitis pigmentosa
Akt	Serine/threonine kinase
Align-GVGD	Align-grantham variation and grantham deviation
AMD	Age related macular degeneration
AMP	Adenosine monophosphate
AMPK	AMP-activated protein kinase
AONs	Antisense oligonucleotides
AP	Autophagosome
AR	Autosomal recessive
Arr	Arrestin
arRP	Autosomal recessive retinitis pigmentosa
ATGs	Autophagy-related genes
BBS	Bardet-Biedl syndrome
Bcl-2	B-cell lymphoma 2
bp	Base pairs
BPCA	Blocking peptide competition assay
BSA	Bovine serum albumin
C8orf37	Chromosome 8 open reading frame 37
Ca^{2+}	Calcium
CADD	Combined annotation dependent depletion
CC	Connecting cilium
CCD	Charged couple device
cDNA	Complementary deoxyribonucleic acid
cGMP	Cyclic guanosine monophosphate
CMA	Chaperone mediated autophagy
CMD	Congenital muscular dystrophy
CNG	Cyclic nucleotide-gated
CNV	Copy number variation
COD	Cone dystrophy

CRALBP	Cellular retinaldyhyde binding protein
Crb	Crumbs homolog 1
CRBP	Cellular retinol-binding protein
CRD	Cone-rod dystrophy
CRISPR	Clustered regularly interspaced short palindromic repeats
CSAP	Centriole and spindle–associated protein
DAPI	4',6-diamidino-2-phenylindole
dbSNP	Single nucleotide polymorphism database
ddH_2O	Double-distilled water
dNTP	Deoxyribose nucleoside triphosphate
DR	Diabetic retinopathy
DRAM2	DNA-damage regulated autophagy modulator protein 2
DSBs	Double-stranded breaks
dsDNA	Double stranded deoxyribonucleic acid
EORD	Early onset retinal dystrophy
ER	Endoplasmic reticulum
ERG	Electroretinogram
ESCs	Embryonic stem cells
EVS	Exome variant server
ExAC	Exome Aggregation Consortium
EYS	Eyes shut homolog
F	Forward
FAF	Fundus autofluorescence
FDFT1	Farnesyl diphosphate farnesyl transferase1
FDR	False discovery rate
ffERG	Full-field electroretinography
FFPE	Formalin-fixed paraffin-embedded
Fs	Frame shift
GAP	GTPase-activating protein
GATK	Genome analysis toolkit
GC	Guanylate cyclase
GCAP	Guanylate-cyclase-activating protein
GCL	Ganglion cell layer
gDNA	Genomic deoxyribonucleic acid
GDP	Guanosine diphosphate
GEF	Guanine nucleotide exchange factor

GNAT2	G Protein subunit alpha transducin 2
GPCRs	G protein–coupled receptors
GRK	G-protein-coupled receptor kinase
Gt	G protein transducin
GTP	Guanosine triphosphate
HDL-C	High-density lipoprotein cholesterol
HDR	Homology directed repair
IBD	Identical by descent
IF	Immunofluorescence
IGV	Integrative genomics viewer
IHC	Immunohistochemistry
IMPDH1	Inosine-5'-monophosphate dehydrogenase 1
INL	Inner nuclear layer
IP3	Inositol trisphosphate
IPL	Inner plexiform layer
IPM	Interphotoreceptor matrix
iPSCs	Induced pluripotent stem cells
IRBP	Interphotoreceptor retinoid-binding protein
IRDs	Inherited retinal dystrophies
kbp	Kilo base pairs
LAMP-2A	Lysosomal associated membrane protein type 2A
LC3	Light chain 3
LCA	Leber congenital amaurosis
LDL-C	Low-density lipoprotein cholesterol
LE	Left eye
LOD	Logarithm of the odds
LRAT	Lecithin retinol acyl transferase
MAF	Minor allele frequency
MAPP	Multivariate analysis of protein polymorphism
MD	Macular dystrophy
MFSD8	Major facilitator superfamily domain-containing protein 8
µg	Micrograms
MKS	Meckel-Gruber syndrome
µl	Microliter
µM	Micromolar
mM	Millimolar

ms	Millisecond
mTOR	Mammalian target of rapamycin
NADPH	Nicotinamide adenine dinucleotide phosphate
NCBI	National center for biotechnology information
NCKX	Na^+/Ca^{2+}, K^+ exchanger
NCLs	Neuronal ceroid lipofuscinosis
ND	Not done
NDK	Nucleoside diphosphate kinase
NGS	Next-generation sequencing
NHEJ	Non homologous end joining
NPs	Nanoparticles
OCT	Optical coherence tomography
OFD1	Oral facial digital syndrome 1
OMIM	Online-Mendelian inheritance in man
ONL	Outer nuclear layer
OPL	Outer plexiform layer
ORF15	Open reading frame 15
OS	Outer segment
OTX2	Orthodenticle homeobox 2
PBS	Phosphate-buffered saline
PCR	Polymerase chain reaction
PDE	Phosphodiesterase
PE	Phosphatidylethanolamine
PFA	Paraformaldehyde
PI3K	Phosphatidylinositol 3-kinase
PIS	Photoreceptor inner segment
PKB	Protein kinase B
PolyPhen-2	Polymorphism Phenotyping v2
POS	Photoreceptor outer segment
PROM1	Prominin 1
PSI-BLAST	Position-specific iterative basic local alignment search tool
PTEN	Phosphatase and tensin homolog
R	Reverse
R/Rho	Rhodopsin
R9AP	Regulator of G protein signalling 9-binding protein
RCD	Rod-cone dystrophy

RD	Retinal dystrophy
RDH	Retinol dehydrogenase
RE	Right eye
RGS9	Regulator of G-protein-signalling isoform 9
RID	RPGR interacting domain
RIPA	Radio immunoprecipitation assay
RP	Retinitis pigmentosa
RPCs	Retinal progenitor cells
RPE	Retinal pigment epithelium
RPGR	Retinitis pigmentosa GTPase regulator
RPGRIP1	Retinitis pigmentosa GTPase regulator interacting protein 1
RPGRIP1L	RPGRIP1-like
RPKM	Reads per kilobase per million mapped reads
RT	Room temperature
RT-PCR	Reverse transcription polymerase chain reaction
SDS	Sodium dodecyl sulphate
SIFT	Sorting intolerant from tolerant
siRNA	Small interfering ribonucleic acid
SLS	Senior-Loken syndrome
SMC	Structural maintenance of chromosomes
SMS	Single molecule sequencing
SNP	Single nucleotide polymorphism
SQSTM1	Sequestosome-1
SRC-1	Steroid receptor coactivator 1
STGD	Stargardt disease
STRs	Short tandem repeats
T	Transducin
TBCC	Tubulin binding cofactor C
TBS	Tris buffered saline
TC	Total cholesterol
TE	Tris-EDTA
TIF2	Transcriptional intermediary factor 2
TM	Transmembrane
T_M	Melting temperature
TMDs	Transmembrane domains
TSC	Tuberous sclerosis complex

TTLL5	Tubulin tyrosine ligase-like family member 5
UCSC	University of California Santa Cruz
USH	Usher syndrome
VA	Visual acuity
VCF	Variant call format
VEGA	Vertebrate genome annotation
WB	Western blot
WGA	Whole genome amplification
WGS	Whole genome sequencing
WWS	Walker–Warburg syndrome
XL	X-linked
XLRP	X-linked retinitis pigmentosa
XMP	Xanthosine monophosphate
Y2H	Yeast-two-hybrid
ZMWs	Zero-mode waveguides

Chapter 1- Introduction

'The eyes are surely the most sensitive, amazing and delicate organs humans possess. They are like a window through which we see the world, and are responsible for most of the information that reaches the brain, which is why humans depend on their sight more than any of the other senses'

1.1 Gross anatomy of the human eye

In simple terms, the eye is made up of three layers; an outer fibrous wall, a middle vascular layer and an inner neuronal layer (Cassin and Solomon, 1990). The outermost layer contains collagen and elastin fibres, and consists of the cornea and sclera. The cornea refracts light, accounting for approximately 70% of the total dioptric power of the eye, while the sclera is the protective coat that gives the eye its white colour. The middle layer consists of the choroid posteriorly, which provides oxygen and nourishment to the innermost layer of the eye, the retina. Anteriorly, the choroid connects with the ciliary body and iris (Figure 1.1).

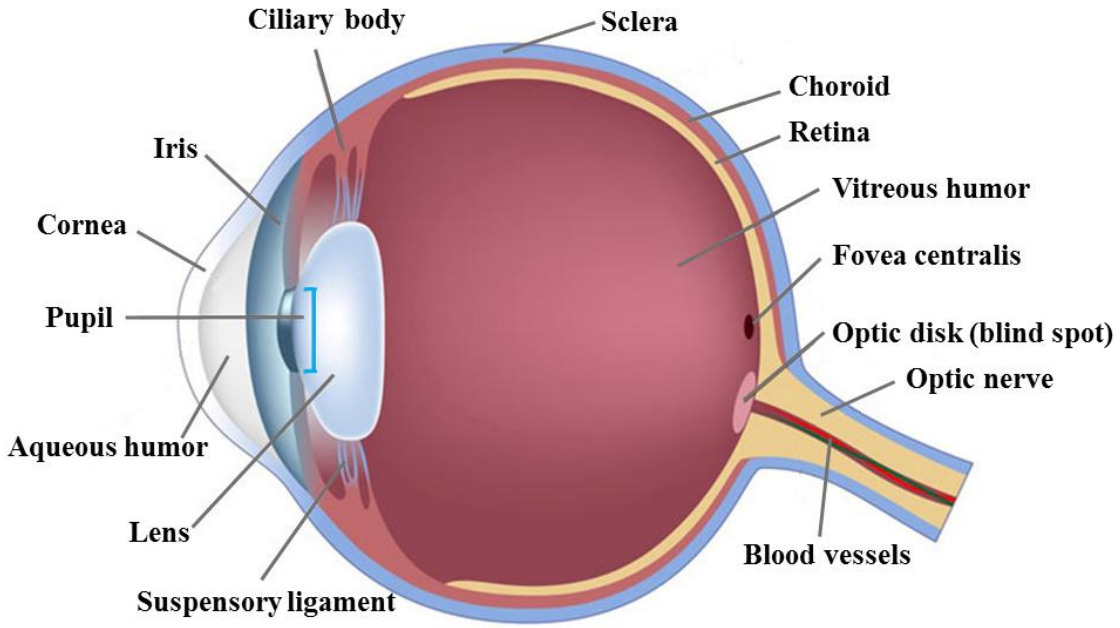

Figure 1.1. Schematic illustration showing the lateral view of a human eye. The diagram shows the three main layers of the eye: the cornea and sclera; the iris, choroid and ciliary body; and the retina (Adapted with a free license from Alila Medical Media, www.alilamedicalmedia.com/).

Images are made up of light reflected from the objects; this light enters the eye through the cornea, creating an upside-down image on the retina. The retina acts like the film in a camera; images come through the eye's lens and are focused onto the retina which converts these images into electrical signals and sends them via the optic nerve to the brain, where the image is translated and perceived in an upright position (Smerdon, 2000).

1.2 Embryonic development of the human eye

1.2.1 Overview

The formation of human eyes takes place between the third and the tenth week of embryonic development. The eye is derived from three key components (Ali and Sowden, 2011) (Figure 1.2). First, the neuroepithelium gives rise to the optic vesicle and optic cup that eventually go on to form the retina, retinal pigment epithelium (RPE), the iris and its smooth muscles, ciliary body, the optic nerve, and part of the eye's vitreous humour. Second, the surface ectoderm gives rise to the lens, the corneal epithelium, conjunctiva and caruncle, the lacrimal apparatus (glands and drainage system) and eyelid skin. Third, the mesenchyme gives rise to the extraocular muscles and the orbital and ocular vascular endothelium.

1.2.2 Development of the optic cup and lens vesicle

The eye begins to form on or about day 22 of embryonic development, when a progressively deepening groove known as the optic sulcus appears in the neural folds on both sides of the developing forebrain. As the neural tube closes, these two sulci become out-pocketings and form optic vesicles that extend toward the surface ectoderm and attenuate to form optic stalks. Interaction between the ectoderm and the optic vesicle induces a thickening of the ectoderm in that area (Weaver and Hogan, 2001) (Figure 1.2A). This in turn invaginates, forming the lens placode (Figure 1.2B) and then a fully enclosed lens vesicle. At the same time, the optic vesicle invaginates to form a bilayered optic cup (Figure 1.2C). A groove on the inferior surfaces of the developing optic vesicle and stalk, known as the optic, or choroidal, fissure, allows blood vessels access to both the optic cup and the lens vesicle. These blood vessels consist of the hyaloid artery and its accompanying vein. Eventually when this fissure fuses, it encloses these vessels inside

the optic stalk. As the pregnancy advances, and the lens matures, the distal end of the hyaloid artery disintegrates, whilst its proximal end forms the central retinal artery.

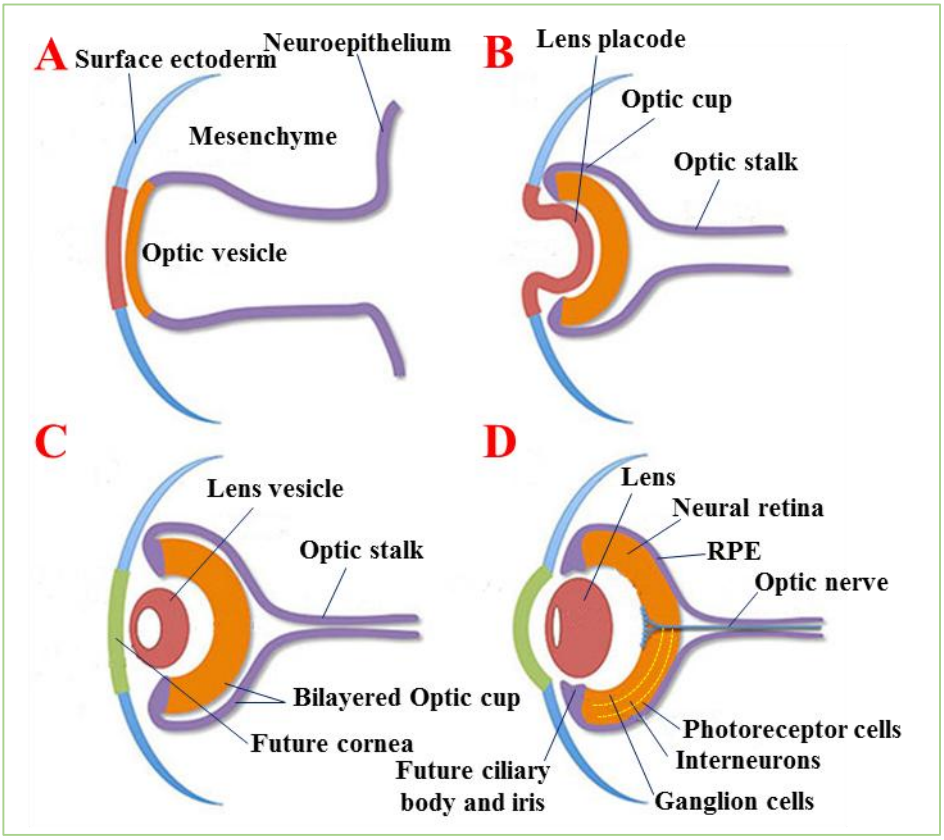

Figure 1.2. Embryonic development of the human eye. The surface ectoderm thickens (A) and invaginates together with the underlying neuroepithelium of the optic vesicle to produce the lens placode (B). The inner layer of the bilayered optic cup (C) produces neural retina whilst the outer layer gives rise to the retinal pigmented epithelium (RPE). When maturation is reached the neural retina comprises three cellular layers: photoreceptors, interneurons and retinal ganglion cells (D). (Adapted with a free license from Brown Lab, https://basicscience.ucdmc.ucdavis.edu/Brown_Lab/index.html, The University of California).

1.2.3 Development of the retina

The bilayer of the optic cup differentiates to produce the outer pigment layer that will eventually form the RPE, whilst the inner layer forms the neural retina of the mature eye (Eiraku et al., 2011). The development of the RPE can be observed shortly after the fourth week, with melanin granules appearing in the cells within this layer. Two weeks later, around day 47 of gestation, the cells adjoining the intraretinal space start to differentiate into the photoreceptors (rods and cones) (Graw, 2003). This is followed by

the development of the interneurons that form the next layer (horizontal, amacrine and bipolar cells). Finally, the innermost layer forms the axons of the ganglion cells that will make up the optic nerve. Also, the cells of the optic cup inner layer generate a range of glia. The macular region is thicker than the rest of the retina until the eighth month, when the macular depression begins to develop. Although cones and rods can be first distinguished at week 15 of gestation and all of these retinal layers appear fully developed and discernible by eight months, the macular development especially for *fovea centralis* (the point of maximum optical resolution) is not complete until few months after birth (Hendrickson and Yuodelis, 1984).

1.2.4 Development of other eye layers

During weeks six and seven, the mesenchyme that surrounds the external surface of the optic cup condenses into the inner vascular layer, the choroid and the outer fibrous layer, the sclera. Mesenchyme anterior to the developing lens splits into two layers that form the anterior chamber of the eye. The inner layer is continuous with the choroid. The outer layer produces the stroma, one of the three layers of the cornea. The other two layers in the cornea, epithelium, and endothelium, develop from surface ectoderm and neural crest cells respectively. Developing neural and pigmented retinas meet at the outer lips of the optic cup where they differentiate into the epithelium of the iris and the ciliary body (Figure 1.2D), while stroma of the iris and the ciliary body develop from neural crest cells migrating into the area (Graw, 2003). The amount of melanin distributed in the stroma of the iris will determine the eye's colour (Sturm and Larsson, 2009). The sphincter and dilator pupillae muscles connected to the iris stroma develop from optic cup neuroectoderm, while the ciliary muscle is formed by invading mesenchyme. Vitreous humour is also formed initially from mesenchymal cells originating in the neural crest. More of this gel-like substance is later added from the neuroectoderm of the optic cup. The eyelids start forming in week six and are derived partially from neural crest cells and partially from surface ectoderm just anterior to the cornea. Beginning as two folds of skin adhering to each other over the cornea, they later separate in the 27^{th} week of development.

1.3 Retina

The retina is a light-sensitive layer at the back of the eye that covers about 65 percent of the eye's interior surface. The retina converts light energy into electrical signals that are carried to the brain by the optic nerve. The retina is a very delicate and complicated structure consisting of two main layers, the RPE and the neural retina.

1.3.1 Retinal pigment epithelium (RPE)

The RPE is a pigmented monolayer of cuboidal cells that are in close proximity to the photoreceptor outer segments. The basal surface of the RPE rests on a prominent basement membrane called the Bruch's membrane, where drusen, which are tiny yellow or white deposits found in dry age-related macular degeneration (AMD), are located. Large confluent drusen are a risk factor for progression of AMD (Davis et al., 2005; Edwards et al., 2005; Klein et al., 2005; Zareparsi et al., 2005; Gold et al., 2006; Yates et al., 2007; Despriet et al., 2009; Fritsche et al., 2013). RPE cells serve numerous diverse functions in the maintenance of retinal homeostasis. They transport ions, water, metabolic end products and nutrients such as glucose and fatty acids between the photoreceptor layer and the choriocapillaris (Rizzolo et al., 2011). During the visual cycle (Section 1.4.4), the RPE maintains the photoreceptor excitability by isomerization of all-*trans*-retinal to 11-*cis*-retinal (Baehr et al., 2003; Thompson and Gal, 2003). Importantly, photoreceptor cells undergo a daily renewal process, in which 10% of the photoreceptor outer segment (POS) is shed and subsequently phagocytosed by adjacent RPE cells. This daily phagocytosis and digestion of POS discs protects photoreceptors from the toxic effects of accumulated photo-oxidative products over a human lifetime (Kevany and Palczewski, 2010). This renewal of POSs is critical for the maintenance of photoreceptor structural integrity and function (LaVail, 1976; Strauss, 2005). A failure of any one of these RPE functions causes degeneration of the retina, loss of visual function and blindness (Marlhens et al., 1997; Morimura et al., 1998; Gal et al., 2000; Thompson et al., 2001; Gibbs et al., 2003; Bonilha, 2008; Sparrow et al., 2010a).

1.3.2 Neural retina

The neural layer of the retina is responsible for trapping the incident light rays and converting their energy into action potentials, which are then transmitted to the brain as

nerve impulses. The neural layer of the retina contains five kinds of cells. Photoreceptor cells, rods and cones, are specialized for light absorption. Bipolar, amacrine and horizontal cells receive information from the photoreceptors, process it in a variety of ways and pass this on to ganglion cells which relay the information to the brain. These cells have a unique 'inverted' arrangement, in which their sensory ends are directed away from incident light as light has to pass through several inner retinal layers before reaching the photoreceptors (Figure 1.3A)

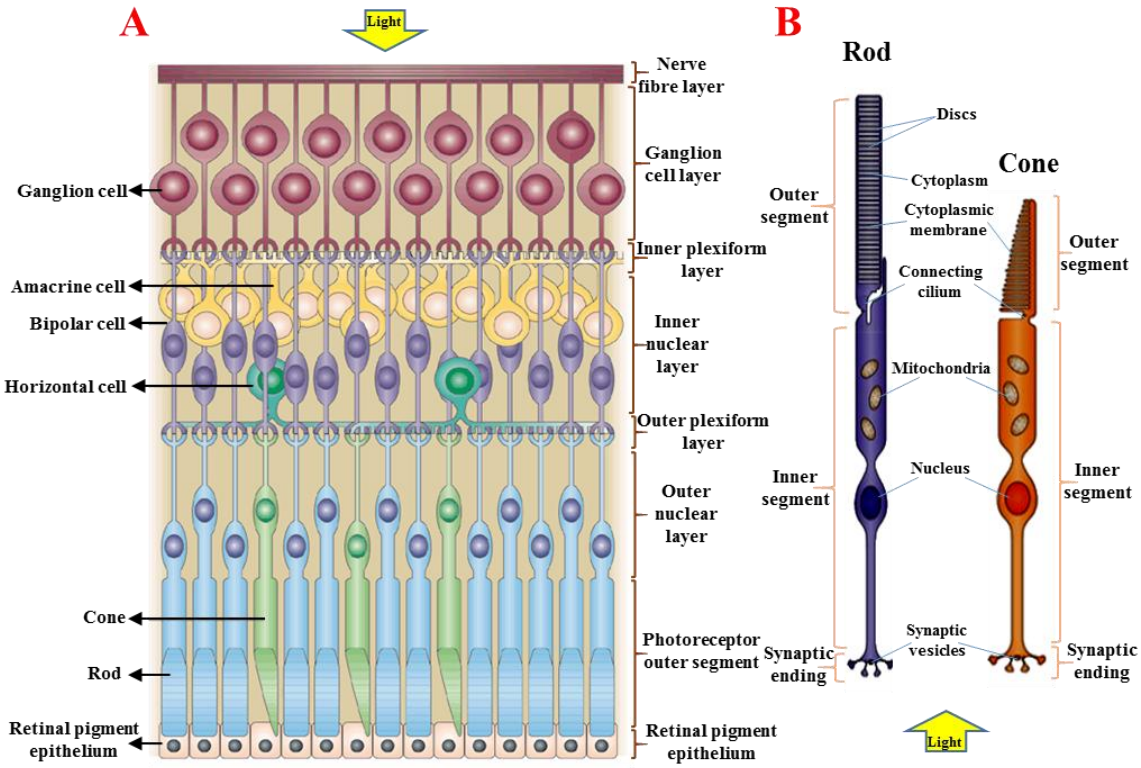

Figure 1.3. The five main cell types in the retina. (A) The arrangement of retinal cells is shown in a cross section. The five cell types in the neural retina are arranged into three layers, the photoreceptor layer (rods and cones), intermediate layer (bipolar, horizontal and amacrine cells) and the internal layer of ganglion cells. (B) The structure of the photoreceptors (rods and cones) consists of three cellular regions: an outer segment, an inner segment and the region of synaptic terminals. (Adapted from Livesey and Cepko (2001) with the permission of Elsevier Copyright Clearance Centre, License number: 3926710001545).

1.3.2.1 Photoreceptors

Human retinal photoreceptors consist of two distinct cell types, rods and cones (Figure 1.3B). Rods are the predominant photoreceptors in the peripheral retina, they

operation under dim light conditions but quickly saturate in bright light, and are mainly responsible for night vision, sensing brightness, contrast and motion (Rodieck and Rushton, 1976). There are relatively few cones at the retinal periphery but they increase in density in the central retina. Cones are relatively insensitive to light requiring relatively high light levels to activate them, and are hence functional in daylight. The cones are responsible for colour discrimination and visual acuity (Sugita and Tasaki, 1988).

Rods and cones differ in their shape, type of photopigment present, retinal distribution and pattern of synaptic connections (Rodieck, 1998; Swaroop et al., 2010). In terms of their shape, both cell types are elongated, highly polarized and have an inner and outer segment connected by a modified cilium. The inner segments (IS) contain numerous elongated mitochondria in addition to endoplasmic reticulum and the Golgi apparatus. The different architectures of their outer segments (OS) represent a major distinctive feature of these two cell types. Rods have a slim rod-shaped OS structure whilst cones are conical-shaped. The OS structures of rods are composed of individualized discs, unconnected to the ciliary plasma membrane, whilst cones have a shorter OS that is composed of a series of discs that are connected to the membrane of the cilium (Arikawa et al., 1992). In terms of type of photopigment, rods contain the visual pigment rhodopsin while cones contain one of the colour opsins. The distribution of rods to cones is not uniform across the surface of the retina (Figure 1.4). The total number of rods in the human retina (91 million) far exceeds the number of cones (roughly 4.5 million). As a result, the density of rods is much greater than cones throughout most of the retina. However, in the fovea, a tiny pit (1.5 mm in diameter) located in the macular region is responsible for sharp central vision. This area has an increased cone density of almost 200-fold, with a sharp decline in the density of rods. In fact, the central 0.35 mm of the fovea, called the foveola, is totally rod-free where all of the photoreceptors are cones (Purves et al., 2001).

The pattern of synaptic connections of rods and cones contributes to the different characteristics of scotopic (rod) and photopic (cone) vision. Each retinal ganglion cell receives input from only one cone bipolar cell, which in turn, is contacted by only a single cone. In contrast, each rod bipolar cell is contacted by a number of rods, and many rod bipolar cells contact a given amacrine cell. More convergence makes the rod system a better detector of light since many rods amplify a small signal to generate a large response

in the bipolar cell. However, such convergence also reduces the spatial resolution of the rod system. The one-to-one relationship of cones to bipolar and ganglion cells is just what is required to maximize visual acuity (Mustafi et al., 2009).

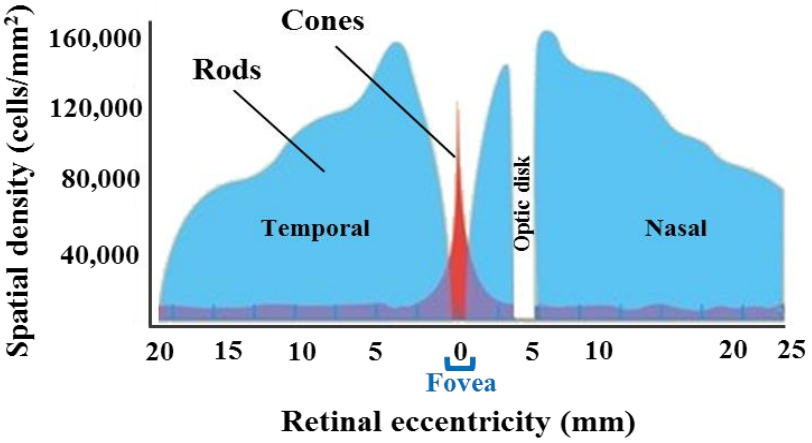

Figure 1.4. Distribution of rods and cones in the human retina. The graph illustrates that rods are present at a higher density throughout most of the retina, with a sharp decline in the fovea. Conversely, cones are present at low density throughout the retina, with a sharp peak in the centre of the fovea. (Adapted from free source: Psyc 2, Biological Foundations, http://mikeclaffey.com/psyc2/)

1.3.2.2 Bipolar cells

Bipolar cells are a type of neuron located in the inner nuclear layer (INL), which receive information from photoreceptors and horizontal cells to pass on to the ganglion and amacrine cells through their axons. Bipolar cells receive synaptic input from either rods or cones, but not both, so the cells can be classified on the basis of their synaptic connections. Morphologically, there are ten distinct sub-types of cone bipolar cells in the mammalian retina, and only one type of rod bipolar cell. Based on how they react to glutamate released by rods or cones, bipolar cells can be further classified into two different groups, ON and OFF bipolar cells (Euler and Schubert, 2015). In the dark, the photoreceptor releases glutamate, which hyperpolarizes (inhibits) the ON bipolar cells and depolarizes (excites) the OFF bipolar cells. However when light hits a photoreceptor cell, the photoreceptor releases less glutamate, and ON bipolar cells respond by depolarizing while OFF bipolar cells respond by hyperpolarizing.

1.3.2.3 Amacrine and horizontal cells

Amacrine cells are interneurons which are synaptically active in the inner plexiform layer (IPL) and serve to integrate, modulate and interpose a temporal domain to the visual message before presentation to the ganglion cell. Amacrine cells are responsible for 70% of the input to the retinal ganglion cells (Farsaii and Connaughton, 1995). There are three types of amacrine cells (mono- bi- or tri-stratified) which contact different types of bipolar and ganglion cells (Cuenca et al., 2002). Horizontal cells are also part of the indirect path of signals that originate from the photoreceptors and transmit to the ganglion cells. Horizontal cells are much less numerous than bipolar cells, which tend to dominate the middle layer of the retina. The horizontal cells smooth the photoreceptor output spatially, providing a negative feedback (lateral inhibition) in a process that sharpens our perception of contrast and colour (Park et al., 2003; Jackman et al., 2011).

1.3.2.4 Ganglion cells

Ganglion cells collect visual information in their dendrites from bipolar and amacrine cells and transmit this to the brain. Based on the dendritic morphologies, at least 13 distinct types of retinal ganglion cells have been identified. All of them vary significantly in terms of their size, interconnections and responses to visual stimulation (ON/OFF) (Wassle, 2004). Photosensitive ganglion cells are important for reflexive responses to bright daylight and play a major role in synchronizing circadian rhythms (Berson et al., 2002).

1.3.2.5 Müller cells

Müller cells are the principal glial cells extending throughout much of the retina. They form the architectural support structures. The apex of the Müller cell is in the photoreceptor layer, whereas the basal aspect is at the inner retinal surface. There are ten million Müller cells in the mammalian retina (Sarthy and Ripps, 2001), which are responsible for the homeostatic and metabolic support of retinal neurons. They express numerous voltage-gated channels and neurotransmitter receptors, which recognize a variety of neuronal signals and trigger cell depolarization and intracellular calcium transport. Recently Müller cells have been implicated in an alternative visual cycle (the cone visual cycle) (Section 1.4.4).

1.4 Visual phototransduction

Phototransduction is the process by which light is converted into a neural signal in rod or cone photoreceptors. The light is first absorbed by visual pigments in the photoreceptor OS, followed by a series of biochemical changes that lead to plasma membrane hyperpolarisation, in which an electric impulse flows through the retina to the bipolar and horizontal cells, followed by the amacrine and ganglion cells. Between each transfer, organization and processing occurs to the signal, and once a ganglion cell is activated, its axon carries the message through the optic nerve to the brain (McBee et al., 2001). A visual pigment (photopigment) consists of two covalently linked components. These are membrane protein moiety, called an opsin, and a chromophore. The opsins are G protein–coupled receptors (GPCRs), also known as seven-transmembrane (7TM) domain receptors, which form a long helix that loops across the membrane bilayer seven times. The chromophore within the looped protein is 11-*cis*-retinal (11-*cis*-retinaldehyde), which is a derivative of vitamin A, the component that actually absorbs the light photon (Menon et al., 2001; Filipek et al., 2003; Koyanagi and Terakita, 2014). All mammals have the same chromophore, but the membrane protein of the photopigments varies in different photoreceptor cell types. In rods the opsin is rhodopsin, whilst each cone will have one of three classes of opsin, Long wave-length, Medium wave-length or Short wave-length (L, M or S), which divide cones into red sensitive L-cones, green sensitive M-cones and blue sensitive S-cones (Okano et al., 1992).

1.4.1 Activation of the phototransduction cascade

Striking of a photon initiates photoisomerization of 11-*cis*-retinal into all-*trans*-retinal (Figure 1.5A) followed by conformational changes in the opsin to make the active intermediate (Meta II). The time scale for the formation of the Meta II is approximately one millisecond (ms) (Menon et al., 2001). Meta II then activates transducin (a heterotrimeric G-protein composed of Gα, Gβ, and Gγ subunits), by prompting the guanosine diphosphate (GDP) - guanosine triphosphate (GTP) exchange on the Gα subunit, leading to the dissociation of the GTP-bound form of Gα (Gα.GTP) from Gβγ (Mase et al., 2012). Gα.GTP in turn stimulates cyclic guanosine monophosphate-phosphodiesterase (cGMP-PDE) to lower the cytoplasmic level of cGMP. PDE is composed of two catalytic subunits (PDE$\alpha\beta$ in rods or two copies of PDEαs in cones) and

two inhibitory subunits (two copies of PDEγs in rods and in cones) (Cote, 2004). Gα·GTP acts by binding to an inhibitory subunit and removing its inhibitory influence on a catalytic subunit. The resulting increase in PDE activity increases the hydrolysis of cGMP to 5'-GMP and closes the cyclic nucleotide-gated (CNG) channels. Closure of the cation channels leads to a photoreceptor membrane hyperpolarization and reduces the glutamate release from the synaptic terminal of the cell.

1.4.2 The termination of phototransduction

Returning to the dark state occurs by the phosphorylation of Meta II by a G-protein-coupled receptor kinase (GRK) followed by the binding of a protein called arrestin to cap the activity of Meta II (Figure 1.5B). Simultaneously, Gα·GTP self-deactivates by its intrinsic GTPase activity, which hydrolyzes the bound GTP to GDP and consequently returns to its inactive Gα·GDP state to be ready for activation again after reassociating with G$\beta\gamma$ (Kleuss et al., 1994). The GTPase activity of Gα·GTP is enhanced by PDEγ, and a GTPase-activating protein (GAP) complex, which consists of regulator of G-protein-signalling isoform 9 (RGS9) with its anchor protein regulator of G protein signalling 9-binding protein (R9AP) and Gβ, another G-protein β-subunit-like protein (Arshavsky, 2013). Transducin deactivation acts by restoration of the inhibitory activity of PDE by its PDEγ. The free cGMP concentration then returns to the dark (high) level because of ongoing activity of the cGMP-synthesizing enzyme, guanylate cyclase (GC). In the dark resting state, there is a steady balance between the synthesis and hydrolysis of cGMP, and a single light flash transiently tips the balance toward hydrolysis (Lamb and Pugh, 2006). Meta II eventually decays to an intrinsically inactive state. The pigment then dissociates into opsin and free all-*trans*-retinal, a process called bleaching. The opsin also loses its bound arrestin and is dephosphorylated by a protein phosphatase 2A.

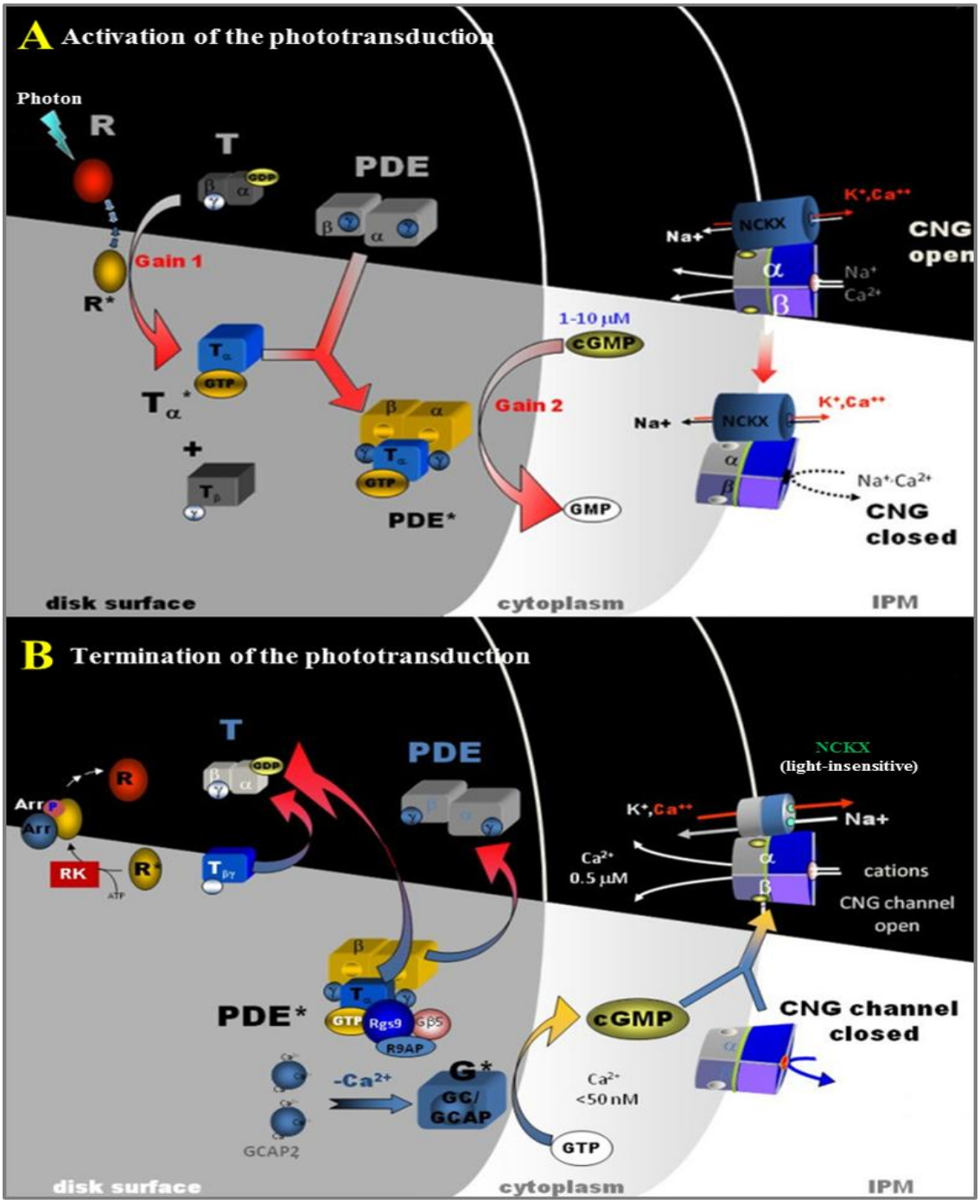

Figure 1.5. Summary of the phototransduction cascade in rods and cones. (A) Activation of the phototransduction cascade that results in the closure of cGMP-gated channels on the plasma membrane (from dark to light state). (B) Recovery of the phototransduction cascade that results in the re-opening of cGMP-gated channels on the plasma membrane (from light to dark state). R= rhodopsin (inactive); R*= rhodopsin (active); T= transducin; PDE= phosphodiesterase (inactive); PDE*= phosphodiesterase (active); NCKX= Na/Ca, K exchanger. IPM= interphotoreceptor matrix; Rgs9= regulator of G protein signalling protein 9; R9AP= regulator of G protein signalling 9-binding protein (RGS9 anchor protein); GC= guanylate-cyclase; Arr= arrestin; GCAP= guanylate-cyclase-activating protein. (Adapted with a free license from Fu (2010)).

1.4.3 Phototransduction components and negative-feedback pathways

Rods are more sensitive to light, and have adapted to detect light at lower levels than cones, whereas cones operate in bright light. Phototransduction for rods and cones has quantitative differences in the process depending on the nature of each subtype of the photoreceptor. There are not only quantitative differences in terms of sensitivity to brightness of light conditions between rod and cone phototransduction processes but there are also differences in protein isoforms that involved in each process (Table 1.1). Calcium (Ca^{2+}) has a critical role in the adaptation of rods or cones to light (Torre et al., 1986). Closure of the CNG channels stops the Ca^{2+} influx, but the Ca^{2+} efflux through the exchanger continues, resulting in a decrease in the free Ca^{2+} concentration in the OS. This Ca^{2+} decrease triggers multiple negative feedback pathways to regulate phototransduction by opposing the effect of light, thus producing active adaptation by the cell to light. The main negative-feedback pathway acts on GC to enhance its activity. The activity of GC is facilitated by guanylate-cyclase-activating proteins (GCAPs), which in turn are controlled by Ca^{2+} in that they act well when not binding Ca^{2+} and poorly when they bind Ca^{2}+ (Dizhoor et al., 2010). Thus, in darkness, the GC activity is only moderate because the high intracellular free Ca^{2+} keeps the GCAPs in check, whereas in the light, the GC activity is enhanced to oppose light because the GCAPs are more active due to lower free Ca^{2+}.

Another pathway is thought to act on the pigment kinase that phosphorylates Meta II to quench the latter's activity, via a Ca^{2+}-binding protein called recoverin. It is thought that recoverin in Ca^{2+}-bound form inhibits the pigment kinase (Gorczyca et al., 2003). Thus, in the light, when Ca^{2+} is relatively low and recoverin loses its bound Ca^{2+}, the kinase quenches Meta II quickly to reduce amplification, again opposing light. A third pathway acts on the CNG channel via calmodulin, which in Ca^{2+}-bound form reduces the affinity of the channel for cGMP (Hsu and Molday, 1993). Thus, in darkness, the Ca^{2+}-calmodulin binds to the CNG channel and lowers its probability of opening. In the light, calmodulin loses its bound Ca^{2+} and dissociates from the channel, as a result of which the CNG channel is more likely to reopen because of its now higher affinity for cGMP, thus opposing the effect of light. Calmodulin, GCAPs, and recoverin are all EF-hand-type Ca^{2+}-binding proteins. Of the three Ca^{2+}-mediated regulatory pathways, the one acting on GC is the most important for low and intermediate light levels, above which the one via

recoverin begins to kick in, becoming increasingly important with still higher light levels. The regulatory pathway on the channel is weak and of minimal importance.

A. Rod component	Gene symbol	Protein Symbol	Activity/function
Rhodopsin	*RHO*	Rho	Light reception; a guanine nucleotide exchange factor (GEF)
Transducin	*GNAT1*	Tα	Activator of rod phosphodiesterase (PDE)
	GNB1	Tβ	Binds phosducin
	GNGT1	Tγ	
Phosphodiesterase (PDE) 6	*PDE6A*	PDE6α	Cyclic guanosine monophosphate (cGMP) hydrolysis
	PDE6B	PDE6β	
	PDEG	PDE6γ	PDE inhibitor
Cation channel	*CNGA1*	CNGA1	cGMP-gated cation channel
	CNGB1	CNGB1	
Exchanger	*SLC24A1*	NCKX1	Cation Exchanger
Guanylate cyclase 2	*GUCY2F*	GC2	Produces cGMP from guanosine triphosphate (GTP)
Arrestin	*SAG*	Arr	Binds to phosphorylated Rho
GC-activating protein 2	*GUCA1B*	GCAP2	Guanylate cyclases (GC) activator at low Ca^{2+}
B. Cone component			
Blue pigment	*OPN1SW*	S-opsin	Light reception; GEF
Green pigment	*OPN1MW*	M-opsin	
Red pigment	*OPN1LW*	L-opsin	
Cone transducin	*GNAT2*	cTα	Activator of cone PDE
	GNB3	Gβ3	
	GNGT2	cTγ	
Cone phosphodiesterase	*PDE6C*	PDE6α′	cGMP hydrolysis
	PDE6H	PDE6γ′	Inhibitor
Cation channel	*CNGA3*	CNGA3	cGMP-gated cation channel
	CNGB3	CNGB3	
Cone exchanger	*SLC24A2*	NCKX2	Cation exchanger
Cone arrestin	*ARR3*	cArr	Binds to phosphorylated cone pigments
Cone pigment kinase	*GPRK7*	GRK7	Phosphorylates cone pigments
GC-activating protein 3	*GUCA1C*	GCAP3	GC activator at low Ca^{2+}
C. Shared component			
Guanylate cyclase 1	*GUCY2D*	GC1	Produces cGMP
GC-activating protein 1	*GUCA1A*	GCAP1	Mediates Ca^{2+} sensitivity of GC1and GC2
PDEδ	*PDE6D*	PrBP/δ	Prenyl binding protein; chaperone in intracellular trafficking
Phosducin	*PDC*	Pdc	Binds to Tβγ
Rhodopsin Kinase	*GRK1*	GRK1	Phosphorylates Rho
GTPase-activating protein regulator of G-protein signalling	*RGS9*	RGS9-1	Accelerates GTP hydrolysis of G protein, transducin (Gt) αGTP (GtαGTP)
RGS9 anchoring protein	*R9AP*	R9AP	RGS9 anchoring protein
G-protein b subunit 5	*GNB5*	Gβ5L	GTPase activity

Table 1.1. Photoreceptor components involved in visual phototransduction. Column 1 = components for rods (A) or cones (B) or shared (C), column 2 = gene symbol, column 3 = protein symbol, column 4 = activity and/or function of the component. **(**Sources: RetNet, https://sph.uth.edu/retnet/home .htm, Purves et al. (2001), Karan et al. (2008) and Yau and Hardie (2009)).

1.4.4 The visual cycle

The visual cycle describes the pathway that occurs in the RPE and photoreceptors to recycle all-*trans*-retinal back to 11-*cis* retinal (Figure1.6). Most of the all-*trans*-retinal dissociates from the opsin complex with phosphatidylethanolamine and is transported to the cytoplasmic disc surface by the retina specific ATP binding cassette subfamily A, member 4 (ABCA4), and released into the cytoplasm as all-*trans*-retinal (Liu et al., 2000; Sparrow et al., 2010b). All-*trans*-retinal in the cytoplasm is reduced to all-*trans*-retinol (Vitamin A) by all-*trans*-retinol dehydrogenase (RDH) in a reversible nicotinamide adenine dinucleotide phosphate (NADPH)-dependent reaction (Palczewski, 2010). All-*trans*-retinol is bound to the interphotoreceptor retinoid-binding protein (IRBP), leaves the photoreceptors and diffuses into the RPE (Jin et al., 2009). In the RPE, all-*trans*-retinol is bound to cellular retinol-binding protein (CRBP) (Bridges et al., 1984) and esterified in a reaction catalyzed by lecithin retinol acyl transferase (LRAT) (Saari and Bredberg, 1989; Saari et al., 1993). These all-*trans*-retinyl esters are then hydrolysed and isomerized to 11-*cis*-retinol by the isomerohydrolase retinal pigment epithelium 65 (RPE65) enzyme (Cai et al., 2009). Cellular retinaldyhyde binding protein (CRALBP) delivers the 11-*cis*-retinol to 11-*cis*-retinol dehydrogenase (11-*cis*-RDH) for oxidization of 11-*cis* retinol to 11-*cis*-retinal using NAD as a cofactor (Haeseleer et al., 2002). Finally 11-cis-retinal is then bound to IRBP and diffuses from the RPE to combine with the opsin proteins ready for another photoisomerization reaction.

This visual cycle is known as the classical cycle and it was associated with rods and is thought to apply to cones also. However more recently it has become known that Muller cells also possess a self-contained chromophore-regenerating mechanism exclusive for the cones. Cones are specialized for functioning in daytime vision where constant light increases the demand for 11-*cis*-retinal. In the proposed cone visual cycle, all-*trans* retinol generated in photoreceptors is transported to Müller cells and isomerized to 11-*cis*-retinol by an unidentified isomerase (Wang and Kefalov, 2011). This theory of the cone-specific retina visual cycle reflects the fact that Müller cells have the ability to generate 11-*cis*-retinol from all-*trans*-retinol (Das et al., 1992; Kanan et al., 2008). In addition, Müller microvilli have visual cycle components such as CRALBP and IRBP (Dyer and Cepko, 2000; Betts-Obregon et al., 2014). However the proposed cone-specific visual cycle pathway has not been proven yet.

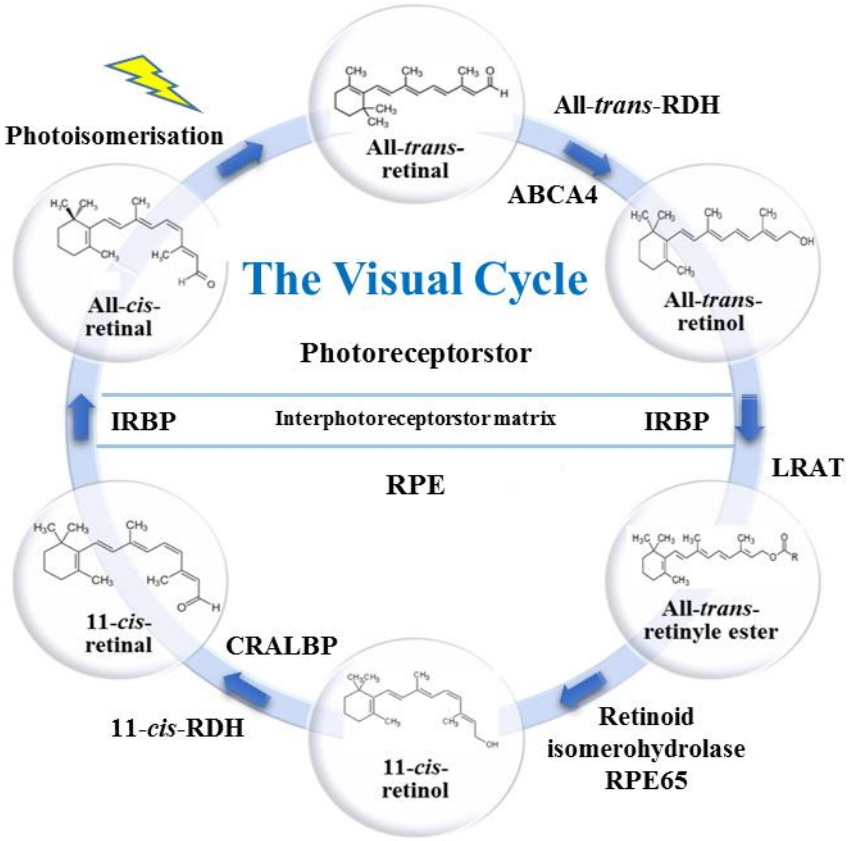

Figure 1.6. The visual cycle. The visual cycle between photoreceptors and retinal pigment epithelium including enzymatic reactions that recycle the retinoids. Activation of the chromophore within the looped opsin by light leads to the isomerization of 11-*cis*-retinal to all-*trans*-retinal. All-*trans* retinal is released, transported to the cytoplasm by ATP-binding cassette, subfamily A, member 4 (ABCA4) and modified to all-*trans*-retinol by all-*trans*-retinol dehydrogenase (all-*trans*-RDH). After that, it is transported to the RPE where it is esterified to all-*trans*-retinyle ester by lecithin retinol acyltransferase (LRAT). All-*trans*-retinyl ester is then isomerized to 11-*cis*-retinol by RPE65 and bound to cellular retinaldyhyde binding protein (CRALBP) for oxidation by 11-*cis*-retinol dehydrogenase (11-*cis*-RDH) to 11-*cis*-retinal. After transport back to the photoreceptor, 11-*cis*-retinal binds to opsin, rendering it sensitive to light. Retinoids are transferred from and to the photoreceptors bound to interstitial retinol-binding protein (IRBP, also known as RBP3).

1.4.5 Phototransduction, visual cycle and retinal disease.

All the components involved in the phototransduction process (Table 1.1) together with all the binding proteins and enzymes involved in the visual cycle or retinoid metabolism, have an important role in human vision. Defects in genes encoding the proteins that are involved in nearly every step of these pathways are responsible for

human-inherited retinal dystrophies (IRDs). For example mutations in *GUCA1A* (Downes et al., 2001a), *GUCY2D* (Kitiratschky et al., 2008), *GUCA1B* (Sato et al., 2005), *PDE6A* (Dryja et al., 1999), *PDE6B* (Shen et al., 2014b), *PDE6C* (Thiadens et al., 2009a), *PDE6G* (Dvir et al., 2010), *PDE6H* (Piri et al., 2005), *CNGB1* (Bareil et al., 2001), *CNGB3* (Nishiguchi et al., 2005), *CNGA1* (Dryja et al., 1995), *PRPH2* (Nakazawa et al., 1994), *RDH12* (Janecke et al., 2004), *LRAT* (Ruiz et al., 2001), RPE65 (Bowne et al., 2011a), *RHO* (Rosenfeld et al., 1992), *SAG* (Nakazawa et al., 1998), *IRBP/RBP3* (den Hollander et al., 2009) and *ABCA4* (Martinez-Mir et al., 1998; Zhang et al., 2015a) are all assosiated with varies types of IRDs (Tables 1.2, 1.3, 1.5 and 1.6).

1.5 Inherited retinal dystrophy

Monogenic retinal dystrophies (RDs) represent the most frequent inherited form of human visual handicap, affecting approximately 1 in 2000 individuals worldwide (Berger et al., 2010). The genetic basis of RDs is extremely heterogeneous. To date, more than 250 genes have been found to have pathogenic mutations giving rise to the different forms of retinal disease (https://sph.uth.edu/retnet/sum-dis.htm#A-genes) and still new mutations and novel genes have yet to be discovered (Audo et al., 2012a; Tiwari et al., 2016). The retinal disorders vary in terms of the cell types affected, the age of onset of visual problems and the inheritance pattern. There is also a wide range of clinical manifestations for these disorders including mild dysfunctions such as night blindness, to severe, early onset (congenital) RDs. The main RDs which form the basis of this study are briefly reviewed here.

1.6 Retinitis pigmentosa (RP)

1.6.1 Overview

Retinitis pigmentosa (RP, OMIM 268000) is the most frequent subtype of inherited RD with a prevalence of approximately 1 in 3,000 to 1 in 5,000 individuals and affecting approximately 1.5 million people worldwide (Ammann et al., 1965; Berson, 1993; Haim, 2002; Shintani et al., 2009; Bowne et al., 2011b). RP is characterized by progressive degeneration of the photoreceptors with subsequent degeneration of the RPE, typically starting in the peripheral retina and advancing towards the macula and fovea (Hamel, 2006; Hartong et al., 2006).

At the cellular level, the peripheral rod cells are affected first causing rod photoreceptor degeneration and RP. Later the effect on central cones often prompts secondary cone degeneration. The photoreceptors die by apoptosis and this is reflected by a reduced outer nuclear layer thickness within the retina (Hartong et al., 2006; Marigo, 2007). The bipolar cells in the retina remain intact and healthy even after rod cell apoptosis at the early stages of disease (Baumgartner, 2000). However, these fully functional bipolar cells try to re-establish communication with nerves of the other photoreceptor subtype (cones) leading to inappropriate signals in the cone cells. These inappropriate signals, over time, lead to cone dystrophy (John et al., 2000). It has been observed that the inner retina is preserved during the course of RP in the *rd* mouse model, as bipolar and horizontal cells are functional even after photoreceptor loss (Strettoi and Pignatelli, 2000).

1.6.2 Clinical manifestation of RP

Visual problems in patients with RP often begin in their early childhood, followed by severe visual impairment by the ages of 40 to 50 years (Mitamura et al., 2012; Wang et al., 2016b). The first symptom is increasing difficulty with night vision (night blindness or nyctalopia), followed by a progressive decrease in the visual fields leading to tunnel vision. Patients with RP suffer from defective light to dark and dark to light adaptation. In general, the earlier the age of onset of defective dark adaptation, the more severe the course of RP (Fahim et al., 2013). Loss of central visual acuity over time correlates with the presence of macular lesions early in the course of the disease (Flynn et al., 2001). Despite the early cone involvement in some cases of RP, the central visual acuity in both eyes is usually preserved for years or even decades until the end stages of the disease course (El-Asrag et al., 2015; Sergouniotis et al., 2015). There is a general correlation between age-related visual acuity and mode of inheritance. X-linked RP (XLRP) represents the worst prognosis for vision (<20/200), especially for male patients older than fifty years old. Autosomal dominant RP (adRP) has the best prognosis for vision (≥20/30) while autosomal recessive RP (arRP) has intermediate prognosis for vision (Fishman, 1978).

In the earliest stages of RP, the fundus appearance appears normal followed by a fine dust-like intraretinal pigmentation (Figure1.7), generalized retinal arteriolar

narrowing and loss of pigment from RPE (Mathijssen et al., 2016). Pigmentation in the retina is a sign that light-sensing rod cells are deteriorating, so it becomes very difficult for the patient to see in dim light. With progression of rod photoreceptor degeneration, there is increasing loss of RPE pigment with intraretinal clumping of melanin, appearing as coarse clumps in the classic bone spicule configuration that predominantly exists in the peripheral retina. Vascular attenuation and waxy pallor of the optic nerve also become more apparent in individuals with RP at this stage (Ma et al., 2015). Later manifestations of RP include cataracts, photophobia, and macular oedema (Jackson et al., 2001). Moreover, some cases reported a serous retinal detachment and retinal lipid deposition (Dave et al., 2016). Patients with RP have diminished or absent a-wave (indicate activity of photoreceptors) and b-wave (derived from ON bipolar cells) in their electroretinograms (ERGs) (Dolan et al., 2002; Hamel, 2006).

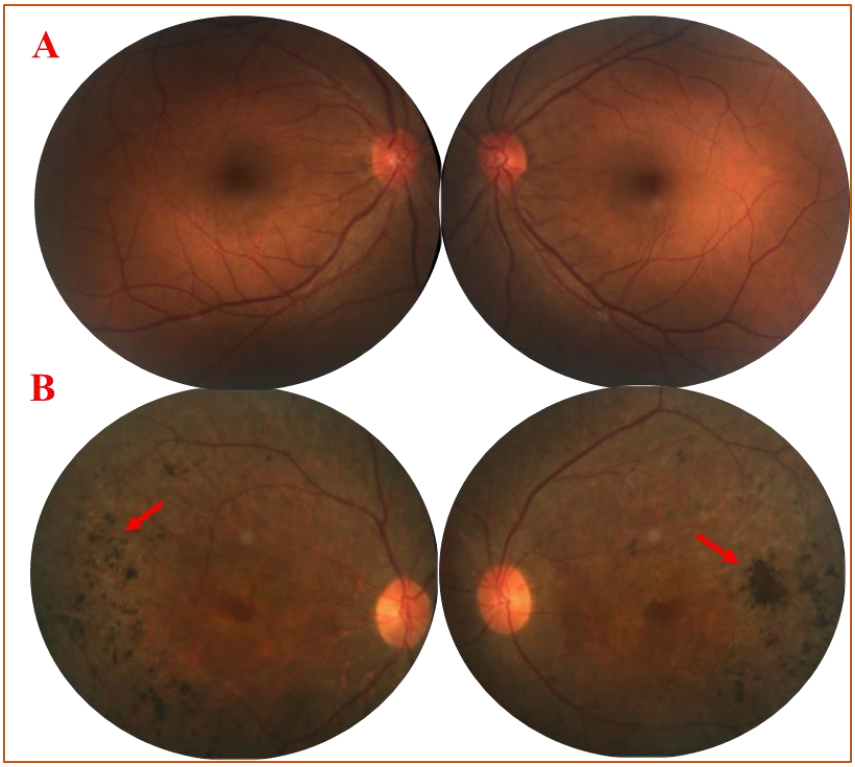

Figure 1.7. Colour fundus photography of patients with typical RP symptoms. Photograph of the right and left eye fundi in a normal individual (A) and affected RP patient (B). The RP patient fundus has peripheral intraretinal pigment deposits in a bone-spicule configuration (arrows), diffuse mottling of the retinal pigmented epithelium, attenuated retinal arterioles, waxy optic discs and a degenerated macula. (Adapted from Gao et al. (2016), no permission is needed).

1.6.3 Genetics of RP

RP can be sub-classified into juvenile RP and late onset RP according to age of onset, while congenital peripheral RD would be classified as Leber congenital amaurosis (LCA, Section 1.8). RP has also been classified according to the distribution of retinal involvement such as central, pericentral, sector, or peripheral. The most common classification is based on the modes of inheritance, dividing RP into X-linked RP (XLRP), autosomal recessive RP (arRP), autosomal dominant RP (adRP) and digenic RP. RP can also be subdivided into non-syndromic and syndromic types. Non-syndromic cases are those in which symptoms and signs are confined to the eye alone, without systemic abnormalities, and these are inherited as an autosomal dominant (20-25%), autosomal recessive (20-30%), X-linked recessive (10-15%) or sporadic/simplex trait (30-40%). 4% of cases are so early in onset that they are grouped as part of LCA. Rarer forms also exist such as X-linked dominant, mitochondrial and digenic RP (Kajiwara et al., 1994). RP can also exist as part of a syndrome that affects other organs and tissues in the body. Most syndromic cases are inherited via an autosomal recessive pattern (Daiger et al., 2007; Ferrari et al., 2011) and the most frequent forms include Usher syndrome (USH) (10%) (Section 1.6.3.5) and Bardet-Biedl syndrome (BBS) (5%) (Section 1.6.3.6).

1.6.3.1 Autosomal recessive RP (arRP)

An autosomal recessive pattern of inheritance means both copies of a gene in each cell have mutations, that these affect men and women equally and that both parents are carriers. As each parent has a 50% chance of passing on the mutation, together they have a 25% chance of having offspring who inherit two mutated copies and are therefore affected (Wang et al., 2005). Consanguinity increases the likelihood that a recessive trait will be manifested. Parents and offspring who carry one copy of a mutated gene (heterozygous), typically do not show any signs and symptoms of disease (Ravesh et al., 2015). arRP is the most frequent inheritance type of RP, with the 57 arRP genes identified to date accounting for approximately 20% to 30% of all RP cases. arRP genes encode proteins with a wide variety of retinal functions including in phototransduction, photoreceptor maintenance and function, the visual cycle, ciliogenesis and cell signalling (Table 1.2).

Gene	Estimated frequency	Potential function	OMIM	Gene	Estimated frequency	Potential function	OMIM
USH2A	12-20%	Cellular structure	613809	***TULP1***	≤1%	Tissue development & maintenance	602280
ABCA4	2-5%	Visual cycle	601718	***ZNF513***	≤1%	Transcription factor	613617
PDE6A	2-5%	Phototransduction	613801	***ARL6***	≤1%	Transmembrane protein	613575
PDE6B	2-8%	Phototransduction	613801	***NR2E3***	Rare	Transcription factor	611131
RPE65	2-5%	Visual cycle	613794	***MAK***	≤1%	Cellular structure	614181
CNGA1	1-2%	Phototransduction	613756	***MERTK***	≤1%	Transmembrane protein	613862
AGBL5	≤1%	posttranslational modification of tubulin	615900	***MVK***	unknown	Visual cycle /unknown	175900
ARL2BP	Unknown	Photoreceptor maintenance and function	615407	***NEK2***	≤1%	Cell division	615565
BBS1	≤1%	Ciliogenesis	209901	***NEUROD1***	≤1%		606394
BBS2	≤1%	Ciliogenesis	616562	***NRL***	≤1%	Tissue development & maintenance	613750
BEST1	≤1%	Anion channel	613194	***PDE6G***	≤1%	Phototransduction	613582
C2orf71	≤1%	Unknown	613428	***POMGNT1***	≤1%	Glycosylation	613157
C8orf37	≤1%	Unknown	614500	***PRCD***	≤1%	Unknown	610599
CLRN1	≤1%	Photoreceptor structure	614180	***PROM1***	≤1%	Cellular structure	612095
CNGB1	≤1%	Phototransduction	613767	***RBP3***	≤1%	Visual cycle	180290
CYP4V2	≤1%	Fatty acid and steroid metabolism	608614	***RGR***	≤1%	Visual cycle	613769
DHDDS	≤1%	Photoreceptor structure	613861	***RHO***	≤1%	Phototransduction	613731
DHX38	unknown	Splicing	605584	***RLBP1***	≤1%	Visual cycle	607475
EMC1	≤1%	Unknown	616846	***RP1***	≤1%	Tissue development & maintenance	603937
FAM161A	≤1%	Tissue development & maintenance	613596	***RP1L1***	≤1%	Tissue development & maintenance	608581
GPR125	≤1%	Unknown	612303	***SLC7A14***	1-2%	Unknown	615725
HGSNAT	≤1%	Unknown	616544	***SPATA7***	≤1%	Unknown	609868
IDH3B	≤1%	Citric acid cycle	612572	***TTC8***	≤1%	Transmembrane protein	613464
IFT140	≤1%	Intraflagellar transport	614620	***ZNF408***	≤1%	Transcription factor	616469
KIZ	≤1% in north African (Sephardic Jews)	Cell division	616394	***EYS***	Common in china, 10-30% in Spain	Cell signaling	612424
IMPG2	≤1%	Cellular structure	613581	***CRB1***	6-7% (Spain)	Tissue development & maintenance	604210
KIAA1549	≤1%	Unknown	613344	***CERKL***	3-4% (Spain)	Cell signaling	608381
IFT172	≤1%	Intraflagellar transport	615780	***SAG***	2-3% in Japan	Phototransduction	613758
LRAT	≤1%	Visual cycle	613341				

Table 1.2. List of genes implicated in autosomal recessive RP (arRP). Gene name, estimated frequency (%) of arRP attributed to mutations in this gene and potential function are listed along with the corresponding OMIM number. (Sources: RetNet, https://sph.uth.edu/retnet/home .htm; OMIM, http: //www.ncbi.nlm.nih.gov/omim; Ruiz et al. (1998); Klevering et al. (2004); Abd El-Aziz et al. (2007); Avila-Fernandez et al. (2010); Daiger et al. (2013); Fahim et al. (2013); Nash et al. (2015))

The most prevalent mutant genes in arRP cases are *USH2A*, the *PDE6A* and *B* genes, *EYS*, *ABCA4* and *RPE65*. *USH2A* is the most commonly mutated gene in Usher

syndrome type 2 (USH2) (Liu et al., 1999; Adato et al., 2000; McGee et al., 2010) (Section 1.6.3.5), but pathogenic variants in this gene also cause 10%-15% of non-syndromic arRP (Rivolta et al., 2000; Xu et al., 2011; Zhao et al., 2014). *USH2A* encodes a protein called usherin that represents an important component of basement membranes. In the human retina, usherin localizes to the connecting cilia of photoreceptors, where it is likely to be involved in cargo delivery from the IS to the OS of the photoreceptor cell (van Wijk et al., 2004; Reiners et al., 2006; Maerker et al., 2008).

More than 36,000 RP cases worldwide are due to defects in components of the heterotetrameric PDE 6 complex, estimated to account for approximately 6-14% of all diagnosed arRP (Ferrari et al., 2011). *PDE6A, PDE6B* and *PDE6G*, mutations in any of which cause RP, encode proteins important in the photoreceptor visual transduction cascade (Tsang et al., 1998) (Section 1.4). The *PDE6* gene has a similar structure to the *PDE5* gene. PDE5 expression is inhibited by sildenafil (Behn and Potter, 2001) and also heterozygous carriers of *PDE6* mutations are at risk of losing vision when excessively inhibiting PDE6 with a commonly used medication for erectile dysfunction such as sildenafil, tadalafil, or vardenafil (Stockman et al., 2007; Tsang et al., 2008).

Mutations in *EYS* (eyes shut homolog) appear to be a prevalent cause of RP in different population-based studies. Pathogenic variants in *EYS* are fairly common in the Chinese population (Abd El-Aziz et al., 2007), and accounts for 10%-30% of Spanish patients with arRP (Barragán et al., 2010). *EYS* is the largest gene that is known to be expressed in the human eye and is likely to have a role in the modelling of retinal architecture (Zelhof et al., 2006).

ABCA4 and *RPE65* encode proteins that are involved in retinoid metabolism (the visual cycle) (Section 1.4.4) and mutations in each of the two genes have been reported to account for between 2-5% of arRP cases. Mutations in *ABCA4* also cause Stargardt disease (STGD) and are responsible for 30 to 60% of cases with autosomal recessive cone-rod dystrophy (CRD) (Section 1.7.3) (Cideciyan et al., 2009), while the *RPE65* gene mutations also account for more than 10% of LCA patients (Section 1.8) (Gu et al., 1997; den Hollander et al., 2008).

1.6.3.2 Autosomal dominant RP (adRP)

Autosomal dominant RP (adRP) affects men and women with equal frequency and severity and there tends to be a known history of the condition in the family, since an affected parent has a 50% chance of passing the defective gene to the offspring. Most cases that have been identified show complete penetrance of the mutation. However, great variation in phenotypes for adRP disease, even within the same pedigree, has been reported (Holopigian et al., 1996). adRP is the second most frequently inherited type of RP, accounting for approximately 15% to 20% of all RP cases, and 29 adRP genes have been identified to date. Like arRP genes, adRP genes encode proteins with a wide variety of retinal functions, including phototransduction, photoreceptor OS structure, tissue development & maintenance, regulation of cell growth and splicing (Table 1.3).

Gene	Estimated frequency	Potential function	OMIM	Gene	Estimated frequency	Potential function	OMIM
RHO	20-30%	Phototransduction	613731	***PRPF3***	≤1%	Splicing	607301
PRPH2	5-10%	Photoreceptor OS structure	606419	***PRPF4***	unknown	Splicing	615922
PRPF31	5-10%	Splicing	608133	***PRPF6***	Rare	Splicing	613983
RP1	3-4%	Tissue development & maintenance	603937	***RDH12***	Unknown	Phototransduction	612712
IMPDH1	2-3%	Regulates cell growth	180105	***ROM1***	Rare	Cellular structure	180721
PRPF8	2-3%	Splicing	607300	***RP63***	One family	Unknown	614494
KLHL7	1-2%	Ubiquitin proteasome protein degeneration	612943	***RP9***	Rare	Splicing	607331
NR2E3	1-2%	Transcription factor	611131	***RPE65***	Rare	Visual cycle	613794
AIPL1	≤1%	Transport, protein trafficking	604392	***SNRNP200***	1-2%	Splicing	610359
ARL3	≤1%	Transport, protein trafficking	604695	***SPP2***	≤1%	Unknown	602637
BEST1	Rare	Anion channel	613194	***TOPORS***	≤1%	Ubiquitin protein ligase	609923
CA4	Rare	Unknown	114760	***GUCA1B***	Rare (4-5% in Japan)	Phototransduction	613827
CRX	1%	Transcription factor	602225	***SEMA4A***	Rare (3-4% in Pakistan)	Tissue development & maintenance	610282
HK1	≤1%	Glucose metabolic	605285	***FSCN2***	Rare (3% in Japan)	Cellular structure	607921
NRL	≤1%	Tissue development & maintenance	613750				

Table 1.3. List of genes implicated in autosomal dominant RP (adRP). Gene name, estimated frequency (%) of adRP attributed to mutation of this gene and potential function are depicted along with the corresponding OMIM number. (Sources: RetNet, https://sph.uth.edu/retnet/ home.htm, OMIM, http: //www.ncbi.nlm.nih.gov/omim; Sohocki et al. (2000), Bowne et al. (2008), Daiger et al. (2008), Davidson et al. (2009), Bowne et al. (2011a), Tanackovic et al. (2011), Daiger et al. (2013), Fahim et al. (2013), Cvackova et al. (2014) and Nash et al. (2015)).

The most prevalent causes of adRP are mutations in *RHO*, *PRPH2*, *PRPF31* and RP1. *RHO*, the first gene found to be mutated in RP (Dryja et al., 1990; Dryja et al., 1991), encodes the rod photoreceptor-specific rhodopsin. Absorption of a photon by this transmembrane protein initiates the visual phototransduction cascade (Section 1.4). More than 100 *RHO* pathogenic mutations have been reported to cause approximately 20-30% of all adRP cases (Wang et al., 2005). While extensive mutational heterogeneity has been characterized in human *RHO* (Lewin et al., 2014), one common founder mutation (NM_000539.3:c.68C>A, p.Pro23His) among Americans of European origin causes 12%-14% of adRP in this population (Sullivan et al., 2006a).

Mutations in *Peripherin2/RDS (PRPH2)* and *PRPF31* are also common causes of adRP, each accounting for between 5%-10% of cases. Peripherin2 is a photoreceptor specific transmembrane glycoprotein necessary for the proper formation of both rod and cone POS. Mutations in *PRPH2* are associated with a wide range of phenotypes including adRP, autosomal dominant macular degeneration (adMD) and complex maculopathies (Cheng et al., 1997; Stuck et al., 2016). *PRPF31* encodes a protein involved in pre-mRNA splicing and genomic rearrangements in this gene account for 5-10% of adRP, this form of adRP shows partial penetrance in that it often skips generations (Sullivan et al., 2006b; Villanueva, 2014).

Known pathogenic variants in *RP1 (*Retinitis Pigmentosa 1) account for 3%-4% of adRP, with two common founder mutations (NM_006269.1: c.2029C>T, p.R677*and c.2285_2289delTAAAT, p.L762Yfs*17) accounting for 2%-3% of all adRP cases. (Payne et al., 2000; Gamundi et al., 2006; Audo et al., 2012b; Fahim et al., 2013). RP1 is a photoreceptor microtubule-associated protein that plays an essential and synergistic role with RP1L1 in OS morphogenesis to maintain the photosensitivity of rod photoreceptors (Yamashita et al., 2009) .

1.6.3.3 X-linked RP

XLRP is the least frequently inherited type of RP, accounting for only 10% to 15% of cases. In XLRP, there is no male to male transmission of the abnormal gene and female carriers have a 50% chance of passing XLRP to their sons, while all female offspring will have a 50% chance of being a carrier. Males with XLRP are characterized by a severe

phenotype during the early stages of disease. A milder phenotype can sometimes occur in female carriers (Comander et al., 2015), probably due to non-random or skewed inactivation of one X chromosome (Friedrich et al., 1993; Carrel and Willard, 2005). Six loci have been mapped on X-chromosome that are responsible for XLRP (*RP6, RP23, RP24, RP34, RP2* and *RPGR*), but only three mutated genes have been identified so far. These are the retinitis pigmentosa GTPase regulator (*RPGR*/*RP3*), the retinitis pigmentosa 2 (*RP2*) and the retinitis pigmentosa 23 (*RP23*) or oral facial digital syndrome 1 (*OFD1*).

Pathogenic mutations in *RPGR* (OMIM 312610) are the most common cause of XLRP accounting for 70 to 75% of all XLRP cases and 15-20% of nonsyndromic RP in North American families (Breuer et al., 2002; Shu et al., 2007; Churchill et al., 2013). *RPGR* has two major transcripts, *RPGRex1-19* that contains 19 exons, encoding 815 amino acids protein, and *RPGR-ORF15* that has 15 exons, encoding 1152 amino acids protein. *RPGR-ORF15* shares exons 1-14 with *RPGRex1-19* plus the exon open reading frame 15 (ORF15) that encodes 567 amino acids with a highly repetitive glycine and glutamic acid-rich domain (Meindl et al., 1996; Vervoort et al., 2000). *RPGR* mutations are associated with XLRP, CRD and MD. Most mutations in this gene are detected in ORF15 region that represent a mutational hotspot, with a mutation rate of 30-60% of all XLRP cases (Vervoort et al., 2000; Pusch et al., 2002; Shu et al., 2008; Branham et al., 2012). RPGR localizes to the POS in human and to photoreceptor connecting cilia in mouse (Mavlyutov et al., 2002; Hong et al., 2003). RPGR is involved in ciliogenesis (Gakovic et al., 2011; Patnaik et al., 2015) and has many interacting partner proteins such as RPGR interacting protein 1 (RPGRIP1), RPGRIP1-like protein (RPGRIP1L), delta subunit of phosphodiesterase (PDEδ), structural maintenance of chromosomes (SMC) 1 and SMC3 (Linari et al., 1999; Hong et al., 2001; Khanna et al., 2005). The role of the RPGR in ciliogenesis was supported by genetic studies where bronchiectasis, respiratory tract infections and sensorineural hearing loss, were associated with XLRP caused by an RPGR mutations with variable penetrance (Iannaccone et al., 2003; Koenekoop et al., 2003; Zito et al., 2003; Moore et al., 2006) . Interestingly, mutations causing syndromic XLRP, to date, are restricted to exons 1–14, suggesting mutations in ORF15 may not be a cause of extraocular phenotypes (Tee et al., 2016).

Approximately 10-15% of XLRP patients have mutations in the *RP2* gene (OMIM 312600). The amino-terminal domain of RP2 has a cofactor C domain that share

homology with tubulin-specific chaperone protein, essential component in tubulin folding (Evans et al., 2006). RP2 has a potential role for in maintaining Golgi cohesion and targeting of proteins to plasma membrane (Evans et al., 2010). Mutations in this gene cause incorrect folding of the photoreceptor or neuron-specific tubulin isoforms followed by progressive retinal degeneration (Bartolini et al., 2002; Patil et al., 2011). *OFD1*/*RP23* (OMIM 311200) is a more recently identified causative gene for XLRP (Webb et al., 2012). OFD1 plays a role in controlling photoreceptor cilium length and number, and protects the photoreceptor from oxidative stress and apoptosis (Wang et al., 2016a). Mutations in *OFD1* also cause a group of ciliopathy related disorders. These include Joubert syndrome (OMIM 300804) (Wentzensen et al., 2016) which is characterised as a neurodevelopmental disorder, with brain abnormalities called the molar tooth sign, respiratory problems in infancy and RD, and oral facial digital type 1 syndrome (OMIM 311200) (Ferrante et al., 2001; Thauvin-Robinet et al., 2006; Tsurusaki et al., 2013), which is an X-linked dominant condition with lethality in males in the first or second trimester pregnancy and is characterized by facial anomalies, abnormalities in oral tissues, digits, brain, and kidney.

1.6.3.4 Digenic and mitochondrial RP

Other rare modes of RP inheritance include digenic RP which was reported as heterozygous mutations in *PRPH2* and *ROM1* (Kajiwara et al., 1994; Goldberg and Molday, 1996; Dryja et al., 1997). Also mitochondrial inheritance was reported in RP (Mansergh et al., 1999) in which mitochondrial DNA defects were transmitted through maternal transmission.

1.6.3.5 Usher syndrome (USH)

Usher syndrome (USH) (OMIM 276900-276902) is an autosomal recessive genetic disease characterized by hearing loss, RP and in some cases vestibular dysfunction (balance problems). The syndrome is the most frequent cause of deaf-blindness, accounting for more than 50% of individuals who are both deaf and blind. It has a prevalence in the range of 1-4 per 25,000 people, and Usher cases represent between 10-15% of all autosomal recessive RP cases (Boughman et al., 1983; Hartong et al., 2006; Kimberling et al., 2010; Millan et al., 2011; Mathur and Yang, 2015). Usher syndrome is

genetically and clinically heterogeneous and can be divided into three clinical subtypes based on severity of hearing loss and age-of-onset of retinal dysfunction.

- Usher syndrome type 1. Congenital, severe-to-profound deafness, lack of development of speech, vestibular areflexia and onset of slowly progressive RP within the first decade of life.
- Usher syndrome type 2. Congenital moderate-to-severe hearing impairment, normal vestibular responses and onset of RP within the second decade of life.
- Usher syndrome type 3. Variable hearing loss, vestibular dysfunction and RP are sporadic and slowly progressive.

RP in USH patients causes night-blindness and loss of peripheral vision due to rod photoreceptor degeneration. As the degeneration of the retina progresses, cone photoreceptors also degenerate and cone density can decrease by nearly 38% before visual acuity becomes abnormal (Sun et al., 2016). Loss of central vision results in USH patients becoming legally blind, and there is no known cure (Nagel-Wolfrum et al., 2014). To date, sixteen loci have been associated with USH: nine are involved in USH1, three in USH2, two in USH3 and two are not specified (Table 1.4) (Keats and Corey, 1999; Ebermann et al., 2010; Puffenberger et al., 2012; Khateb et al., 2014; Mathur and Yang, 2015). From these loci, thirteen genes have been identified. They include six USH1, three USH2, two USH3, one USH modifier (*PDZD7*) and one a typical USH gene (*CEP250*).

USH type	locus	Gene	Potential function	Estimated frequency
USH1	USH1B/DFNB2/DFNA1	*MYO7A*	Actin-based motor protein	53%-63%
	USH1C/DFNB18	*USH1C*	PDZ scaffold protein	1%-15%
	USH1D/DFNB12	*CDH23*	Cell adhesion	7%-20%
	USH1E	unknown	Unknown	unknown
	USH1F/DFNB23	*PDCH15*	Cell adhesion	7%-12%
	USH1G	*USH1G*	Scaffold protein	0%-4%
	USH1H	unknown	Unknown	unknown
	USH1J	*CIB2*	Ca2+ and integrin binding	unknown
	USH1K	unknown	Unknown	unknown
USH2	USH2A/RP	*USH2A*	Cell adhesion	57%-79%
	USH2C	*GPR98/ ADGRV1*	G-protein coupled receptor	6.6%-19%
	USH2D/DFNB31	*DNFB31/WHRN*	PDZ scaffold protein	0%-9.5%
USH3	USH3A	*CLRN1*	Auxiliary subunit of ion channels	unknown
	USH3B	*HARS*	Synthesis of histidyl-transfer RNA	unknown
unknown	unknown	*PDZD7*	PDZ scaffold protein	unknown
unknown	unknown	*CEP250*	Centrosomal activity	unknown

Table 1.4. Genetics of Usher syndrome (USH). USH loci, genes, potential function and proportion of each USH subtype attributed to pathogenic variants in this gene. (Sources: RetNet, https://sph.uth.edu/retnet/ home .htm, Lentz and Keats (1993a), Lentz and Keats (1993b), Daiger et al. (2013), Mathur and Yang, (2015).

1.6.3.6 Bardet-Biedl syndrome (BBS)

Bardet-Biedl syndrome (BBS) (OMIM 209900) is an autosomal recessive multisystemic genetic disorder characterised by heterogeneous clinical manifestations. These include primary features of the disease (obesity, renal anomalies, polydactyly, retinal degeneration, learning difficulties and hypogenitalism) and secondary features (speech deficit, hearing loss, developmental delay, cardiovascular anomalies, dental defects, hypertension, olfactory deficit and diabetes mellitus) (M'Hamdi et al., 2014; Khan et al., 2016b; Suspitsin and Imyanitov, 2016). The severity of BBS varies greatly even among individuals within the same family and symptoms may not be present at birth but usually develop in the first decade of life. The retinal degeneration in BBS patients is typically rod-cone dystrophy (RCD), which is reported to affect 93-100% of BBS patients (Suspitsin and Imyanitov, 2016). Fundus photographs of BBS patients usually show mid-peripheral bone spicule formation with early macular atrophy involvement (Adams et al., 2007). Night blindness is usually evident by age 7-8 years and most patients are legally blind by the second or third decade (Heon et al., 2005; Azari et al., 2006).

BBS is a rare autosomal recessive genetic disorder with estimated frequency 1:100,000 in the European and North America populations (Forsythe and Beales, 2013). Unusual higher incidence has been reported in isolated populations, such as 1:3,700 in Faroe Islands (Hjortshoj et al., 2009), 1:18,000 in Newfoundland (Moore et al., 2005) and 1:13,500 in some Bedouin communities at Middle East (Farag and Teebi, 1989; M'Hamdi et al., 2011). This is likely to reflect the presence of local founder mutations or a high level of cousin-marriage in these populations.

Twenty BBS genes have been identified so far (Suspitsin and Imyanitov, 2016), and all of them are involved in primary cilia functioning. 23% of BBS morbidity has been attributed to *BBS1* (Muller et al., 2010), 8% to *BBS2* (Fattahi et al., 2014), 0.4% to *BBS3/ARL6* (Fan et al., 2004), 2% to *BBS4* (Mykytyn et al., 2001), 0.4% *BBS5* (Li et al., 2004), 6% to *BBS6/MKKS* (Slavotinek et al., 2000), 2% to *BBS7* (Badano et al., 2003), 1% to *BBS8/TTC8* (Ansley et al., 2003), 6% to *BBS9/ B1* (Nishimura et al., 2005), 20% to *BBS10 /C12orf58* (Stoetzel et al., 2006), 0.1% to *BBS11/TRIM32* (Chiang et al., 2006), 5% to *BBS12/C4orf24* (Stoetzel et al., 2007), 4.5% *BBS13 /MKS1* (Leitch et al., 2008), 1% to *BBS14/CEP290* (Leitch et al., 2008), 1% to *BBS15/ C2orf86* (Kim et al., 2010),

1% to *BBS16 /SDCCAG8* (Billingsley et al., 2012) and unknown proportions to *BBS17/ LZTFL1*(Schaefer et al., 2014), *BBS18/BBIP1* (Scheidecker et al., 2014), *BBS19/IFT27* (Aldahmesh et al., 2014), and *BBS20/IFT172* (Schaefer et al., 2016).

1.7 Macular and cone related disorders.

1.7.1 Overview

Inherited macular and cone related disorders are a rare group of inherited eye diseases of the cone, or cone and rod photoreceptors, or RPE, that are associated with various forms of stationary or progressive visual impairment. Cone related degeneration is a clinically heterogeneous disease category within which the cone photoreceptors are primarily affected. Macular dystrophy (MD) is a diagnosis based on the anatomical area of the retina affected. Patients show a localised abnormality of the neuro retina at the macula whereas the retinal periphery is spared. In contrast, cone dystrophy (COD) and cone-rod dystrophy (CRD) affect a particular category of photoreceptor throughout the retina. All patients with these diseases suffer from difficulties in detecting colour vision, facial recognition and reading (Hamel, 2007). These diseases are commonly divided into sub groups of retinal dystrophy, including achromatopsia (ACHM), COD, CRD, MD and other cone related disorders. All modes of Mendelian inheritance, i.e. autosomal recessive (AR), autosomal dominant (AD) and X-linked (XL) forms exist, and the disease can present as non-syndromic and syndromic forms. An AR inheritance pattern represents the main mode of inheritance, accounting for more than two third of all cases. AD inheritance accounts for 20-25% of all cases while X-linked inheritance represents only 1-5 % (Roosing et al., 2014).

1.7.2 Achromatopsia (ACHM)

Achromatopsia is an inherited retinal disease characterized by severely impaired or complete colour blindness. Patients present with significantly reduced visual acuity (<20/200), nystagmus and severe photophobia (Zelinger et al., 2015; Kohl et al., 2016). Most affected individuals with ACHM show normal rod responses but complete absence of cone responses on full-field electroretinography (ffERG). Sometimes the phenotype is described as incomplete ACHM with milder symptoms since residual cone function can be demonstrated by residual cone responses on ffERG (Kohl et al., 2000; Thiadens et al.,

2009b). ACHM was thought to be a congenital and stationary disorder, but a progressive form of the disease has been reported with a changing macular appearance over time ranging from no apparent abnormalities to atrophic lesions (Thiadens et al., 2010; Kohl et al., 2012).

The estimated prevalence of ACHM is 1:40,000 individuals and it is exclusively inherited in an AR manner. To date, six genes have been shown to be associated with ACHM. Five genes encode proteins that are involved in cone phototransduction, including 2 subunits of the cone cyclic guanosine monophosphate–regulated cation channel (*CNGA3* and *CNGB3*) (Kohl et al., 1998; Sundin et al., 2000; Chen et al., 2015; Liang et al., 2015), the alpha subunit of the cone-specific G-protein transducin (*GNAT2*) (Kohl et al., 2002; Ouechtati et al., 2011), and the active and inhibitory γ subunits of the cone-specific phosphodiesterase *PDE6C* and *PDE6H*, respectively (Thiadens et al., 2009c; Kohl et al., 2012). The sixth ACHM gene is *ATF6*, which encodes a transcription factor that acts as a key regulator of the unfolded protein response and cellular endoplasmic reticulum homeostasis (Ansar et al., 2015; Kohl et al., 2015). Mutations in *CNGB3* represent the most common cause of AR ACHM, accounting for more than 40% of all cases, mainly owing to a single frameshift mutation (c.1148delC), which is found in approximately 70% of all *CNGB3* disease-causing alleles (Kohl et al., 2005). *CNGA3* is mutated in about 25% of ACHM cases. Mutations in *GNAT2*, *PDE6C*, PDE6H and *ATF6* are rare (Grau et al., 2011).

1.7.3 Cone and cone-rod dystrophies (COD and CRD)

1.7.3.1 Overview

COD and CRD have an estimated worldwide prevalence of 1:30.000 to 1:40.000, display all types of Mendelian inheritance and are characterized by predominantly retinal pigment deposits to the macular region (Michaelides et al., 2004; Roosing et al., 2013). Patients with COD have normal cone function at birth, but develop progressive loss of cones and central vision during the first or second decade of life. Photophobia may also be observed but because the cone function is initially normal in COD, nystagmus does not usually exist. Fundus appearance varies from normal to a bull's eye maculopathy and the optic nerve may have variable degrees of temporal pallor (Perrault et al., 1998). Reduced cone responses with preserved rod responses on ERG are an important clinical

hallmark for the diagnosis of COD (Michaelides et al., 2006). Both diseases are characterized by loss of cone photoreceptors and a progressive visual decline, but CRD can be distinguished from COD by subsequent or simultaneous loss of rod photoreceptors (Roosing et al., 2014).

An RD would thus be called a CRD in a patient who experienced a progressive inherited retinal disorder characterized by a primary loss of cone photoreceptors followed by involvement of rod photoreceptors. This is distinguished from COD by loss of both cones and rods on ERG (Scholl and Kremers, 2003). Symptoms resemble those of COD but patients with CRD also may experience nyctalopia caused by rod dysfunction. Fundus appearance in patients with CRD shows retinal vascular attenuation and peripheral pigment deposits. The course of CRD is generally more severe than COD. Disease symptoms usually become apparent in childhood with a rapid decline of the visual function to legal blindness before the age of 50. COD and CRD are clinically overlapping diseases and often difficult to distinguish at the advanced stage, and indeed CRD might be difficult to differentiate from RP based on clinical signs alone, but complete blindness is a more frequent occurrence in CRD than RP (Thiadens et al., 2012; Yokochi et al., 2012).

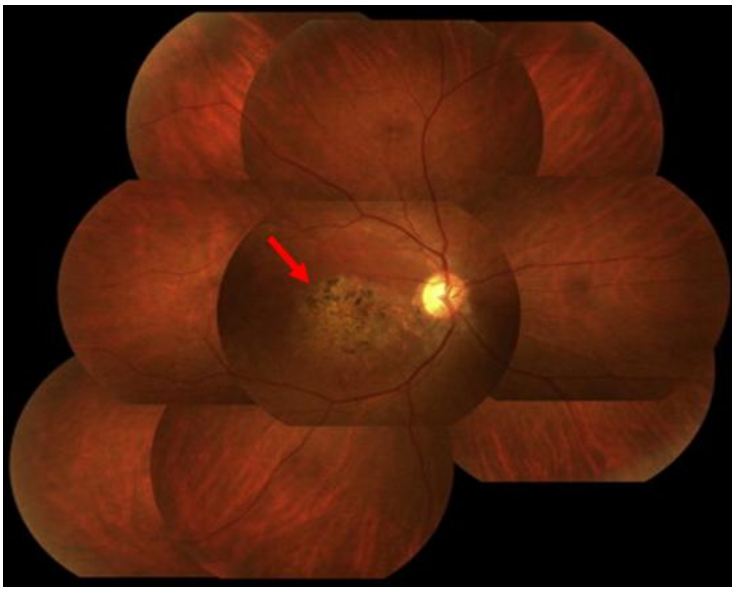

Figure 1.8. Colour fundus photography of CRD patient. Fundus changes with macular dystrophies show pigment deposits in the central macular area (arrow) and attenuated retinal arteries. (Adapted from Huang et al. (2012) with the permission of Elsevier Copyright Clearance Centre, License number: 3940440860754).

1.7.3.2 Genetics of COD and CRD

Unlike ACHM, in which mutations in only six genes can explain the majority of the cases, Mendelian mutations in 33 genes are known to cause COD/CRD. 21 of these genes account for autosomal recessive COD/CRD, while 10 genes are responsible for autosomal dominant disease. In addition, two genes have been found to be responsible for X-linked COD/CRD (Table 1.5). CRD/COD genes encode proteins that are involved in multiple functions, including phototransduction, the visual cycle, cilia function and protein trafficking. The four major genes involved in the pathogenesis of COD/CRD are *ABCA4* in AR COD/CRD, *GUCY2D* and *CRX* in AD COD/CRD and *RPGR* in X-linked COD/CRD (Hamel, 2007).

Gene	Inheritance	Potential function	OMIM
PDE6C	Recessive	Phototransduction	600827
PDE6H	Recessive	Phototransduction	601190
CNGB3	Recessive	Phototransduction	605080
ABCA4	Recessive	Visual cycle	601691
RDH5	Recessive	Visual cycle	601617
RAX2	Recessive	Transcription	610362
RPGRIP1	Recessive	Interacts with RPGR	605446
ADAM9	Recessive	Cell/matrix interaction	602713
TTLL5	Recessive	Cilia function	612268
CACNA2D4	Recessive	Ion channel	608171
KCNV2	Recessive	Ion channel subunit	607604
CDHR1	Recessive	Cellular structure	609502
C21orf2	Recessive	Unknown	603191
C8orf37	Recessive	Unknown	614477
CNNM4	Recessive	Unknown	607805
RAB28	Recessive	Unknown	612994
CERKL	Recessive	Cell signaling	608381
ATF6	Recessive	Transcription factors	605537
CNGA3	Recessive	Phototransduction	600053
GNAT2	Recessive	Phototransduction	139340
POC1B	Recessive	Centriole duplication and/or maintenance	614784
PROM1	Dominant	Cellular structure	604365
GUCA1A	Dominant	Phototransduction	600364
GUCY2D	Dominant	Phototransduction	600179
PRPH2	Dominant	Phototransduction	179605
CRX	Dominant	Transcription factor	602225
AIPL1	Dominant	Transport, protein trafficking	604392
HRG4	Dominant	Neurotransmitter release	604011
RIMS1	Dominant	Neurotransmitter release	606629
PITPNM3	Dominant	Transport	608921
SEMA4A	Dominant	Axon guidance	607292
RPGR	X-Linked	Intraflagellar transport	312610
CACNA1F	X-Linked	Calcium channel	300110

Table 1.5. List of genes implicated in cone or cone-rod dystrophy (COD/CRD). Gene name, mode of inheritance and potential function are depicted along with the corresponding OMIM number. (Sources: RetNet, https://sph.uth.edu/retnet/home.htm; OMIM, http://www.ncbi.nlm.nih.gov/ omim).

The *ABCA4* gene encodes an ATP-binding cassette (ABC) superfamily transmembrane protein that is expressed exclusively in retinal photoreceptors and is involved in retinoid metabolism (Section 1.4.4). Mutations in *ABCA4* cause STGD disease and are responsible for 30 to 60% of the cases with AR COD/CRD (Hamel, 2007; Cideciyan et al., 2009).

GUCY2D (LCA1) encodes retinal guanylate cyclase 1 (RetGC-1), which is one of a group of proteins that are important in determining how rods and cones can return to the resting state after being stimulated by light (Figure 1.5B, Table 1.1) (Perrault et al., 2000; Tucker et al., 2004). Defects in this gene leave the eye unable to respond to light, which ultimately leads to RD. Biallelic mutations in *GUCY2D* are the most common cause of arLCA, accounting 12-21% of all disease cases, while monoallelic mutations are a common cause of COD/CRD/MD. Mutations in *GUCY2D* account for more than a third of cases with dominant form of COD/CRD/MD. Pathogenic variants in *GUCY2D* have been associated with RD characterized by photophobia, high hyperopia and poor but stable vision with no visual improvement (Perrault et al., 1999; Hanein et al., 2004). For the *GUCY2D*-LCA phenotype, more than half of the mutations identified in patients are truncating mutations that cause complete loss of retGC-1 catalytic activity and lead to loss of the outer nuclear layer and abnormal inner retinal and synaptic organization (Rozet et al., 2001; Milam et al., 2003). For the *GUCY2D*-COD/CRD/MD phenotype, the majority of the pathogenic missense mutations map in the catalytic domain of the protein causing dramatic consequences on protein activity (Jiang et al., 2015; Lazar et al., 2015).

The *CRX* gene encodes the cone-rod homeobox protein, a transcription factor expressed in rod and cone photoreceptors in the retina and pinealocytes in the brain (Chen et al., 1997; Furukawa et al., 1997). CRX plays an essential role in the development and maintenance of functional mammalian rod and cone photoreceptors (Furukawa et al., 1999). It interacts with transcription co-regulators including the rod-specific transcription factors NRL, NR2E3 and general co-activator proteins GCN5, CBP and p300 to control photoreceptor gene expression and induce rhodopsin promoter activity (Mitton et al., 2000; Peng et al., 2005; Roduit et al., 2009; Nichols et al., 2010). Photoreceptors in homozygous *Crx* knock-out mice ($Crx^{-/-}$) fail to form POS (Sanyal and Jansen, 1981; Humphries et al., 1997; Furukawa et al., 1999), leading to progressive degeneration

(Blackshaw et al., 2001; Morrow et al., 2005; Hsiau et al., 2007). Mutations in human *CRX* have been associated with adLCA, adCRD, adRP and arLCA with different ages of onset and severity (Sohocki et al., 1998; Dharmaraj et al., 2000; Rivolta et al., 2001; Nichols et al., 2010; Walia et al., 2010; Huang et al., 2012). Disease-causing human *CRX* mutations can be divided into two groups. One group is mostly monoallelic frameshift mutations or amino acid substitutions within the DNA binding homeodomain. This group of mutations shows a dominant-negative effect on the wild-type allele activity (Mitton et al., 2000; Peng et al., 2005; Roduit et al., 2009; Nichols et al., 2010), and leads to a severe dominant retinal phenotype adCRD/adLCA (Sohocki et al., 1998; Paunescu et al., 2007; Wang et al., 2007; den Hollander et al., 2008; Huang et al., 2012). The other group of mutations also demonstrate a reduced ability of CRX to bind to the targeted protein (Nichols et al., 2010), but these mutations appear to represent hypomorphic alleles and are more likely to be associated with either autosomal recessive Leber congenital amaurosis (LCA) or less severe forms of dominant *CRX*-associated disease adRP (Swaroop et al., 1999).

1.8 Leber congenital amaurosis (LCA)

1.8.1 Overview

Leber congenital amaurosis (LCA; OMIM 204000), first described by Theodor Leber in 1869 (Leber, 1869), represents the most severe and earliest form of IRDs, causing blindness in infants and children (Perrault et al., 1999). LCA is a rare disease with a population frequency between 1 in 30,000 to 1 in 81,000 (Koenekoop, 2004; Stone, 2007), although the condition is more frequent in consanguineous populations or isolated communities (Sherwin et al., 2008). LCA represents almost 5% of all retinal dystrophies and 20% of children with visual impairment in special schools (Koenekoop et al., 2007). This dystrophy is highly heterogeneous, has complex genetic and clinical features and overlaps with the more severe forms of RP and COD/CRD (den Hollander et al., 2008).

1.8.2 Clinical manifestation of LCA

For the LCA infant, although blind at birth, the features usually first manifest at around the age of 6 weeks, when the parents notice the child's eyes oscillating (nystagmus) (Zahn, 1978). LCA is characterized by severe and early visual impairment

and visual acuity among LCA patients ranges from 20/200 to perception of light only or no perception of light. Generally patients with LCA do not achieve visual acuity better than 20/400 (Cremers et al., 2002). Sluggish or near-absent pupillary responses reflecting severe retinal dysfunction and absence of electrical signals on ERG are also clinical hallmarks for LCA (Franceschetti and Dieterle, 1954; Chung and Traboulsi, 2009). The appearance of the fundus is extremely variable in patients. The retina may initially appear normal, but fundus abnormalities are frequently present later in life (Figure 1.9) including white dots at the level of the RPE, retinal vascular attenuation, bone-spicule pigment migration, macular coloboma or maculopathy. Refractive errors, photophobia and nyctalopia are also commonly detected (den Hollander et al., 2008; Chung and Traboulsi, 2009; Hull et al., 2014; Chacon-Camacho and Zenteno, 2015).

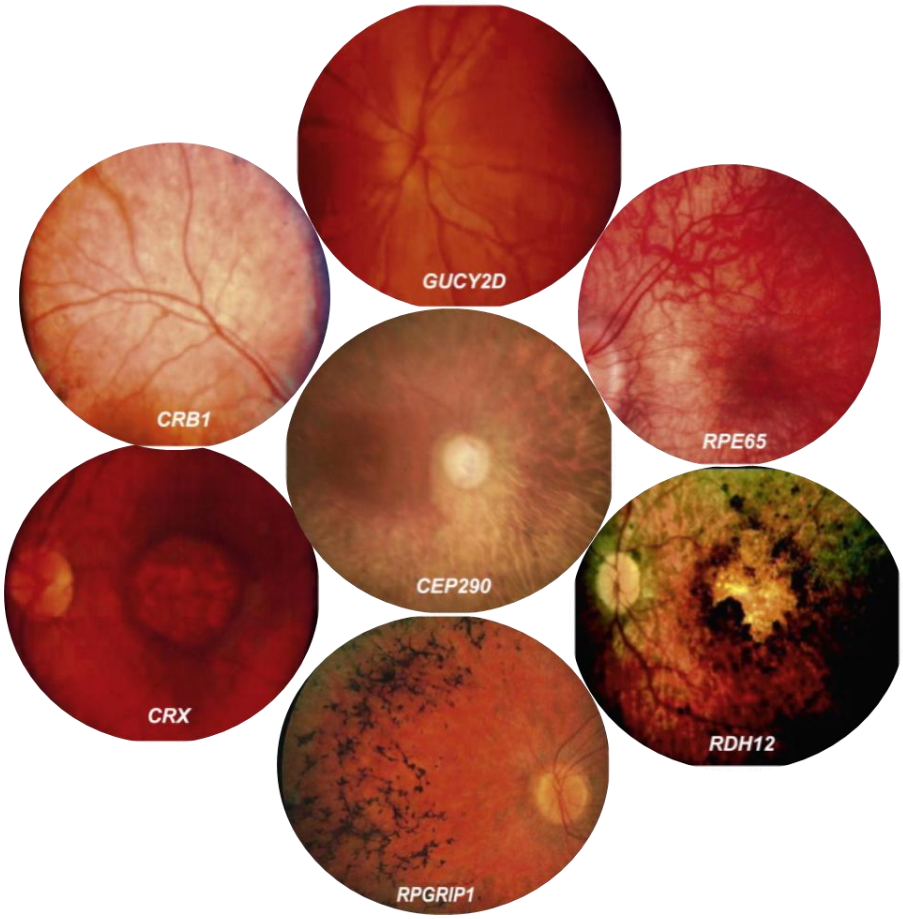

Figure 1.9. Colour fundus photography of LCA patients with known genotypes. LCA associated with a *CEP290* mutation has marked choroidal sclerosis, pale optic discs, barely visible retinal vessels and relative preservation of the posterior pole. *CRX*-associated LCA manifests as a prominent maculopathy with relatively normal appearing vessels and optic disc. The fundus in *CRB1*-associated LCA reveals a preserved para-arteriolar RPE (PPRPE) and nummular pigment changes. *GUCY2D*-associated LCA patients have a relatively normal retinal appearance including

retinal colour, retinal vessel calibre, and optic disc appearance. *RPE65*-associated LCA leads to RPE translucency but with relatively normal vessel calibre and a normal optic disc appearance. *RDH12*-associated LCA is characterised by nystagmus, nyctalopia and a prominent maculopathy. *RPGRIP1*-associated LCA patients have a retinal pigment epithelium degeneration with bone spicules and vessel dragging. (Adapted from den Hollander et al. (2008) with the permission of Elsevier Copyright Clearance Centre, License number: 3926710489180).

1.8.3 Genetics of LCA

LCA is genetically heterogeneous and can result from mutations in 24 genes (Table 1.6). In most cases, LCA is inherited in an autosomal recessive manner and LCA genes encode proteins that play a variety of roles in the development and function of the retina such as normal development of photoreceptors, phototransduction, normal function of the cilia and protein trafficking.

Locus	Gene	inheritance	Potential function	Estimated frequency	OMIM
LCA1	***GUCY2D***	Recessive	Phototransduction	12-21%	601777
LCA2	***RPE65***	Recessive	Visual cycle	3-16%	204100
LCA3	***SPATA7***	Recessive	Unknown	2-4%	609868
LCA4	***AIPL1***	Recessive	Transport, protein trafficking	4-8%	604393
LCA5	***LCA5***	Recessive	Centrosome protein with ciliary function	1-7%	611408
LCA6	***RPGRIP1***	Recessive	Interacts with RPGR	4-6%	613826
LCA7	***CRX***	Dominant & Recessive	Transcription factor	2-3%	613829
LCA 8	***CRB1***	Recessive	Tissue development and maintenance	9-13%	613835
LCA9	***NMNAT1***	Recessive	Photoreceptor maintenance	5%	608700
LCA 10	***CEP290***	Recessive	Centrosomal & ciliary protein	20 -25%	611755
LCA 11	***IMPDH1***	Dominant	Regulates cell growth	Rare	613837
LCA12	***RD3***	Recessive	Splicing	Rare	610612
LCA13	***RDH12***	Recessive	Phototransduction	4%	612712
LCA 14	***LRAT***	Recessive	Retinal metabolism	≤1%	613341
LCA 15	***TULP1***	Recessive	Tissue development & maintenance	1-2%	613843
LCA 16	***KCNJ13***	Recessive	Potassium channel	Unknown	614186
LCA 17	***GDF6***	Recessive	Growth factor	Unknown	615360
LCA18	***PRPH2/ /RDS***	Recessive	Phototransduction	Unknown	179605
---	***CABP4***	Recessive	Unknown	Cell signalling	610427
---	***IQCB1***	Recessive	Interacts with RPGR & connecting cilia	Unknown	09254
---	***IFT140***	Recessive	Intraflagellar transport	≤1%	614620
---	***CLUAP1***	Recessive	Ciliogenesis	Unknown	616787
---	***DTHD1***	Recessive	Unknown	Unknown	616979
---	***OTX2***	Dominant	Transcription factor	Rare	600037

Table 1.6. List of genes implicated in Leber congenital amaurosis (LCA). Locus, gene name, mode of inheritance and potential function and estimated frequency are depicted along with the corresponding OMIM number ‘Sources: RetNet, https://sph.uth.edu/retnet/home.htm; OMIM, http: //www.ncbi.nlm .nih.gov/omim; Weleber et al. (2013); Nash et al. (2015).

Mutations in the *CEP290*, *CRB1*, *GUCY2D* and *RPE65* genes are the most common causes of the disorder and only three genes *CRX*, *IMPDH1* and *OTX2* cause adLCA. Mutations in the other genes generally account for a smaller percentage of cases.

CEP290 is the most frequently mutated gene in LCA and accounts for 20-25% of all cases (den Hollander et al., 2006; Perrault et al., 2007; Coppieters et al., 2010a). CEP290 encodes a centrosomal protein that is thought to play an important role in protein trafficking and ciliogenesis in many different cell types including retinal photoreceptor cells (Chang et al., 2006; Sayer et al., 2006; Craige et al., 2010). Interestingly, one intronic mutation (c.2991+1655A>G) accounts for up to 15% of all LCA cases in some European and North-American populations (den Hollander et al., 2006; Coppieters et al., 2010a). This deep-intronic *CEP290* mutation creates a splice donor site that allows the insertion of a 128-bp cryptic exon to approximately 50% of the *CEP290* transcripts, resulting in a premature termination of protein synthesis (den Hollander et al., 2006; Collin et al., 2012). Mutations in the *CEP290* gene have also been associated with a wide range of ciliopathies including Joubert syndrome (JBTS5, OMIM 610188), Senior–Loken syndrome (SLSN6, OMIM: 610189), Meckel syndrome (MKS4, OMIM 611134) and Bardet–Biedl syndrome (BBS14, 615991) (Baala et al., 2007; Brancati et al., 2007; Helou et al., 2007; Leitch et al., 2008; Coppieters et al., 2010b). The majority of the reported CEP290 mutations are truncating in all phenotypes with only a few missense mutations reported (Valente et al., 2006; Tory et al., 2007). Moreover there appears to be no genotype-phenotype correlation for CEP290 mutations leading to all these different diseases. The only genotype-phenotype correlation observed is with the common founder mutation (c.2991+1655A>G) which so far has only been seen in patients with isolated LCA (den Hollander et al., 2006; Perrault et al., 2007).

RPE65 (retinal pigment epithelium 65) encodes a retinoid isomerohydrolase with an essential role in the visual cycle (Figure 1.6) (Moiseyev et al., 2005). RPE65 is essential for the conversion of activated all-*trans*-retinal to 11-*cis*–retinal, the universal chromophore of the visual pigments in both cone and rod photoreceptors (Section 1.4.4). More than 70 different point mutations in *RPE65* are associated with severe early onset retinal dystrophies LCA (3-16%), RP (2-5%) and approximately 11% of early onset RCD (Gu et al., 1997; Marlhens et al., 1997; Thompson et al., 2000; den Hollander et al., 2008; Bowne et al., 2011a; Hull et al., 2016). All patients with *RPE65* mutations had reduced

central vision at infancy or early childhood with nyctalopia as a prominent feature and varying degrees of nystagmus. The fundus appearance is usually normal in infancy but small subretinal white dots might appear later in childhood, possibly as a result of abnormal accumulation of retinyl esters (Lorenz et al., 2000; Galvin et al., 2005; Weleber et al., 2011). Thinning of the outer nuclear layer on optical coherence tomography (OCT) and low signal on fundus autofluorescence (FAF) are also common in patients with *RPE65* mutations (Lorenz et al., 2004; Jacobson et al., 2008b). Electrophysiology demonstrates absent rod function but there may be residual cone function in childhood (Jacobson et al., 2009). This may reflect the alternative source of 11-*cis*-retinol that cones obtain from Müller cells (Kaylor et al., 2014). Mice lacking RPE65 ($Rpe65^{-/-}$) cannot synthesize 11-*cis*-retinol and all-*trans*-retinyl esters over-accumulate in the RPE, whereas 11-cis-retinyl esters are absent. As a result, photoreceptors in these mice lose sensitivity to light (Redmond et al., 1998; Cottet et al., 2006; Fan et al., 2008; Feathers et al., 2008).

CRB1 is a human homologue of the *Drosophila melanogaster* gene coding for the protein crumbs (Crb). *CRB1* is expressed in the retina and the brain, and is involved in photoreceptor morphogenesis (den Hollander et al., 1999). Mutations in the *CRB1* gene are associated with variable RD phenotypes, ranging from congenital blindness in LCA to early-onset progressive visual impairment in early onset retinal dystrophy (EORD) and early onset RP (EORP) (Booij et al., 2005; Yzer et al., 2006; Vallespin et al., 2007a; Tosi et al., 2009; Henderson et al., 2011; Bujakowska et al., 2012). Among arLCA genes, *CRB1* mutations represent one of the most frequent causes, accounting for between 9-13% of all LCA cases (den Hollander et al., 2004; den Hollander et al., 2008; Benayoun et al., 2009). LCA and RP resulting from *CRB1* mutations may be accompanied by specific fundus features. These include preservation of the para-arteriolar retinal pigment epithelium (PPRPE), which is a relative preservation of RPE adjacent to the retinal arterioles despite a panretinal RPE degeneration (Heckenlively, 1982), retinal telangiectasia/Coats-like vasculopathy, a condition in which abnormally permeable blood vessels lead to exudation and retinal detachment (Cahill et al., 2001; den Hollander et al., 2001) and an increased retina thickness with altered laminar organization (Jacobson et al., 2003).

IMPDH1 (inosine-5'-monophosphate dehydrogenase 1) is a housekeeping gene encoding a protein subunit that forms active homotetramers and catalyzes the rate-

limiting step in *de novo* guanine synthesis. IMPDH1 performs this by converting inosine monophosphate (IMP) to xanthosine monophosphate (XMP) with the reduction of NAD (Senda and Natsumeda, 1994; Hedstrom, 1999). IMPDH1 levels are higher in the retina than in any other tissue and the protein is localized to the photoreceptor IS at synaptic terminals (Bowne et al., 2006). Mutations in *IMPDH1* cause adRP or adLCA due to photoreceptor degeneration as reduced enzyme activity leads to reduced guanine nucleotide concentrations in the retina (Bowne et al., 2002; Coussa et al., 2015).

OTX2 (orthodenticle homeobox 2) encodes a transcription factor that is critical for the development of the forebrain and eye. It is expressed in the neuroepithelium of most of the forebrain and midbrain, including the eye domain (Simeone et al., 1993). The protein plays a critical role in retinal photoreceptor development and maintenance, and is required for the development of the RPE (Martinez-Morales et al., 2003; Rath et al., 2007). Mutations in *OTX2* have been reported to cause adLCA and adMD (Vincent et al., 2014). In mice, homozygous mutants ($Otx2^{-/-}$) are embryonically lethal. Heterozygous mice show a wide phenotypic variability, including craniofacial malformation, known as otocephaly (Matsuo et al., 1995; Hide et al., 2002).

1.9 Autozygosity mapping and genetic markers

A consanguineous marriage is a union between two individuals who are related by a common ancestor. It can be a deeply rooted social trend that is widely practiced in some countries for economic benefit and for cultural reasons (Jaber et al., 1998; Na'amnih et al., 2014). Individuals from consanguineous marriages are at increased risk of developing a recessive condition (Hamamy, 2012; Shawky et al., 2013; Salway et al., 2016). This phenomena was first observed in children from a first cousin marriage who had alkaptonuria and albinisim (Garrod, 1902). Garrod's observations were named homozygosity-by-descent by William Bateson in 1902. Using modern genetics analyses, affected patients in such families have been shown to have an increased frequency of uninterrupted homozygous segments in their genome. Such chromosomal segments come about as both segments have been passed down through separate branches of the family but are derived from a common ancestor and come together in the children, meaning these autozygous segments are identical by descent (IBD) from a common ancestor (Figure 1.10). As the mutation and immediate surrounding DNA passes through successive

generations without recombination, IBD regions around a disease-causing allele can be used to map the mutation that causes recessive disease in a family (Lander and Botstein, 1987). This was first demonstrated in Leeds, by Prof. Bob Mueller who used autozygosity mapping to identify disease-causing genes in local consanguineous Pakistani families (Mueller and Bishop, 1993).

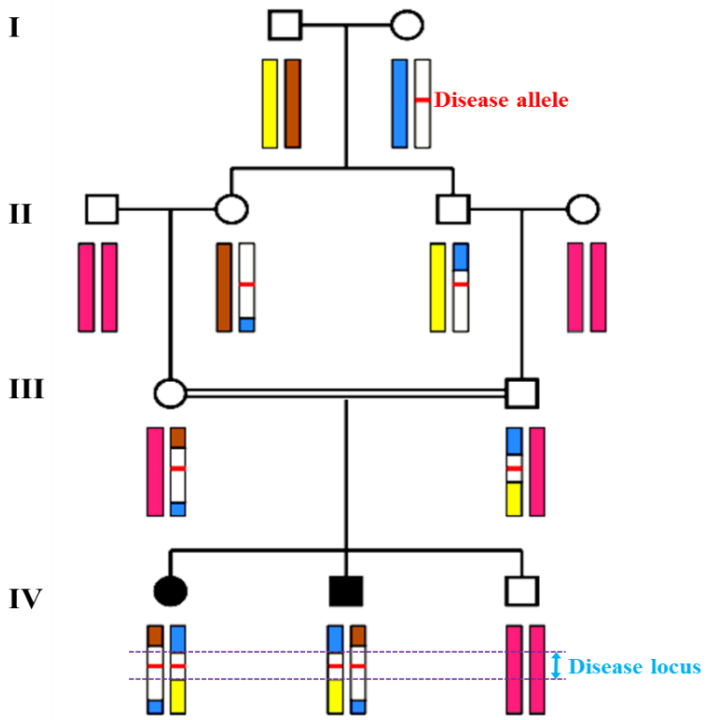

Figure 1.10. Principle of autozygosity mapping. First-cousin consanguineous pedigree showing the inheritance of a disease allele (red) through the generations. Affected children (IV.1 and IV.2) have inherited disease alleles and the surrounding haplotype from a common ancestor (I.2). Mapping of the disease locus can be achieved by locating the homozygous region shared by all affected individuals in the family.

Before the human genome sequence became available, linkage maps were fundamental tools for many genetic studies. These had been created over the years using various types of polymorphic markers, since their conception by Sturtevant (Sturtevant, 1913). Genetic linkage maps determine the linear position of genes or markers on a chromosome and can be used to search for IBD loci. As knowledge of the human genome sequence became available (Lander et al., 2001), a wide range of molecular markers have been used in studies. Before the completion of the human genome project, genetic maps were made using Random Amplified Polymorphic DNA (RAPDs), Restriction Fragment Length Polymorphisms (RFLPs), Amplified Fragment Length Polymorphisms (AFLPs) and microsatellites, also known as short tandem repeats (STRs). With access to the first

human genome sequence, more detailed maps were based on single nucleotide polymorphisms (SNPs).

The three criteria considered essential for the development of linkage maps were ensuring a spread of markers across the genome, for the markers to be highly polymorphic and having a low genotyping error rate. STRs and SNPs are the markers most commonly used for the identification of loci for autosomal recessive diseases in consanguineous families (Acland et al., 1998; Bellingham et al., 1998; Aligianis et al., 2002; Ball et al., 2010; Saqib et al., 2015). Microsatellites, which are di-, tri-, or tetra nucleotide tandem repeats, are variable in populations of DNA and within the alleles of an individual. They were until recently the genetic markers of choice as they are highly polymorphic and interspersed throughout the entire genome (Tian et al., 2008; Pemberton et al., 2009). However, despite being informative, STR genotyping is relatively complicated, time consuming, expensive, and can involve problematic PCRs which may lead to human errors in sizing the alleles. Furthermore, microsatellites account for about 3% of the genome and cannot be used for high resolution mapping (Ellegren, 2004). Advances in high-throughput DNA sequencing and bioinformatics, have led to the emergence of SNPs as genetic markers (Sachidanandam et al., 2001; Heaton et al., 2002). Despite the biallelic nature of SNPs that provide relatively less informativity, SNPs have a genetic stability, higher density, simpler nomenclature and can be suitably automated for data analysis and interpretation (Slate et al., 2009; Ball et al., 2010; Fernández et al., 2013). Moreover, modern SNP genotyping is almost fully automated and error rates tend to be much lower. Platforms such as the Affymetrix SNP Array 6.0 are now used, which includes more than 906,600 SNPs to allow high-resolution genotyping.

1.10 Sequence of the DNA sequencing

Over the course of six decades, large amounts of time and resources have been invested in developing and improving the technologies that underpin genetic research. DNA sequencing is one method that has seen a vast improvement over the years. When considering the history of this technique, researchers have gone from being able to sequence only a short oligonucleotide of a single gene to the whole genome sequencing (WGS) that is available now. DNA sequencing can be summarised in two generations from the genesis of this field to the starting time of this study.

1.10.1 First-generation DNA sequencing

Over two decades elapsed from the discovery of the double helix structure of DNA (Watson and Crick, 1953) to the introduction of several influential DNA sequencing protocols. Initial efforts at sequencing were met with limited success since the methods employed could only determine the nucleotide composition but were not powerful enough to determine the order of the nucleotides (Holley et al., 1961). However, the mid-1970s represent the real start of 'first-generation' DNA sequencing by widely adopted the plus and minus and the chemical cleavage techniques (Sanger and Coulson, 1975; Maxam and Gilbert, 1977). This method used radio-labelled DNA treated with chemicals designed to cleave fragments of the chain at specific bases, followed by migrating the labelled fragments through a polyacrylamide gel to determine the length and position of the nucleotides.

Sanger's 'chain-termination' or dideoxy technique (Sanger et al., 1977) represented the most significant development amongst the first generation of DNA sequencing methods. This technique used polymerase-based copying of single-stranded DNA, but included a small proportion of radio-labelled chemical analogues of the nucleotides, chain-terminating dideoxynucleotides (ddNTPs), in each of four parallel reactions. The products were then run in adjacent lanes on a polyacrylamide gel to produce radioactive bands in the lanes, the positions of which corresponded to the sequence of nucleotides. Over time further improvements were made to this technique. Fluorescent dyes (Smith et al., 1986) were used instead of radioactive labelling to tag the different chain terminating analogues, allowing all four nucleotides to be resolved in a single lane. Capillary electrophoresis instead of a polyacrylamide gels, together with the use of laser induced fluorescence detection, allowed longer reads and avoided the need to cast new gels for each sequence. (Ruiz-Martinez et al., 1993; Hebenbrock et al., 1995). The polymerase chain reaction (PCR) replaced DNA cloning from libraries as the main method to generate the sequencing templates (Saiki et al., 1985; Saiki et al., 1988) and automated Sanger sequencing by capillary electrophoresis was established (Hunkapiller et al., 1991). This allowed 500-1000bp of DNA sample to be sequenced in 6–8 hours. This method is the gold-standard DNA sequencing technique that is still used in laboratories today to sequence short pieces of DNA.

1.10.2 Second-generation DNA sequencing

The emergence of a new technique known as pyrosequencing (Roche GS FLX) paved the way for 'next-generation sequencing' (NGS) technologies for high-throughput sequencing. In this method, an enzymatic reaction occurs in which ATP sulfurylase converts pyrophosphate into ATP, which subsequently serves as the substrate for luciferase, meaning that the light produced is proportional to the amount of pyrophosphate (Nyrén and Lundin, 1985). The amount of incorporation is monitored by luminometric detection of the quantity of pyrophosphate released as each nucleotide is washed through the system in turn over the template DNA affixed to a solid phase. This signal is then used to infer DNA sequences (Hyman, 1988). The weakness with this technique though, is that errors can be caused by misjudging the length of homopolymer runs in this process, which may result in false single-base insertions or deletions (indels) in the DNA sequence readout (Ronaghi et al., 1998).

The sequencing machines developed by different companies during the first decade of the new millennium dramatically increased the amount of DNA that could be sequenced, ranging from five hundred million bases of raw sequence (Roche) to billions of bases in a single run (Illumina, ABI SOLiD technology). These machines relied on performing massive numbers of parallel sequencing reactions on a micrometer scale on clonal beads (Roche and ABI SOLiD) or clonal bridges (Illumina). (Shendure and Ji, 2008). Over the last decade, these three platforms are commercially leading second generation NGS platforms (Pareek et al., 2011).

Here at Leeds the NGS facility (a partnership between the University of Leeds and the Leeds Teaching Hospitals NHS Trust) uses the Illumina NGS platform. For the Illumina Genome Analyser, sample preparation involves fragmentation of the DNA sample, enzymatically repairing the staggered ends, adding adenines (A) to the 3-ends of the DNA fragments and ligating adapters, followed by library amplification (Myllykangas et al., 2012). Solid-phase amplification is used to produce randomly distributed, clonally amplified clusters from fragments or mate-pair templates on a glass slide. The sequencing library is immobilised on the surface of a flow cell onto which a "lawn" of high-density forward and reverse primers has been covalently attached to the slide to create an ultra-dense primer field. The primer functionalised flow cell surface

serves as a support for amplification of the immobilised sequencing library by a process also known as “Bridge-PCR” (Figure 1.11A). The resulting bridged double-strand DNA is freed using a denaturing reagent. Repeated reagent flush cycles generate groups of thousands of DNA molecules, also known as “clusters,” on each flow cell lane. DNA clusters are then unbound from the complementary DNA strand (linearization), followed by blocking the free 3’-ends of the clusters and hybridising a sequencing primer.

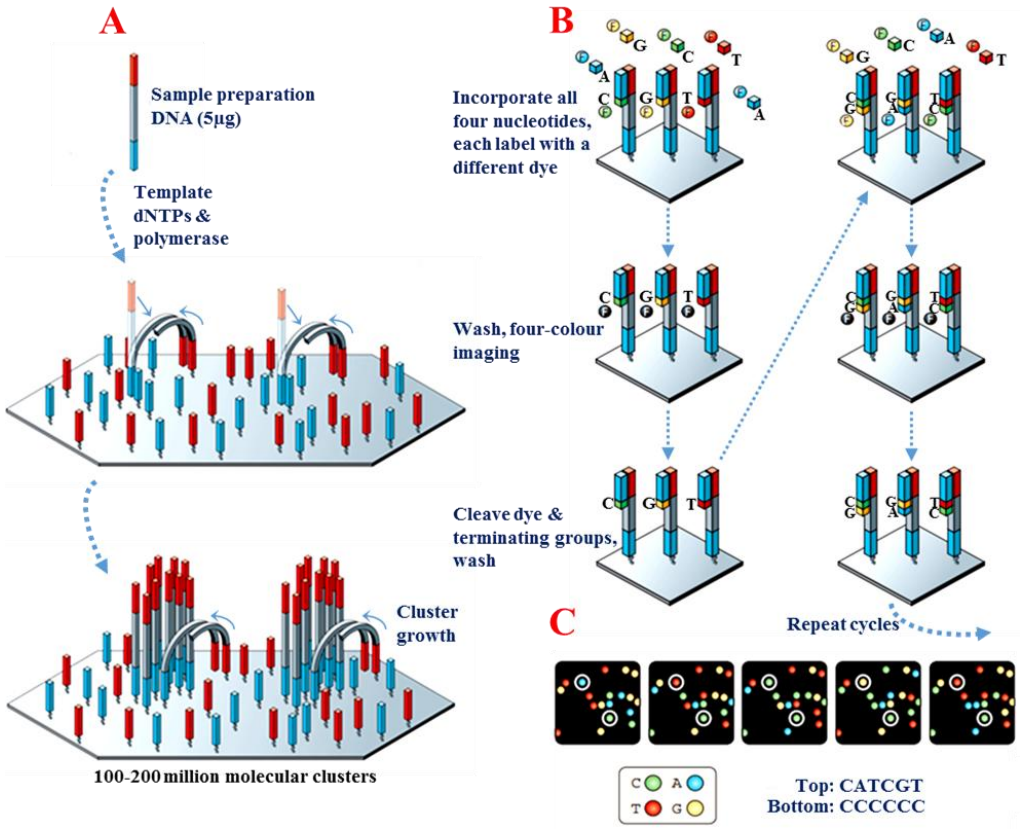

Figure 1.11. Illumina solid-phase amplification and four-colour cyclic reversible termination sequencing method. Illumina solid-phase amplification (A) is achieved through two basic steps, these being initial priming and extending of the single stranded single-molecule template, followed by bridge amplification of the immobilised template with immediately adjacent primers to form clusters. The four-colour cyclic reversible termination (B) uses Illumina’s 3′-O-azidomethyl reversible terminator chemistry on solid-phase-amplified template clusters. Following incorporation, a cleavage step removes the fluorescent dyes and regenerates the 3′-OH group using the reducing agent Tris (2-carboxyethyl) phosphine. (C) The four-colour images highlight the sequencing data from two clonally amplified templates. (Adapted from Metzker (2010) with the permission of Elsevier Copyright Clearance Centre, License number: 3940451410070).

Cyclic reversible termination is the method employed by Illumina for sequencing-by-synthesis. Firstly, a DNA polymerase bound to the primed template incorporates just one fluorescently modified nucleotide, which represents the complement of the template base. Following incorporation, the remaining unincorporated nucleotides are washed away (Figure 1.11B). Secondly the four colours of the four nucleotides are detected by total internal reflection fluorescence imaging using two lasers (Figure 1.11C). The synchronous extension of the sequencing strand by one nucleotide per cycle ensures that homopolymer stretches can be accurately sequenced. However, failure to incorporate a nucleotide during a sequencing cycle results in an off-phasing effect, and as the sequence extends, gradually more and more molecules lag behind in the extension so that the generalised signal derived from each cluster deteriorates over many cycles. Therefore, Illumina sequencing accuracy declines as the read length increases, which limits this technology to short sequence reads (Myllykangas et al., 2012).

1.11 Aims

There were two aims for this research project, both of which involved finding and characterising new mutations and genes involved in inherited retinal dystrophies using NGS technologies.

The first approach described the Retinome project, which used targeted exome sequencing against all the known retinal dystrophy genes to attempt to identify the pathogenic mutation in twenty multiplex families with various different inherited retinal dystrophies. This approach identified mutations in known retinal dystrophy genes but also highlighted families in whom the pathogenic mutation could not be identified, suggesting that their Mendelian cause of retinal dystrophy may be in a gene that has not yet been implicated.

The second approach used whole exome next generation sequencing from affected members in six families, each with a different inherited retinal disease, to identify the pathogenic mutation.

Chapter 2 - Materials and Methods

2.1 Patient ascertainment

Affected patients and their relatives were recruited in the ophthalmology clinics of the Eye Department, St. James's University Hospital, Leeds, UK following their informed consent using a process that adhered to the tenets of the Declaration of Helsinki and was approved by the Leeds East Research Ethics committee (Project number 03/362). The patients underwent an eye examination by an experienced ophthalmologist to confirm their diagnosis of retinal dystrophy and the full clinical family history was taken. Peripheral blood or saliva was collected from the patient and where possible from additional family members for DNA extraction (Section 2.2).

2.2 Genomic DNA extraction

DNA was extracted from peripheral blood or saliva according to the following methods.

2.2.1 Extraction of DNA from blood using phenol-chloroform extraction

To extract DNA from a blood sample, 9ml of red cell lysis buffer [10mM/ml Potassium Bicarbonate ($KHCO_3$), 155mM/ml Ammonium Chloride (NH_4C1) and 1mM/ml Ethylenediaminetetraacetic acid (EDTA)] was added to 3ml of whole blood and mixed by inversion for 10 minutes. The sample was centrifuged at 2,000 x g for 15 minutes. After removing the supernatant, 500µl of cell lysis buffer [20ug/m1 RNAase A, 0.25% [v/v] SDS, 10mM/ml Tris pH 8.0 and 100mM/ml EDTA] was added to the white cell pellet and incubated at 37°C for one hour. Proteinase K was then added at a final concentration of 100µg/ml and the sample was incubated at 55°C for one hour. An equal volume of phenol-chloroform (phenol: chloroform: isoamyl alcohol, 25: 24: 1) was added to the sample and mixed vigorously for 1 minute until an emulsion was produced. The aqueous and organic phases were then separated by centrifugation at 14,000 x g for 1 minute. The upper aqueous phase was transferred to a new test tube and an equal volume of chloroform (chloroform: isoamyl alcohol, 24:1) was added. The nucleic acid in the upper aqueous phase was then precipitated from the solution by the addition of 0.1 volume

of 0.3M sodium chloride and 2.5 volumes of 100% ethanol. After mixing, the precipitated material was collected by centrifugation at 3,000 x g for 15 minutes. The ethanol supernatant was discarded and the nucleic acid pellet was washed with 70% ethanol. After centrifugation, the ethanol wash was removed and the pellet was air-dried for 5 minutes before re-dissolving in 30-50µl of 1 x Tris-EDTA (TE) buffer [10mM/ml Hydroxymethyl aminomethane hydrochloride (Tris-HCl) (pH 7.5) and 1mM/ml EDTA].

2.2.2 Extraction of DNA from blood using salt precipitation technique

A salt precipitation technique was performed to extract DNA from fresh non-frozen blood samples. Briefly, 3ml of whole blood was aliquoted into a polypropylene tube and 9ml of red cell lysis solution added. The samples were then mixed for 10 minutes at room temperature (RT) and then centrifuged at 2,000 x g for 10 minutes. The supernatant was removed and the remaining white cell pellet was re-suspended in 3ml white cell lysis solution by pipetting. To remove any contaminating protein, 1ml of protein precipitation solution (10M ammonium acetate) was added, and samples were vortexed for 20 seconds then centrifuged at 2,000 x g for 10 minutes. The supernatant was transferred into a fresh tube and the DNA was precipitated using 3m1 of isopropanol, followed by centrifugation for 10 minutes at 2,000 x g. The pellet was then washed twice in 70% ethanol and left to air dry. The precipitated DNA was dissolved in 1x TE buffer.

2.2.3 Extraction of DNA from saliva

Saliva samples were collected using Oragene® DNA sample collection kits (DNA Genotek Inc.) and the DNA extracted according to the manufacturer's protocol. Briefly, 30µl of PT-L2P reagent (provided with kits) was added to 750µl of saliva and incubated on ice for 10 minutes. The sample was then centrifuged at RT for 10 minutes at 3500 x g. 600µl of the supernatant was transferred to a fresh tube and 720µl of 100% ethanol was added. The mix was inverted 10 times. The samples were then incubated for 10 minutes at RT and centrifuged for 10 minutes at 3500 x g. The pellet was washed in 500µl of 70% ethanol for 1 minute at RT. After drying, the pellet was re-dissolved in 50µl TE buffer then stored at -20°C.

2.3 Determining the concentration of purified nucleic acid

The concentration of purified nucleic acids was measured using a Qubit® Fluorometer (Invitrogen) and the appropriate dsDNA/RNA assay kits according to the manufacturer's instructions. Briefly, 1-10µl of sample were added to the Qubit dsDNA/RNA dilution reagent to make a final volume of 200µl and samples were vortexed and incubated for 2 minutes at RT. The Qubit® Fluorometer was calibrated using standards provided in each assay kit and the samples processed. A NanoDrop spectrophotometer (Thermo Scientific) was also used for measuring optical densities of DNA/RNA samples at 260/280 nm ratio ($A_{260/280}$).

2.4 The polymerase chain reaction (PCR)

2.4.1 Primer design for standard PCR analysis

Oligonucleotide primer pairs were designed to amplify products of 200-550 base pairs (bp) in size. The genomic DNA sequence for the region of interest (ROI) was obtained from Ensembl (http://www.ensembl.org) and UCSC Genome Browser (http://genome.ucsc.edu/) in the FASTA format with all exons in upper case and everything else in lower case. The primers were designed using the Primer3 program (http://bioinfo.ut.ee/primer3-0.4.0/) with length of 20 bp (range 18-27 bp), a primer melting temperature of 60°C (range 57-63°C) and GC% between 20% and 80%. Primer sequences were checked using the BLAT tool in the UCSC Genome Browser in order to check for unique primers for species-specific regions and to avoid known SNPs over the binding site. Primers used for RT-PCR were designed using the same methods described above, but in this case mRNA sequence was used as template and primers designed to span an exon-exon junction.

For gene screening, the primers were designed to amplify the exonic region and at least 50 bp from the intron-exon boundary using the automated ExonPrimer tool (https://ihg.helmholtz-muenchen.de/cgi-bin/primer/ExonPrimerUCSC.pl?db=hg19&acc=uc009wfy.3) with the following settings: minimal distance between primer and exon (50-bp), primer region (70-bp), maximal target size (500-bp), overlap for large exon (50-bp), annealing temperature (60°C), GC content (50%), primer size (17-[20]-27bp) and maximum length of mononucleotide repeat (4-bp).

2.4.2 Primer design for Gateway® cloning

Cloning PCR primers were designed according to the guidelines provided by the Gateway® Technology protocol (Invitrogen) to amplify the full coding sequence of genes of interest, and to add gateway *att*B1 and *att*B2 restriction enzyme sequences to the 5' and 3' ends of a gene fragment. The Kozak sequence was also added to ensure protein expression. For 5' primer, the *att*B1 sequence was added, followed by the Kozak sequence including ATG initiation codon, then 18-22 nucleotides at the start of the gene. For 3' primer, the *att*B2 sequence was added, followed by 18-22 gene-specific nucleotides, while the stop codon was removed to allow an in-frame read with the *att*B2 sequence (C-terminal fusion). The GC content, GC clamp and melting temperature (TM) of gene-specific nucleotides for gateway *att*B primers was adjusted using an online oligonucleotide properties calculator (http://biotools.nubic. northwestern. edu/ Oligo Calc.html) (Kibbe, 2007). Finally for the 3` primer, the reverse complement of the sequence was used (http://www.bioinformatics.org/sms2/rev _comp.html).

2.4.3 Standard PCR

PCR was typically performed in 25µl volumes containing 20-50ng genomic DNA (gDNA) with the following reagents at the specified concentrations:1x PCR reaction buffer [20mM Ammonium sulphate ($(NH_4)_2SO_4$), 20mM Tris-HCL (pH 8.4), 0.01% [v/v] Tween20 and 1.5 mM Magnesium chloride ($MgCl_2$)], 10 picomoles of each of the F(forward) and R(reverse) primers, 200µM of each dATP, dGTP, dCTP and dTTP nucleotides and 1 unit Taq DNA polymerase (Invitrogen Ltd., Renfrew, UK). Thermal cycling was performed on this mixture with an initial denaturing step at 96ºC for 3 minutes, followed by 35 cycles of 92ºC for 30 seconds (denaturing), 55-65ºC for 30 seconds (annealing) and 72ºC for 30 seconds (extension). The final extension step was performed at 72ºC for 10 minutes.

2.4.4 Hot-Shot master mix PCR

20-50ng of gDNA was amplified in a 10 µl reaction volume, containing 50% [v/v] Hotshot Diamond PCR Master Mix (Clent Life Science, Stourbridge, UK), 5-10% [v/v] dimethyl sulphoxide (DMSO) and 10 picomoles of each primer. Touchdown PCR cycle was then performed on the mixture through the following ten steps:

1	95ºC for 10.00 mins (initial denaturing)
2	95ºC for 0.30 mins (denaturing)
3	67.5ºC for 0.30 mins (annealing) "Decrease by 0.5ºC every cycle"
4	72ºC for 0.30 mins (extension)
5	Go to step 2, repeat 13 times
6	95ºC for 0.30 mins (denaturing)
7	60 or 65ºC for 0.30 mins (annealing)
8	72ºC for 0.30 mins (extension)
9	Go to step 6, repeat 29 times
10	72ºC for 7.00 mins (final extension)

2.4.5 Cloning PCR

For cloning purposes, PCR reactions were performed with the designed cloning primers using platinum Pfx DNA polymerase (Invitrogen). The reactions were typically carried out on 60ng template DNA in a 50µl final volume that included 0.4µl of platinum Pfx DNA polymerase, 5µl of 10 x Pfx amplification buffer, 1.5µl of 10µM forward and reverse primer mix, 1.5µl of 10mM dNTPs, 1µl of 50mM magnesium sulphate ($MgSO_4$) and 1µl of DNA template. Initial denaturation was performed at 94ºC for 5 minutes followed by 30 cycles of three steps: denaturation at 94ºC for 15 seconds, annealing at 58ºC for 30 seconds and the extension step at 68ºC for 5 minutes. A final extension was performed at 68ºC for 10 minutes.

2.5 Agarose gel electrophoresis

Agarose gel electrophoresis was used to analyse the presence and size of PCR products from the samples. Gels usually contained between 1.0% and 1.5% [w/v] of ultra-pure agarose (Fisher Scientific). To prepare a gel, the desired amount of agarose was first dissolved in 0.5 x TBE buffer [44.5 mM Hydroxymethyl aminomethane (Tris), 44.5 mM Boric acid (H_3BO_3) and 1.25 mM EDTA (pH 8.0)], a process that was hastened by heating in a microwave oven. The solution was cooled to 55ºC, mixed with ethidium bromide (final concentration 0.5µg/ml), and then poured into a gel tray with gel combs inserted, to a depth of between 5 and 8 mm. When solidified, the gel was submerged under 0.5 x TBE buffer, in an electrophoresis tank. The combs were removed to create wells. Wells

within the gel were next filled with 2µl PCR product that had been mixed with 8µl of 1 x DNA loading dye [0.01% w/v Xylene cyanol, 0.01% w/v Bromophenol blue, 10% v/v Glycerol and 2x TBE buffer]. DNA molecular weight markers (Bioline) were also loaded alongside the samples. The gel was then run at 120 V for 30 minutes. Ethidium bromide stained DNA within the gel and was visualized using the ChemiDoc™ MP System (Bio-Rad Life Science) under UV light (wavelength 320 nm). The image was analysed using Image Lab™ software (Bio-Rad Life Science).

2.6 DNA extraction from agarose gels

DNA bands of the correct size were excised from agarose gels using Qiagen's QIAquick Gel Extraction kit protocol. Briefly, a DNA band was excised with a clean scalpel under long wave-length UV light using a Mineralight UVGL-58 lamp. Gel fragments were subsequently weighed and melted in QG buffer at 37°C for 15 minutes. The mixture containing DNA was centrifuged using a QIAquick column, following a wash with PE buffer, containing 70% ethanol. Finally, the DNA was re-dissolved in 1 x TE buffer.

2.7 Genotyping

2.7.1 Microsatellite marker genotyping

Microsatellite markers were used for genotyping by standard PCR with the addition of a 5'-FAM (blue) fluorescent dye on the forward primers. The markers were selected and their genetic locations within given regions were identified using the UCSC Genome Browser (http://genome.ucsc.edu/) or NCBI Map Viewer (http://www.ncbi.nlm.nih.gov /map view/). PCR was performed according to the description in Section 2.4 using a 5' fluorescently labelled forward primer. PCR products were visualised on a 1.5% agarose gel. 1µl diluted product was then added to a mixture of 0.5µl ROX-500 size standard (Applied Biosystems) and 8.5µl Hi-Di formamide (Applied Biosystems). Fragments were resolved and separated via electrophoresis on an ABI3130xl Genetic Analyzer (Applied Biosystems) using a 36cm array, POP7 polymer and the Fragment Analysis 36_pop7_1 module (Applied Biosystems). Sizing of the microsatellite alleles was performed using Gene Mapper v.4 software (Applied Biosystems).

2.7.2 Affymetrix SNP chip genotyping

Patient samples were SNP genotyped using the commercial service providers GeneService (London, UK) or AROS Applied Biotechnology (Denmark). Low-resolution genotyping (250,000 SNPs) was undertaken by sending 500ng of gDNA at a concentration of 50ng/µl to GeneService for genotyping using a 250K Affymetrix SNP chip. For high-resolution genotyping (1 million SNPs), 1µg gDNA was sent to AROS for hybridization to the Affymetrix 6.0 chip.

The resulting Affymetrix SNP chip genotyping data were returned as CEL files, which were annotated by using Affymetrix Genotyping Console Software (http://www.affymetrix.com/estore/browse/level_seven_software_products_only.jsp?productId=131535#1) into Microsoft Excel files containing SNP ID, chromosome, physical position and resulting allele call for each SNP assayed. Annotated genotype data was then analysed to identify potential autozygous regions using either AutoSNPa software (Carr et al., 2006), IBDfinder software (Carr et al., 2009) or SNP Viewer (http://snpviewer.sourceforge.net/) software using the default settings. Homozygous regions were exported to Microsoft Excel/Word for manual analysis. To visualise the SNP data at the genome level, or to combine the SNP chip genotyping data with SNP data generated from WES data (Section 2.12), either AgileMultiIdeogram (http:// dna.leeds.ac.uk/ agile/AgileMultiIdeogram/) or AutoIdeogram (http://dna.leeds.ac.uk/AutoIdeogram/) software were used.

2.8 Sanger sequencing

2.8.1 PCR product preparation prior to sequencing

Prior to performing the sequencing reaction, PCR products were either purified using Qiagen's QIAQuick PCR Purification columns or treated with ExoSAP-IT (Affymetrix, Santa Clara, USA) consisting of Exonuclease I and Shrimp Alkaline Phosphatase for the removal of unincorporated dNTPs and primers. Each clean-up reaction of 7µl (2µl ExoSAP-IT and 5µl PCR product) lasted for 45 minutes (30 minutes at 37 ºC for treatment and 15 minutes at 80 ºC for inactivation).

2.8.2 Dye terminator sequencing on the AB13130xl Genetic Analyser

Purified PCR products were sequenced using the BigDye® Terminator Cycle Sequencing Kit v3.1 (Applied Biosystems). Each sequencing reaction contained 1µl of purified PCR product, 0.5µl of BigDye® terminator v3.1 (Applied Biosystems), 1.5µl 5 x BigDye® terminator sequencing buffer (Applied Biosystems), 6µl distilled water and 1µl (1.6 picomoles) of the sequencing primer, giving a final reaction volume of 10µl. The sequencing reaction mixture was denatured initially for 1 minute at 96ºC, followed by 25 cycles of 96ºC for 30 seconds, 50ºC for 5 seconds, and 60ºC for 4 minutes, with all temperatures ramped at 1ºC/second. DNA was then ethanol precipitated by adding 5µl of 125mM EDTA and 60µl 100% ethanol to the sequencing product. Samples were mixed and underwent centrifugation for 30 minutes at 3,000 x g at 22ºC, followed by an inverted spin for 40 seconds at 200 x g. Next, 60µl of freshly prepared 70% ethanol was added, and samples were centrifuged for 15 minutes at 800 x g at 4ºC. Finally, an inverted spin was performed for 40 seconds at 200 x g and samples were left to air dry at RT for 15 minutes. Pellets were re-dissolved in 10µl of Hi-Di formamide loading buffer (Applied Biosystems) and resolved at 60ºC using a 36cm array, POP-7 polymer and the default RapidSeq 36 POP7 module on an ABI3130xl Genetic Analyser (Applied Biosystems). The sequences produced were analysed using the Sequence Analysis v5.2 and SeqScape v2.5 software packages (Applied Biosystems).

2.9 Whole genome amplification (WGA)

WGA of gDNA was carried out using the GenomiPhi V2 kit (GE Healthcare, USA) according to the manufacturer's guidelines, however half the recommended volumes were used. 0.5µl of the DNA sample was mixed with 4.5µl of the sample buffer followed by denaturation for 3 minutes at 95ºC. On ice, 4.5µl of reaction buffer and 0.5µl of the enzyme mix was added to each sample followed by incubation at 30ºC for two hours. The enzyme was then inactivated at 65ºC for 10 minutes. Amplified samples were diluted 1 in 50 in distilled water and 2 µl from each sample was amplified in subsequent PCR reactions.

2.10 Whole exome sequencing (WES)

2.10.1 Library preparation

WES was carried out using commercial kits from Agilent Technologies: SureSelect XT Library Preparation kit ILM, SureSelect Target Enrichment and Herculase II Fusion DNA Polymerase, SureSelect XT Human All Exon V4 Capture or SureSelect XT Human All Exon V5 Capture Libraries. The standard Illumina protocol "SureSelect XT Target Enrichment System for Illumina Paired-End Sequencing Library" was followed (available from http://www.agilent.com/cs/library/usermanuals/ Public/G7530-90000_SureSelect_IlluminaXTMultiplexed_1.8.pdf). Briefly, each DNA sample was quantified using the Qubit® dsDNA (Broad-Range) Assay (Invitrogen) (Section 2.3). 3µg of gDNA was diluted in 1 x TE buffer to a final volume of 250µl and added to a clearly labelled T6-30 glass tube (Covaris, USA). The DNA was then sheared in a water bath at 20°C to fragment sizes of 150 to 200 bp using the Covaris system (Covaris S220 Sonicator and SonoLite software). This sheared DNA sample was then purified using Agencourt AMPure XP magnetic beads (Beckman Coulter Genomics, South Plainfield, USA) and analysed using a DNA 1000 Bioanalyzer^{TM} (Agilent Technologies) to assess the distribution of DNA fragment sizes between 150-200 bp.

The creation of blunt-ended fragments and 5'-phosphorylation of the ends were the next steps. 48µl of the purified sample was mixed with 35.2µl of nuclease-free water, 10µl of 10 x end repair buffer, 1.6µl of dNTP mix, 1µl of T4 DNA polymerase, 2.2µl of T4 Polynucleotide Kinase, and 2 µl Klenow DNA Polymerase. This mixture was incubated in a thermal cycler for 30 minutes at 20°C, then the DNA fragments were again purified using Agencourt AMPure XP magnetic beads. After the fragment ends were repaired, adenosine overhangs were added to their 3' ends (3'-dA overhangs) by incubation of 30µl of the sample with 3 µl of Exo(-) Klenow, 5µl of 10 × Klenow polymerase buffer, 11µl of nuclease-free water and 1µl dATP for 30 minutes at 37°C.

The sample was then purified a third time using the magnetic beads. Paired-end adaptors were ligated on by adding 1.5µl T4 DNA Ligase, 10µl of 5 x T4 DNA ligase

buffer, 10µl of diluted SureSelect adaptor oligo mix and 15.5µl of nuclease-free water to 13µl of the DNA sample, followed by incubating for 15 minutes at RT. Next, the sample was purified using the magnetic beads again and the adapter-ligated library was amplified in a 50µl PCR containing, 15µl of DNA sample, 1.25µl of SureSelect ILM indexing pre-capture PCR reverse primer, 1.25µl SureSelect primer, 10µl of 5 x Herculase II reaction buffer, 1 µl of Herculase II fusion DNA polymerase, 0.5µl of 100mM dNTP mix, and 21µl of nuclease-free water. The PCR mix was loaded into a thermal cycler with the following program: 98°C for 2 minutes (denaturation) and 6 cycles of 98°C for 30 seconds, 65°C for 30 seconds and 72°C for 1 minute, followed by a final extension step of 72°C for 10 minutes. The amplified library was purified using the magnetic beads and analysed using a DNA 1000 Bioanalyzer^{TM} assay. Only samples with an electropherogram reading showing a single peak around 250 to 275 bp were taken through to the hybridisation steps.

Each amplified library was quantified using the PicoGreen® double stranded DNA (dsDNA) quantitation assay (Invitrogen) according to the manufacturer's instructions. The library was then hybridized and the exome was captured individually prior to addition of the indexing tag. For each hybridization reaction, 40µl of the hybridization buffer and 5.6µl of SureSelect block mix were prepared according to the manufacturer's protocol. 750ng of the library DNA with a maximum volume of 3.4µl was added to 5.6µl of prepared SureSelect block mix then incubated for 5 minutes at 95°C. In a PCR plate maintained at 65°C, the prepared library was mixed with 13µl of the prepared hybridization buffer and 7µl of SureSelect capture library of biotinylated RNA oligonucleotide probes (5µl of SureSelectXT Human All Exon V4/V5 and 2µl of 25% RNase block), followed by incubation for 24 hours at 65°C in a thermal cycler with a heated lid at 105°C. The captured library was fished out using streptavidin-coated magnetic beads (Dynabeads MyOne Streptavidin T1, Invitrogen) on a magnetic separator according to the protocol guidelines. Subsequently, index tags were added to the captured library by post-hybridization amplification. 14µl of each DNA sample and 1µl of the appropriate index PCR primer were mixed with 35µl of Herculase II master mix (10µl of 5 x Herculase II reaction buffer, 1µl of Herculase II fusion DNA polymerase, 0.5µl of 100mM dNTP mix, 22.5µl of nuclease-free water and 1µl of SureSelect ILM Indexing post capture forward PCR primer), followed by loading into a thermal cycler for 2 minutes at 98°C, then 12 cycles of 30 seconds at 98°C, 30 seconds at 57°C and 1 minute at 72°C.

Final extension was at 72°C for 10 minutes. The samples were then purified using Agencourt AMPure XP beads and analysed using the 2100 Bioanalyzer™ high sensitivity DNA assay (Agilent Technologies) which was expected to achieve a normal distribution around a peak ranging from approximately 300 to 400 bp. Six samples were pooled together in a final volume of 50µl, with each sample having a final concentration of 10nM. Finally, the cluster amplification was performed at the NGS facility (University of Leeds), followed by NGS using paired-end 100 bp reads on an Illumina 2500 HiSeq sequencer (Illumina Inc. UK).

2.10.2 Analysis of WES data.

The computational analysis of the WES data was performed using Unix console commands (Appendix 1) and a wide range of online servers. The quality of the raw data coming from the Illumina high throughput sequencing was determined by using FASTQC tools run on the Galaxy platform (Blankenberg et al., 2010). Quality scores across all bases, GC content per sequence, sequence length distribution and duplication levels were evaluated before any further analysis. After sequence quality monitoring, the sequencing data was aligned against the reference genome (hg19/GRCh37) using either the Bowtie2 program (Langmead and Salzberg, 2012) or NovoAlign software (http://www.novocraft .com/ products/novoalign/). NovoAlign was preferred in exome depth and fishing CNV analysis or filtering the sample against in-house samples that had been analysed using the same aligner. Otherwise the Bowtie2 aligner was more widely used. The aligned files were sorted, indexed and processed in SAM/BAM format using the SAMtools suite of programs (Li et al., 2009) (http://samtools. sourceforge.net/). PCR duplicates were removed by Picard tools (http://broadinstitute. github.io/ picard/). The mean depth of reads per base was observed and the variants were then realigned locally and recalibrated using the Genome Analysis Toolkit (GATK) (https://www. broadinstitute. org/gatk, version 3.3-0). Indel and single nucleotide variants were called in the variant call format (VCF) format using the Unified Genotyper function of GATK (DePristo et al., 2011). The Integrative Genomics Viewer (IGV) (https://www. broadinstitute.org/igv/) (Robinson et al., 2011) was used for visualization and interactive exploration of the aligned data files. The variant list of each individual was annotated using ANNOVAR software (http://annovar. openbioinformatics.org/en/latest/) and filtered using the following criteria: selecting only DNA variants in coding regions, splice donor and

acceptor sites (±2 bp), removing synonymous changes, selecting variants with a greater than depth of coverage of 10 reads, filtering out exome variants that have a minor allele frequency (MAF) of greater than 1% in either dbSNP 138 (http://www.ncbi. nlm.nih.gov/SNP/), the 1000 Genomes (Abecasis et al., 2012), the exome variant server (EVS) or the Exome Aggregation Consortium (ExAC) databases (Section 2.14.4). For VCF files of patients of Pakistani origin, an additional filtering step was used to filter out all variants with MAF greater than 5% in a cohort of 3222 exomes of British Pakistani adults (Narasimhan et al., 2016) (http://www.genesandhealth.org/research/scientific-data-downloads), this step was used through a perl script (Appendix 1) developed by Dr David Parry, University of Leeds. The final variant lists were initially compared to the known retinal dystrophy genes in the RetNet database (URL: https://sph.uth. edu/retnet/). The pathogenicity of variants was also assessed using a number of software either integrated in the ANNOVAR or used separately (Section 2.14.2).

2.11 Targeted capture NGS

2.11.1 Target design and library construction

In order to enrich for specific targets from patient gDNA, a liquid-phase reagent comprising 'SureSelect Target Enrichment' biotinylated cRNA baits was designed against regions of interest using the Agilent Technologies eArray platform (http://www.genomics.agilent.com) (Agilent Technologies UK Limited, Wokingham, UK). For the library preparation, gDNA from each patient was sheared using the Covaris S220 sonicator (Applied Biosystems). Illumina sequencing adapters, containing 6 bp sequence tags were ligated to the samples, with each DNA sample being ligated to a different tag. The tagged DNA libraries were then captured using the SureSelect custom baits. Hybridization reaction, post-hybridization amplification, indexing and purification and pooling were done as previously descried (Section 2.10.1). The cluster amplification was performed at the NGS facility (University of Leeds) followed by NGS using single-end 80 bp reads on an Illumina GAIIx Sequencer (Illumina Inc. UK).

2.11.2 Targeted sequencing analysis and variant detection

Sequence data were generated in qseq format and barcode sorted by their unique 5′ tag using NovoSort (http://www.novocraft.com/). Output data were aligned to the

reference human genome sequence, hg19, using NovoAlign software (v2.08.01) (http:// www. novocraft.com/products/novoalign/). Following realignment around indels using the GATK (v2.0.34) (https://www.broadinstitute.org/gatk, version 2.0-34). Unified Genotyper (DePristo et al., 2011) was used for variant calling. The output VCF files were annotated using ANNOVAR software (http://annovar.openbioinformatics.org/en/latest/). Analysis of read depth was performed using BED Tools (v2.15.0) (http://bedtools. readthedocs.io/en/latest/) and the GATK Count Reads walker (https://software. broadinstitute.org/gatk/gatkdocs/org_broadinstitute_gatk_tools_walkers_qc_CountRead s.php). VCF file filtration was carried out as mentioned above (Section 2.10.2). Unix console commands used for the targeted sequencing analysis can be found in Appendix 1.

2.12 Homozygosity mapping using WES data

Detection of homozygous regions from NGS data was performed using AgileGenotyper (Carr et al., 2013). The genome annotation file and exome SNP database were downloaded from AgileGenotyper (http//dna.leeds.ac.uk/agile/AgileGenotyper/ download.php) and then loaded with the aligned sequence data file of the sample to the software. Exported genotype data in text format was analysed using AutoSNPa software (Carr et al., 2006), and the locations of homozygous regions were displayed by using either AutoIdeogram (http://dna.leeds.ac.uk/AutoIdeogram/) or AgileMultiIdeogram (http://dna.leeds.ac.uk/agile/AgileMultiIdeogram/) software.

2.13 Detection of copy number variation (CNV) using WES data

Fishing CNV was used to compare the distribution of the depth of coverage between the sample and a large batch of control samples that sequenced in different sequencing run according to method described by Shi and Majewski (2013). Briefly the fastq file of the sample was processed as described above (Section 2.10.2) without duplicates removing step by Picard. The sample indexed Bam file was then treated by GATK's Depth Of Coverage command with a minimum 10 value as base quality. Reads per kilobase per million mapped reads (RPKM) files were generated for the sample and seventy eight pooled control samples. The analysis was then performed on R package

FishingCNV (http://sourceforge.net/projects/fishingcnv/). False discovery rate (FDR) adjusted P-value of 0.05 was used as the threshold of detection and smaller values indicative of more confident calls.

ExomeDepth analysis was to compare the read depths between the sample and a small batch of control samples that sequenced in the same sequencing run with the same version of the SureSelect Human All Exon capture reagent according to method described by Plagnol et al. (2012).The fastq files of all samples were processed as described for fishing CNV method up to indexing of the Bam file then analysed using the R package ExomeDepth (https://cran.r-project.org/web/packages/ExomeDepth/index.html). The output csv file prioritised according the highest Bayes factor (the log10 of the likelihood ratio of data for the CNV call divided by that of the normal copy number call). The read ratios of 0, 1, 1.5 and 2 indicated a homozygous deletion, a heterozygous deletion, a heterozygous duplication and a homozygous duplication respectively. Unix and R commands used for detection of CNV using WES data can be found in Appendix 2.

2.14 Bioinformatics and computational biology

The fields of bioinformatics and computational biology were widely used to investigate questions about biological composition, structure and function of gene/protein involved in this study. These approaches allow large-scale analysis (such as WES and targeted NGS analysis, Sections 2.10.2 and 2.11.2), designing (such as primer design, Section 2.4.1), prediction (such as software for predicting mutation pathogenicity, Section 2.14.2) and obtaining data from many disciplines. The list of bioinformatics tools used in this study are listed below.

2.14.1 Genetic, phenotypic and functional data sources

The basic information about the candidate genes including genomic sequence, intron-exon structure, location of polymorphisms and amino acid conservation was obtained using the UCSC Genome Browser (http://genome.ucsc.edu/), while information about disease phenotypes was collected using Online Mendelian Inheritance in Man database (OMIM - http://www.ncbi.nlm.nih. aov/omim). Literature searches of techniques, genes and proteins were carried out using PubMed (http://www.ncbi.nlm.

nih.gov/pubmed), Genecards (http://www.genecards.org/), the Ensembl Genome Browser (http://www.ensembl.org/index.html) and NCBI site (http://www.ncbi.nlm.nih.gov/gene/).

2.14.2 Software for predicting mutation pathogenicity

A large number of *in-silico* tools have been developed to predict the effect of an unclassified variant on the protein function. These software tools play a key role in prioritizing the causative mutation candidates. Some of these tools are discussed below.

2.14.2.1 Polymorphism phenotyping v2 (PolyPhen-2)

PolyPhen-2 is a freely available, web-based program used to predict the possible impact of a non-synonymous variant on the stability and function of the protein (http://genetics.bwh.harvard.edu/pph2 /index.shtml). This tool integrates the indexes of UCSC Genome Browser's human genome annotations together with the Vertebrate Genome Annotation (VEGA) database. The software estimates the probability score based on a combination of structural properties, comparative evolutionary profiles, the differences between all functionally known damaging alleles with non-damaging and the differences present between human and vertebrate orthologues (Adzhubei et al., 2010). The differences between human disease-causing mutations in the UniProt knowledgebase (UniProtKB) (http://www.uniprot.org/help/uniprotkb) and common human non-synonymous single nucleotide polymorphisms (nsSNPs) with MAF>1% and no disease-associated annotation are also considered in the prediction. PolyPhen-2 scores between 0 and 1.00 are interpreted to give qualitative predictions as follows: <0.15 = benign substitution prediction, 0.15-0.85 = possibly damaging, and 0.85-1.00 = probably damaging.

2.14.2.2 Sorting intolerant from tolerant (SIFT)

SIFT is a web-based program that classifies the amino acid substitutions as tolerated or deleterious (http://sift.jcvi.org/). The probability matrix is calculated according to the degree of conservation of amino acid residues in multiple sequence alignments collected from homologues with similar functions using PSI-BLAST (Position-Specific Iterative Basic Local Alignment Search Tool). The software has a default cut-off threshold of 0.05.

SNPs with SIFT scores higher than this threshold are regarded as tolerated (Ng and Henikoff, 2003).

2.14.2.3 The BLOSUM62 matrix

The BLOSUM62 substitution matrix can score all the possible exchanges of one amino acid with another (http://www.ncbi.nlm.nih.gov/Class/FieldGuide/BLOSUM62 .txt). The matrix is derived from about 2,000 blocks of aligned sequence segments characterizing more than 500 groups of related proteins. The classification of protein patterns into families depends mainly on the regions thought to be important to protein function (motifs) in addition to how often the amino acid is substituted within the block of human related proteins. The "star-tree" score model ranges from -4 to +3 for non-synonymous amino acid substitutions. A score of -4 means a big change in property when switching from one of the two amino acids in question to the other, which would be likely to alter protein function, so the amino acid substitution is highly unlikely to be benign. Conversely, a score of +3 means the substitution is between two amino acids with very similar properties, and is therefore likely to be benign. The Blosum62 substitution matrix should be used alongside other pathogenicity prediction tools because the data upon which it is based is restricted to a subset of conserved domains (Henikoff and Henikoff, 1992).

2.14.2.4 Align-GVGD program

The Align-GVGD program (Align-Grantham Variation and Grantham Deviation) is a web server that can localize the missense substitutions in genes of interest into a spectrum ranging from enriched neutral to enriched deleterious (http://agvgd.iarc.fr/ index.php). The program works on the combination of protein multiple sequence alignments (in FASTA format) and the biophysical characteristics of amino acids. The biophysical variation at each alignment position is converted to a Grantham Variation score. The prediction classes form a spectrum (C0, C15, C25, C35, C45, C55 and C65) with C65 most likely to affect the protein function and C0 least likely (Tavtigian et al., 2006).

2.14.2.5 MAPP program

Multivariate Analysis of Protein Polymorphism (MAPP) is one of the missense prediction tools that can be downloaded and run locally (http://mendel. stanford.edu/SidowLab/downloads/MAPP/index.html). This application can be used to predict if the effect of the mutation will have a good or bad effect on the physicochemical properties of the protein including polarity, volume and hydropathy (Stone and Sidow, 2005).

2.14.2.6 Mutation taster

Mutation taster is a fast web-based program (http://www.mutationtaster.org) used to evaluate different types of DNA mutations: synonymous, non-synonymous, nonsense and frameshift. The software integrates various data sources such as HapMap, Ensembl, dbSNP and SwissProt/UniProt. For this study, the scripts were downloaded and integrated into ANNOVAR software to run locally on a Unix-based system. A prediction is given as either 'disease-causing' or 'polymorphism' along with a P value indicating the security of the prediction (with 1 being most secure) (Schwarz et al., 2014).

2.14.2.7 CADD score

Combined Annotation-Dependent Depletion (CADD) is a novel functional meta-annotation tool (http://cadd.gs.washington.edu/) that can evaluate and score the deleteriousness of a large number of single nucleotide substitutions and indel variants (Kircher et al., 2014). CADD works as a framework that integrates data from 63 existing tools into one calculated metric score called the C-score of the variant. Unlike other annotation tools, CADD does not rely solely on the conservation information of the amino acid residues but also on the functional genomic data such as *DNase I* hypersensitivity and transcription factor binding; protein-level scores such as PolyPhen, SIFT and Align-GVGD; expression levels in commonly studied cell lines and exon-intron boundaries determined by transcript data. The C-score is calculated according to a combination of all of these data. A scaled CADD score of 10 means that a variant is amongst the top 10% of deleterious variants in the human genome. A scaled CADD score of 20 means that the variant is in the top 1%. A scaled CADD score of 30 means that the variant is in the top 0.1%.

2.14.3 Splice site prediction tools

In-silico splice prediction tools were used for the interpretation of intronic and exonic mutations that can lead to splicing defects. Two web based programs were used, Berkeley Drosophila Genome Project (http://www.fruitfly.org/seq_tools /splice.html) and NetGene2 (http://www.cbs.dtu.dk/services/NetGene2/) (Hebsgaard et al., 1996; Reese et al., 1997). These tools work as neural network based programs to find possible 5' and 3' splice sites. For each variant, two data sheets of reference and variant sequences including the surrounding genomic sequence of two or more exons were uploaded separately to the program. The output data of the possible splice acceptor and splice donor sites with the confidence scores were compared between the reference and variant sequences.

2.14.4 db SNP, 1000 Genomes, the EVS Server and ExAC database

The single nucleotide polymorphism database (dbSNP) is a public-domain archive for a broad collection of simple genetic polymorphisms for a variety of organisms, maintained at the National Center for Biotechnology Information (NCBI) (http://www. ncbi.nlm.nih.gov/ SNP/). The 1000 genomes project is a public catalogue of human variation and genotype data of over 1,000 unidentified individuals from around the world (US, UK, China and Germany) (http://www.1000genomes.org/). The Exome Variant Server (EVS) (http://evs.gs.washington.edu/EVS/) and Exome Aggregation Consortium (ExAC) (http://exac.broadinstitute.org/) are two different databases that collect frequencies of variants in populations from multiple studies. EVS based on WES data of 6503 well-phenotyped individuals from various ethnicities, while ExAC includes a larger cohort of 60,706 unrelated individuals sequenced as part of various disease-specific and population genetic studies. The data of individuals affected by severe paediatric disease has been removed from ExAC shared datasets, so these have been frequently used as a control population for calculating allele frequencies and filtering out potential benign variants observed at a relatively common frequency in the databases (Song et al., 2016).

2.14.5 Protein bioinformatics tools

Interactive protein analysis servers were used to perform basic bioinformatics analysis on any candidate protein. ExPASy translate tool is an online tool (http://web.expasy.org/translate/) that was used for translating a nucleotide sequence (DNA/RNA) to a protein sequence. ClustalW (http://www.ebi.ac.uk/Tools/msa /clustalw2/) and Clustal Omega (http://www.ebi.ac.uk/Tools/msa/clustalo/) are fast web-based programs that were used for multiple sequence alignments of amino acids in a protein. NCBI reference sequences of interest and orthologous protein sequences in FASTA format were pasted into this software. The output of multiple sequence alignment was arranged from top to bottom according to the degree of similarity indicating the conservation of an amino acid of interest and of the surrounding amino acid residues. Finally, the Protter tool was used for visualization of proteoforms (http://wlab.ethz.ch/protter/start/) and predicting protein sequence features (Omasits et al., 2014).

2.14.6 Linkage analysis

Two-point linkage analysis was carried out using Superlink (http://bioinfo.cs. technion.ac.il/superlink-online/) (Silberstein et al., 2006). This method uses a Bayesian network model to compute the likelihood scores for complex pedigrees, such as consanguineous pedigrees with multiple inbreeding loops. The software requires a pedigree (ped) file, describing the details and genotyping results of the individuals to be analysed in each pedigree, and a data (dat) file, describing the type of analysis required and allele frequencies. The resulting data is given as the logarithm of the odds (LOD) score.

2.15 RNA extraction

Total RNA was extracted using the TRIzol RNA extraction kit (Invitrogen) according to the manufacturers' instructions. Before starting, the equipment was sterilized by treatment with 3% hydrogen peroxide solution (H_2O_2) for 30 minutes prior to use. The deionized water was treated with 0.1% [v/v] diethyl pyrocarbonate (DEPC) (Sigma) for at least 16 hours and then autoclaved. For tissues, the sample was homogenized with a pellet pestle motor in the presence of the 1ml TRIzol/100mg tissue until the tissue was

completely dissolved in solution. For cells, 1ml TRIzol per 10cm^2 of the culture dish was used to lyse the cells, followed by incubation at RT for 5 minutes. Homogenised tissue or lysed cells were then transferred to a microfuge tube and 200µl chloroform was added per 1ml of TRIzol reagent. Samples were then vortexed for 5 seconds followed by incubation for 3 minutes at RT, and then spun at 12,000 x g for 15 minutes at 4°C. The aqueous phase was then transferred to a fresh tube and the RNA was precipitated by adding 500µl isopropanol per 1ml of TRIzol. Samples were incubated at RT for 10 minutes, then centrifuged at 12,000 x g for 10 minutes at 4°C. The RNA pellet was then washed with 1ml 75% ethanol per 1ml TRIzol used, and centrifuged at 7500 x g for 5 minutes at 4°C. The air-dried RNA pellet was re-dissolved in DEPC-treated water. Total human RNA from adult and fetal tissues was purchased from ClonTech (Catalog No. 636643, Mountain View, USA).

2.16 Reverse transcriptase PCR (RT-PCR) for first strand cDNA synthesis

Complementary DNA (cDNA) was synthesised from total RNA using Moloney Murine Leukemia Virus reverse transcriptase (MMLV RT) (Invitrogen). 1µl (100ng) of random primers (Invitrogen) was incubated with 0.5µg of total RNA and 10µl of DEPC-treated water at 70°C for 10 minutes, followed by chilling on ice. 4µl 5 x MMLV RT buffer (Invitrogen), 2µl 10mM dNTPs (Invitrogen), 2µl 0.1M DTT (dithiothreitol) (Invitrogen) and 10U (0.25µl) of RNAsin (Promega, USA) were then added to each reaction which was incubated at 37°C for a further 2 minutes. 0.5µl (100U) MMLV RT was added to each sample followed by incubation at 37°C for 1 hour then denaturation of the enzyme at 95°C for 5 minutes. Finally, samples were stored in the freezer at -20°C until required for PCR amplification with specific primers.

2.17 Histology and immuno-staining

2.17.1 Harvesting mouse eyes and embryos

The most humane way to euthanize male and pregnant female mice, as defined in schedule 1 of the Animal Scientific Procedures Act, 1986, was used to obtain mouse embryos and adults for histology and immune-staining. Embryos at E11.5 or later embryonic stages were dissected out from the uterus and yolk sac in cold 1 x phosphate-

buffered saline (PBS) [one PBS tablet (Sigma-Aldrich)/200ml ddH_2O]. Adult mouse eyes were carefully dissected using micro-scissors and 45 degree forceps under a dissecting microscope (Section 2.18).

2.17.2 Preparation of frozen sections

Whole embryos and eyes were transferred to fixative solution 0.4% [w/v] paraformaldehyde (PFA) in 1 x PBS for 4-24 hours, followed by cryoprotection incubation in 30% [w/v] sucrose in 1 x PBS for two hours. Using round cork discs, embryos and eyes were embedded in "Optimum Cutting Temperature (OCT)" (Raymond A Lamb Limited, UK) solution followed by snap freezing in isopentane supercooled over liquid nitrogen. The tissues were sectioned at 5µm thickness using a CM30505 cryostat (Leica). The specimen temperature of the cryostat was set to -21±3°C. Thin sections were placed onto SuperFrost plus slides (Menzel Glaser, Germany) and stored at -80°C until required.

2.17.3 Preparation of paraffin sections

Dissected embryos and mouse eyes were fixed by overnight immersion in 4% [w/v] PFA in 1 x PBS at 4°C. Following three washes in 1 x PBS solution, the tissues were processed using an automated system. The tissues were initially dehydrated by immersion in 70%, 90% and 100% ethanol; each three times for 30 minutes at RT followed by three immersions in xylene for 20 minutes each at RT. The tissues were then embedded in paraffin wax (58-60 ºC), two changes, 1.5 hour each. The blocks of paraffin embedded tissues were sliced at 4µm thickness using an RM2255 microtome (Leica). These tissue sections were placed onto SuperFrost plus slides (Menzel Glaser, Germany) and allowed to dry overnight at RT. The sections were later stored either at RT or for long-term storage at 2-8°C.

2.17.4 Haematoxylin and eosin (H&E) staining

Hematoxylin-eosin (H&E) staining was used for a proper evaluation of paraffin-embedded or frozen tissue sections. For paraffin sections, air-dried slides were initially placed directly on a hot plate at 60°C for 15 minutes, followed by de-paraffinization 4 times in fresh xylene for 3 minutes each. The slides were rehydrated by immersion in a

series of descending dilutions of ethanol (100%, 75% [v/v], 50% [v/v] and 25% [v/v]). Each was immersed twice for 3 minutes per immersion and then finally washed under running tap water for 2 minutes. The slides were stained with Mayer's haematoxylin stain [0.05g/ml Aluminum potassium sulphate, 0.001g/ml Hematoxylin, 0.0002g/ml Sodium iodate and 2%[v/v] Glacial acetic acid] for 2 minutes and washed under running tap water for 2 minutes. They were then immersed in Scott's tap water (pH = 8) containing 0.2% [v/v] sodium bicarbonate ($NaHCO_3$) and 1% [v/v] $MgSO_4$ for a few seconds, followed by immersion in tap water for a further minute, then stained in eosin for 2 minutes and washed in tap water for 2 minutes. The tissue sections were dehydrated in ascending grades of ethanol, each twice for 3 minutes and finally immersed three times in xylene, 3 minutes per immersion. For frozen tissue sections, only steps from staining of Mayer's haematoxylin to the staining of eosin were performed. The slide containing the specimen was protected under a coverslip using DPX mounting media (Solmedia ltd, Shrewsbury, UK) which was allowed to dry at RT before examining under light microscope (Section 2.18).

2.17.5 lmmunohistochemistry (IHC)

Immunohistochemical staining on slides containing paraffin-embedded tissues was carried out using the Novolink TM Max Polymer Detection system (Leica) according to the manufacturer's guidelines. The specimens were initially de-waxed using xylene then rehydrated in decreasing concentrations of ethanol as described previously (section 2.17.4). Antigen retrieval pre-treatment was performed in a pressure cooker by boiling slides in a solution containing 1mM EDTA in distilled water for 2 minutes at 121°C and maximum pressure at 15psi (103.4kPa). The slides were then allowed to cool down for an additional 2 minutes in tap water prior to continuing the staining procedure. In a humidity chamber, the endogenous peroxidase activity was blocked by incubating each slide for 5 minutes with 100 µl (2 drops) of 3% hydrogen peroxide (H_2O_2) provided with the kit. This was followed by three washes in 1 x Tris buffered saline (TBS) (pH 7.5) [50mM Tris, 0.8% [w/v] Sodium chloride (NaCl), 0.02% [w/v] Potassium chloride (KCl) and 6.0M Hydrochloric acid (HCl)] for 3 minutes each. 100 µl (2 drops) of protein blocker [0.4% [w/v] Casein, 0.2% [w/v] Bronidox and 1x PBS] was added to each slide for 5 minutes to block the non-specific antigenic sites, followed by three washes in 1 x TBS for 3 minutes each. The slides were then incubated for 2 hours at 4°C in primary antibody

diluted to the recommended concentration in antibody diluent solution [250mg bovine serum albumin (BSA), 50 ml 1x TBS and 0.01% NaN_3]. The antibodies that were used in these experiments are listed in Table 2.1. Following incubation, three washes in 1 x TBS-Tween [1x TBS-T (pH 7.5) and 0.1% [v/v] of Tween20] were performed for 5 minutes each, before a 30 minute incubation was carried out with 100µl (2 drops) of "Post Primary Block" provided with the kit (10% [v/v] animal serum in TBS/0.9% ProClin^{TM} 950) to facilitate the penetration of the subsequent polymer reagent. A further three washes in 1 x TBS-Tween were performed for 5 minutes each.

Next, sections were incubated for 30 minutes with 100µl (2 drops) of NovoLink Polymer (Anti-goat/rabbit IgG-poly-HRP, 8.0µg/m1) provided with the kit and specific to the species of animal the primary antibody was raised in. This was followed by three washes in 1 x TBS-Tween, for 5 minutes each. A high-sensitivity diaminobenzidine (DAB) substrate-chromagen system (Nonvocastra DAB chromogen and NovoLink DAB substrate) was prepared according to the manufacturer's instructions for the brown end-product at the site of the targeted antigen. 100µl of prepared DAB was used per slide, followed by incubation for 5 minutes, then three washes in 1 x TBS each for 3 minutes. Counterstaining was performed in Mayer's haematoxylin for 2 minutes 30 seconds followed by dehydration in increasing concentrations of ethanol (25%, 50%, 75% and 100%) for 3 minutes each followed by three rounds of 3 minute washes in xylene. DAB stained sections were mounted by a coverslip using DPX mounting media (Sigma) and left to air dry overnight before examining under the light microscope (Section 2.18).

Antibody name	Raised in	Recommended for	Dilution used (1/x)			Incubation times	Source
			IF	WB	IHC		
DRAM2 (M-12)	Goat	Mouse and Rat	100	-	50	2 hours	Santa Cruz Biotechnology
DRAM2	Rabbit	Human	-	200	-	16 hours	Novus Biologicals
MFSD8 (S14)	Goat	Mouse, Rat and Human	100	-	-	16 hours	Santa Cruz Biotechnology
LARGE (Y-14)	Goat	Mouse, Rat, Human and Chicken	50	-	-	16 hours	Santa Cruz Biotechnology
Rhodopsin	Rabbit	Mouse, Rat and Human	300	500	-	2-16 hours	Sigma-Aldrich
Alexa Fluor 568-conjugated	Donkey	Goat immunoglobulins	500	-	-	1 hour	Molecular Probes Incorporation
Alexa Fluor 488-conjugated	Chicken	Rabbit immunoglobulins	500	-	-	1 hour	Sigma-Aldrich
Rabbit Immunoglobulins (HRP)	Rabbit	Goat immunoglobulins	-	2,000	-	1 hour	Dako Cytomation
Goat Immunoglobulins (HRP)	Goat	Rabbit immunoglobulins	-	-	2,000	1 hour	Dako Cytomation

Table 2.1. List of antibodies used in this study. Names of antibodies, species in which they were raised, species recommended for, used dilutions for immunofluorescence (IF), western blotting (WB) & immunohistochemistry (IHC), incubation times and the commercial source.

2.17.6 Immunofluorescent (IF) staining on frozen tissue sections

Before commencing the IF protocol, frozen tissue sections were thawed for 20 minutes at RT, then washed twice in PBS for 5 minutes each. Slides were fixed either in ice-cold methanol for 5 minutes or 2% paraformaldehyde (PFA) at RT for 20 minutes. They were then incubated in a humidity chamber with blocking solution (1% w/v Marvel (non-fat milk) powder in PBS-T) [1xPBS and 0.1% [v/v] of Tween20] for one hour at RT. At the same time, primary and secondary antibodies were prepared in the same blocking solution according to the recommended dilutions and centrifuged at 10,000 x g for 5 minutes. Following blocking, slides were incubated with the primary antibody (100µl per slide) for 2 hours at 4°C, then washed three times in PBS-T for 5 minutes each. A solution of fluorophore conjugated secondary antibody was used to detect the primary antibody, whilst 4',6-diamidino-2-phenylindole (DAPI) at a final concentration of 1µg/ml was added for nuclear staining. After one hour of incubation in a dark chamber, the slides were washed three times in 1 x PBS-T for 5 minutes each, followed by mounting the slide with a coverslip and Mowiol® 488 mounting medium (Calbiochem®, Hertfordshire, UK). Slides were left to dry in a dark chamber at RT for at least 18 hours before examination under the confocal microscope (Section 2.18).

2.17.7 Immunofluorescent (IF) staining on paraffin-embedded tissues

This method of immunofluorescence labelling was carried out using primary antibodies that were recommended for work with formalin-fixed paraffin-embedded (FFPE) tissues. Slides containing sections of the paraffin-embedded tissue were placed on a hot plate at 60°C for 15 minutes, deparaffinized in fresh xylene and rehydrated by immersion in a series of descending grades of ethanol as previously described (Section 2.17.4). Heat induced retrieval of antigen was performed as previously described (Section 2.17.5). Slides were then incubated in a humidity chamber with blocking solution (1% w/v Marvel (non-fat milk) powder in PBS-T) for 60 minutes at RT. The incubation steps for primary and secondary antibodies were performed as described above (Section 2.17.6), except that the incubation time for the primary antibodies was 16-18 hours. After mounting the coverslip as described above (Section 2.17.6) the slides were examined by confocal microscopy (Section 2.18).

2.17.8 The blocking peptide competition assay (BPCA)

The Blocking Peptide Competition Assay (BPCA) was used to show the specificity of the primary antibody binding to the antigen. Primary antibodies were diluted to the recommended working concentration in the blocking solution. A master mix solution of 1 to 20 molar ratio of antibody to peptide was incubated overnight on a rotator at 4°C. The prepared solutions were then used for staining as described previously.

2.18 Microscopy

2.18.1 Light microscopy

Investigation and imaging of stained sections by immunohistochemistry (IHC) and H&E eosin were performed using a Nikon Eclipse TE-2000-E light microscope.

2.18.2 Confocal microscopy

IF stained tissue sections were visualized using a Nikon Eclipse Ti-E inverted microscopes. Slides were first viewed using wide-field epifluorescence with the DAPI blue filter (340-380nm excitation, 400nm emission), FITC green filter (460-500nm excitation, 505nm emission) and TRITC red filter (528-553nm excitation, 565nm emission). Image capturing and z-stacks were done using scanning confocal microscopy with 408nm BD (brilliant™ blue dye), 488nm Ar (argon) and 543nm helium-neon (G-HeNe) lasers and 515/30 (blue), 540/50 (green) and 650LP (red) spectral detectors. Confocal images were processed using Nikon EZ-C1 3.50 software.

2.18.3 Dissecting microscopy

A Zeiss Stemi 2000-C stereo microscope supplied with a 10X/23 focusing eyepiece and auxiliary objectives was used for dissection of the mouse eye and isolation of the whole retina from the mouse eye (Section 2.19.1).

2.19 Isolation of mouse/cow retina and protein extraction

2.19.1 Isolation of the mouse/cow retina

Dissected adult mouse eyes were washed twice in PBS (Sigma-Aldrich) before proceeding to extract the retina. Under the dissecting microscope, a small hole in the posterior of the limbus was made by an 18 gauge needle. After puncturing the limbus, tissue at the circumference of the limbus was cut and the cornea, iris, lens and sclera were removed using autoclaved micro-scissors and forceps. Next, the vitreous humour was extracted and the retina was carefully separated from the eyecup using two autoclaved micro-forceps. Snap frozen cow eyes provided by Mr Mike Shires, University of Leeds. Eyes were left at RT to defrost, then washed twice in PBS. The cow retina was then extracted using a similar method to the one described above except that the dissecting microscope was not required.

2.19.2 Preparation of the protein extract from the mouse/cow retina

Total protein from either the mouse or the cow retina was prepared by adding 2 ml of protein lysis buffer [20mM HEPES, 150mM NaCl, 1mM EDTA, 1x Protease inhibitor cocktail and 10% [W/V] Dodecylmaltoside (DM)] to each extracted retina. The tissue solution was homogenised with a pellet pestle motor and then incubated on an overhead shaker for 30 minutes at 4°C. The solution was then centrifuged at 16,000 x g for 10 minutes at 4°C to pellet cell debris. The resulting supernatant was transferred to a new eppendorf tube. The protein concentration was determined using Bradford assay (Section 2.19.3) and samples were used for western blot analysis (Section 2.20) and pull-down assays (Sections 2.21).

2.19.3 Measuring protein concentration

The amount of extracted protein was quantified using the Bradford Assay (DC protein assay, Bio-rad). Before starting the assay, the following reagents were prepared using either the protein lysis buffer described before (Section 2.19.2) or radio immunoprecipitation assay (RIPA) buffer [50mM Tris-HCl pH 8, 150mM NaCl, 1% NP-40, 0.5% Sodium deoxycholate, 0.1% SDS, 5mM EDTA and 1x Protease inhibitor cocktail]. Reagents of 10% protein lysis/RIPA buffer in ddH_2O, 2µg/ml BSA solution in

10% protein lysis/RIPA buffer and seven different BSA standards as a dilution series ranging from 0.1 to 2µg/µl prepared in 10% protein lysis/RIPA buffer.

Using a flat bottomed 96-well plate, 5µl of 10% protein lysis/RIPA was added once as a blank to correct the background absorbance, 5µl of each BSA standard was added in triplicate to the plate and 5µl of protein extract was also added to the plate in triplicate. 20µl of Reagent S was added to 1ml of Reagent A, then 25µl of this Reagent, SA, was added to each well. Then 200µl of Reagent B was added to each well. The plate was incubated for 15 minutes on a shaker at RT, and then the absorbance at 690nm was read using a multiscan microplate reader (Titertek-Berthold®, Germany). Absorbance readings were analysed in Microsoft Excel by interpolation on a complete standard curve and consideration of the dilution factor to calculate volumes required for western blotting and pull-down assays.

2.20 Western blotting

Approximately 20µg of total protein was denatured by incubating at 95°C for 5 minutes with 2 x Sodium Dodecyl Sulphate (SDS) western loading buffer [100mM Tris-HCL (pH 6.8), 200mM β-mercaptoethanol, 20% [v/v] glycerol and 4% [w/v] SDS]. After denaturating, the samples were loaded onto a NuPAGE® gradient (4-12%) Bis-Tris PAGE gel (Invitrogen) alongside a SeeBlue Plus2 pre-stained protein marker (Invitrogen). The gel was run in an X-Cell SureLock electrophoresis tank filled with a 1 x NuPAGE® MES-SDS running buffer (Invitrogen) at 120V for 90 minutes. An Invitrolon polyvinylidene difluoride (PVDF) membrane (Invitrogen) was activated by soaking in 100% methanol for 30 seconds followed by submerging in 1 x NuPAGE® transfer buffer (Invitrogen) containing 10% methanol for 5 minutes. In the X-Cell SureLock Blot module (Invitrogen), the SDS-PAGE gel and the activated PVDF membrane were sandwiched between blotting paper and a number of sponges soaked in 1 x NuPAGE® transfer buffer (Invitrogen) containing 10% [v/v] methanol. The module was filled with l x transferring buffer whilst the surrounding tank was filled with cold distilled water, and the transfer was run at 30V for 60-90 minutes. Following transfer, the membrane was rinsed with PBS-T, then the membrane was incubated with western blocking solution (5% [w/v] Marvel dried non-fat milk powder in PBS-T) for between 1 and 18 hours at 4°C with gentle agitation. The membrane was then incubated on a tube

roller with the primary antibody (diluted in blocking solution) for 2-18 hours at 4°C depending on the antibody used (Table 2.1). This was followed by three washes of PBS-T of 5 minutes each. Next the membrane was incubated with the HRP conjugated-secondary antibody (diluted in blocking solution) for 1 hour at RT with agitation. After three washes of 5 minutes each in PBS-T, the membrane was then placed on an acetate sheet and incubated with Femto Super Signal West reagent® (Thermo Scientific) according to the manufacturer's guidelines to develop the immune-positive bands. Membranes were visualised on the ChemiDoc™ MP System with Image Lab™ software (Bio-Rad Life Science). If the membrane was to be re-used, it was first stripped in 0.2M sodium hydroxide prepared in distilled water for 5 minutes then the protocol was started again from the blocking step.

2.21 Pull down assay

The pulling down of protein complexes out of solution was attempted using Protein A plus agarose beads (Thermo Fisher Scientific). Approximately 1 mg of the protein was incubated on a rotating mixer with 2.5µg of the antibody and 600µl of immunoprecipitation (IP) washing buffer [150mM NaCl, 1% [v/v] NP40, 50 mM Tris-HCl pH8.0, 10% [v/v] glycerol and 2mM EDTA] for 2 hours at 4°C. Meanwhile, 50µl of the beads were washed three times, with the first wash in 1 x TBS followed by centrifugation at 1,000 x g for 1 minute at 4°C, and the second and third washes were performed by adding 500µl of IP washing buffer followed by centrifugation at 1,000 x g for 1 minute each at 4°C. 25µl of the washed beads were added to the antibody-protein solution and then incubated overnight on the rotating mixer at 4°C. 60µl Neutralisation buffer (1M Tris, pH8) was added to the mixture before eluting three times in MicroSpin G-25 columns (GE Healthcare Life Sciences) using 200µl Elution buffer (200mM glycine, pH 2.5) for 20 minutes each at 4°C. The solution was then neutralized using the Neutralization buffer. Before the protein precipitation step, the sample was checked by silver staining (Section 2.22). Protein precipitation was achieved using a methanol (MeOH)/chloroform ($CHCl_3$) mixture. 800µl MeOH was added to the sample which was then vortexed, followed by centrifugation at 9,000x g for 30 seconds, then 200µl $CHCl_3$ was added to the pellet and it was vortexed again, followed by centrifugation at 9,000x g for 30 second. The supernatant was carefully discarded, then 600µl of MeOH was added to the pellet, followed by vortexing and centrifugation at 16,000 x g for 2 minutes. Finally

the pellet was dried at RT for 5 minutes. The sample was then ready for analysis by mass spectrometry.

2.22 Silver staining

Prior to silver staining of proteins in polyacrylamide gels, the protein was denatured, loaded onto a NuPAGE® gel and run at 120V for 1.5 hours as described previously (Section 2.20). The gel was then fixed in a solution containing 50% [v/v] methanol and 5% [v/v] acetic acid for 20 minutes, washed in 50% methanol for 10 minutes then washed in double-distilled water (ddH_2O) for 10 minutes. For sensitizing, the gel was incubated with 0.02% [v/v] sodium thiosulphate for 1 minute, followed by rinsing twice in ddH_2O for 1 minute per rinse. For the silver reaction, the gel was submerged in 0.1% [v/v] silver nitrate for 20 minutes, followed by two rinses in ddH_2O for 1 minute each. For developing, the gel was incubated with 2% [v/v] sodium carbonate with 0.04% [v/v] formalin until the desired intensity of staining was produced. The developer solution was replaced with fresh solution when it turned yellow. The staining was terminated in 5% [v/v] acetic acid for 10 minutes. The gel was then washed twice in ddH_2O, 5 minutes per wash, and imaged using an Olympus C-7070 digital camera which reflected light from a cold light source.

2.23 Gateway® cloning technology

The DNA fragment of interest was cloned into the plasmid vector pC-TAP GW332 (Figure 2.1) provided by Prof. Colin Johnson, using the Gateway® cloning system (Invitrogen). Briefly, cloning PCR primers were designed to add gateway attB restriction enzyme sequences to the 5' and 3' ends of a gene fragment (Section 2.4.2). The PCR was carried out to amplify the full coding sequence of the gene of interest using Platinum *Pfx* DNA polymerase (Section 2.4.5). The PCR product was run on a 1.5% agarose gel and the DNA bands were excised from the agarose gel and purified using the Qiagen's QIAquick Gel Extraction kit protocol (Section 2.6) according to the manufacturer's recommendations. The entry clone was created by *in-vitro* recombination reaction using the enzyme BP Clonase® (Invitrogen). This entry clone was then used in an LR Clonase® reaction (Invitrogen) with the destination vector (pC-TAP GW332) to create the desired expression clone (Eg. pDRAM2-C-TAP).

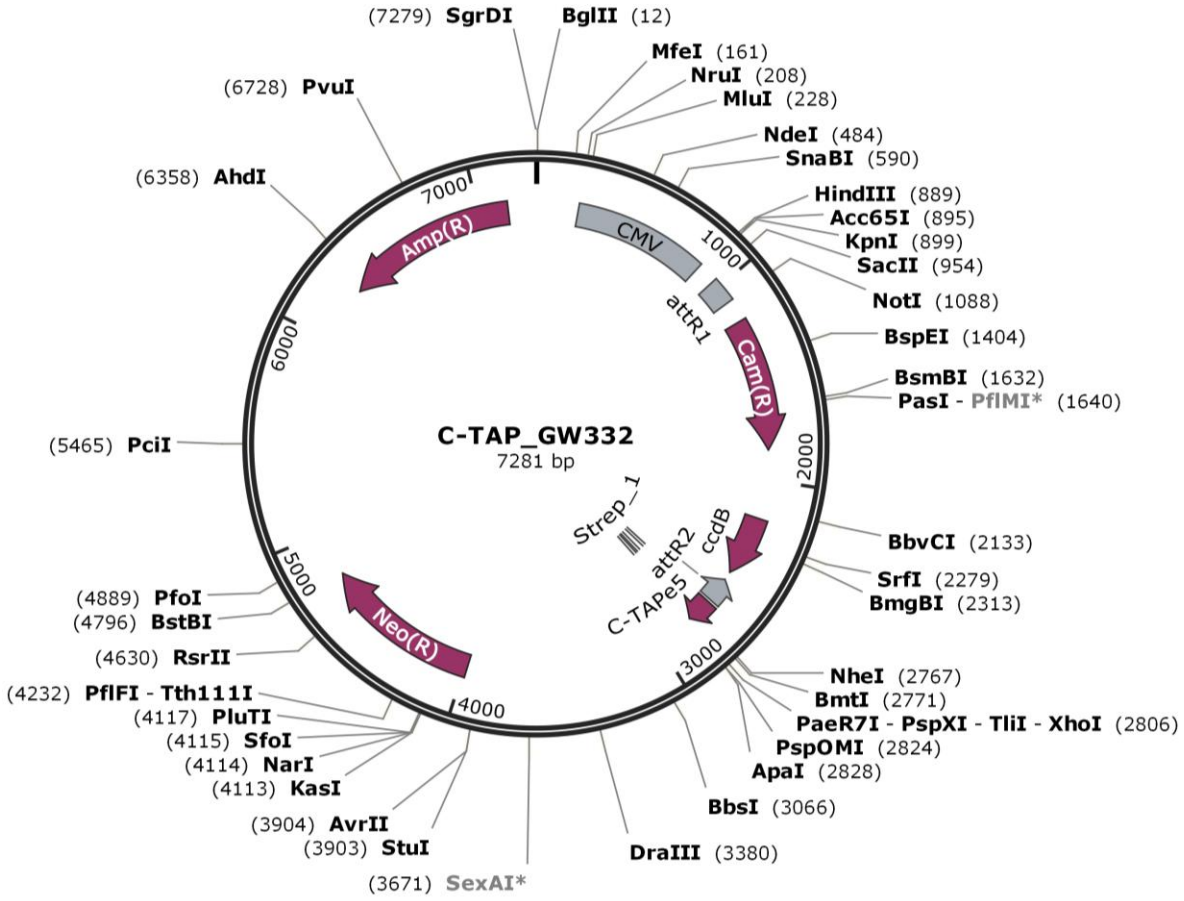

Figure 2.1. Map of the C-TAP GW332 plasmid.

2.24 Bacterial transformation and cell culture

10-40ng of plasmid DNA was transfected into One Shot® *ccd*B Survival™ 2T1^{R} Chemically Competent Cells (Invitrogen) using heat shock. The DNA was added into a vial of defrosted One Shot® cells and mixed gently, followed by incubation on ice for 30 minutes. The cells were heat-shocked for 30 seconds at 42°C without shaking, then placed on ice for 2 minutes. 250µl of pre-warmed Super Optimal Broth with Catabolite repression (SOC) medium (Invitrogen) was added to each vial followed by horizontal shaking at 37°C for 1 hour at 225 rpm. After incubation, 25µl from each transformation was then spread onto LB agar plates containing the appropriate antibiotic and incubated overnight at 37ºC. A single colony was picked from the agar plate using a sterile 1µl loop and inoculated with 5ml of Luria-Bertani (LB) broth [Tryptone Yeast Extract Sodium Chloride (NaCl), 1.5% [w/v] agar and 50mg/ml Ampicillin] containing the appropriate

amount of desired antibiotic. The bacterial culture was then allowed to grow for 16 hours at 37^{o}C with 225 rpm shaking. Only 1.5 ml of the culture was used for Miniprep plasmid DNA isolation, whilst the remaining culture was stored at 4^{o}C for any further use.

2.25 Plasmid DNA isolation and purification

The Qiagen QIAprep® miniprep kit was used for small-scale plasmid DNA isolation and purification according to the manufacturer's protocol. Cells from 1.5ml of bacterial culture were pelleted by centrifugation at 3220 x g then resuspended in neutral buffer containing RNAse A, followed by mixing with equal volume of alkaline lysis buffer. The lysis was then neutralized by addition of high salt neutralization buffer. Lysates containing DNA in a high salt solution were applied to a spin column and centrifuged at 3220 x g. The DNA was then washed by an ethanol buffer and eluted in 50µl by buffer ddH_2O.

Chapter 3. Screening for variants causing inherited retinal dystrophy using customized targeted capture and next-generation sequencing

3.1 Introduction

According to current knowledge, hereditary retinal dystrophies (RDs) are the most genetically heterogeneous group of diseases in humans. The genetic screening of patients with inherited retinal dystrophies is particularly challenging since all modes of inheritance are possible and conditions such as LCA, COD/CRD, RP and MD can be caused by mutations in any one of more than 250 genes (see RetNet, https://sph.uth.tmc.edu/retnet/). The genetic causes of many hereditary cases remain unknown (Wang et al., 2005; Daiger et al., 2010; Perez-Carro et al., 2016; Weisschuh et al., 2016). The large number of genes implicated in RD means that mutation detection by Sanger sequencing of individual genes is highly labour intensive and inefficient.

In the last six years, the introduction of next-generation sequencing (NGS) technologies has made it possible to simultaneously sequence multiple genes in one experiment. The work described in this chapter was initiated in the early days of applying NGS to find the pathogenic mutations in inherited eye diseases. A customised SureSelect solution-based targeted capture reagent was designed by a colleague, Dr David Parry (Section of Genetics, University of Leeds), which is hereafter referred to as the "Retinome" reagent. This reagent simultaneously captures all the exons and flanking splice site junctions of the 162 genes that had been shown to harbour mutations causing RD at the time of design, based on the RetNet database in July 2010. The full list of genes that were selected is shown in Appendix 3. Patient genomic DNA was sheared, tagged and pooled before hybridisation to the targeted reagent (Section 2.11). Probes could not be designed against 9 exons (Appendix 4) that have highly repetitive and purine rich sequences. The captured DNA from the pull-down experiment was analysed by next-generation sequencing.

This customised targeted reagent was first tested by Dr Parry on a cohort of four RD patients with known causative mutations in order to validate the capture reagent and

establish the pipeline for variant detection. The results confirmed that the pipeline used to identify pathogenic mutations was robust (Appendix 5). After validation of the capture reagent, libraries were prepared from genomic DNA of 20 patients selected from 20 unrelated families diagnosed with various retinal degenerations for which no mutation had yet been identified. The families were recruited by Dr Martin McKibbin (Eye Department, St. James's University Hospital), the library preparation was done by Dr Christopher Watson (Yorkshire Regional Genetics, St. James's University Hospital) while the families analysed were chosen by Prof Chris Inglehearn, Dr Carmel Toomes and Dr Manir Ali (Section of Ophthalmology & Neuroscience, University of Leeds). These libraries were then pooled in pools of four samples, each with its own unique tag for later deconvolution, then this mix was hybridized to the Retinome capture reagent. The DNA captured was then subjected to NGS (Section 2.11.1). The 20 families included in this study, the diagnoses of the affected cases, possible inheritance patterns, ethnicity and summary information regarding numbers of affected cases and members available for sampling are recorded in Table 3.1.

The output data from this experiment was analysed by the author as described in Section 2.11.2 and the list of candidate gene variants from each family was filtered on the basis of variant type (deletion, insertion, nonsense, missense, non-synonymous/ synonymous), population frequency, conservation, pathogenicity prediction and phenotype match. The major steps in the pipeline and the data filtration criteria used in the Retinome project are illustrated in Figure 3.1. Primers were designed against plausible candidate variants (Section 2.4.1), and these were PCR amplified (Sections 2.4.3 and 2.4.4) and Sanger sequenced (Section 2.8) to confirm presence of the variants in the original samples and assess segregation in additional family members. The primer pairs used in this study are listed in Appendix 6. The results of these findings are presented in this chapter and contributed to publications Watson et al., 2014 and Shevach et al., 2015.

ID	Ethnicity	Diagnosis	Inheritance pattern	Number of affected cases	Number of affected cases sampled	Number of unaffected cases Sampled
MA1[a]	Asian	LCA	Recessive	4	2	0
MA2[a]	Asian	CRD	Recessive /Dominant	5	3	0
MA3[a]	Asian	RP	Recessive	3	2	0
MA4[a]	Asian	RP	Recessive	2	2	0
MA5	European	CRD/MD	Dominant	2	2	0
MA6[a]	Asian	RP	Recessive	2	1	0
MA7	European	CRD	Dominant	12	8	4
MA8	European	RP with Maculopathy	Dominant /X-linked	10	9	5
MA9	European	CRD/MD	Dominant	18	12	2
MA10[a]	Asian	CRD	Recessive	6	6	1
MA11[a]	European	RP	Recessive	2	2	0
MA12[a]	Asian	CRD	Recessive	9	6	9
MA13[a]	Asian	RP	Recessive	2	2	4
MA14[a]	Asian	RP	Recessive	2	2	0
MA15[a]	Asian	CRD	Recessive	4	4	7
MA16[a]	Asian	LCA	Recessive	2	2	0
MA17[a]	Asian	RCD	Recessive	2	2	0
MA18	Asian	CRD	Recessive	3	3	4
MA19[a]	Asian	RCD	Recessive	8	3	3
MA20[a]	Asian	RP	Recessive	2	2	5

Table 3.1. Summary of specific details of families that were studied in the Retinome project. The family ID, diagnosis, ethnicity, inheritance pattern, number of cases and numbers sampled are shown. [a] = consanguineous family, LCA = Leber congenital amaurosis, CRD = cone-rod dystrophy, RP = retinitis pigmentosa, MD = macular dystrophy and RCD = rod-cone dystrophy. (Adapted from Watson et al., 2014).

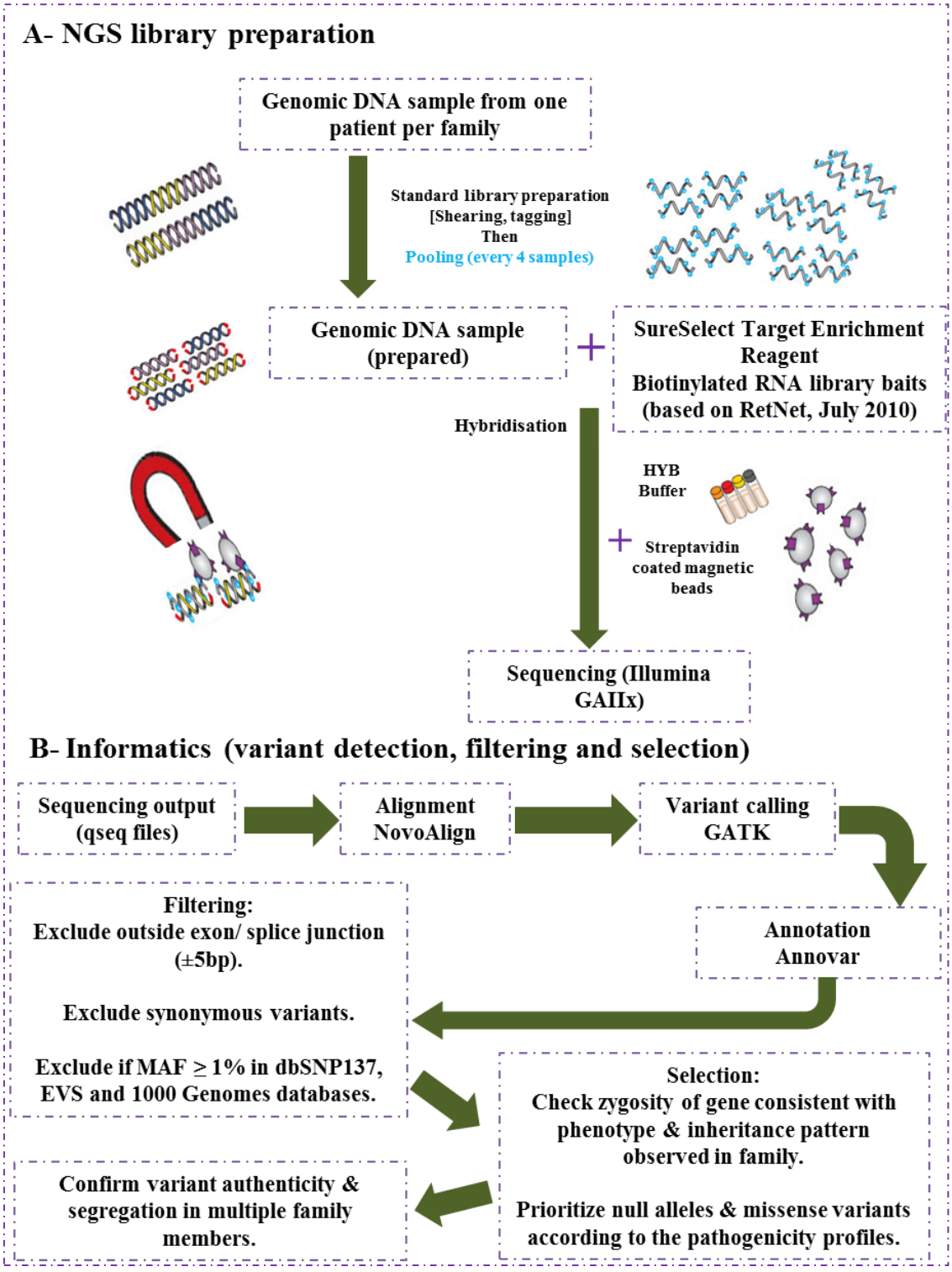

Figure 3.1. Schematic representation of the targeted NGS and variant detection data pipeline used in the Retinome project described in chapter 3. The flowchart illustrates the major steps of the pipeline, beginning with NGS library preparation (A) (Modified from http://www.genomics.agilent.com/article.jsp?pageId=3083) and ending with informatics for variant detection, filtering and selection (B).

3.2 Results

3.2.1 Inherited retinal dystrophy families in whom the pathogenic mutation was found using the retinome reagent.

3.2.1.1 Genetic analysis of family MA1

For family MA1, the affected cases were diagnosed with LCA, while the family structure suggested recessive inheritance caused by an autozygous mutation (Figure 3.2A). Based on the zygosity, the filtered variant list generated from the analysis of patient 2906 (Table 3.2) highlighted three homozygous variants in *HMCN1*, *CRB1* and *TRPM1* and three compound heterozygous mutations in *USH2A*, *GPR98* and *TOPORS*. A novel homozygous deletion of 23 base pairs including part of exon 8 of *CRB1* (NM_201253.2:c.2832_2842+ 23del) (Figure 3.2B) was the only candidate variant that was consistent with the diagnosis (LCA) in the family. Sanger sequencing of this truncating *CRB1* mutation in the other affected case from whom DNA was available (2907) provided further confirmation that the mutation is the pathogenic cause of disease.

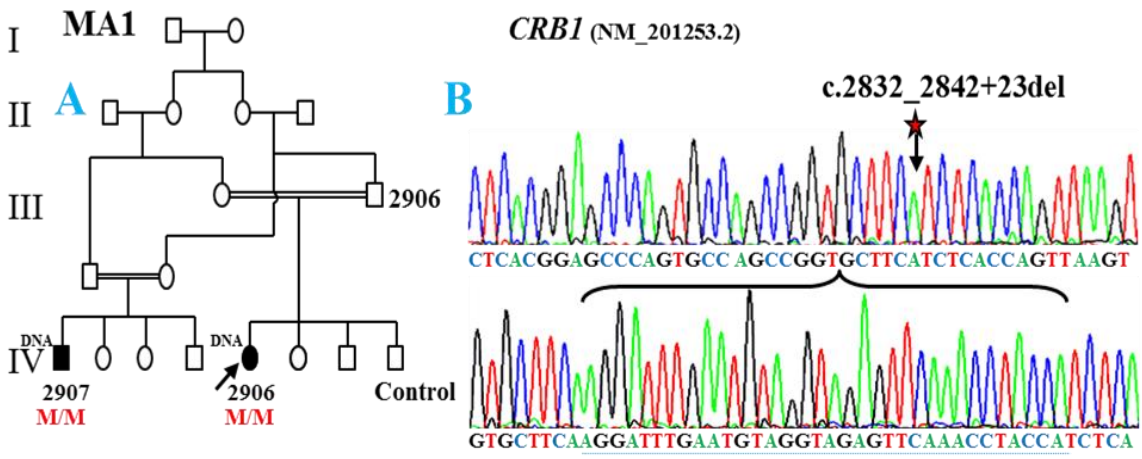

Figure 3.2. Molecular analysis of family MA1. (A) The pedigree of family MA1. Individuals from whom DNA was available are numbered and the proband is indicated by an arrow. (B) Sanger DNA sequencing chromatograms of a control subject and an affected family member (2906) with the *CRB1* mutation. (Adapted from Watson et al., 2014)

Chr	Position	Gene	Coding Effect	cDNA change	Protein change	BLOSUM 62	AGVGD class	SIFT prediction	MAPP prediction	Zygosity	Protein Domain	Segregates
1	186010250	*HMCN1*	missense	NM_031935.2:c.6286A>G	p.Ile2096Val	3	C0	Tolerated	good	Homo	Immunoglobulin I-set	
1	**197398744**	***CRB1***	**frameshift**	**NM_201253.2:c.2832_2842+23del**	**p.?**	**NA**	**NA**	**NA**	**NA**	**Homo**		**YES**
1	215820993	*USH2A*	missense	NM_206933.2:c.14662A>T	p.Thr4888Ser	1	C0	Tolerated	good	Het	Fibronectin, type III	
1	216405368	*USH2A*	missense	NM_206933.2:c.2920G>A	p.Asp974Asn	1	C15	Deleterious	bad	Het	EGF-like, laminin	
1	216496929	*USH2A*	missense	NM_206933.2:c.1437C>A	p.Phe479Leu	0	C15	Deleterious	bad	Het	Laminin, N-terminal	
3	63981343	*ATXN7*	missense	NM_001177387.1:c.1845C>G	p.Ser615Arg	-1	C0	Tolerated	good	Het		
4	122766846	*BBS7*	missense	NM_176824.2:c.1043A>G	p.Glu348Gly	-2	C65	Deleterious	bad	Het	BBS7 protein	
5	89925326	*GPR98*	missense	NM_032119.3:c.1809C>A	p.Phe603Leu	0	C15	Deleterious	bad	Het		
5	90149261	*GPR98*	missense	NM_032119.3:c.17365A>G	p.Lys5789Glu	1	C0	Tolerated	good	Het		
7	33545217	*BBS9*	missense	NM_198428.2:c.2258A>T	p.Glu753Val	-2	C0	Deleterious	bad	Het		
7	92140266	*PEX1*	missense	NM_000466.2:c.1579A>G	p.Thr527Ala	0	C0	Tolerated	good	Het		
8	38869207	*ADAM9*	missense	NM_003816.2:c.226G>A	p.Glu76Lys	1	C0	Tolerated	good	Het	Peptidase M12B, propeptide	
9	32542056	*TOPORS*	missense	NM_005802.4:c.2467A>G	p.Ser823Gly	0	C0	Tolerated	good	Het		
9	32542166	*TOPORS*	missense	NM_005802.4:c.2357G>A	p.Arg786Gln	1	C0	Tolerated	good	Het		
10	50669416	*ERCC6*	missense	NM_000124.2:c.3965G>T	p.Gly1322Val	-3	C65	Deleterious	bad	Het		
10	73573082	*CDH23*	missense	NM_022124.5:c.9715T>C	p.Ser3239Pro	-1	C0	Deleterious	bad	Het		
15	31342673	*TRPM1*	missense	NM_002420.4:c.1310G>T	p.Gly437Val	-3	C0	Deleterious	bad	Homo		
X	49076224	*CACNA1F*	In-frame	NM_005183.2:c.2439_2444dupTCCTCC	p.Glu824_Glu825dup	NA	NA	NA	NA	Het		

Table 3.2. List of candidate variants after alignment, variant calling and filtering for patient 2906 (female) for family MA1. The likely causative variant is orange shaded. Chr = chromosome, NA = not annotated, Homo = homozygous and Het = heterozygous. (Adapted from Watson et al., 2014).

The identification of this mutation was also consistent with linkage analysis data previously generated by Dr Ali for this family through Affymetrix 6.0 SNP homozygosity mapping on patients (2906 and 2907). This genotyping showed that there were four regions of homozygosity greater than 5 Mb shared between the two affected individuals; chr1:174,370,600-203,208,400 (28.8Mb), chr12:15,094,230-24,477,660 (9.4Mb, hg19), chr12:57,021,120-92,472,930 (35.5Mb, hg19) and chr15:69,828,190-89,825,460 (20.0Mb, hg19). *CRB1* (chr1:197,237,334-197,447,585; hg 19) is located in the second largest region.

3.2.1.2 Genetic analysis of family MA2

For family MA2, the pedigree structure, with both parents unaffected and in a consanguineous marriage, suggested a recessive mode of inheritance (Figure 3.3A). The clinical history and examination of the affected cases indicated CRD. Based on the zygosity, the variant list after next-generation sequencing analysis (Table 3.3) and Sanger sequencing of patient 2844 highlighted only one homozygous mutation in *ABCA4* (NM_000350.2:c.6088C>T, p.R2030*) (Figure 3.3B). Segregation analysis revealed this nonsense mutation in a heterozygous form in the affected offspring 2843 and 2845, suggesting that they both had another unidentified *ABCA4* mutation on the other allele, which they had inherited from their mother. The c.6088C>T, p.R2030* mutation was previously reported in a family with affected cases that had early-onset non-syndromic RD (Singh et al., 2006).

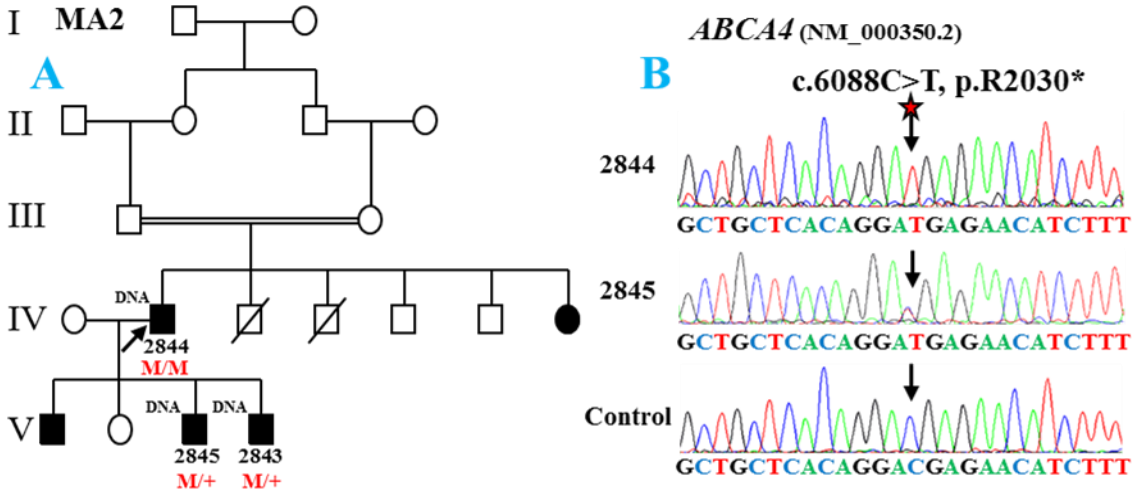

Figure 3.3. Molecular analysis of family MA2. (A) The pedigree of family MA2. Individuals from whom DNA was available are numbered and the proband is indicated by an arrow. (B) Sanger DNA sequencing chromatograms of a control subject and affected family members (2844 and 2845) with the *ABCA4* mutation. (Adapted from Watson et al., 2014).

3.2.1.3 Genetic analysis of family MA3

For family MA3, the family history suggested RP in the affected cases with a recessive mode of inheritance (Figure 3.4A). Targeted capture and next-generation sequence analysis on the index case 2908 identified only one homozygous variant (Table 3.4). This variant was a novel homozygous missense mutation in *USH2A* (NM_206933.2: c.12874A>G, p.N4292D) (Figure 3.4B) which had a high pathogenicity profile with C15 class by AGVGD, predicted to have a severe effect on the physicochemical of the protein by MAPP software and to be a deleterious mutation by SIFT. The amino acid residues are evolutionarily fully conserved from human to zebrafish (Figure 3.4C) and Sanger sequencing confirmed the mutation in both affected cases 2908 and 2909 from whom DNA was available.

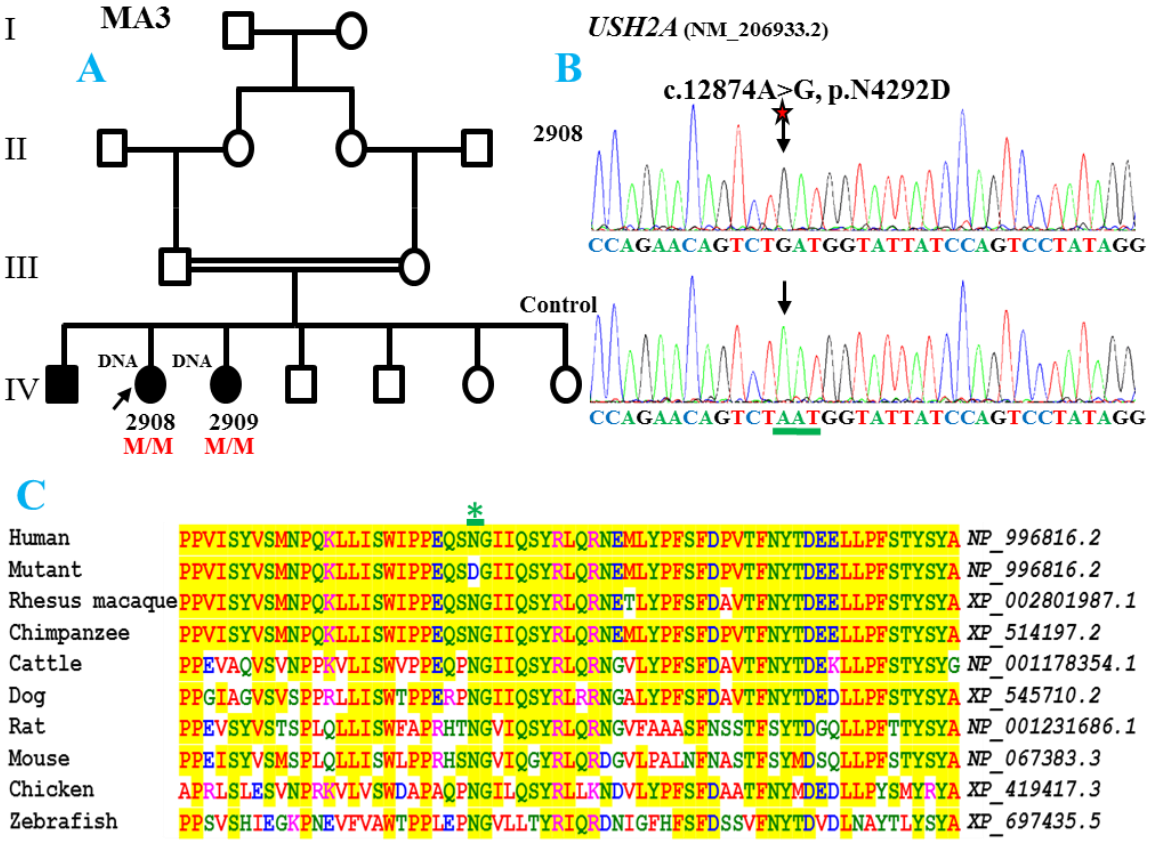

Figure 3.4. Molecular analysis of family MA3. (A) The pedigree of family MA3. Individuals from whom DNA was available are numbered and the proband is indicated by an arrow. (B) Sanger DNA sequencing chromatograms of a control subject and an affected family member (2908) with the *USH2A* mutation are shown. (Adapted from Watson et al., 2014). (C) Evolutionary conservation of the part of the USH2A polypeptide that contains the missense mutation p.N4292D.

Chr	Position	Gene	Coding Effect	cDNA change	Protein change	BLOSUM 62	AGVGD class	SIFT prediction	MAPP prediction	Zygosity	Protein Domain	Segregates
1	5925272	*NPHP4*	missense	NM_015102.3:c.3706G>A	p.Val1236Met	1	C0	Deleterious	bad	Het		
1	**94471056**	***ABCA4***	**nonsense**	**NM_000350.2:c.6088C>T**	**p.Arg2030***	**NA**	**NA**	**NA**	**NA**	**Homo**	**ABC transporter-like**	**YES**
1	186120461	*HMCN1*	missense	NM_031935.2:c.14738C>A	p.Thr4913Asn	0	C0	Deleterious	bad	Het	G2 nidogen/fibulin G2F	
1	215914751	*USH2A*	missense	NM_206933.2:c.11677C>A	p.Pro3893Thr	-1	C35	Deleterious	bad	Het	Fibronectin, type III	
2	96950323	*SNRNP200*	missense	NM_014014.4:c.4165G>A	p.Val1389Ile	3	C0	Tolerated	good	Het	DEAD/DEAH box type, N-terminal	
4	15554873	*CC2D2A*	missense	NM_001080522.2:c.2431G>A	p.Glu811Lys	1	C0	Deleterious	unknown	Het		
6	65596607	*EYS*	missense	NM_001142800.1:c.2975G>T	p.Cys992Phe	-2	C0	Deleterious	unknown	Het	Epidermal growth factor-like, type 3	
10	73405717	*CDH23*	missense	NM_022124.5:c.1270G>A	p.Val424Met	1	C0	Deleterious	bad	Het	Cadherin	
12	76740134	*BBS10*	missense	NM_024685.3:c.1631A>G	p.Asn544Ser	1	C0	Tolerated	good	Het		
12	88480262	*CEP290*	missense	NM_025114.3:c.4208G>C	p.Arg1403Thr	-1	C0	Tolerated	good	Het		

Table 3.3. List of candidate variants after alignment, variant calling and filtering for patient 2844 (male) for family MA2. The likely causative variant is orange shaded. Chr = chromosome, NA = not annotated, Homo = homozygous and Het = heterozygous. (Adapted from Watson et al., 2014).

Chr	Position	Gene	Coding Effect	cDNA change	Protein change	BLOSUM 62	AGVGD class	SIFT prediction	MAPP prediction	Zygosity	Protein Domain	Segregates
1	68910315	*RPE65*	missense	NM_000329.2:c.394G>A	p.Ala132Thr	0	C0	Tolerated	good	Het	Carotenoid oxygenase	
1	**215848379**	***USH2A***	**missense**	**NM_206933.2:c.12874A>G**	**p.Asn4292Asp**	**1**	**C15**	**Deleterious**	**bad**	**Homo**	**Fibronectin, type III**	**YES**
6	137193331	*PEX7*	splicing?	NM_000288.3:c.748-5dupT	p.?	NA	NA	NA	NA	Het		
9	120475185	*TLR4*	missense	NM_138554.3:c.779T>C	p.Leu260Pro	-3	C25	Deleterious	bad	Het	Toll-like receptor	
9	139333568	*INPP5E*	missense	NM_019892.3:c.304G>T	p.Asp102Tyr	-3	C0	Deleterious	good	Het		
10	73537449	*CDH23*	missense	NM_022124.5:c.4858G>A	p.Val1620Met	1	C15	Deleterious	bad	Het	Cadherin	
11	66291004	*BBS1*	missense	NM_024649.4:c.908T>C	p.Val303Ala	0	C25	Deleterious	good	Het	WD40 repeat-like domain	
16	56536660	*BBS2*	missense	NM_031885.3:c.865A>G	p.Ile289Val	3	C0	Tolerated	good	Het	BBS2 protein	
X	13774746	*OFD1*	missense	NM_003611.2:c.1271A>G	p.Asn424Ser	1	C0	Deleterious	good	Het		

Table 3.4. List of candidate variants after alignment, variant calling and filtering for patient 2908 (female) for family MA3. The likely causative variant is orange shaded. Chr = chromosome, NA = not annotated, Homo = homozygous and Het = heterozygous. (Adapted from Watson et al., 2014).

3.2.1.4 Genetic analysis of family MA6

For family MA6, the family history suggested recessive inheritance of RP caused by an autozygous mutation (Figure 3.5A). Targeted capture and next-generation sequencing of case 2771 (Table 3.5) highlighted two homozygous variants in *PROM1* and *RDH12*. *PROM1* has a splice variant that is not predicted to cause defective splicing using software described in Section 2.14.3. However, both variant were test for segregation by confirmatory Sanger sequencing. This excluded the *PROM1* variant and instead highlighted the missense mutation in exon five of *RDH12* (NM_152443.2: c.601T>C, p.C201R) (Figure 3.5B). This homozygous mutation was previously reported by (Sun et al., 2007) in a family with LCA. Bioinformatics analysis of this mutation revealed a high pathogenicity profile with -3, C0, 0.03 and bad prediction scores in BLOSUM62, AGVGD, SIFT and MAPP respectively.

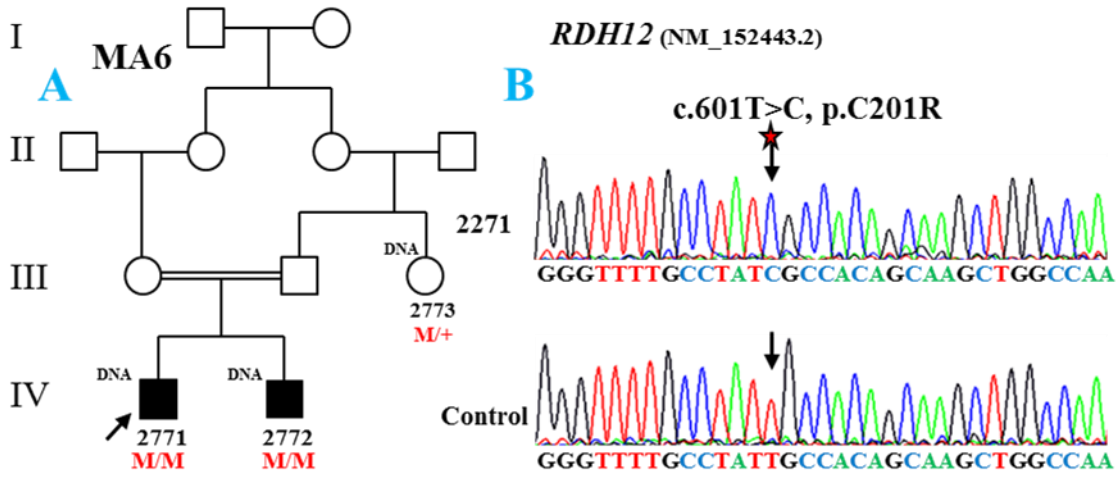

Figure 3.5. Molecular analysis of family MA6. (A) The pedigree of family MA6. Individuals from whom DNA was available are numbered and the proband is indicated by an arrow. (B) Sanger DNA sequencing chromatograms of a control subject and an affected family member (2271) with the *RDH12* mutation. (Adapted from Watson et al., 2014).

3.2.1.5 Genetic analysis of family MA7

For family MA7, the pedigree structure suggested dominant inheritance with affected members being diagnosed with CRD (Figure 3.6A). Targeted capture and next-generation sequencing analysis of patient 114 identified four candidate heterozygous mutations; three pathogenic missense variants in *MERTK*, *PROM1*, *GRM6* and one possible splicing variant in *EYS* (Table 3.6). Based on the available literature, the

heterozygous missense mutation in *PROM1* (NM_006017.2: c.1117C>T, p.R373C) (Figure 3.6B) was the only variant consistent with the phenotype and mode of inheritance. This substitution was previously identified in patients with disease symptoms of adCRD (Yang et al., 2008; Michaelides et al., 2010). It is predicted to be pathogenic with -3 score for BLOSUM62, C0 for AGVGD, 0.03 (deleterious) for SIFT and bad for MAPP. Sanger sequence validation of the mutation confirmed segregation with the disease in the members from whom DNA was available.

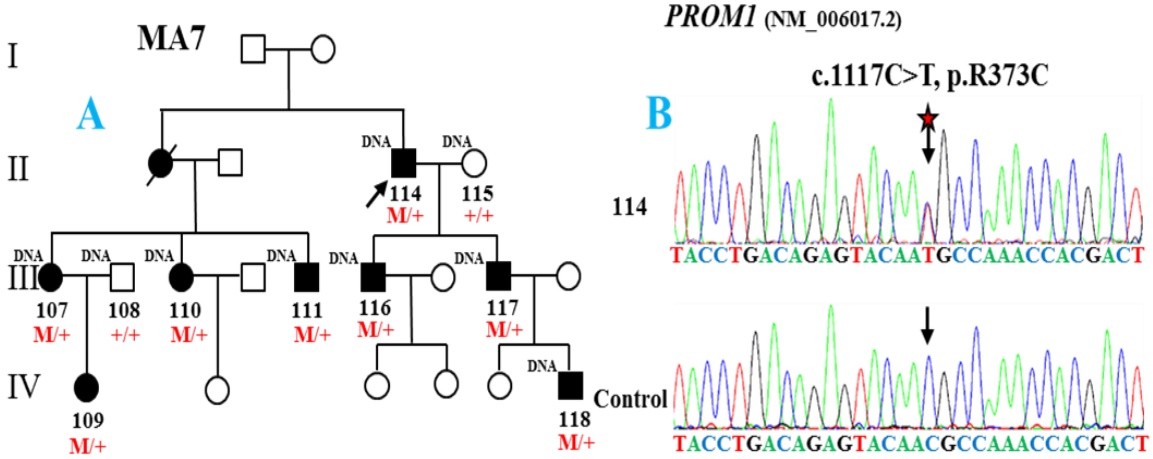

Figure 3.6. Molecular analysis of family MA7. (A) The pedigree of family MA7. Individuals from whom DNA was available are numbered and the proband is indicated by an arrow. (B) Sanger DNA sequencing chromatograms of a control subject and an affected family member (114) with the *PROM1* mutation. (Adapted from Watson et al., 2014).

3.2.1.6 Genetic analysis of family MA8

For family MA8, all affected members had RP with macular involvement and the family structure suggested a dominant or X-linked mode of inheritance (Figure 3.7A). The final variant list produced from targeted capture and next-generation sequence analysis of patient 40 included 11 variants (Table 3.7). Three candidate variants in *RP2*, *NR2E3* and *RPGR* were consistent with the phenotype and mode of the inheritance observed the family. Segregation analysis on genomic DNA from eight affected and three unaffected family members showed that only the novel splicing variant in *RP2* (NM_006915.2:c.884-1G>T) (Figure 3.7B) followed disease symptoms as expected for an X-linked dominant condition.

Chr	Position	Gene	Coding Effect	cDNA change	Protein change	BLOSUM 62	AGVGD class	SIFT prediction	MAPP prediction	Zygosity	Protein Domain	Segregates
1	186007997	*HMCN1*	missense	NM_031935.2:c.5888G>T	p.Gly1963Val	-3	C0	Tolerated	good	Het		
4	15982163	*PROM1*	splicing?	NM_006017.2:c.2374-4dupG	p.?	NA	NA	NA	NA	Homo		No
5	82836537	*VCAN*	missense	NM_004385.4:c.7715C>T	p.Ser2572Leu	-2	C65	Deleterious	bad	Het	Immunoglobulin I-set	
10	86008700	*RGR*	missense	NM_002921.3:c.271G>A	p.Gly91Ser	0	C55	Deleterious	good	Het		
14	**68193850**	***RDH12***	**missense**	**NM_152443.2:c.601T>C**	**p.Cys201Arg**	**-3**	**C0**	**Deleterious**	**bad**	**Homo**	**GPCR, rhodopsin-like, 7TM**	**YES**
15	73029831	*BBS4*	missense	NM_033028.3:c.1463C>A	p.Thr488Lys	-1	C0	Tolerated	good	Het	Short-chain dehydrogenase/reductase SDR	

Table 3.5. List of candidate variants after alignment, variant calling and filtering for patient 2771 (male) for family MA6. The likely causative variant is orange shaded. Chr = chromosome, NA = not annotated, Homo = homozygous and Het = heterozygous. (Adapted from Watson et al., 2014).

Chr	Position	Gene	Coding Effect	cDNA change	Protein change	BLOSUM 62	AGVGD class	SIFT prediction	MAPP prediction	Zygosity	Protein Domain	Segregates
2	71134	*ALMS1*	missense	NM_015120.4:c.5362A>G	p.Asn1788Asp	1	C0	Tolerated	unknown	Het		
2	112722801	*MERTK*	missense	NM_006343.2:c.791C>G	p.Ala264Gly	0	C55	Deleterious	bad	Het	Immunoglobulin-like	
4	**16014922**	***PROM1***	**missense**	**NM_006017.2:c.1117C>T**	**p.Arg373Cys**	**-3**	**C0**	**Deleterious**	**bad**	**Het**	**Prominin**	**YES**
5	178413684	*GRM6*	missense	NM_000843.3:c.1571C>T	p.Pro524Leu	-3	C65	Deleterious	bad	Het	GPCR, family 3, nine cysteines domain	
6	66063346	*EYS*	splicing?	NM_001142800.1:c.1459+5C>T	p.?	NA	NA	NA	NA	Het		
16	53692694	*RPGRIP1L*	missense	NM_015272.2:c.1340T>C	p.Leu447Ser	-2	C0	Tolerated	good	Het		

Table 3.6. List of candidate variants after alignment, variant calling and filtering for patient 114 (male) for family MA7. The likely causative variant is orange shaded. Chr = chromosome, NA = not annotated and Het = heterozygous. (Adapted from Watson et al., 2014).

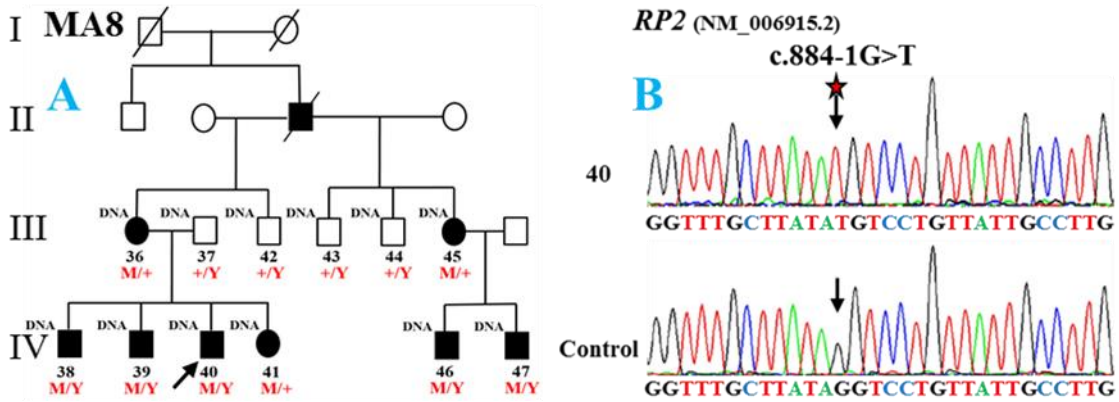

Figure 3.7. Molecular analysis of family MA8. (A) The pedigree of family MA8. Individuals from whom DNA was available are numbered and the proband is indicated by an arrow. (B) Sanger DNA sequencing chromatograms of a control subject and an affected family member (40) with the *RP2* mutation. (Adapted from Watson et al., 2014).

3.2.1.7 Genetic analysis of family MA9

For MA9, diagnosis of the affected family members and family history revealed a macular dystrophy phenotype with a dominant mode of inheritance (Figure 3.8A). The variant list derived from analysis of genomic DNA from patient 530 included seven variants (Table 3.8), from which two heterozygous variants in *HMCN1* and *GUCY2D* were highlighted as possible candidate variants consistent with the phenotype and mode of inheritance. Segregation analysis using additional family members from whom DNA was available excluded the *HMCN1* variant as a cause of adMD in this family, but confirmed segregation of the previously reported *GUCY2D* mutation (c.2512C>T, p.R838C) (Figure 3.8B) (Van Ghelue et al., 2000; Wilkie et al., 2000) with the disease phenotype.

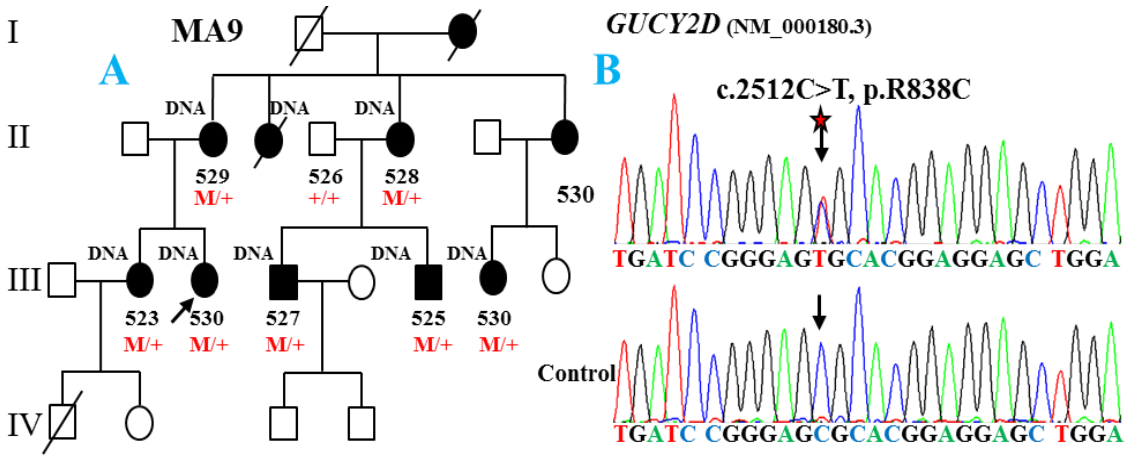

Figure 3.8. Molecular analysis of family MA9. (A) The pedigree of family MA9. Individuals from whom DNA was available are numbered and the proband is indicated by an arrow. (B) Sanger DNA sequencing chromatograms of a control subject and an affected family member (530) with the *GUCY2D* mutation. (Adapted from Watson et al., 2014).

3.2.1.8 Genetic analysis of family MA10

Family MA10 is a large consanguineous family with six affected members diagnosed with autosomal recessive CRD (Figure 3.9A). After analyzing patient 1857, the filtered vcf file that was generated highlighted only one homozygous candidate variant (Table 3.9), a null variant in *RPGRIP1* (NM_020366.3:c.3565C>T, p.R1189*). This mutation had previously been reported as a pathogenic cause of the disease (Abu-Safieh et al., 2013) and segregation analysis on seven family members for whom DNA was available confirmed this mutation as the cause of disease symptoms in this family (Figure 3.9B).

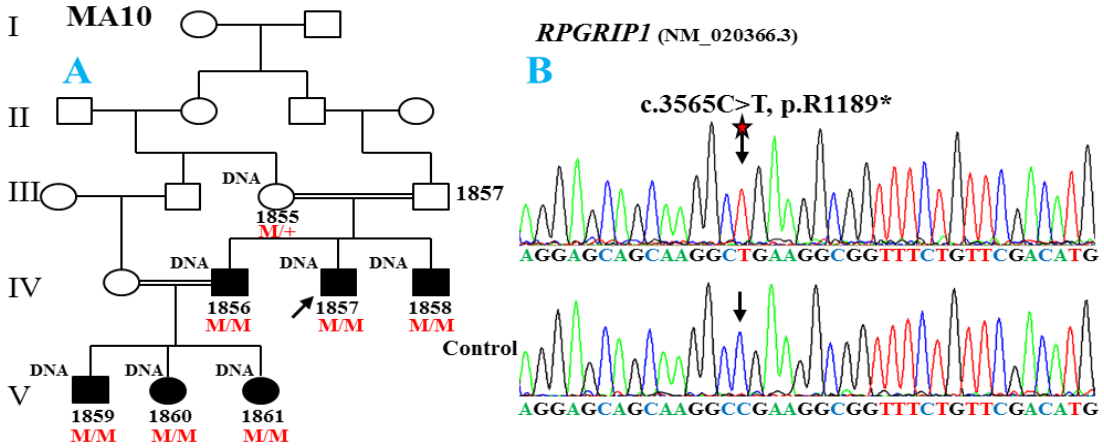

Figure 3.9. Molecular analysis of family MA10. (A) The pedigree of family MA10. Individuals from whom DNA was available are numbered and the proband is indicated by an arrow. (B) Sanger DNA sequencing chromatograms of a control subject and an affected family member (1857) with the *RPGRIP1* mutation. (Adapted from Watson et al., 2014).

Chr	Position	Gene	Coding Effect	cDNA change	Protein change	BLOSUM 62	AGVGD class	SIFT prediction	MAPP prediction	Zygosity	Protein Domain	Segregates
1	103400669	*COL11A1*	missense	NM_080629.2:c.3475G>A	p.Gly1159Ser	0	C55	Deleterious	good	Het		
1	215844373	*USH2A*	missense	NM_206933.2:c.14074G>A	p.Gly4692Arg	-2	C65	Deleterious	bad	Het	Fibronectin, type III	
4	15982163	*PROM1*	splicing?	NM_006017.2:c.2374-4dupG	p.?	NA	NA	NA	NA	Het		
5	89969880	*GPR98*	missense	NM_032119.3:c.4939A>G	p.Ile1647Val	3	C0	Tolerated	good	Het	Na-Ca exchanger/ integrin-beta4	
10	13320305	*PHYH*	in-frame	NM_006214.3:c.1010_1012dupGAT	p.Asn337_Leu338insHis	NA	NA	NA	NA	Het		
11	119216627	*MFRP*	missense	NM_031433.2:c.283G>A	p.Ala95Thr	0	C0	Tolerated	good	Het		
15	31294159	*TRPM1*	missense	NM_002420.4:c.4678G>A	p.Val1560Met	1	C0	Deleterious	good	Het		
15	6267	*NR2E3*	nonsense	NM_014249.2:c.300C>A	p.Cys100*	NA	NA	NA	NA	Het	Zinc finger, nuclear hormone receptor-type	NO
X	18674770	*RS1*	splicing?	NM_000330.3:c.184+3G>T	p.?	NA	NA	NA	NA	Het		A
X	38182144	*RPGR*	missense	NM_001034853.1:c.209G>A	p.Gly70Glu	-2	C0	Deleterious	bad	Het	Regulator of chromosome condensation, RCC1	A
X	**46736939**	***RP2***	**splicing**	**NM_006915.2:c.884-1G>T**	**p.?**	**NA**	**NA**	**NA**	**NA**	**Hemi**		**YES**

Table 3.7. List of candidate variants after alignment, variant calling and filtering for patient 40 (male) for family MA8. The likely causative variant is orange shaded. Chr = chromosome, NA = not annotated. Hemi= hemizygous, Het = heterozygous and A = artefact. (Adapted from Watson et al., 2014).

Chr	Position	Gene	Coding Effect	cDNA change	Protein change	BLOSUM 62	AGVGD class	SIFT prediction	MAPP prediction	Zygosity	Protein Domain	Segregates
1	186141213	*HMCN1*	missense	NM_031935.2:c.15764T>C	p.Ile5255Thr	-1	C65	Deleterious	bad	Het	EGF-like calcium-binding	NO
1	216172258	*USH2A*	missense	NM_206933.2:c.6628C>G	p.Pro2210Ala	-1	C25	Deleterious	bad	Het	Fibronectin, type III	
4	15982163	*PROM1*	splicing?	NM_006017.2:c.2374-4dupG	p.?	NA	NA	NA	NA	Homo		
16	53653005	*RPGRIP1L*	missense	NM_015272.2:c.3548C>G	p.Ala1183Gly	0	C0	Deleterious	bad	Het		
16	53683031	*RPGRIP1L*	splicing?	NM_015272.2:c.2153-4G>C	p.?	NA	NA	NA	NA	Het		
17	**7918018**	***GUCY2D***	**missense**	**NM_000180.3:c.2512C>T**	**p.Arg838Cys**	**-3**	**C65**	**Deleterious**	**bad**	**Het**	**Haem NO binding associated**	**YES**
20	10393439	*MKKS*	missense	NM_170784.1:c.724G>T	p.Ala242Ser	1	C15	Deleterious	good	Het	Chaperonin Cpn60/TCP-1	

Table 3.8. List of candidate variants after alignment, variant calling and filtering for patient 530 (female) for family MA9. The likely causative variant is orange shaded. Chr = chromosome, NA = not annotated, Homo = homozygous and Het = heterozygous. (Adapted from Watson et al., 2014).

Chr	Position	Gene	Coding Effect	cDNA change	Protein change	BLOSUM 62	AGVGD class	SIFT prediction	MAPP prediction	Zygosity	Protein Domain	Segregates
1	215960153	*USH2A*	missense	NM_206933.2:c.10246T>G	p.Cys3416Gly	-3	C65	Deleterious	bad	Het	Fibronectin, type III	
1	216062306	*USH2A*	missense	NM_206933.2:c.7685T>C	p.Val2562Ala	0	C0	Tolerated	good	Het	Fibronectin, type III	
2	96942928	*SNRNP200*	missense	NM_014014.4:c.5983G>A	p.Ala1995Thr	0	C0	Tolerated	good	Het	Sec63 domain	
5	82835550	*VCAN*	missense	NM_004385.4:c.6728C>G	p.Thr2243Arg	-1	C0	Tolerated	good	Het		
9	139326278	*INPP5E*	missense	NM_019892.3:c.1547A>G	p.Lys516Arg	2	C0	Tolerated	good	Het	Endo-/Exo-nuclease phosphatase	
10	73337684	*CDH23*	missense	NM_022124.5:c.767G>A	p.Arg256His	0	C0	Deleterious	bad	Het	Cadherin	
11	17531058	*USH1C*	missense	NM_153676.3:c.1858C>T	p.Arg620Cys	-3	C0	Deleterious	unknown	Het		
12	2022196	*CACNA2D4*	missense	NM_172364.4:c.419C>G	p.Ala140Gly	0	C0	Deleterious	good	Het		
14	**21813304**	***RPGRIP1***	**nonsense**	**NM_020366.3:c.3565C>T**	**p.Arg1189***	**NA**	**NA**	**NA**	**NA**	**Homo**	**-**	**YES**
15	73028295	*BBS4*	missense	NM_033028.3:c.1236A>T	p.Glu412Asp	2	C0	Tolerated	good	Het		
16	53698905	*RPGRIP1L*	missense	NM_015272.2:c.1120C>T	p.His374Tyr	2	C15	Deleterious	good	Het		
17	79503621	*FSCN2*	missense	NM_001077182.2:c.1151C>A	p.Ala384Glu	-1	C0	Not scored	unknown	Het		

Table 3.9. List of candidate variants after alignment, variant calling and filtering for patient 1857 (female) for family MA10. The probable causative variant is orange shaded. Chr = chromosome, NA = not annotated, Homo = homozygous and Het = heterozygous. (Adapted from Watson et al., 2014).

3.2.1.9 Genetic analysis of family MA11

For MA11, family history suggested recessive inheritance of RP with an autozygous mutation (Figure 3.10A). The variant list derived from analysing the index case 1267 included only one homozygous missense variant in *BBS2* (NM_031885.3:c.1895G>C, p.R632P) (Table 3.10), which was considered the most likely causative variant based on mode of inheritance of the family. Sanger sequencing confirmed the presence of the mutation in the second affected family member 2093 for whom DNA was available (Figure 3.10B). This mutation is likely to be pathogenic as it is predicted to have a deleterious effect on the protein by MAPP, it scores -3 on the BLOSUM62 matrix and C15 for AGVGD. Furthermore the amino acid residues are conserved through evolution from human to brown algae.

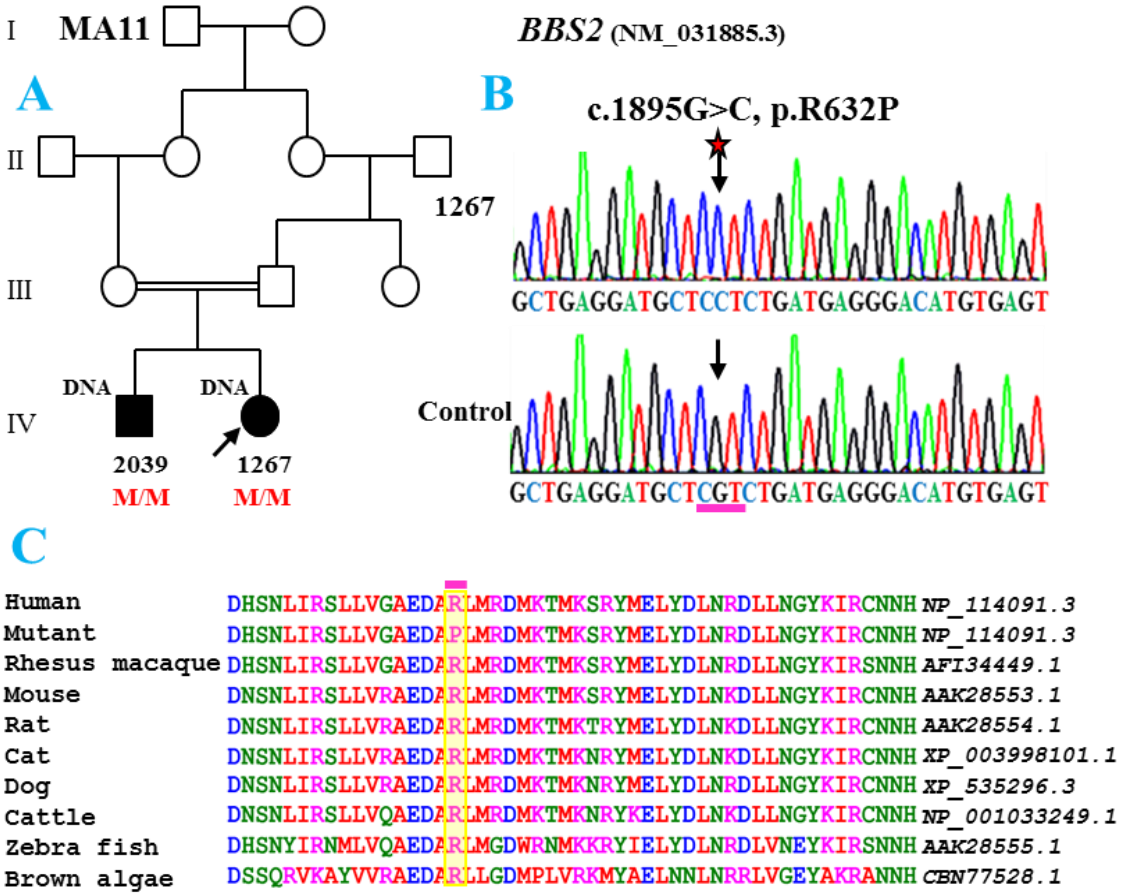

Figure 3.10. Molecular analysis of family MA11. (A) The pedigree of family MA11. Individuals from whom DNA was available are numbered and the proband is indicated by an arrow. (B) Sanger DNA sequencing chromatograms of a control subject and an affected family member (1267) with the *BBS2* mutation. (Adapted from Watson et al., 2014). (C) Evolutionary conservation of the part of the BBS2 polypeptide that contains the missense mutation p.R632P.

Chr	Position	Gene	Coding Effect	cDNA change	Protein change	BLOSUM 62	AGVGD class	SIFT prediction	MAPP prediction	Zygosity	Protein Domain	Segregates
1	6012898	*NPHP4*	splicing	NM_015102.3:c.674-2A>G	p.?	NA	NA	NA	NA	Het		
1	94467548	*ABCA4*	missense	NM_000350.2:c.6148G>C	p.Val2050Leu	1	C25	Deleterious	bad	Het	ABC transporter-like	
1	216011442	*USH2A*	missense	NM_206933.2:c.9262G>A	p.Glu3088Lys	1	C55	Deleterious	bad	Het	Fibronectin, type III	
4	16077349	*PROM1*	missense	NM_006017.2:c.181A>G	p.Ile61Val	3	C0	Tolerated	good	Het	Prominin	
6	42153428	*GUCA1B*	missense	NM_002098.5:c.465G>T	p.Glu155Asp	2	C0	Tolerated	good	Het	EF-HAND 2	
6	80626456	*ELOVL4*	missense	NM_022726.3:c.814G>C	p.Glu272Gln	2	C0	Tolerated	good	Het	GNS1/SUR4 membrane protein	
9	2718127	*KCNV2*	missense	NM_133497.3:c.388A>C	p.Thr130Pro	-1	C0	Deleterious	bad	Het	Potassium channel, voltage dependent, Kv, tetramerisation	
9	120476583	*TLR4*	missense	NM_138554.3:c.2177G>T	p.Gly726Val	-3	C65	Deleterious	bad	Het	Toll/interleukin-1 receptor homology domain	
11	76883864	*MYO7A*	missense	NM_000260.3:c.1868G>A	p.Arg623His	0	C0	Deleterious	good	Het	Myosin head, motor domain	
12	1908849	*CACNA2D4*	missense	NM_172364.4:c.2987T>C	p.Phe996Ser	-2	C0	Tolerated	unknown	Het		
16	53686789	*RPGRIP1L*	missense	NM_015272.2:c.1810G>A	p.Glu604Lys	1	C0	Deleterious	bad	Het	Protein of unknown function DUF3250	
16	**56530894**	***BBS2***	**missense**	**NM_031885.3:c.1895G>C**	**p.Arg632Pro**	**-2**	**C15**	**Tolerated**	**bad**	**Homo**	**BBS2 protein**	**YES**
X	49082958	*CACNA1F*	missense	NM_005183.2:c.1409T>C	p.Leu470Pro	-3	C0	Deleterious	bad	Het		A

Table 3.10. List of candidate variants after alignment, variant calling and filtering for patient 1267 (female) for family MA11. The likely causative variant is orange shaded. Chr = chromosome, NA = not annotated, Homo = homozygous, Het = heterozygous and A = artefact. (Adapted from Watson et al., 2014).

This result was consistent with the homozygosity mapping that was previously carried by Dr Ali on both affected individuals (1267 and 2093). That analysis revealed that *BBS2* (chr16:56,518,259-56,554,008, hg19) localizes in the largest of three shared homozygous regions detected; one on chromosome 11 (45.6-55.4 Mb, for a total of 9.8 Mb, hg19) and two on chromosome 16 (19.0-26.1 Mb, for a total of 7.1 Mb, hg19 and 54.2-73.8 Mb, for a total of 19.6 Mb, hg19).

These data represent for the first time the association between missense mutations in the *BBS2* gene and partially penetrant RP. Family patients and their clinical notes were re-examined by Mr McKibbin in light of these findings. The index case (1267) first presented in an ophthalmic clinic with high myopia and poor visual acuity (VA) of 0.5 at five years of age. The VA deteriorated gradually to 0.25 at the age of 37 and 0.1 by the age of 45. Along with the abnormal retinal pigmentation, polydactyly in one hand (removed in childhood) and some learning difficulties were also reported. The second patient (2039) had only a mild ocular phenotype with bone spicule-like pigmentation but VA continued to gradually deteriorate over time, being 1.0, 0.3 and 0.01 by the age of 39, 50 and 56 years respectively.

3.2.1.10 Genetic analysis of family MA15

For MA15, family structure suggested a consanguineous recessive mode of inheritance, with three affected members diagnosed with CRD (Figure 3.11A).The variant list generated from targeted sequencing of patient 3283 (Table 3.11) included 16 variants. Based on the zygosity and phenotype observed in the family, the candidate variants of *VCAN, GPR98, EYS, MYO7A* were excluded, while the a nonsense mutation in *SPATA7* (NM_018418.4:c.253C>T, p.R85*) (Figure 3.11B) was the most likely candidate. This homozygous truncating mutation segregated with the disease symptoms in the three affected family members and was heterozygous in eight unaffected family members for whom DNA was available. This homozygous mutation was previously reported in a family with LCA by (Mackay et al., 2011b).

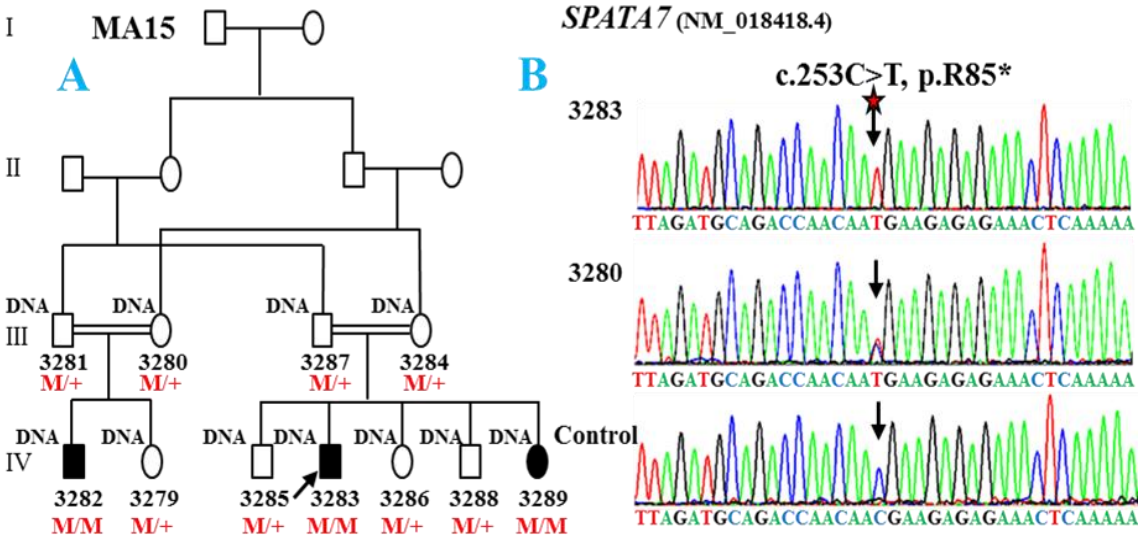

Figure 3.11. Molecular analysis of family MA15. (A) The pedigree of the family MA15. Individuals from whom DNA was available are numbered and the proband is indicated by an arrow. (B) Sanger DNA sequencing chromatograms of a control subject, an affected (3283) and carrier (3280) family members with the *SPATA7* mutation. (Adapted from Watson et al., 2014).

3.2.1.11 Genetic analysis of family MA16

The diagnosis in two members of family MA16 was LCA, and the presence of a consanguinity loop suggested a recessive mode of inheritance (Figure 3.12A). 18 variants were included in the final list produced after targeted sequencing, alignment, variant calling and filtering in the index case 3341 (Table 3.12). Based on the zygosity and phenotype, a homozygous missense mutation was identified in exon five of *RDH12* (NM_152443.2:c.506G>A, p.R169Q), as described previously by (Mackay et al., 2011a). This mutation was also present in the second affected member 3340 for whom DNA was available (Figure 3.12B). It is almost certainly pathogenic as it has been published before as a cause of arLCA, segregates with the disease in the family and is predicted to be deleterious (zero score) by SIFT, bad by MAPP, C35 by AGVGD and scores +1 for BLOSUM62.

Chr	Position	Gene	Coding Effect	cDNA change	Protein change	BLOSUM 62	AGVGD class	SIFT prediction	MAPP prediction	Zygosity	Protein Domain	Segregates
1	94473807	*ABCA4*	missense	NM_000350.2:c.5882G>A	p.Gly1961Glu	-2	C65	Deleterious	bad	Het	ABC transporter-like	
5	82817313	*VCAN*	missense	NM_004385.4:c.3188T>C	p.Leu1063Pro	-3	C0	Deleterious	bad	Homo		
5	89948189	*GPR98*	missense	NM_032119.3:c.3443G>A	p.Gly1148Asp	-1	C65	Deleterious	bad	Homo		
6	64431505	*EYS*	missense	NM_001142800.1:c.8422G>A	p.Ala2808Thr	0	C0	Deleterious	unknown	Het	Laminin G, subdomain 2	
6	65300160	*EYS*	missense	NM_001142800.1:c.5600C>T	p.Ser1867Phe	-2	C0	Deleterious	unknown	Het		
8	55538820	*RP1*	missense	NM_006269.1:c.2378G>T	p.Arg793Ile	-3	C15	Deleterious	bad	Het		
9	117266673	*DFNB31*	missense	NM_015404.3:c.409G>C	p.Glu137Gln	2	C0	Tolerated	good	Het		
9	139333403	*INPP5E*	missense	NM_019892.3:c.469G>T	p.Gly157Trp	-2	C0	Tolerated	good	Het		
11	66291279	*BBS1*	missense	NM_024649.4:c.1036G>A	p.Val346Ile	3	C25	Deleterious	bad	Het	WD40 repeat-like-containing domain	
11	68115675	*LRP5*	missense	NM_002335.2:c.452A>C	p.Asp151Ala	-2	C65	Deleterious	bad	Het	LDLR class B repeat	
11	76891457	*MYO7A*	missense	NM_000260.3:c.2624C>G	p.Ala875Gly	0	C0	Tolerated	bad	Het		
11	76891460	*MYO7A*	missense	NM_000260.3:c.2627A>G	p.Glu876Gly	-2	C0	Deleterious	bad	Het		
12	1906632	*CACNA2D4*	missense	NM_172364.4:c.3065C>T	p.Pro1022Leu	-3	C0	Tolerated	unknown	Het		
14	**88883069**	***SPATA7***	**nonsense**	**NM_018418.4:c.253C>T**	**p.Arg85***	**NA**	**NA**	**NA**	**NA**	**Homo**	**-**	**YES**
17	63221207	*RGS9*	missense	NM_003835.3:c.1495T>C	p.Ser499Pro	-1	C0	Deleterious	unknown	Het		
20	10622214	*JAG1*	missense	NM_000214.2:c.2810G>A	p.Arg937Gln	1	C0	Tolerated	good	Het		

Table 3.11. List of candidate variants after alignment, variant calling and filtering for patient 3283 (male) for family MA15. The probable causative variant is orange shaded. Chr = chromosome, NA = not annotated, Homo = homozygous and Het = heterozygous. (Adapted from Watson et al., 2014).

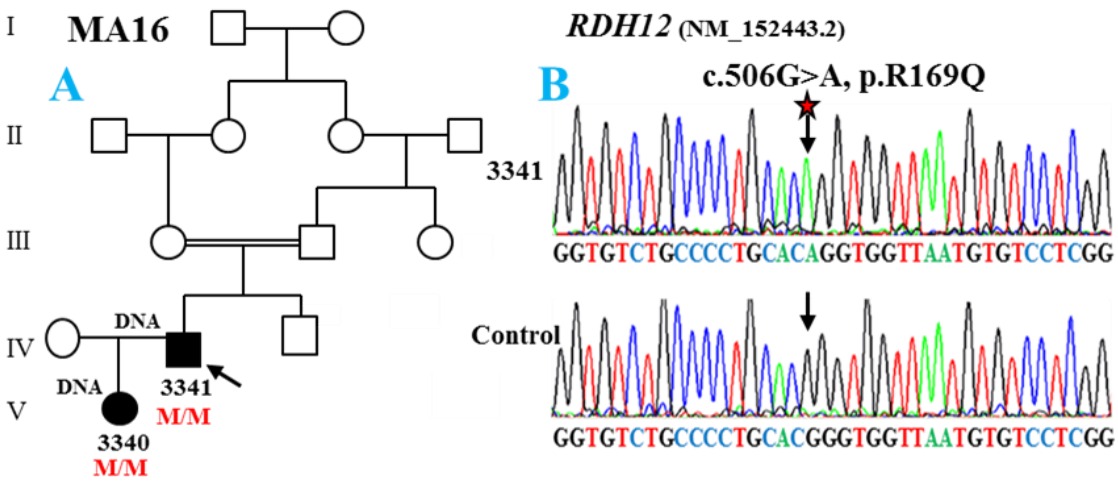

Figure 3.12. Molecular analysis of family MA16. (A) The pedigree of family MA16. Individuals from whom DNA was available are numbered and the proband is indicated by an arrow. (B) Sanger DNA sequencing chromatograms of a control subject and an affected family member with the *RDH12* mutation. (Adapted from Watson et al., 2014).

3.2.1.12 Genetic analysis of family MA18

Affected members of family MA18 were diagnosed with CRD and the family history suggested recessive inheritance, though there was no evidence of consanguinity (Figure 3.13A). Based on the zygosity, analysis of the variant list of patient 1484 (Table 3.13) highlighted compound heterozygous variants in two genes, *ABCA4* and *RBP3*. Even though *RBP3* did not appear to fit the observed phenotype well, both variants were segregated in the three affected and four unaffected family members for whom DNA was available. Segregation analysis excluded *RBP3* and confirmed the *ABCA4* (NM_000350.2) compound heterozygous mutations. The first was a novel splicing mutation that alters the splice donor site of exon 25 (c.3328+1G>C), while the second mutation was a previously reported missense change (c.5882 G>A, p.G1961E) (Figure 3.13B) (Cella et al., 2009; Burke et al., 2012). The missense variant was predicted to be pathogenic [SIFT (damaging, zero score), BLOSUM62 (-2), MAPP (bad) and AGVGD (C65)].

Chr	Position	Gene	Coding Effect	cDNA change	Protein change	BLOSUM 62	AGVGD class	SIFT prediction	MAPP prediction	Zygosity	Protein Domain	Segregates
1	186072648	*HMCN1*	missense	NM_031935.2:c.10618G>A	p.Val3540Ile	3	C25	Deleterious	bad	Het	Immunoglobulin I-set	
2	110187	*ALMS1*	missense	NM_015120.4:c.8983G>A	p.Val2995Ile	3	C0	Tolerated	unknown	Het		
2	169521	*ALMS1*	missense	NM_015120.4:c.9917A>G	p.Asn3306Ser	1	C0	Deleterious	unknown	Het		
3	121518211	*IQCB1*	missense	NM_001023570.2:c.598C>A	p.Leu200Ile	2	C0	Tolerated	good	Het		
3	132423114	*NPHP3*	missense	NM_153240.4:c.1452A>G	p.Ile484Met	1	C0	Deleterious	good	Het		
5	90149261	*GPR98*	missense	NM_032119.3:c.17365A>G	p.Lys5789Glu	1	C0	Tolerated	good	Het		
5	178418555	*GRM6*	missense	NM_000843.3:c.727G>T	p.Val243Phe	-1	C0	Tolerated	good	Het	Extracellular ligand-binding receptor	
6	64431505	*EYS*	missense	NM_001142800.1:c.8422G>A	p.Ala2808Thr	0	C0	Deleterious	unknown	Het	Laminin G, subdomain 2	
7	92157661	*PEX1*	missense	NM_000466.2:c.89A>C	p.His30Pro	-2	C0	Tolerated	bad	Het	Peroxisome biogenesis factor 1, alpha/beta	
8	38880817	*ADAM9*	missense	NM_003816.2:c.887G>A	p.Arg296Gln	1	C0	Tolerated	good	Het	Peptidase M12B, ADAM/reprolysin	
10	95400223	*PDE6C*	missense	NM_006204.3:c.1646T>C	p.Met549Thr	-1	C45	Deleterious	bad	Het		
10	95405722	*PDE6C*	missense	NM_006204.3:c.1853C>T	p.Thr618Met	-1	C0	Tolerated	good	Het	3'-5'-cyclic nucleotide phosphodiesterase, catalytic domain	
11	76891457	*MYO7A*	missense	NM_000260.3:c.2624C>G	p.Ala875Gly	0	C0	Tolerated	bad	Het		
14	**68193755**	***RDH12***	**missense**	**NM_152443.2:c.506G>A**	**p.Arg169Gln**	**1**	**C35**	**Deleterious**	**bad**	**Homo**	**Short-chain dehydrogenase/reductase SDR**	**YES**
15	31325130	*TRPM1*	missense	NM_002420.4:c.2648A>G	p.Glu883Gly	-2	C0	Deleterious	bad	Het	Ion transport	
16	16295863	*ABCC6*	missense	NM_001171.5:c.1171A>G	p.Arg391Gly	-2	C0	Deleterious	bad	Het	transmembrane domain	
17	63221207	*RGS9*	missense	NM_003835.3:c.1495T>C	p.Ser499Pro	-1	C0	Deleterious	unknown	Het		
20	10389422	*MKKS*	missense	NM_170784.1:c.1015A>G	p.Ile339Val	3	C0	Tolerated	good	Het	Chaperonin Cpn60/TCP-1	

Table 3.12. List of candidate variants after alignment, variant calling and filtering for patient 3341 (male) for family MA16. The likely causative variant is orange shaded. Chr = chromosome, Homo = homozygous and Het = heterozygous. (Adapted from Watson et al., 2014).

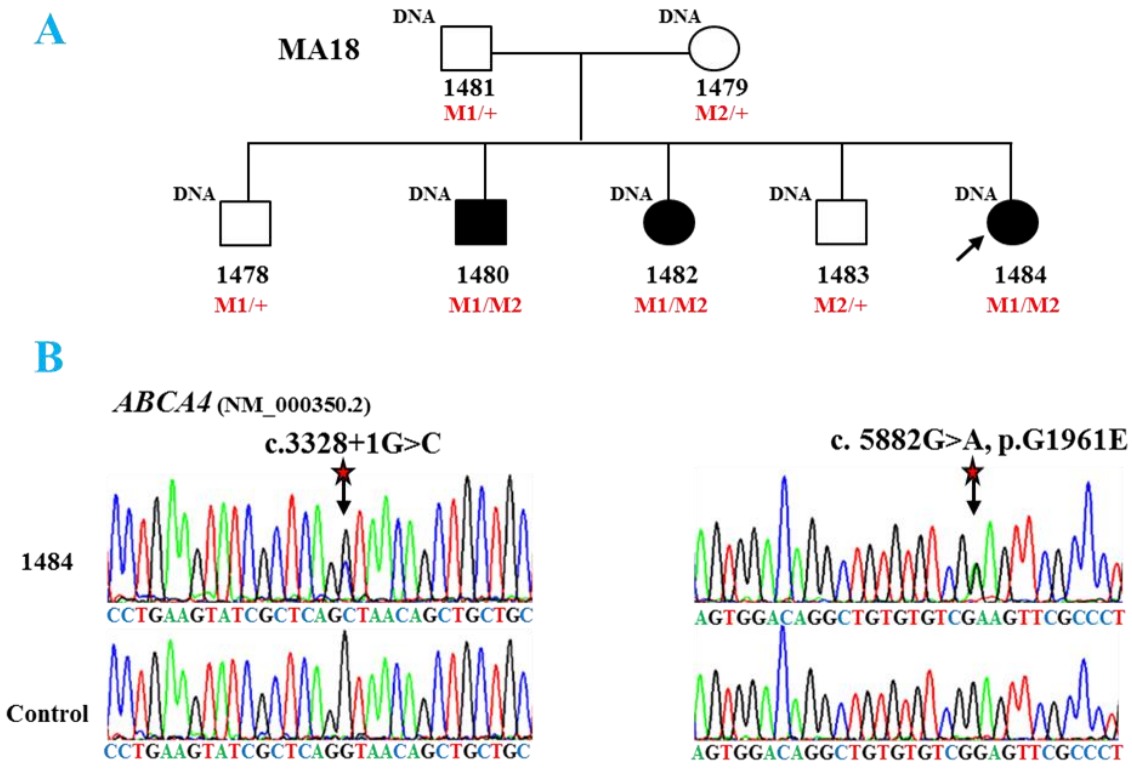

Figure 3.13. Molecular analysis of family MA18. (A) The pedigree of family MA18. Individuals from whom DNA was available are numbered and the proband is indicated by an arrow. (B) Sanger DNA sequencing chromatograms of a control subject and an affected family member (1484) with the *ABCA4* mutation. (Adapted from Watson et al., 2014).

3.2.2 Inherited retinal dystrophy families in whom variants of unknown significance were found

3.2.2.1 Genetic analysis of family MA4

For family MA4, the diagnosis of the affected patients was RP and the presence of consanguinity suggests a recessive inheritance pattern (Figure 3.14A). Targeted capture and next-generation sequence analysis of case 2833 (Table 3.14) identified a variant list with two homozygous missense variants in *EYS* (NM_001142800.1: c.7558A>G p.F2520L & c.334C>T, p.V112I) as possible candidates. Sanger sequencing validation in the other affected case 2910 confirmed the presence of both *EYS* variants in the homozygous state.

However both variants gave low pathogenicity profile scores with unknown effects on protein function by MAPP and zero scores in BLOSUM62, SIFT and AGVGD. Public

Chr	Position	Gene	Coding Effect	cDNA change	Protein change	BLOSUM 62	AGVGD class	SIFT prediction	MAPP prediction	Zygosity	Protein Domain	Segregates
1	6007259	*NPHP4*	missense	NM_015102.3:c.1024C>T	p.Arg342Cys	-3	C0	Deleterious	bad	Het		
1	68904660	*RPE65*	missense	NM_000329.2:c.963T>G	p.Asn321Lys	0	C0	Deleterious	good	Het	Carotenoid oxygenase	
1	**94508316**	***ABCA4***	**splicing**	**NM_000350.2:c.3328+1G>C**	**p.?**	**NA**	**NA**	**NA**	**NA**	**Het**		**YES**
1	**94473807**	***ABCA4***	**missense**	**NM_000350.2:c.5882G>A**	**p.Gly1961Glu**	**-2**	**C65**	**Deleterious**	**bad**	**Het**	**ABC transporter-like**	**YES**
2	96950323	*SNRNP200*	missense	NM_014014.4:c.4165G>A	p.Val1389Ile	3	C0	Tolerated	good	Het	DEAD/DEAH box type, N-terminal	
4	15982163	*PROM1*	splicing?	NM_006017.2:c.2374-4dupG	p.?	NA	NA	NA	NA	Het		
6	14945	*C2*	missense	NM_000063.4:c.1103G>A	p.Arg368Gln	1	C35	Deleterious	bad	Het	von Willebrand factor, type A	
10	48389479	*RBP3*	missense	NM_002900.2:c.1399C>T	p.Pro467Ser	-1	C0	Deleterious	bad	Het	Interphotoreceptor retinol-binding	No
10	48389841	*RBP3*	missense	NM_002900.2:c.1037G>A	p.Arg346His	0	C0	Deleterious	bad	Het		No
10	73551036	*CDH23*	missense	NM_022124.5:c.6197G>A	p.Arg2066Gln	1	C0	Tolerated	good	Het	Cadherin	
12	76742114	*BBS10*	missense	NM_024685.3:c.25G>T	p.Gly9Trp	-2	C0	Tolerated	unknown	Het		
12	88508951	*CEP290*	frameshift	NM_025114.3:c.1833delA	p.Leu612Phefs*5	NA	NA	NA	NA	Het		
14	89307227	*TTC8*	missense	NM_144596.2:c.284A>G	p.Lys95Arg	2	C0	Tolerated	good	Het		
15	31318408	*TRPM1*	missense	NM_002420.4:c.3497A>T	p.His1166Leu	-3	C0	Tolerated	good	Het		
17	6329946	*AIPL1*	missense	NM_014336.3:c.773G>A	p.Arg258Gln	1	C0	Tolerated	good	Het	Tetratricopeptide repeat-containing	
20	10393438	*MKKS*	missense	NM_170784.1:c.725C>T	p.Ala242Val	0	C0	Tolerated	good	Het	Chaperonin Cpn60/TCP-1	
X	31462606	*DMD*	missense	NM_004006.2:c.9076C>T	p.Leu3026Phe	0	C0	Deleterious	good	Het	Spectrin repeat	
X	153418535	*OPN1LW*	missense	NM_020061.4:c.532A>G	p.Ile178Val	3	C0	Tolerated	good	Homo	GPCR, rhodopsin-like, 7TM	

Table 3.13. List of candidate variants after alignment, variant calling and filtering for patient 1484 (female) for family MA18. The probable causative variants are orange shaded. Chr = chromosome, NA = not annotated, Homo = homozygous and Het = heterozygous. (Adapted from Watson et al., 2014).

variant databases were checked to determine the frequencies of both alleles (Section 2.14.4). The variant c.7558A>G was found at a frequency of 0.1% (5/5008) in dbSNP142 (rs527486914), a frequency of 0.1% (5/5000) in 1000 Genomes and at a frequency of 0.1623 % (35/21568) in the ExAC database including (34/7860, 0.4326%) in the south Asian population with only one reported homozygous state. The second variant c.334C>T was found at a frequency of 0.859% (43/5008) in dbSNP142 (rs112609906), a frequency of 0.86% (43/5000) in 1000 Genomes and at a frequency of 0.86 % (1048/121362) in the ExAC database including (534/16512, 3.32%) in the south Asian population with ten homozygous alleles. Moreover, a lack of amino acid conservation of the F2520 and V112 residues in vertebrates suggests that these variants may be benign.

Sanger sequencing of the terminal exon of *EYS*, which was not covered by the capture reagent, failed to identify any other variants in the genomic DNA of the affected case However, it was noted that one of the *EYS* variants (c.7558A>G, p.F2520L) disrupts the second laminin G subdomain which is essential for normal protein function (Khan et al., 2010). Furthermore, previously generated Affymetrix 6.0 SNP chip analysis showed that there were two large regions of homozygosity shared between the two affected individuals (2833 and 2910): chr6: 47,001,610 - 88,893,510 in hg19, with a size of 41.9 Mb and chr16: 31,656,080 - 48,554,250 in hg19, with a size of 16.9 Mb. *EYS* was in the largest region spanning chr6:64,429,876-65,531,616 in hg19, suggesting that one or both of these *EYS* variants may be the pathogenic cause of disease in these cases. These results were considered to be uncertain and remain to be proven.

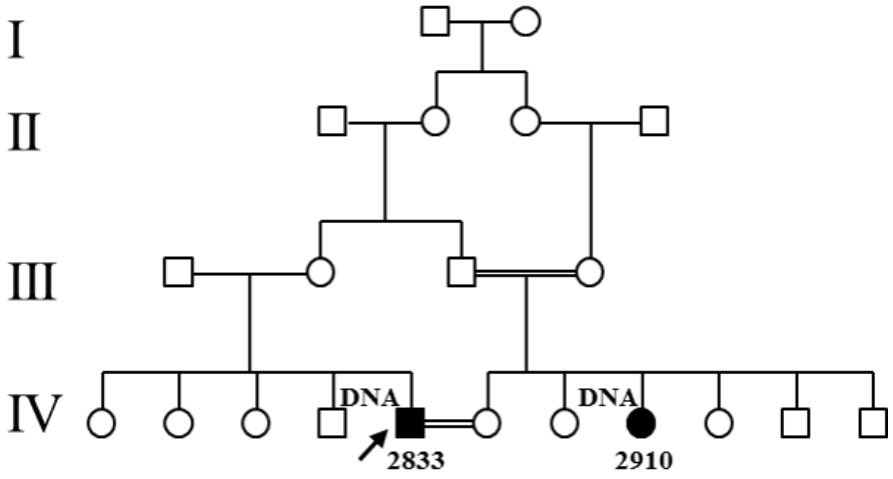

Figure 3.14. Pedigree of family MA4. Individuals from whom DNA was available are numbered and the proband is indicated by an arrow. (Adapted from Watson et al., 2014).

Chr	Position	Gene	Coding Effect	cDNA change4	Protein change	BLOSUM 62	AGVGD class	SIFT prediction	MAPP prediction	Zygosity	Protein Domain	Segregates
1	5969225	*NPHP4*	missense	NM_015102.3:c.1490C>G	p.Pro497Arg	-2	C0	Deleterious	bad	Het		
1	94544183	*ABCA4*	missense	NM_000350.2:c.1319A>G	p.Tyr440Cys	-2	C15	Tolerated	good	Het	Rim ABC transporter	
1	197297965	*CRB1*	missense	NM_201253.2:c.484G>A	p.Val162Met	1	C0	Tolerated	good	Het	EGF	
1	215848645	*USH2A*	missense	NM_206933.2:c.12608A>G	p.Gln4203Arg	1	C0	Tolerated	good	Het	Fibronectin, type III	
4	123663048	*BBS12*	start loss	NM_152618.2:c.1A>C	p.?	NA	NA	NA	NA	Het		
4	187118692	*CYP4V2*	missense	NM_207352.3:c.610G>A	p.Ala204Thr	0	C0	Deleterious	bad	Het	Cytochrome P450	
6	**64498971**	***EYS***	**missense**	**NM_001142800.1:c.7558A>G**	**p.Phe2520Leu**	**0**	**C0**	**Tolerated**	**unknown**	**Homo**	**Laminin G, subdomain 2**	**YES**
6	**66204970**	***EYS***	**missense**	**NM_001142800.1:c.334C>T**	**p.Val112Ile**	**3**	**C0**	**Tolerated**	**good**	**Homo**		**YES**
6	135726089	*AHI1*	frameshift	NM_017651.4:c.2988delT	p.Val997Serfs*20	NA	NA	NA	NA	Het		
8	87645092	*CNGB3*	missense	NM_019098.4:c.1208G>A	p.Arg403Gln	1	C0	Deleterious	bad	Het		
9	103059231	*INVS*	missense	NM_014425.2:c.2819G>A	p.Arg940Gln	1	C0	Tolerated	good	Het	IQ motif, EF-hand binding site	
10	73537449	*CDH23*	missense	NM_022124.5:c.4858G>A	p.Val1620Met	1	C15	Deleterious	bad	Het	Cadherin	
11	76893481	*MYO7A*	missense	NM_000260.3:c.3121G>T	p.Val1041Phe	-1	C0	Deleterious	good	Het	MyTH4 domain	
12	48371141	*COL2A1*	missense	NM_001844.4:c.3235G>A	p.Ala1079Thr	0	C0	Tolerated	good	Het		
15	12084	*NR2E3*	missense	NM_014249.2:c.1186G>A	p.Gly396Arg	-2	C65	Deleterious	unknown	Het	Retinoid X receptor	
17	63221207	*RGS9*	missense	NM_003835.3:c.1495T>C	p.Ser499Pro	-1	C0	Deleterious	unknown	Het		
17	72916365	*USH1G*	missense	NM_173477.2:c.566G>A	p.Arg189Gln	1	C0	Tolerated	good	Het		
17	79502218	*FSCN2*	missense	NM_001077182.2:c.967G>A	p.Ala323Thr	0	C0	Tolerated	good	Het	Fascin domain	
X	32509447	*DMD*	missense	NM_004006.2:c.2569C>T	p.Pro857Ser	-1	C0	Tolerated	good	Hemi	Spectrin repeat	

Table 3.14. List of candidate variants after alignment, variant calling and filtering for patient 2833 (male) for family MA4. Teasted variants of uncertain significance are orange shaded**.** Chr = chromosome, NA = not annotated, Homo = homozygous, Het = heterozygous and Hemi = hemizygous. (Adapted from Watson et al., 2014).

3.2.2.2 Genetic analysis of family MA5

For family MA5, the history suggests dominant inheritance of a CRD phenotype (Figure 3.15) but X-linked inheritance is also possible. The filtered variant list following analysis of patient 2278 included six variants (Table 3.15). Based on the phenotype and mode of inheritance, none were highlighted as possible causative variants for CRD in this family. However, all variants were tested for segregation and all were either shown to be sequencing artefacts or they did not segregate with the disease phenotype in the family.

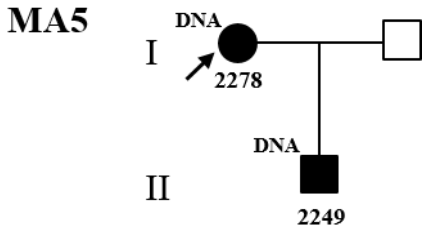

Figure 3.15. Pedigree of family MA5. Individuals from whom DNA was available are numbered and the proband is indicated by an arrow. (Adapted from Watson et al., 2014).

3.2.2.3 Genetic analysis of family MA12

For family MA12, the family history suggested consanguineous recessive inheritance and affected individuals were diagnosed with CRD (Figure 3.16). According to the zygosity of variants generated from targeted sequencing of case 1024 (Table 3.16), one homozygous splice variant in *PROM1* and two heterozygous missense variants in *CDH23* were highlighted as possible candidate causative variants for the disease. Neither though are a perfect fit for the phenotype. Recessive mutations in *PROM1* cause severe RP with macular involvement (Zhang et al., 2007) and recessive mutations in *CDH23* usually cause USH (Bork et al., 2001). The absence of segregation in other family members suggested that these variants were not the pathogenic cause of disease in this family.

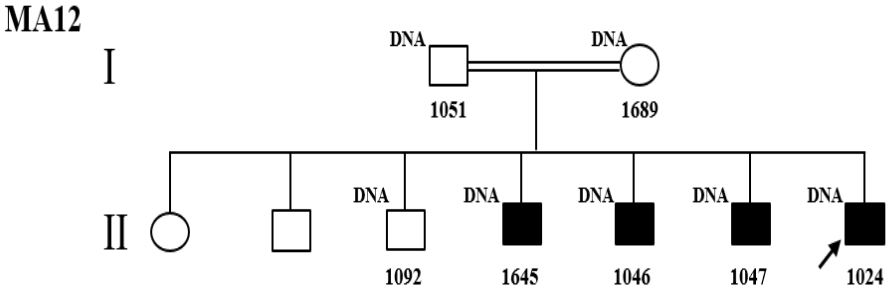

Figure 3.16. Pedigree of family MA12. Individuals from whom DNA was available are numbered and the proband is indicated by an arrow. (Adapted from Watson et al., 2014).

Chr	Position	Gene	Coding Effect	cDNA change	Protein change	BLOSUM 62	AGVGD class	SIFT prediction	MAPP prediction	Zygosity	Protein Domain	Segregates
1	215844373	*USH2A*	missense	NM_206933.2:c.14074G>A	p.Gly4692Arg	-2	C65	Deleterious	bad	Het	Fibronectin, type III	No
2	96942978	*SNRNP200*	missense	NM_014014.4:c.5933G>C	p.Gly1978Ala	0	C0	Tolerated	good	Het	Sec63 domain	No
10	13336486	*PHYH*	missense	NM_006214.3:c.356C>T	p.Thr119Met	-1	C0	Deleterious	bad	Het	Phytanoyl-CoA dioxygenase	No
16	16284103	*ABCC6*	missense	NM_001171.5:c.1553G>A	p.Arg518Gln	1	C0	Tolerated	good	Het	transmembrane domain	No
16	53653005	*RPGRIP1L*	missense	NM_015272.2:c.3548C>G	p.Ala1183Gly	0	C0	Deleterious	bad	Homo		No
X	49076224	*CACNA1F*	In-frame	NM_005183.2:c.2442_2444dupTCC	p.Glu825dup	NA	NA	NA	NA	Het		A

Table 3.15. List of candidate variants after alignment, variant calling and filtering for patient 2278 (female) for family MA5. Chr = chromosome, NA = not annotated. Homo = homozygous. Het = heterozygous and A = artefact. (Adapted from Watson et al., 2014).

Chr	Position	Gene	Coding Effect	cDNA change12	Protein change	BLOSUM 62	AGVGD class	SIFT prediction	MAPP prediction	Zygosity	Protein Domain	Segregates
4	15982163	*PROM1*	splicing?	NM_006017.2:c.2374-4dupG	p.?	NA	NA	NA	NA	Homo		NO
6	5304	*CFB*	missense	NM_001710.5:c.26T>A	p.Leu9His	-3	C0	Deleterious	bad	Het	Complement B/C2	
9	2718127	*KCNV2*	missense	NM_133497.3:c.388A>C	p.Thr130Pro	-1	C0	Deleterious	bad	Het	Potassium channel, voltage dependent, Kv, tetramerisation	
10	73553052	*CDH23*	missense	NM_022124.5:c.6367G>A	p.Gly2123Arg	-2	C65	Deleterious	bad	Het	Cadherin	NO
10	73563067	*CDH23*	missense	NM_022124.5:c.7762G>C	p.Glu2588Gln	2	C0	Tolerated	good	Het	Cadherin	NO
12	76740134	*BBS10*	missense	NM_024685.3:c.1631A>G	p.Asn544Ser	1	C0	Tolerated	good	Het		
12	88454728	*CEP290*	missense	NM_025114.3:c.6401T>C	p.Ile2134Thr	-1	C0	Deleterious	bad	Het		
16	56534761	*BBS2*	splicing?	NM_031885.3:c.1397+5C>G	p.?	NA	NA	NA	NA	Het		
17	63221207	*RGS9*	missense	NM_003835.3:c.1495T>C	p.Ser499Pro	-1	C0	Deleterious	unknown	Het		
17	72916338	*USH1G*	missense	NM_173477.2:c.593A>C	p.His198Pro	-2	C0	Tolerated	bad	Het		
20	10625830	*JAG1*	missense	NM_000214.2:c.2188A>G	p.Met730Val	1	C0	Tolerated	bad	Het	EGF, extracellular	

Table 3.16. List of candidate variants after alignment, variant calling and filtering for patient 1024 (male) for family MA12. Chr = chromosome, NA = not annotated, Homo = homozygous and Het = heterozygous. (Adapted from Watson et al., 2014).

3.2.2.4 Genetic analysis of family MA13

For MA13, family history suggested recessive inheritance of RP (Figure 3.17). On the basis of zygosity and assumed recessive inheritance, the variant list generated from case 863 (Table 3.17) identified missense variants in *GPR98* and *MYO7A* as the best candidates, though mutations in these genes usually cause recessive Usher syndrome (Jacobson et al., 2008a). Segregation analysis confirmed that these variants were not the cause of disease symptoms in this family.

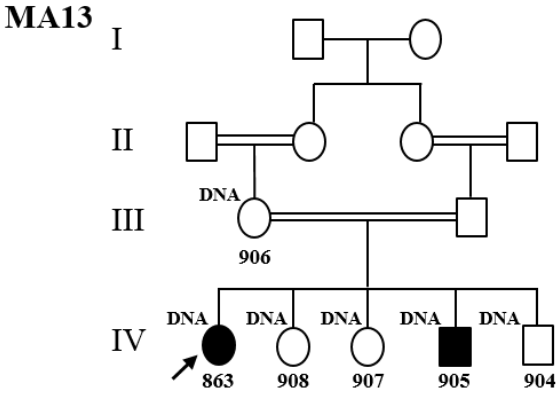

Figure 3.17. Pedigree of family MA13. Individuals from whom DNA was available are numbered and the proband is indicated by an arrow. (Adapted from Watson et al., 2014).

3.2.2.5 Genetic analysis of family MA14

For MA14, family history suggested RP with recessive inheritance due to an autozygous mutation in each case (Figure 3.18). The variant lists for patient 1518 (Table 3.18) identified two heterozygous variants in *BBS12* and one in *FSCN2* as possible candidates though neither option appeared to fit the observed phenotype perfectly. Following analysis of the other affected sibling (1527) these variants were shown to be either sequencing artefacts or they did not segregate with the disease phenotype and so were unlikely to be the pathogenic cause of disease in this family.

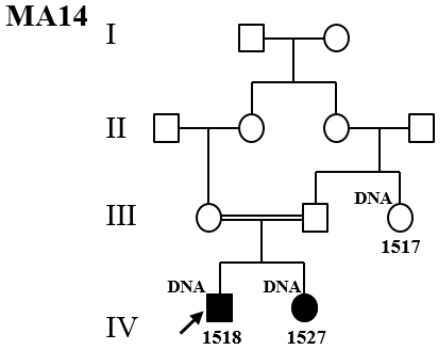

Figure 3.18. Pedigree of family MA14. Individuals from whom DNA was available are numbered and the proband is indicated by an arrow. (Adapted from Watson et al., 2014).

Chr	Position	Gene	Coding Effect	cDNA change	Protein change	BLOSUM 62	AGVGD class	SIFT prediction	MAPP prediction	Zygosity	Protein Domain	Segregates
4	100503136	*MTTP*	missense	NM_000253.2:c.136C>G	p.Arg46Gly	-2	C0	Tolerated	good	Het	Lipid transport protein, N-terminal	
5	89924514	*GPR98*	missense	NM_032119.3:c.1374T>A	p.Phe458Leu	0	C15	Deleterious	bad	Het		No
5	90149261	*GPR98*	missense	NM_032119.3:c.17365A>G	p.Lys5789Glu	1	C0	Tolerated	good	Het		A
9	2718127	*KCNV2*	missense	NM_133497.3:c.388A>C	p.Thr130Pro	-1	C0	Deleterious	bad	Het	K channel, voltage dependent, K tetramerization	
9	117266942	*DFNB31*	missense	NM_015404.3:c.140C>A	p.Thr47Asn	0	C0	Tolerated	good	Het		
11	76891457	*MYO7A*	missense	NM_000260.3:c.2624C>G	p.Ala875Gly	0	C0	Tolerated	bad	Het		No
11	76910630	*MYO7A*	missense	NM_000260.3:c.4619C>T	p.Ala1540Val	0	C0	Tolerated	unknown	Het	FERM domain	No

Table 3.17. List of candidate variants after alignment, variant calling and filtering for patient 863 (female) for family MA13. Chr = chromosome, Het = heterozygous and A = artefact. (Adapted from Watson et al., 2014).

Chr	Position	Gene	Coding Effect	cDNA change14	Protein change	BLOSUM 62	AGVGD class	SIFT prediction	MAPP prediction	Zygosity	Protein Domain	Segregates
4	15517532	*CC2D2A*	missense	NM_001080522.2:c.922T>C	p.Phe308Leu	0	C0	Tolerated	good	Het		
4	123664710	*BBS12*	missense	NM_152618.2:c.1663G>A	p.Glu555Lys	1	C0	Tolerated	good	Het	Chaperonin Cpn60/TCP-1	A
4	123665061	*BBS12*	missense	NM_152618.2:c.2014G>A	p.Ala672Thr	0	C55	Deleterious	bad	Het		No
5	178418549	*GRM6*	missense	NM_000843.3:c.733A>G	p.Ile245Val	3	C15	Tolerated	bad	Homo	Extracellular ligand-binding receptor	
6	72892193	*RIMS1*	missense	NM_014989.4:c.1019C>T	p.Ala340Val	0	C0	Tolerated	good	Het		
6	137193331	*PEX7*	splicing?	NM_000288.3:c.748-5dupT	p.?	NA	NA	NA	NA	Het		
9	2718127	*KCNV2*	missense	NM_133497.3:c.388A>C	p.Thr130Pro	-1	C0	Deleterious	bad	Het	K channel, voltage dependent, K tetramerization	
11	66283020	*BBS1*	missense	NM_024649.4:c.442G>A	p.Asp148Asn	1	C0	Tolerated	good	Het		
11	119216338	*MFRP*	missense	NM_031433.2:c.433G>A	p.Gly145Arg	-2	C25	Deleterious	bad	Het	CUB	
16	53705492	*RPGRIP1L*	missense	NM_015272.2:c.1033C>A	p.Gln345Lys	1	C0	Tolerated	good	Het		
17	63221207	*RGS9*	missense	NM_003835.3:c.1495T>C	p.Ser499Pro	-1	C0	Deleterious	unknown	Het		
17	79495853	*FSCN2*	missense	NM_001077182.2:c.296G>T	p.Arg99Leu	-2	C0	Deleterious	bad	Het	Fascin domain	A

Table 3.18. List of candidate variants after alignment, variant calling and filtering for patient 1518 (female) for family MA14. Chr = chromosome, NA = not annotated, Homo = homozygous, Het = heterozygous and A = artefact. (Adapted from Watson et al., 2014).

3.2.2.6 Genetic analysis of family MA17

For family MA17, the family history suggested recessive inheritance of RCD caused by an autozygous mutation (Figure 3.19). Based on the zygosity, no obvious candidates could be identified from the final variant list of patient 3347 (Table 3.19).

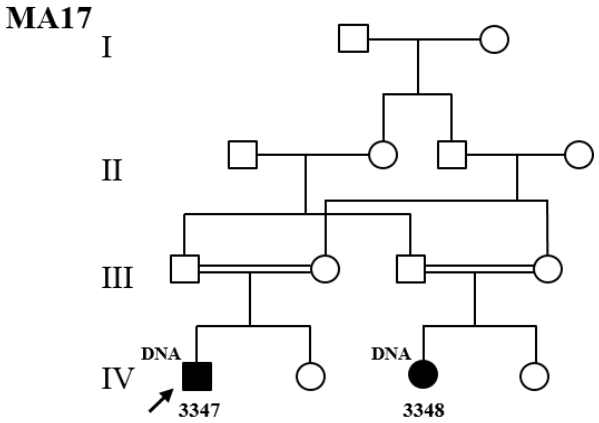

Figure 3.19. Pedigree of family MA17. Individuals from whom DNA was available are numbered and the proband is indicated by an arrow. (Adapted from Watson et al., 2014).

3.2.2.7 Genetic analysis of family MA19

For family MA19, the family history suggested recessive inheritance of RCD with an autozygous mutation (Figure 3.20). The variant list of patient 1885 (Table 3.20) identified compound heterozygous variants in *CC2D2A* and *PCDH15* as well as a variant in *WFS1* with a high pathogenicity profile as possible candidates although none of the options appeared to fit the observed phenotype perfectly. Analysis of family members from whom DNA was available confirmed three of the putative variants were artefacts and the remaining ones in CC2D2A and WFS1 did not segregate with disease.

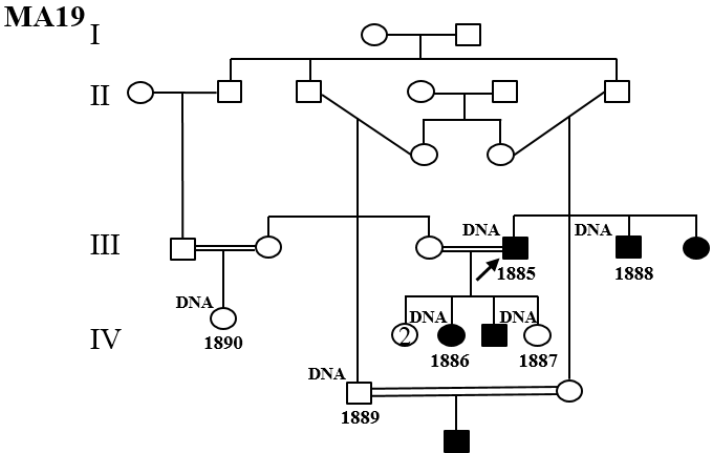

Figure 3.20. Pedigree of family MA19. Individuals from whom DNA was available are numbered and the proband is indicated by an arrow. (Adapted from Watson et al., 2014).

Chr	Position	Gene	Coding Effect	cDNA change17	Protein change	BLOSUM 62	AGVGD class	SIFT prediction	MAPP prediction	Zygosity	Protein Domain	Segregates
1	5969225	*NPHP4*	missense	NM_015102.3:c.1490C>G	p.Pro497Arg	-2	C0	Deleterious	bad	Het		
1	185976299	*HMCN1*	missense	NM_031935.2:c.4515C>G	p.Asp1505Glu	2	C0	Tolerated	good	Het	Immunoglobulin I-set	
1	216348809	*USH2A*	missense	NM_206933.2:c.4412G>C	p.Arg1471Thr	-1	C0	Tolerated	good	Het		
1	243652316	*SDCCAG8*	missense	NM_006642.3:c.1986G>T	p.Arg662Ser	-1	C0	Deleterious	bad	Het		
5	82816753	*VCAN*	missense	NM_004385.4:c.2628T>A	p.His876Gln	0	C0	Deleterious	bad	Het		
5	90024663	*GPR98*	missense	NM_032119.3:c.10339G>A	p.Glu3447Lys	1	C0	Tolerated	good	Het	EAR	
7	92147143	*PEX1*	missense	NM_000466.2:c.686A>G	p.Asn229Ser	1	C0	Tolerated	unknown	Het		
9	2718127	*KCNV2*	missense	NM_133497.3:c.388A>C	p.Thr130Pro	-1	C0	Deleterious	bad	Het	K channel, voltage dependent, K tetramerization	
9	120475128	*TLR4*	missense	NM_138554.3:c.722A>G	p.Asn241Ser	1	C0	Tolerated	good	Het	Toll-like receptor	
10	102568919	*PAX2*	missense	ENST00000370296.1:c.914C>T	p.Ser305Leu	-2	C0	Tolerated	good	Het	Paired-box protein 2 C-terminal	
11	86662343	*FZD4*	missense	NM_012193.3:c.1455G>T	p.Leu485Phe	0	C0	Deleterious	bad	Het	Frizzled protein	
12	88472996	*CEP290*	missense	NM_025114.3:c.5237G>A	p.Arg1746Gln	1	C0	Tolerated	good	Het		
X	13765025	*OFD1*	missense	NM_003611.2:c.781G>A	p.Val261Ile	3	C0	Tolerated	good	Hemi		

Table 3.19. List of candidate variants after alignment, variant calling and filtering for patient 3347 (male) for family MA17. Chr = chromosome, Hemi = hemizygous and Het = heterozygous. (Adapted from Watson et al., 2014).

Chr	Position	Gene	Coding Effect	cDNA change19	Protein change	BLOSUM 62	AGVGD class	SIFT prediction	MAPP prediction	Zygosity	Protein Domain	Segregates
1	216270422	*USH2A*	splicing?	NM_206933.2:c.4758+3A>G	p.?	NA	NA	NA	NA	Het		
4	15982163	*PROM1*	splicing?	NM_006017.2:c.2374-4dupG	p.?	NA	NA	NA	NA	Het		
4	6303810	*WFS1*	missense	NM_006005.3:c.2288A>C	p.His763Pro	-2	C15	Deleterious	bad	Het		NO
4	15513014	*CC2D2A*	in-frame	NM_001080522.2:c.685_687delGAA	p.Glu229del	NA	NA	NA	NA	Het		NO
4	15539735	*CC2D2A*	missense	NM_001080522.2:c.1978G>C	p.Val660Leu	1	C0	Tolerated	good	Het		A
4	123665061	*BBS12*	missense	NM_152618.2:c.2014G>A	p.Ala672Thr	0	C55	Deleterious	bad	Het		
5	90149261	*GPR98*	missense	NM_032119.3:c.17365A>G	p.Lys5789Glu	1	C0	Tolerated	good	Het		
6	135787297	*AHI1*	missense	NM_017651.4:c.404A>C	p.Gln135Pro	-1	C0	Tolerated	unknown	Het		
8	87645092	*CNGB3*	missense	NM_019098.4:c.1208G>A	p.Arg403Gln	1	C0	Deleterious	bad	Het		
9	120476570	*TLR4*	missense	NM_138554.3:c.2164A>G	p.Ile722Val	3	C25	Deleterious	bad	Het	Toll/interleukin-1 receptor homology domain	
10	55582584	*PCDH15*	frameshift	NM_001142763.1:c.4923delT	p.Glu1642Argfs*5	NA	NA	NA	NA	Het		A
10	55721600	*PCDH15*	missense	NM_001142763.1:c.2936A>C	p.Tyr979Ser	-2	C0	Deleterious	good	Het	Cadherin	A
12	76740134	*BBS10*	missense	NM_024685.3:c.1631A>G	p.Asn544Ser	1	C0	Tolerated	good	Het		
X	31854856	*DMD*	missense	NM_004006.2:c.7179A>C	p.Lys2393Asn	0	C0	Deleterious	bad	Het	Dystrophin/utrophin	A

Table 3.20. List of candidate variants after alignment, variant calling and filtering for patient 1885 (male) for family MA19. Chr = chromosome, NA = not annotated, Het = heterozygous and A= artefact. (Adapted from Watson et al., 2014).

3.2.2.8 Genetic analysis of family MA20

For family MA20, the history suggested RP with recessive inheritance due to an autozygous mutation (Figure 3.21). The variant list of case 472 (Table 3.21) identified a single homozygous missense variant in *TRPM1* as well as compound heterozygous variants in *CEP290* and a variant in *CA4*, though none of these candidates appeared to exactly fit the observed phenotype. As suspected, these variants were either artefacts or failed to segregate with disease in this family, suggesting that the pathogenic cause of disease has yet to be identified.

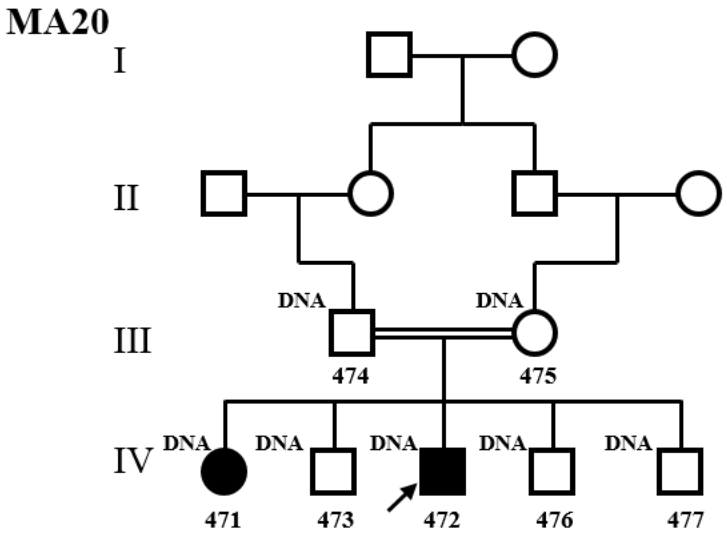

Figure 3.21. Pedigree of family MA20. Individuals from whom DNA was available are numbered and the proband is indicated by an arrow. (Adapted from Watson et al., 2014).

Chr	Position	Gene	Coding Effect	cDNA change20	Protein change	BLOSUM 62	AGVGD class	SIFT prediction	MAPP prediction	Zygosity	Protein Domain	Segregates
2	110904416	NPHP1	splicing?	NM_000272.3:c.1438-4C>T	p.?	NA	NA	NA	NA	Het		
2	96955677	SNRNP200	missense	NM_014014.4:c.2800A>G	p.Thr934Ala	0	C0	Tolerated	good	Het		
5	90149261	GPR98	missense	NM_032119.3:c.17365A>G	p.Lys5789Glu	1	C0	Tolerated	good	Het		
6	42689868	PRPH2	missense	NM_000322.4:c.205G>T	p.Val69Leu	1	C0	Tolerated	good	Het	Tetraspanin	
6	135776946	AHI1	missense	NM_017651.4:c.1270A>G	p.Ile424Val	3	C0	Tolerated	good	Het		
11	76891457	MYO7A	missense	NM_000260.3:c.2624C>G	p.Ala875Gly	0	C0	Tolerated	bad	Het		
12	88472996	CEP290	missense	NM_025114.3:c.5237G>A	p.Arg1746Gln	1	C0	Tolerated	good	Het		A
12	88519039	CEP290	missense	NM_025114.3:c.1173G>T	p.Glu391Asp	2	C0	Tolerated	good	Het		A
15	31318408	TRPM1	missense	NM_002420.4:c.3497A>T	p.His1166Leu	-3	C0	Tolerated	good	Homo		NO
17	58233966	CA4	missense	NM_000717.3:c.158C>T	p.Pro53Leu	-3	C65	Deleterious	bad	Het	Alpha carbonic anhydrase	A
17	63221207	RGS9	missense	NM_003835.3:c.1495T>C	p.Ser499Pro	-1	C0	Deleterious	unknown	Het		
X	32459413	DMD	missense	NM_004006.2:c.3805C>A	p.His1269Asn	1	C0	Tolerated	good	Het	Spectrin/alpha-actinin	A
X	38163895	RPGR	missense	NM_001034853.1:c.927G>T	p.Leu309Phe	0	C0	Deleterious	good	Het	Regulator of chromosome condensation, RCC1	A

Table 3.21. List of candidate variants after alignment, variant calling and filtering for patient 472 (male) for family MA20. Chr = chromosome, NA = not annotated, Homo = homozygous, Het = heterozygous and A = artefact. (Adapted from Watson et al., 2014).

3.3 Discussion

In the work described in this chapter, the genetic basis of retinal dystrophy was investigated in twenty families using targeted capture enrichment and next-generation sequencing technology. Likely pathogenic mutations were identified in 12 out of 20 cases (60%). A list of these mutations is highlighted in Table 3.22. The mutations consisted of previously reported mutations of clinical significance in *ABCA4* (c.6088C>T, p.R2030* and c.5882G>A, p.G1961E), *RDH12* (c.601T>C, p.C201R and c.506G>A, p.R169Q), *PROM1* (c.1117C>T, p.R373C), *GUCY2D* (c.2512C>T, p.R838C), *RPGRIP1* (c.3565C>T, p.R1189*), *BBS2* (c.1895G>C, p.R632P) and *SPATA7* (c.253C>T, p.R85*); and new mutations in *CRB1* (c.2832_2842+23del), *USH2A* (c.12874A>G, p.N4292D), *RP2* (c.884-1G>T) and *ABCA4* (c.3328+1G>C). In eight cases the pathogenic mutation could not be unambiguously identified.

3.3.1. How useful was the targeted capture reagent?

The approach used in this study differed from previously described methods (Harakalova et al., 2011, which usually pool the samples after the hybridization step to multiplex onto one lane of the sequencer. Instead the samples were tagged and pooled in batches of four prior to enrichment. This approach refined the use of the targeted capture technology, facilitating the enrichment of exons from pooled samples using a single aliquot of capture reagent. This technology contributes to the development of a RD diagnostic screening method that might benefit RD patients by reducing costs associated with using a single aliquot of capture reagent to successfully analyse up to four samples in a single experiment.

The strategy used in this chapter succeeded in detecting the causative mutations in 60% (12/20) of the patients tested. The mutations included single nucleotide (missense, nonsense and splice site mutations) and indel (insertion and deletion) changes that existed in homozygous or heterozygous (dominant and compound heterozygous) forms. The use of targeted next-generation sequencing for retinal disease diagnosis has been previously described, using a range of target enrichment methods. Studies detailing a range of approaches are listed in Table 3.23.

ID	Diagnosis	Inheritance Pattern	Chr	Position	Gene	Coding effect	cDNA change	Protein change	BLOSUM62	AGVGD class	SIFT prediction	MAPP prediction	Zygosity
MA1	LCA	Rec.	1	197398744	*CRB1*	FS	NM_201253.2:c.2832_2842+23del	p.?	NA	NA	NA	NA	Homo
MA2	CRD	Rec/Dom.	1	94471056	*ABCA4*	NS	NM_000350.2:c.6088C>T	p.Arg2030*	NA	NA	NA	NA	Homo
MA3	RP	Rec.	1	215848379	*USH2A*	MS	NM_206933.2:c.12874A>G	p.Asn4292Asp	1	*C15*	*Deleterious*	bad	Homo
MA4	RP	Rec.	None confirmed										
MA5	CRD/MD	Dom.	None confirmed										
MA6	RP	Rec.	14	68193850	*RDH12*	MS	NM_152443.2:c.601T>C	p.Cys201Arg	*-3*	C0	*Deleterious*	bad	Homo
MA7	CRD	Dom.	4	16014922	*PROM1*	MS	NM_006017.2:c.1117C>T	p.Arg373Cys	*-3*	C0	*Deleterious*	bad	Het
MA8	RP with Maculopathy	Dom./ X-linked	X	46736939	*RP2*	SP	NM_006915.2:c.884-1G>T	p.?	NA	NA	NA	NA	Homo
MA9	CRD/MD	Dom.	17	7918018	*GUCY2D*	MS	NM_000180.3:c.2512C>T	p.Arg838Cys	*-3*	*C65*	*Deleterious*	bad	Het
MA10	CRD	Rec.	14	21813304	*RPGRIP1*	NS	NM_020366.3:c.3565C>T	p.Arg1189*	NA	NA	NA	NA	Homo
MA11	RP	Rec.	16	56530894	*BBS2*	MS	NM_031885.3:c.1895G>C	p.Arg632Pro	*-2*	*C15*	Tolerated	bad	Homo
MA12	CRD	Rec.	None confirmed										
MA13	RP	Rec.	None confirmed										
MA14	RP	Rec.	None confirmed										
MA15	CRD	Rec.	14	88883069	*SPATA7*	NS	NM_018418.4:c.253C>T	p.Arg85*	NA	NA	NA	NA	Homo
MA16	LCA	Rec.	14	68193755	*RDH12*	MS	NM_152443.2:c.506G>A	p.Arg169Gln	1	*C35*	*Deleterious*	bad	Homo
MA17	RCD	Rec.	None confirmed										
MA18	CRD	Rec.	1	94508316	*ABCA4*	SP	NM_000350.2:c.3328+1G>C	p.?	NA	NA	NA	NA	Het
				94473807	*ABCA4*	MS	NM_000350.2:c.5882G>A	p.Gly1961Glu	*-2*	*C65*	*Deleterious*	bad	Het
MA19	RCD	Rec.	None confirmed										
MA20	RP	Rec.	None confirmed										

Table 3.22. List of confirmed likely pathogenic mutations in the 20 patients study. The family ID and diagnosis of the cases studied as well as the chromosome and position of the mutation according to the human genome assembly hg19, gene, coding effect, cDNA and protein nomenclature, BLOSUM62, AGVGD class, SIFT prediction, MAPP prediction, and zygosity are shown. Rec.= recessive, Dom.= dominant, NA = not annotated, Homo = homozygous, Het = heterozygous, FS = frameshift. NS = nonsense, MS = missense and SP = splicing. (Adapted from Watson et al., 2014).

Authors	Detecting phenotypes	Library preparation		NGS instrument	Number of independent samples tested	Pathogenic mutation identified (%)
		Gene number	Method			
(Bowne et al., 2011b)	adRP	46	PCR amplicons	454GS FLX Titanium (Roche) & GAIIx (Illumina)	21	5 (24%)
(Simpson et al., 2011)	RP	45	Solid phase customised capture array (NimbleGen)	GAIIx (Illumina)	5	3 (60%)
(Shanks et al., 2013)	RP & CRD	73	Solid phase customised capture array (NimbleGen)	454GS FLX Titanium (Roche)	36	9 (25%)
(Neveling et al., 2012)	RP	111	Solid phase customised capture array (NimbleGen)	454GS FLX Titanium (Roche)	100	36 (36%)
(O'Sullivan et al., 2012)	RDs	105	Liquid phase targeted SureSelect capture (Agilent)	SOLiD 4 (Life Technologies)	50	21 (42%)
(Audo et al., 2012a)	RDs	254	Liquid phase targeted SureSelect capture (Agilent)	GAIIx (Illumina)	13	7 (54%)
(Coppieters et al., 2012)	LCA	16	PCR amplicons	GAIIx (Illumina)	17	3 (18%)
Retinome project (Watson et al., 2014)	**RDs**	**162**	**Liquid phase targeted SureSelect capture (Agilent)**	**GAIIx (Illumina)**	**20**	**12 (60%)**
(Fernandez-San Jose et al., 2015)	adRP	73	Liquid phase targeted SureSelect capture (Agilent)	Illumina MiSeq	59	27% (16/59)
(Oishi et al., 2016)	COD & CRD	193	Liquid phase targeted SureSelect capture (Agilent)	Illumina HiSeq 2500	43	12 (27.9%)
(Perez-Carro et al., 2016)	RP	75	Liquid phase targeted SureSelect capture (Agilent)	Illumina MiSeq	47	27(57.4%)

Table 3.23. Comparison of the methodological approaches in key recent publications that have used targeted high throughput NGS for retinal disease diagnosis. Retinome project is orange shaded**.** adRP = autosomal dominant retinitis pigmentosa, RP = retinitis pigmentosa, CRD = cone-rod dystrophy, COD = cone dystrophy, LCA = Leber congenital amaurosis and RDs = retinal dystrophies.

These previous studies included solid phase capture arrays (Simpson et al., 2011; Neveling et al., 2012; Shanks et al., 2013) or liquid phase capture arrays (Audo et al., 2012a; O'Sullivan et al., 2012; Fernandez-San Jose et al., 2015; Oishi et al., 2016; Perez-Carro et al., 2016). PCR amplicon-based approaches (Bowne et al., 2011b; Coppieters et al., 2012) have also been used. These methods are followed by sequencing on various machines including the ABI SOLiD (O'Sullivan et al., 2012), the Illumina Genome Analyser (Simpson et al., 2011; (Bowne et al., 2011b; Audo et al., 2012a; Coppieters et al., 2012; Fernandez-San Jose et al., 2015; Oishi et al., 2016; Perez-Carro et al., 2016) or the Roche 454 (Bowne et al., 2011b; Neveling et al., 2012; Shanks et al., 2013). In these studies of RD screening, the success rate in identifying the pathogenic mutation has varied from 18% (3 out of 17 cases studied) (Coppieters et al., 2012) to 60% (3 out of 5 cases studied) (Simpson et al., 2011) with no correlation between the identification of the pathogenic mutation rates and the library preparation methods or machines used for these studies.

A 60% success rate (12 out of 20 cases studied) places the Retinome project at the higher end of mutation rate detection (Table 3.23). One possible reason for this relatively high mutation rate detection may be that the retinome project focused on studying families with multiple affected members rather than single cases with no family history. This allowed us to assess the pathogenicity of candidate disease-causing variants by following the transmission of the mutation with the disease phenotype. It is interesting to note when studying isolated cases that several examples of *de novo* mutations have been demonstrated to be the cause of disease (Neveling et al., 2012; Shanks et al., 2013). Another possible reason for the increased detection rate in this study is the high number of consanguineous cases in the local Yorkshire population, which allows filtering on the basis of zygosity.

Although the targeted capture approach is often used, it has a several limitations. These include suboptimal capturing efficiency at repetitive regions due to binding interference of the target DNA to homologous sequences, and lack of flexibility if new regions need to be captured (Chou et al., 2010; Raca et al., 2010). In the current reagent, 9 exons, including the *RPGR-ORF15* that is known to be a hot spot for RD mutations (Pusch et al., 2002; Yang et al., 2002), could not be covered because of repetitive nature

of the sequence, suggesting that these exons may have to be analysed using alternative methods. In terms of data analysis, we observed a number of sequencing artefacts that may be due to low coverage as a result of pooling the DNA samples, low sequence quality or inaccurate variant calling. In order to reduce the number of false negative results, the stringency of variant calling algorithms was relaxed and the use of hard variant calibration and filtering was avoided. This conservative approach to capture all possible variants inevitably meant that there were also a number of false positives in the annotated variant lists. Moreover, with the rapid evolution of next generation sequencing technologies and the costs coming down, the customized targeted approach described in this chapter is no longer a cost effective method compared to WES.

3.3.2. The genes in which a pathogenic mutation was identified in the families following customized targeted capture and NGS

3.3.2.1. A *CRB1* mutation was identified in family MA1 with a diagnosis of LCA

A novel frameshift (deletion) mutation (c.2832_2842+23del) in *CRB1* gene was identified as the likely causative mutation for LCA in family MA1. CRB1 is one of three human homologues of the *Drosophila* transmembrane protein Crumbs (den Hollander et al., 1999). *Drosophila* Crumbs is required for the maintenance of apico-basal cell polarity and the adherens junction in embryonic ectodermal epithelia and has a similar function in adult fly retina (Tepass et al., 2001; Izaddoost et al., 2002). CRB1 is named after its function in the fly since a homozygous loss-of-function mutation in the gene causes a failure in cuticle development resulting in only a few "crumbs" of cuticle of the *Drosophila* embryo (Tepass and Knust, 1990). In humans, *CRB1* is located on the long arm of chromosome 1 (1q31.1). It encodes a 1406 amino acid transmembrane protein with a predicted size of 154 kDa and includes a short intracellular component as well as a transmembrane domain and a long extracellular component that contains a signal peptide, 19 EGF-like domains and three laminin A G-like domains. The N-linked glycosylation motifs in the extracellular domain of CRB1 are responsible for N-glycosylation (Kantardzhieva et al., 2005; Gosens et al., 2008).

CRB1 protein is expressed exclusively in the brain and retina (den Hollander et al., 2002) and required for appropriate photoreceptor morphogenesis. Mouse mutant models of *CRB1* show disruptions in the outer limiting membrane and loss of adhesion between photoreceptors and Muller cells. This leads to the displacement of photoreceptors and progressive retinal degeneration (Aleman et al., 2011). *Crb1*$^{-/-}$ mice also have an irregular number and size of Muller glia cell villi (van de Pavert et al., 2007). The existence of genetic modifiers is strongly suspected in *CRB1* mutant mice where the photoreceptor degeneration varies strongly according to the genetic background (Mehalow et al., 2003). This might explain why mutations in this single gene have been associated with a wide-range of retinal phenotypes that have been described including LCA, EORD, RP and autosomal recessive familial foveal retinoschisis (arFFR). No clear genotype-phenotype relationship has been established in CRB1 disease (den Hollander et al., 2004; Ehrenberg et al., 2013). For example, p.Cys948Tyr and p.Arg764Cys variants have been previously associated with LCA, EORD, RP and arFFR in both homozygous and compound heterozygous forms in patients of different ethnicities (den Hollander et al., 1999; den Hollander et al., 2001; Lotery et al., 2001; Booij et al., 2005; Tosi et al., 2009; Bujakowska et al., 2012; Srilekha et al., 2015; Vincent et al., 2016). This suggests that genetic and/or environmental factors modify the expression of the *CRB1* phenotype. However, increased retinal thickness with loss of lamination is a relatively constant feature of *CRB1*-related human diseases (Jacobson et al., 2003; Henderson et al., 2011).

Here a novel frameshift mutation is reported as causing LCA in family MA1. Among the LCA genes, *CRB1* is one of the most frequently mutated genes, representing 9-13% of all LCA cases (den Hollander et al., 2008) (Table 1.6). Almost all *CRB1* mutations that cause LCA, including the one reported here, occur in the long extracellular component of the protein; 17 mutations occur in the EGF-like domains, 17 in the laminin G-like domains, while only 2 are outside of these regions (den Hollander et al., 2004; den Hollander et al., 2008; Vincent et al., 2016) (see the public domain, www.uniprot.org), while the intracellular domain forms complexes with intracellular proteins that result in the Crumbs protein complex (Kantardzhieva et al., 2005; Bulgakova and Knust, 2009).

3.3.2.2. *ABCA4* mutations were identified in families MA2 and MA18 with a diagnosis of CRD

Screening of families MA2 and MA18 diagnosed with CRD showed that *ABCA4* was the causative gene for these cases. The *ABCA4* gene encodes the ATP-binding cassette sub-family A member 4, a membrane transporter located in the outer segment disc membranes of rods and cones (Illing et al., 1997; Molday et al., 2000). The structure of ABCA4 consists of two transmembrane domains (TMDs), two large glycosylated extracellular domains (ECD) and two internal nucleotide-binding domains (NBDs) (Linton and Higgins, 2007). ABCA4 plays a significant role in visual phototransduction, it prevents accumulation of the toxic retinoid derivative N-retinylidene-phosphatidylethanolamine (*N*-retinylidene-PE) inside the disks by transporting it across the photoreceptor outer segment disk membranes into the cytosol where it can dissociate, allowing the released all-*trans*-retinal to enter the visual cycle (Section 1.4.4) (Beharry et al., 2004; Tsybovsky et al., 2010).

Mutations in the gene encoding *ABCA4* represent the most common cause of CRD, accounting for 30% of all reported cases (Maugeri et al., 2000; Burke and Tsang, 2011). More than 800 mutations in the *ABCA4* gene have been implicated in three autosomal recessive retinal phenotypes, CRD, STGD and RP. It is also associated with AMD (Allikmets et al., 1997a; Cremers et al., 1998; Martinez-Mir et al., 1998; Fishman et al., 2003; Molday, 2015). There is no clear genotype phenotype correlation in *ABCA4* mutations. However the clinical manifestations for *ABCA4* mutation usually arRP or arCRD with severe mutations, STGD with two mild or moderate mutations and AMD with one milder heterozygous mutation (Rozet et al., 1998; Cideciyan et al., 2004; Lorenz and Preising, 2005; Valverde et al., 2007; Burke and Tsang, 2011; Riveiro-Alvarez et al., 2013). Here, a homozygous nonsense mutation (p.R2030*) in one family, and compound heterozygous mutations consist of a novel splicing mutation (c.3328+1G>C) and a missense mutation (p.G1961E) were identified as the likely cause of CRD in families MA2 and MA18 respectively. The grading system of *ABCA4* retinopathy seems consistent with the results reported here. p.R2030* is located in the second nucleotide-binding domain of the ABCA4 protein and is predicted to either lead to inactive protein or instability of the messenger RNA due to nonsense-mediated mRNA decay (Singh et al., 2006); while the G1961E allele is associated with macular atrophy and a trend to

delayed onset of symptoms, relative to other manifestations of *ABCA4* mutations (Cella et al., 2009).

3.3.2.3. An *USH2A* mutation was identified in family MA3 with a diagnosis of RP

A novel missense mutation in *USH2A* was identified as causing an RP phenotype in family MA3. Located on chromosome 1q41, *USH2A* has two alternatively spliced isoforms. The short *USH2A* isoform a consists of 21 exons and the long *USH2A* isoform b consists of 51 additional exons at the 3′ end of *USH2A* (Eudy et al., 1998). The protein usherin, encoded by *USH2A* isoform b, is a transmembrane protein of 5,202 amino acids (van Wijk et al., 2004). Usherin is expressed in the developing cochlear hair cells and the photoreceptor connecting cilium between the inner and outer segments where it is required for the maintenance of retinal photoreceptors (Liu et al., 2007).

Mutations in the *USH2A* gene were frequently reported in patients with Usher syndrome type IIA that is one of the subtypes of Usher syndrome, an autosomal recessive condition in which patients have both RP and sensorineural hearing loss (Section 1.6.3.5). More than 300 mutations including more than 70 different null alleles and several different missense mutations have been identified in the two isoforms of the *USH2A* gene in patients with USH2 (http://www.umd.be/ USH2A/gene. shtml) (Baux et al., 2007; Dreyer et al., 2008). The *USH2A* gene appears to be the major cause of USH2, accounting for approximately 50% to 75% of USH2 cases. Furthermore, 12% to 20% of non-syndromic RP patients carry mutations in *USH2A*, making it also the most frequently mutated genes in recessive RP (McGee et al., 2010). The genotype–phenotype correlations have not been very distinct in patients with *USH2A* mutations. However, certain mutations in *USH2A*, such as p.Glu767Serfs*21, have been associated mainly with the syndromic phenotype, while p.Cys759Phe has been linked with non-syndromic RP (Le Quesne Stabej et al., 2012; Blanco-Kelly et al., 2015; Lenassi et al., 2015).

The reason why some mutations in *USH2A* lead to Usher syndrome type IIA and others to nonsyndromic RP remains unknown. Among all the mutations that have been identified, only one common mutation (p. Glu767Serfs*21) has been reported frequently in several populations and has been found to have been derived from a common ancestor

(Dreyer et al., 2001), while the majority are unique pathogenic mutations observed only in one family (McGee et al., 2010). In addition, most patients have compound heterozygous mutations and in some cases, the affected siblings have the same phenotype with differences in the severity of the disease (Lenassi et al., 2015). This suggests that each phenotype may be caused by a distinct set of genotypes.

3.3.2.4. *RDH12* mutations were identified in families MA6 and MA16 with a diagnosis of RP and LCA respectively

RDH12, located on chromosome 14q23, has 7 exons and encodes an NADPH-dependent retinal reductase, belonging to a sub-family of retinol dehydrogenases that metabolize both all-*trans*-retinal and 11-*cis* retinal to their corresponding retinols (Haeseleer et al., 2002). They are also involved in the metabolism of other non-retinoid alcohols/aldehydes (Belyaeva et al., 2005). RDH12 localizes to the inner segment of rod and cone photoreceptors (Maeda et al., 2006) , where it plays this critical role in the visual cycle (Haeseleer et al., 2002; Kurth et al., 2007) (Section 1.4.4). Mutations in this gene increase susceptibility to light-induced photoreceptor apoptosis, leading to severe forms of visual impairment such as LCA13 and EORD (Janecke et al., 2004; Perrault et al., 2004; Maeda et al., 2006; Chacon-Camacho et al., 2013; Kuniyoshi et al., 2014). Patients with *RDH12* mutations showed severe loss of VA at an early age and severe reductions in ffERG amplitudes, while *RDH12*$^{-/-}$ mice showed decreasing RDH activity, slowing in the kinetics of all-*trans*-retinal reduction, delaying dark adaptation and loss of the photoreceptor outer segment after intense light (Maeda et al., 2006; Sun et al., 2007).

Five recessive mutations in *RDH12* were first reported in patients with EORD (Janecke et al., 2004), closely followed by identification of eleven distinct *RDH12* recessive mutations in patients with LCA (Perrault et al., 2004). To date, over than 60 different *RDH12* mutations have been identified accounting for approximately 3–7% of autosomal recessive RD cases (Thompson et al., 2005; Fingert et al., 2008; Valverde et al., 2009; Mackay et al., 2011a; Yucel-Yilmaz et al., 2014). These have been reported predominantly in LCA patients (Janecke et al., 2004; Perrault et al., 2004; Schuster et al., 2007; Valverde et al., 2009; Avila-Fernandez et al., 2010; Walia et al., 2010; Chacon-Camacho et al., 2013; Beryozkin et al., 2014; Yucel-Yilmaz et al., 2014) but also in EORD (Janecke et al., 2004; Valverde et al., 2009; Walia et al., 2010; Mackay et al.,

2011a; Beryozkin et al., 2014; Katagiri et al., 2014) in families with autosomal recessive inheritance pattern and in a family with autosomal dominant RP (Fingert et al., 2008) with no evidence for genotype/phenotype correlation in this gene. In our study, we found two missense mutations that had been described previously; one in the exon five of *RDH12* (p.C201R) (Sun et al., 2007) causing RP in family MA6 and the other in the same exon (p.R169Q) (Mackay et al., 2011a) causing LCA in family MA16.

3.3.2.5. A *PROM1* mutation was identified in family MA7 with a diagnosis of CRD

In family MA7 with affected members that have CRD a previously reported missense mutation in *PROM1* (p.R373C) (Yang et al., 2008; Michaelides et al., 2010) was identified to be the pathogenic cause of disease. The prominin 1 (*PROM1*) gene encodes a 5–transmembrane domain protein containing 2 large, highly glycosylated extracellular loops and a cytoplasmic tail (Corbeil et al., 2001). *PROM1* localizes at the base of the photoreceptor outer segment and interacts with protocadherin-21 (*PCDH21*) and with actin filaments, both of which play critical roles in photoreceptor disc membrane morphogenesis (Yang et al., 2008). In addition to family MA7 reported here, five other families with a heterozygous p.R373C mutation in the *PROM1* gene have been identified in previous studies (Kniazeva et al., 1999; Michaelides et al., 2003; Yang et al., 2008; Michaelides et al., 2010). In all of these families, the p.R373C mutation produces an autosomal dominant, fully penetrant retinopathy characterized by the consistent finding of bull's-eye maculopathy. There have also been cases of variable rod or rod-cone dysfunction associated with this mutation, displaying marked intra- and interfamilial variability, where the phenotypes ranged from isolated maculopathy without generalized photoreceptor dysfunction to a very severe rod-cone dysfunction and MD.

3.3.2.6. A *RP2* mutation was identified in family MA8 with a diagnosis of RP

A novel splicing variant in *RP2* causes RP with macular involvement in family MA8. The *RP2* gene encodes a polypeptide of 350 amino acids with a tubulin binding cofactor C (TBCC) homology domain and a C-terminal nucleoside diphosphate kinase (NDK) homology domain (Schwahn et al., 1998; Chapple et al., 2000). RP2 has a potentially distinct functional relevance in maintaining Golgi cohesion, targets proteins to the plasma membrane and acts as a GTPase activating protein (GAP) for ARL3, to

control protein trafficking to the primary cilia (Evans et al., 2006; Evans et al., 2010; Patil et al., 2011; Schwarz et al., 2012).

Mutations in *RP2* cause XLRP with an early age of onset and rapid disease progression (Section 1.6.3.3). Mutations in the *RPGR* gene are the most common cause of XLRP, accounting for over 70% of all cases (Vervoort et al., 2000; Breuer et al., 2002; Branham et al., 2012), while mutations in the *RP2* gene account for approximately 15-20% of XLRP cases (Hardcastle et al., 1999; Breuer et al., 2002; Branham et al., 2012). Patients with *RP2* mutations developed night blindness as an early symptom of the disease, followed by peripheral retinal degeneration and, eventually, loss of central vision. Moreover, females can be affected as severely as their male counterparts (Jayasundera et al., 2010; Churchill et al., 2013; Misky et al., 2016). Unlike *RPGR*, disease-causing mutations in *RP2* are found to be spread more uniformly throughout the gene, than those that are caused by mutations in *RPGR-ORF15*. The majority of pathogenic *RP2* mutations are null mutations, and it is likely that the novel splice mutation found in this study is also a null mutation. Most of the missense mutations found in *RP2* are in the TBCC homology domain and a pathogenic missense mutation in NDK domain has been also reported (Hardcastle et al., 1999; Sharon et al., 2003; Pelletier et al., 2007; Churchill et al., 2013). Mutations in *RP2* gene have been associated with only ocular phenotypes, however RP2 is ubiquitously expressed in human tissues. This suggests that RP2 has either a unique isoform-specific function in the retina or a redundant role in other tissues (Evans et al., 2006).

3.3.2.7. A *GUCY2D* mutation was identified in family MA9 with a diagnosis of MD

A previously reported *GUCY2D* mutation (p.R838C) (Van Ghelue et al., 2000; Wilkie et al., 2000) has been identified as causing dominant MD in family MA9. The *GUCY2D* gene (Section 1.7.4) comprises 18 coding exons, that encode a 1103 amino acid (120kD) membrane guanylate cyclase RetGC-1 (retinal guanylyl cyclase-1). This enzyme and its associated activator proteins (GCAPs) are involved in the cGMP resynthesis that is required for the recovery of the dark state after phototransduction (Section 1.4) (Kelsell et al., 1998; Hunt et al., 2010). *GUCY2D* is expressed specifically in the retina where it localizes to the nuclei and inner segments of rod and cone photoreceptors, but its

expression is much higher in cones than in rods (Dizhoor et al., 1994; Liu et al., 1994). RetGC-1 knockout (GC1ko) mice develop a cone dystrophy (Yang et al., 1999; Boye et al., 2010).

To date, more than 130 mutations of the *GUCY2D* gene have been identified as being responsible for retinal degenerations (Kelsell et al., 1998; Gregory-Evans et al., 2000; Weigell-Weber et al., 2000; Downes et al., 2001b; Payne et al., 2001; Cremers et al., 2002; Udar et al., 2003; Ito et al., 2004a; Ito et al., 2004b; Yoshida et al., 2006; Smith et al., 2007; den Hollander et al., 2008; Kitiratschky et al., 2008; Auz-Alexandre et al., 2009; Ugur Iseri et al., 2010; Garcia-Hoyos et al., 2011; Xiao et al., 2011; Xu et al., 2013; Zhao et al., 2013b; Jiang et al., 2015; Lazar et al., 2015; Oishi et al., 2016). Homozygous or compound heterozygous mutations of the *GUCY2D* gene are one of the most frequent causes of recessive LCA, accounting for 12 to 21% of this disorder, depending on the population studied (Cremers et al., 2002; den Hollander et al., 2008; Auz-Alexandre et al., 2009). Some recessive *GUCY2D* missense mutations in the catalytic domain such as p.Pro858Ser and p.Leu954Pro, surprisingly showed *in vitro* a dominant-negative effect in heterozygous carriers, indicating by a severe reduction in guanylyl cyclase activities (Tucker et al., 2004). Heterozygous *GUCY2D* mutations are one of the major causes of dominant COD/CRD/MD, and over 35% of patients with these types of dystrophies have mutations in this gene (Payne et al., 2001; Kitiratschky et al., 2008).

LCA-associated *GUCY2D* mutations are scattered across the *GUCY2D* gene, while almost all the mutations detected in COD/CRD/MD are located in exon 13 (Kelsell et al., 1998; Gregory-Evans et al., 2000; Van Ghelue et al., 2000; Weigell-Weber et al., 2000; Downes et al., 2001b; Payne et al., 2001; Udar et al., 2003; Ito et al., 2004b; Yoshida et al., 2006; Kitiratschky et al., 2008; Hunt et al., 2010; Garcia-Hoyos et al., 2011; Xiao et al., 2011; Xu et al., 2013; Zhao et al., 2013b; Jiang et al., 2015; Lazar et al., 2015). The only dominant CRD causing mutations that are not located in exon 13 are a complex mutation p.I915T/p.G917R in exon 14 (Ito et al., 2004a) and a homozygous mutation p.I949T in exon 15 (Ugur Iseri et al., 2010). Moreover, the majority of the mutations in exon 13 are clustered at codon 838 in which five distinct variants (p.R838→C/G/H/P/S) have been identified (Kelsell et al., 1998; Gregory-Evans et al., 2000; Van Ghelue et al., 2000; Weigell-Weber et al., 2000; Wilkie et al., 2000; Downes et al., 2001b; Payne et al., 2001; Udar et al., 2003; Ito et al., 2004b; Yoshida et al., 2006; Smith et al., 2007;

Kitiratschky et al., 2008; Hunt et al., 2010; Garcia-Hoyos et al., 2011; Xiao et al., 2011; Xu et al., 2013; Jiang et al., 2015; Lazar et al., 2015). Haplotype analysis has shown codon 838 to be a mutation hot spot (Payne et al., 2001; Kitiratschky et al., 2008) and the mutation that has been identified for MA9 (p.R838C) in this study is also located in this hot spot.

3.3.2.8. A *RPGRIP1* mutation was identified in family MA10 with a diagnosis of CRD

In family MA10, the affected members with CRD harbored a previously reported nonsense mutation in *RPGRIP1* (p.R1189*) (Abu-Safieh et al., 2013). Patients with *RPGRIP1* mutations develops a degeneration of both rod and cone photoreceptors with a severe loss of central VA and nystagmus early in life (Dryja et al., 2001). The RP GTPase regulator interacting protein 1, encoded by *RPGRIP1*, has different splice variants with the largest encoding a protein of 1259 amino acids with a predicted molecular weight of 144 kDa (Lu and Ferreira, 2005). *RPGRIP1* contains two-coiled coil domains that are homologous to those found in proteins involved in vesicular trafficking (Hong et al., 2001). The central region of *RPGRIP1* contains two C2 domains. Most LCA-associated missense mutations in *RPGRIP1* are located in the segment that encodes these two Ca^{2+} binding C2 domains (Roepman et al., 2005). *RPGRIP1* binds directly to the RPGR with its C-terminal RPGR interacting domain (RID) (Boylan and Wright, 2000). *RPGR* is mutated in the majority of patients with XLRP and disease-associated missense mutations in the RCC1-like domain of RPGR disrupt the interaction between RPGR and RPGRIP1, suggesting that this defect underlies the pathogenesis of RD (Roepman et al., 2000).

Previous studies (Roepman et al., 2000; Hong et al., 2001; Mavlyutov et al., 2002; Lu and Ferreira, 2005; Shu et al., 2005) have shown a prominent localization of both RPGR and RPGRIP1 proteins in the ciliary structure that connects the inner and outer segments of rod and cone photoreceptors. Studies of the retina of *RPGRIP1*$^{-/-}$and RPGR$^{-/-}$ mice showed that *RPGRIP1* prominently localized to the connecting cilium (CC) without RPGR, but that the opposite was not the case, since RPGR is absent in the CC of photoreceptors lacking RPGRIP1, indicating that RPGR is dependent on RPGRIP1 to be anchored to the connecting cilium (Zhao et al., 2003). This expression pattern of RPGRIP1 explains why mutations in the ubiquitously expressed RPGR only cause a

photoreceptor-specific phenotype (Hong et al., 2001). Missense mutations in the RID of RPGRIP1 could lead to a gain- or loss-of-binding to RPGR (Lu et al., 2005). Recessive truncating mutations in *RPGRIP1,* such as the nonsense mutation that has been found in this study in family MA10, are the most common mutations form that cause LCA6 and account for 4% to 6% of the total LCA patient population (Li, 2015).

3.3.2.9. A *BBS2* mutation was identified in family MA11 with a diagnosis of RP

A homozygous missense mutation in the *BBS2* gene was identified in family MA11, linking mutations in the *BBS2* gene with partially penetrant RP. Recessive mutations in *BBS2* have previously been associated with BBS (Section 1.6.3.6) (Forsythe and Beales, 1993; Fattahi et al., 2014; Bee et al., 2015). *BBS2* is one of the twenty BBS genes that have been identified and the majority of them are essential for the function of the BBSome, the stable core of a protein complex involved in transporting membrane proteins into and from cilia (Nachury et al., 2007; Aldahmesh et al., 2014; Scheidecker et al., 2014). Mutations in the BBS genes can account for more than 80% of BBS patients while 20% of them still lack a molecular diagnosis (Redin et al., 2012).

Mutations in *BBS2* were identified in 2001 as a cause of BBS (Nishimura et al., 2001). Since then, more than 25 mutations have been identified as causing BBS. Interestingly, specific *BBS2* mutations were reported to be involved in triallelic inheritance with the presence of three mutant alleles in both *BBS2* and *BBS6* in affected individuals in four BBS families (Katsanis et al., 2001). In the same study, two individuals who carried two *BBS2* mutations but not a *BBS6* mutation were phenotypically normal, suggesting that *BBS2* may act as a modifier in contributing to complex disease. It is interesting to note that one of the patients (AR171) reported in the previous study (Katsanis et al., 2001) was a compound heterozygote in *BBS2* for p.D104A and the mutation that we found here, p.R632P (mistakenly reported as p.R634P by Katsanis et al., 2001). This individual had also exhibited some of the clinical features of BBS including obesity and polydactyly. The p.R632P mutation reported here produced polydactyly in only one patient while the second has only RP, a result that further demonstrates the complexity of the *BBS2*-related phenotypes and the probable involvement of modifier genes. It is known that mutations in five BBS genes can cause

non-syndromic or partially penetrant retinal degeneration: *BBS1* mutations cause a wide spectrum of phenotypes ranging from non-syndromic RP to BBS (Estrada-Cuzcano et al., 2012a), a *BBS3* missense mutation was reported to cause non-syndromic RP in a single family (Aldahmesh et al., 2009a), a splice-site *BBS8* mutation was reported to cause non-syndromic RP in a single family (Riazuddin et al., 2010), a nonsense *BBS12* mutation was reported to cause late-onset retinal dysfunction with postaxial polydactyly in a single family (Pawlik et al., 2010) and *CEP290* mutations can also cause non-syndromic LCA (den Hollander et al., 2006; Vallespin et al., 2007b). The results reported here highlighted *BBS2* as a sixth BBS gene that can cause partially penetrant retinal degeneration when mutated.

3.3.2.10. A *SPATA7* mutation was identified in family MA15 with a diagnosis of CRD

In family MA15, affected members with CRD had a previously described nonsense mutation in *SPATA7* (p.R85*) (Mackay et al., 2011b). The spermatogenesis-associated protein 7 (*SPATA7*) is located on chromosome 14 at the LCA3 locus (Wang et al., 2009b) and encodes to a protein expressed in the retina, brain and many other tissues, and especially in the testes where it was first identified (Zhang et al., 2003). Despite the apparent importance of *SPATA7* in human eye disease, it has only one conserved protein domain for a predicted coiled-coil domain at amino acids 49-77 (SMART: http://smart.emblheidelberg.de; ID=Q6FI63_HUMAN).

SPATA7 directly interacts with the coiled-coil domain of RPGRIP1 at the connecting cilium of photoreceptor cells where both ciliary proteins are co-localized. In the homozygous knockout mutant mice (*Spata7*$^{-/-}$) the level of *RPRGIP1* in the retina is greatly reduced at the connecting cilium and mislocalized to the inner segment followed by mislocalization of the RHO and apoptotic photoreceptor cell death (Eblimit et al., 2015) . This functional interaction between SPATA7 and RPGRIP1 plays a key role in RPGRIP1-mediated protein trafficking across the connecting cilium between the inner and outer segment of photoreceptor cells. The apoptotic degeneration of these cells triggered by protein mislocalization is the most likely mechanism of disease pathogenesis associated with *SPATA7* mutations (Eblimit et al., 2015).

Recessive mutations in the *SPATA7* gene are associated with many types of inherited RDs including LCA3, CRD and juvenile RP, accounting for about 1.7 to 4.6% of LCA patients in British and Chinese populations respectively (Perrault et al., 2010; Li et al., 2011; Mackay et al., 2011b; Kannabiran et al., 2012; Matsui et al., 2016). The mutation identified here in *SPATA7* has been reported previously in six subjects from three consanguineous families of Pakistani and Bangladeshi origin diagnosed with LCA or severe autosomal recessive RD (Mackay et al., 2011b). All the patients who have this mutation including the patients of MA15 family have the onset of symptoms before six years of age, suggesting that, this nonsense mutation may be associated with the early onset of the disease.

3.3.3. What of the negative cases after customized targeted capture and NGS

The work described in this chapter leaves a residual cohort of patients and families with RD that could not be resolved using the methods described. The mutations causing RD in these patients may be in the RD genes known in 2010 when the retinome reagent was made, but within regions that were not targeted, such as the regulatory or deep intronic regions or one of the 9 exons of repetitive sequence not covered by the retinome reagent. Also, the mutation may be a cryptic splice site created by one of the synonymous variants that were removed during filtering. Alternatively, the mutation may be in one of the 89 additional genes that have been added to RetNet since the capturing reagent was manufactured, or it may be in a new gene that has never been implicated in RD. Nevertheless, this cohort serves as a powerful resource for further gene identification studies. Following WES of genomic DNA samples from these patients, several examples of the latter two possibilities are described in the next chapter.

Chapter 4. Using whole exome sequencing to find the pathogenic mutations in pre-screened inherited retinal dystrophy families

4.1 Introduction

The introduction of NGS has enabled large scale sequencing experiments to be undertaken in individual institutes. Although it took an international consortium 13 years to generate the first draft sequence of the human genome, it is now possible to generate the same amount of data in a matter of days at a fraction of the cost. This development in sequencing technology has revolutionized gene identification studies as it is now possible to identify mutations by sequencing the exome or genome of affected patients. Although commercial sequencing providers now provide WGS services, it remains a considerable bioinformatic challenge to annotate all the non-coding data that is generated, and in particular to filter variants of potential significance from the huge amount of sequence variation carried by each individual. Thus, the slightly cheaper option of sequencing only the encoding parts of the genome, WES, is a widely used research tool in gene identification projects. The technology used for this is the same as that used in the Retinome project (Chapter 3) but the capture array reagent targets all the exons in the genome, as well as other regions of interest such as microRNAs, rather than just a subset of genes known to be involved in inherited RDs. This chapter describes how this technology was used successfully to identify the pathogenic mutations causing inherited RDs.

The work in this chapter focuses on analysing those families in which the causative pathogenic mutation(s) was not identified by the targeted NGS strategy used in the Retinome project (Chapter 3). Unfortunately, there was insufficient DNA for any of the patients from family MA20 to allow further testing. Furthermore, the pedigree structure of family MA12 (Figure 3.16, Chapter 3) looks like X-linked inheritance and possibly a mutation in ORF15 could account for the disease in this family. The exon ORF15 of *RPGR* is a mutational hot spot for XLRP and one form of cone dystrophies (Vervoort et al., 2000; Breuer et al., 2002; Pusch et al., 2002; Sharon et al., 2003; Branham et al., 2012). However, ORF15 is difficult to sequence using traditional Sanger methods due to

a large segment of highly repetitive purine rich sequences in this exon. NGS technologies are also currently unable to generate reliable sequence for this exon, which is why ORF15 was not targeted in the Retinome project (Appendix 4). Due to these technical difficulties, it was decided to leave family MA12 to one side. Families MA12 and MA20 were therefore excluded from this study.

One or more affected members from each of the five remaining unsolved families (MA5, MA13, MA14, MA17 and MA19) were screened using WES. Prior to screening, microsatellite genotyping was performed to verify the pedigree structure of each family using the methods described in Section 2.7.1. The WES library preparation was performed following the methods described in Section 2.10.1. A representative examples of the bioanalyser analysis after samples shearing, and before and after hybridisation steps are illustrated in Appendix 7. The WES analyses were carried out according the steps described in Section 2.10.2 and the major steps in the pipeline and the WES data filtration criteria are illustrated in Figure 4.1. Genomic DNA from one affected member of MA14 and MA17 was also sent to AROS Applied Biotechnology (Denmark) for hybridization to Affymetrix 6.0 SNP chips. The genotype data obtained from this was analysed as described in Section 2.7.2.

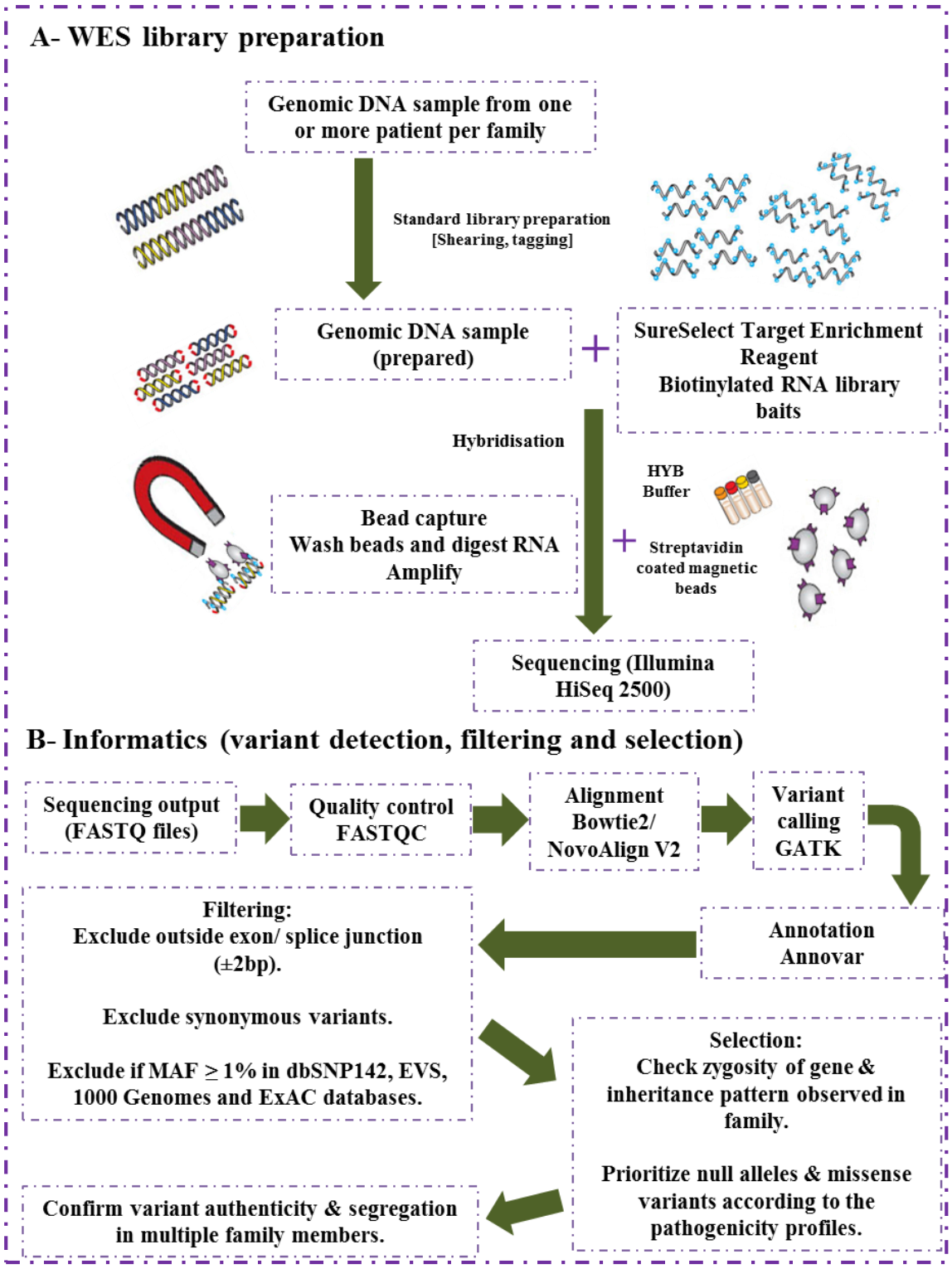

Figure 4.1. Schematic representation of the WES and variant detection data pipeline used in chapter 4. The flowchart illustrates the major steps in the pipeline including (A) WES library preparation (modified from http://www.genomics.agilent.com/article.jsp?pageId=3083) and (B) the informatics for variant detection, filtering and selection.

4.2 Results

4.2.1 WES analysis of family MA5 identifies compound heterozygous mutations in *MFSD8* causing non-syndromic retinal disease

4.2.1.1 Clinical features of the affected members in family MA5

Family MA5 is a non-consanguineous Caucasian family with three affected siblings (two males and one female) who have been diagnosed with MD (Figure 4.2). A summary of the clinical features reported is shown in Table 4.1. All three patients had experienced a progressive decline in visual acuity (VA) by the third or fourth decade of life, followed by discomfort in bright light and delayed adaptation to dark. Night vision was reported to be normal. Electrophysiological testing identified localised macular dysfunction with a normal ffERG (n=2). None of the individuals reported or displayed signs of neurological symptoms. Fundus examination revealed central outer retinal atrophy, confirmed by OCT, with a normal periphery in all cases (Figure 4.3). FAF was reduced in the central macula surrounded by a rim of increased autofluorescence. Examination findings for all siblings were consistent with a clinical diagnosis of presumed autosomal recessive MD.

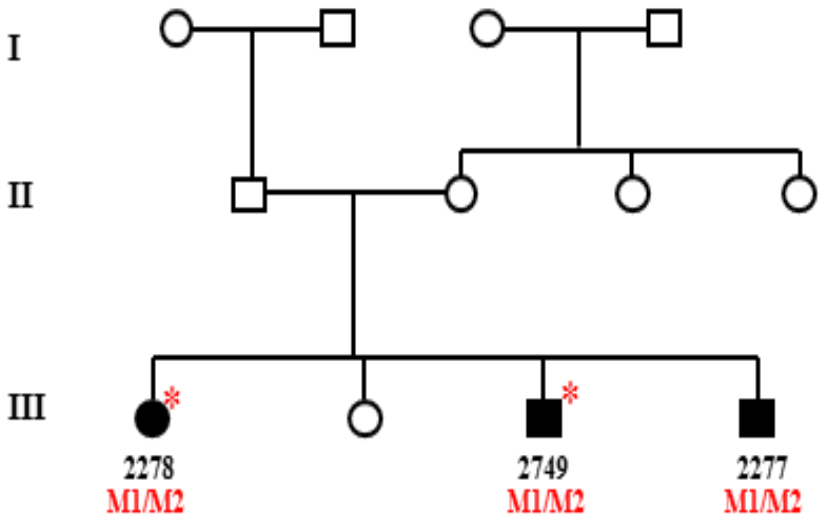

Figure 4.2. Pedigree of family MA5. The pedigree shows three generations of the family, with three affected children in the lower generation born to unrelated, unaffected parents of Caucasian origin. Individuals from whom DNA was available are numbered. * = family members for whom DNA was analysed by WES, M1= c.1394G>A, p.R465Q and M2= c.1006G>C, p.E336Q.

Patient	2278	2749	2277
Ethnicity	Caucasian		
Age of onset	30	28	Early 30s
Symptoms at onset	Gradual binocular reduction in visual acuity		
Visual Acuity	BCVA (6/18 BE); final BCVA (6/24 BE); MSE (-1D BE)	BCVA (RE 6/9, LE 6/18); final BCVA (RE 6/36, LE 6/60) with pin hole; MSE (-1D BE)	Final BCVA (6/60 BE); MSE (RE -3D, LE -3.5D)
Neurological symptoms	None		
Electrophysiology (Slit lamp biomicroscopy)	Central macular dysfunction only	Central macular dysfunction only	ND
Working diagnosis	Recessive macular dystrophy		
Fundus photograph	BE: ill-demarcated area of central macular atrophy (1-1.5 DD) with paracentral area of hyperpigmentation.	ND	BE: Well demarcated circular area with a golden sheen measuring 1.5-2 DD
OCT	ND	BE: Outer retinal atrophy at macula	
Fundus autofluorescence (FAF)	ND	Smaller circular (RE) and larger oval (LE) shaped areas of decreased FAF surrounded by halos of increased FAF towards the periphery.	BE: Circular area of reduced FAF centrally surrounded by a ring of increased FAF on edges

Table 4.1. Summary of clinical data from the three patients 2278, 2749 and 2277 from family MA5. BCVA = best corrected visual acuity, MSE = mean spherical equivalent, RE = right eye, LE = left eye, BE = both eyes, DD = disc diameters, OCT = optical coherence tomography, FAF = fundus autofluorescence, ERG = electroretinogram and ND= not done.

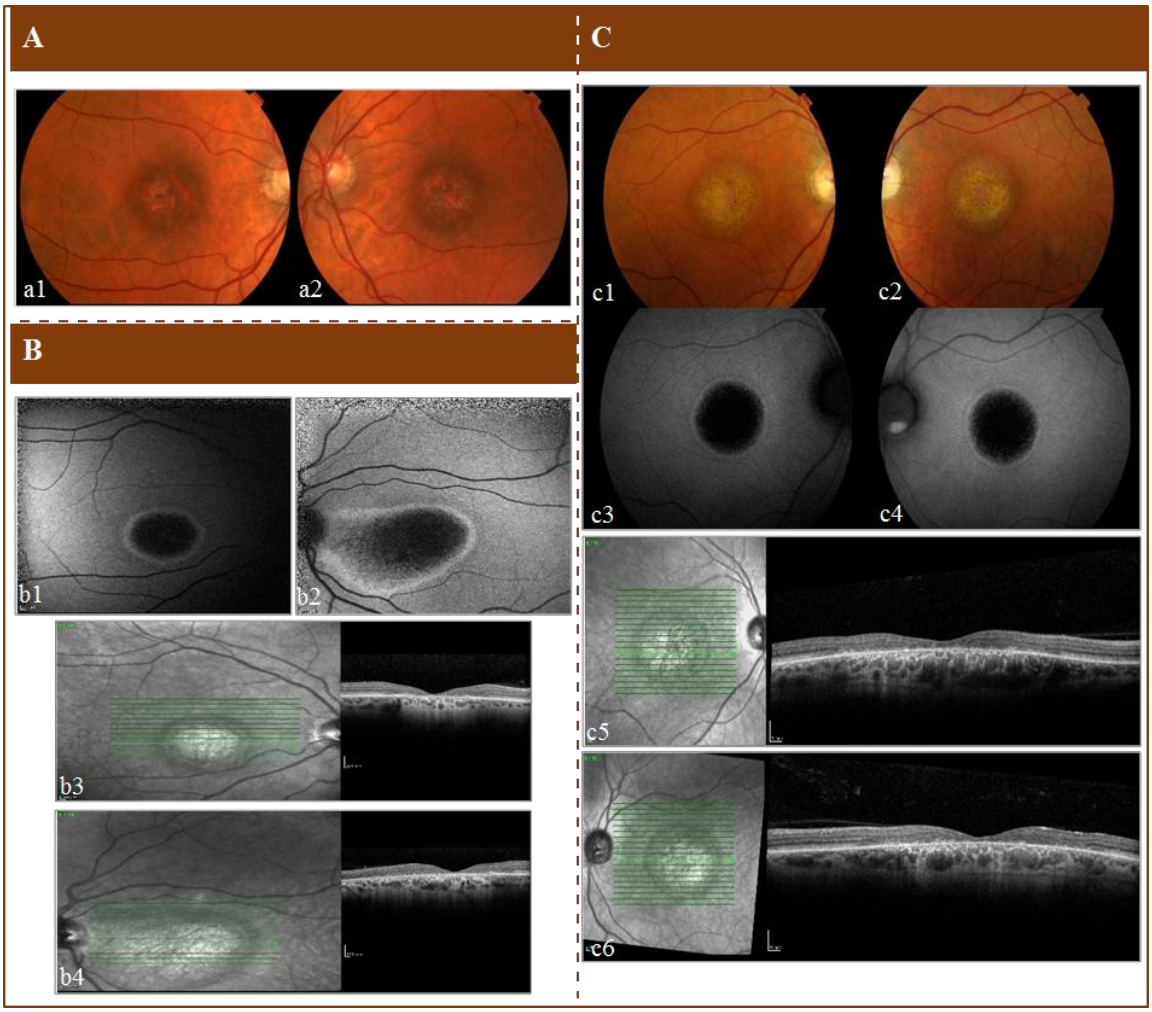

Figure 4.3. Retinal imaging of patients 2278 (A), 2749 (B) & 2277 (C) from family MA5. For 2278 (A), colour photographs of the fundus for right eye (RE, a1) and for left eye (LE, a2) show ill-demarcated areas of central macular atrophy with a paracentral area of hyperpigmentation. For 2749 (B), fundus autofluorescence (FAF) images show smaller circular (RE, b1) and larger oval-shaped (LE, b2) areas of decreased FAF surrounded by halos of increased FAF towards the periphery. For 2277 (C), colour photographs of fundus (RE, c1 and LE, c2) showed well-demarcated circular area with a golden sheen, while AF images (RE, c3 and LE, c4) showed a circular area of reduced FAF centrally surrounded by a ring of increased FAF on edges. Optical coherence tomography (OCT) for 2749 (RE, b3 and LE, b4) and 2277 (RE, c5 and LE, c6) showed outer retinal atrophy at the macula. Images courtesy of Mr Martin McKibbin (St James Hospital, Leeds).

4.2.1.2 Genetic analysis of family MA5

Genomic DNA from two affected family members (subjects 2278 and 2749, Figure 4.2) was analysed by WES. The library preparation was performed using the SureSelectXT Human All Exon reagent version 5 as described in Section 2.10.1. The WES analysis of both individuals was carried out independently according to methods described in 2.10.2. The quality of the output data was determined using FastQC tools on the Galaxy platform. A representative example of the quality control report for sample 2278 is shown in Figure 4.4. After quality control monitoring, the sequencing data was aligned against the reference genome (hg19/GRCh37) using the Bowtie 2 program. The data was then processed in SAM/BAM format using SAMtools and GATK, and a mean depth of 56.43 and 59.68 reads per base was observed for subjects 2278 and 2749 respectively.

After annotation by ANNOVAR, 57,612 and 63,757 variants were detected for patients 2278 and 2749 respectively, including both heterozygous and homozygous changes. Filtration of variant lists was done according to the strategy described in Figure 4.1. For subject 2278, a total of 20,259 variants were detected in the exonic/splice (±2bp) regions, but only 9,508 were non-synonymous or indel variants and only 827 of these were found to have a MAF ≤1% in dbSNP142, EVS, 1000 Genomes and ExAC databases. The same filtering criteria were applied to the list of variants for subject 2749, producing a total of 20,779 variants in the exonic/splice (±2bp) regions, including 9,751 non-synonymous and indel variants of which 926 were found to have a MAF ≤1%. The CADD pathogenicity score was determined for each variant listed, and 121 and 201 candidate variants with a CADD score >10 were identified respectively in patients 2278 and 2749. None of these variants occurred in genes that had previously been listed in the RetNet database (accessed February 2015). Assuming a recessive mode of inheritance from the pedigree structure, there were 15 homozygous variants and 4 genes with compound heterozygous variants that were shared between both these individuals. It was noted that one of these genes was *MFSD8* (encoding the Major Facilitator Superfamily Domain-containing protein 8) that was previously reported to have caused non-syndromic recessive MD in two families (Roosing et al., 2015). *MFSD8* therefore became the top candidate in this family.

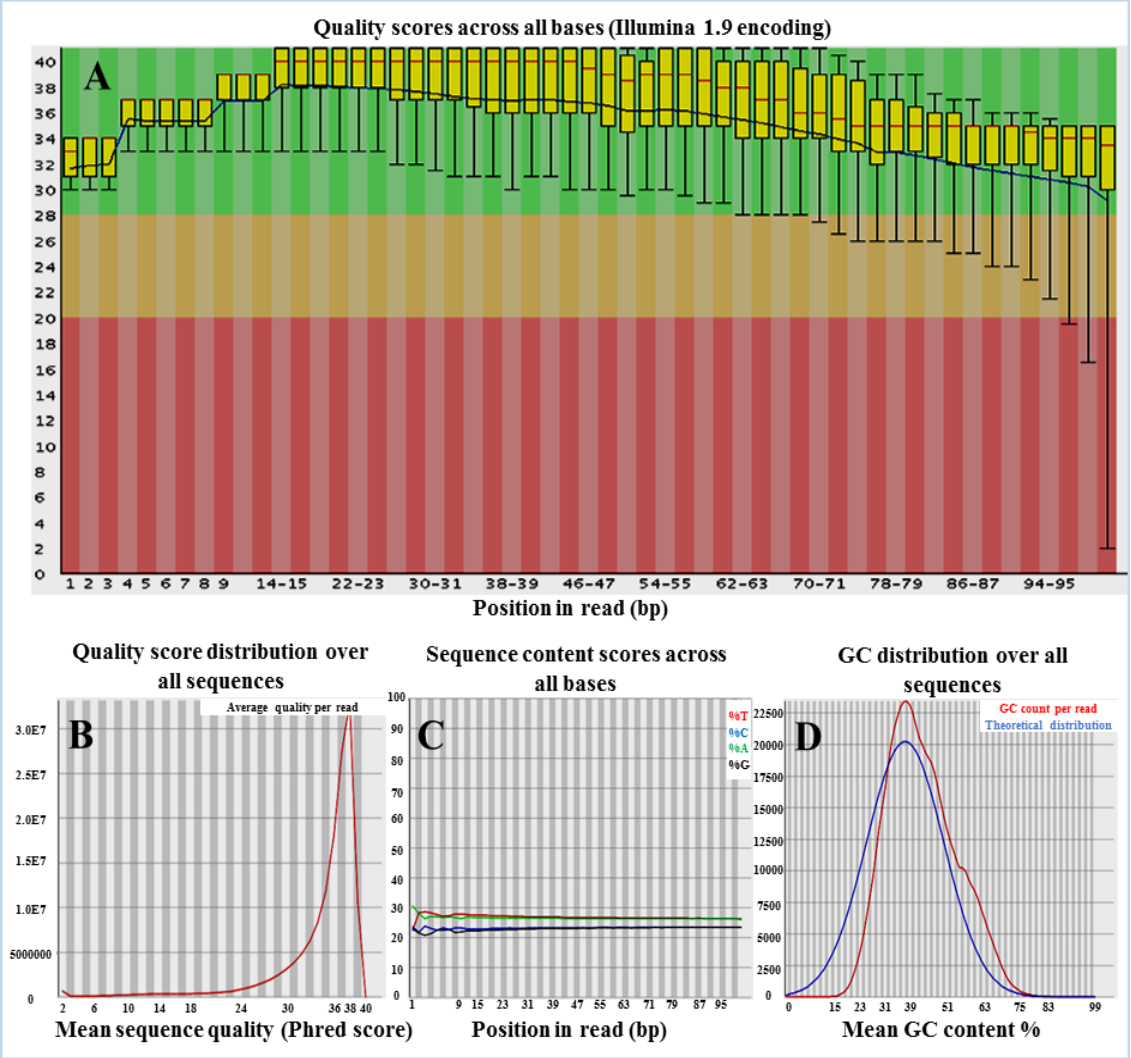

Figure 4.4. FastQC quality analysis report for sample 2278 from family MA5. A shows an overview of the range of quality values across all bases at each position in the FastQC file. A box whisker-type plot is drawn for each position. Red lines show the median value, yellow boxes represent the inter-quartile range (25-75%), upper and lower whiskers indicate 10% and 90% points, and the blue line represents the mean quality. The y-axis on the graph shows the quality scores. The higher the score, the better the base call. The coloured zones on the graph divide the y-axis into very good quality calls (green), reasonable quality calls (orange) and poor quality calls (red). B shows the average quality per read. C shows the sequence content of each base position in a file for which each of the four normal DNA bases have been called. D shows the GC content across the whole length of each sequence in a file and compares it to a modelled normal distribution of GC content. Sample 2278 represented here had very good quality calls (green zone) with zero flagged as poor quality from a total of 143,313,139 sequences , 39 average quality per read, little to no difference between the different bases of a sequence run and a normal GC distribution curve over all sequences.

The compound heterozygous variants in *MFSD8* identified in MA5 were c.1006G>C, p.E336Q in exon 11 and c.1394G>A, p.R465Q in exon 13. To determine if the variants were likely to be pathogenic they were assessed using five different pathogenic prediction tools (Section 2.14.2). Four out of five tools predicted that the missense variants were probably damaging (Table 4.2). Next, public variant databases were checked to determine the frequencies of both alleles (Section 2.14.4). The variant c.1006G>C was found at a frequency of 0.04% (2/5008) in dbSNP142 (rs150418024), a frequency of 0.19% (25/12981) in EVS, a frequency of 0.04% (2/5000) in 1000 Genomes and at a frequency of 0.25% (287/115508) in WES data from 60,706 unrelated individuals in the ExAC database, while no c.1394G>A alleles were found in any of these databases. Both alleles are therefore rare, compatible with a role in recessive disease.

Variant	PolyPhen2	MutationTaster	SIFT	Blosum62*	CADD**
p.E336Q	Probably damaging (score 1.000)	Disease causing (prediction probability 0.9999)	Damaging (score 0.00)	Score +2	Scaled C-score = 35
p.R465Q	Probably damaging (score 0.892)	Disease causing (prediction probability 0.9921)	Damaging (score 0.03)	Score +1	Scaled C-score = 33

Table 4.2. Pathogenic prediction scores for MFSD8 identified in family MA5. The scores for five different prediction software tools are shown for the two *MFSD8* missense variants. *Blosum62 scores range from +3 to -3 and negative scores are more likely to be damaging substitutions. **CADD scores are reported as scaled C-scores and values ≥ 20 represent the 1% most deleterious changes predicted in the human genome.

To confirm the mutations and to segregate them in the family, primer pairs were designed to PCR across the candidate variants (Sections 2.4.1). PCR (Section 2.4.3), agarose gel electrophoresis (Section 2.5) and Sanger sequencing (Section 2.8) showed that the *MFSD8* variants segregated with the disease phenotype in a recessive manner in the three family members tested (Figures 4.2 and 4.5A). The evolutionary conservation of the mutated amino acids was assessed using ClustalW alignment (Section 2.14.5) and the normal amino acid residues were fully conserved from human to mosquitoes (Figure 4.5B). These results indicate that these *MFSD8* mutations are the cause of the MD phenotype in family MA5.

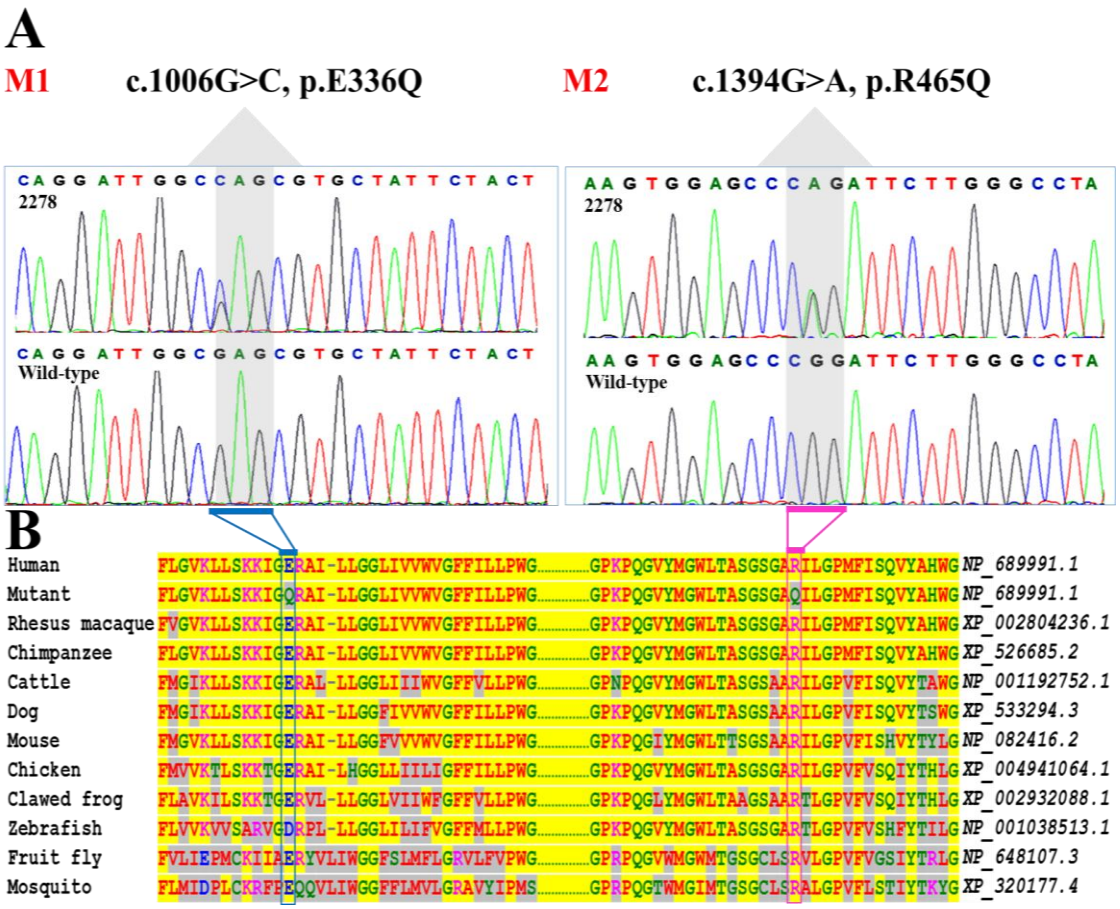

Figure 4.5. Mutations in *MFSD8* identified in family MA5. A. Electropherograms of *MFSD8* (NM_152778) sequence around the compound heterozygous mutations of M1 (c.1006G>C, p.E336Q) and M2 (c.1394G>A, p.R465Q) in patient 2278 from family MA5 and a wild type control. B. ClustalW alignment of the normal amino acid sequence of MFSD8 showing evolutionary conservation of the glutamic acid and arginine residues at positions 336 and 465 respectively.

4.2.1.3 Immunofluorescent localization of MFSD8 in the retina

In light of the recent findings that mutations in *MFSD8* can cause non-syndromic retinal disease, the localization of MFSD8 in the retina was investigated using IF staining and confocal microscopy on mouse retinal sagittal sections. Mouse eyes from adult age P30 wild-type mice were harvested, cryosections were prepared and IF staining performed as previously described (Section 2.17). The primary antibody of a goat polyclonal anti-MFSD8 was used at a final dilution of 1:100 followed by the secondary antibody, Alexa Fluor 568-conjugated donkey anti-goat immunoglobulin at a final dilution of 1:500. The nuclei were counterstained with DAPI at a final dilution of 1:1000.

In addition, an independent section was stained with secondary antibody only. Confocal images were analysed using EZ-C1 3.50 (Nikon) software (Section 2.18). The results show that MFSD8 is predominantly localized to the outer plexiform layer (OPL) in the mouse retina (Figure 4.6). The secondary antibody control showed that the labelling observed was not due to non-specific binding of the secondary antibody.

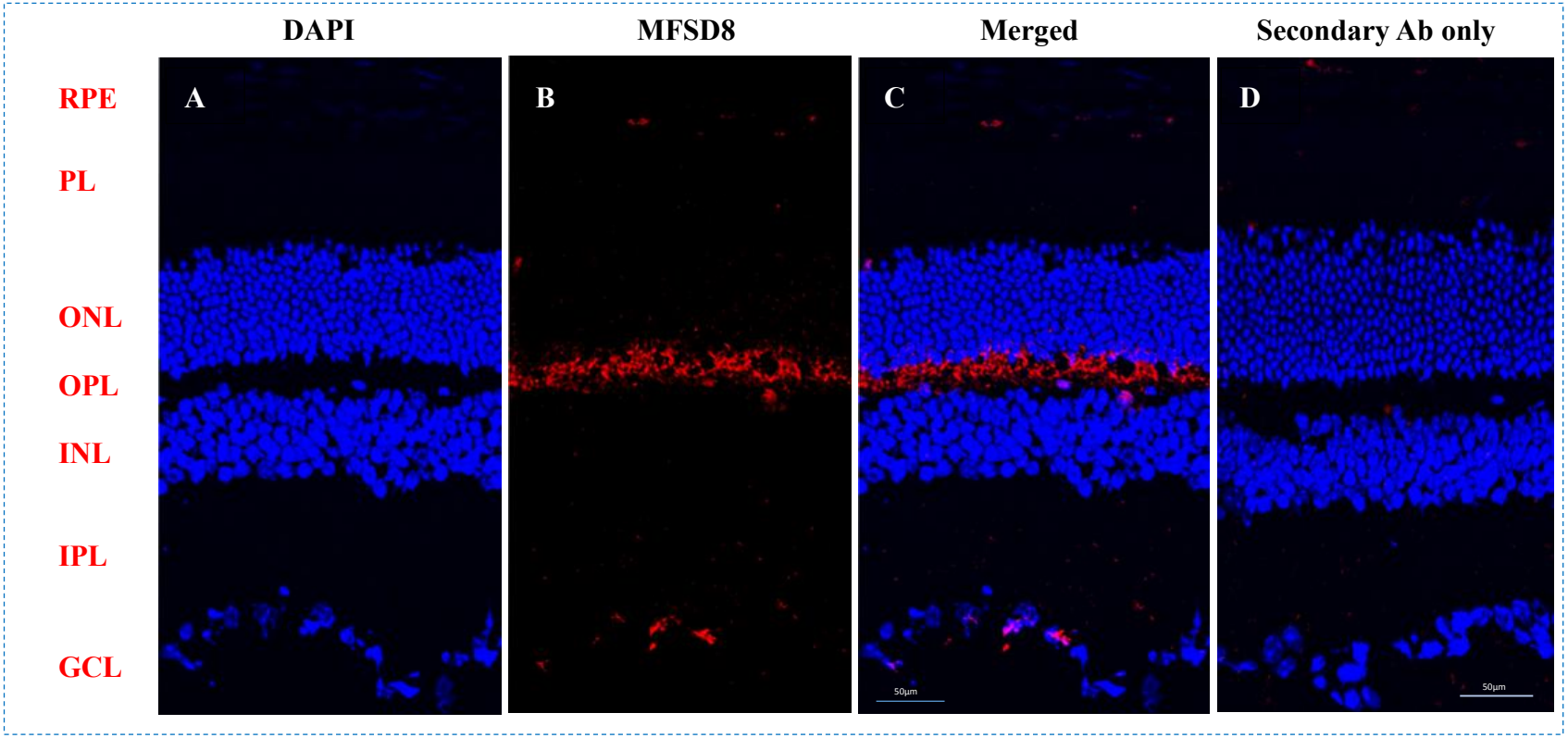

Figure 4.6. Immuno-localisation of MFSD8 to the mouse retina. Immunofluorescence and confocal microscopy images of mouse retinal sections showing that MFSD8 is predominantly localized to the outer plexiform layer (OPL) in the retina. Photomicrographs of P30 s mouse retinal sections stained for MFSD8 (red) antibody are shown in separate channels and merged images (A, B & C) compared to negative control (secondary antibody (Ab) only) (D). RPE = retinal pigment epithelium, PL = photoreceptor layer, ONL = outer nuclear layer, INL = inner nuclear layer, IPL = inner plexiform layer and GCL = ganglion cell layer. Scale bar = 50µM.

4.2.2 WES analysis of family MA13 identifies a novel homozygous *C8orf37* mutation causing RP

4.2.2.1 Clinical features of the affected members of family MA13

Family MA13 is a consanguineous UK family of Pakistani origin with two affected (one male and one female) and three unaffected (one male and two females) siblings. These subjects were recruited through the eye clinic at St. James's University Hospital, Leeds, UK. The pedigree structure is depicted in Figure 4.7. The patients, aged 12 to 27 years old at the time of the initial examination, were diagnosed with RP after ophthalmic assessment by Mr McKibbin. Apart from problems with their vision they had no other obvious abnormalities. Peripheral blood was collected from the affected patients, one of their parents, and unaffected siblings and genomic DNA was extracted from peripheral blood leukocytes (Section 2.2).

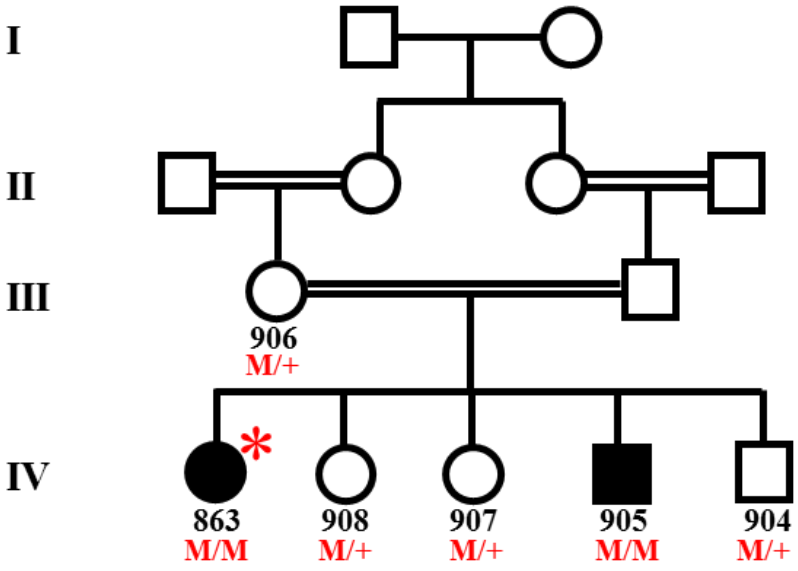

Figure 4.7. Pedigree of family MA13. The pedigree shows a four-generation consanguineous family with two affected members born to unaffected parents of Pakistani origin. Individuals from whom DNA was available are numbered, * = Family member from whom DNA was exome sequenced, + = wild type allele and **M** = c.555G>A, p.W185*.

4.2.2.2 Genetic analysis of family MA13

In family MA13, genomic DNA from the proband 863 was analyzed using WES (Section 2.10), the library preparation was performed using using the SureSelectXT Human All Exon reagent version 4. The output files were processed to generate 47,391 variants, all has a minimum read depth of 10. According to strategy described in Figure 4.1, these variants were filtered to exclude those not within exons or the conserved two base pair flanking splice-site junctions, and those that have a MAF≤ 1% in the public DNA databases (dbSNP 142, EVS and 1000 Genomes). After synonymous variants were excluded, 73 homozygous variants remained in the filtered list. One of these variants was a null allele in exon 6 of *C8orf37* (c.555G>A, p.W185*), a gene previously implicated in RD (Estrada-Cuzcano et al., 2012b). This mutation was therefore highly likely to be the cause of the RP phenotype in this family. The mutation was confirmed using Sanger sequencing (Figure 4.8) and shown to segregate in a recessive manner with the disease in the family (Figure 4.7). Public variant databases were checked for the allele (Section 2.14.4) and it was not reported in EVS, dbSNP137 and 1000 genomes, while it was reported once in ExAC (1/121316) which included 16488 unrelated subjects of South Asian origin.

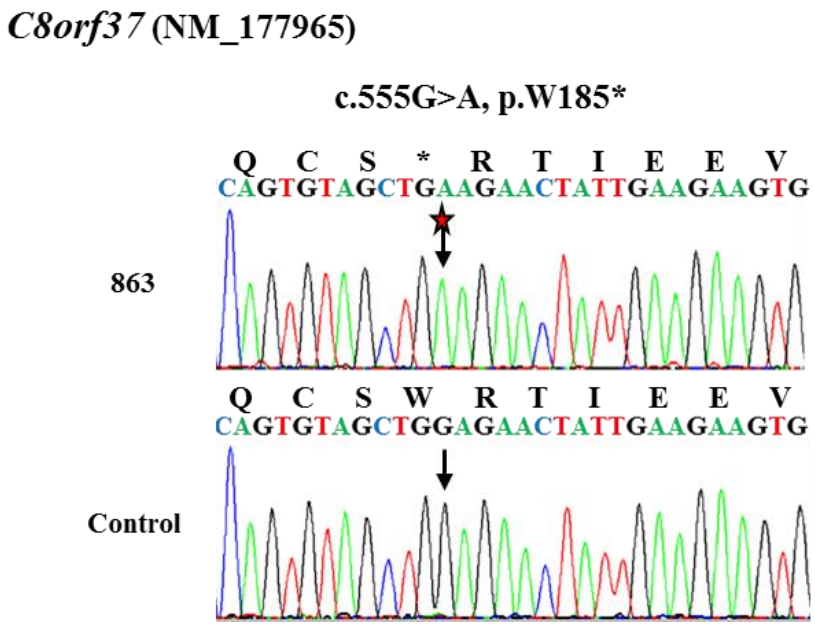

Figure 4.8. Mutation in *C8orf37* identified in family MA13. Electropherograms of *C8orf37* (NM_177965) sequence around the homozygous c.555G>A, p.W185* mutation in patient 863 from family MA13 and a wild type control.

In order to identify the size of the homozygous region in which the *C8orf37* gene mapped, the WES data of subject 863 was analysed as described in Section 2.12 to locate the homozygous regions at the genome level using AutoIdeogram (Figure 4.9). The homozygous intervals with a minimum threshold of 1 Mbp are shown in Table 4.3. The results showed that *C8orf37* (chr8:96,257,141-96,281,462, hg19) maps within the second largest homozygous region (~27.2 Mbp) of the patient.

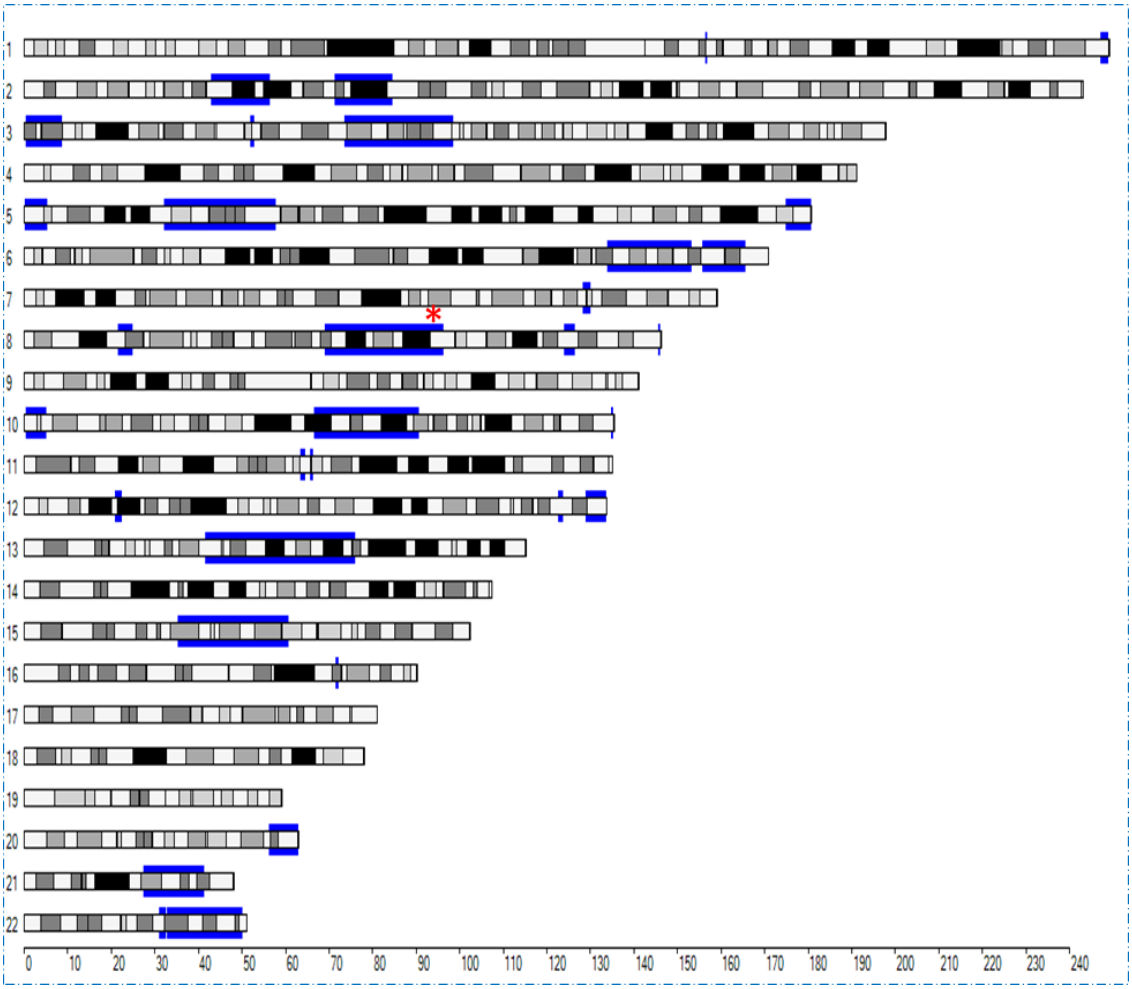

Figure 4.9. Homozygous regions in the WES data from subject 863 of family MA13. Detected homozygous regions are shown in blue. Y-axis shows the chromosome numbers 1-22 and the x-axis shows the genomic size in mega base pairs (Mbp). * = *C8orf37* gene location**.**

Chromosome	Start	End	Length (bp)
13	41495924	73650117	32154193
8	69104521	96300181	27195660
5	32058115	57750267	25692152
15	35149008	60678328	25529320
3	73437112	98536571	25099459
10	68040325	90771829	22731504
6	133827354	153332926	19505572
22	30927975	50018069	19090094
21	27326859	41165566	13838707
2	71297982	84771480	13473498
2	43015719	56411817	13396098
6	155750035	165693624	9943589
3	386247	8667896	8281649
20	56186884	62905090	6718206
5	174937193	180687428	5750235
5	163260	5200281	5037021
10	282897	5260812	4977915
12	128900005	133778796	4878791
8	21984650	24811064	2826414
2	208986385	211481257	2494872
8	123964431	126445544	2481113
1	247150740	249110906	1960166
7	128371206	130021488	1650282
12	20801855	22354921	1553066
11	63313644	64598944	1285300

Table 4.3. Homozygous intervals in the WES data from subject 863 of family MA13. The homozygous intervals (UCSC version hg19) are arranged according to the length in base pairs (bp). The *C8orf37* gene is located at chr8:96,257,141-96,281,462, hg19 which maps within the second largest homozygous region in the patient (shaded orange).

4.2.3 WES analysis of family MA14 identifies a homozygous mutation in *LARGE* as the potential cause of non-syndromic retinal dystrophy.

4.2.3.1 Clinical features of the affected members in family MA14

Family MA14 is a large consanguineous UK family of Pakistani origin with seven family members recruited for this study by Mr Martin McKibbin (Figure 4.10). The affected individuals were diagnosed with RP and apart from problems with their vision they had no other obvious abnormalities based on family history and assessment in clinic. Retinal imaging of patient 1527 showed peripheral retinal atrophy with perifoveal loss of the photoreceptors and RPE (Figure 4.11).

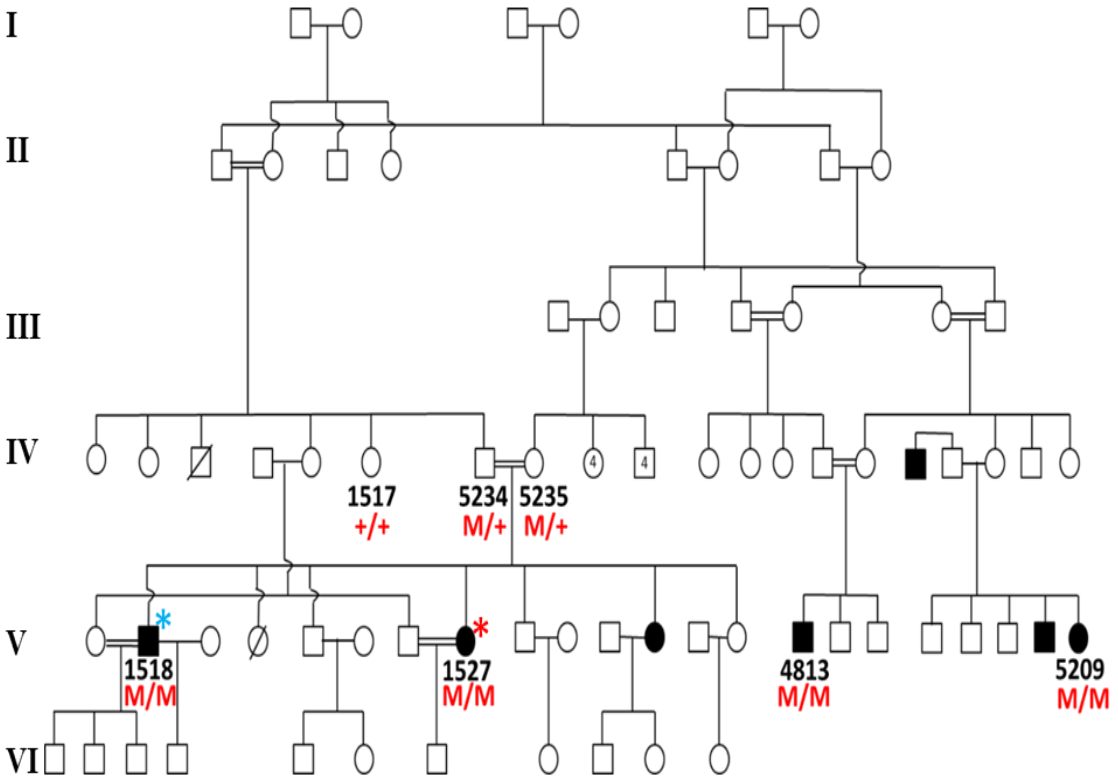

Figure 4.10. Pedigree of family MA14. The pedigree shows a six-generation consanguineous family with multiple affected members by arRP. Individuals from whom DNA was available are numbered. * = family members from whom DNA was exome sequenced, * = family member whose DNA was SNP chipped, + = wild type allele and M = c.2089G>T, p.V697L.

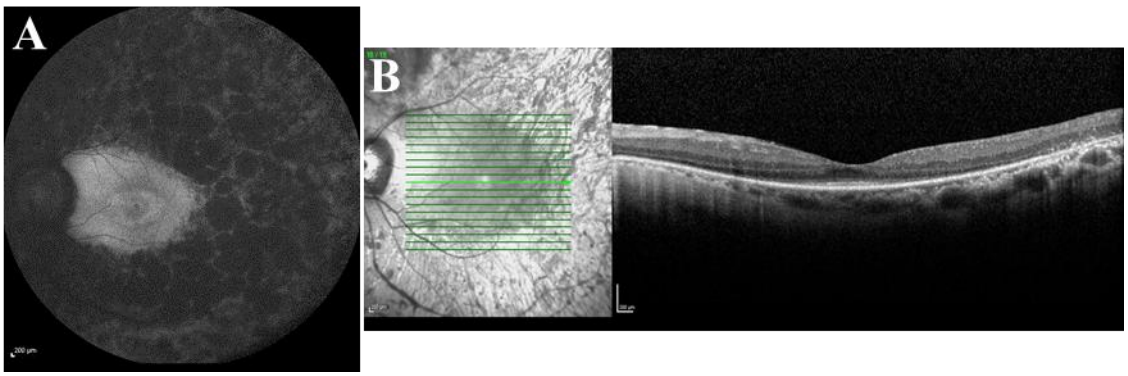

Figure 4.11. Retinal imaging of patient 1527 from family MA14. A. Fundus autofluorescence (FAF) image of the left eye (LE) shows intensive peripheral retinal atrophy with decreasing FAF in the peripheral retina. B. Optical coherence tomography (OCT) of LE shows that most of the outer retina has been lost, with perifoveal loss of the photoreceptors and RPE. Images courtesy of Mr Martin McKibbin (St James Hospital, Leeds).

4.2.3.2 Genetic analysis of family MA14

WES was performed on the proband, individual 1527, in family MA14. The genomic DNA was sequenced using the SureSelectXT Human All Exon reagent version 4 following the standard protocol (Figure 4.1, Section 2.10). Novoalign V2 program was used for the data alignment against the reference genome (hg19/GRCh37). Individual 1527 contained a total of 6,118 variants with a MAF ≤ 1% in dbSNP 142, EVS, 1000 Genomes and the ExAC databases and MAF ≤ 5% in a cohort of 3222 exomes of British Pakistani adults. 227 were exonic or within the two base pair conserved splice donor/acceptor sites, and were non-synonymous or indels with a minimum depth of coverage 10. Based on consanguinity in the family and hence assuming a recessive mode of inheritance and autozygosity, only 43 variants were homozygous. When this variant list was compared to the RD genes in the RetNet database (accessed February 2015), none were contained within known RD genes. The genomic DNA of patient 1518 in family MA14 was analysed by SNP genotyping using the Affymetrix 6.0 chips (Section 2.7.2). The locations of the homozygous regions are displayed by a MultiIdeogram (Figure 4.12) and the intervals described in Table 4.4.

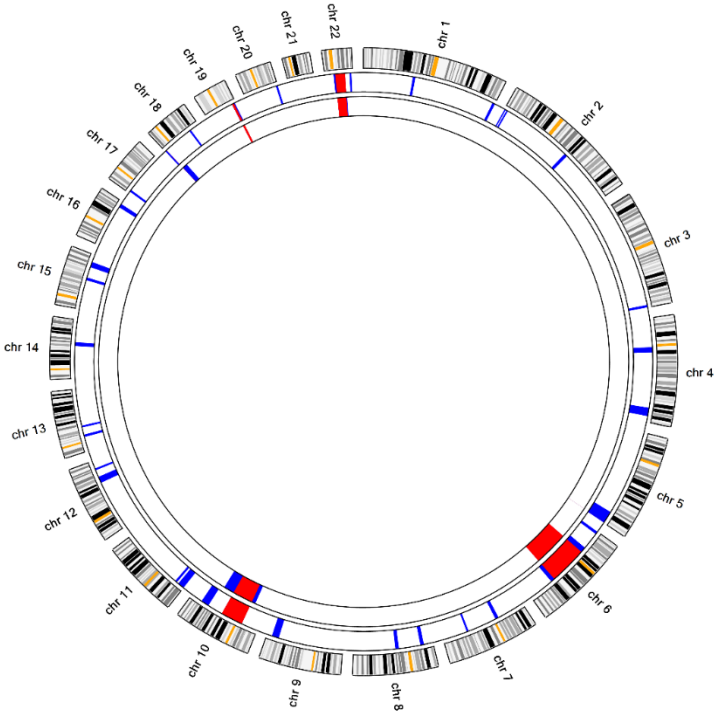

Figure 4.12. Autozygosity mapping in family MA14. All detected autozygous regions from SNP data of patient 1518 and WES data of patient 1527 were visualized from outside to the centre respectively. The homozygous regions observed in each individual are shown in blue. The shared autozugous regions are shown in red.

Chromosome	Start	End	Length (bp)
6	**37287936**	**124427719**	**87139783**
10	**30264550**	**71338247**	**41073697**
5	157777400	180692833	22915433
22	**16055171**	**37117055**	**21061884**
4	164560459	179961720	15401261
10	99868961	114742835	14873874
9	118957282	132150041	13192759
11	198510	12566917	12368407
12	91429973	103248017	11818044
15	79462776	89415247	9952471
4	53169664	62771716	9602052
16	78700674	85820521	7119847
14	59554796	66553683	6998887
8	16663961	23179226	6515265
8	63106536	69524413	6417877
7	50335232	56559512	6224280
19	**51374047**	**57258916**	**5884869**
2	137148547	142978639	5830092
6	203249	5391286	5188037
15	54570348	59694505	5124157
1	244273096	249198692	4925596
1	90559712	95202007	4642295
3	193277513	197856433	4578920
13	26611827	31158331	4546504
11	15887004	19921293	4034289
17	2899292	6872983	3973691
12	116263512	119857079	3593567
7	110429011	113995296	3566285
20	59347665	62912463	3564798
13	44538352	48049494	3511142
18	57451692	60840128	3388436
22	45457915	48824664	3366749
18	11543	316863	3157094
2	4162616	6958384	2795768
2	15703	2424495	2408792

Table 4.4. Autozygosity mapping in family MA14. The homozygous intervals (UCSC version hg19) detected from SNP data of patient 1518. Shared autozygous regions detected from combining SNP data of patient 1518 with WES data of patient 1527 are shaded orange.

Of the 43 rare homozygous variants that were identified in subject 1527, only 15 were located in regions of homozygosity listed in Table 4.4 generated from sibling 1518 (Table 4.5). When these were limited to the homozygous regions identified from the WES-SNP data of individual 1527, only nine variants remained making these the most promising candidates for potentially causing RP in this family (Table 4.5). The WES of individual 1527 was manually inspected using IGV (Section 2.10.1) around the remaining 6 variants to confirm the presence of heterozygous alleles. This confirmed the exclusion of 6 alleles. Moreover, CNV detection using Fishing CNV and ExomeDepth analysis according to methods described in Section 2.13 using WES data from individual 1527 did

not reveal any significance homozygous CNV over the homozygous regions identified from the SNP data of patient 1518.

However, given the porous nature of the WES SNP data, primer pairs (Appendix 6) were designed to PCR across all the fifteen variants to confirm and segregate them in the available family members using Sanger sequencing (Section 2.8). The only variant which segregated in a recessive manner with the disease phenotype was the missense mutation in exon 15 of the *LARGE* gene (NM_133642: c.2089G>T, p.V697L) (Figures 4.13A and 4.10). *LARGE* gene (chr22: 33,669,062-34,316,416, hg19) was located in one of the shared autozygous regions patients 1518 and 1527 that was 21.06 Mbp in size (Table 4.4). Identified missense variant in *LARGE* was not reported in dbSNP, EVS, ExAC or 1000 Genomes databases. The normal amino acid residue was fully conserved from human to roundworm (Figure 4.13B), whilst the substitution was predicted to be pathogenic by several prediction programs (Figure 4.13C).

Chr	Position (hg19)	Gene	Mutation	AAChange.refGene
1	94057835	*BCAR3*	ns SNV	NM_001261410:exon2:c.G200A:p.R67H
3	195501121	*MUC4*	fs Del	NM_138297:exon2:c.138delG:p.R46fs
5	179331789	*TBC1D9B*	ns SNV	NM_015043:exon2:c.G142A:p.V48M,
6	**38906708**	***DNAH8***	**ns SNV**	**NM_001206927:exon79:c.A11951T:p.K3984M**
6	**47251773**	***TNFRSF21***	**sg SNV**	**NM_014452:exon3:c.C1144T:p.Q382X**
6	**56422262**	***DST***	**ns SNV**	**NM_015548:exon40:c.A6626G:p.E2209G**
6	**76023033**	***FILIP1***	**ns SNV**	**NM_015687:exon5:c.C2515T:p.R839W**
6	**110636619**	***METTL24***	**sg SNV**	**NM_001123364:exon3:c.G483A:p.W161X**
8	17814914	*PCM1*	ns SNV	NM_006197:exon12:c.C1788G:p.N596K
8	21978365	*HR*	ns SNV	NM_005144:exon11:c.G2474A:p.R825H
10	103871253	*LDB1*	ns SNV	NM_001113407:exon2:c.G66T:p.E22D
19	**52448349**	***ZNF613***	**ns SNV**	**NM_001031721:exon6:c.T1213C:p.C405R**
19	**54758804**	***LILRB5***	**ns SNV**	**NM_001081443:exon5:c.T749G:p.I250R**
19	**55527078**	***GP6***	**ns SNV**	**NM_001256017:exon6:c.A694C:p.S232R**
22	**33670595**	***LARGE***	**ns SNV**	**NM_133642:exon15:c.G2089T:p.V697L**

Table 4.5. List of 15 candidate genes for MA14. 15 candidate variants generated after filtering of the WES data of patient 1527 against the homozygous regions identified by SNP genotyping of patient 1518. Only 9 variants (bold) from the list were limited to the homozygous regions identified from the WES-SNP data of individual 1527. Chr = chromosome number, nsSNV = non-synonymous single nucleotide variant, sg SNV = stop gain single nucleotide variant and fs Del = frameshift deletion.

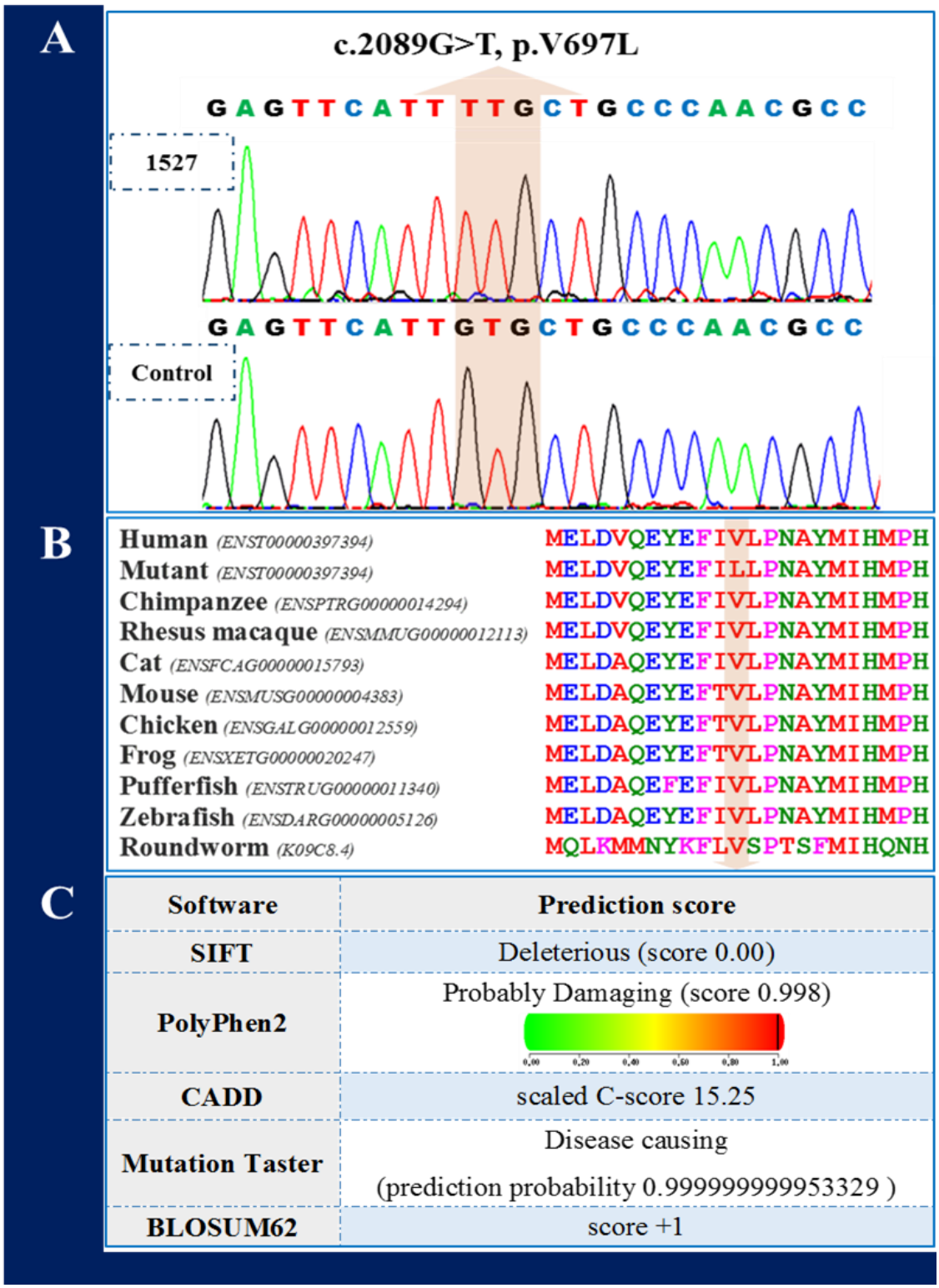

Figure 4.13. Analysis of the missense variant c.2089G>T, p.V697L in *LARGE* that identified in family MA14. A. Sanger sequence chromatograms from an affected family member (1527) and a normal unaffected control subject. B. ClustalW alignment of the normal amino acid sequence of LARGE showing evolutionary conservation of the valine residue at position 697. C. Summary of bioinformatic analyses to predict pathogenicity of the variant in *LARGE*.

4.2.3.3 LOD score for family MA14.

Linkage analysis was performed between the mutation (c.G2089T) and the disease in family MA14 members using Superlink (Section 2.14.6). A maximum two point LOD score of 5.16 was obtained by using the mutation as a genetic marker with a MAF of 0.01%, and the disease was assumed to segregate in the family in a recessive fashion with full penetrance.

4.2.3.4 Immunofluorescent localization of LARGE in the retina

In order to define the precise localization of LARGE within the retina, IF staining and confocal microscopy were used on mouse retinal sagittal sections. Sections of 4% paraformaldehyde-fixed wild-type mouse eyes from adult age P30 mice were prepared (Section 2.17.3) followed by IF staining (Section 2.17.7). Sections were labelled with a goat polyclonal anti-LARGE (at a final dilution of 1:50) and a rabbit polyclonal anti-Rhodopsin (at a final dilution of 1:300) followed by the secondary antibodies Alexa Fluor 568-conjugated donkey anti-goat immunoglobulin (red) (at a final dilution of 1:500) and Alexa Fluor 488-conjugated chicken anti-rabbit immunoglobulin (green) (at a final dilution of 1:500) respectively. The nuclei were counterstained with DAPI (at a final dilution of 1:1000). An independent section stained with both secondary antibodies only and another with peptide competition against the LARGE primary antibody according to BPCA described in Section 2.17.8 to serve as negative controls in the experiment. Confocal images were analyzed using EZ-C1 3.50 (Nikon) software (Section 2.18). The results showed that LARGE is predominantly localized to the photoreceptor inner segment (PIS), outer nuclear layer (ONL) and outer plexiform layer (OPL) in the retina, while, as expected, Rhodopsin localised to the outer segment of the photoreceptor layer (POS) (Figure 4.14). Negative controls sections confirmed the specificity of the primary antibody for staining LARGE protein.

4.2.3.5 Screening for additional cases of *LARGE* related retinopathy

In an attempt to identify further families with *LARGE*-associated retinopathy, the fourteen coding *LARGE* exons and their flanking splice sites were PCR amplified and Sanger sequenced in a panel of 60 patients diagnosed with RDs. In addition, the last four coding exons of *LARGE* and their flanking splice sites were screened in a panel of 254 patients diagnosed with RDs. Part of the panel was prepared by WGA method described

in Section 2.9. The primer pairs are shown in Appendix 6. The screening did not reveal other cases with mutations in *LARGE*.

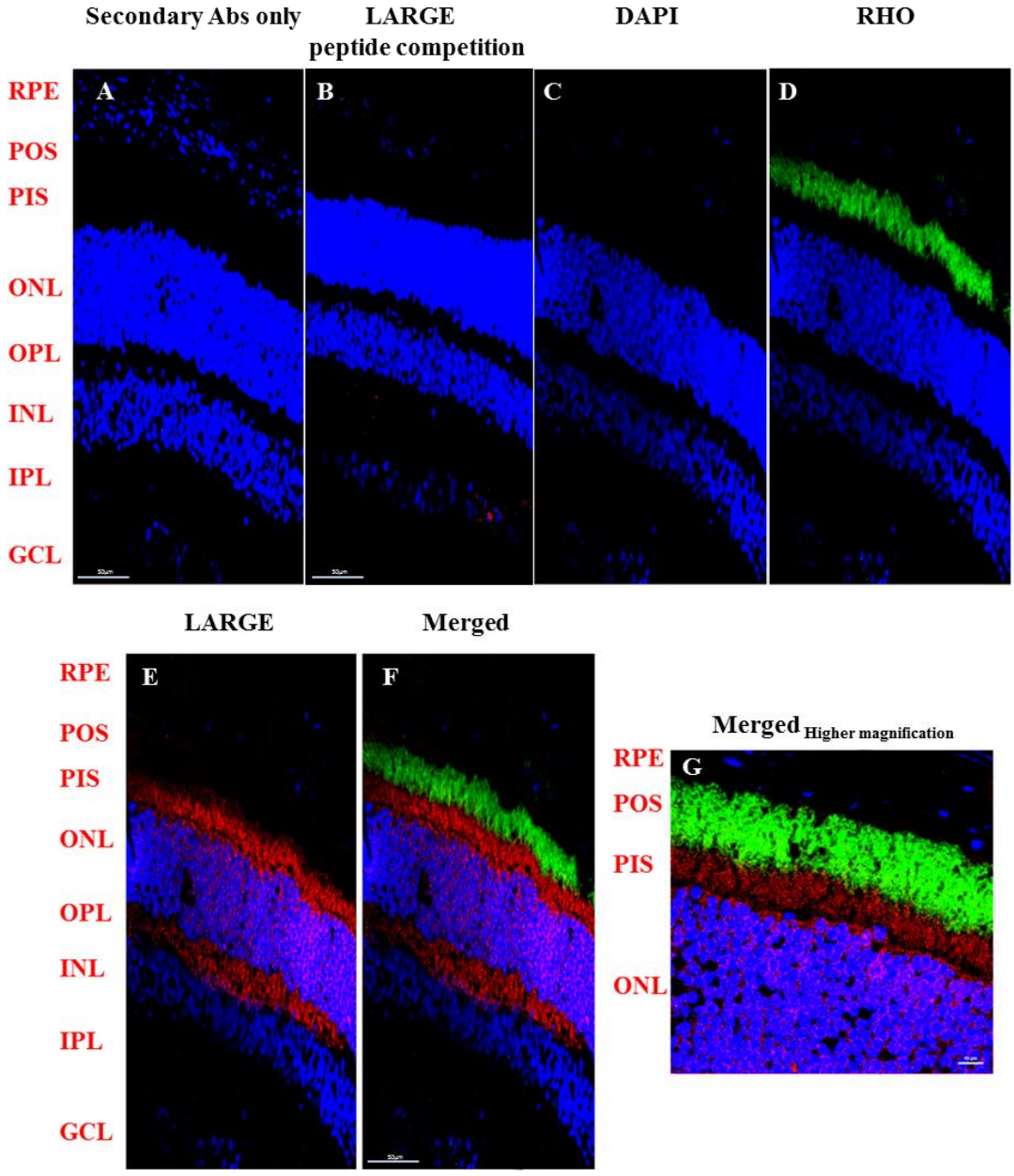

Figure 4.14. Immuno-localisation of LARGE to the mouse retina. Immunofluorescence and confocal microscopy images of mouse retinal sections showing that LARGE is predominantly localized to photoreceptor inner segment (PIS), outer nuclear layer (ONL) and outer plexiform layer (OPL) in the retina. Photomicrographs of P30 sagittal mouse retinal sections stained for LARGE (red) and rhodopsin (RHO) (green) antibodies are shown in separate channels and merged images (C, D, E, & F) and higher magnification (G) compared to negative controls with secondary antibodies only (A) and peptide competition against the LARGE primary antibody (B). RPE = retinal pigment epithelium, POS = photoreceptor outer segment, INL = inner nuclear layer, IPL = inner plexiform layer and GCL = ganglion cell layer. Scale bars = 50µM (A, B, C, D,E &F) and 10µM (G).

4.2.4 WES analysis of family MA17 identifies a homozygous mutation in *FDFT1* as the potential cause of RCD.

4.2.4.1 Clinical features of the affected members in family MA17

Family MA17 is a five-generation UK family of Pakistani origin with two affected patients, male and female siblings, from whom DNA was available. They were both recruited by Mr McKibbin through the eye clinic at St. James's University Hospital, Leeds, UK. This family (Figure 3.19) was previously analysed in the Retinome project, however after revisiting the patient's family it was established that the original pedigree structure was incorrect. The updated pedigree structure is depicted in Figure 4.15. The family structure is consistent with recessive inheritance and there is evidence of consanguinity in the pedigree, but the parents of the sampled patients were not knowingly related. The patients were diagnosed as having rod cone dystrophy after ophthalmic assessment. Apart from problems with their vision they had no other obvious abnormalities. Retinal imaging of patient 3347 showed peripheral retinal atrophy with relatively preserved macula is preserved that has a peripheral ring of depigmentation (Figure 4.16).

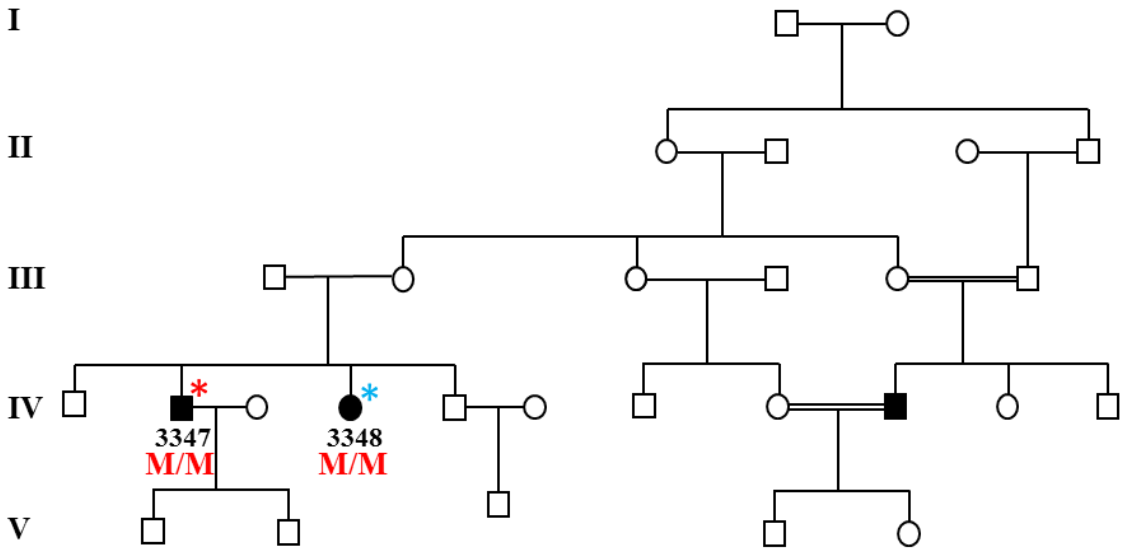

Figure 4.15. Pedigree of family MA17. The pedigree shows a five-generation family with three affected members born to unaffected parents of Pakastani origin. Individuals from whom DNA was available are numbered. * = family member from whom DNA was exome sequenced, * = family member from whom DNA was SNP chipped and M = c.930C>G, p.F310L.

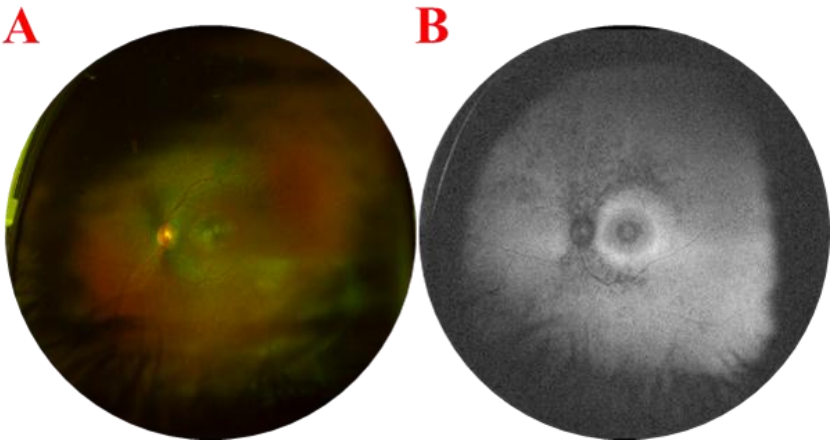

Figure 4.16. Retinal imaging of patient 3347 from family MA17. A. Colour fundus photograph shows temporal pallor and severely attenuated retinal vessels in the peripheral retina along with peripheral retinal atrophy. The macula is preserved but has a peripheral ring of depigmentation. B. Fundus autofluorescence (FAF) image showing absence of FAF in the midperiphery with a central ring of reduced FAF centrally, surrounded by a ring of increased FAF on edges. Images courtesy of Mr Martin McKibbin (St James Hospital, Leeds).

4.2.4.2 Genetic analysis of family MA17

WES was used to identify the causative mutation for rod cone dystrophy in family MA17. A library was prepared from the genomic DNA of patient 3347 using the SureSelectXT Human All Exon reagent version 5 as described previously with Novoalign V2 aligner program (Section 2.10, Figure 4.1). WES analysis of patient 3347 revealed 50,771 variants after quality filtering with a minimum depth of coverage 10. Of these, 21,193 were exonic or presumed splice altering (within 2 bp of exon-intron junctions). 16,185 remained after removing the synonymous variants, and of these 426 had an allele frequency of ≤1% in the dbSNP 142, EVS, 1000 Genomes, ExAC and ≤5% in a cohort of 3222 exomes of British Pakistani adults. The absence of a family history of eye disease and the non-consanguinity of the parents suggested autosomal recessive inheritance and either homozygous or compound heterozygous disease alleles. Filtering for variants that fitted this hypothesis identified 66 homozygous and 2 compound heterozygous variants, none of which occurred in genes already implicated in retinal disease according to the RetNet database (accessed April 2015). The genomic DNA of patient 3348 was analysed by SNP genotyping using the Affymetrix 6.0 chips (Section 2.7.2). The resulting data were analysed and the homozygous regions are displayed in Figure 4.17 whilst the intervals are listed in Table 4.6.

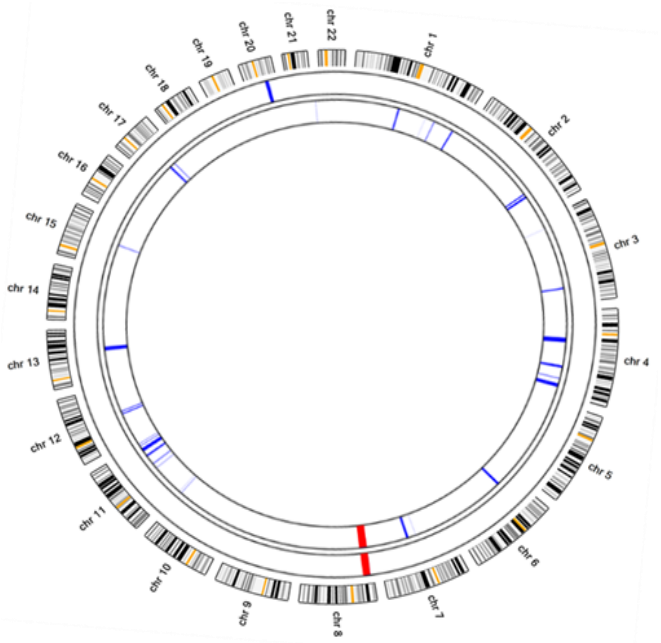

Figure 4.17. Autozygosity mapping in family MA17. All detected autozygous regions from SNP data of patient 3348 and WES data of patient 3347 were visualized from outside to the centre respectively. The homozygous regions observed in each individual are shown in blue. The shared autozugous region is shown in red.

Chromosome	Start	End	Length (bp)
8	1363663	12995633	11631970
20	24336365	31573320	7236955

Table 4.6. Autozygosity mapping in family MA17. The homozygous intervals (UCSC version hg19) detected from SNP data of patient 3348. Shared autozygous region detected from combining SNP data of patient 3348 with WES data of patient 3347 is shaded orange.

WES in combination with homozygosity mapping utilizing SNP chip genotyping reduced the candidate list to five potentially causative homozygous variants in *MYT1 YWHAB, CST1*, *DLC1* and *FDFT1*. Sanger sequencing using primer pairs designed across the candidate mutations identified that the missense mutation, NM_004462: c.930C>G, p.F310L, in exon 7 of the *FDFT1* gene was the only variant of the five candidates that both patients 3347 and 3348 have in a homozygous form (Figure 4.18A). This variant is absent in dbSNP 142, EVS, 1000 Genomes and the in-house database of 3222 exomes of British Pakistani adults, while it occurs only in a heterozygous form at a frequency of 0.07078 % (87/122918) in the ExAC browser. The amino acid residue was fully conserved from human to lamprey (Figure 4.18B) and the substitution is predicted to be damaging using a range of in-silico pathogenicity prediction tests (Figure 4.18C).

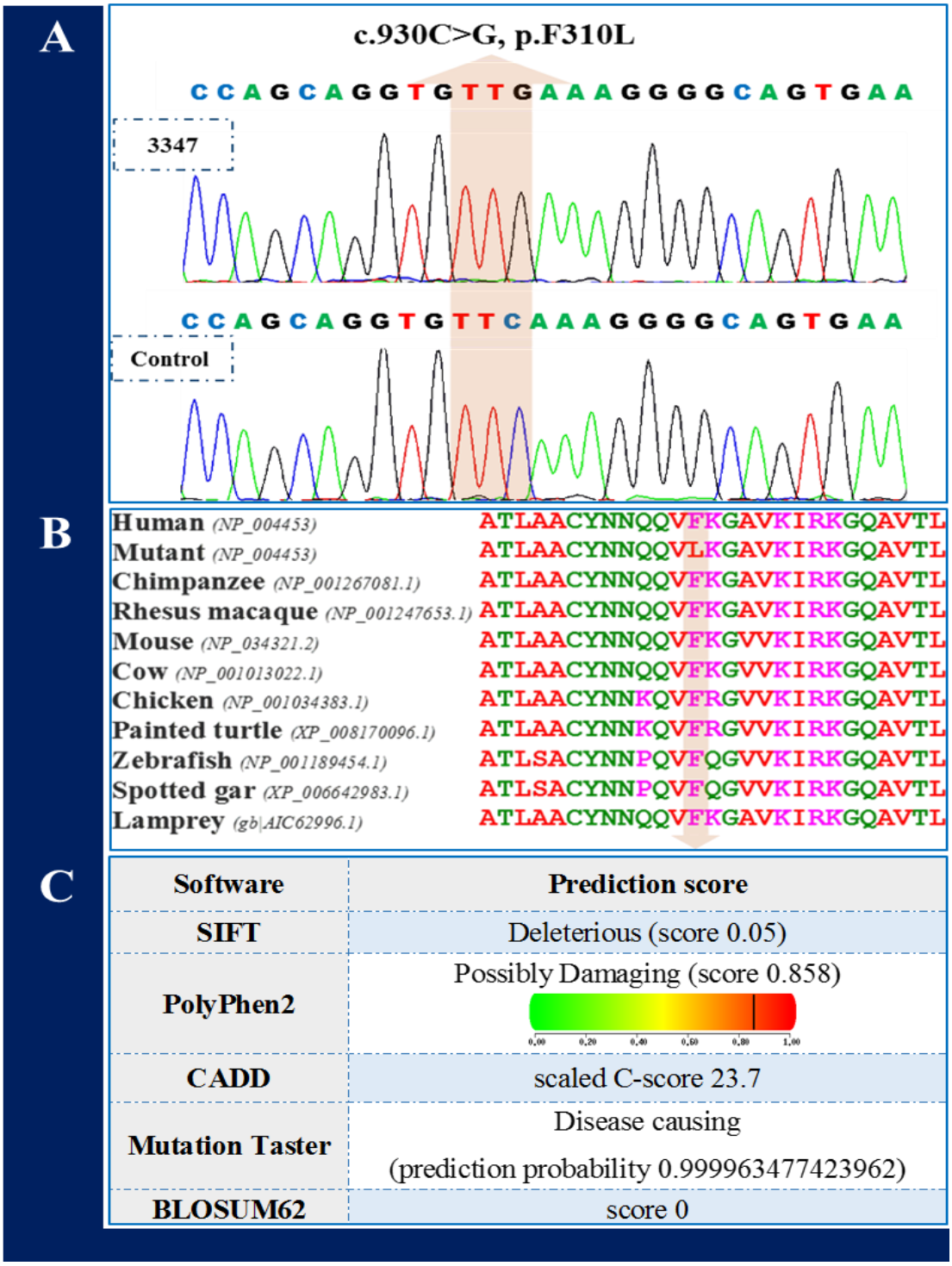

Figure 4.18. Analysis of the missense mutation, c.930C>G, p.F310L, in *FDFT1* that identified in family MA17. A. Sanger sequence chromatograms of an affected individual from family MA17 and a normal control subject. B. ClustalW alignment of the normal amino acid sequence of FDFT1 showing evolutionary conservation of the phenylalanine residue at position 310. C. Summary of the bioinformatic analyses to predict the pathogenic nature of the *FDFT1* variant.

To further support the hypothesis that the variant in *FDFT1* is the most plausible candidate cause of disease symptoms in the affected members of family MA17, three confirmatory steps were applied. First, the WES data from patient 3347 was converted to homozygosity data according to the methods described in Section 2.12. The locations of the autozygous regions common to both individuals are displayed (Figure 4.17, Table 4.6). These results show that only one homozygous region was shared between these two patients 3347 and 3348, *FDFT1* was located in this shared regions on chromosome 8 that was 11.36 Mbp in size. Second, segregation analysis for the two compound heterozygous candidates in *SLC45A1* and *KLF5* excluded both variants. Furthermore, CNV detection using Fishing CNV and ExomeDepth analysis according to methods described in Section 2.13 using WES data from individual 3347 did not reveal any significance homozygous CNV over the homozygous regions identified from the SNP data of patient 3348.

4.2.4.3 Screening for additional cases of *FDFT1*-related retinopathy

The coding *FDFT1* exons and their flanking splice sites were PCR amplified and Sanger sequenced in a panel of 303 patients diagnosed with RDs. The primer pairs are shown in Appendix 6 and a representative agarose gel electrophoresis image for the PCR for the sixth coding exon of *FDFT1* on the panel of sixty patients is depicted in Figure 4.19. The screen results reveal a heterozygous missense mutation in exon 8: c.1173G>T, p.M391I in a female case (4673) with a diagnosis of RP but no family history of eye disease (Figure 4.20A). The amino acid residue was conserved from human to western clawed frog and the substitution is predicted to be damaging using a range of in-silico pathogenicity prediction tests (Figure 4.20B).

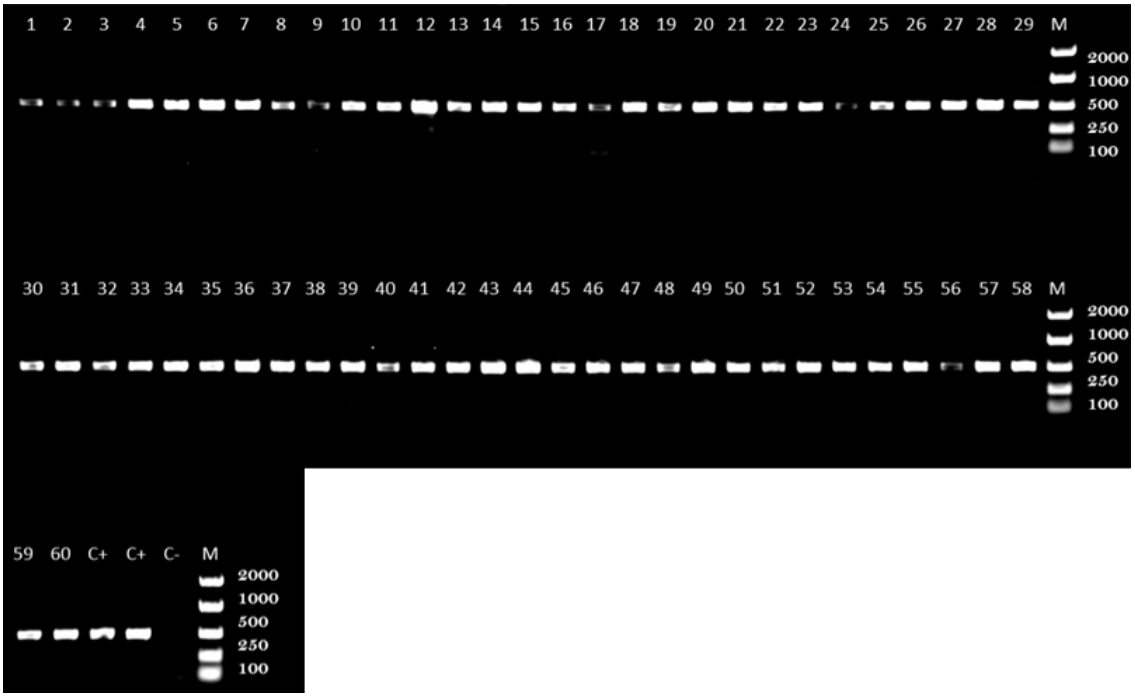

Figure 4.19. Example of agarose gel electrophoresis used in *FDFT1* screening. The gel shows the PCR products of the sixth coding exon of *FDFT1* amplified from genomic DNA of 60 RD patients. Lanes 1-60 = patient samples; lanes C+ = positive control, lane C- = negative control; lanes M = EasyLadder I, a DNA molecular weight marker (100bp-2000bp).The PCR product size for this reaction was 488 bp.

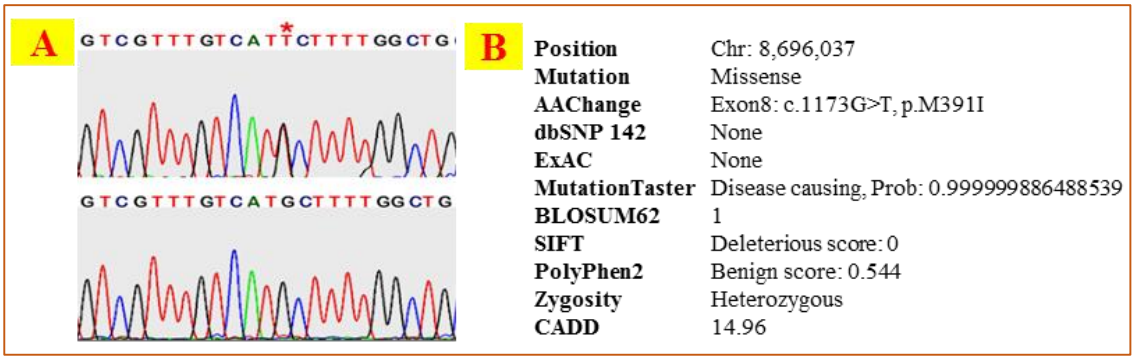

Figure 4.20. Analysis of the heterozygous variant c.1173G>T, p.M391I in *FDFT1* that identified in case 4673 with a diagnosis of RP. A. Sanger sequence chromatograms from case 4673 and a normal unaffected control subject. B. Summary of bioinformatic analyses to predict pathogenicity of the variant.

4.2.5 WES analysis of family MA19 identifies a previously described homozygous missense mutation in *TTLL5* causing RCD

4.2.5.1 Clinical features of the affected members in family MA19

Family MA19 is a four-generation Pakistani family with multiple affected members. Genomic DNA was available from three affected (two males and one female) and three unaffected (one male and two females) family members who were recruited for this study. Pedigree structure is depicted in Figure 4.21.

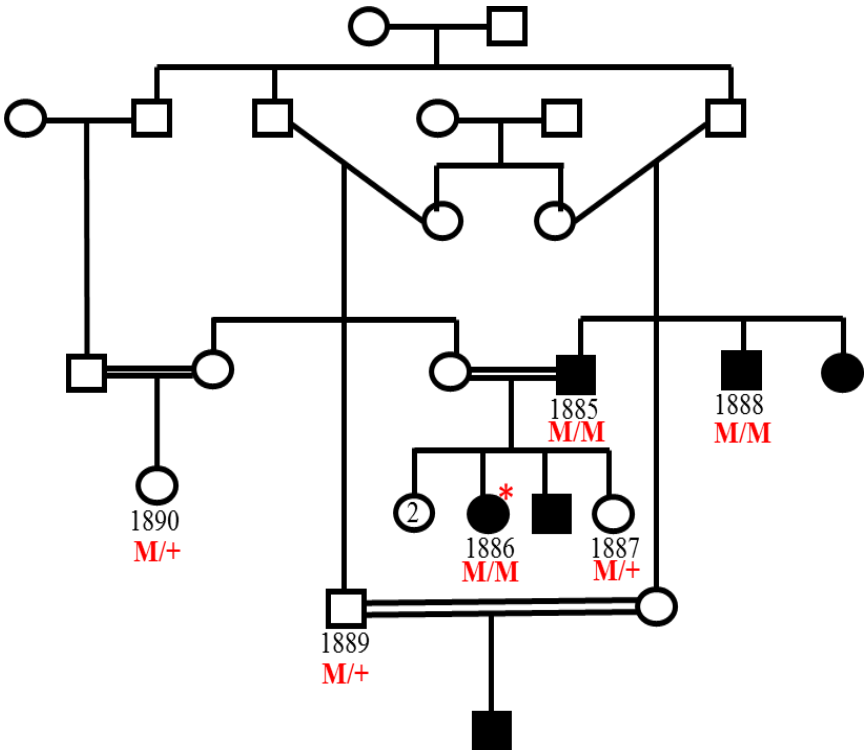

Figure 4.21. Pedigree of family MA19. The pedigree shows a four-generation family with multiple affected members who are Pakistani in origin. Individuals from whom DNA was available are numbered, * = family member from whom DNA was exome sequenced, + = wild type allele and M = c.1627G>A, p.E543K.

The patients were aged between 18 and 53 years old at the time of the initial examination. Patient 1885, a 53 year old, who had a phthisical right eye, said he had good vision in his left eye till his 30s but his visual acuity at the time of examination was perception of light only. There was high myopia (-8DS) and evidence of rod-cone dystrophy with central atrophy and peripheral pigmentary changes. Patient 1888, a 38

year-old male, said that his visual acuity was good until he was 30. He was also short sighted (-5DS) and had similar features to patient 1885 but with a posterior subcapsular cataract. Patient 1886, an 18 year–old female, had high myopia (-12DS) but the retina had a fairly normal appearance. Her visual acuity could not be improved beyond 6/60, although she denied suffering from night or day blindness. DNA was not taken from two other individuals. The first of these is the affected sister of patients 1885 and 1888. She had high myopia (-8DS) but no other clinical details recorded. The second was the son of patient 1889, aged 10, who was highly myopic but with good visual acuity (6/4 in each eye) and a normal retina. The diagnosis given to the family by the recruiting Ophthalmologist, Mr McKibbin, was that this is a type of RCD with high myopia as an early feature.

4.2.5.2 Genetic analysis of family MA19

In order to identify the mutation causing rod-cone dystrophy in family MA19, WES was performed on genomic DNA from proband 1886. A library was prepared from the genomic DNA using the SureSelectXT Human All Exon reagent version 4 (Section 2.10.1). The output FastQC file was aligned against the reference genome (hg19/ GRCh37) using the Bowtie 2 program, then processed in SAM/BAM format using the SAMtools and GATK suite of programmes (Section 2.10.2). The combined vcf file of SNPs and indels was annotated using ANNOVAR and all variants with MAF ≥1% in dbSNP 142, EVS, 1000 Genomes, ExAC database were excluded. Of the remaining 4658 variants, 786 were exonic or within the 2bp splice consensus sequences, were non-synonymous missense variants or indels and had a minimum depth of coverage 10. Based on known familial consanguinity, a recessive mode of inheritance was considered most likely and homozygous variants were prioritised. The final list of 128 variants was compared to the retinal dystrophy genes in the RetNet database and one missense variant in the *BBS10* gene (NM_024685:c.A1631G:p.N544S) was detected but did not segregate with the disease phenotype in the other family members from whom DNA was available. The aligned file in SAM format of subject 1886 was used to identify the homozygous regions using AgileGenotyper (Section 2.12); the locations of the homozygous regions are displayed by AutoIdeogram in Figure 4.22 and the intervals were exported into Table 4.7.

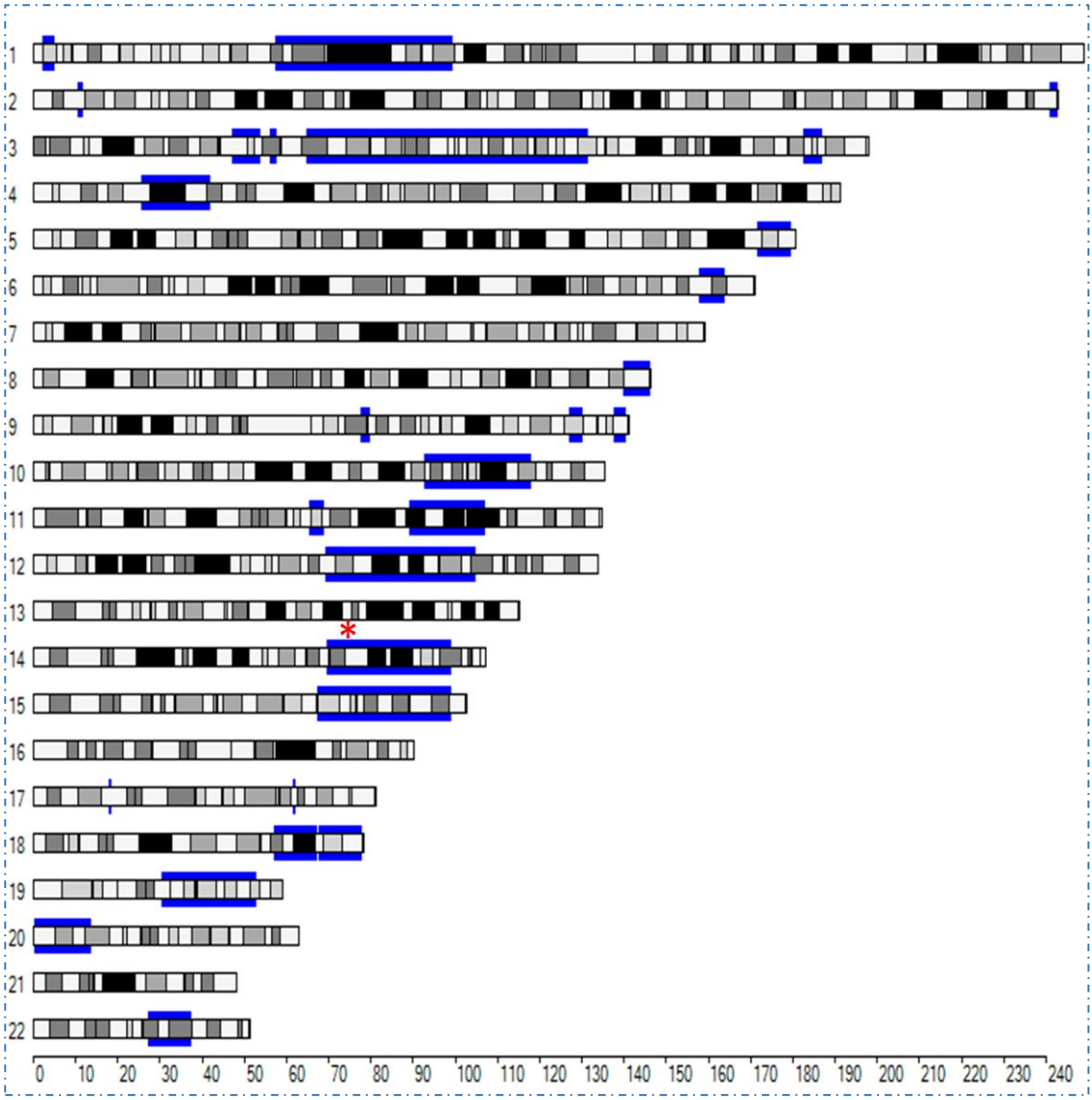

Figure 4.22. Homozygosity mapping in family MA19. Homozygous regions detected from the WES data of patient 1886 are represented by an AutoIdeogram. The y-axis shows the chromosome numbers 1-22 and x-axis shows the genomic size in mega base pairs (Mbp). * = *TTLL5* gene location.

Chromosome	Start	End	Length (bp)
3	64640206	131415340	66775134
1	57340727	99418911	42078184
12	69141678	104698582	35556904
15	67358478	98995081	31636603
14	69376623	92530551	23153928
10	92672564	114884950	22212386
11	89223616	107224225	18000609
4	25678199	42025284	16347085
20	76962	13747441	13670479
19	36351768	47774772	11423004
22	27021457	37271882	10250425
18	57134152	67345034	10210882

18	67718688	77927028	10208340
5	171760544	179780340	8019796
3	46899516	53926017	7026501
14	92549586	99182559	6632973
6	157713777	163987389	6273612
8	139736933	145578296	5841363
19	30500118	36322601	5822483
19	47778221	52887904	5109683
3	182511351	186954285	4442934
11	65480768	68834968	3354200
9	127101924	130164818	3062894
1	2005740	4834606	2828866
9	137593099	140374861	2781762
9	77676285	79922845	2246560
3	55886573	57743246	1856673
2	240981262	242814463	1833201
2	10563233	11853988	1290755
17	17682484	18541915	859431
8	145579953	146229161	649208
17	61559923	62152611	592688

Table 4.7. Homozygosity mapping in family MA19. The homozygous intervals detected from the WES data of patient 1886 in family MA19. The regions are arranged according to their length in base pairs (bp). The *TTLL5* gene maps to chr14:76,127,551-76,421,425, hg19, which is located within the fifth largest homozygous region in patient 1886 (shaded orange).

34 variants out of the 128 were located within the homozygous regions. It was noted that there was a homozygous missense change in *TTLL5*, c.1627G>A, p.E543K, present in the final list. This gene had only recently been reported as a cause of RD, and indeed this specific mutation had been reported as disease causing (Sergouniotis et al., 2014). Primers designed to amplify across the variant, confirmed this variant was present and clarified the co-segregation with the disease phenotype in the family (Figure 4.21and 4.23A). The amino acid of the normal glutamic acid residue at position 543 is evolutionary conserved from human to lizard (Figure 4.23B).

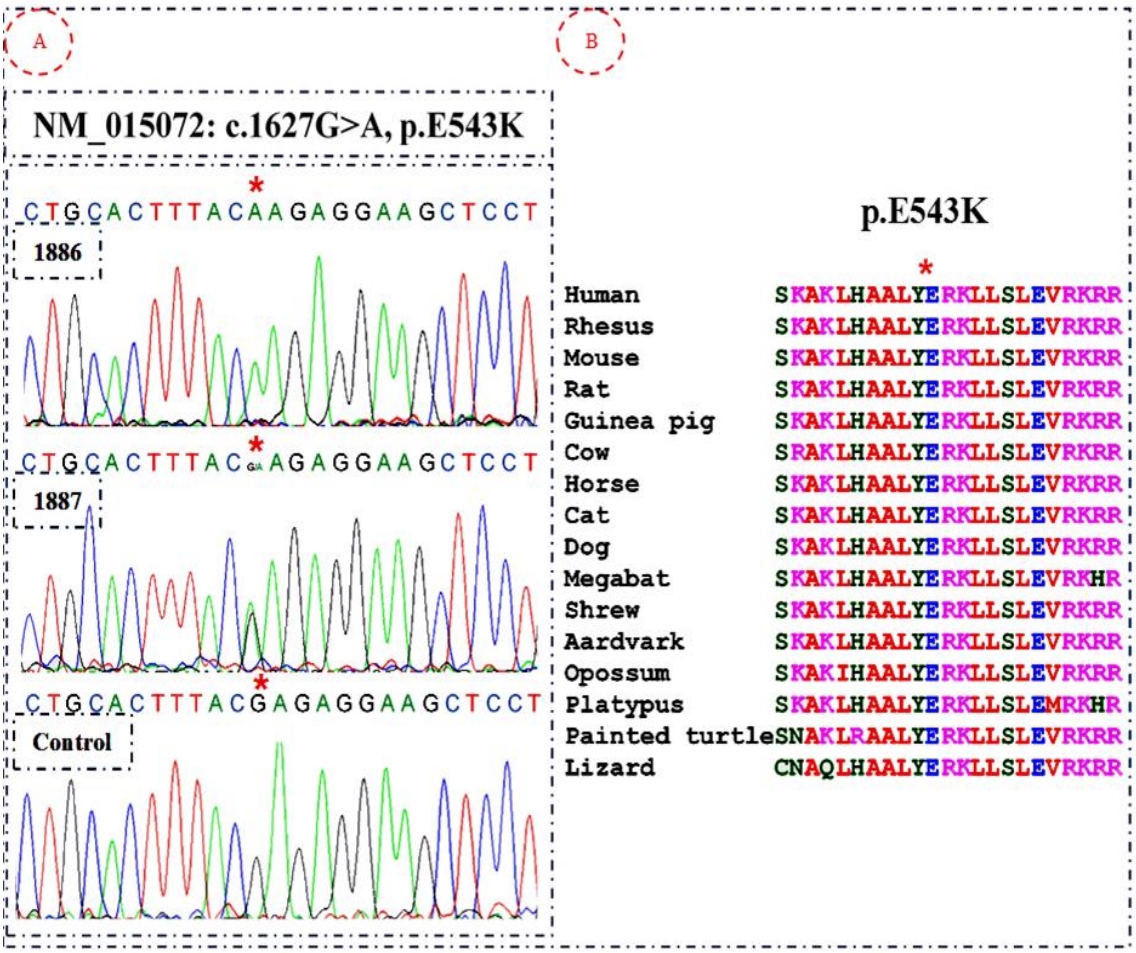

Figure 4.23. Sanger sequence chromatograms of the missense mutation, c.1627G>A, p.E543K, in the *TTLL5* gene and evolutionary conservation of the normal amino acid residue. A. The sequence chromatograms shown are from the DNA of a carrier, an affected member of family MA17 and a normal unaffected subject as control. B. ClustalW alignment of amino acid sequence around the TTLL5 mutation showing evolutionary conservation of the normal glutamic acid residue at position 543.

4.3 Discussion

In this chapter, five families with an autosomal recessive pattern of inheritance are described. Four of these families were large consanguineous pedigrees of Pakistani origin whereas one was a non-consanguineous Caucasian family. Each of these families had been pre-screened using the "retinome" reagent but were found to be negative for changes in the targeted genes (ie all genes on RetNet in 2010). WES technologies were therefore applied on one or more patient samples from each family in order to try to identify the most likely, causative variant(s) associated with the disease phenotype in each case. This

approach was used independently or combined with homozygosity mapping and leading to the identification of mutations in three known causes of RD (*C8orf37*, *MFSD8* and *TTLL5*) and convincing mutations in potentially two new RD genes (*LARGE* and *FDFT1)*.

4.3.1 Confirmation that mutations in *MFSD8* cause non-syndromic recessive retinal disease.

In family MA5, compound heterozygous missense variants c.1006G>C, p.E336Q and c.1394G>A, p.R465Q in *the major facilitator superfamily domain-containing protein 8* (*MFSD8,* OMIM 611124) gene were identified as the most likely causative mutations for MD in three affected siblings, born to unrelated Caucasian parents. Biallelic mutations in *MFSD8* were initially described as causing a variant of late-infantile neuronal ceroid lipofuscinosis (vLINCL, CLN7, OMIM 610951) (Siintola et al., 2007; Aiello et al., 2009; Kousi et al., 2009). The neuronal ceroid lipofuscinoses (NCLs) are collectively the most common childhood neurodegenerative disorders (Haltia, 2003). They are characterised by lysosomal accumulation of autofluorescent lipopigments, neuronal inflammation and subsequent brain atrophy (Haltia, 2003; Mole et al., 2005). Symptoms of vLINCL usually start between the ages of 3-6 years, with seizures and developmental regression, followed by speech failure, ataxia, visual loss, myoclonus and ultimately premature death (Kousi et al., 2009). As a group, NCLs result from dysfunction of lysosome-related proteins or enzymes (Kida et al., 2001; Haltia, 2006). *MFSD8* is thought to function as a lysosomal transporter protein (Siintola et al., 2007). More recently, recessive mutations in *MFSD8* have also been shown to cause non-syndromic MD in two families (Roosing et al., 2015). Prior to this finding, *MFSD8* mutations had not been associated with non-syndromic retinal dysfunction. The work in this chapter confirms the finding of Roosing and are the second report of *MFSD8* mutations cause non-syndromic RD.

The majority of the reported mutations in *MFSD8* are "private" mutations specific to each case or family, and are often null variants. In most cases of syndromic *MFSD8*-related disease the clinical phenotype is relatively uniform, in keeping with a loss of gene function. The ophthalmic features present in conjunction with syndromic disease are consistent with a severe, early onset generalised retinal dystrophy (Siintola et al., 2007; Aiello et al., 2009; Aldahmesh et al., 2009b; Kousi et al., 2009). It is worth highlighting

that one of the *MFSD8* missense mutations, p.E336Q, exists in a heterozygous state in all three families with non-syndromic MD including family MA5. Based on the pathogenicity prediction scores and location of all the *MFSD8* missense mutations identified so far, there is no obvious correlation between the mutations and whether the patient develops vLINCL or non-syndromic RD (Figure 4.24). p.E336Q allele may act as a modifier of disease symptoms resulting in the less severe phenotype when paired with a null variant (Roosing et al., 2015) or when paired with a missense mutation such as p.R465Q reported herein. p.E336Q is close to the edge of the transporting domain and the cytoplasmic surface of the protein (Figure 4.24), and may reduce the transporter function of MFSD8 on the cytoplasmic surface of the lysosome.

Immunolocalization MFSD8 to OPL of the retina, in a region containing a dense network of ribbon synapses between photoreceptors and the dendrites of horizontal and bipolar cells (tom Dieck and Brandstatter, 2006) together with the presence of a post phototransduction ERG (b-wave) abnormality in patients with *MFSD8* mutations (Roosing et al., 2015) strongly suggests association between MFSD8 function and the signal transmission process at the ribbon synapse. Moreover, synaptic alterations have previously been suggested as initiating events causing NCL in a mouse model of lysosomal disease due to a defect in cathepsin D function (CLN10) (Partanen et al., 2008) and in the CLN5-knockout sheep (Amorim et al., 2015). Furthermore, it was reported that reduction in the levels of proteins that are essential for the proper structure and function of the ribbon synapse e.g. pikachurin causes RD with a clinical hallmark of an abnormal b-wave on the ERG and Pikachurin null-mutant mice showed improper apposition of the bipolar cell dendrites to the photoreceptor ribbon synapses, resulting in alterations in synaptic signal transmission and visual function (Sato et al., 2008; Nagaya et al., 2015; Sugita et al., 2015).

The localization of MFSD8 to OPL and the supposed synaptic alterations by *MFSD8* mutations may also explain why the condition is MD with more cone involvement. Extra-macular photoreceptors are the next most vulnerable, with cortical neurons being the most resistant of the affected cell types. There are anatomical and

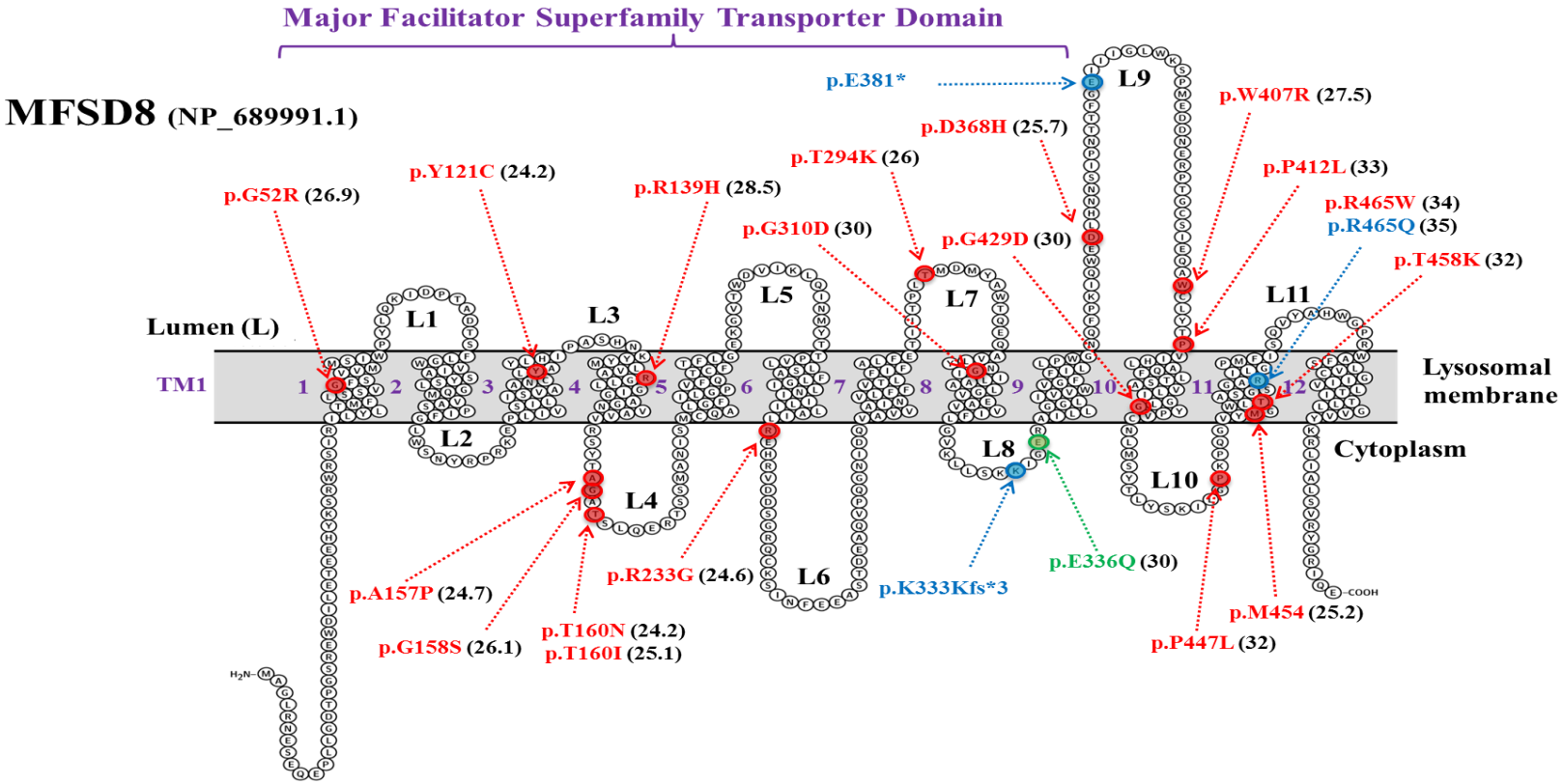

Figure 4.24. Topology prediction diagram of MFSD8 showing the location of pathogenic missense mutations identified to date (July 2016). The twelve transmembrane domain protein (TM), spanning the lysosomal membrane, was visualized using methods described in Section 2.14.5 using the protein sequence with accession code NP_689991.1. The major facilitator superfamily transporter domain motif is highlighted. Pathogenic missense mutations that give rise to vLINCL are depicted in red. Mutations highlighted in blue were reported as either causing vLINCL or combining with the predicted milder mutation p.E336Q (highlighted in green) to cause non-syndromic MD. Number in brackets corresponds to CADD scaled C-scores for the mutation and values ≥ 20 and ≥ 10 respectively represent the 1% and 10% most deleterious changes predicted in the human genome.

physiological differences between photoreceptor and conventional synapses that could account for this differential vulnerability. Photoreceptor terminals release neurotransmitter continuously, with light turning off vesicle release, whereas cortical neurons are usually switched off and are only triggered by action potentials and photoreceptor terminals contain many more synaptic vesicles of which ~85% are freely mobile, actively participating in glutamate release, compared to ~20% in conventional synapses (Pyle et al., 2000; Richards et al., 2003; Rea et al., 2004; Choi et al., 2005). Furthermore, photoreceptor termini possess a synaptic ribbon for vesicle docking, necessary for maintaining the higher rates of neurotransmitter release over a sustained period of time (Sterling and Matthews, 2005). It is also relevant that peripheral cones contain twice as many ribbons as central cones (Chun et al., 1996), suggesting that this, or a similar synaptic modification, may underlie the different photoreceptor sensitivities. Indeed, as observed in some other cells, the lysosomes may even have a role as 'non-professional' synaptic vesicles, directly releasing neurotransmitter themselves (Andrews, 2000; Luzio et al., 2007). The consequences of lysosomal dysfunction at the synapse could therefore be either disordered neurotransmitter release, or inadequate reuptake, and this may result in local excitotoxicity. Whatever this mechanism may be, it appears that the photoreceptors in particular are exquisitely sensitive to this.

To conclude, this study describes patients with isolated retinal disease due to bilallelic mutations in *MFSD8*, mutations in which are usually associated with NCL. The data suggest that the genotype influences the phenotype, with a mild reduction in MFSD8 function results in an isolated later onset maculopathy whilst a severe reduction caused by functionally null alleles results in central nervous system pathology. This study provides an insight into the underlying pathology of disease and contributed to a paper that is currently under review at the journal Investigative Ophthalmology and Visual Science (IOVS).

4.3.2 A novel *C8orf37* homozygous mutation causes RP in a consanguineous family of Pakistani origin

In family MA13, a novel homozygous *C8orf37* (OMIM 614477) mutation, c.555G>A, p.W185* was identified in the affected patients who had a diagnosis of non-syndromic RP. *C8orf37* spans 23,203 nucleotides of genomic DNA and consists of six

exons that encode a 207 amino acid protein (chromosome 8 open reading frame 37) of unknown function with a predicted molecular mass of approximately 23kDa. It has no significant overall sequence homology with any other human proteins. C8orf37 is ubiquitously expressed and immunolocalization studies on human and mouse retinal cross-sections have shown that C8orf37 co-localizes with polyglutamylated tubulin, acetylated α-tubulin and γ-tubulin, the basal body markers at the base of the connecting cilium, between the outer and inner segments in the photoreceptor layer (Estrada-Cuzcano et al., 2012b). The basal body acts as the organizing centre for the cilium and permits trafficking of proteins and lipids by the intraflagellar transport system from the inner to the outer segment, a process necessary for the formation of the outer segment discs (Qin et al., 2004; Wright et al., 2010).

C8orf37 mutations were first identified as a cause of RD in 2012 when Estrada-Cuzcano and colleagues reported three mutations in four families with either CRD or RP with early macular involvement (Estrada-Cuzcano et al., 2012b). Since this study more mutations have been reported in *C8orf37* but they are rare and account for only ≤1% of all unrelated RD cases that have been identified (Fahim et al., 2013; Nash et al., 2015). Studies on the clinical features seen in patients with mutations in this gene described eight patients with a diagnosis of CRD and seven with RP with early macular involvement (Estrada-Cuzcano et al., 2012b; van Huet et al., 2013; Jinda et al., 2014; Lazar et al., 2015; Katagiri et al., 2016). RP (Section 1.6) and CRD (Section 1.7.3) differ in terms of the predominant photoreceptor cell type involved, but there can be some overlap between these diagnoses depending on the age of the patients and the testing carried out. The prevalence of CRD is 1 in 40,000 individuals and for RP, 1 in 4,000 individuals (Haim, 2002; Hamel, 2007). Distinguishing between RP, in which patients experience night blindness followed by progressive visual field constriction, and CRD, where the symptoms are photophobia, loss of visual acuity, and central vision, depends on recognizing the early symptoms and examination of electroretinography data (van Huet et al., 2013). However, in severe end-stage disease there may be considerable phenotypic overlap on presentation, making it difficult to diagnose these progressive conditions. Sometimes when features of both conditions are present at the early stages it may be difficult to assign a disease category (Berger et al., 2010; den Hollander et al., 2010).

Of the 81 genes that have mutations leading to RP and the 33 genes that have defects leading to COD/CRD (RetNet, May 2016), mutations in only eight genes, including *C8orf37*, account for patients with either diagnosis. These genes affect a wide variety of molecular pathways and processes and include dominant mutations in *CRX* (OMIM 120970) (Sohocki et al., 1998), *SEMA4A* (OMIM 607292) (Abid et al., 2006) and *PRPH2* (OMIM 179605) (Kajiwara et al., 1991; Nakazawa et al., 1994); recessive mutations in *ABCA4* (OMIM 601691) (Allikmets et al., 1997b; Martinez-Mir et al., 1998; Maugeri et al., 2000) and *CERKL* (OMIM 608381) (Tuson et al., 2004; Aleman et al., 2009); X-linked mutations in *RPGR* (OMIM 312610) (Meindl et al., 1996; Yang et al., 2002), and mutations in *PROM1* (OMIM 604365) that show a genotype-phenotype correlation. A dominant missense mutation, p.Arg373Cys (dbSNP: rs137853006) causes CRD (Yang et al., 2008) whereas recessive mutations lead to RP (Maw et al., 2000; Yang et al., 2008).

Recently, *C8orf37* mutations have been linked twice with BBS (Heon et al., 2016; Khan et al., 2016a). Khan et al. (2016) identified a previously reported homozygous mutation, c.529C>T, p.R177W, in a 6 year old child with BBS from Saudi Arabia. The child has obesity, hypodontia, irregular dental spacing, postaxial polydactyly, high myopia and CRD. Furthermore, Heon et al. (2016) identified a novel loss-of-function homozygous *C8orf37* mutation (c.304A>T, p.K102*) in a 17-year-old Caucasian female, born to consanguineous parents. She had a slowly progressive CRD, high myopia and BBS features that included obesity (with a BMI of 29.1), three-limb post-axial polydactyly, a mild learning difficulty, horseshoe kidney, abnormally positioned uterus and elevated liver enzymes. This association was confirmed by C8orf37 knockdown in *Danio rerio* (zebrafish) that resulted in impaired visual function and BBS-related phenotypes such as such as defects in a ciliated Kuppfer's vesicle (KV), delays in melanosome transport and impairment in visual behaviour (Heon et al., 2016). Patients in family MA13 need to a specifically check for ciliopathy features as it is easy to miss some of the features of ciliopathies as being overweight is common and the clinician can't see kidney defects and don't look unless there is a problem.

A summary of all the *C8orf37* mutations found in patients with RD to date, together with the available clinical information in each case was compiled to deduce any phenotype/genotype correlation (Estrada-Cuzcano et al., 2012b; van Huet et al., 2013; Jinda et al., 2014; Lazar et al., 2015; Ravesh et al., 2015; Heon et al., 2016; Katagiri et

al., 2016; Khan et al., 2016a; Rahner et al., 2016) (Figure 4.25). The clinical features of night blindness, visual field constriction and progressive loss of vision appeared to be consistent in all patients with *C8orf37* mutations, whether the patients had a missense mutation or a null allele, suggesting that there does not appear to be an obvious correlation between genotype and phenotype. However, all affected patients who harbouring splice site mutations affecting intron 1 of *C8orf37* have postaxial polydactyly as additional feature (Estrada-Cuzcano et al., 2012b; van Huet et al., 2013; Rahner et al., 2016). BBS-related phenotypes as an additional feature with CRD, together with the known cellular localisation, all serve to suggest that this condition is a ciliopathy (Estrada-Cuzcano et al., 2012b; Heon et al., 2016; Rahner et al., 2016).

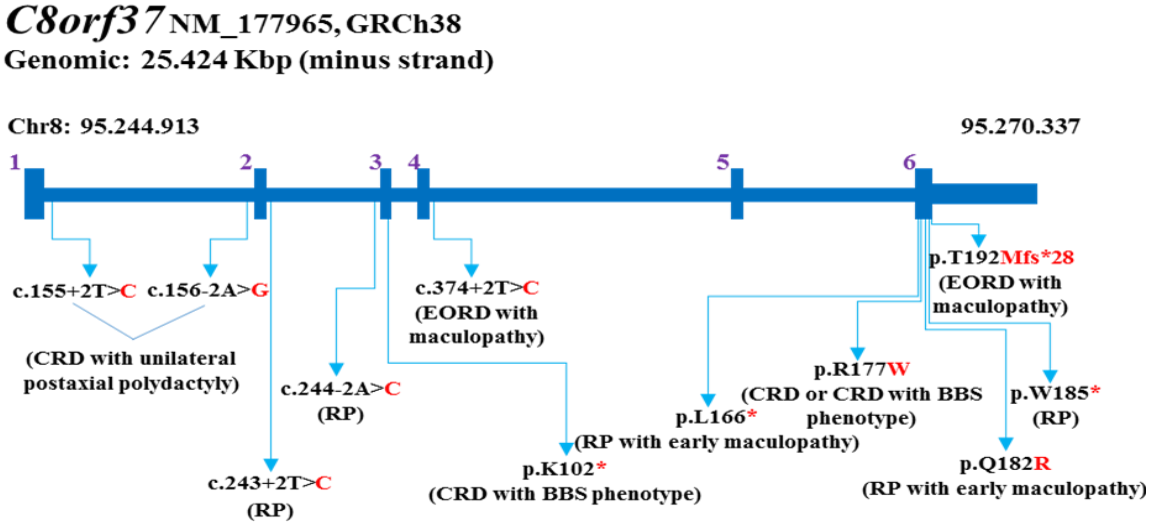

Figure 4.25. Diagram showing *C8orf37* mutations identified to date (July 2016) together with diagnosis of the patient(s) in whom they were found. The six coding exons of *C8orf37* are shown. The mutations are annotated relative to the transcript with accession number NM_177965 and protein sequence with accession NP_808880.1

To summarize, a novel *C8orf37* mutation has been identified in a consanguineous family who originated in Pakistan. These findings contribute further data on the phenotype and the spectrum of mutations in this form of RP. This work contributed to a paper that was published in the journal Molecular Vision (Ravesh et al., 2015).

4.3.3 Exome sequencing identified *LARGE* as a new candidate gene for non-syndromic retinal dystrophy

In family MA14, a homozygous missense mutation in *LARGE* was identified as the most likely candidate variant for causing RP in the affected members of family MA14.

The *LARGE* gene is located at the long arm of chromosome 22 (22q12.3) and spans more than 647 kilobases (kbp) (chr22: 33,669,062-34,316,416, hg19) of genomic DNA. *LARGE* is the fifth largest gene in the human genome (hence its name '*LARGE'*). It contains 15 exons that encode a 756 amino acid protein containing an amino-terminal transmembrane domain, a coiled-coil domain and two catalytic domains of N-acetylgalactos-aminyl-transferases (Brockington et al., 2005).

The LARGE protein is involved in protein glycosylation, a post-translational modification when sugar molecules are added to certain proteins. The amino-terminal transmembrane domain of LARGE interacts with the mucin-like domain of alpha-dystroglycan (α-dystroglycan), defining an intracellular enzyme-substrate recognition motif necessary for the post-translational modification of α-dystroglycan which is required for the functional glycosylation of α-dystroglycan (Kanagawa et al., 2004). This modification acts through two glycosyltransferase activities of the LARGE protein (xylosyltransferase and glucuronyl transferase) that allow xylose and glucuronic acid containing glycan structures to be added to α-dystroglycan. Addition of a glycan allows glycosylated α-dystroglycan to bind laminin-G-domain-containing extracellular matrix ligands, which are required for the normal function of skeletal muscle basement membranes and neuromuscular junctions (Inamori et al., 2012). Lack of the transmembrane domain causes mislocalization of LARGE at the Golgi apparatus, while lack of catalytic domains causes inhibition of the glycosyltransferase activities of LARGE and prevents α-dystroglycan hyperglycosylation (Brockington et al., 2005). The LARGE protein acts on α-dystroglycan which is localized to the outer plexiform layer (OPL) (Montanaro et al., 1995). This is consistent with the IF staining results that showed localization of LARGE to OPL, PIS and ONL in the mouse retina (Section 4.2.3.4).

Mutations in the *LARGE* gene have previously been shown to cause dystroglycanopathy in a myodystrophy mouse model carrying a null mutation (100-kb genomic deletion) in *LARGE* (Grewal et al., 2001). The *LARGE*^{myd} was then used as a model for congenital muscular dystrophy (CMD). The phenotypic studies of this model showed a sharp decrease in glycosylated α-dystroglycan in muscular dystrophy. They also revealed a defect in retinal transmission, with abnormalities of b-wave characteristics for ON bipolar cells and the Muller cells, abnormal neuronal migration, and defective laminar

architecture of the cerebrum and the cerebellum cortices (Holzfeind et al., 2002; Michele et al., 2002).

The first human biallelic mutation in *LARGE* was identified in 2003 (Longman et al., 2003) in a 17-year-old girl with congenital muscular dystrophy, mental retardation, structural brain abnormalities and a moderate reduction in the level of glycosylated α-dystroglycan in muscle sections. This phenotype was named congenital muscular dystrophy 1D (MDC1D) and represented one of a heterogeneous group of human muscle-eye-brain disorders that are characterized by severe CMD, eye abnormalities and central nervous system neuronal migration defects. These also include Fukuyama-type CMD and Walker–Warburg syndrome (WWS). These diseases result from mutations in one of six genes which encode glycosylation enzymes (*POMT1, POMT2, POMGnT1, fukutin, FKRP* and *LARGE*) (Muntoni et al., 2007).

To date, only 15 patients in 12 families have been reported to have mutations in *LARGE* (Table 4.8) (Longman et al., 2003; Godfrey et al., 2007; van Reeuwijk et al., 2007; Clement et al., 2008; Mercuri et al., 2009; Clarke et al., 2011; Vuillaumier-Barrot et al., 2011; Meilleur et al., 2014). Analysis of the mutation spectrum identified in *LARGE* shows association between the pathogenicity of the disease-causing mutation and the severity of the phenotype ranging from milder MDC1D to a severe form of CMD (WWS). Patients who had a compound heterozygous combination of a frameshift indel or nonsense variant with a missense mutation showed a milder phenotype MDC1D or Fukuyama-type CMD, with sufficient motor ability to walk or climb stairs and a moderate reduction of glycosylated α-dystroglycan. A complete loss of *LARGE* function due to the presence of two nonsense or frameshift indel mutations leads to a severe phenotype of WWS with more severe motor inability and sharply decreased glycosylated α-dystroglycan. This result was consistent with the findings of Goddeeris et al. (2013) who reported a direct association between *LARGE*-glycan extension and its binding capacity for extracellular matrix ligands and knocking out of *LARGE* produced a dystroglycan with minimal *LARGE*-glycan repeats that led to immature neuromuscular junctions and a less compact basement membrane.

Family ID	Number of patients	Mutation	Zygosity	Phenotype	Eye Involvement	Reference
1	1	c.1999insT (p.693X); c.1525G>A (p.Glu509Lys)	C-Hetero	MDC1D	Nystagmus	Longman et al. (2003)
2	1	c.1548C>G (p.Trp516X)	Hetero	WWS	Retinal detachment	Godfrey et al. (2007)
3	2	63-kb del (introns 8-10) resulting in premature stop codon	Homo	WWS	Bilateral leukocornia, retinal dysplasia, posterior synechia	van Reeuwijk et al. (2007)
4	1	c.253_259dup (p.Gln87fs); c.992C>T (p.Ser331Phe)	C-Hetero	MEB-like	Myopia	(Clement et al., 2008)
5	1	c.1483T>C (Trp495Arg)	Homo	WWS	NR	Mercuri et al. (2009)
6	2	Insertion between exons 10 and 11 deletion (3-4 kb) in intron 10	Homo	MEB-like	Mild myopia, strabismus	Clarke et al. (2011)
7	2	c.871+27358_1132- 21850del42152insT; 252-kb dup of exons 2-4	C-Hetero	WWS	Bulging eyes, horizontal narrow palpebral slit	Vuillaumier-Barrot et al. (2011)
8	1	c.106+6361_408-6628del122058insGTGTG; c.615+24218_788-42869del105083insAATG	C-Hetero	WWS	No retinal dysplasia or other eye involvement	
9	1	74-kb deletion flanking exons 4-6, c.1525G>A (p.Glu509Lys)	C-Hetero	Fukuyama CMD	Amblyopia, microtropia	Meilleur et al. (2014)
10	1	c.1328_1329delGCinsAT (p.Cys443Tyr)	Homo	WWS	Thin optic nerves, severe atrophy of ganglion cells and very thin nerve fibre layer	
11	1	330.6-kb deletion of exons 3-7; 74.3-kb deletion of exon 7	C-Hetero	WWS	Complete retinal detachment on the right and poor retinal development on the left	
12	1	108-kb homozygous deletion of exons 4-7	Homo	WWS	Bilateral retinal detachment and blindness	

Table 4.8. Summary of all case reports of *LARGE* mutations identified to date (July 2016). Family ID, number of patients studied, mutation, zygosity, phenotype and extent of eye involvement. C-Hetero = compound heterozygous, Homo = homozygous, Hetero = heterozygous, MDC1D = Congenital Muscular Dystrophy type 1D, MEB = muscle-eye-brain disease, WWS = Walker–Warburg syndrome, Fukuyama CMD = Fukuyama-type Congenital Muscular Dystrophy and NR = not recorded.

In summary, in this study a novel homozygous missense mutation was identified that segregates with non-syndromic RP in a large consanguineous family, giving a very significant LOD score. This finding strongly suggests that the phenotype found in this family represents the less severe end of the phenotype spectrum of mutations in the *LARGE* gene, causing non-syndromic RP. This mutation is localized in the second catalytic domain of the protein and is expected to have minimum effects on the *LARGE*-glycan extension. However modelling of the effects of this mutation, screening patients' blood for glycosylation defects, searching for more mutations among RD patients are all potential ways to strengthen this finding.

4.3.4 Exome sequencing identified *FDFT1* as a potential new candidate for retinal dystrophy

In family MA17, a novel homozygous missense mutation in *FDFT1* (NM_004462: c.930C>G, p.F310L) was identified as a potential case of the RCD phenotype in the family. Farnesyl diphosphate farnesyl transferase1 (FDFT1, OMIM 184420), or squalene synthase, is a membrane-associated enzyme located at the branch point in the mevalonate pathway. FDFT1 catalyses the conversion of two molecules of farnesyl diphosphate to squalene in the first step in the cholesterol biosynthetic pathway (McKenzie et al., 1992; Stamellos et al., 1993). *FDFT1* is ubiquitously expressed in human tissues (Tansey and Shechter, 2001). Targeted disruption of *FDFT1* in mice causes embryonic lethality in the homozygotes, while the heterozygous mice have phenotypically normal plasma levels of total cholesterol (TC), low-density lipoprotein cholesterol (LDL-C) and high-density lipoprotein cholesterol (HDL-C) (Tozawa et al., 1999).

Previous studies have shown association of non-synonymous SNPs such as p.K45R of *FDFT1* with plasma cholesterol levels (Do et al., 2008), while targeted-overexpression of *FDFT1* in the mouse liver caused increased plasma TC, LDL-C, and HDL-C levels (Okazaki et al., 2006) confirming a strong effect of *FDFT1* in regulating plasma cholesterol levels (Do et al., 2008). Cholesterol is an essential lipid constituent of cell membranes, and cholesterol biosynthesis is required to make vitamin D. There are two known pathways of cholesterol input into the retina, *in situ* cholesterol biosynthesis that accounts for the majority (72%) of retinal cholesterol input in the mouse, and tissue uptake of cholesterol from the systemic circulation (Lin et al., 2016). Some cholesterol-

related genes (*ABCA1*, *APOE*, *CETP* and *LIPC*) are risk factors for AMD (Peter et al., 2011; Yu et al., 2011; Paun et al., 2015), but the link between cholesterol homeostasis in the retina and retinal degeneration are poorly understood (Fliesler and Bretillon, 2010; Pikuleva and Curcio, 2014).

In the work described here, a variant in *FDFT1* was shown to be the most likely cause of non-syndromic retinal disease. However in the absence of the finding of further mutations, this link remains unproven. Work to further substantiate the link between *in situ* cholesterol biosynthesis and inherited retinal degeneration could include modelling of the effect of the F310L variant and blood testing in patients to look for an imbalance of the cholesterol metabolism. Also the second case with *FDFT1* heterozygous mutation need first a full clinical examination to check whether her phenotype similar to that in the family MA17. Then it might be worth doing WGS on this case to check for the other missing heterozygous variant that may be large indel or deep intronic change.

4.3.5 A *TTLL5* homozygous mutation causes rod-cone dystrophy in a consanguineous family of Pakistani origin

The *TTLL5* (tubulin tyrosine ligase-like family member 5, OMIM 612268) gene, also called *STAMP* (SRC1 and TIF2-associated modulatory protein), encodes a glucocorticoid receptor that is one of 13 members of the tubulin tyrosine ligase-like superfamily (TTLLs) (He and Simons, 2007; Bosch Grau et al., 2013). *TTLL5* has been mapped to chromosome 14q24.3 and has 32 exons that encode a 1,281 amino acid protein with an approximately 400 amino acid carboxy-terminal residue, making it one of the longest carboxy-terminal extensions in the TTLL family of proteins (van Dijk et al., 2007). This protein is expressed in many tissues, with the highest expression profile in heart and testes (http://www.proteinatlas.org/ENSG00000119685-TTLL5/tissue) and lower expression in eye and the brain. Protein topology predicts a highly homologous core amino-terminus tubulin tyrosine ligase domain, three carboxy-terminal receptor interaction domains and one carboxy-terminal coactivator interaction domain (Janke et al., 2005; Lee et al., 2013).

Multiple activities have been associated with *TTLL5*. The carboxy-terminal extension is a transcription cofactor and has polyglutamylation activities (He and Simons, 2007; van Dijk et al., 2008). Polyglutamylation is a post-translation modification associated with sequential attachment of glutamic acids to an internal glutamate residue of the target proteins (Edde et al., 1990; Janke et al., 2008). TTLL5 interacts with two glucocorticoid receptor coactivators, namely, transcriptional intermediary factor 2 (TIF2) and steroid receptor coactivator 1 (SRC-1) to mediate gene induction and repression. It also has a function as an alpha tubulin (α-tubulin) polyglutamylase and is required for centriole and spindle–associated protein (CSAP) localization to both spindle and cilia microtubules (van Dijk et al., 2008). Disruption of *TTLL5* leads to male infertility in mice. Mutant *STAMP*$^{tm/tm}$ mice that lack the carboxy-terminal extension but retain the TTLL domain, showed a sharp reduction in the level of polyglutamylation of α-tubulin in sperm, correlating with reduced levels of a truncated protein retaining the structural features to permit polyglutamylation (Lee et al., 2013). Reduced α-tubulin polyglutamylation resulted in abnormal axonemal structures with loss of tubulin doublets in sperm tails and defective sperm motility. This reduced fertility in male mice, while female mice were apparently normal (Lee et al., 2013). Lastly, *TTLL5* was localized to the base of the connecting cilium between the basal body and the adjacent daughter centriole in the photoreceptor cells of the mouse and human retina (Sergouniotis et al., 2014), so it is thought to be responsible for the tubulin polyglutamination in the microtubule triplets of the centrioles, increasing the centriole stability.

Recently, biallelic *TTLL5* mutations have been shown to cause RD (Sergouniotis et al., 2014). These authors identified five patients with *TTLL5* mutations from four unrelated families, each showing either early or late onset cone dystrophy. The five mutations that had been identified consisted of frameshift mutations, p.L134Rfs*45 and p.E529Vfs*2, nonsense mutations, p.E543* and p.W1118*, and a missense mutation, p.E543K. The missense mutation identified in family MA19 (p.E543K) was a reported in this study in a 53-year-old man with adult-onset cone dystrophy. Interestingly, male patients of the family MA19 (1885 and 1888) are both fertile (five offspring each). This is consistent with the fact that the E543K missense mutation is outside the carboxy-terminal tail of TTLL5 that is thought to play an essential role in normal male fertility (Lee et al., 2013). Also, all 5 RD patients described in the published report were diagnosed with cone or cone-rod dystrophy, whilst patients of family MA19 showed a rod first form

of the RD, suggesting that disruption of TTLL5 polyglutamylation activities can lead to primary loss of either cone or rod photoreceptors in the human retina. This work contributed to a paper that the published at Human Molecular Genetics journal (Bedoni et al., 2016).

Chapter 5. An atypical late-onset retinal dystrophy with early macular involvement is caused by biallelic mutations in the autophagy regulator *DRAM2*.

5.1 Introduction

In clinics at the Eye Department of St. James's University Hospital, Leeds, consultant ophthalmologist Mr Martin McKibbin saw a family, designated ES1, of Pakistani origin, with multiple affected members diagnosed as having an atypical RD. The family tree is illustrated in Figure 5.1.

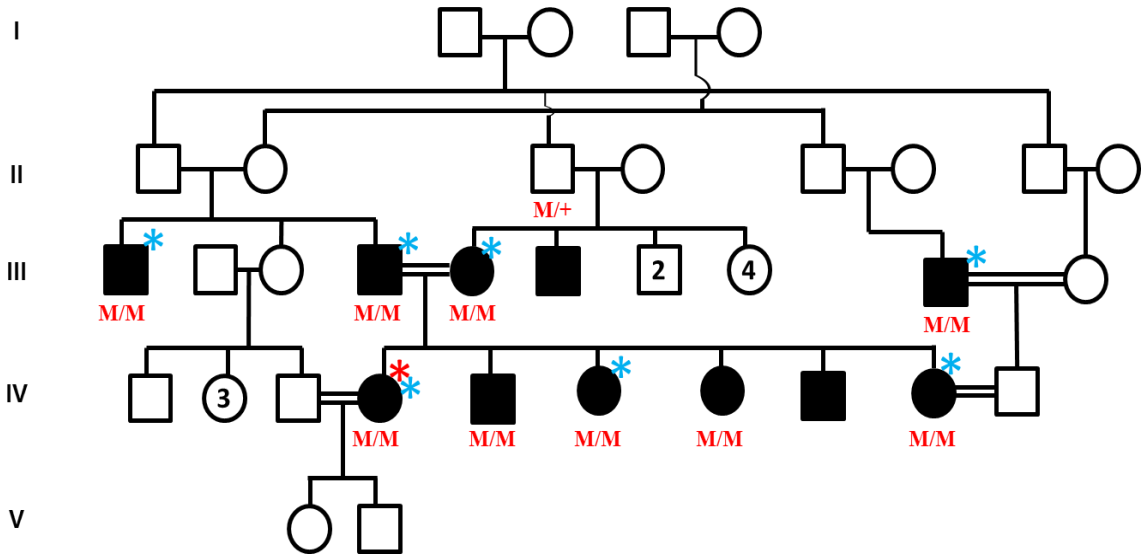

Figure 5.1. Pedigree of family ES1. Affected individuals are shaded black. The genotypes for all tested family members are shown below each individual; + = wild type allele and M = c.140delG, p.G47Vfs*3. * = Family member for whom DNA was exome sequenced and * = Family member for whom DNA was SNP chipped. (Adapted from El-Asrag et al. (2015) with the permission of Elsevier Copyright Clearance Centre, License number: 3919040428835).

The phenotype observed in this family was unusual, with an adult-onset retinal dystrophy with early macular involvement. Mr McKibbin has extensive experience of a wide range of retinal dystrophies, and was of the view that this represented a condition likely to be distinct from any other he had observed. Affected individuals presented with symptoms in the second or third decade, describing increasing difficulty with close visual

tasks. Neither light sensitivity nor night blindness were significant early symptoms, though there was progressive loss of visual acuity in all symptomatic individuals. However light sensitivity and difficulty seeing in dim illumination were inconsistent features of advanced disease. A summary of the clinical features are shown in Table 5.1.

Patient (sex)	Presenting symptom	Age of Onset	LogMAR VA RE/LE	Fundus examination	Fundus AF	OCT
III:1 (M) III:4 (M) III:13 (M)	Central visual loss Central visual loss Central visual loss	16 23 25	2.3/2.3 2.0/2.0 2.0/2.0	Central macular atrophy with pigment clumping and surrounding granular appearance; midperipheral bone spicule pigmentation; attenuated vessels **(48, 56, 46)**	ND	ND
III:5 (F)	Central visual loss	28	1.0/2.0	Central macular atrophy with surrounding granular appearance; pigment clumping in left macula only; minimal peripheral changes **(51)**	ND	ND
III:6 (M) IV:8 (F) IV:11 (F)	Central visual loss Central visual loss Central visual loss	25 21 27	1.3/1.3 0.8/0.8 1.0/1.0	Granular macular atrophy with associated yellow dots **(37, 24, 29)**	ND	ORL loss **(37, 24, 29)**
IV:6 (F)	Central visual loss	26	0.8/0.8	Granular macular atrophy with associated yellow dots and pigment clumping; irregular reflex extending beyond the macula **(32)**	ND	ORL loss **(32)**
IV:7 (M)	Central visual loss	22	0.2/0.2	Irregular foveal reflex **(23)**	ND	ORL loss **(23)**
IV:9 (F)	Central visual loss	22	1.0/1.0	Granular macular atrophy with yellow dots at its temporal edge **(25)**	Hyper AF ring around central area of hypo AF **(25)**	Reduced foveal thickness **(21)**; ORL loss **(25)**
IV:10 (M)	Asymptomatic	19	0.0/0.0	Within normal limits **(19)**	ND	Reduced foveal thickness, disruption of the ellipsoid zone **(19)**

Table 5.1. Summary of clinical data from eleven patients from family ES1. VA = visual acuity, RE = right eye, LE = left eye, OCT = optical coherence tomography, AF = autofluorescence, ORL = outer retinal layer and ND = not done. Number in brackets corresponds to the age (years) at which the patient was tested.

As the disease progressed, subjects III:4, III:13, IV:9 and IV:6 developed photophobia, while subject III:13 complained of night vision problems. Fundus examination revealed maculopathy in all symptomatic individuals tested, with peripheral retinal degeneration being a frequent finding in older subjects. Notably, OCT imaging in a pre-symptomatic individual (subject IV.9) suggested early central photoreceptor cell loss (Figure 5.2) in the second decade of life.

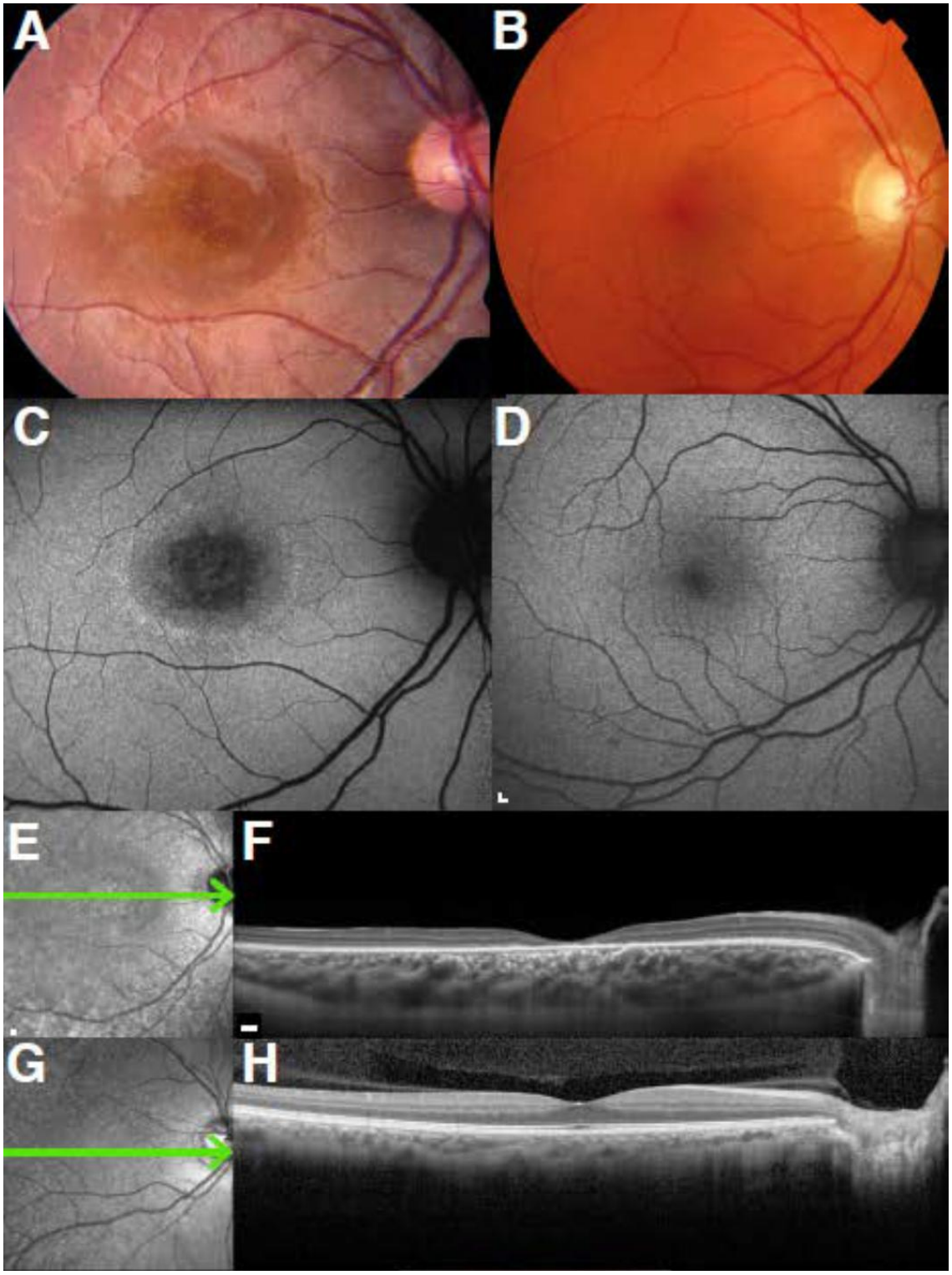
A
B
C
D
E
F
G
H

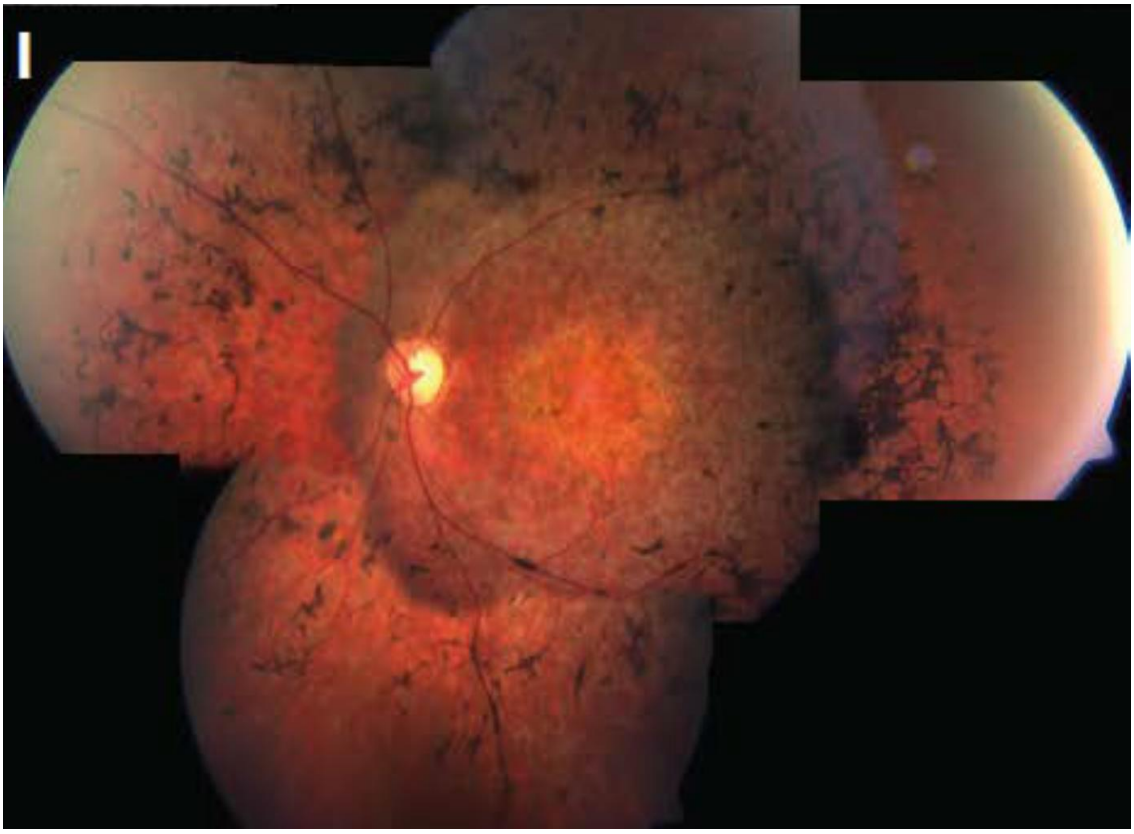

Figure 5.2. Retinal imaging of individuals (IV.9 and III.1) from family ES1. Colour fundus photograph (A), fundus AF (C), infra-red reflectance (E) and OCT (F) images from the right eye of case IV.9 at 25 years. Corresponding images from an unaffected individual are provided for comparison (B, D, G and H). Macular atrophy with white dots at its temporal edge are observed on fundus photography. On AF imaging, there is a central area of reduced AF surrounded by a hyper AF ring. On OCT imaging, there is significant thinning in the foveal region consistent with photoreceptor loss. A composite color photograph from the left eye of case III.1, at the age of 48, is also shown (I). This reveals macular atrophy, mid-peripheral bone-spicule pigmentation and attenuated retinal vessels. On the infra-red reflectance images, the horizontal green lines indicate the position and direction of the corresponding OCT scan. AF = autofluorescence and OCT = optical coherence tomography. (Reused from El-Asrag et al. (2015) with the permission of Elsevier Copyright Clearance Centre, License number: 3919040428835).

Peripheral blood was collected from the affected individuals, parents and their unaffected relatives where they consented and were available. Genomic DNA was extracted from blood leukocytes as described in Section 2.2. DNA from seven affected family members (III.1, III.4, III.5, III.13, IV.6, IV.8 and IV.11; Figure 5.1) was sent away to the company MRC GeneService (London, UK) for SNP genotyping using the Affymetrix 250K SNP array. This chapter describes the identification of the genetic basis

of RD in the affected members of family ES1 and contributed to publications by El-Asrag et al. (2015) and Sergouniotis et al. (2015).

5.2 Results

5.2.1 Analysis of SNP genotyping data by homozygosity mapping

The multiple consanguineous marriages in the family suggested that an autosomal recessive inheritance pattern for retinal dystrophy was the most likely mode of inheritance in this family. Analysis was therefore carried out on the assumption that the condition was caused by a recessive mutation inherited from a common ancestor, and that this allele and the chromosomal region around it would be homozygous in each affected individual. Homozygosity mapping of SNP array genotyping data was therefore considered a useful method to locate and identify the disease gene. The SNP genotyping data from seven affected individuals (III.1, III.4, III.5, III.13, IV.6, IV.8 and IV.11; Figure 5.1) were annotated individually by using Affymetrix Genotyping Console Software and then analysed using AutoSNPa software to identify regions of homozygosity that overlapped in multiple affected individuals and would represent an autozygous region (Section 2.12). The output data files were then imported to AgileMultiIdeogram to display the regions of homozygosity shared between all the affected individuals at the genome level (Figure 5.3).

Two homozygous regions were shared among all seven affected individuals: a 10.1Mb interval on chromosome 1 between rs6677953 and rs814987 and a 2.9Mb region on chromosome 7 between rs17140297 and rs12706292. The two homozygous regions that were shared among all seven affected individuals of family ES1 contained 167 RefSeq genes. The larger region on chromosome 1 (Chr1:106188422-116250460, hg38) contained 160 RefSeq genes, while the smaller region on chromosome 7 (Chr7:117088307-119982844, hg38) contained only 7 genes (Figure 5.4). None of the genes within these homozygous intervals had been reported previously to be associated with retinal dystrophy (RetNet, accessed February 2015).

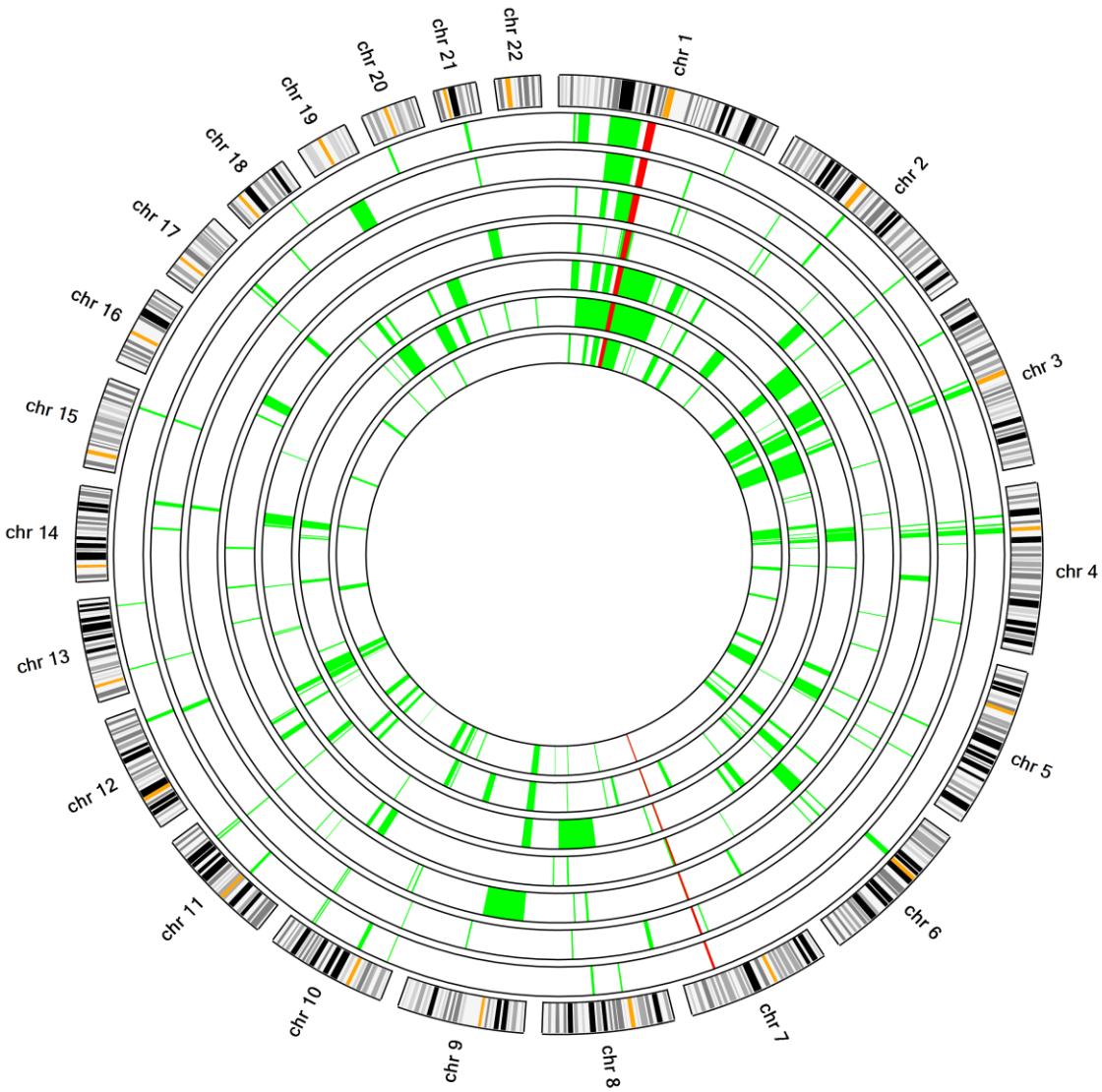

Figure 5.3. Homozygosity mapping in family ES1. The figure displays the locations of the homozygous regions identified by SNP genotyping data of multiple individuals against a circular ideogram of chromosomes 1–22. Data for individuals III.1, III.4, III.5, III.13, IV.6, IV.8 and IV.11 are displayed in that order as white circular bands toward the center of the ideogram. The homozygous regions in each family member are shown in green. The common autozygous regions identified in all affected family members are highlighted in red. (Adapted from El-Asrag et al. (2015) with the permission of Elsevier Copyright Clearance Centre, License number: 3919040428835).

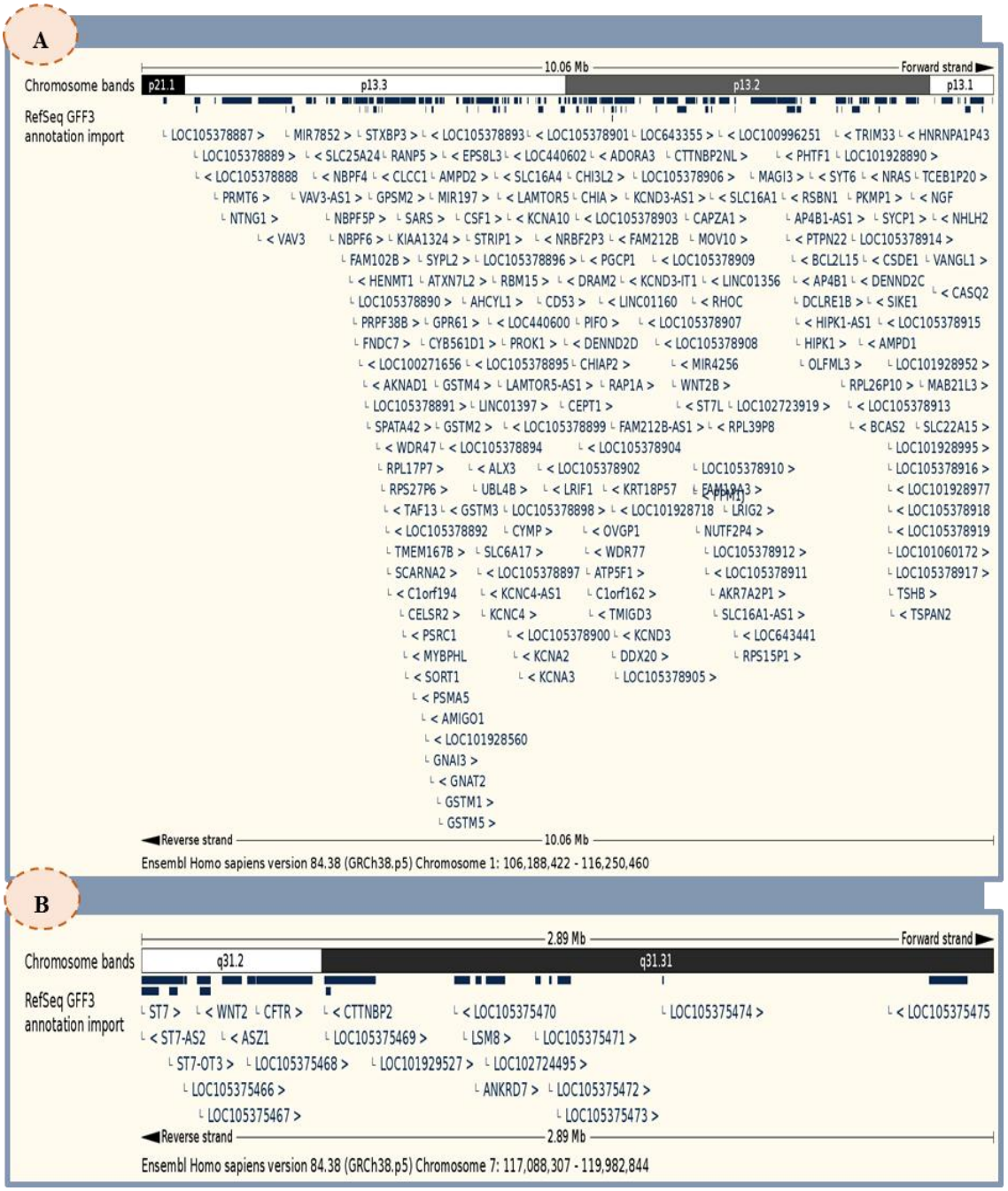

Figure 5.4. RefSeq genes in homozygous regions identified in family ES1. Ensembl genome browser output displaying the list of genes in the two homozygous regions shared among all seven affected individuals III.1, III.4, III.5, III.13, IV.6, IV.8 and IV.11 of family ES1. 160 genes were found in the region on chromosome 1 (Chr1:106188422-116250460, hg38) (A), while only 7 genes were found in the region on chromosome 7 (Chr7:117088307-119982844, hg38) (B).

5.2.2 Analysis of WES of patient IV.6 from family ES1

WES was utilized to identify the molecular pathology in the family. DNA from one affected family member (subject IV.6, family ES1; Figure 5.1) was extracted (Section 2.2) and the concentration of purified DNA was estimated (Section 2.3). 3µg of genomic DNA was prepared for whole exome sequencing using the SureSelectXT Human All Exon V4 target enrichment reagent, and paired-end sequencing was completed on a HiSeq2500 system (Section 2.10.1). The quality of the raw sequence data files was checked using FastQC tools and sequencing reads with quality scores less than 20 were removed. The FastQ files were then aligned to the human reference genome sequence (hg19/GRCh37) using Bowtie2 and a total of 34,490,556 reads were obtained. The sequence file was then processed in SAM/BAM format according to methods described in Section 2.10.2. Quality score recalibration was achieved and 13.81% of the sample reads were removed as PCR duplicates. The annotated VCF file was then filtered by removing all variants that lay outside the exons and flanking two base-pair splice donor and acceptor sites, synonymous variants, variants with a read depth of less than 5 and variants with a MAF ≥1% in dbSNP142, the EVS, the 1000 Genomes or ExAC databases. Filtering on the basis that the condition was likely to have a recessive mode of transmission from a common ancestor and so the pathogenic variant was likely to be homozygous identified a list of 33 homozygous variants (Table 5.2).

Chr	Gene	Effect	cDNA change	Protein change
1	***HMGB4***	Missense	NM_145205:exon2:c.C345A	p.N115K
1	***GJB5***	Missense	NM_005268:exon2:c.C166T	p.R56C
1	***DRAM2***	Frameshift deletion	NM_178454:exon4:c.140delG	p.G47fs
1	***LY9***	Missense	NM_001261456:exon5:c.A1238G	p.N413S
2	***NEB***	Missense	NM_004543:exon131:c.T17909C	p.I5970T
2	***LY75***	Missense	NM_001198759:exon12:c.C1960T	p.L654F
3	***LOC401052***	Missense	NM_001008737:exon4:c.A287C	p.H96P
5	***SPEF2***	Missense	NM_024867:exon5:c.A601G	p.R201G
5	***BRD8***	Missense	NM_139199:exon9:c.C671T	p.S224F
6	***CD109***	Missense	NM_001159588:exon4:c.A385G	p.I129V
6	***ZNF292***	Missense	NM_015021:exon8:c.A8132G	p.D2711G
7	***FZD1***	Missense	NM_003505:exon1:c.G1578T	p.K526N
10	***GPRIN2***	Missense	NM_014696:exon3:c.A724G	p.R242G
10	***ADAMTS14***	Missense	NM_080722:exon16:c.C2363T	p.A788V
10	***RRP12***	Missense	NM_001145114:exon24:c.G2847C	p.K949N
10	***GBF1***	Missense	NM_001199378:exon3:c.C112A	p.P38T

11	***OR51V1***	Missense	NM_001004760:exon1:c.G286C	p.G96R
11	***OR52H1***	Missense	NM_001005289:exon1:c.G3T	p.M1I
12	***PLEKHG6***	Nonsense	NM_001144857:exon9:c.C1023G	p.Y341X
12	***TAPBPL***	Missense	NM_018009:exon1:c.G49A	p.G17R
12	***NUAK1***	Missense	NM_014840:exon1:c.A32G	p.D11G
16	***SOCS1***	Missense	NM_003745:exon2:c.C116G	p.P39R
17	***CD300C***	Missense	NM_006678:exon2:c.G103C	p.V35L
19	***PLIN4***	Missense	NM_001080400:exon3:c.A2200G	p.I734V
19	***OR10H3***	Missense	NM_013938:exon1:c.G293T	p.C98F
19	***OR10H4***	Missense	NM_001004465:exon1:c.G293T	p.C98F
19	***ZNF773***	Missense	NM_198542:exon4:c.C290A	p.A97E
21	***USP16***	Missense	NM_001001992:exon14:c.A1829G	p.E610G
X	***SHROOM2***	Missense	NM_001649:exon4:c.C2725G	p.Q909E
X	***APEX2***	Missense	NM_001271748:exon5:c.G509A	p.R170H
X	***CYLC1***	Missense	NM_001271680:exon1:c.G14C	p.R5T
X	***TCEAL5***	Missense	NM_001012979:exon3:c.C246A	p.D82E
X	***MAGEA10***	Missense	NM_021048:exon4:c.A1014C	p.E338D

Table 5.2. List of variants identified after filtering WES data from patient IV.6 of family ES1. (Adapted from El-Asrag et al. (2015) with the permission of Elsevier Copyright Clearance Centre, License number: 3919040428835).

5.2.3 Using the SNP genotype data to further filter the WES analysed data.

WES identified 33 homozygous sequence variants after filtration. SNP genotyping data identified 2 homozygous regions in common with the 7 affected members that were analysed. By combining these datasets, it was identified that only one of the homozygous variants identified by WES mapped within the shared homozygous regions. This was a single-base deletion in *DRAM2* (DNA-damage regulated autophagy modulator protein 2, OMIM 613360), NM_178454.4: c.140delG, p.G47Vfs*3. This variant created a frameshift mutation and was predicted to lead to premature protein truncation. This change was not present in dbSNP142, the EVS or 1000 Genomes databases. It was found once in a heterozygous state in WES data from 61,486 unrelated individuals present in the ExAC dataset. Notably, no homozygous presumed loss-of-function variants in *DRAM2* were present in the ExAC dataset. Sanger DNA sequencing of *DRAM2* exon 4

(Section 2.8, primer pairs in Appendix 6) confirmed the presence of the mutation in the index case (Figure 5.5) and showed that the mutation segregated with the disease in the family (Figure 5.1). Sanger sequencing in a control DNA panel of ethnically-matched individuals excluded this frameshift mutation from 159 controls.

5.2.4 Calculation of a LOD score for family ES1.

With the c.140delG variant as a genetic marker, and assuming a minor allele frequency of 0.01% and full penetrance in the family according to a recessive manner, a LOD score was calculated using the Superlink program, via. the Superlink-online website. By analysing nine genotyped family members, a maximum two-point LOD score of 2.4 was achieved.

5.2.5 Screening for *DRAM2* mutations to identify more independent cases with the same disease

In an attempt to identify further cases with *DRAM2*-associated retinopathy, panels of genomic DNA from RD patients were screened by PCR (primer pairs in Appendix 6) and Sanger sequencing of the seven coding exons of *DRAM2* and their flanking splice sites junctions. The panels consisted of 74 individuals diagnosed with RP, 154 with CRD or MD and 94 with infantile-onset retinal dystrophy (LCA). The screen identified one additional case in the CRD/MD panel that could be accounted by mutations in *DRAM2*. An isolated female case (subject 1325; Figure 5.6A) of European ancestry was identified who was a compound heterozygote for a nonsense mutation in exon 6 of *DRAM2*, c.494G>A, p.W165*, and a missense variant in exon 3 of *DRAM2*, c.131G>A, p.S44N (Figure 5.5).

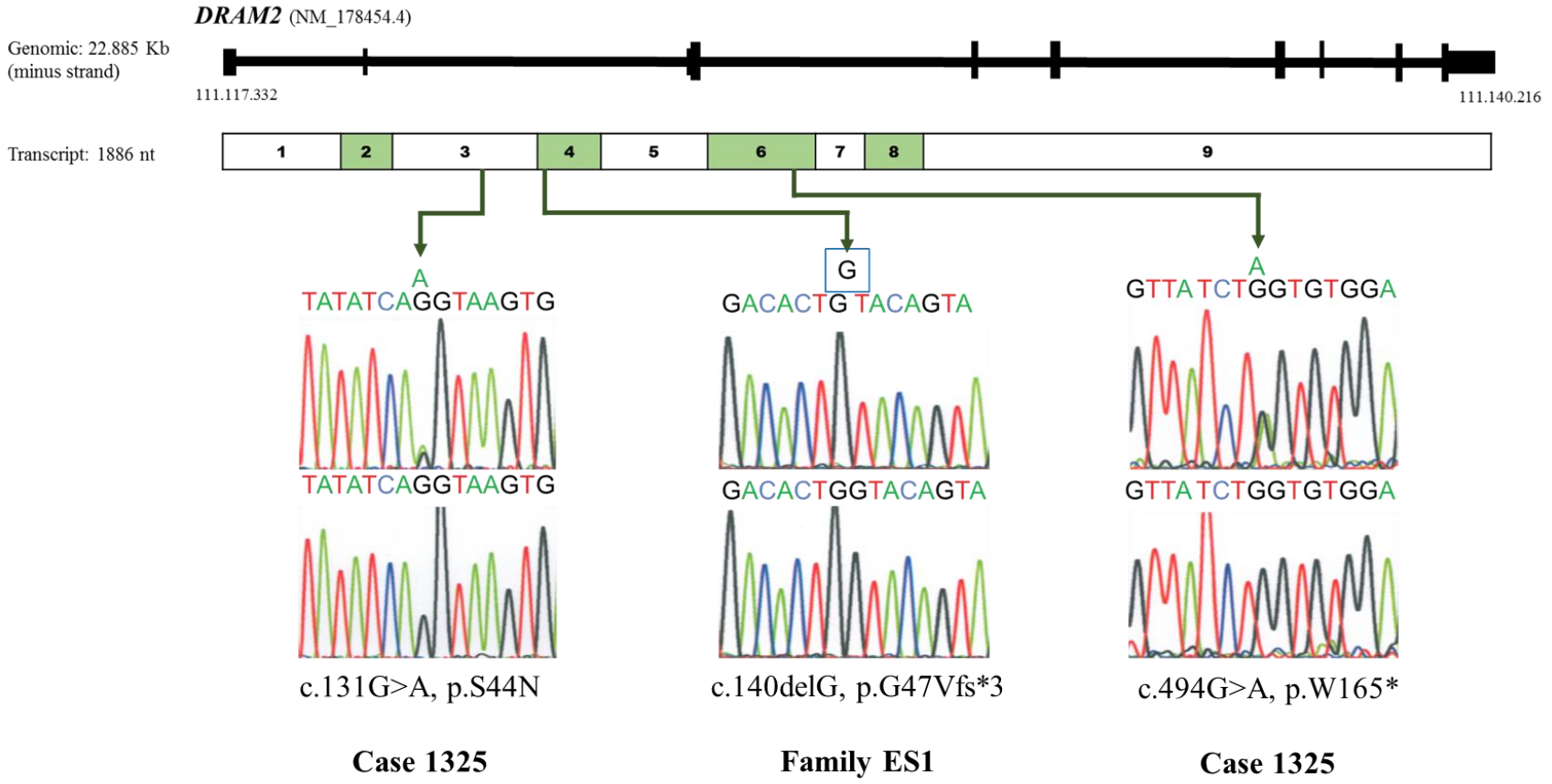

Figure 5.5. Schematic representation of the *DRAM2* genomic structure and major transcript (NM_178454.4), showing the location and sequence traces of the three disease-causing variants identified in this study. (Adapted from El-Asrag et al. (2015) with the permission of Elsevier Copyright Clearance Centre, License number: 3919040428835).

The missense change was predicted to be pathogenic by a number of bioinformatic prediction tools (Table 5.6B) and was not present in dbSNP142, EVS or ExAC databases. Note that the variant affects a serine residue that is conserved from human to zebrafish, suggesting that the normal residue may be important for protein structure or function (Figure 5.6C). The other mutation, a c.494G>A change, is an annotated variant in dbSNP142 (rs201422368), with a MAF of 0.008% (1/13,003) in EVS and 0.003% (3/118,572) in ExAC. It is however only reported in the heterozygous state in these databases.

A

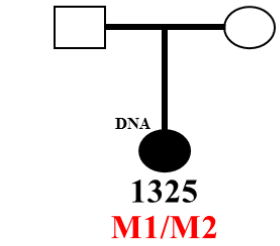

B

Software	Prediction score
PolyPhen2	Probably damaging (score 0.999)
MutationTaster	Disease causing (prediction probability 0.9999)
SIFT	Damaging (score 0.000)
Blosum62*	Score +1
CADD**	Scaled C-score = 22.5
PROVEAN	Deleterious (score -2.650)
MutPred	Deleterious mutation (prediction probability 0.879)

C

Figure 5.6. Genetic analysis of Case 1325. (A) Case 1325 family structure. The genotype for the tested case is shown below the individual, with M1 representing c.131G>A, p.S44N and M2 representing c.494G>A, p.W165*. (B) Summary of bioinformatic analyses to predict the pathogenic nature of the missense variant c.131G>A, p.S44N in *DRAM2*. (C) ClustalW alignment of DRAM2 amino acid sequences around the missense mutation, p.S44N, showing a highly conserved serine residue at position 44 in the protein. Accession numbers for DRAM2 protein are human NP_848549.3, gorilla XP_004026374.1, rhesus AFI36263.1, mouse NP_080289.1, rat NP_001020189.1, rabbit XP_008262917.1, cow NP_001070464.1, horse XP_005610395.1, dog XP_005621847.1, ferret XP_004816269.1, shrew XP_004620147.1, opossum XP_007485185.1, pigeon XP_005505369.1, chicken XP_003642762.1, painted turtle XP_005309999.1, lizard XP_003220625.1 and zebrafish NP_001002135.1.

5.2.6 Clinical features of case 1325

Subject 1325, who is a compound heterozygote for *DRAM2* mutations, had been examined and recruited by Mr Martin McKibbin at a retinal dystrophy clinic in the Eye Department, St. James's University Hospital. In light of genetics findings, her case notes were requested and an updated ophthalmic assessment was performed. She had experienced blurred vision at the age of 29 and was soon after found to have maculopathy on fundus examination. At the age of 35, she also complained of problems with night vision and sensitivity to light. Fundus examination revealed mild peripheral retinal degeneration in addition to central macular atrophy, with grey dots in the temporal macula and intra-retinal pigment migration. At the age of 46, she had acuity of 1.0 logMAR in each eye and electrophysiology revealed severely attenuated or absent ffERGs and pattern ERGs (Figure 5.7).

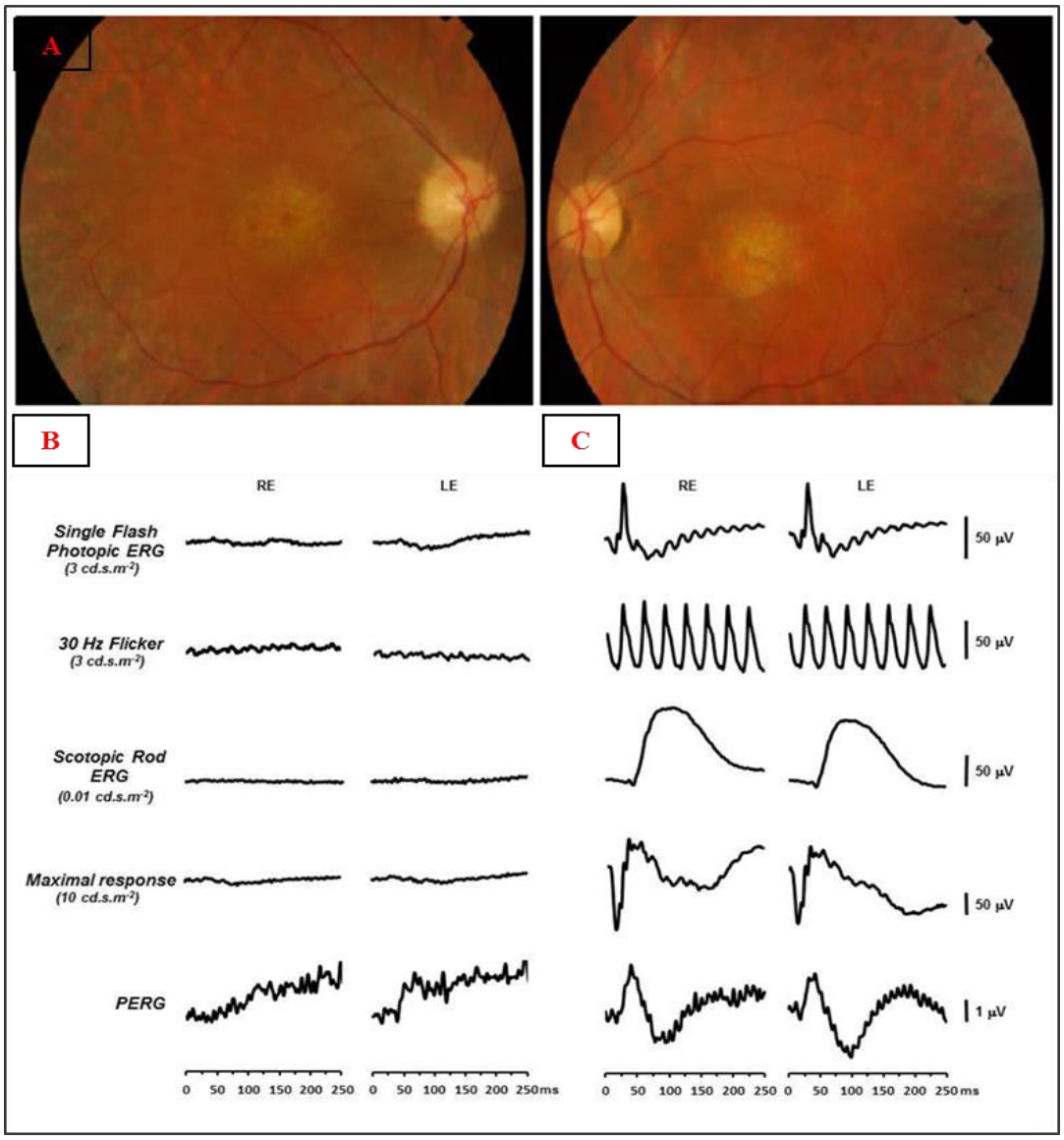

Figure 5.7. Clinical features of Case 1325. Fundus photographs of the right and left eyes at 35 years of age (A) show central macular atrophy with grey dots in the temporal macula with intra-retinal pigment migration. Flash and pattern electroretinography (ERG and PERG) of the case (at 46 years of age) (B) and a normal control individual (C) were recorded to ISCEV standard protocols for the right (RE) and left (LE) eyes. Light-adapted single flash photopic ERG, 30Hz flicker (cone-isolating) ERG, dark-adapted scotopic rod ERG and PERG traces were all severely attenuated or absent compared to the normal control values suggesting a generalised rod-cone dysfunction. The attenuated PERGs indicate that the central macular region is affected by this condition. (Reused from El-Asrag et al. (2015) with the permission of Elsevier Copyright Clearance Centre, License number: 3919040428835).

5.2.7 Mapping the mutations on the DRAM2 protein

Previous overexpression studies in HEK293 cells have localised DRAM2 to lysosomal membranes (O'Prey et al., 2009; Park et al., 2009). However apart from these studies, DRAM2 has not been extensively characterised. Bioinformatics analyses were used (Section 2.14.5) to visualize the normal DRAM2 protein structure. The analysis revealed that the *DRAM2* gene encodes a 266 amino acid protein containing six putative transmembrane domains (Figure 5.8). The mutations identified in human patients have been mapped onto the protein schematic and the missense mutation p.S44N maps within a loop between the first and second transmembrane domains suggesting that this loop may have an important functional role in DRAM2.

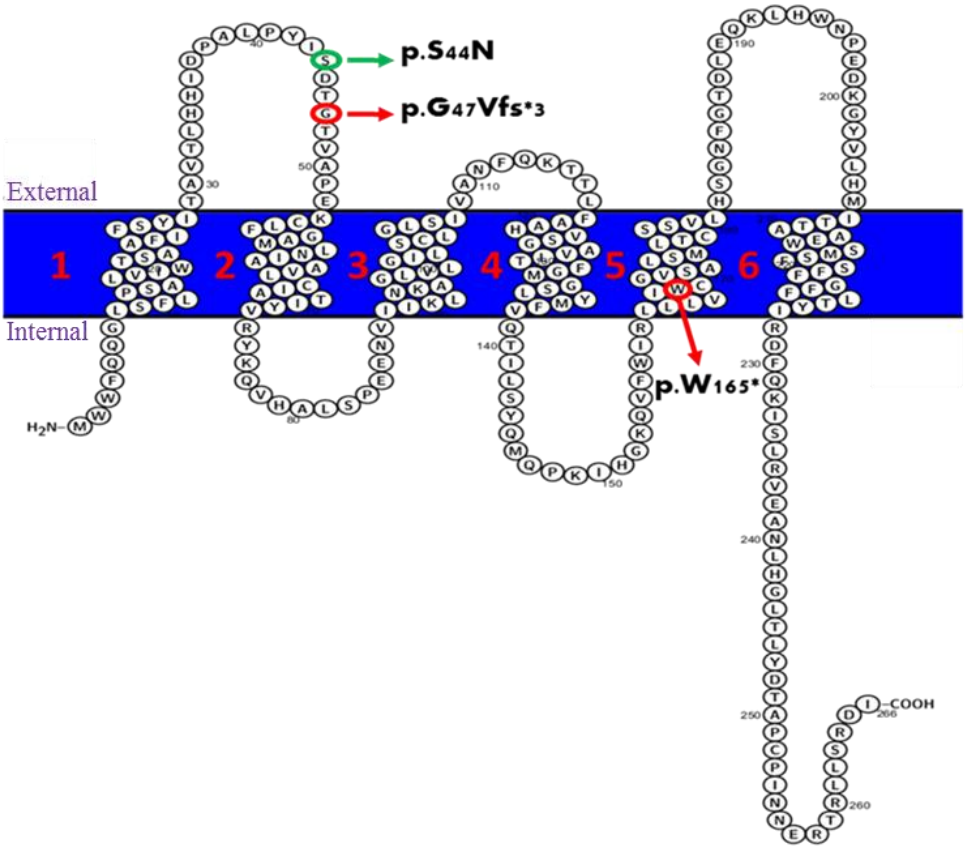

Figure 5.8. Schematic diagram of the DRAM2 transmembrane protein. The proteoform shows six putative transmembrane domains, and the location of the mutations that were identified in human RD patients are shown.

5.2.8 Gene expression profile of *DRAM2* in multiple human tissues

In order to investigate the expression profile of *DRAM2*, reverse transcription PCR (Section 2.16) and agarose gel electrophoresis (Section 2.5) was performed on total RNA that had been extracted from various human tissues (Sections 2.15). In order to amplify *DRAM2* cDNA, a forward sense primer was designed (Section 2.4) to exon 6, whilst the reverse antisense primer bound to exon 7. As a control in the PCR, primer pairs against the housekeeping gene P53 were used. Primer pairs used in this study are listed in Appendix 6. After RT-PCR and agarose gel electrophoresis, *DRAM2* was shown to be ubiquitously expressed in all the tissues that were analysed (Figure 5.9).

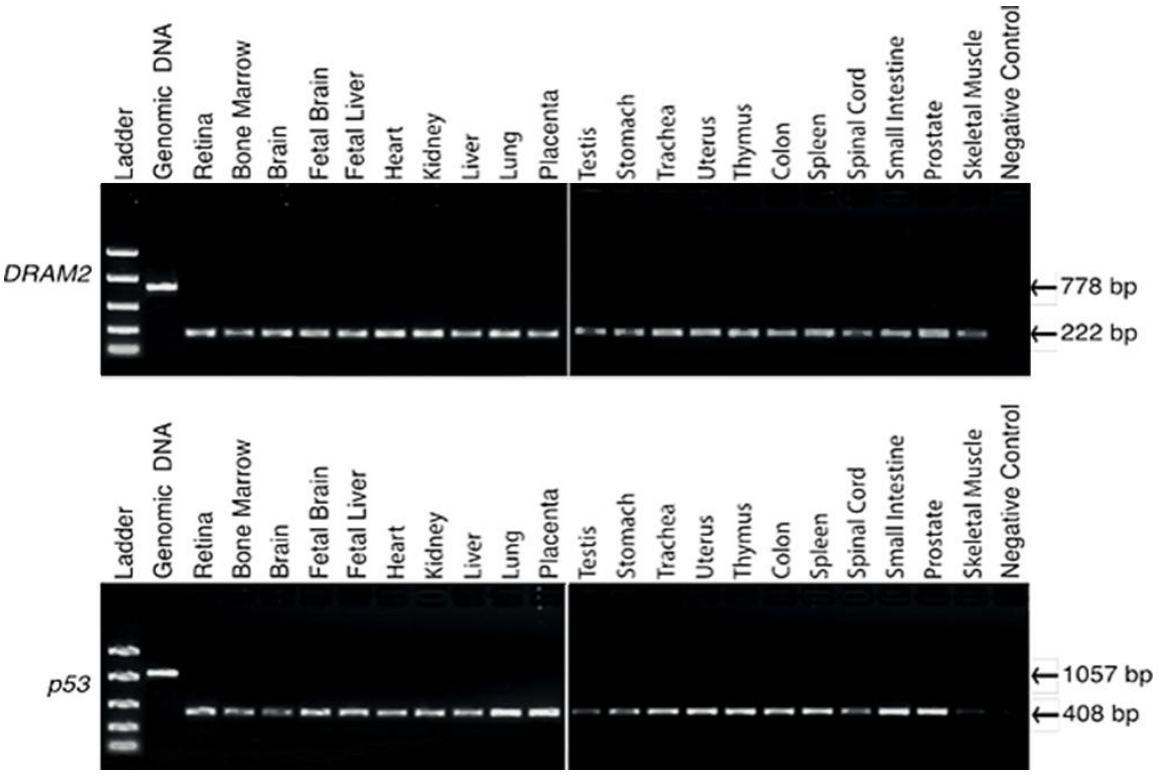

Figure 5.9. *DRAM2* mRNA is ubiquitously expressed in all the 21 tissues analysed. cDNA was prepared from human adult and fetal tissue total RNA. The retinal cDNA was purchased from Clontech. A 222-bp fragment of *DRAM2* spanning intron 6 was amplified from the cDNAs (genomic PCR expected size = 778 bp). P53 control primers amplified a cDNA product size 408 bp or genomic PCR size 1057 bp. (Reused from El-Asrag et al. (2015) with the permission of Elsevier Copyright Clearance Centre, License number: 3919040428835).

5.2.9 Immuno-localisation of DRAM2 to the mouse eye

As pathogenic mutations in *DRAM2* cause retinal dystrophy in human patients, it was important to investigate the precise localization of normal DRAM2 protein in the retina. First, paraffin fixed cross eye sections of mouse embryo (Postnatal zero (Po)/E21) were prepared and stained according to methods described in Sections 2.17.1 and 2.17.3 followed by IHC staining (Sections 2.17.4 and 2.17.5) using goat DARM2 polyclonal antibody at a final dilution 1:50 for 2 hours at 4 °C followed by polyclonal rabbit anti-goat immunoglobulins/HRP at a final dilution 1:2000 and counterstained with haematoxylin. The results showed nonspecific staining to DRAM2 in the eye layers (Appendix 8).

IF staining was the performed on sagittal frozen sections of adult mouse retina that were labeled with goat anti-DRAM2 (at a final dilution of 1:100) followed by a secondary Alexa Fluor 568-conjugated donkey anti-goat immunoglobulin (red). As a positive control, the sections were also stained with rabbit anti-Rhodopsin (at a final dilution of 1:500) and Alexa Fluor 488-conjugated chicken anti-rabbit immunoglobulin (green) as secondary. The nuclei were counterstained with DAPI (Figure 5.10A-C). The immunofluorescence was visualised by confocal microscopy (Section 2.18) and showed that DRAM2 localised to the inner segment of the photoreceptor layer (PIS) and the retinal pigment epithelium (RPE). The rhodopsin protein localised to the outer segment of the photoreceptor layer (POS) as expected. An independent section stained with both secondary antibodies only and another with peptide competition against the DRAM2 primary antibody (Section 2.17.8) served as negative controls in the experiment and confirmed the specificity of the primary antibody for staining DRAM2 protein (Figure 5.10D&E).

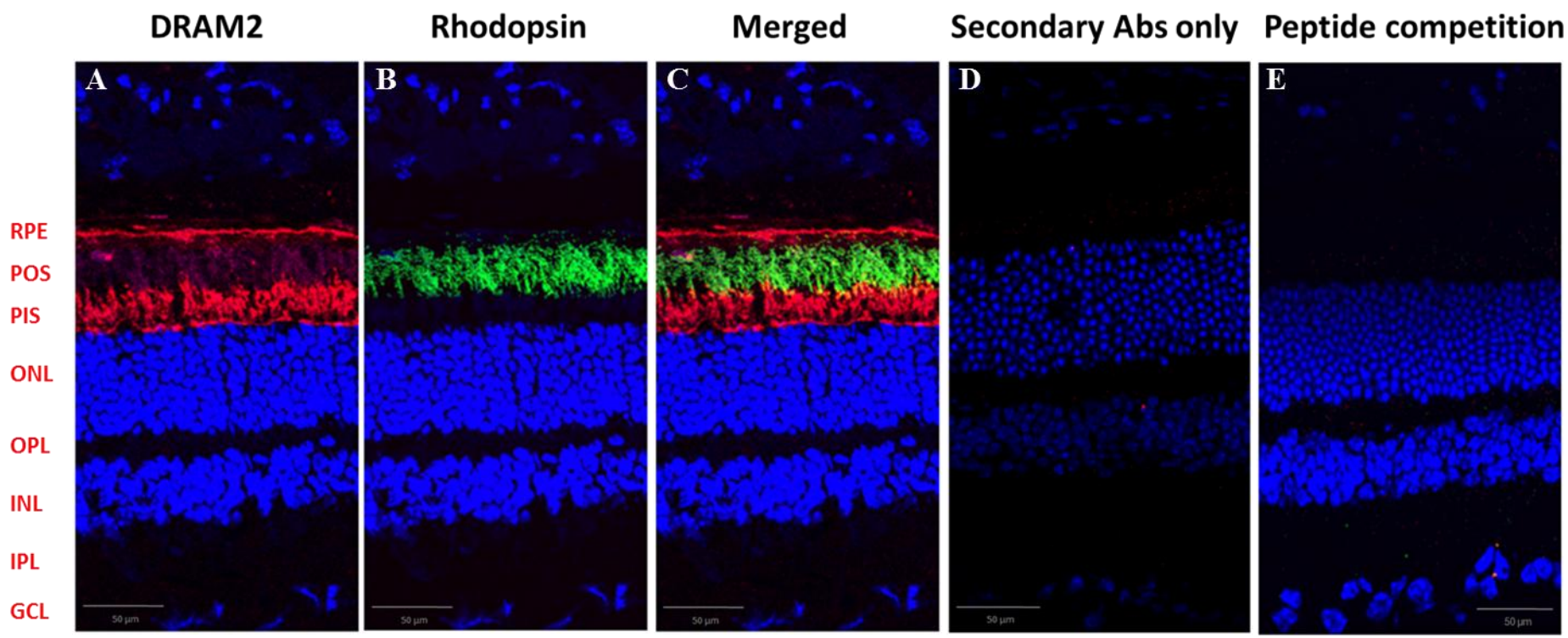

Figure 5.10. Immuno-localisation of DRAM2 to the mouse retina. Immunofluorescence and confocal microscopy images of mouse retinal sections showing DRAM2 predominantly localises to the photoreceptor inner segment (PIS) and the retina pigment epithelium (RPE). Immunofluorescence photomicrographs of P30 coronal mouse retinal sections stained with antibodies against DRAM2 (red) and Rhodopsin (green) in separate channels and in merged images (A, B & C) compared to negative controls of secondary antibodies only (D) and peptide competition against the DRAM2 primary antibody (E). POS = photoreceptor outer segment, ONL = outer nuclear layer, OPL = outer plexiform layer, INL = inner nuclear layer, IPL = inner plexiform layer and GCL = ganglion cell layer. Scale bar: 50µM. (Reused from El-Asrag et al. (2015) with the permission of Elsevier Copyright Clearance Centre, License number: 3919040428835).

5.2.10 Immunoprecipitation analysis of the DRAM2 protein to identify protein interactants

Many biological processes require direct physical interactions between proteins. Identifying and characterizing protein-protein interactions could provide important insights into molecular function. Using existing databases, that are based on yeast-2-hybrid, such as IntAct (http://www.ebi.ac.uk/intact/b,) (Orchard et al., 2014) and MINT (http://mint.bio. uniroma2.it/) (Licata et al., 2012) revealed that no interactant binding partners for DRAM2 have been identified so far. In order to attempt to identify DRAM2 interactant partners, an immunoprecipitation strategy with mass spectrometry was considered.

To minimise the number of false-positives in the assay, endogenous levels of DRAM2 were pulled-down using a polyclonal anti-DRAM2. Initially retina was isolated from mouse eyes or snap frozen cow eye. 1 ml of retinal cell lysates were prepared separately from mouse and cow eyes according to methods described in Sections 2.19.1 and 2.19.2. The two mouse lysates from the same mice were pooled together. The protein concentrations were measured using the Bradford assay (Section 2.19.3). These highlighted that the amount of protein extracted from the mouse retina was 0.35 to 0.48 µg/µl while for the cow retina the amount was 2.94 to 4.82 µg/µl.

Given that a minimum of 1 mg was required to perform the pull down assays, there was insufficient material available from the mouse retina and so the extract from the cow retina was analysed further. Before performing the pull-down experiment, the epitope sequence of rabbit anti-DRAM2 was checked against the cow protein sequence and showed 88.24% similarity. Then 20 µg of the lysate was investigated by western blotting (Section 2.20) against rabbit anti-DRAM2 (with a final dilution 1/200) and rabbit anti-Rhodopsin (at a final dilution 1/200) with 16 hours incubation time. The secondary antibody was anti-rabbit IgG (HRP) used at a final dilution 1/2000 for 60 minutes. The purpose of using rhodopsin alongside DRAM2 was to confirm that the lysate is retinal in origin, which is an important step, given the difficulty in separating the retina from other eye tissues. The results confirmed the presence of DRAM2 and rhodopsin in the retinal lysate at the expected band sizes and that the antibody does detect cow DRAM2 (Figure 5.11).

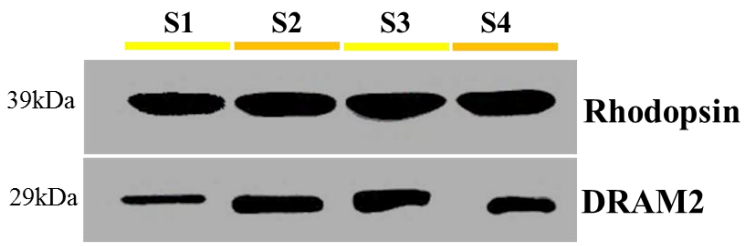

Figure 5.11. Western blot analysis of cow retinal lysates. Two bands are visible for each sample from four retinal lysate samples (S1 to S4) isolated from 2 different cow eyes. These were incubated with anti-DRAM2 and anti-rhodopsin. A band at 29 kDa highlights DRAM2 and a band at 39 kDa indicates rhodopsin.

For the pull-down experiment, 1 mg of the cow retinal lysate was incubated with 2.5µg polyclonal rabbit anti-DRAM2 and 30µl Protein A plus agarose beads according to the methods described in Section 2.21. The pulldown results were checked by migration through a polyacrylamide gel and silver staining (Section 2.22). No protein appeared to be detected after the pull down assay. However an unexpected band at ~98 KDa was found in all samples after the pull down (Figure 5.12).

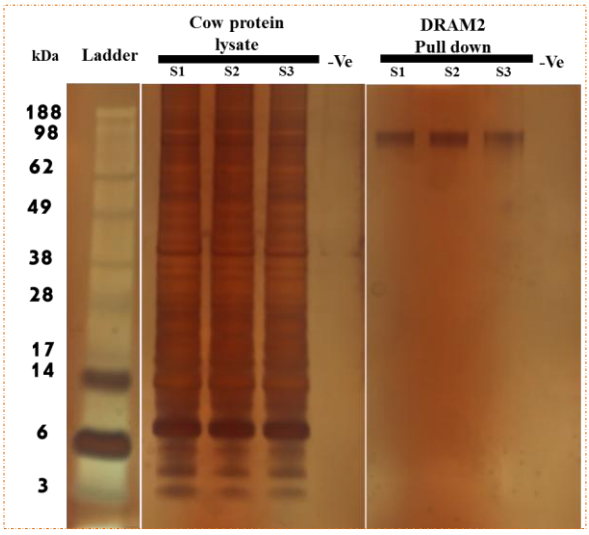

Figure 5.12. A representative image of silver stained polyacrylamide gel. The gel showing cow retinal lysates before and after the pull-down experiment with rabbit anti-DRAM2 antibody. The experiments were performed in triplicate. The staining highlights consistent protein composition amongst the lysates, but no protein was detected after the DRAM2 antibody pull-down except an unexpected band at ~98 KDa, which was found in all the tested samples (S1, S2 and S3).

This experiment was replicated four times with increasing parameters of incubations times (2-48 hours), concentration of antibodies (2.5-5µg) and protein A/G plus agarose beads (25-50 µl). The same results were still detected after the pull-down in each case. Moreover western blotting analysis of all samples after the pull down using rabbit anti-DRAM2 did not highlight any protein bands suggesting that the experiment did not work under the experimental conditions that were tested. Given that analysis by mass spectrometry is very expensive ($1000 per sample), no further work was carried out on this aspect of the project.

An attempt was then planned to obtain DRAM2 interactant data via an alternative approach. This involved transfecting a DRAM2 expression construct into a cell expressing little or no endogenous DRAM2, followed by a pull-down assay in the lysate of the transfected cells. This avoids the difficulties of performing pull-down experiments against endogenous proteins in their native state. DRAM2 cDNA was cloned using the Gateway system into a tagged expression construct according to methods described in Sections 2.23, 2.24 and 2.25, to create a clone denoted pDRAM2-C-TAP GW332 that was verified by Sanger sequencing. In addition, DRAM2 expression was investigated by RT-PCR in various cell lines, using the previously designed primers (Section 5.2.8) on total RNA extracted (Section 2.15) from the cell lines. Human cell lines tested included MCF7, RPE, RPE1 SS (Serum starved), U2OS, H2B, HRT18, HCT116, MT29, SW480, Sh5Y differentiated, Sh5Y undifferentiated, MCF10A, HDF, and HEK293. DRAM2 was expressed in all of these cell lines (Figure 5.14).The next step planned will be transfection into one or more of these cell lines followed by pull down experiments with anti-C-TAP antibody, western blot analysis and mass spectrometry.

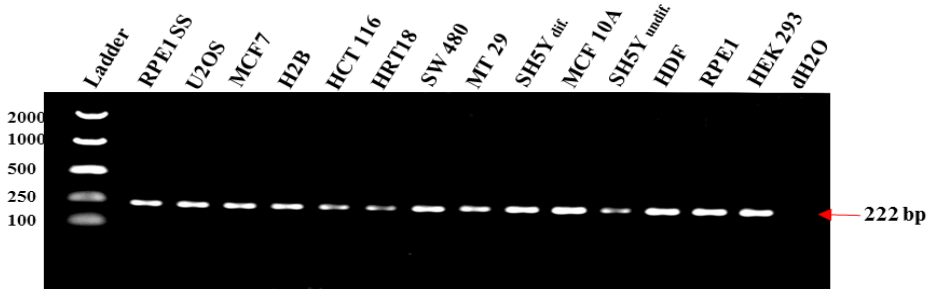

Figure 5.13. *DRAM2* mRNA is ubiquitously expressed in all the 13 cell lines analysed. cDNA was prepared from cell lines total RNA. A 222-bp fragment of DRAM2 spanning intron 6 was amplified from the cDNAs.

5.3 Discussion

5.3.1 Combining homozygosity mapping with WES to identify disease-causing genes.

The study of consanguineous families with multiple affected individuals has proved a successful approach in determining the causes of autosomal recessive retinal disease. The children of consanguineous individuals will have more homozygous DNA than the offspring of an outbred marriage (Section 1.9). This leads to an increased likelihood of rare, recessive disease-causing variants being inherited from both parents, known as identical by descent (IBD) (Modell and Darr, 2002). Homozygosity mapping locates regions of the genome containing large stretches of homozygosity that are shared between affected individuals to represent the disease loci. However these regions usually contain large numbers of genes. WES is an effective way to identify the RD causing gene and mutation in such cases, but this approach alone tends to identify long lists of candidate variants which are then challenging to filter and exclude. Combining data from these two approaches allows the researcher to narrow down the candidate genes and potentially to identify the most likely variant that causes disease in any given family. In this chapter, these combined approaches were used to identify *DRAM2*, a novel RD gene.

5.3.2 Further *DRAM2* mutations and any possible genotype–phenotype correlation.

Given that affected members of family ES1 are homozygous for a *DRAM2* variant that is likely to lead either to nonsense-mediated decay of the encoded mRNA or to a truncated protein of only 47 amino acids, the molecular pathology of the disease is likely to be loss of DRAM2 function. This speculation is further supported by the independent finding of five disease-causing variants that have been identified in four RD cases by the UK Inherited Retinal Disease Consortium and the European Retinal Disease Consortium (ERDC) (El-Asrag et al., 2015; Sergouniotis et al., 2015). Two of these cases (gc17004 and gc4728) were identified through a gene-based case-control association analysis that was performed on 18 families from the inherited retinal disease clinics at Moorfields Eye Hospital (London), utilizing 1,917 unrelated control samples generated by a consortium of UK-based researchers ("UCL-exomes"). The first (gc17004) was a 37-year-old female of European ancestry who was compound heterozygote for a missense variant (c.79T>C,

p.Y27H) and an in-frame deletion (c.217_225del, p.V73_Y75del). The second was a 47-year-old male of South Asian origin who had a homozygous missense change (c.362A>T, p.H121L). The third and fourth cases (BL1 and PCI1) were identified by WES. Both are in their early forties, one of Indian and the other of Turkish origins, and both have a homozygous variant, c.64_66del, p.A22del and c.169G>C, p.G57R respectively. The phenotype of these cases was notably similar to the affected members of family ES1 and subject 1325.

Interestingly, most the mutations that have been identified so far (Figure 5.14) are truncating mutations or severe missense mutations in the transmembrane domains. p.S44N is the only missense mutation that has been identified within a loop between the first and second transmembrane domains. This variant is identified in compound heterozygous Leeds case 1325, who also carries the nonsense mutation p.W165*. No precise genotype–phenotype correlations of *DRAM2* mutations can be observed from the few cases that have been identified. However, affected members of family ES1, and also subject 1325 who harbour at least one presumed loss-of-function variant in DRAM2, appear to manifest symptoms of retinal disease earlier than the remaining cases (gc17004, gc4728, BL1 and PCI1), who harbour only missense changes or in-frame deletions and became symptomatic at a later age (El-Asrag et al., 2015; Sergouniotis et al., 2015).

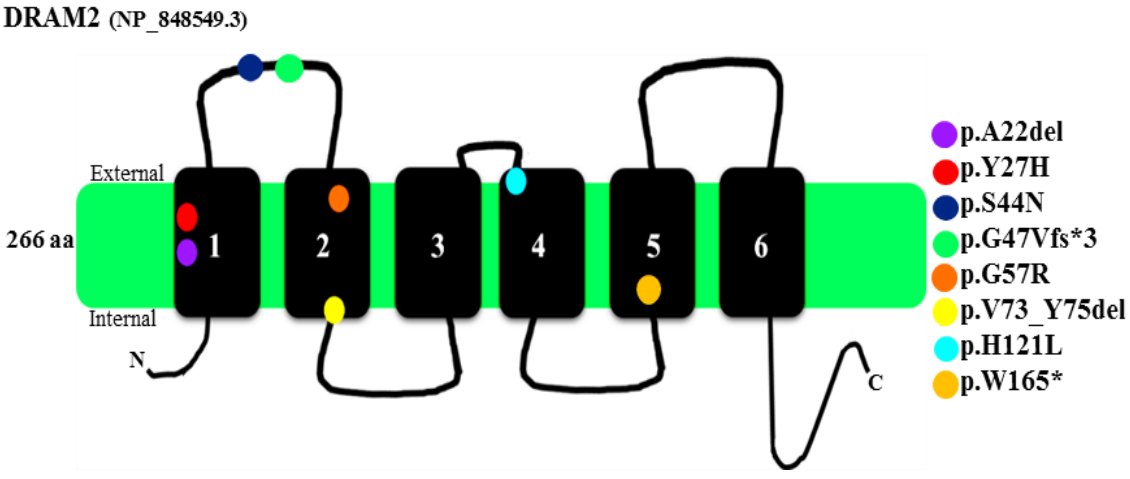

Figure 5.14. Schematic diagram of DRAM2 showing the protein domains and the location of the affected amino acids identified in patients with DRAM2 retinopathy.

5.3.3 DRAM2 is an autophagy regulator

During autophagy, a cytosolic form of LC3-I (microtubule-associated protein light chain 3) conjugates with phosphatidylethanolamine (PE) to form LC3-II (LC31/PE conjugate), which is recruited to autophagosomal membranes. DRAM2 overexpression studies in HEK293 have shown that it initiates the conversion of endogenous LC3-I to LC3-II, the general autophagosome marker protein in the lysosome. These studies showed that overexpression of DRAM2 increased GFP-LC3 punctate that represent the extent of autophagy. Also, siRNA knockdown of endogenous DRAM2 results in reduced conversion to LC3-II in cells subject to starvation-induced autophagy. This suggests that DRAM2 may act as a positive regulator of autophagy (Park et al., 2009; Yoon et al., 2012).

Autophagy is a natural cell survival mechanism triggered in response to stress stimuli such as light-induced damage, nutrient starvation or the accumulation of damaged organelles. It is responsible for degrading and recycling cytoplasmic proteins and lipids as well as organelles within the cell (Levine and Klionsky, 2004). Depending on the mode of cargo delivery to the lysosome, autophagy can be subdivided into three categories, macroautophagy, microautophagy and chaperone mediated autophagy (CMA) (Mizushima and Komatsu, 2011) (Figure 5.15).

Microautophagy and CMA directly involve the lysosome. During the microautophagic process, cytosolic components are transported into the lysosome by direct invagination of the lysosomal membrane, followed by budding off of the vesicle formed into the lysosomal lumen (Kunz et al., 2004; Sahu et al., 2011). During CMA, the substrate proteins are targeted to the lysosomal membrane through recognition of a targeting motif (a KFERQ-like motif) by a chaperone complex composed of hsc70 and its co-chaperones. This substrate chaperone complex is delivered to the lysosomal membrane, where it interacts with lysosomal associated membrane protein type 2A (LAMP-2A) and is directly translocated across the membrane into the lysosomal lumen (Massey et al., 2006; Xilouri et al., 2016).

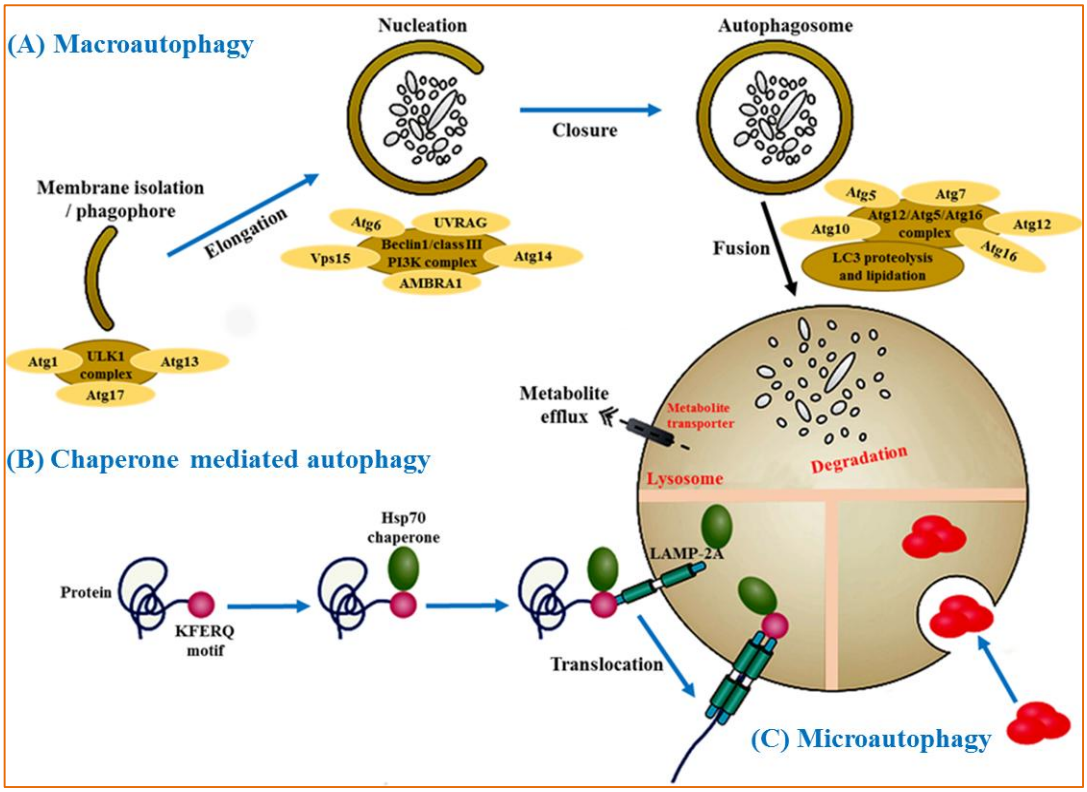

Figure 5.15. Different types of autophagy. (A) Macroautophagy begins with the formation of a phagophore which is also called an isolation membrane (nucleation step), followed by the engulfment step, which is either nonspecific, involving bulk of cytoplasm, or selective, involving specific cargoes. The autophagosome is then formed by elongation of the phagophore and fusion of its edges to form the autophagosome (elongation and completion steps). The outer membrane of the autophagosome then fuses with the lysosome (fusion step) followed by lysis of the autophagosome inner membrane and breakdown of the contents (degradation step). Autophagy-related genes (Atg) and protein complexes that are involved in each step are shown. (B) chaperone mediated autophagy (CMA) refers to the recognition of proteins carrying the pentapeptide KFERQ-like sequence by the Hsc70 chaperone, followed by association with the integral lysosome membrane receptor LAMP-2A, which leads to the translocation of the bound protein into the lysosomal lumen. (C) Microautophagy refers to the sequestration of cytosolic targeted components directly by lysosomes through invaginations in their limiting membrane. After all three types of autophagy, the resultant degradation products can be used for different purposes, such as new protein synthesis and energy production. (Adapted from Boya et al. (2013) with the permission of Elsevier Copyright Clearance Centre, License number: 3934340352393)

On the other hand, macroautophagy, the most common form of autophagy, begins with isolation of the macromolecules and organelles within the cytoplasm into single membrane vesicles, which fuse together to produce an autophagosome (AP). This AP

subsequently fuses with a lysosome containing acid hydrolases, to form a double-membrane autolysosome (Yoshimori, 2004; Kroemer and Jaattela, 2005). APs are generated on or in close proximity to the endoplasmic reticulum (ER) (Mizushima et al., 2011). Recent studies suggest that the plasma membrane, ER, Golgi complex and mitochondria are all possible membrane sources for APs (Hailey et al., 2010; Hamasaki and Yoshimori, 2010; Ravikumar et al., 2010; Tooze and Yoshimori, 2010). Macroautophagy is a highly complex process, dividing into several steps, including the formation of autophagosome by membrane isolation, nucleation, elongation and autophagosome-vacuole fusion, followed by fusion of autophagosomes with lysosomes for degradation of the autophagosomal content. Approximately 30 autophagy-related genes (ATGs) were first identified in yeast and have orthologs in humans. The proteins encoded by these genes are involved in the regulation of every step of this process (Hamasaki and Yoshimori, 2010).

The serine/threonine kinase UNC-51-like kinase -1 (ULK1), which plays a similar role as the yeast Atg1 protein, forms a ULK1 complex with mATG13 (a mammalian ortholog of yeast Atg13) and FIP200 (a mammalian ortholog of yeast Atg17) to promote the membrane isolation which represents the first step in autophagosome generation (Ganley et al., 2009; Hosokawa et al., 2009). LC3 (a mammalian ortholog of yeast Atg8) binds directly to ULK1 and enhances its activity in autophagy (Kraft et al., 2012). Beclin1-class III PI3K complex containing: hVps34, Beclin-1 (a mammalian ortholog of yeast Atg6), p150 (a mammalian ortholog of yeast Vps15) and Atg14-like protein (Atg14L), AMBRA1 (activating molecule in Beclin1-regulated autophagy protein 1) and UVRAG (UV radiation resistance associated gene), are all associated with nucleation of the phagophore (Itakura et al., 2008; Simonsen and Tooze, 2009; Li et al., 2012). Atg12-Atg5-Atg16 complex together with Atg8-phosphatidylethanolamine (Atg8-PE) complex (LC3-II), participate in the elongation and enclosure step for autophagosome formation (Yorimitsu and Klionsky, 2005). Atg12 is conjugated to Atg5 through Atg7 and Atg10 (Mizushima et al., 1998). Atg8/LC3 is cleaved by Atg4 to form the cytosolic soluble LC3-I, then activation by Atg7 and transferring to the E2-like Atg3 where lipidation by conjugation to the lipid PE take place and converting to a membrane-associated form LC3-II (Kabeya et al., 2000). LC3-II remains on the mature autophagosomes until fusion with lysosomes is completed. Thus, it is commonly used as a marker for the mammalian

autophagosome together with LAMP1, a lysosome associated membrane protein 1 (Weidberg et al., 2011).

5.3.4 Possible role of DRAM2 in regulatory signalling pathways that lead to autophagy

The process of autophagy is controlled by activation/inhibition cascades (Figure 5.16). The mammalian rapamycin (mTOR), a phosphatidylinositol 3-kinase (PI3K) and a serine/threonine kinase (Akt) also known as protein kinase B (PKB), are key regulators in various cellular functions in autophagy regulation (Schmelzle and Hall, 2000). mTOR consists of two protein complexes, mTORC1 and mTORC2, and activation of the mTOR by nutrients or growth factors inhibits autophagy.

Growth factors such as insulin and insulin-like growth factor bind to their receptor tyrosine kinases, leading to receptor autophosphorylation and activation of PI3K-Akt/PKB, which then phosphorylates the tuberous sclerosis complex (TSC2) and prevents the formation of TSC1/2. TSC1/2 acts as a GTPase-activating protein for Rheb (Ras (small GTPase) homolog enriched in brain). Blocking the activity of TSC1/2 leads to Rheb-GTP accumulation which activates mTOR (Proud, 2007). Activation of mTOR inhibits autophagy by inhibiting the association between Atg1/Ulk1 and Atg13/mATG13 by mTORC1 (Kamada et al., 2010). Under conditions of starvation or rapamycin treatment, inactivation of mTOR1 leads to dephosphorylation and activation of Atg1/Ulk1 that induces autophagy (Shang et al., 2011). Phosphatase and tensin homolog (PTEN) is an activator of autophagy by inhibition of the Akt/PKB signaling pathway (Shaw and Cantley, 2006).

Adenosine monophosphate (AMP)-activated protein kinase (AMPK) is an important regulator of autophagy. It induces autophagy by suppression of mTOR, either by enhancing the functions of TSC2 that lead to suppression of mTORC1, or by directly phosphorylating the mTOR binding partner Raptor (regulatory associated protein of mTOR), leading to inactivation of Raptor and mTORC1 (Gwinn et al., 2008; Herrero-Martin et al., 2009). AMPK also can directly induce autophagy by phosphorylation of the Atg1/Ulk1 complex (Mack et al., 2012). B-cell lymphoma 2 (Bcl-2) apoptotic family proteins also act as autophagy regulators. The anti-apoptotic Bcl-2 family members

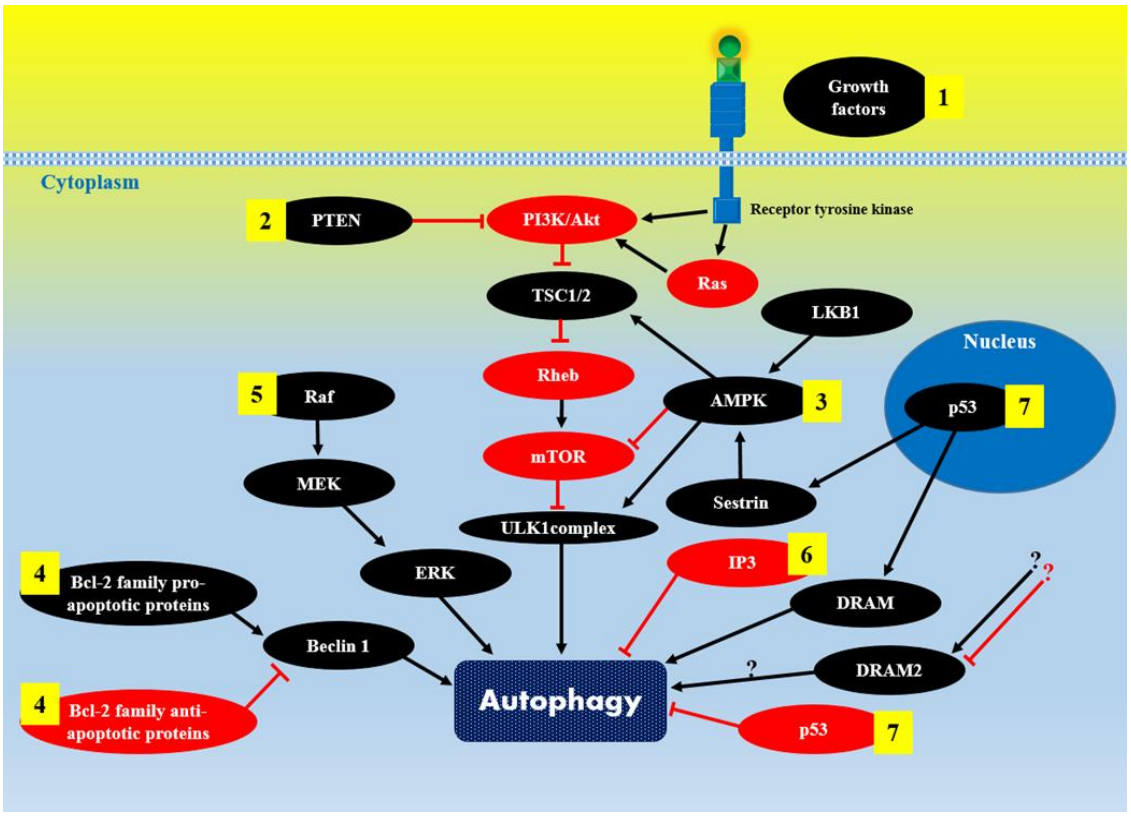

Figure 5.16. The regulatory signaling pathways in autophagy. (1) Growth factors bind to their receptor tyrosine kinase which stimulates PI3K/Akt directly or through Ras. PI3K inhibits the TSC1/2 complex, leading to Rheb-GTP accumulation, which in turn activates mTORC1 and causes autophagy inhibition by inhibiting ULK1 complex formation. (2) PTEN inhibits PI3K/Akt/ mTOR signaling. (3) AMPK can be activated by LKB1, causing activation of TSC1/2, inactivation of mTOR and induction of autophagy. AMPK can also cause inactivation of mTOR by directly phosphorylating the mTOR binding partner Raptor. AMPK also can directly induce autophagy through ULK1 upregulation. (4) The Bcl-2 family anti-apoptotic proteins have inhibitory effects on autophagy by interaction with Atg6/Beclin1, while pro-apoptotic proteins have stimulatory effects on autophagy by disrupting the association of anti-apoptotic proteins with Atg6/Beclin1. (5) The Raf/MEK1/ERK1 signaling cascade causes the activation of autophagy. (6) Intracellular IP3 negatively regulates autophagy via an mTOR-independent mechanism. (7) Cytoplasmic p53 is responsible for the inhibition of autophagy. By contrast, nuclear p53 stimulates autophagy in a transcription-dependent fashion by activating the expression of DRAM and sestrin. Red ovals = autophagy inhibitory and Black ovals = autophagy stimulatory. (Sources: Ravikumar et al. (2004), He and Klionsky (2009), Mizushima and Komatsu (2011), Peracchio et al. (2012) and Cheng et al. (2013)).

members (Bcl-2, Bcl-XL, Bcl-wl, and Mcl-1) inhibit autophagy, while pro-apoptotic Bcl-2 homology 3 (BH3) proteins (BNIP3L, Bad, Noxa, Puma, BimEL22, and Bik) stimulate autophagy (Maiuri et al., 2009). These proteins act through interaction with Atg6/Beclin1 (Pattingre et al., 2005). The Raf/MEK/ERK pathway also promotes autophagy by the disassembly mTORC1 (Wang et al., 2009c). Inositol trisphosphate (IP3) can negatively regulate autophagy via an mTOR-independent mechanism (Khan and Joseph, 2010).

Many autophagy inducers, such as starvation and rapamycin, stimulate degradation of cytoplasmic p53. Inactivation of cytoplasmic p53 can trigger autophagy (Tasdemir et al., 2008). On the other hand, nuclear p53 can stimulate autophagy in a transcription-dependent fashion by activating the expression of DRAM (DNA-damage regulated autophagy modulator) (Crighton et al., 2006) and sestrin (Budanov and Karin, 2008). DRAM belongs to a family of five proteins thought to act as modulators of autophagy, which also includes DRAM2, DRAM4, DRAM5a and DRAM5b. DRAM2 is by far the most closely related human protein to DRAM and shares 45% identity and 67% conservation at the amino acid level (O'Prey et al., 2009). Both DRAM and DRAM2 are transmembrane proteins, localized in lysosomes, and the expression of both is generally down-regulated in tumours. However DRAM2 is different from DRAM in that it not induced by p53 (Park et al., 2009). Examination of medical histories in the reported subjects with DRAM2-associated RD provided no evidence of increased susceptibility to cancer. To conclude, the autophagy is the end target of many different complex and interconnected pathways. It seems likely that DRAM2, like its paralog DRAM, is likely to fit into these pathways but which one, is unknown yet.

5.3.5 Autophagy and the RPE

Autophagy proteins are particularly highly expressed in the retinal layers that have a high metabolic demand, such as the ganglion cell layer (GCL), inner nuclear layer (INL), ONL, PIS and RPE (Mitter et al., 2012; Mitter et al., 2014). DRAM2 immunolocalisation to the inner segment of the photoreceptor layer and the apical surface of the RPE is consistent with a role for DRAM2 in photoreceptor autophagy. A high level of autophagy is also expected to take place in the RPE. These cells have a key role in processing shed photoreceptor outer segment discs and consequently, in removing toxic metabolites and recycling phototransduction components. The process of disc shedding

and phagocytosis by the RPE causes up to 10% photoreceptor volume loss each day. It is achieved by an atypical autophagy pathway involving the proteins Atg5 and LC3, which trigger phagosome fusion with the lysosome, resulting in POS degradation. This process is entrained to the circadian rhythm (Young and Bok, 1969; Nguyen-Legros and Hicks, 2000). Indeed there is increasing interest in the role of autophagy in preserving photoreceptor function in connection with the circadian cycle (Yao et al., 2014), the aging process (Rodriguez-Muela et al., 2013) and retinal disease pathology (Metrailler et al., 2012). Autophagy is a housekeeping process that plays an important role in survival, development and homeostasis of the ocular tissues and autophagy dysregulation is involved in a group of eye diseases such as AMD (Wang et al., 2009a), cataract (Morishita and Mizushima, 2016), glaucoma (Wang et al., 2015), diabetic retinopathy (DR) (Lu and Xu, 2012) and photoreceptor degeneration (Mellen et al., 2008; Mustafi et al., 2011; Chen et al., 2013). It is therefore likely that the absence of DRAM2 in the retina reduces the efficiency of autophagy in recycling cell components, which in turn reduces photoreceptor renewal, leading to the thin photoreceptor layer observed on OCT, which is the first presenting feature in pre-symptomatic patients with *DRAM2*-induced retinopathy.

5.3.6 Autophagy and ciliogenesis

Influencing ciliogenesis is another possible consequence of DRAM2 retinopathy. Photoreceptor outer segments are in a constant state of renewal by ciliogenesis in response to light-induced damage. Recent studies have suggested that there is interplay between ciliogenesis and autophagy. In one study, it was shown that disruption of ciliogenesis partially inhibited autophagy, while blocking autophagy enhanced primary cilia growth and cilia-associated signalling during normal nutritional conditions. The authors therefore proposed that basal autophagy regulated ciliary growth through the degradation of proteins required for intraflagellar transport (Pampliega et al., 2013). In another study, the protein OFD1 (oral facial digital syndrome 1), which accumulated at centriolar satellites located close to the base of the cilium, was rapidly degraded by serum starvation-induced autophagy. This led to ciliary growth suggesting that OFD1 normally inhibited ciliogenesis (Tang et al., 2013).

5.3.7 What are the DRAM2 interacting binding partners in the retina?

Future work could involve pull down assays and mass spectrometry of the attached proteins to find DRAM2 interacting partners and determine the autophagy pathway defects that lead to RD. One possible reason for the failure of the endogenous DRAM2 pulldown experiments presented in this thesis may be that the rabbit anti-DRAM2 may have limited affinity for the DRAM2 protein in its native state, and that it can only detect the protein after denaturation with SDS in western blotting. Another possibility could be that the protein concentration after the pull down assay was too low to detect by silver staining or western blotting. Alternatively, given that the DRAM2 is a transmembrane protein that it may pose significant challenges in terms of solubilization without disrupting the protein-protein interactions.

In the evolution of this work, the next step could be to transfect human embryonic kidney (HEK293) or RPE cell lines with the pDRAM2-C-TAP expression construct. Then extract a cell lysate from these transfected cells and use the expressed epitope tagged protein as a pull down with an anti-C-TAP antibody. The resultant protein mix could then be separated on a polyacrylamide gel for silver staining andon a duplicate gel for western blot analysis. If DRAM2 protein can be detected, the mix would then be prepared for mass spectrometry analysis to try and identify the protein interacting partners of DRAM2.

Another way that to identify DRAM2 interacting partners could be to use a yeast-two-hybrid (Y2H) approach (Brückner et al., 2009). With this approach, two fusion proteins (hybrids) would be constructed, one between the protein of interest and containing the DNA-binding domain (DB) of a transcription factor, while the other would contain the activation domain (AD) of the transcription factor combined with a library of test proteins. Both hybrids would be co-transfected into yeast cells. If the test protein and library protein interact, bringing the DB and AD domains into proximity, activation of the transcription of the reporter gene (such as HIS3 and LacZ) is initiated, enabling the yeast colony to grow. A great advantage of this system is that it is scalable and can be used to identify many interacting proteins in a relatively short time. However Y2H has two major disadvantages. The first is the potential for misfolding of the proteins of interest inside the yeast cells and secondly, the yeast as a heterologous system and some interactions depend upon post-translational modifications that may not occur in yeast.

Such modifications are frequent and include the formation of disulfide bridges, glycosylation and most commonly phosphorylation (Scott and Pawson, 2009).

5.3.8 Can the new knowledge about DRAM2 be used in therapy to modulate retinal disease?

A *Dram2* knockout mouse could help determine the mechanism by which dysregulated autophagy, due to the absence of Dram2, leads to an RD phenotype. With the current methods that are available for monitoring autophagy such as measuring autophagy flux using sequestosome-1 (SQSTM1) or LC3-II (Klionsky et al., 2008), this would allow confirmation of an autophagy defect in Dram2 knockout mice. This could also be used to monitor the effects of potential therapeutic agents on the mouse model of DRAM2 retinopathy. Many drugs and compounds that modulate autophagy are currently receiving considerable attention as potential therapies for diverse diseases (Rubinsztein et al., 2012; Cheng et al., 2013). These include, autophagy inhibitors, such as chloroquine (Fedorko, 1967) and hydroxychloroquine (Amaravadi et al., 2011), PIK3C3 inhibitors (Miller et al., 2010) and also autophagy inducers such as the mTORC1 inhibitor rapamycin (Ravikumar et al., 2004), mTOR kinase inhibitors (Torin) (Thoreen et al., 2009), carbamazepine (Hidvegi et al., 2010) and tat-beclin 1 (Shoji-Kawata et al., 2013). It is interesting that hydroxychloroquine, widely prescribed in the treatment of autoimmune diseases such as systemic lupus erythematosus, can be associated with retinal toxicity (Cheng et al., 2013; Marmor and Melles, 2015). In particular, central retinal thinning and loss of the ellipsoid zone in the perifoveal area on OCT testing are features of DRAM2-retinopathy, and are also frequently observed in hydroxychloroquine toxicity (Cukras et al., 2015). Intravitreal administration of rapamycin has been attempted in patients with AMD and posterior uveitis (Ibrahim et al., 2015; Petrou et al., 2015). The role of these drugs in DRAM2-retinopathy can be tested on an animal model if one was available. Understanding how DRAM2, autophagy and RD link together and the development of therapeutic compounds may be an avenue for future research.

Chapter 6. General discussion and concluding remarks

6.1 Summary of key findings

The work outlined in this thesis has described the use of NGS technologies to identify new mutations and genes involved in inherited retinal dystrophies.

Chapter three describes the Retinome project, in which a customised targeted exome capture reagent was used to produce an enriched NGS template targeting all the exons and flanking splice site junctions of the 162 genes known to cause RD at the time of reagent design (2010). After capturing the RD gene exons from patients' genomic DNA, the enriched sample was sequenced by massively parallel NGS to produce a list of exonic variants that differed from the reference sequence in each patient sample. Each variant list was then filtered to exclude common variants or those unlikely to be biologically significant, leading to the identification of the pathogenic mutation in many cases. Twenty RD families were studied in this project. Each family included multiple members affected with the same type of RD, while the twenty families reflected a range of different RD diagnoses. The detection rate for identifying the pathogenic mutation was 60%, meaning that in 12 out of 20 cases the likely causative mutation was identified (Watson et al., 2014; Shevach et al., 2015). The mutations identified consisted of previously reported mutations of known clinical significance in *ABCA4*, *RDH12*, *PROM1*, *GUCY2D*, *RPGRIP1*, *BBS2* and *SPATA7*, and new mutations in *CRB1*, *USH2A*, *RP2* and *ABCA4*. This relatively high detection rate may be because the analysis involved working on families with multiple affected members rather than single cases with no family history, which permitted follow up work to check for segregation of possible pathogenic variants in other family members.

Chapter four of this thesis focused on analysing five families in which the causative pathogenic mutations could not be identified using the targeted NGS strategy employed in Chapter three. WES technologies were therefore applied to one or more patient's genomic DNA from each family in order to try and identify the most likely causative variant(s) associated with the disease phenotype in each case. This approach was used independently or combined with homozygosity mapping. The pathogenic mutations or

best candidates causing inherited RD were identified in all five families and included known mutations in *TTLL5* (Bedoni et al., 2016) and *MFSD8*, a novel mutation in *C8orf37* (Ravesh et al., 2015), and putative pathogenic mutations in possibly two new RD-causing genes, *LARGE* and *FDFT1*. These data were supported with IF staining of mouse retina sagittal-sections that revealed localization of MFSD8 to the OPL and of LARGE to the PIS, ONL and OPL in the retina. Moreover, the calculated two-point LOD score of 5.16 for the RP family with the *LARGE* mutation was highly significant.

Chapter five describes genetic analysis of a large family with an atypical diagnosis of late-onset RD with early macular involvement. This family was not included in the Retinome analysis but was analysed in parallel. WES was combined with homozygosity mapping to identify a biallelic frameshift mutation in *DRAM2* as a novel RD gene (El-Asrag et al., 2015; Sergouniotis et al., 2015). This data was supported by another RD case with compound heterozygous changes identified by screening for mutations in *DRAM2* among 322 unrelated probands with RD. These results are further supported by the additional five likely disease-causing variants identified in four RD cases by collaborators in the UK Inherited Retinal Disease Consortium and the European Retinal Disease Consortium (ERDC). The clinical features and the course of the retinal degeneration were highly similar among affected individuals. DRAM2 is a ubiquitously expressed protein and IF staining showed its expression to be particularly strong in the PIS and at the apical surface of the RPE. Previous studies suggest that DRAM2 acts as a positive regulator of autophagy and this study suggests that DRAM2 is essential for the normal function of the retina and photoreceptor survival. Further studies are needed to provide insights into its precise role in the retina. This may include identifying DRAM2 binding partners using pull downs and mass spectrometry.

6.2 Future prospects in inherited eye disease diagnostic research

Patients with inherited RD believe that genetic testing is important (Stone, 2007) although various factors may motivate personal decisions to seek genetic testing (Willis et al., 2013). Individuals may see many different eye specialists before a definitive diagnosis can be made but genetic testing can provide an accurate diagnosis quickly. It can confirm the way in which the condition is inherited, giving a clearer picture of the

risk to patients and helping with family planning decisions. Genetic testing can help with disease prevention strategies and provide patients with an accurate guide to likely future function. With all this information, an individual can make informed decisions regarding education, employment and lifestyle.

During the last four years, since this project was started, efforts have been made to apply NGS technology for mutation detection in RD in a diagnostic setting (http://www.cmft.nhs.uk/saint-marys/our-services/manchester-centre-for-genomic-medicine) (Audo et al., 2012a; Shanks et al., 2013; Ellingford et al., 2016; Weisschuh et al., 2016). Some groups, including the Leeds Vision Research Group, have tested custom reagents for screening RD genes in order to sequence a predetermined list of known disease genes. These targeted capture NGS approaches require careful design, as they are not readily available pre-made panels, though this approach is a significant advance in mutation detection technologies compared to the previous laborious gene by gene Sanger sequencing approach. By pooling samples before targeted capture, the approach using the Retinome reagent, saves the researcher a further 75% on costs for the capturing step. However, the approach of using pooled samples poses challenges in data analysis due to the small sample size and sequencing artefacts that are detected due to low coverage, low sequence quality or variant calling. The stringency of variant calling algorithm was relaxed in the Retinome data analysis, to reduce the number of false negative results and the filtering pipeline used is very conservative, even though this causes some false positive variants to be short-listed. Furthermore, only examining known disease genes in the capture reagent limits the flexibility of the reagent to test for more disease genes as they are discovered. Another limitation may be that the capture reagent is relatively inefficient at detecting copy number variants.

As the costs of WES have decreased, customised targeted sequencing approaches have been replaced with a more broad-based NGS strategy that offers more flexibility to examine newly identified disease genes, to find variants in genes not previously associated with disease and to have greater capacity to identify copy number and structural variations (Plagnol et al., 2012; Zhao et al., 2013a; Zhang et al., 2015b). Moreover, competition between commercial companies investing in various types of NGS platforms have encouraged regular product improvements and lowering of costs, making this a more viable diagnostic strategy. Looking forward as costs become even

cheaper, WGS may be the future of DNA sequencing. WGS covers the whole genome at more consistent coverage than WES, can provide more accurate detection of structural variants (Belkadi et al., 2015) and does not rely on the accuracy of the genome annotation. Also with the new WGS library preparation kits such as TruSeq® DNA Library Prep kit (Illumina), areas that are traditionally difficult to sequence as high GC-rich regions, promoters, and repetitive elements are superiorly covered. Moreover the ability to prepare a PCR-free library eliminates the biases, gaps and errors associated with previous methods (Meynert et al., 2014).Illumina's HiSeq X Ten system are the first sequencing platforms to break the $1000 barrier for 30× coverage of WGS with ≥ 75% of bases above quality 30 and less than three days per run (Watson, 2014; Warr et al., 2015). However, cost is not the only consideration and at the moment this technology still has some limitations including data challenges in bioinformatic analysis and secure data storage, interpretation of results and ethical dilemmas (Chrystoja and Diamandis, 2014).

Some of these dilemmas also exist in the application of current NGS approaches to the diagnostic setting. For example, it is sometimes difficult to interpret the variant lists given that in some cases it may not be possible to identify an obvious pathogenic mutation based on existing knowledge of the disease phenotype. In such circumstances, even though a clear pathogenic cause cannot be established, variants of unknown significance are likely to be present and can still be reported back to the clinician who is looking after the patients, though their interpretation ought to be treated with caution. Another issue is that of incidental findings and how these are reported back to the patient. Secondary findings could be a mutation in a gene related to cancer susceptibility or heart disease such as *BRCA1, BRCA2* or *ACTA2* (Regalado et al., 2015; Metcalfe et al., 2016). Though these were not the target of the original test, patients ought to be offered the choice as to whether they want to know the result of secondary findings as they could have a major impact on them. There are also legal issues around the confidential nature of genetic findings and whether disclosure may lead to discrimination at the social level in terms of job-hunting or applications for health insurance. Best practice for these difficult dilemmas is being debated by the patients, scientists and health care professionals.

In terms of where a person is treated, there are considerable differences between patients with an inherited disease depending on whether they are living in the UK or abroad. Whilst families of Pakistani origin living in the UK have access to appropriate

infrastructure for counselling and support such as ophthalmologists, clinical geneticists and social services through the National Health Service, there are no specialized genetic counselling services in the healthcare system in Pakistan, and often it is left to the practicing physician to perform the genetic counselling duties (Hussain and Bittles, 1998; Ashfaq et al., 2013). Approximately 60% of marriages in Pakistan are consanguineous and 80% of these are between first cousins (Hussain and Bittles, 1998; Qidwai et al., 2003), making this one of the highest consanguinity rates in the world. This is likely to contribute to the high burden of recessively inherited genetic disease in this population (Bittles and Black, 2010). While this results in large families that permit gene/mutation identification studies, as shown in this thesis, it also highlights how important it is that the health care system is improved in poorer countries.

In the research presented in this thesis, two generations of DNA sequencing were used. Sanger sequencing represents the first generation, with targeted NGS and WES representing the second. Inevitably, this raises the question of what comes next in DNA sequencing. Whilst it is relatively simple to identify the divide between first and second generation DNA sequencing technologies, there is no general agreement concerning whether we have already entered the third generation of developments. However, claims have been made that single molecule sequencing (SMS) and the possibility of real-time sequencing may be the defining characteristics of the third generation (Macaulay and Voet, 2014; Grün and van Oudenaarden, 2015; Lee et al., 2016).Currently, the single molecule real time (SMRT) platform (Pacific Biosciences) is the most commonly used third-generation technology (van Dijk et al., 2014; Heather and Chain, 2016). This system employs so-called zero-mode waveguides (ZMWs) which are microfabricated nanostructures used to create an illuminated observation volume small enough to allow the monitoring of a single nucleotide being incorporated by DNA polymerase. Individual DNA polymerase molecules are deposited inside the illuminated region within the ZMWs, then the relevant DNA library and fluorescently labelled dNTPs are washed over, a different fluorescent dye being used for each of the four DNA bases. The DNA sequence is determined via a charged couple device (CCD) sensor on the basis of fluorescence nucleotide detection. Following incorporation of the nucleotide by the DNA polymerase, this dye is cleaved away, ending the detectable fluorescence signal for that position. The SMRT process not only facilitates very rapid single-molecule sequencing but is also

capable of producing extremely long reads of over 10 kb in length and scoring of the microsatellite length (Liljegren et al., 2016).

It is anticipated that nanopore sequencing (Oxford Nanopore Technologies) will also prove to be another key technology in third-generation DNA sequencing, eventually providing high accuracy long read, non-amplified sequence data at a faster speed and lower cost than was previously thought possible (Magierowski et al., 2016). In simple terms, this method involves passing an ionic current through nanopores embedded in a synthetic membrane. Double-stranded DNA is denatured enzymatically then single-stranded DNA is passed through the nanopore while the different bases prevent ionic flow in a distinctive manner. The DNA sequence can then be identified on the basis of the data provided by the change in current (Loose et al., 2016). The fact that this new generation of nanopore sequencers such as MinION is available as a small USB device that can be used in the field, outside the laboratory setting, will radically change not only the type of data that can be produced, but where and when it can be produced, and by whom (Check Hayden, 2015).Third-generation sequencing platforms will offer many theoretical benefits relating to reduced cost, increased speed and removal of PCR-bias; however, this technology is still maturing and it is likely to be a few years yet before such platforms seriously rival the second-generation instruments and enter mainstream diagnostic use.

As we move into the third generation of DNA sequencing, our understanding of genetics and the genome has been greatly enhanced by this rapid revolution in sequencing technology in recent years. As a consequence, novel RD genes continue to be discovered, improving diagnostic service provision and giving further insights into retinal function. The question now is can these genetic findings in RD research help contribute to developing therapies for these patients?

6.3 Future directions in eye disease therapeutics

Diagnosing RD patients using molecular analysis not only stratifies the patients into disease categories but may also influence their future prospects as new treatments and therapies are developed. Gene replacement therapy is one of a number of the developing therapies that depend on the delivery of a normal copy of the mutated gene to restore function. The last decade has witnessed significant success in the application of gene

replacement therapies to RD using animal models (Acland et al., 2001; Black et al., 2014; Pellissier et al., 2015). For these and other therapies to undergo clinical trials, it is essential to identify groups of genotyped patients with mutations in each gene and at various stages of the disease process. This is one of the major drivers for the development of diagnostic testing.

The first successful clinical example was for RPE65, the visual cycle protein in which gene mutations cause congenital blindness in 6-16% of all LCA patients. Animal model studies in the *Rpe65* knockout (KO) mouse and RPE65-deficient Briard dogs (Acland et al., 2001; Bemelmans et al., 2006; Pang et al., 2006; Le Meur et al., 2007; Bemelmans et al., 2008) were successful and used to develop the treatment in human patients (Cideciyan et al., 2013; Ku and Pennesi, 2015; Bennett et al., 2016; Grob et al., 2016). These human trials have successfully delivered the target gene(s) to the retina via adeno-associated virus (AAV) vectors.

Other examples of RD gene therapy trials that have shown promising results using a similar approach include the following. AAV-mediated *BBS4* delivery to the BBS mouse model *(Bbs4*-KO) was shown to prevent photoreceptor death by rescuing rhodopsin mislocalization, whilst preserving the normal-appearing architecture of rod outer segments (Simons et al., 2011). The accumulation of lipofuscin pigment A2E in the retina of *Abca4*-KO mice as a model of STGD was sharply reduced by delivering the intact human *ABCA4* gene by AAV (Kong et al., 2008). Treatment for ACHM was also successful in *CNGA3*-KO and *CNGB3*-KO mice (Carvalho et al., 2011; Pang et al., 2012). Gene therapy has also proved successful in rescuing defects in *Peripherin2*-KO (Schlichtenbrede et al., 2003), *Aipl1*-KO (Sun et al., 2010), *Mertk*-KO (LaVail et al., 2016) and *Crb1*-KO (Pellissier et al., 2015) mice. These and other mouse models have been used for testing the efficacy of gene therapy for RD-specific genes before clinical gene therapy trials that have already begun in patients with retinal diseases (Bainbridge et al., 2015; Edwards et al., 2016) (www.clinical trials.gov, NCT00481546, NCT01367444, NCT01505062 and NCT01482195).

Genome editing technologies represent a promising new approach for the treatment of RD in human patients, offering the hope that one day it might be possible to correct the defect in a patient's cells, either in culture for re-implantation or in-vivo. The clustered

regularly interspaced short palindromic repeats (CRISPR)/Cas9 system is the most advanced of these technologies, whereby targeting a precise genomic position is possible with the use of synthetic guide RNAs (Mali et al., 2013). The system edits the genome by inducing double-stranded breaks (DSBs) using a nuclease which can then be repaired by one of two different pathways that operate in nearly all cell types and organisms: non homologous end joining (NHEJ) and homology directed repair (HDR). NHEJ can lead to the efficient introduction of insertion/deletion mutations (indels) of various lengths from a single-stranded or double-stranded DNA donor template. This therefore provides a means of generating knockouts by disrupting the translational reading frame of a coding sequence. While the HDR pathway allows precise editing resulting in the newly modified target still being in its same position so still under the influence of its endogenous control elements such as promoters, enhances and repressors. This is particularly important as it prevents incorrect or inappropriate levels of expression of the newly modified gene, while allowing introduction of exact changes. Furthermore, a modified version of the CRISPR-Cas9 system has been developed to induce only a single-strand break, or nick (Shen et al., 2014a), as opposed to DSBs where significant misalignment and mispairing has been reported. The single-strand break approach allows for the endogenous base excision repair pathway to facilitate repair and results in more specific and efficient modification, thereby reducing the off target effects (Ran et al., 2013; Hsu et al., 2014). The HDR pathway therefore opens up the possibility of engineering exact disease models in animal models, or possibly of exact correction to wild-type in cells from patients with specific mutations. Progress in developing CRISPR/Cas9 into a set of tools for cell and molecular biology research has been remarkable and the application of the CRISPR/Cas9 system in conjunction with stem cell technologies is likely to pave the way for new treatments of genetic diseases.

Another therapeutic approach depends on the use of antisense oligonucleotides (AONs) that can be delivered either as naked oligonucleotides or expressed by viral vectors (Evers et al., 2015). This development is not applicable to all mutations, but AONs are ideally suited for targeting splicing mutations that cause activation of cryptic splice sites. This approach can potentially block these abnormal splicing events, and hence restore normal splicing. Among RD genes, the best known example of such a mutation is the intronic c.2991+1655A>G variant in *CEP290* which accounts for up to 20% of all LCA cases (Section 1.8.3) (den Hollander et al., 2006; Coppieters et al.,

2010a). AON-based therapy for CEP290-associated LCA has shown promising results, as it redirected normal splicing of *CEP290* in patient derived lymphoblast cells, creating an increase in correctly spliced CEP290 mRNA and a decrease in levels of aberrantly spliced CEP290 in a dose-dependent manner (Collin et al., 2012).Other examples where AON-based therapy can be applied are deep intronic mutations in *OFD1* (IVS9+705A>G) that causes XLRP (RP23) (Webb et al., 2012) or in *ABCA4 (*c.4539+2001G>A) that causes STGD (Bauwens et al., 2015).

In terms of viral vectors for therapeutic delivery, AAV appears to be safe and can be used to deliver genes to both photoreceptors and RPE. However, AAV has a limitation in that it cannot accommodate genes over 5 kb in length. Therefore, other methods of delivery are being explored. For example, non-viral nanoparticles (NPs) have been used to deliver plasmid vectors containing either RS1 or RPE65 to the retina (Delgado et al., 2012; Koirala et al., 2013). Although AAV-based therapies typically have a better transfection efficiency than NP-based systems (Han et al., 2012a), NP technology has a number of advantages. NPs can accommodate large vectors with sizes up to 20 kbp, are easy to synthesize, have low production cost compared to AAV systems and possess a safety profile with low immunogenicity and off-target risk of insertion mutagenesis into the genome (Rajala et al., 2014). NPs that have been formulated for gene therapy can be divided into three categories (Adijanto and Naash, 2015): metal NPs (gold NPS), lipid NPs (liposomes and solid lipid NPs) and polymer NPs which are composed of different monomers either proteins such as gelatin and albumin, carbohydrates such as dextran and chitosan, or small chemical compounds such as poly-lactic acid (PLA) and poly-lactic-co-glycolic acid (PLGA).

Of all the NPs that have been tested, a modified polymer-based NP (CK30-PEG) (a 30-mer cationic polylysine conjugated with 10 kDa polyethylene glycol) has proved to be the most successful for gene therapeutic delivery (Boylan et al., 2012; Kim et al., 2014; Adijanto and Naash, 2015). Generally, the effectiveness of a NP-based gene delivery system is dependent on key factors such as cellular uptake, escaping from endosomal vesicles into the cytosol, and delivery of the plasmid DNA into the nucleus. In term of cellular uptake, rod-shaped CK30-PEG NPs can effectively transfect both photoreceptor cells and the RPE, while in terms of escaping from endosomal vesicles and transfer to the nucleus, CK30-PEG NPs are directly transported into the nucleus by a unique nucleolin-

dependent endocytic process (Chen et al., 2008). Importantly, CK30-PEG NPs were found to be non-toxic to the retina even after repeated delivery (Ding et al., 2009; Han et al., 2012c). Unsurprisingly, CK30-PEG compacted DNA NPs have been extensively tested as a gene therapy for RD, and this was successfully used for the delivery of a gene-therapy plasmid carrying the human *ABCA4* gene into the retina of *abca4*$^{-/-}$ mice that was stably expressed and rescued many features of the Stargardt-associated RD (Han et al., 2012b). It was also found to promote phenotypic rescue in the *rpe65*$^{-/-}$mouse model of LCA (Koirala et al., 2013) and in rhodopsin knockout (RKO) mouse model of RP (Han et al., 2015). Recent advances in NPs technology suggested that the time may have come to rethink of using only AVV as the standard in gene delivery.

Advances in stem cell technology are the catalysing factor for the cell-based therapies that are currently being explored in the context of retinal diseases. Stem cells can be induced to differentiate into specific retinal cell types (Idelson et al., 2009; Li et al., 2013). Embryonic stem cells (ESCs), induced pluripotent stem cells (iPSCs) and retinal progenitor cells (RPCs) can be isolated and have been injected into the eye to successfully target the RPE, in mouse models of RD, and show regeneration (Tucker et al., 2011; Barnea-Cramer et al., 2016; Santos-Ferreira et al., 2016). The iPSC- derived from an affected adult's fibroblasts can differentiate into retinal cells when cultured under specific conditions. When reintroduced, such cells will have reduced risk of immune system rejection. In a mouse model this allows delivery of retinal cells derived from its own stem cells, and in which the defect has been corrected by gene therapy or genome editing, back in the mouse, facilitating the repair and restoration of function. Work is also now focusing on using IPCS to replace disease-affected retinal cells in humans (Mellough et al., 2014; Yvon et al., 2015). ESCs have also shown success in both transplantation and restoration of retinal function in mouse models (Mead et al., 2015). These experiments have led the way to the launch the first-in-human clinical trial in which RPE-differentiated cells derived from human EECs, have been transplanted into the sub-retinal space of patients with AMD or STGD. Initial results appear promising with visual acuity improvement and confirming that human ESC-derived cells could serve as a potentially safe new source for regenerative medicine (Schwartz et al., 2015; Song et al., 2015).

It is reasonable to ask, why was the RPE rather than the photoreceptor cell layer chosen as the initial target for the cell based therapy trials? This is due in part to the

involvement of the former in diseases such as AMD and RP (Ramsden et al., 2013). Importantly, it is much easier to derive from iPSCs cells that display the morphological characteristics of RPE cells, and cell replacement in this case would not require the formation of neuronal connectivity. Also the fact that RPE can be grown, whereas photoreceptors are end differentiated so cannot be amplified in culture. Moving forward in cell-based therapy for photoreceptors is dependent on future studies explaining the development, maintenance and function of photoreceptor synapses. Additional investigations are also required to elucidate complex interactions among retinal neurons and supportive retinal Müller glia (Vecino et al., 2016).

Retinal implants (prosthetics), sometimes referred to as 'bionic eyes' is also an area that is currently being developed. This approach can work in patients who have lost all photoreceptors, a group for whom other therapies are likely to prove ineffective as they can generally only preserve any remaining limited vision the patient may have (Rizzo et al., 2014).The retinal implant uses microchip electrodes surgically implanted into the retina and connected to micro-photodiode arrays, utilising the remaining intact neural network in order to transmit signals to the visual centres of the brain (Chuang et al., 2014). This technology has been successfully applied to RP patients with varying stages of disease progression and has resulted in some restoration of visual perception and improvements in light detection (da Cruz et al., 2016; Matet et al., 2016).

6.4 Filling the gap between genetics and therapy

Identification of genes and mutations associated with RD, both before and after the development of NGS technology, have considerably improved our knowledge of protein and cellular functions in the retina over the last decade. At the same time, treatment for genetic diseases is constantly moving forward at a steady pace. However, there is still a gap between these parallel trends and this begs the question: how this gap between genetics and therapy can be filled? Some researchers believe that the gap is between the mutation and the disease. What are the molecular mechanisms and how exactly do changes in ABCA4 or rhodopsin or DRAM2 kill cells? Whilst others have the view that time will fill this gap. Soon all the genes causing Mendelian disease will be identified, and new therapeutic methods will come through increased understanding of the genetics.

In reality it will be a combination of both approaches, though a well-structured personalized medicine programme would contribute to bridging this gap.

Personalized medicine is a phrase describing the use of specific information about a person, including their genetic make-up, to determine which treatment will work best for that person. The introduction of personal genomics into clinical practice has been slow and many factors have created this gap between genetic knowledge and clinical application (Anaya et al., 2016). Funding to support genetic testing is a key factor since this is usually expensive and implementation of new testing programs are often limited. Despite the decreasing cost of NGS, it is still not possible to apply this to every patient in the NHS since the cost of interpreting the sequencing data, then the counselling, and all further tests on the patient's relatives need to be considered. In practise, this can prove very expensive, at least in the first instance as the infrastructure is set up. Though once established and widely available, it might lead to indirect savings, and possibly save lives.

The heterogeneity and complexity of genomic risk information, points to the need for strategies to select and deliver the information most appropriate for particular clinical needs (Burke and Korngiebel, 2015). To fill this gap, efforts are needed to improve the body of evidence addressing clinical outcomes for genomics, to apply these scientific advances in personal genomics, and to develop realistic goals for genomic risk assessment. Smart cards such as electronic health records (EHR) and Genome (G) cards represent a new approach for personalized medicine, helping every individual to have a unique health identity (Jauhari and Rizvi, 2015). The DNA analysis for each individual is uploaded, whilst patients themselves can add lifestyle information, such as eating habits, exercise and metabolic activities, quantity and quality of sleep, and meditation. Environmental data such as pollution and air condition can also be uploaded onto the card. When needed, this data will be accessible to the healthcare researcher to analysis and compare with the results of other similar cases, as well as being available to healthcare professional in order to provide valuable prescriptions to the patient and decipher the key to good health.

6.5 Concluding remarks

NGS technology, especially WGS, needs further development in terms of bioinformatic analysis and results interpretation, and careful consideration also needs to be given to the ethical dilemmas it may pose. The CRISPR-Cas9 system needs to be developed to ensure strategies that avoid off-target effects, and combined with iPSC technology that might be used to efficiently engineer the genome to correct the pathogenic mutations. Moving forward in the various RD therapeutic approaches will mainly depend on future studies of the photoreceptor synapses. However it is possible that in the not too distant future, RD patients will all have treatment initiated with the collection of blood and skin samples to identify the pathogenic mutation and to generate a fibroblast cell line from which iPSCs can be derived. Once the mutation is identified by DNA sequencing, the most effective therapy and treatment options can be determined and applied by adopting a personalized medicine strategy. The chosen therapeutic approach may first be tested in the iPSC-derived relevant cell-line if necessary to examine its efficiency, then genome editing will be used to correct the DNA mutation, followed by transplanting these into the affected retina. This strategy is one of the most promising avenues of future research to be explored. The unanswered question is how soon will it be possible to achieve these goals?

Bibliography

Abd El-Aziz MM, El-Ashry MF, Chan WM, Chong KL, Barragan I, Antinolo G, Pang CP and Bhattacharya SS (2007). A novel genetic study of Chinese families with autosomal recessive retinitis pigmentosa. Ann Hum Genet 71(Pt 3): 281-294.

Abecasis GR, Auton A, Brooks LD, DePristo MA, Durbin RM, Handsaker RE, Kang HM, Marth GT and McVean GA (2012). An integrated map of genetic variation from 1,092 human genomes. Nature 491(7422): 56-65.

Abid A, Ismail M, Mehdi SQ and Khaliq S (2006). Identification of novel mutations in the SEMA4A gene associated with retinal degenerative diseases. J Med Genet 43(4): 378-381.

Abu-Safieh L, Alrashed M, Anazi S, Alkuraya H, Khan AO, Al-Owain M, Al-Zahrani J, Al-Abdi L, Hashem M, Al-Tarimi S, Sebai MA, Shamia A, Ray-Zack MD, Nassan M, Al-Hassnan ZN, Rahbeeni Z, Waheeb S, Alkharashi A, Abboud E, Al-Hazzaa SA and Alkuraya FS (2013). Autozygome-guided exome sequencing in retinal dystrophy patients reveals pathogenetic mutations and novel candidate disease genes. Genome Res 23(2): 236-247.

Acland GM, Ray K, Mellersh CS, Gu W, Langston AA, Rine J, Ostrander EA and Aguirre GD (1998). Linkage analysis and comparative mapping of canine progressive rod–cone degeneration (prcd) establishes potential locus homology with retinitis pigmentosa (RP17) in humans. Proc Natl Acad Sci U S A 95(6): 3048-3053.

Acland GM, Aguirre GD, Ray J, Zhang Q, Aleman TS, Cideciyan AV, Pearce-Kelling SE, Anand V, Zeng Y, Maguire AM, Jacobson SG, Hauswirth WW and Bennett J (2001). Gene therapy restores vision in a canine model of childhood blindness. Nat Genet 28(1): 92-95.

Adams NA, Awadein A and Toma HS (2007). The retinal ciliopathies. Ophthalmic Genet 28(3): 113-125.

Adato A, Weston MD, Berry A, Kimberling WJ and Bonne-Tamir A (2000). Three novel mutations and twelve polymorphisms identified in the USH2A gene in Israeli USH2 families. Hum Mutat 15(4): 388.

Adijanto J and Naash MI (2015). Nanoparticle-based technologies for retinal gene therapy. European Journal of Pharmaceutics and Biopharmaceutics 95, Part B: 353-367.

Adzhubei IA, Schmidt S, Peshkin L, Ramensky VE, Gerasimova A, Bork P, Kondrashov AS and Sunyaev SR (2010). A method and server for predicting damaging missense mutations. Nat Methods 7(4): 248-249.

Aiello C, Terracciano A, Simonati A, Discepoli G, Cannelli N, Claps D, Crow YJ, Bianchi M, Kitzmuller C, Longo D, Tavoni A, Franzoni E, Tessa A, Veneselli E, Boldrini R, Filocamo M, Williams RE, Bertini ES, Biancheri R, Carrozzo R, Mole SE and Santorelli FM (2009). Mutations in MFSD8/CLN7 are a frequent cause of variant-late infantile neuronal ceroid lipofuscinosis. Hum Mutat 30(3): E530-540.

Aldahmesh MA, Abu Safieh L, Alkuraya H, Al-Rajhi A, Shamseldin H, Hashem M, Alzahrani F, Khan AO, Alqahtani F, Rahbeeni Z, Alowain M, Khalak H, Al-Hazzaa S, Meyer BF and Alkuraya FS (2009a). Molecular characterization of retinitis pigmentosa in Saudi Arabia. Mol Vis 15: 2464-2469.

Aldahmesh MA, Al-Hassnan ZN, Aldosari M and Alkuraya FS (2009b). Neuronal ceroid lipofuscinosis caused by MFSD8 mutations: a common theme emerging. Neurogenetics 10(4): 307-311.

Aldahmesh MA, Li Y, Alhashem A, Anazi S, Alkuraya H, Hashem M, Awaji AA, Sogaty S, Alkharashi A, Alzahrani S, Al Hazzaa SA, Xiong Y, Kong S, Sun Z and Alkuraya FS (2014). IFT27, encoding a small GTPase component of IFT particles, is mutated in a consanguineous family with Bardet-Biedl syndrome. Hum Mol Genet 23(12): 3307-3315.

Aleman TS, Soumittra N, Cideciyan AV, Sumaroka AM, Ramprasad VL, Herrera W, Windsor EA, Schwartz SB, Russell RC, Roman AJ, Inglehearn CF, Kumaramanickavel G, Stone EM, Fishman GA and Jacobson SG (2009). CERKL mutations cause an autosomal recessive cone-rod dystrophy with inner retinopathy. Invest Ophthalmol Vis Sci 50(12): 5944-5954.

Aleman TS, Cideciyan AV, Aguirre GK, Huang WC, Mullins CL, Roman AJ, Sumaroka A, Olivares MB, Tsai FF, Schwartz SB, Vandenberghe LH, Limberis MP, Stone EM, Bell P, Wilson JM and Jacobson SG (2011). Human CRB1-associated retinal degeneration: comparison with the rd8 Crb1-mutant mouse model. Invest Ophthalmol Vis Sci 52(9): 6898-6910.

Ali RR and Sowden JC (2011). Regenerative medicine: DIY eye. Nature 472(7341): 42-43.

Aligianis IA, Forshew T, Johnson S, Michaelides M, Johnson CA, Trembath RC, Hunt DM, Moore AT and Maher ER (2002). Mapping of a novel locus for achromatopsia (ACHM4) to 1p and identification of a germline mutation in the alpha subunit of cone transducin (GNAT2). J Med Genet 39(9): 656-660.

Allikmets R, Shroyer NF, Singh N, Seddon JM, Lewis RA, Bernstein PS, Peiffer A, Zabriskie NA, Li Y, Hutchinson A, Dean M, Lupski JR and Leppert M (1997a). Mutation of the Stargardt disease gene (ABCR) in age-related macular degeneration. Science 277(5333): 1805-1807.

Allikmets R, Singh N, Sun H, Shroyer NF, Hutchinson A, Chidambaram A, Gerrard B, Baird L, Stauffer D, Peiffer A, Rattner A, Smallwood P, Li Y, Anderson KL, Lewis RA, Nathans J, Leppert M, Dean M and Lupski JR (1997b). A photoreceptor cell-specific ATP-binding transporter gene (ABCR) is mutated in recessive Stargardt macular dystrophy. Nat Genet 15(3): 236-246.

Amaravadi RK, Lippincott-Schwartz J, Yin XM, Weiss WA, Takebe N, Timmer W, DiPaola RS, Lotze MT and White E (2011). Principles and current strategies for targeting autophagy for cancer treatment. Clin Cancer Res 17(4): 654-666.

Ammann F, Klein D and Franceschetti A (1965). Genetic and epidemiological investigations on pigmentary degeneration of the retina and allied disorders in Switzerland. J Neurol Sci 2(2): 183-196.

Amorim IS, Mitchell NL, Palmer DN, Sawiak SJ, Mason R, Wishart TM and Gillingwater TH (2015). Molecular neuropathology of the synapse in sheep with CLN5 Batten disease. Brain Behav 5(11): e00401.

Anaya J-M, Duarte-Rey C, Sarmiento-Monroy JC, Bardey D, Castiblanco J and Rojas-Villarraga A (2016). Personalized medicine. Closing the gap between knowledge and clinical practice. Autoimmunity Reviews 15(8): 833-842.

Andrews NW (2000). Regulated secretion of conventional lysosomes. Trends Cell Biol 10(8): 316-321.

Ansar M, Santos-Cortez RL, Saqib MA, Zulfiqar F, Lee K, Ashraf NM, Ullah E, Wang X, Sajid S, Khan FS, Amin-ud-Din M, Smith JD, Shendure J, Bamshad MJ, Nickerson DA, Hameed A, Riazuddin S, Ahmed ZM, Ahmad W and Leal SM (2015). Mutation of ATF6 causes autosomal recessive achromatopsia. Hum Genet 134(9): 941-950.

Ansley SJ, Badano JL, Blacque OE, Hill J, Hoskins BE, Leitch CC, Kim JC, Ross AJ, Eichers ER, Teslovich TM, Mah AK, Johnsen RC, Cavender JC, Lewis RA, Leroux MR, Beales PL and Katsanis N (2003). Basal body dysfunction is a likely cause of pleiotropic Bardet-Biedl syndrome. Nature 425(6958): 628-633.

Arikawa K, Molday LL, Molday RS and Williams DS (1992). Localization of peripherin/rds in the disk membranes of cone and rod photoreceptors: relationship to disk membrane morphogenesis and retinal degeneration. J Cell Biol 116(3): 659-667.

Arshavsky VY (2013). Timing Is Everything: GTPase Regulation in Phototransduction. 54(12): 7725-7733.

Ashfaq M, Amanullah F, Ashfaq A and Ormond KE (2013). The views of Pakistani doctors regarding genetic counseling services - is there a future? J Genet Couns 22(6): 721-732.

Audo I, Bujakowska KM, Leveillard T, Mohand-Said S, Lancelot ME, Germain A, Antonio A, Michiels C, Saraiva JP, Letexier M, Sahel JA, Bhattacharya SS and Zeitz C (2012a). Development and application of a next-generation-sequencing (NGS) approach to detect known and novel gene defects underlying retinal diseases. Orphanet J Rare Dis 7: 8.

Audo I, Mohand-Said S, Dhaenens CM, Germain A, Orhan E, Antonio A, Hamel C, Sahel JA, Bhattacharya SS and Zeitz C (2012b). RP1 and autosomal dominant rod-cone dystrophy: novel mutations, a review of published variants, and genotype-phenotype correlation. Hum Mutat 33(1): 73-80.

Auz-Alexandre CL, Vallespin E, Aguirre-Lamban J, Cantalapiedra D, Avila-Fernandez A, Villaverde-Montero C, Ainse E, Trujillo-Tiebas MJ and Ayuso C (2009). Novel human pathological mutations. Gene symbol: GUCY2D. Disease: Leber congenital amaurosis. Hum Genet 125(3): 349.

Avila-Fernandez A, Cantalapiedra D, Aller E, Vallespin E, Aguirre-Lamban J, Blanco-Kelly F, Corton M, Riveiro-Alvarez R, Allikmets R, Trujillo-Tiebas MJ, Millan JM, Cremers FP and Ayuso C (2010). Mutation analysis of 272 Spanish families affected by autosomal recessive retinitis pigmentosa using a genotyping microarray. Mol Vis 16: 2550-2558.

Azari AA, Aleman TS, Cideciyan AV, Schwartz SB, Windsor EA, Sumaroka A, Cheung AY, Steinberg JD, Roman AJ, Stone EM, Sheffield VC and Jacobson SG (2006). Retinal disease expression in Bardet-Biedl syndrome-1 (BBS1) is a spectrum from maculopathy to retina-wide degeneration. Invest Ophthalmol Vis Sci 47(11): 5004-5010.

Baala L, Audollent S, Martinovic J, Ozilou C, Babron MC, Sivanandamoorthy S, Saunier S, Salomon R, Gonzales M, Rattenberry E, Esculpavit C, Toutain A, Moraine C, Parent P, Marcorelles P, Dauge MC, Roume J, Le Merrer M, Meiner V, Meir K, Menez F, Beaufrere AM, Francannet C, Tantau J, Sinico M, Dumez Y, MacDonald F, Munnich A, Lyonnet S, Gubler MC, Genin E, Johnson CA, Vekemans M, Encha-Razavi F and Attie-Bitach T (2007). Pleiotropic effects of CEP290 (NPHP6) mutations extend to Meckel syndrome. Am J Hum Genet 81(1): 170-179.

Badano JL, Ansley SJ, Leitch CC, Lewis RA, Lupski JR and Katsanis N (2003). Identification of a novel Bardet-Biedl syndrome protein, BBS7, that shares structural features with BBS1 and BBS2. Am J Hum Genet 72(3): 650-658.

Baehr W, Wu SM, Bird AC and Palczewski K (2003). The retinoid cycle and retina disease. Vision Res 43(28): 2957-2958.

Bainbridge JW, Mehat MS, Sundaram V, Robbie SJ, Barker SE, Ripamonti C, Georgiadis A, Mowat FM, Beattie SG, Gardner PJ, Feathers KL, Luong VA, Yzer S, Balaggan K, Viswanathan A, de Ravel TJ, Casteels I, Holder GE, Tyler N, Fitzke FW, Weleber RG, Nardini M, Moore AT, Thompson DA, Petersen-Jones SM, Michaelides M, van den Born LI, Stockman A, Smith AJ, Rubin G and Ali RR (2015). Long-term effect of gene therapy on Leber's congenital amaurosis. N Engl J Med 372(20): 1887-1897.

Ball AD, Stapley J, Dawson DA, Birkhead TR, Burke T and Slate J (2010). A comparison of SNPs and microsatellites as linkage mapping markers: lessons from the zebra finch (Taeniopygia guttata). BMC Genomics 11(1): 1-15.

Bareil C, Hamel CP, Delague V, Arnaud B, Demaille J and Claustres M (2001). Segregation of a mutation in CNGB1 encoding the beta-subunit of the rod cGMP-gated channel in a family with autosomal recessive retinitis pigmentosa. Hum Genet 108(4): 328-334.

Barnea-Cramer AO, Wang W, Lu S-J, Singh MS, Luo C, Huo H, McClements ME, Barnard AR, MacLaren RE and Lanza R (2016). Function of human pluripotent stem cell-derived photoreceptor progenitors in blind mice. Sci Rep 6: 29784.

Barragán I, Borrego S, Pieras JI, Pozo M, Santoyo J, Ayuso C, Baiget M, Millan Jé M, Mena M, El-Aziz MMA, Audo I, Zeitz C, Littink KW, Dopazo J, Bhattacharya SS and Antiñolo G (2010). Mutation Spectrum of EYS in Spanish Patients with Autosomal Recessive Retinitis Pigmentosa. Hum Mutat 31(11): E1772-1800.

Bartolini F, Bhamidipati A, Thomas S, Schwahn U, Lewis SA and Cowan NJ (2002). Functional overlap between retinitis pigmentosa 2 protein and the tubulin-specific chaperone cofactor C. J Biol Chem 277(17): 14629-14634.

Baumgartner WA (2000). Etiology, pathogenesis, and experimental treatment of retinitis pigmentosa. Med Hypotheses 54(5): 814-824.

Bauwens M, De Zaeytijd J, Weisschuh N, Kohl S, Meire F, Dahan K, Depasse F, De Jaegere S, De Ravel T, De Rademaeker M, Loeys B, Coppieters F, Leroy BP and De Baere E (2015). An augmented ABCA4 screen targeting noncoding regions reveals a deep intronic founder variant in Belgian Stargardt patients. Hum Mutat 36(1): 39-42.

Baux D, Larrieu L, Blanchet C, Hamel C, Ben Salah S, Vielle A, Gilbert-Dussardier B, Holder M, Calvas P, Philip N, Edery P, Bonneau D, Claustres M, Malcolm S and Roux AF (2007). Molecular and in silico analyses of the full-length isoform of usherin identify new pathogenic alleles in Usher type II patients. Hum Mutat 28(8): 781-789.

Bedoni N, Haer-Wigman L, Vaclavik V, Tran HV, Farinelli P, Balzano S, Royer-Bertrand B, El-Asrag ME, Bonny O, Ikonomidis C, Litzistorf Y, Nikopoulos K, Yioti G, Stefaniotou M, McKibbin M, Ellingford J, Booth AP, Black G, Toomes C, Inglehearn CF, Hoyng CB, Bax N, Klaver CCW, Thiadens AA, Murisier F, Schorderet DF, Ali M, Cremers FPM, Andréasson S, Munier FL and Rivolta C (2016). Mutations in the polyglutamylase gene TTLL5, expressed in photoreceptor cells and spermatozoa, are associated with cone-rod degeneration and reduced male fertility. Hum Mol Genet.

Bee YM, Chawla M and Zhao Y (2015). Whole Exome Sequencing Identifies a Novel and a Recurrent Mutation in BBS2 Gene in a Family with Bardet-Biedl Syndrome. Biomed Res Int 2015: 524754.

Beharry S, Zhong M and Molday RS (2004). N-retinylidene-phosphatidylethanolamine is the preferred retinoid substrate for the photoreceptor-specific ABC transporter ABCA4 (ABCR). J Biol Chem 279(52): 53972-53979.

Behn D and Potter MJ (2001). Sildenafil-mediated reduction in retinal function in heterozygous mice lacking the gamma-subunit of phosphodiesterase. Invest Ophthalmol Vis Sci 42(2): 523-527.

Belkadi A, Bolze A, Itan Y, Cobat A, Vincent QB, Antipenko A, Shang L, Boisson B, Casanova JL and Abel L (2015). Whole-genome sequencing is more powerful than whole-exome sequencing for detecting exome variants. Proc Natl Acad Sci U S A 112(17): 5473-5478.

Bellingham J, Gregory-Evans CY and Gregory-Evans K (1998). Microsatellite markers for the cone-rod retinal dystrophy gene, CRX, on 19q13.3. J Med Genet 35(6): 527.

Belyaeva OV, Korkina OV, Stetsenko AV, Kim T, Nelson PS and Kedishvili NY (2005). Biochemical properties of purified human retinol dehydrogenase 12 (RDH12): catalytic efficiency toward retinoids and C9 aldehydes and effects of cellular retinol-binding protein type I (CRBPI) and cellular retinaldehyde-binding protein (CRALBP) on the oxidation and reduction of retinoids. Biochemistry 44(18): 7035-7047.

Bemelmans AP, Kostic C, Crippa SV, Hauswirth WW, Lem J, Munier FL, Seeliger MW, Wenzel A and Arsenijevic Y (2006). Lentiviral gene transfer of RPE65 rescues survival and function of cones in a mouse model of Leber congenital amaurosis. PLoS Med 3(10): e347.

Bemelmans AP, Kostic C, Cachafeiro M, Crippa SV, Wanner D, Tekaya M, Wenzel A and Arsenijevic Y (2008). Lentiviral gene transfer-mediated cone vision restoration in RPE65 knockout mice. Adv Exp Med Biol 613: 89-95.

Benayoun L, Spiegel R, Auslender N, Abbasi AH, Rizel L, Hujeirat Y, Salama I, Garzozi HJ, Allon-Shalev S and Ben-Yosef T (2009). Genetic heterogeneity in two consanguineous families segregating early onset retinal degeneration: the pitfalls of homozygosity mapping. Am J Med Genet A 149a(4): 650-656.

Bennett J, Wellman J, Marshall KA, McCague S, Ashtari M, DiStefano-Pappas J, Elci OU, Chung DC, Sun J, Wright JF, Cross DR, Aravand P, Cyckowski LL, Bennicelli JL, Mingozzi F, Auricchio A, Pierce EA, Ruggiero J, Leroy BP, Simonelli F, High KA and Maguire AM (2016). Safety and durability of effect of contralateral-eye administration of AAV2 gene therapy in patients with childhood-onset blindness caused by RPE65 mutations: a follow-on phase 1 trial. Lancet 388(10045): 661-672.

Berger W, Kloeckener-Gruissem B and Neidhardt J (2010). The molecular basis of human retinal and vitreoretinal diseases. Prog Retin Eye Res 29(5): 335-375.

Berson DM, Dunn FA and Takao M (2002). Phototransduction by retinal ganglion cells that set the circadian clock. Science 295(5557): 1070-1073.

Berson EL (1993). Retinitis pigmentosa. The Friedenwald Lecture. Invest Ophthalmol Vis Sci 34(5): 1659-1676.

Beryozkin A, Zelinger L, Bandah-Rozenfeld D, Shevach E, Harel A, Storm T, Sagi M, Eli D, Merin S, Banin E and Sharon D (2014). Identification of mutations causing inherited retinal degenerations in the israeli and palestinian populations using homozygosity mapping. Invest Ophthalmol Vis Sci 55(2): 1149-1160.

Betts-Obregon BS, Gonzalez-Fernandez F and Tsin AT (2014). Interphotoreceptor retinoid-binding protein (IRBP) promotes retinol uptake and release by rat Muller cells (rMC-1) in vitro: implications for the cone visual cycle. Invest Ophthalmol Vis Sci 55(10): 6265-6271.

Billingsley G, Vincent A, Deveault C and Heon E (2012). Mutational analysis of SDCCAG8 in Bardet-Biedl syndrome patients with renal involvement and absent polydactyly. Ophthalmic Genet 33(3): 150-154.

Bittles AH and Black ML (2010). Evolution in health and medicine Sackler colloquium: Consanguinity, human evolution, and complex diseases. Proc Natl Acad Sci U S A 107 Suppl 1: 1779-1786.

Black A, Vasireddy V, Chung DC, Maguire AM, Gaddameedi R, Tolmachova T, Seabra M and Bennett J (2014). Adeno-associated virus 8-mediated gene therapy for choroideremia: preclinical studies in in vitro and in vivo models. J Gene Med 16(5-6): 122-130.

Blackshaw S, Fraioli RE, Furukawa T and Cepko CL (2001). Comprehensive analysis of photoreceptor gene expression and the identification of candidate retinal disease genes. Cell 107(5): 579-589.

Blanco-Kelly F, Jaijo T, Aller E, Avila-Fernandez A, Lopez-Molina MI, Gimenez A, Garcia-Sandoval B, Millan JM and Ayuso C (2015). Clinical aspects of Usher syndrome and the USH2A gene in a cohort of 433 patients. JAMA Ophthalmol 133(2): 157-164.

Blankenberg D, Gordon A, Von Kuster G, Coraor N, Taylor J and Nekrutenko A (2010). Manipulation of FASTQ data with Galaxy. Bioinformatics 26(14): 1783-1785.

Bonilha VL (2008). Age and disease-related structural changes in the retinal pigment epithelium. Clin Ophthalmol 2(2): 413-424.

Booij JC, Florijn RJ, ten Brink JB, Loves W, Meire F, van Schooneveld MJ, de Jong PT and Bergen AA (2005). Identification of mutations in the AIPL1, CRB1, GUCY2D, RPE65, and RPGRIP1 genes in patients with juvenile retinitis pigmentosa. J Med Genet 42(11): e67.

Bork JM, Peters LM, Riazuddin S, Bernstein SL, Ahmed ZM, Ness SL, Polomeno R, Ramesh A, Schloss M, Srisailpathy CRS, Wayne S, Bellman S, Desmukh D, Ahmed Z, Khan SN, Kaloustian VMD, Li XC, Lalwani A, Riazuddin S, Bitner-Glindzicz M, Nance WE, Liu XZ, Wistow G, Smith RJH, Griffith AJ, Wilcox ER, Friedman TB and Morell RJ (2001). Usher Syndrome 1D and Nonsyndromic Autosomal Recessive Deafness DFNB12 Are Caused by Allelic Mutations of the Novel Cadherin-Like Gene CDH23. Am J Hum Genet 68(1): 26-37.

Bosch Grau M, Gonzalez Curto G, Rocha C, Magiera MM, Marques Sousa P, Giordano T, Spassky N and Janke C (2013). Tubulin glycylases and glutamylases have distinct functions in stabilization and motility of ependymal cilia. J Cell Biol 202(3): 441-451.

Boughman JA, Vernon M and Shaver KA (1983). Usher syndrome: Definition and estimate of prevalence from two high-risk populations. Journal of Chronic Diseases 36(8): 595-603.

Bowne SJ, Sullivan LS, Blanton SH, Cepko CL, Blackshaw S, Birch DG, Hughbanks-Wheaton D, Heckenlively JR and Daiger SP (2002). Mutations in the inosine monophosphate dehydrogenase 1 gene (IMPDH1) cause the RP10 form of autosomal dominant retinitis pigmentosa. Hum Mol Genet 11(5): 559-568.

Bowne SJ, Liu Q, Sullivan LS, Zhu J, Spellicy CJ, Rickman CB, Pierce EA and Daiger SP (2006). Why Do Mutations in the Ubiquitously Expressed Housekeeping Gene IMPDH1 Cause Retina-Specific Photoreceptor Degeneration? Invest Ophthalmol Vis Sci 47(9): 3754-3765.

Bowne SJ, Sullivan LS, Gire AI, Birch DG, Hughbanks-Wheaton D, Heckenlively JR and Daiger SP (2008). Mutations in the TOPORS gene cause 1% of autosomal dominant retinitis pigmentosa. Mol Vis 14: 922-927.

Bowne SJ, Humphries MM, Sullivan LS, Kenna PF, Tam LC, Kiang AS, Campbell M, Weinstock GM, Koboldt DC, Ding L, Fulton RS, Sodergren EJ, Allman D, Millington-Ward S, Palfi A, McKee A, Blanton SH, Slifer S, Konidari I, Farrar GJ, Daiger SP and Humphries P (2011a). A dominant mutation in RPE65 identified by whole-exome sequencing causes retinitis pigmentosa with choroidal involvement. Eur J Hum Genet 19(10): 1074-1081.

Bowne SJ, Sullivan LS, Koboldt DC, Ding L, Fulton R, Abbott RM, Sodergren EJ, Birch DG, Wheaton DH, Heckenlively JR, Liu Q, Pierce EA, Weinstock GM and Daiger SP (2011b). Identification of disease-causing mutations in autosomal dominant retinitis pigmentosa (adRP) using next-generation DNA sequencing. Invest Ophthalmol Vis Sci 52(1): 494-503.

Boya P, Reggiori F and Codogno P (2013). Emerging regulation and functions of autophagy. Nat Cell Biol 15(7): 713-720.

Boye SE, Boye SL, Pang J, Ryals R, Everhart D, Umino Y, Neeley AW, Besharse J, Barlow R and Hauswirth WW (2010). Functional and behavioral restoration of vision by gene therapy in the guanylate cyclase-1 (GC1) knockout mouse. PLoS One 5(6): e11306.

Boylan NJ, Suk JS, Lai SK, Jelinek R, Boyle MP, Cooper MJ and Hanes J (2012). Highly compacted DNA nanoparticles with low MW PEG coatings: in vitro, ex vivo and in vivo evaluation. J Control Release 157(1): 72-79.

Brancati F, Barrano G, Silhavy JL, Marsh SE, Travaglini L, Bielas SL, Amorini M, Zablocka D, Kayserili H, Al-Gazali L, Bertini E, Boltshauser E, D'Hooghe M, Fazzi E, Fenerci EY, Hennekam RC, Kiss A, Lees MM, Marco E, Phadke SR, Rigoli L, Romano S, Salpietro CD, Sherr EH, Signorini S, Stromme P, Stuart B, Sztriha L, Viskochil DH, Yuksel A, Dallapiccola B, Valente EM and Gleeson JG (2007). CEP290 mutations are frequently

identified in the oculo-renal form of Joubert syndrome-related disorders. Am J Hum Genet 81(1): 104-113.

Branham K, Othman M, Brumm M, Karoukis AJ, Atmaca-Sonmez P, Yashar BM, Schwartz SB, Stover NB, Trzupek K, Wheaton D, Jennings B, Ciccarelli ML, Jayasundera KT, Lewis RA, Birch D, Bennett J, Sieving PA, Andreasson S, Duncan JL, Fishman GA, Iannaccone A, Weleber RG, Jacobson SG, Heckenlively JR and Swaroop A (2012). Mutations in RPGR and RP2 account for 15% of males with simplex retinal degenerative disease. Invest Ophthalmol Vis Sci 53(13): 8232-8237.

Breuer DK, Yashar BM, Filippova E, Hiriyanna S, Lyons RH, Mears AJ, Asaye B, Acar C, Vervoort R, Wright AF, Musarella MA, Wheeler P, MacDonald I, Iannaccone A, Birch D, Hoffman DR, Fishman GA, Heckenlively JR, Jacobson SG, Sieving PA and Swaroop A (2002). A comprehensive mutation analysis of RP2 and RPGR in a North American cohort of families with X-linked retinitis pigmentosa. Am J Hum Genet 70(6): 1545-1554.

Bridges CD, Alvarez RA, Fong SL, Gonzalez-Fernandez F, Lam DM and Liou GI (1984). Visual cycle in the mammalian eye. Retinoid-binding proteins and the distribution of 11-cis retinoids. Vision Res 24(11): 1581-1594.

Brockington M, Torelli S, Prandini P, Boito C, Dolatshad NF, Longman C, Brown SC and Muntoni F (2005). Localization and functional analysis of the LARGE family of glycosyltransferases: significance for muscular dystrophy. Hum Mol Genet 14(5): 657-665.

Brückner A, Polge C, Lentze N, Auerbach D and Schlattner U (2009). Yeast Two-Hybrid, a Powerful Tool for Systems Biology. Int J Mol Sci 10(6): 2763-2788.

Budanov AV and Karin M (2008). The p53-regulated Sestrin gene products inhibit mTOR signaling. Cell 134(3): 451-460.

Bujakowska K, Audo I, Mohand-Said S, Lancelot ME, Antonio A, Germain A, Leveillard T, Letexier M, Saraiva JP, Lonjou C, Carpentier W, Sahel JA, Bhattacharya SS and Zeitz C (2012). CRB1 mutations in inherited retinal dystrophies. Hum Mutat 33(2): 306-315.

Bulgakova NA and Knust E (2009). The Crumbs complex: from epithelial-cell polarity to retinal degeneration. J Cell Sci 122(Pt 15): 2587-2596.

Burke TR and Tsang SH (2011). Allelic and Phenotypic Heterogeneity in ABCA4 mutations. Ophthalmic Genet 32(3): 165-174.

Burke TR, Fishman GA, Zernant J, Schubert C, Tsang SH, Smith RT, Ayyagari R, Koenekoop RK, Umfress A, Ciccarelli ML, Baldi A, Iannaccone A, Cremers FP, Klaver CC and Allikmets R (2012). Retinal phenotypes in patients homozygous for the G1961E mutation in the ABCA4 gene. Invest Ophthalmol Vis Sci 53(8): 4458-4467.

Burke W and Korngiebel DM (2015). Closing the Gap between Knowledge and Clinical Application: Challenges for Genomic Translation. PLoS Genet 11(2): e1004978.

Cahill M, O'Keefe M, Acheson R, Mulvihill A, Wallace D and Mooney D (2001). Classification of the spectrum of Coats' disease as subtypes of idiopathic retinal telangiectasis with exudation. Acta Ophthalmol Scand 79(6): 596-602.

Cai X, Conley SM and Naash MI (2009). RPE65: Role in the visual cycle, human retinal disease, and gene therapy. Ophthalmic Genet 30(2): 57.

Carr IM, Flintoff KJ, Taylor GR, Markham AF and Bonthron DT (2006). Interactive visual analysis of SNP data for rapid autozygosity mapping in consanguineous families. Hum Mutat 27(10): 1041-1046.

Carr IM, Sheridan E, Hayward BE, Markham AF and Bonthron DT (2009). IBDfinder and SNPsetter: tools for pedigree-independent identification of autozygous regions in individuals with recessive inherited disease. Hum Mutat 30(6): 960-967.

Carr IM, Bhaskar S, O'Sullivan J, Aldahmesh MA, Shamseldin HE, Markham AF, Bonthron DT, Black G and Alkuraya FS (2013). Autozygosity mapping with exome sequence data. Hum Mutat 34(1): 50-56.

Carrel L and Willard HF (2005). X-inactivation profile reveals extensive variability in X-linked gene expression in females. Nature 434(7031): 400-404.

Carvalho LS, Xu J, Pearson RA, Smith AJ, Bainbridge JW, Morris LM, Fliesler SJ, Ding XQ and Ali RR (2011). Long-term and age-dependent restoration of visual function in a mouse model of CNGB3-associated achromatopsia following gene therapy. Hum Mol Genet 20(16): 3161-3175.

Cassin B and Solomon S (1990). Dictionary of Eye Terminology, Triad Publishing Company.

Cella W, Greenstein VC, Zernant-Rajang J, Smith TR, Barile G, Allikmets R and Tsang SH (2009). G1961E mutant allele in the Stargardt disease gene ABCA4 causes bull's eye maculopathy. Exp Eye Res 89(1): 16-24.

Chacon-Camacho OF, Jitskii S, Buentello-Volante B, Quevedo-Martinez J and Zenteno JC (2013). Exome sequencing identifies RDH12 compound heterozygous mutations in a family with severe retinitis pigmentosa. Gene 528(2): 178-182.

Chacon-Camacho OF and Zenteno JC (2015). Review and update on the molecular basis of Leber congenital amaurosis. World J Clin Cases 3(2): 112-124.

Chang B, Khanna H, Hawes N, Jimeno D, He S, Lillo C, Parapuram SK, Cheng H, Scott A, Hurd RE, Sayer JA, Otto EA, Attanasio M, O'Toole JF, Jin G, Shou C, Hildebrandt F, Williams DS, Heckenlively JR and Swaroop A (2006). In-frame deletion in a novel centrosomal/ciliary protein CEP290/NPHP6 perturbs its interaction with RPGR and results in early-onset retinal degeneration in the rd16 mouse. Hum Mol Genet 15(11): 1847-1857.

Chapple JP, Hardcastle AJ, Grayson C, Spackman LA, Willison KR and Cheetham ME (2000). Mutations in the N-terminus of the X-linked retinitis pigmentosa protein RP2 interfere with

the normal targeting of the protein to the plasma membrane. Hum Mol Genet 9(13): 1919-1926.

Check Hayden E (2015). Pint-sized DNA sequencer impresses first users. Nature 521(7550): 15-16.

Chen S, Wang QL, Nie Z, Sun H, Lennon G, Copeland NG, Gilbert DJ, Jenkins NA and Zack DJ (1997). Crx, a novel Otx-like paired-homeodomain protein, binds to and transactivates photoreceptor cell-specific genes. Neuron 19(5): 1017-1030.

Chen X, Kube DM, Cooper MJ and Davis PB (2008). Cell surface nucleolin serves as receptor for DNA nanoparticles composed of pegylated polylysine and DNA. Mol Ther 16(2): 333-342.

Chen XT, Huang H, Chen YH, Dong LJ, Li XR and Zhang XM (2015). Achromatopsia caused by novel missense mutations in the CNGA3 gene. Int J Ophthalmol 8(5): 910-915.

Chen Y, Sawada O, Kohno H, Le Y-Z, Subauste C, Maeda T and Maeda A (2013). Autophagy Protects the Retina from Light-induced Degeneration. J Biol Chem 288(11): 7506-7518.

Cheng T, Peachey NS, Li S, Goto Y, Cao Y and Naash MI (1997). The effect of peripherin/rds haploinsufficiency on rod and cone photoreceptors. J Neurosci 17(21): 8118-8128.

Cheng Y, Ren X, Hait WN and Yang JM (2013). Therapeutic targeting of autophagy in disease: biology and pharmacology. Pharmacol Rev 65(4): 1162-1197.

Chiang AP, Beck JS, Yen HJ, Tayeh MK, Scheetz TE, Swiderski RE, Nishimura DY, Braun TA, Kim KY, Huang J, Elbedour K, Carmi R, Slusarski DC, Casavant TL, Stone EM and Sheffield VC (2006). Homozygosity mapping with SNP arrays identifies TRIM32, an E3 ubiquitin ligase, as a Bardet-Biedl syndrome gene (BBS11). Proc Natl Acad Sci U S A 103(16): 6287-6292.

Choi SY, Borghuis BG, Rea R, Levitan ES, Sterling P and Kramer RH (2005). Encoding light intensity by the cone photoreceptor synapse. Neuron 48(4): 555-562.

Chou LS, Liu CS, Boese B, Zhang X and Mao R (2010). DNA sequence capture and enrichment by microarray followed by next-generation sequencing for targeted resequencing: neurofibromatosis type 1 gene as a model. Clin Chem 56(1): 62-72.

Chrystoja CC and Diamandis EP (2014). Whole genome sequencing as a diagnostic test: challenges and opportunities. Clin Chem 60(5): 724-733.

Chuang AT, Margo CE and Greenberg PB (2014). Retinal implants: a systematic review. Br J Ophthalmol 98(7): 852-856.

Chun M-H, GrÜNert U, Martin PR and WÄSsle H (1996). The Synaptic Complex of Cones in the Fovea and in the Periphery of the Macaque Monkey Retina. Vision Research 36(21): 3383-3395.

Chung DC and Traboulsi EI (2009). Leber congenital amaurosis: clinical correlations with genotypes, gene therapy trials update, and future directions. J aapos 13(6): 587-592.

Churchill JD, Bowne SJ, Sullivan LS, Lewis RA, Wheaton DK, Birch DG, Branham KE, Heckenlively JR and Daiger SP (2013). Mutations in the X-linked retinitis pigmentosa genes RPGR and RP2 found in 8.5% of families with a provisional diagnosis of autosomal dominant retinitis pigmentosa. Invest Ophthalmol Vis Sci 54(2): 1411-1416.

Cideciyan AV, Aleman TS, Swider M, Schwartz SB, Steinberg JD, Brucker AJ, Maguire AM, Bennett J, Stone EM and Jacobson SG (2004). Mutations in ABCA4 result in accumulation of lipofuscin before slowing of the retinoid cycle: a reappraisal of the human disease sequence. Hum Mol Genet 13(5): 525-534.

Cideciyan AV, Swider M, Aleman TS, Tsybovsky Y, Schwartz SB, Windsor EA, Roman AJ, Sumaroka A, Steinberg JD, Jacobson SG, Stone EM and Palczewski K (2009). ABCA4 disease progression and a proposed strategy for gene therapy. Hum Mol Genet 18(5): 931-941.

Cideciyan AV, Jacobson SG, Beltran WA, Sumaroka A, Swider M, Iwabe S, Roman AJ, Olivares MB, Schwartz SB, Komáromy AM, Hauswirth WW and Aguirre GD (2013). Human retinal gene therapy for Leber congenital amaurosis shows advancing retinal degeneration despite enduring visual improvement. Proc. Natl. Acad. Sci. U.S.A. 110(6): E517-E525.

Clarke NF, Maugenre S, Vandebrouck A, Urtizberea JA, Willer T, Peat RA, Gray F, Bouchet C, Manya H, Vuillaumier-Barrot S, Endo T, Chouery E, Campbell KP, Megarbane A and Guicheney P (2011). Congenital muscular dystrophy type 1D (MDC1D) due to a large intragenic insertion/deletion, involving intron 10 of the LARGE gene. Eur J Hum Genet 19(4): 452-457.

Clement E, Mercuri E, Godfrey C, Smith J, Robb S, Kinali M, Straub V, Bushby K, Manzur A, Talim B, Cowan F, Quinlivan R, Klein A, Longman C, McWilliam R, Topaloglu H, Mein R, Abbs S, North K, Barkovich AJ, Rutherford M and Muntoni F (2008). Brain involvement in muscular dystrophies with defective dystroglycan glycosylation. Ann Neurol 64(5): 573-582.

Collin RWJ, den Hollander AI, van der Velde-Visser SD, Bennicelli J, Bennett J and Cremers FPM (2012). Antisense Oligonucleotide (AON)-based Therapy for Leber Congenital Amaurosis Caused by a Frequent Mutation in CEP290. Mol Ther Nucleic Acids 1(3): e14-.

Comander J, Weigel-DiFranco C, Sandberg MA and Berson EL (2015). Visual Function in Carriers of X-Linked Retinitis Pigmentosa. Ophthalmology 122(9): 1899-1906.

Coppieters F, Casteels I, Meire F, De Jaegere S, Hooghe S, van Regemorter N, Van Esch H, Matuleviciene A, Nunes L, Meersschaut V, Walraedt S, Standaert L, Coucke P, Hoeben H, Kroes HY, Vande Walle J, de Ravel T, Leroy BP and De Baere E (2010a). Genetic screening of LCA in Belgium: predominance of CEP290 and identification of potential modifier alleles in AHI1 of CEP290-related phenotypes. Hum Mutat 31(10): E1709-1766.

Coppieters F, Lefever S, Leroy BP and De Baere E (2010b). CEP290, a gene with many faces: mutation overview and presentation of CEP290base. Hum Mutat 31(10): 1097-1108.

Coppieters F, De Wilde B, Lefever S, De Meester E, De Rocker N, Van Cauwenbergh C, Pattyn F, Meire F, Leroy BP, Hellemans J, Vandesompele J and De Baere E (2012). Massively parallel sequencing for early molecular diagnosis in Leber congenital amaurosis. Genet Med 14(6): 576-585.

Corbeil D, Roper K, Fargeas CA, Joester A and Huttner WB (2001). Prominin: a story of cholesterol, plasma membrane protrusions and human pathology. Traffic 2(2): 82-91.

Cote RH (2004). Characteristics of photoreceptor PDE (PDE6): similarities and differences to PDE5. Int J Impot Res 16 Suppl 1: S28-33.

Cottet S, Michaut L, Boisset G, Schlecht U, Gehring W and Schorderet DF (2006). Biological characterization of gene response in Rpe65−/− mouse model of Leber's congenital amaurosis during progression of the disease. The FASEB Journal 20(12): 2036-2049.

Coussa RG, Chakarova C, Ajlan R, Taha M, Kavalec C, Gomolin J, Khan A, Lopez I, Ren H, Waseem N, Kamenarova K, Bhattacharya SS and Koenekoop RK (2015). Genotype and Phenotype Studies in Autosomal Dominant Retinitis Pigmentosa (adRP) of the French Canadian Founder Population. Invest Ophthalmol Vis Sci 56(13): 8297-8305.

Craige B, Tsao CC, Diener DR, Hou Y, Lechtreck KF, Rosenbaum JL and Witman GB (2010). CEP290 tethers flagellar transition zone microtubules to the membrane and regulates flagellar protein content. J Cell Biol 190(5): 927-940.

Cremers FP, van de Pol DJ, van Driel M, den Hollander AI, van Haren FJ, Knoers NV, Tijmes N, Bergen AA, Rohrschneider K, Blankenagel A, Pinckers AJ, Deutman AF and Hoyng CB (1998). Autosomal recessive retinitis pigmentosa and cone-rod dystrophy caused by splice site mutations in the Stargardt's disease gene ABCR. Hum Mol Genet 7(3): 355-362.

Cremers FP, van den Hurk JA and den Hollander AI (2002). Molecular genetics of Leber congenital amaurosis. Hum Mol Genet 11(10): 1169-1176.

Crighton D, Wilkinson S, O'Prey J, Syed N, Smith P, Harrison PR, Gasco M, Garrone O, Crook T and Ryan KM (2006). DRAM, a p53-induced modulator of autophagy, is critical for apoptosis. Cell 126(1): 121-134.

Cuenca N, Deng P, Linberg KA, Lewis GP, Fisher SK and Kolb H (2002). The neurons of the ground squirrel retina as revealed by immunostains for calcium binding proteins and neurotransmitters. J Neurocytol 31(8-9): 649-666.

Cukras C, Huynh N, Vitale S, Wong WT, Ferris FL, 3rd and Sieving PA (2015). Subjective and objective screening tests for hydroxychloroquine toxicity. Ophthalmology 122(2): 356-366.

Cvackova Z, Mateju D and Stanek D (2014). Retinitis pigmentosa mutations of SNRNP200 enhance cryptic splice-site recognition. Hum Mutat 35(3): 308-317.

da Cruz L, Dorn JD, Humayun MS, Dagnelie G, Handa J, Barale PO, Sahel JA, Stanga PE, Hafezi F, Safran AB, Salzmann J, Santos A, Birch D, Spencer R, Cideciyan AV, de Juan E, Duncan JL, Eliott D, Fawzi A, Olmos de Koo LC, Ho AC, Brown G, Haller J, Regillo C, Del Priore LV, Arditi A and Greenberg RJ (2016). Five-Year Safety and Performance Results from the Argus II Retinal Prosthesis System Clinical Trial. Ophthalmology.

Daiger S, Sullivan L and Bowne S (2013). Genes and mutations causing retinitis pigmentosa. Clin Genet 84(2).

Daiger SP, Bowne SJ and Sullivan LS (2007). Perspective on genes and mutations causing retinitis pigmentosa. Arch Ophthalmol 125(2): 151-158.

Daiger SP, Sullivan LS, Gire AI, Birch DG, Heckenlively JR and Bowne SJ (2008). Mutations in known genes account for 58% of autosomal dominant retinitis pigmentosa (adRP). Adv Exp Med Biol 613: 203-209.

Daiger SP, Sullivan LS, Bowne SJ, Birch DG, Heckenlively JR, Pierce EA and Weinstock GM (2010). Targeted high-throughput DNA sequencing for gene discovery in retinitis pigmentosa. Adv Exp Med Biol 664: 325-331.

Das SR, Bhardwaj N, Kjeldbye H and Gouras P (1992). Muller cells of chicken retina synthesize 11-cis-retinol. Biochem J 285(Pt 3): 907-913.

Dave VP, Jalali S, Nayaka A, Pappuru RR, Pathengay A and Das T (2016). CLINICAL PRESENTATIONS AND OUTCOMES OF RHEGMATOGENOUS RETINAL DETACHMENT IN RETINITIS PIGMENTOSA. Retina 36(7): 1345-1348.

Davidson AE, Millar ID, Urquhart JE, Burgess-Mullan R, Shweikh Y, Parry N, O'Sullivan J, Maher GJ, McKibbin M, Downes SM, Lotery AJ, Jacobson SG, Brown PD, Black GC and Manson FD (2009). Missense mutations in a retinal pigment epithelium protein, bestrophin-1, cause retinitis pigmentosa. Am J Hum Genet 85(5): 581-592.

Davis MD, Gangnon RE, Lee LY, Hubbard LD, Klein BE, Klein R, Ferris FL, Bressler SB and Milton RC (2005). The Age-Related Eye Disease Study severity scale for age-related macular degeneration: AREDS Report No. 17. Arch Ophthalmol 123(11): 1484-1498.

Delgado D, Gascon AR, Del Pozo-Rodriguez A, Echevarria E, Ruiz de Garibay AP, Rodriguez JM and Solinis MA (2012). Dextran-protamine-solid lipid nanoparticles as a non-viral vector for gene therapy: in vitro characterization and in vivo transfection after intravenous administration to mice. Int J Pharm 425(1-2): 35-43.

den Hollander AI, Ten Brink JB, De Kok YJM, Van Soest S, Van Den Born LI, Van Driel MA, Van De Pol DJR, Payne AM, Bhattacharya SS, Kellner U, Hoyng CB, Westerveld A, Brunner HG, Bleeker-Wagemakers EM, Deutman AF, Heckenlively JR, Cremers FPM and

Bergen AAB (1999). Mutations in a human homologue of Drosophila crumbs cause retinitis pigmentosa (RP12). Nat. Genet 23(2): 217-221.

den Hollander AI, Heckenlively JR, van den Born LI, de Kok YJ, van der Velde-Visser SD, Kellner U, Jurklies B, van Schooneveld MJ, Blankenagel A, Rohrschneider K, Wissinger B, Cruysberg JR, Deutman AF, Brunner HG, Apfelstedt-Sylla E, Hoyng CB and Cremers FP (2001). Leber congenital amaurosis and retinitis pigmentosa with Coats-like exudative vasculopathy are associated with mutations in the crumbs homologue 1 (CRB1) gene. Am J Hum Genet 69(1): 198-203.

den Hollander AI, Ghiani M, de Kok YJ, Wijnholds J, Ballabio A, Cremers FP and Broccoli V (2002). Isolation of Crb1, a mouse homologue of Drosophila crumbs, and analysis of its expression pattern in eye and brain. Mech Dev 110(1-2): 203-207.

den Hollander AI, Davis J, van der Velde-Visser SD, Zonneveld MN, Pierrottet CO, Koenekoop RK, Kellner U, van den Born LI, Heckenlively JR, Hoyng CB, Handford PA, Roepman R and Cremers FP (2004). CRB1 mutation spectrum in inherited retinal dystrophies. Hum Mutat 24(5): 355-369.

den Hollander AI, Koenekoop RK, Yzer S, Lopez I, Arends ML, Voesenek KE, Zonneveld MN, Strom TM, Meitinger T, Brunner HG, Hoyng CB, van den Born LI, Rohrschneider K and Cremers FP (2006). Mutations in the CEP290 (NPHP6) gene are a frequent cause of Leber congenital amaurosis. Am J Hum Genet 79(3): 556-561.

den Hollander AI, Roepman R, Koenekoop RK and Cremers FP (2008). Leber congenital amaurosis: genes, proteins and disease mechanisms. Prog Retin Eye Res 27(4): 391-419.

den Hollander AI, McGee TL, Ziviello C, Banfi S, Dryja TP, Gonzalez-Fernandez F, Ghosh D and Berson EL (2009). A homozygous missense mutation in the IRBP gene (RBP3) associated with autosomal recessive retinitis pigmentosa. Invest Ophthalmol Vis Sci 50(4): 1864-1872.

den Hollander AI, Black A, Bennett J and Cremers FPM (2010). Lighting a candle in the dark: advances in genetics and gene therapy of recessive retinal dystrophies. J Clin Invest 120(9): 3042-3053.

DePristo MA, Banks E, Poplin R, Garimella KV, Maguire JR, Hartl C, Philippakis AA, del Angel G, Rivas MA, Hanna M, McKenna A, Fennell TJ, Kernytsky AM, Sivachenko AY, Cibulskis K, Gabriel SB, Altshuler D and Daly MJ (2011). A framework for variation discovery and genotyping using next-generation DNA sequencing data. Nat Genet 43(5): 491-498.

Despriet DD, van Duijn CM, Oostra BA, Uitterlinden AG, Hofman A, Wright AF, ten Brink JB, Bakker A, de Jong PT, Vingerling JR, Bergen AA and Klaver CC (2009). Complement component C3 and risk of age-related macular degeneration. Ophthalmology 116(3): 474-480.e472.

Dharmaraj SR, Silva ER, Pina AL, Li YY, Yang JM, Carter CR, Loyer MK, El-Hilali HK, Traboulsi EK, Sundin OK, Zhu DK, Koenekoop RK and Maumenee IH (2000). Mutational analysis and clinical correlation in Leber congenital amaurosis. Ophthalmic Genet 21(3): 135-150.

Ding X-Q, Quiambao AB, Fitzgerald JB, Cooper MJ, Conley SM and Naash MI (2009). Ocular Delivery of Compacted DNA-Nanoparticles Does Not Elicit Toxicity in the Mouse Retina. PLoS One 4(10): e7410.

Dizhoor AM, Lowe DG, Olshevskaya EV, Laura RP and Hurley JB (1994). The human photoreceptor membrane guanylyl cyclase, RetGC, is present in outer segments and is regulated by calcium and a soluble activator. Neuron 12(6): 1345-1352.

Dizhoor AM, Olshevskaya EV and Peshenko IV (2010). Mg(2+)/Ca(2+) cation binding cycle of guanylyl cyclase activating proteins (GCAPs): role in regulation of photoreceptor guanylyl cyclase. Mol Cell Biochem 334(1-2): 117-124.

Do R, Pare G, Montpetit A, Hudson TJ, Gaudet D and Engert JC (2008). K45R variant of squalene synthase increases total cholesterol levels in two study samples from a French Canadian population. Hum Mutat 29(5): 689-694.

Dolan FM, Parks S, Hammer H and Keating D (2002). The wide field multifocal electroretinogram reveals retinal dysfunction in early retinitis pigmentosa. Br J Ophthalmol 86(4): 480-481.

Downes SM, Holder GE, Fitzke FW, Payne AM, Warren MJ, Bhattacharya SS and Bird AC (2001a). Autosomal dominant cone and cone-rod dystrophy with mutations in the guanylate cyclase activator 1A gene-encoding guanylate cyclase activating protein-1. Arch Ophthalmol 119(1): 96-105.

Downes SM, Payne AM, Kelsell RE, Fitzke FW, Holder GE, Hunt DM, Moore AT and Bird AC (2001b). Autosomal dominant cone-rod dystrophy with mutations in the guanylate cyclase 2D gene encoding retinal guanylate cyclase-1. Arch Ophthalmol 119(11): 1667-1673.

Dreyer B, Tranebjaerg L, Brox V, Rosenberg T, Moller C, Beneyto M, Weston MD, Kimberling WJ, Cremers CW, Liu XZ and Nilssen O (2001). A common ancestral origin of the frequent and widespread 2299delG USH2A mutation. Am J Hum Genet 69(1): 228-234.

Dreyer B, Brox V, Tranebjaerg L, Rosenberg T, Sadeghi AM, Moller C and Nilssen O (2008). Spectrum of USH2A mutations in Scandinavian patients with Usher syndrome type II. Hum Mutat 29(3): 451.

Dryja TP, McGee TL, Hahn LB, Cowley GS, Olsson JE, Reichel E, Sandberg MA and Berson EL (1990). Mutations within the rhodopsin gene in patients with autosomal dominant retinitis pigmentosa. N Engl J Med 323(19): 1302-1307.

Dryja TP, Hahn LB, Cowley GS, McGee TL and Berson EL (1991). Mutation spectrum of the rhodopsin gene among patients with autosomal dominant retinitis pigmentosa. Proc Natl Acad Sci U S A 88(20): 9370-9374.

Dryja TP, Finn JT, Peng YW, McGee TL, Berson EL and Yau KW (1995). Mutations in the gene encoding the alpha subunit of the rod cGMP-gated channel in autosomal recessive retinitis pigmentosa. Proc Natl Acad Sci U S A 92(22): 10177-10181.

Dryja TP, Hahn LB, Kajiwara K and Berson EL (1997). Dominant and digenic mutations in the peripherin/RDS and ROM1 genes in retinitis pigmentosa. Invest Ophthalmol Vis Sci 38(10): 1972-1982.

Dryja TP, Rucinski DE, Chen SH and Berson EL (1999). Frequency of mutations in the gene encoding the alpha subunit of rod cGMP-phosphodiesterase in autosomal recessive retinitis pigmentosa. Invest Ophthalmol Vis Sci 40(8): 1859-1865.

Dryja TP, Adams SM, Grimsby JL, McGee TL, Hong DH, Li T, Andréasson S and Berson EL (2001). Null RPGRIP1 Alleles in Patients with Leber Congenital Amaurosis. Am J Hum Genet 68(5): 1295-1298.

Dvir L, Srour G, Abu-Ras R, Miller B, Shalev SA and Ben-Yosef T (2010). Autosomal-recessive early-onset retinitis pigmentosa caused by a mutation in PDE6G, the gene encoding the gamma subunit of rod cGMP phosphodiesterase. Am J Hum Genet 87(2): 258-264.

Dyer MA and Cepko CL (2000). Control of Muller glial cell proliferation and activation following retinal injury. Nat Neurosci 3(9): 873-880.

Ebermann I, Phillips JB, Liebau MC, Koenekoop RK, Schermer B, Lopez I, Sch, xE, fer E, Roux A-F, Dafinger C, Bernd A, Zrenner E, Claustres M, Blanco B, xFc, rnberg G, xFc, rnberg P, Ruland R, Westerfield M, Benzing T and Bolz HJ (2010). PDZD7 is a modifier of retinal disease and a contributor to digenic Usher syndrome. J Clin Invest 120(6): 1812-1823.

Eblimit A, Nguyen TMT, Chen Y, Esteve-Rudd J, Zhong H, Letteboer S, Van Reeuwijk J, Simons DL, Ding Q, Wu KM, Li Y, Van Beersum S, Moayedi Y, Xu H, Pickard P, Wang K, Gan L, Wu SM, Williams DS, Mardon G, Roepman R and Chen R (2015). Spata7 is a retinal ciliopathy gene critical for correct RPGRIP1 localization and protein trafficking in the retina. Hum Mol Genet 24(6): 1584-1601.

Edde B, Rossier J, Le Caer JP, Desbruyeres E, Gros F and Denoulet P (1990). Posttranslational glutamylation of alpha-tubulin. Science 247(4938): 83-85.

Edwards AO, Ritter R, 3rd, Abel KJ, Manning A, Panhuysen C and Farrer LA (2005). Complement factor H polymorphism and age-related macular degeneration. Science 308(5720): 421-424.

Edwards TL, Jolly JK, Groppe M, Barnard AR, Cottriall CL, Tolmachova T, Black GC, Webster AR, Lotery AJ, Holder GE, Xue K, Downes SM, Simunovic MP, Seabra MC and

MacLaren RE (2016). Visual Acuity after Retinal Gene Therapy for Choroideremia. N Engl J Med 374(20): 1996-1998.

Ehrenberg M, Pierce EA, Cox GF and Fulton AB (2013). CRB1: one gene, many phenotypes. Semin Ophthalmol 28(5-6): 397-405.

Eiraku M, Takata N, Ishibashi H, Kawada M, Sakakura E, Okuda S, Sekiguchi K, Adachi T and Sasai Y (2011). Self-organizing optic-cup morphogenesis in three-dimensional culture. Nature 472(7341): 51-56.

El-Asrag ME, Sergouniotis PI, McKibbin M, Plagnol V, Sheridan E, Waseem N, Abdelhamed Z, McKeefry D, Van Schil K, Poulter JA, Johnson CA, Carr IM, Leroy BP, De Baere E, Inglehearn CF, Webster AR, Toomes C and Ali M (2015). Biallelic mutations in the autophagy regulator DRAM2 cause retinal dystrophy with early macular involvement. Am J Hum Genet 96(6): 948-954.

Ellegren H (2004). Microsatellites: simple sequences with complex evolution. Nat Rev Genet 5(6): 435-445.

Ellingford JM, Barton S, Bhaskar S, O'Sullivan J, Williams SG, Lamb JA, Panda B, Sergouniotis PI, Gillespie RL, Daiger SP, Hall G, Gale T, Lloyd IC, Bishop PN, Ramsden SC and Black GCM (2016). Molecular findings from 537 individuals with inherited retinal disease. J Med Genet.

Estrada-Cuzcano A, Koenekoop RK, Senechal A, De Baere EB, de Ravel T, Banfi S, Kohl S, Ayuso C, Sharon D, Hoyng CB, Hamel CP, Leroy BP, Ziviello C, Lopez I, Bazinet A, Wissinger B, Sliesoraityte I, Avila-Fernandez A, Littink KW, Vingolo EM, Signorini S, Banin E, Mizrahi-Meissonnier L, Zrenner E, Kellner U, Collin RW, den Hollander AI, Cremers FP and Klevering BJ (2012a). BBS1 mutations in a wide spectrum of phenotypes ranging from nonsyndromic retinitis pigmentosa to Bardet-Biedl syndrome. Arch Ophthalmol 130(11): 1425-1432.

Estrada-Cuzcano A, Neveling K, Kohl S, Banin E, Rotenstreich Y, Sharon D, Falik-Zaccai TC, Hipp S, Roepman R, Wissinger B, Letteboer SJ, Mans DA, Blokland EA, Kwint MP, Gijsen SJ, van Huet RA, Collin RW, Scheffer H, Veltman JA, Zrenner E, den Hollander AI, Klevering BJ and Cremers FP (2012b). Mutations in C8orf37, encoding a ciliary protein, are associated with autosomal-recessive retinal dystrophies with early macular involvement. Am J Hum Genet 90(1): 102-109.

Eudy JD, Weston MD, Yao S, Hoover DM, Rehm HL, Ma-Edmonds M, Yan D, Ahmad I, Cheng JJ, Ayuso C, Cremers C, Davenport S, Moller C, Talmadge CB, Beisel KW, Tamayo M, Morton CC, Swaroop A, Kimberling WJ and Sumegi J (1998). Mutation of a gene encoding a protein with extracellular matrix motifs in Usher syndrome type IIa. Science 280(5370): 1753-1757.

Euler T and Schubert T (2015). Multiple Independent Oscillatory Networks in the Degenerating Retina. Front Cell Neurosci 9: 444.

Evans JR, Hardcastle AJ and Cheetham ME (2006). Focus on Molecules: X-linked Retinitis Pigmentosa 2 protein, RP2. Exp Eye Res 82(4): 543-544.

Evans RJ, Schwarz N, Nagel-Wolfrum K, Wolfrum U, Hardcastle AJ and Cheetham ME (2010). The retinitis pigmentosa protein RP2 links pericentriolar vesicle transport between the Golgi and the primary cilium. Hum Mol Genet 19(7): 1358-1367.

Evers MM, Toonen LJA and van Roon-Mom WMC (2015). Antisense oligonucleotides in therapy for neurodegenerative disorders. Adv. Drug Deliv. Rev. 87: 90-103.

Fahim AT, Daiger SP and Weleber RG (2013). Retinitis Pigmentosa Overview. GeneReviews(R). R A Pagon, M P Adam, H H Ardinger et al. Seattle (WA), University of Washington, Seattle.

Fan J, Rohrer B, Frederick JM, Baehr W and Crouch RK (2008). Rpe65(−/−) and Lrat(−/−) Mice: Comparable Models of Leber Congenital Amaurosis. Invest Ophthalmol Vis Sci 49(6): 2384-2389.

Fan Y, Esmail MA, Ansley SJ, Blacque OE, Boroevich K, Ross AJ, Moore SJ, Badano JL, May-Simera H, Compton DS, Green JS, Lewis RA, van Haelst MM, Parfrey PS, Baillie DL, Beales PL, Katsanis N, Davidson WS and Leroux MR (2004). Mutations in a member of the Ras superfamily of small GTP-binding proteins causes Bardet-Biedl syndrome. Nat Genet 36(9): 989-993.

Farag TI and Teebi AS (1989). High incidence of Bardet Biedl syndrome among the Bedouin. Clin Genet 36(6): 463-464.

Farsaii M and Connaughton VP (1995). AII Amacrine Cells. Webvision: The Organization of the Retina and Visual System. H Kolb, E Fernandez and R Nelson. Salt Lake City (UT), University of Utah Health Sciences Center.

Fattahi Z, Rostami P, Najmabadi A, Mohseni M, Kahrizi K, Akbari MR, Kariminejad A and Najmabadi H (2014). Mutation profile of BBS genes in Iranian patients with Bardet-Biedl syndrome: genetic characterization and report of nine novel mutations in five BBS genes. J Hum Genet 59(7): 368-375.

Feathers KL, Lyubarsky AL, Khan NW, Teofilo K, Swaroop A, Williams DS, Pugh EN and Thompson DA (2008). Nrl-Knockout Mice Deficient in Rpe65 Fail to Synthesize 11-cis Retinal and Cone Outer Segments. Invest Ophthalmol Vis Sci 49(3): 1126-1135.

Fedorko M (1967). Effect of chloroquine on morphology of cytoplasmic granules in maturing human leukocytes--an ultrastructural study. J Clin Invest 46(12): 1932-1942.

Fernandez-San Jose P, Corton M, Blanco-Kelly F, Avila-Fernandez A, Lopez-Martinez MA, Sanchez-Navarro I, Sanchez-Alcudia R, Perez-Carro R, Zurita O, Sanchez-Bolivar N, Lopez-Molina MI, Garcia-Sandoval B, Riveiro-Alvarez R and Ayuso C (2015). Targeted

Next-Generation Sequencing Improves the Diagnosis of Autosomal Dominant Retinitis Pigmentosa in Spanish Patients. Invest Ophthalmol Vis Sci 56(4): 2173-2182.

Fernández ME, Goszczynski DE, Lirón JP, Villegas-Castagnasso EE, Carino MH, Ripoli MV, Rogberg-Muñoz A, Posik DM, Peral-García P and Giovambattista G (2013). Comparison of the effectiveness of microsatellites and SNP panels for genetic identification, traceability and assessment of parentage in an inbred Angus herd. GENET MOL BIOL 36(2): 185-191.

Ferrante MI, Giorgio G, Feather SA, Bulfone A, Wright V, Ghiani M, Selicorni A, Gammaro L, Scolari F, Woolf AS, Sylvie O, Bernard L, Malcolm S, Winter R, Ballabio A and Franco B (2001). Identification of the gene for oral-facial-digital type I syndrome. Am J Hum Genet 68(3): 569-576.

Ferrari S, Di Iorio E, Barbaro V, Ponzin D, Sorrentino FS and Parmeggiani F (2011). Retinitis Pigmentosa: Genes and Disease Mechanisms. Curr Genomics 12(4): 238-249.

Filipek S, Teller DC, Palczewski K and Stenkamp R (2003). The crystallographic model of rhodopsin and its use in studies of other G protein-coupled receptors. Annu Rev Biophys Biomol Struct 32: 375-397.

Fingert JH, Oh K, Chung M, Scheetz TE, Andorf JL, Johnson RM, Sheffield VC and Stone EM (2008). Association of a novel mutation in the retinol dehydrogenase 12 (RDH12) gene with autosomal dominant retinitis pigmentosa. Arch Ophthalmol 126(9): 1301-1307.

Fishman GA (1978). Retinitis pigmentosa. Visual loss. Arch Ophthalmol 96(7): 1185-1188.

Fishman GA, Stone EM, Eliason DA, Taylor CM, Lindeman M and Derlacki DJ (2003). ABCA4 gene sequence variations in patients with autosomal recessive cone-rod dystrophy. Arch Ophthalmol 121(6): 851-855.

Fliesler SJ and Bretillon L (2010). The ins and outs of cholesterol in the vertebrate retina. J Lipid Res 51(12): 3399-3413.

Flynn MF, Fishman GA, Anderson RJ and Roberts DK (2001). Retrospective longitudinal study of visual acuity change in patients with retinitis pigmentosa. Retina 21(6): 639-646.

Forsythe E and Beales PL (1993). Bardet-Biedl Syndrome. GeneReviews(R). R A Pagon, M P Adam, H H Ardinger et al. Seattle (WA), University of Washington, Seattle

University of Washington, Seattle. All rights reserved.

Forsythe E and Beales PL (2013). Bardet-Biedl syndrome. Eur J Hum Genet 21(1): 8-13.

Franceschetti A and Dieterle P (1954). [Diagnostic and prognostic importance of the electroretinogram in tapetoretinal degeneration with reduction of the visual field and hemeralopia]. Confin Neurol 14(2-3): 184-186.

Friedrich U, Warburg M and Jorgensen AL (1993). X-inactivation pattern in carriers of X-linked retinitis pigmentosa: a valuable means of prognostic evaluation? Hum Genet 92(4): 359-363.

Fritsche LG, Chen W, Schu M, Yaspan BL, Yu Y, Thorleifsson G, Zack DJ, Arakawa S, Cipriani V, Ripke S, Igo RP, Jr., Buitendijk GH, Sim X, Weeks DE, Guymer RH, Merriam JE, Francis PJ, Hannum G, Agarwal A, Armbrecht AM, Audo I, Aung T, Barile GR, Benchaboune M, Bird AC, Bishop PN, Branham KE, Brooks M, Brucker AJ, Cade WH, Cain MS, Campochiaro PA, Chan CC, Cheng CY, Chew EY, Chin KA, Chowers I, Clayton DG, Cojocaru R, Conley YP, Cornes BK, Daly MJ, Dhillon B, Edwards AO, Evangelou E, Fagerness J, Ferreyra HA, Friedman JS, Geirsdottir A, George RJ, Gieger C, Gupta N, Hagstrom SA, Harding SP, Haritoglou C, Heckenlively JR, Holz FG, Hughes G, Ioannidis JP, Ishibashi T, Joseph P, Jun G, Kamatani Y, Katsanis N, C NK, Khan JC, Kim IK, Kiyohara Y, Klein BE, Klein R, Kovach JL, Kozak I, Lee CJ, Lee KE, Lichtner P, Lotery AJ, Meitinger T, Mitchell P, Mohand-Said S, Moore AT, Morgan DJ, Morrison MA, Myers CE, Naj AC, Nakamura Y, Okada Y, Orlin A, Ortube MC, Othman MI, Pappas C, Park KH, Pauer GJ, Peachey NS, Poch O, Priya RR, Reynolds R, Richardson AJ, Ripp R, Rudolph G, Ryu E, Sahel JA, Schaumberg DA, Scholl HP, Schwartz SG, Scott WK, Shahid H, Sigurdsson H, Silvestri G, Sivakumaran TA, Smith RT, Sobrin L, Souied EH, Stambolian DE, Stefansson H, Sturgill-Short GM, Takahashi A, Tosakulwong N, Truitt BJ, Tsironi EE, Uitterlinden AG, van Duijn CM, Vijaya L, Vingerling JR, Vithana EN, Webster AR, Wichmann HE, Winkler TW, Wong TY, Wright AF, Zelenika D, Zhang M, Zhao L, Zhang K, Klein ML, Hageman GS, Lathrop GM, Stefansson K, Allikmets R, Baird PN, Gorin MB, Wang JJ, Klaver CC, Seddon JM, Pericak-Vance MA, Iyengar SK, Yates JR, Swaroop A, Weber BH, Kubo M, Deangelis MM, Leveillard T, Thorsteinsdottir U, Haines JL, Farrer LA, Heid IM and Abecasis GR (2013). Seven new loci associated with age-related macular degeneration. Nat Genet 45(4): 433-439, 439e431-432.

Fu Y (2010). Phototransduction in Rods and Cones. The Organization of the Retina and Visual System Kolb H, Fernandez E and Nelson R. University of Utah Health Sciences Center, Salt Lake City (UT), USA, Webvision.

Furukawa T, Morrow EM and Cepko CL (1997). Crx, a novel otx-like homeobox gene, shows photoreceptor-specific expression and regulates photoreceptor differentiation. Cell 91(4): 531-541.

Furukawa T, Morrow EM, Li T, Davis FC and Cepko CL (1999). Retinopathy and attenuated circadian entrainment in Crx-deficient mice. Nat Genet 23(4): 466-470.

Gakovic M, Shu X, Kasioulis I, Carpanini S, Moraga I and Wright AF (2011). The role of RPGR in cilia formation and actin stability. Hum Mol Genet 20(24): 4840-4850.

Gal A, Li Y, Thompson DA, Weir J, Orth U, Jacobson SG, Apfelstedt-Sylla E and Vollrath D (2000). Mutations in MERTK, the human orthologue of the RCS rat retinal dystrophy gene, cause retinitis pigmentosa. Nat Genet 26(3): 270-271.

Galvin JA, Fishman GA, Stone EM and Koenekoop RK (2005). Evaluation of genotype-phenotype associations in leber congenital amaurosis. Retina 25(7): 919-929.

Gamundi MJ, Hernan I, Martínez-Gimeno M, Maseras M, García-Sandoval B, Ayuso C, Antiñolo G, Baiget M and Carballo M (2006). Three novel and the common Arg677Ter RP1 protein truncating mutations causing autosomal dominant retinitis pigmentosa in a Spanish population. BMC Medical Genetics 7(1): 1-10.

Ganley IG, Lam du H, Wang J, Ding X, Chen S and Jiang X (2009). ULK1.ATG13.FIP200 complex mediates mTOR signaling and is essential for autophagy. J Biol Chem 284(18): 12297-12305.

Gao M, Zhang S, Liu C, Qin Y, Archacki S, Jin L, Wang Y, Liu F, Chen J, Liu Y, Wang J, Huang M, Liao S, Tang Z, Guo AY, Jiang F and Liu M (2016). Whole exome sequencing identifies a novel NRL mutation in a Chinese family with autosomal dominant retinitis pigmentosa. Mol Vis 22: 234-242.

Garcia-Hoyos M, Auz-Alexandre CL, Almoguera B, Cantalapiedra D, Riveiro-Alvarez R, Lopez-Martinez MA, Gimenez A, Blanco-Kelly F, Avila-Fernandez A, Trujillo-Tiebas MJ, Garcia-Sandoval B, Ramos C and Ayuso C (2011). Mutation analysis at codon 838 of the Guanylate Cyclase 2D gene in Spanish families with autosomal dominant cone, cone-rod, and macular dystrophies. Mol Vis 17: 1103-1109.

Garrod AE (1902). The incidence of alkaptonuria: a study in chemical individuality. 1902 [classical article]. Yale J Biol Med 75(4): 221-231.

Gibbs D, Kitamoto J and Williams DS (2003). Abnormal phagocytosis by retinal pigmented epithelium that lacks myosin VIIa, the Usher syndrome 1B protein. Proc Natl Acad Sci U S A 100(11): 6481-6486.

Goddeeris MM, Wu B, Venzke D, Yoshida-Moriguchi T, Saito F, Matsumura K, Moore SA and Campbell KP (2013). LARGE glycans on dystroglycan function as a tunable matrix scaffold to prevent dystrophy. Nature 503(7474): 136-140.

Godfrey C, Clement E, Mein R, Brockington M, Smith J, Talim B, Straub V, Robb S, Quinlivan R, Feng L, Jimenez-Mallebrera C, Mercuri E, Manzur AY, Kinali M, Torelli S, Brown SC, Sewry CA, Bushby K, Topaloglu H, North K, Abbs S and Muntoni F (2007). Refining genotype–phenotype correlations in muscular dystrophies with defective glycosylation of dystroglycan. Brain 130(10): 2725-2735.

Gold B, Merriam JE, Zernant J, Hancox LS, Taiber AJ, Gehrs K, Cramer K, Neel J, Bergeron J, Barile GR, Smith RT, Hageman GS, Dean M and Allikmets R (2006). Variation in factor B (BF) and complement component 2 (C2) genes is associated with age-related macular degeneration. Nat Genet 38(4): 458-462.

Goldberg AF and Molday RS (1996). Defective subunit assembly underlies a digenic form of retinitis pigmentosa linked to mutations in peripherin/rds and rom-1. Proc Natl Acad Sci U S A 93(24): 13726-13730.

Gorczyca WA, Kobialka M, Kuropatwa M and Kurowska E (2003). Ca2+ differently affects hydrophobic properties of guanylyl cyclase-activating proteins (GCAPs) and recoverin. Acta Biochim Pol 50(2): 367-376.

Gosens I, den Hollander AI, Cremers FPM and Roepman R (2008). Composition and function of the Crumbs protein complex in the mammalian retina. Exp Eye Res 86(5): 713-726.

Grau T, Artemyev NO, Rosenberg T, Dollfus H, Haugen OH, Cumhur Sener E, Jurklies B, Andreasson S, Kernstock C, Larsen M, Zrenner E, Wissinger B and Kohl S (2011). Decreased catalytic activity and altered activation properties of PDE6C mutants associated with autosomal recessive achromatopsia. Hum Mol Genet 20(4): 719-730.

Graw J (2003). The genetic and molecular basis of congenital eye defects. Nat Rev Genet 4(11): 876-888.

Gregory-Evans K, Kelsell RE, Gregory-Evans CY, Downes SM, Fitzke FW, Holder GE, Simunovic M, Mollon JD, Taylor R, Hunt DM, Bird AC and Moore AT (2000). Autosomal dominant cone-rod retinal dystrophy (CORD6) from heterozygous mutation of GUCY2D, which encodes retinal guanylate cyclase. Ophthalmology 107(1): 55-61.

Grewal PK, Holzfeind PJ, Bittner RE and Hewitt JE (2001). Mutant glycosyltransferase and altered glycosylation of alpha-dystroglycan in the myodystrophy mouse. Nat Genet 28(2): 151-154.

Grob SR, Finn A, Papakostas TD and Eliott D (2016). Clinical Trials in Retinal Dystrophies. Middle East Afr J Ophthalmol 23(1): 49-59.

Grün D and van Oudenaarden A (2015). Design and Analysis of Single-Cell Sequencing Experiments. Cell 163(4): 799-810.

Gu SM, Thompson DA, Srikumari CR, Lorenz B, Finckh U, Nicoletti A, Murthy KR, Rathmann M, Kumaramanickavel G, Denton MJ and Gal A (1997). Mutations in RPE65 cause autosomal recessive childhood-onset severe retinal dystrophy. Nat Genet 17(2): 194-197.

Gwinn DM, Shackelford DB, Egan DF, Mihaylova MM, Mery A, Vasquez DS, Turk BE and Shaw RJ (2008). AMPK phosphorylation of raptor mediates a metabolic checkpoint. Mol Cell 30(2): 214-226.

Haeseleer F, Jang GF, Imanishi Y, Driessen CA, Matsumura M, Nelson PS and Palczewski K (2002). Dual-substrate specificity short chain retinol dehydrogenases from the vertebrate retina. J Biol Chem 277(47): 45537-45546.

Hailey DW, Rambold AS, Satpute-Krishnan P, Mitra K, Sougrat R, Kim PK and Lippincott-Schwartz J (2010). Mitochondria Supply Membranes for Autophagosome Biogenesis during Starvation. Cell 141(4): 656-667.

Haim M (2002). Epidemiology of retinitis pigmentosa in Denmark. Acta Ophthalmol Scand Suppl(233): 1-34.

Haltia M (2003). The neuronal ceroid-lipofuscinoses. J Neuropathol Exp Neurol 62(1): 1-13.

Haltia M (2006). The neuronal ceroid-lipofuscinoses: From past to present. Biochim Biophys Acta 1762(10): 850-856.

Hamamy H (2012). Consanguineous marriages: Preconception consultation in primary health care settings. J Community Genet 3(3): 185-192.

Hamasaki M and Yoshimori T (2010). Where do they come from? Insights into autophagosome formation. FEBS Letters 584(7): 1296-1301.

Hamel C (2006). Retinitis pigmentosa. Orphanet J Rare Dis 1: 40.

Hamel CP (2007). Cone rod dystrophies. Orphanet J Rare Dis 2: 7.

Han Z, Conley SM, Makkia R, Guo J, Cooper MJ and Naash MI (2012a). Comparative Analysis of DNA Nanoparticles and AAVs for Ocular Gene Delivery. PLoS One 7(12): e52189.

Han Z, Conley SM, Makkia RS, Cooper MJ and Naash MI (2012b). DNA nanoparticle-mediated ABCA4 delivery rescues Stargardt dystrophy in mice. J. Clin. Invest. 122(9): 3221-3226.

Han Z, Koirala A, Makkia R, Cooper MJ and Naash MI (2012c). Direct gene transfer with compacted DNA nanoparticles in retinal pigment epithelial cells: Expression, repeat delivery and lack of toxicity. Nanomedicine 7(4): 521-539.

Han Z, Banworth MJ, Makkia R, Conley SM, Al-Ubaidi MR, Cooper MJ and Naash MI (2015). Genomic DNA nanoparticles rescue rhodopsin-associated retinitis pigmentosa phenotype. The FASEB Journal 29(6): 2535-2544.

Hanein S, Perrault I, Gerber S, Tanguy G, Barbet F, Ducroq D, Calvas P, Dollfus H, Hamel C, Lopponen T, Munier F, Santos L, Shalev S, Zafeiriou D, Dufier JL, Munnich A, Rozet JM and Kaplan J (2004). Leber congenital amaurosis: comprehensive survey of the genetic heterogeneity, refinement of the clinical definition, and genotype-phenotype correlations as a strategy for molecular diagnosis. Hum Mutat 23(4): 306-317.

Hardcastle AJ, Thiselton DL, Van Maldergem L, Saha BK, Jay M, Plant C, Taylor R, Bird AC and Bhattacharya S (1999). Mutations in the RP2 gene cause disease in 10% of families with familial X-linked retinitis pigmentosa assessed in this study. Am J Hum Genet 64(4): 1210-1215.

Hartong DT, Berson EL and Dryja TP (2006). Retinitis pigmentosa. Lancet 368(9549): 1795-1809.

He C and Klionsky DJ (2009). Regulation Mechanisms and Signaling Pathways of Autophagy. Annu Rev Genet 43: 67-93.

He Y and Simons SS, Jr. (2007). STAMP, a novel predicted factor assisting TIF2 actions in glucocorticoid receptor-mediated induction and repression. Mol Cell Biol 27(4): 1467-1485.

Heather JM and Chain B (2016). The sequence of sequencers: The history of sequencing DNA. Genomics 107(1): 1-8.

Heaton MP, Harhay GP, Bennett GL, Stone RT, Grosse WM, Casas E, Keele JW, Smith TP, Chitko-McKown CG and Laegreid WW (2002). Selection and use of SNP markers for animal identification and paternity analysis in U.S. beef cattle. Mamm Genome 13(5): 272-281.

Hebenbrock K, Williams PM and Karger BL (1995). Single strand conformational polymorphism using capillary electrophoresis with two-dye laser-induced fluorescence detection. Electrophoresis 16(8): 1429-1436.

Hebsgaard SM, Korning PG, Tolstrup N, Engelbrecht J, Rouze P and Brunak S (1996). Splice site prediction in Arabidopsis thaliana pre-mRNA by combining local and global sequence information. Nucleic Acids Res 24(17): 3439-3452.

Heckenlively JR (1982). Preserved para-arteriole retinal pigment epithelium (PPRPE) in retinitis pigmentosa. Br J Ophthalmol 66(1): 26-30.

Hedstrom L (1999). IMP dehydrogenase: mechanism of action and inhibition. Curr Med Chem 6(7): 545-560.

Helou J, Otto EA, Attanasio M, Allen SJ, Parisi MA, Glass I, Utsch B, Hashmi S, Fazzi E, Omran H, O'Toole JF, Sayer JA and Hildebrandt F (2007). Mutation analysis of NPHP6/CEP290 in patients with Joubert syndrome and Senior-Loken syndrome. J Med Genet 44(10): 657-663.

Henderson RH, Mackay DS, Li Z, Moradi P, Sergouniotis P, Russell-Eggitt I, Thompson DA, Robson AG, Holder GE, Webster AR and Moore AT (2011). Phenotypic variability in patients with retinal dystrophies due to mutations in CRB1. Br J Ophthalmol 95(6): 811-817.

Hendrickson AE and Yuodelis C (1984). The morphological development of the human fovea. Ophthalmology 91(6): 603-612.

Henikoff S and Henikoff JG (1992). Amino acid substitution matrices from protein blocks. Proc Natl Acad Sci U S A 89(22): 10915-10919.

Heon E, Westall C, Carmi R, Elbedour K, Panton C, Mackeen L, Stone EM and Sheffield VC (2005). Ocular phenotypes of three genetic variants of Bardet-Biedl syndrome. Am J Med Genet A 132a(3): 283-287.

Heon E, Kim G, Qin S, Garrison JE, Tavares E, Vincent A, Nuangchamnong N, Scott CA, Slusarski DC and Sheffield VC (2016). Mutations in C8ORF37 cause Bardet Biedl syndrome (BBS21). Hum Mol Genet.

Herrero-Martin G, Hoyer-Hansen M, Garcia-Garcia C, Fumarola C, Farkas T, Lopez-Rivas A and Jaattela M (2009). TAK1 activates AMPK-dependent cytoprotective autophagy in TRAIL-treated epithelial cells. EMBO J 28(6): 677-685.

Hide T, Hatakeyama J, Kimura-Yoshida C, Tian E, Takeda N, Ushio Y, Shiroishi T, Aizawa S and Matsuo I (2002). Genetic modifiers of otocephalic phenotypes in Otx2 heterozygous mutant mice. Development 129(18): 4347-4357.

Hidvegi T, Ewing M, Hale P, Dippold C, Beckett C, Kemp C, Maurice N, Mukherjee A, Goldbach C, Watkins S, Michalopoulos G and Perlmutter DH (2010). An autophagy-enhancing drug promotes degradation of mutant alpha1-antitrypsin Z and reduces hepatic fibrosis. Science 329(5988): 229-232.

Hjortshoj TD, Gronskov K, Brondum-Nielsen K and Rosenberg T (2009). A novel founder BBS1 mutation explains a unique high prevalence of Bardet-Biedl syndrome in the Faroe Islands. Br J Ophthalmol 93(3): 409-413.

Holley RW, Apgar J, Merrill SH and Zurkoff PL (1961). Nucleotide and oligonucleotide compositions of the alanine-, valine-, and tyrosine-acceptor "soluble" ribonucleic acids of yeast [3]. ACS Symp. Ser 83(23): 4861-4862.

Holopigian K, Greenstein V, Seiple W and Carr RE (1996). Rates of change differ among measures of visual function in patients with retinitis pigmentosa. Ophthalmology 103(3): 398-405.

Holzfeind PJ, Grewal PK, Reitsamer HA, Kechvar J, Lassmann H, Hoeger H, Hewitt JE and Bittner RE (2002). Skeletal, cardiac and tongue muscle pathology, defective retinal transmission, and neuronal migration defects in the Large(myd) mouse defines a natural model for glycosylation-deficient muscle - eye - brain disorders. Hum Mol Genet 11(21): 2673-2687.

Hong DH, Yue G, Adamian M and Li T (2001). Retinitis pigmentosa GTPase regulator (RPGRr)-interacting protein is stably associated with the photoreceptor ciliary axoneme and anchors RPGR to the connecting cilium. J Biol Chem 276(15): 12091-12099.

Hong DH, Pawlyk B, Sokolov M, Strissel KJ, Yang J, Tulloch B, Wright AF, Arshavsky VY and Li T (2003). RPGR isoforms in photoreceptor connecting cilia and the transitional zone of motile cilia. Invest Ophthalmol Vis Sci 44(6): 2413-2421.

Hosokawa N, Hara T, Kaizuka T, Kishi C, Takamura A, Miura Y, Iemura S, Natsume T, Takehana K, Yamada N, Guan JL, Oshiro N and Mizushima N (2009). Nutrient-dependent mTORC1 association with the ULK1-Atg13-FIP200 complex required for autophagy. Mol Biol Cell 20(7): 1981-1991.

Hsiau TH, Diaconu C, Myers CA, Lee J, Cepko CL and Corbo JC (2007). The cis-regulatory logic of the mammalian photoreceptor transcriptional network. PLoS One 2(7): e643.

Hsu PD, Lander ES and Zhang F (2014). Development and Applications of CRISPR-Cas9 for Genome Engineering. Cell 157(6): 1262-1278.

Hsu YT and Molday RS (1993). Modulation of the cGMP-gated channel of rod photoreceptor cells by calmodulin. Nature 361(6407): 76-79.

Huang L, Xiao X, Li S, Jia X, Wang P, Guo X and Zhang Q (2012). CRX variants in cone-rod dystrophy and mutation overview. Biochem Biophys Res Commun 426(4): 498-503.

Hull S, Arno G, Plagnol V, Chamney S, Russell-Eggitt I, Thompson D, Ramsden SC, Black GCM, Robson A, Holder GE, Moore AT and Webster AR (2014). The Phenotypic Variability of Retinal Dystrophies Associated With Mutations in CRX, With Report of a Novel Macular Dystrophy PhenotypeRetinal Dystrophies and Mutations in CRX. Invest Ophthalmol Vis Sci 55(10): 6934-6944.

Hull S, Holder GE, Robson AG, Mukherjee R, Michaelides M, Webster AR and Moore AT (2016). Preserved visual function in retinal dystrophy due to hypomorphic RPE65 mutations. Br J Ophthalmol.

Humphries MM, Rancourt D, Farrar GJ, Kenna P, Hazel M, Bush RA, Sieving PA, Sheils DM, McNally N, Creighton P, Erven A, Boros A, Gulya K, Capecchi MR and Humphries P (1997). Retinopathy induced in mice by targeted disruption of the rhodopsin gene. Nat Genet 15(2): 216-219.

Hunkapiller T, Kaiser RJ, Koop BF and Hood L (1991). Large-scale and automated DNA sequence determination. Science 254(5028): 59-67.

Hunt DM, Buch P and Michaelides M (2010). Guanylate cyclases and associated activator proteins in retinal disease. Mol Cell Biochem 334(1-2): 157-168.

Hussain R and Bittles AH (1998). The prevalence and demographic characteristics of consanguineous marriages in Pakistan. J Biosoc Sci 30(2): 261-275.

Hyman ED (1988). A new method of sequencing DNA. Anal. Biochem. 174(2): 423-436.

Iannaccone A, Breuer DK, Wang XF, Kuo SF, Normando EM, Filippova E, Baldi A, Hiriyanna S, MacDonald CB, Baldi F, Cosgrove D, Morton CC, Swaroop A and Jablonski MM (2003). Clinical and immunohistochemical evidence for an X linked retinitis pigmentosa syndrome with recurrent infections and hearing loss in association with an RPGR mutation. J Med Genet 40(11): e118.

Ibrahim MA, Sepah YJ, Watters A, Bittencourt M, Vigil EM, Do DV and Nguyen QD (2015). One-Year Outcomes of the SAVE Study: Sirolimus as a Therapeutic Approach for UVEitis. Transl Vis Sci Technol 4(2): 4.

Idelson M, Alper R, Obolensky A, Ben-Shushan E, Hemo I, Yachimovich-Cohen N, Khaner H, Smith Y, Wiser O, Gropp M, Cohen MA, Even-Ram S, Berman-Zaken Y, Matzrafi L, Rechavi G, Banin E and Reubinoff B (2009). Directed Differentiation of Human Embryonic Stem Cells into Functional Retinal Pigment Epithelium Cells. Cell Stem Cell 5(4): 396-408.

Illing M, Molday LL and Molday RS (1997). The 220-kDa rim protein of retinal rod outer segments is a member of the ABC transporter superfamily. J Biol Chem 272(15): 10303-10310.

Inamori K, Yoshida-Moriguchi T, Hara Y, Anderson ME, Yu L and Campbell KP (2012). Dystroglycan function requires xylosyl- and glucuronyltransferase activities of LARGE. Science 335(6064): 93-96.

Itakura E, Kishi C, Inoue K and Mizushima N (2008). Beclin 1 forms two distinct phosphatidylinositol 3-kinase complexes with mammalian Atg14 and UVRAG. Mol Biol Cell 19(12): 5360-5372.

Ito S, Nakamura M, Nuno Y, Ohnishi Y, Nishida T and Miyake Y (2004a). Novel complex GUCY2D mutation in Japanese family with cone-rod dystrophy. Invest Ophthalmol Vis Sci 45(5): 1480-1485.

Ito S, Nakamura M, Ohnishi Y and Miyake Y (2004b). Autosomal dominant cone-rod dystrophy with R838H and R838C mutations in the GUCY2D gene in Japanese patients. Jpn J Ophthalmol 48(3): 228-235.

Izaddoost S, Nam S-C, Bhat MA, Bellen HJ and Choi K-W (2002). Drosophila Crumbs is a positional cue in photoreceptor adherens junctions and rhabdomeres. Nature 416(6877): 178-183.

Jaber L, Halpern GJ and Shohat M (1998). The impact of consanguinity worldwide. Community Genet 1(1): 12-17.

Jackman SL, Babai N, Chambers JJ, Thoreson WB and Kramer RH (2011). A positive feedback synapse from retinal horizontal cells to cone photoreceptors. PLoS Biol 9(5): e1001057.

Jackson H, Garway-Heath D, Rosen P, Bird AC and Tuft SJ (2001). Outcome of cataract surgery in patients with retinitis pigmentosa. Br J Ophthalmol 85(8): 936-938.

Jacobson SG, Cideciyan AV, Aleman TS, Pianta MJ, Sumaroka A, Schwartz SB, Smilko EE, Milam AH, Sheffield VC and Stone EM (2003). Crumbs homolog 1 (CRB1) mutations result in a thick human retina with abnormal lamination. Hum Mol Genet 12(9): 1073-1078.

Jacobson SG, Cideciyan AV, Aleman TS, Sumaroka A, Roman AJ, Gardner LM, Prosser HM, Mishra M, Bech-Hansen NT, Herrera W, Schwartz SB, Liu XZ, Kimberling WJ, Steel KP and Williams DS (2008a). Usher syndromes due to MYO7A, PCDH15, USH2A or GPR98 mutations share retinal disease mechanism. Hum Mol Genet 17(15): 2405-2415.

Jacobson SG, Cideciyan AV, Aleman TS, Sumaroka A, Windsor EAM, Schwartz SB, Heon E and Stone EM (2008b). Photoreceptor Layer Topography in Children with Leber Congenital Amaurosis Caused by RPE65 Mutations. Invest Ophthalmol Vis Sci 49(10): 4573-4577.

Jacobson SG, Aleman TS, Cideciyan AV, Roman AJ, Sumaroka A, Windsor EAM, Schwartz SB, Heon E and Stone EM (2009). Defining the Residual Vision in Leber Congenital Amaurosis Caused by RPE65 Mutations. Invest Ophthalmol Vis Sci 50(5): 2368-2375.

Janecke AR, Thompson DA, Utermann G, Becker C, Hubner CA, Schmid E, McHenry CL, Nair AR, Ruschendorf F, Heckenlively J, Wissinger B, Nurnberg P and Gal A (2004). Mutations in RDH12 encoding a photoreceptor cell retinol dehydrogenase cause childhood-onset severe retinal dystrophy. Nat Genet 36(8): 850-854.

Janke C, Rogowski K, Wloga D, Regnard C, Kajava AV, Strub JM, Temurak N, van Dijk J, Boucher D, van Dorsselaer A, Suryavanshi S, Gaertig J and Edde B (2005). Tubulin polyglutamylase enzymes are members of the TTL domain protein family. Science 308(5729): 1758-1762.

Janke C, Rogowski K and van Dijk J (2008). Polyglutamylation: a fine-regulator of protein function? 'Protein Modifications: beyond the usual suspects' review series. EMBO Rep 9(7): 636-641.

Jauhari S and Rizvi SAM (2015). An Indian eye to personalized medicine. Compu Biol Med 59: 211-220.

Jayasundera T, Branham KE, Othman M, Rhoades WR, Karoukis AJ, Khanna H, Swaroop A and Heckenlively JR (2010). RP2 phenotype and pathogenetic correlations in X-linked retinitis pigmentosa. Arch Ophthalmol 128(7): 915-923.

Jiang F, Xu K, Zhang X, Xie Y, Bai F and Li Y (2015). GUCY2D mutations in a Chinese cohort with autosomal dominant cone or cone-rod dystrophies. Doc Ophthalmol 131(2): 105-114.

Jin M, Li S, Nusinowitz S, Lloyd M, Hu J, Radu RA, Bok D and Travis GH (2009). The role of interphotoreceptor retinoid-binding protein on the translocation of visual retinoids and function of cone photoreceptors. J Neurosci 29(5): 1486-1495.

Jinda W, Taylor TD, Suzuki Y, Thongnoppakhun W, Limwongse C, Lertrit P, Suriyaphol P, Trinavarat A and Atchaneeyasakul LO (2014). Whole exome sequencing in Thai patients with retinitis pigmentosa reveals novel mutations in six genes. Invest Ophthalmol Vis Sci 55(4): 2259-2268.

John SK, Smith JE, Aguirre GD and Milam AH (2000). Loss of cone molecular markers in rhodopsin-mutant human retinas with retinitis pigmentosa. Mol Vis 6: 204-215.

Kabeya Y, Mizushima N, Ueno T, Yamamoto A, Kirisako T, Noda T, Kominami E, Ohsumi Y and Yoshimori T (2000). LC3, a mammalian homologue of yeast Apg8p, is localized in autophagosome membranes after processing. EMBO J 19(21): 5720-5728.

Kajiwara K, Hahn LB, Mukai S, Travis GH, Berson EL and Dryja TP (1991). Mutations in the human retinal degeneration slow gene in autosomal dominant retinitis pigmentosa. Nature 354(6353): 480-483.

Kajiwara K, Berson EL and Dryja TP (1994). Digenic retinitis pigmentosa due to mutations at the unlinked peripherin/RDS and ROM1 loci. Science 264(5165): 1604-1608.

Kamada Y, Yoshino K, Kondo C, Kawamata T, Oshiro N, Yonezawa K and Ohsumi Y (2010). Tor directly controls the Atg1 kinase complex to regulate autophagy. Mol Cell Biol 30(4): 1049-1058.

Kanagawa M, Saito F, Kunz S, Yoshida-Moriguchi T, Barresi R, Kobayashi YM, Muschler J, Dumanski JP, Michele DE, Oldstone MB and Campbell KP (2004). Molecular recognition by LARGE is essential for expression of functional dystroglycan. Cell 117(7): 953-964.

Kanan Y, Kasus-Jacobi A, Moiseyev G, Sawyer K, Ma JX and Al-Ubaidi MR (2008). Retinoid processing in cone and müller cell lines. Exp Eye Res 86(2): 344-354.

Kannabiran C, Palavalli L and Jalali S (2012). Mutation of SPATA7 in a family with autosomal recessive early-onset retinitis pigmentosa. J Mol Genet Med 6: 301-303.

Kantardzhieva A, Gosens I, Alexeeva S, Punte IM, Versteeg I, Krieger E, Neefjes-Mol CA, den Hollander AI, Letteboer SJ, Klooster J, Cremers FP, Roepman R and Wijnholds J (2005). MPP5 recruits MPP4 to the CRB1 complex in photoreceptors. Invest Ophthalmol Vis Sci 46(6): 2192-2201.

Karan S, Zhang H, Li S, Frederick JM and Baehr W (2008). A model for transport of membrane-associated phototransduction polypeptides in rod and cone photoreceptor inner segments. Vision Research 48(3): 442-452.

Katagiri S, Akahori M, Sergeev Y, Yoshitake K, Ikeo K, Furuno M, Hayashi T, Kondo M, Ueno S, Tsunoda K, Shinoda K, Kuniyoshi K, Tsurusaki Y, Matsumoto N, Tsuneoka H and Iwata T (2014). Whole exome analysis identifies frequent CNGA1 mutations in Japanese population with autosomal recessive retinitis pigmentosa. PLoS One 9(9): e108721.

Katagiri S, Hayashi T, Yoshitake K, Akahori M, Ikeo K, Gekka T, Tsuneoka H and Iwata T (2016). Novel C8orf37 Mutations in Patients with Early-onset Retinal Dystrophy, Macular Atrophy, Cataracts, and High Myopia. Ophthalmic Genet 37(1): 68-75.

Katsanis N, Ansley SJ, Badano JL, Eichers ER, Lewis RA, Hoskins BE, Scambler PJ, Davidson WS, Beales PL and Lupski JR (2001). Triallelic inheritance in Bardet-Biedl syndrome, a Mendelian recessive disorder. Science 293(5538): 2256-2259.

Kaylor JJ, Cook JD, Makshanoff J, Bischoff N, Yong J and Travis GH (2014). Identification of the 11-cis-specific retinyl-ester synthase in retinal Müller cells as multifunctional O-acyltransferase (MFAT). Proc. Natl. Acad. Sci. U.S.A. 111(20): 7302-7307.

Keats BJB and Corey DP (1999). The Usher syndromes. Am. J. Med. Genet. 89(3): 158-166.

Kelsell RE, Gregory-Evans K, Payne AM, Perrault I, Kaplan J, Yang RB, Garbers DL, Bird AC, Moore AT and Hunt DM (1998). Mutations in the retinal guanylate cyclase (RETGC-1) gene in dominant cone-rod dystrophy. Hum Mol Genet 7(7): 1179-1184.

Kevany BM and Palczewski K (2010). Phagocytosis of retinal rod and cone photoreceptors. Physiology 25(1): 8-15.

Khan AO, Decker E, Bachmann N, Bolz HJ and Bergmann C (2016a). C8orf37 is mutated in Bardet-Biedl syndrome and constitutes a locus allelic to non-syndromic retinal dystrophies. Ophthalmic Genet: 1-4.

Khan MI, Collin RWJ, Arimadyo K, Micheal S, Azam M, Qureshi N, Faradz SMH, den Hollander AI, Qamar R and Cremers FPM (2010). Missense mutations at homologous positions in the fourth and fifth laminin A G-like domains of eyes shut homolog cause autosomal recessive retinitis pigmentosa. Mol Vis 16: 2753-2759.

Khan MT and Joseph SK (2010). Role of inositol trisphosphate receptors in autophagy in DT40 cells. J Biol Chem 285(22): 16912-16920.

Khan SA, Muhammad N, Khan MA, Kamal A, Rehman ZU and Khan S (2016b). Genetics of human Bardet-Biedl syndrome, an updates. Clin Genet 90(1): 3-15.

Khanna H, Hurd TW, Lillo C, Shu X, Parapuram SK, He S, Akimoto M, Wright AF, Margolis B, Williams DS and Swaroop A (2005). RPGR-ORF15, which is mutated in retinitis pigmentosa, associates with SMC1, SMC3, and microtubule transport proteins. J Biol Chem 280(39): 33580-33587.

Khateb S, Zelinger L, Mizrahi-Meissonnier L, Ayuso C, Koenekoop RK, Laxer U, Gross M, Banin E and Sharon D (2014). A homozygous nonsense CEP250 mutation combined with a heterozygous nonsense C2orf71 mutation is associated with atypical Usher syndrome. Journal of Medical Genetics 51(7): 460-469.

Kibbe WA (2007). OligoCalc: an online oligonucleotide properties calculator. Nucleic Acids Res 35(Web Server issue): W43-46.

Kida E, Golabek AA and Wisniewski KE (2001). 2 Cellular pathology and pathogenic aspects of neuronal ceroid lipofuscinoses. Adv Genet. **45:** 35-68.

Kim AJ, Woodworth GF, Boylan NJ, Suk JS and Hanes J (2014). Highly compacted pH-responsive DNA nanoparticles mediate transgene silencing in experimental glioma. J. Mater. Chem. B 2(46): 8165-8173.

Kim SK, Shindo A, Park TJ, Oh EC, Ghosh S, Gray RS, Lewis RA, Johnson CA, Attie-Bittach T, Katsanis N and Wallingford JB (2010). Planar cell polarity acts through septins to control collective cell movement and ciliogenesis. Science 329(5997): 1337-1340.

Kimberling WJ, Hildebrand MS, Shearer AE, Jensen ML, Halder JA, Trzupek K, Cohn ES, Weleber RG, Stone EM and Smith RJH (2010). Frequency of Usher syndrome in two pediatric populations: Implications for genetic screening of deaf and hard of hearing children. Genet Med 12(8): 512-516.

Kircher M, Witten DM, Jain P, O'Roak BJ, Cooper GM and Shendure J (2014). A general framework for estimating the relative pathogenicity of human genetic variants. Nat Genet 46(3): 310-315.

Kitiratschky VB, Wilke R, Renner AB, Kellner U, Vadala M, Birch DG, Wissinger B, Zrenner E and Kohl S (2008). Mutation analysis identifies GUCY2D as the major gene responsible for autosomal dominant progressive cone degeneration. Invest Ophthalmol Vis Sci 49(11): 5015-5023.

Klein RJ, Zeiss C, Chew EY, Tsai JY, Sackler RS, Haynes C, Henning AK, SanGiovanni JP, Mane SM, Mayne ST, Bracken MB, Ferris FL, Ott J, Barnstable C and Hoh J (2005). Complement factor H polymorphism in age-related macular degeneration. Science 308(5720): 385-389.

Kleuss C, Raw AS, Lee E, Sprang SR and Gilman AG (1994). Mechanism of GTP hydrolysis by G-protein alpha subunits. Proc Natl Acad Sci U S A 91(21): 9828-9831.

Klevering BJ, Yzer S, Rohrschneider K, Zonneveld M, Allikmets R, van den Born LI, Maugeri A, Hoyng CB and Cremers FP (2004). Microarray-based mutation analysis of the ABCA4 (ABCR) gene in autosomal recessive cone-rod dystrophy and retinitis pigmentosa. Eur J Hum Genet 12(12): 1024-1032.

Klionsky DJ, Abeliovich H, Agostinis P, Agrawal DK, Aliev G, Askew DS, Baba M, Baehrecke EH, Bahr BA, Ballabio A, Bamber BA, Bassham DC, Bergamini E, Bi X, Biard-Piechaczyk M, Blum JS, Bredesen DE, Brodsky JL, Brumell JH, Brunk UT, Bursch W, Camougrand N, Cebollero E, Cecconi F, Chen Y, Chin LS, Choi A, Chu CT, Chung J, Clarke PG, Clark RS, Clarke SG, Clave C, Cleveland JL, Codogno P, Colombo MI, Coto-Montes A, Cregg JM, Cuervo AM, Debnath J, Demarchi F, Dennis PB, Dennis PA, Deretic V, Devenish RJ, Di Sano F, Dice JF, Difiglia M, Dinesh-Kumar S, Distelhorst CW, Djavaheri-Mergny M, Dorsey FC, Droge W, Dron M, Dunn WA, Jr., Duszenko M, Eissa NT, Elazar Z, Esclatine A, Eskelinen EL, Fesus L, Finley KD, Fuentes JM, Fueyo J, Fujisaki K, Galliot B, Gao FB, Gewirtz DA, Gibson SB, Gohla A, Goldberg AL, Gonzalez R, Gonzalez-Estevez C, Gorski S, Gottlieb RA, Haussinger D, He YW, Heidenreich K, Hill JA, Hoyer-Hansen M, Hu X, Huang WP, Iwasaki A, Jaattela M, Jackson WT, Jiang X, Jin S, Johansen T, Jung JU, Kadowaki M, Kang C, Kelekar A, Kessel DH, Kiel JA, Kim HP, Kimchi A, Kinsella TJ, Kiselyov K, Kitamoto K, Knecht E, Komatsu M, Kominami E, Kondo S, Kovacs AL, Kroemer G, Kuan CY, Kumar R, Kundu M, Landry J, Laporte M, Le W, Lei HY, Lenardo MJ, Levine B, Lieberman A, Lim KL, Lin FC, Liou W, Liu LF, Lopez-Berestein G, Lopez-Otin C, Lu B, Macleod KF, Malorni W, Martinet W, Matsuoka K, Mautner J, Meijer AJ, Melendez A, Michels P, Miotto G, Mistiaen WP, Mizushima N, Mograbi B, Monastyrska I, Moore MN, Moreira PI, Moriyasu Y, Motyl T, Munz C, Murphy LO, Naqvi NI, Neufeld TP, Nishino I, Nixon RA, Noda T, Nurnberg B, Ogawa M, Oleinick NL, Olsen LJ, Ozpolat B, Paglin S, Palmer GE, Papassideri I, Parkes M, Perlmutter DH, Perry G, Piacentini M, Pinkas-Kramarski R, Prescott M, Proikas-Cezanne T, Raben N, Rami A, Reggiori F, Rohrer B, Rubinsztein DC, Ryan KM,

Sadoshima J, Sakagami H, Sakai Y, Sandri M, Sasakawa C, Sass M, Schneider C, Seglen PO, Seleverstov O, Settleman J, Shacka JJ, Shapiro IM, Sibirny A, Silva-Zacarin EC, Simon HU, Simone C, Simonsen A, Smith MA, Spanel-Borowski K, Srinivas V, Steeves M, Stenmark H, Stromhaug PE, Subauste CS, Sugimoto S, Sulzer D, Suzuki T, Swanson MS, Tabas I, Takeshita F, Talbot NJ, Talloczy Z, Tanaka K, Tanaka K, Tanida I, Taylor GS, Taylor JP, Terman A, Tettamanti G, Thompson CB, Thumm M, Tolkovsky AM, Tooze SA, Truant R, Tumanovska LV, Uchiyama Y, Ueno T, Uzcategui NL, van der Klei I, Vaquero EC, Vellai T, Vogel MW, Wang HG, Webster P, Wiley JW, Xi Z, Xiao G, Yahalom J, Yang JM, Yap G, Yin XM, Yoshimori T, Yu L, Yue Z, Yuzaki M, Zabirnyk O, Zheng X, Zhu X and Deter RL (2008). Guidelines for the use and interpretation of assays for monitoring autophagy in higher eukaryotes. Autophagy 4(2): 151-175.

Kniazeva MF, Chiang MF, Cutting GR, Zack DJ, Han M and Zhang K (1999). Clinical and genetic studies of an autosomal dominant cone-rod dystrophy with features of Stargardt disease. Ophthalmic Genet 20(2): 71-81.

Koenekoop RK, Loyer M, Hand CK, Al Mahdi H, Dembinska O, Beneish R, Racine J and Rouleau GA (2003). Novel RPGR mutations with distinct retinitis pigmentosa phenotypes in French-Canadian families. Am J Ophthalmol 136(4): 678-687.

Koenekoop RK (2004). An overview of leber congenital amaurosis: A model to understand human retinal development. Surv Ophthalmol 49(4): 379-398.

Koenekoop RK, Lopez I, den Hollander AI, Allikmets R and Cremers FP (2007). Genetic testing for retinal dystrophies and dysfunctions: benefits, dilemmas and solutions. Clin Experiment Ophthalmol 35(5): 473-485.

Kohl S, Marx T, Giddings I, Jägle H, Jacobson SG, Apfelstedt-Sylla E, Zrenner E, Sharpe LT and Wissinger B (1998). Total colourblindness is caused by mutations in the gene encoding the α-subunit of the cone photoreceptor cGMP-gated cation channel. Nat Genet 19(3): 257-259.

Kohl S, Baumann B, Broghammer M, Jagle H, Sieving P, Kellner U, Spegal R, Anastasi M, Zrenner E, Sharpe LT and Wissinger B (2000). Mutations in the CNGB3 gene encoding the beta-subunit of the cone photoreceptor cGMP-gated channel are responsible for achromatopsia (ACHM3) linked to chromosome 8q21. Hum Mol Genet 9(14): 2107-2116.

Kohl S, Baumann B, Rosenberg T, Kellner U, Lorenz B, Vadalà M, Jacobson SG and Wissinger B (2002). Mutations in the cone photoreceptor G-protein α-subunit gene GNAT2 in patients with achromatopsia. Am J Hum Genet 71(2): 422-425.

Kohl S, Varsanyi B, Antunes GA, Baumann B, Hoyng CB, Jägle H, Rosenberg T, Kellner U, Lorenz B, Salati R, Jurklies B, Farkas A, Andreasson S, Weleber RG, Jacobson SG, Rudolph G, Castellan C, Dollfus H, Legius E, Anastasi M, Bitoun P, Lev D, Sieving PA, Munier FL, Zrenner E, Sharpe LT, Cremers FPM and Wissinger B (2005). CNGB3

mutations account for 50% of all cases with autosomal recessive achromatopsia. Eur. J. Hum. Genet 13(3): 302-308.

Kohl S, Coppieters F, Meire F, Schaich S, Roosing S, Brennenstuhl C, Bolz S, van Genderen Maria M, Riemslag Frans CC, Lukowski R, den Hollander Anneke I, Cremers Frans PM, De Baere E, Hoyng Carel B and Wissinger B (2012). A Nonsense Mutation in PDE6H Causes Autosomal-Recessive Incomplete Achromatopsia. Am. J. Hum. Genet 91(3): 527-532.

Kohl S, Zobor D, Chiang WC, Weisschuh N, Staller J, Gonzalez Menendez I, Chang S, Beck SC, Garcia Garrido M, Sothilingam V, Seeliger MW, Stanzial F, Benedicenti F, Inzana F, Heon E, Vincent A, Beis J, Strom TM, Rudolph G, Roosing S, Hollander AI, Cremers FP, Lopez I, Ren H, Moore AT, Webster AR, Michaelides M, Koenekoop RK, Zrenner E, Kaufman RJ, Tsang SH, Wissinger B and Lin JH (2015). Mutations in the unfolded protein response regulator ATF6 cause the cone dysfunction disorder achromatopsia. Nat Genet 47(7): 757-765.

Kohl S, Jagle H and Wissinger B (2016). Achromatopsia. GeneReviews(R). R A Pagon, M P Adam, H H Ardinger et al. Seattle (WA), University of Washington, Seattle

University of Washington, Seattle. All rights reserved.

Koirala A, Conley SM, Makkia R, Liu Z, Cooper MJ, Sparrow JR and Naash MI (2013). Persistence of non-viral vector mediated RPE65 expression: case for viability as a gene transfer therapy for RPE-based diseases. J Control Release 172(3): 745-752.

Kong J, Kim SR, Binley K, Pata I, Doi K, Mannik J, Zernant-Rajang J, Kan O, Iqball S, Naylor S, Sparrow JR, Gouras P and Allikmets R (2008). Correction of the disease phenotype in the mouse model of Stargardt disease by lentiviral gene therapy. Gene Ther 15(19): 1311-1320.

Kousi M, Siintola E, Dvorakova L, Vlaskova H, Turnbull J, Topcu M, Yuksel D, Gokben S, Minassian BA, Elleder M, Mole SE and Lehesjoki AE (2009). Mutations in CLN7/MFSD8 are a common cause of variant late-infantile neuronal ceroid lipofuscinosis. Brain 132(Pt 3): 810-819.

Koyanagi M and Terakita A (2014). Diversity of animal opsin-based pigments and their optogenetic potential. Bba-Bioenergetics 1837(5): 710-716.

Kraft C, Kijanska M, Kalie E, Siergiejuk E, Lee SS, Semplicio G, Stoffel I, Brezovich A, Verma M, Hansmann I, Ammerer G, Hofmann K, Tooze S and Peter M (2012). Binding of the Atg1/ULK1 kinase to the ubiquitin-like protein Atg8 regulates autophagy. EMBO J 31(18): 3691-3703.

Kroemer G and Jaattela M (2005). Lysosomes and autophagy in cell death control. Nat Rev Cancer 5(11): 886-897.

Ku CA and Pennesi ME (2015). Retinal Gene Therapy: Current Progress and Future Prospects. Expert Rev Ophthalmol 10(3): 281-299.

Kuniyoshi K, Sakuramoto H, Yoshitake K, Abe K, Ikeo K, Furuno M, Tsunoda K, Kusaka S, Shimomura Y and Iwata T (2014). Longitudinal clinical course of three Japanese patients with Leber congenital amaurosis/early-onset retinal dystrophy with RDH12 mutation. Doc Ophthalmol 128(3): 219-228.

Kunz JB, Schwarz H and Mayer A (2004). Determination of four sequential stages during microautophagy in vitro. J Biol Chem 279(11): 9987-9996.

Kurth I, Thompson DA, Ruther K, Feathers KL, Chrispell JD, Schroth J, McHenry CL, Schweizer M, Skosyrski S, Gal A and Hubner CA (2007). Targeted disruption of the murine retinal dehydrogenase gene Rdh12 does not limit visual cycle function. Mol Cell Biol 27(4): 1370-1379.

Lamb TD and Pugh JEN (2006). Phototransduction, Dark Adaptation, and Rhodopsin Regeneration The Proctor Lecture. Invest Ophthalmol Vis Sci 47(12): 5138-5152.

Lander ES and Botstein D (1987). Homozygosity mapping: a way to map human recessive traits with the DNA of inbred children. Science 236(4808): 1567-1570.

Lander ES, Linton LM, Birren B, Nusbaum C, Zody MC, Baldwin J, Devon K, Dewar K, Doyle M, FitzHugh W, Funke R, Gage D, Harris K, Heaford A, Howland J, Kann L, Lehoczky J, LeVine R, McEwan P, McKernan K, Meldrim J, Mesirov JP, Miranda C, Morris W, Naylor J, Raymond C, Rosetti M, Santos R, Sheridan A, Sougnez C, Stange-Thomann Y, Stojanovic N, Subramanian A, Wyman D, Rogers J, Sulston J, Ainscough R, Beck S, Bentley D, Burton J, Clee C, Carter N, Coulson A, Deadman R, Deloukas P, Dunham A, Dunham I, Durbin R, French L, Grafham D, Gregory S, Hubbard T, Humphray S, Hunt A, Jones M, Lloyd C, McMurray A, Matthews L, Mercer S, Milne S, Mullikin JC, Mungall A, Plumb R, Ross M, Shownkeen R, Sims S, Waterston RH, Wilson RK, Hillier LW, McPherson JD, Marra MA, Mardis ER, Fulton LA, Chinwalla AT, Pepin KH, Gish WR, Chissoe SL, Wendl MC, Delehaunty KD, Miner TL, Delehaunty A, Kramer JB, Cook LL, Fulton RS, Johnson DL, Minx PJ, Clifton SW, Hawkins T, Branscomb E, Predki P, Richardson P, Wenning S, Slezak T, Doggett N, Cheng JF, Olsen A, Lucas S, Elkin C, Uberbacher E, Frazier M, Gibbs RA, Muzny DM, Scherer SE, Bouck JB, Sodergren EJ, Worley KC, Rives CM, Gorrell JH, Metzker ML, Naylor SL, Kucherlapati RS, Nelson DL, Weinstock GM, Sakaki Y, Fujiyama A, Hattori M, Yada T, Toyoda A, Itoh T, Kawagoe C, Watanabe H, Totoki Y, Taylor T, Weissenbach J, Heilig R, Saurin W, Artiguenave F, Brottier P, Bruls T, Pelletier E, Robert C, Wincker P, Smith DR, Doucette-Stamm L, Rubenfield M, Weinstock K, Lee HM, Dubois J, Rosenthal A, Platzer M, Nyakatura G, Taudien S, Rump A, Yang H, Yu J, Wang J, Huang G, Gu J, Hood L, Rowen L, Madan A, Qin S, Davis RW, Federspiel NA, Abola AP, Proctor MJ, Myers RM, Schmutz J, Dickson

M, Grimwood J, Cox DR, Olson MV, Kaul R, Raymond C, Shimizu N, Kawasaki K, Minoshima S, Evans GA, Athanasiou M, Schultz R, Roe BA, Chen F, Pan H, Ramser J, Lehrach H, Reinhardt R, McCombie WR, de la Bastide M, Dedhia N, Blocker H, Hornischer K, Nordsiek G, Agarwala R, Aravind L, Bailey JA, Bateman A, Batzoglou S, Birney E, Bork P, Brown DG, Burge CB, Cerutti L, Chen HC, Church D, Clamp M, Copley RR, Doerks T, Eddy SR, Eichler EE, Furey TS, Galagan J, Gilbert JG, Harmon C, Hayashizaki Y, Haussler D, Hermjakob H, Hokamp K, Jang W, Johnson LS, Jones TA, Kasif S, Kaspryzk A, Kennedy S, Kent WJ, Kitts P, Koonin EV, Korf I, Kulp D, Lancet D, Lowe TM, McLysaght A, Mikkelsen T, Moran JV, Mulder N, Pollara VJ, Ponting CP, Schuler G, Schultz J, Slater G, Smit AF, Stupka E, Szustakowki J, Thierry-Mieg D, Thierry-Mieg J, Wagner L, Wallis J, Wheeler R, Williams A, Wolf YI, Wolfe KH, Yang SP, Yeh RF, Collins F, Guyer MS, Peterson J, Felsenfeld A, Wetterstrand KA, Patrinos A, Morgan MJ, de Jong P, Catanese JJ, Osoegawa K, Shizuya H, Choi S, Chen YJ and Szustakowki J (2001). Initial sequencing and analysis of the human genome. Nature 409(6822): 860-921.

Langmead B and Salzberg SL (2012). Fast gapped-read alignment with Bowtie 2. Nat Methods 9(4): 357-359.

LaVail MM (1976). Rod outer segment disk shedding in rat retina: relationship to cyclic lighting. Science 194(4269): 1071-1074.

LaVail MM, Yasumura D, Matthes MT, Yang H, Hauswirth WW, Deng WT and Vollrath D (2016). Gene Therapy for MERTK-Associated Retinal Degenerations. Adv Exp Med Biol 854: 487-493.

Lazar CH, Mutsuddi M, Kimchi A, Zelinger L, Mizrahi-Meissonnier L, Marks-Ohana D, Boleda A, Ratnapriya R, Sharon D, Swaroop A and Banin E (2015). Whole exome sequencing reveals GUCY2D as a major gene associated with cone and cone-rod dystrophy in Israel. Invest Ophthalmol Vis Sci 56(1): 420-430.

Le Meur G, Stieger K, Smith AJ, Weber M, Deschamps JY, Nivard D, Mendes-Madeira A, Provost N, Pereon Y, Cherel Y, Ali RR, Hamel C, Moullier P and Rolling F (2007). Restoration of vision in RPE65-deficient Briard dogs using an AAV serotype 4 vector that specifically targets the retinal pigmented epithelium. Gene Ther 14(4): 292-303.

Le Quesne Stabej P, Saihan Z, Rangesh N, Steele-Stallard HB, Ambrose J, Coffey A, Emmerson J, Haralambous E, Hughes Y, Steel KP, Luxon LM, Webster AR and Bitner-Glindzicz M (2012). Comprehensive sequence analysis of nine Usher syndrome genes in the UK National Collaborative Usher Study. J Med Genet 49(1): 27-36.

Leber T (1869). Ueber Retinitis pigmentosa und angeborene Amaurose. Archiv für Ophthalmologie 15(3): 1-25.

Lee G-S, He Y, Dougherty EJ, Jimenez-Movilla M, Avella M, Grullon S, Sharlin DS, Guo C, Blackford JA, Awasthi S, Zhang Z, Armstrong SP, London EC, Chen W, Dean J and Simons SS (2013). Disruption of Ttll5/Stamp Gene (Tubulin Tyrosine Ligase-like Protein 5/SRC-1 and TIF2-associated Modulatory Protein Gene) in Male Mice Causes Sperm Malformation and Infertility. J Biol Chem 288(21): 15167-15180.

Lee H, Gurtowski J, Yoo S, Nattestad M, Marcus S, Goodwin S, McCombie WR and Schatz M (2016). Third-generation sequencing and the future of genomics. bioRxiv.

Leitch CC, Zaghloul NA, Davis EE, Stoetzel C, Diaz-Font A, Rix S, Alfadhel M, Lewis RA, Eyaid W, Banin E, Dollfus H, Beales PL, Badano JL and Katsanis N (2008). Hypomorphic mutations in syndromic encephalocele genes are associated with Bardet-Biedl syndrome. Nat Genet 40(4): 443-448.

Lenassi E, Vincent A, Li Z, Saihan Z, Coffey AJ, Steele-Stallard HB, Moore AT, Steel KP, Luxon LM, Heon E, Bitner-Glindzicz M and Webster AR (2015). A detailed clinical and molecular survey of subjects with nonsyndromic USH2A retinopathy reveals an allelic hierarchy of disease-causing variants. Eur J Hum Genet 23(10): 1318-1327.

Lentz J and Keats B (1993a). Usher Syndrome Type II. GeneReviews(R). R A Pagon, M P Adam, H H Ardinger et al. Seattle (WA), University of Washington, Seattle

University of Washington, Seattle. All rights reserved.

Lentz J and Keats BJB (1993b). Usher Syndrome Type I. GeneReviews(R). R A Pagon, M P Adam, H H Ardinger et al. Seattle (WA), University of Washington, Seattle

University of Washington, Seattle. All rights reserved.

Levine B and Klionsky DJ (2004). Development by self-digestion: molecular mechanisms and biological functions of autophagy. Dev Cell 6(4): 463-477.

Lewin AS, Rossmiller B and Mao H (2014). Gene Augmentation for adRP Mutations in RHO. Cold Spring Harb Perspect Med 4(9): a017400.

Li H, Handsaker B, Wysoker A, Fennell T, Ruan J, Homer N, Marth G, Abecasis G and Durbin R (2009). The Sequence Alignment/Map format and SAMtools. Bioinformatics 25(16): 2078-2079.

Li JB, Gerdes JM, Haycraft CJ, Fan Y, Teslovich TM, May-Simera H, Li H, Blacque OE, Li L, Leitch CC, Lewis RA, Green JS, Parfrey PS, Leroux MR, Davidson WS, Beales PL, Guay-Woodford LM, Yoder BK, Stormo GD, Katsanis N and Dutcher SK (2004). Comparative genomics identifies a flagellar and basal body proteome that includes the BBS5 human disease gene. Cell 117(4): 541-552.

Li L, Xiao X, Li S, Jia X, Wang P, Guo X, Jiao X, Zhang Q and Hejtmancik JF (2011). Detection of variants in 15 genes in 87 unrelated Chinese patients with Leber congenital amaurosis. PLoS One 6(5): e19458.

Li T, Lewallen M, Chen S, Yu W, Zhang N and Xie T (2013). Multipotent stem cells isolated from the adult mouse retina are capable of producing functional photoreceptor cells. Cell Res 23(6): 788-802.

Li T (2015). Leber congenital amaurosis caused by mutations in RPGRIP1. Cold Spring Harb Perspect Med 5(4).

Li X, He L, Che KH, Funderburk SF, Pan L, Pan N, Zhang M, Yue Z and Zhao Y (2012). Imperfect interface of Beclin1 coiled-coil domain regulates homodimer and heterodimer formation with Atg14L and UVRAG. Nat Commun 3: 662.

Liang X, Dong F, Li H, Li H, Yang L and Sui R (2015). Novel CNGA3 mutations in Chinese patients with achromatopsia. Br J Ophthalmol 99(4): 571-576.

Licata L, Briganti L, Peluso D, Perfetto L, Iannuccelli M, Galeota E, Sacco F, Palma A, Nardozza AP, Santonico E, Castagnoli L and Cesareni G (2012). MINT, the molecular interaction database: 2012 update. Nucleic Acids Res 40(Database issue): D857-861.

Liljegren MM, de Muinck EJ and Trosvik P (2016). Microsatellite Length Scoring by Single Molecule Real Time Sequencing - Effects of Sequence Structure and PCR Regime. PLoS One 11(7): e0159232.

Lin JB, Mast N, Bederman IR, Li Y, Brunengraber H, Bjorkhem I and Pikuleva IA (2016). Cholesterol in mouse retina originates primarily from in situ de novo biosynthesis. J Lipid Res 57(2): 258-264.

Linari M, Ueffing M, Manson F, Wright A, Meitinger T and Becker J (1999). The retinitis pigmentosa GTPase regulator, RPGR, interacts with the delta subunit of rod cyclic GMP phosphodiesterase. Proc Natl Acad Sci U S A 96(4): 1315-1320.

Linton KJ and Higgins CF (2007). Structure and function of ABC transporters: the ATP switch provides flexible control. Pflugers Arch 453(5): 555-567.

Liu J, Itagaki Y, Ben-Shabat S, Nakanishi K and Sparrow JR (2000). The biosynthesis of A2E, a fluorophore of aging retina, involves the formation of the precursor, A2-PE, in the photoreceptor outer segment membrane. J Biol Chem 275(38): 29354-29360.

Liu X, Seno K, Nishizawa Y, Hayashi F, Yamazaki A, Matsumoto H, Wakabayashi T and Usukura J (1994). Ultrastructural localization of retinal guanylate cyclase in human and monkey retinas. Exp Eye Res 59(6): 761-768.

Liu X, Bulgakov OV, Darrow KN, Pawlyk B, Adamian M, Liberman MC and Li T (2007). Usherin is required for maintenance of retinal photoreceptors and normal development of cochlear hair cells. Proc Natl Acad Sci U S A 104(11): 4413-4418.

Liu XZ, Hope C, Liang CY, Zou JM, Xu LR, Cole T, Mueller RF, Bundey S, Nance W, Steel KP and Brown SD (1999). A mutation (2314delG) in the Usher syndrome type IIA gene: high prevalence and phenotypic variation. Am J Hum Genet 64(4): 1221-1225.

Livesey FJ and Cepko CL (2001). Vertebrate neural cell-fate determination: lessons from the retina. Nat Rev Neurosci 2(2): 109-118.

Longman C, Brockington M, Torelli S, Jimenez-Mallebrera C, Kennedy C, Khalil N, Feng L, Saran RK, Voit T, Merlini L, Sewry CA, Brown SC and Muntoni F (2003). Mutations in the human LARGE gene cause MDC1D, a novel form of congenital muscular dystrophy with severe mental retardation and abnormal glycosylation of alpha-dystroglycan. Hum Mol Genet 12(21): 2853-2861.

Loose M, Malla S and Stout M (2016). Real-time selective sequencing using nanopore technology. Nat Methods 13(9): 751-754.

Lorenz B, Gyürüs P, Preising M, Bremser D, Gu S, Andrassi M, Gerth C and Gal A (2000). Early-Onset Severe Rod–Cone Dystrophy in Young Children with RPE65 Mutations. Invest Ophthalmol Vis Sci 41(9): 2735-2742.

Lorenz B, Wabbels B, Wegscheider E, Hamel CP, Drexler W and Preising MN (2004). Lack of fundus autofluorescence to 488 nanometers from childhood on in patients with early-onset severe retinal dystrophy associated with mutations in RPE65. Ophthalmology 111(8): 1585-1594.

Lorenz B and Preising MN (2005). Age matters--thoughts on a grading system for ABCA4 mutations. Graefes Arch Clin Exp Ophthalmol 243(2): 87-89.

Lotery AJ, Jacobson SG, Fishman GA, Weleber RG, Fulton AB, Namperumalsamy P, Heon E, Levin AV, Grover S, Rosenow JR, Kopp KK, Sheffield VC and Stone EM (2001). Mutations in the CRB1 gene cause Leber congenital amaurosis. Arch Ophthalmol 119(3): 415-420.

Lu X and Ferreira PA (2005). Identification of Novel Murine- and Human-Specific RPGRIP1 Splice Variants with Distinct Expression Profiles and Subcellular Localization. Invest Ophthalmol Vis Sci 46(6): 1882-1890.

Lu X, Guruju M, Oswald J and Ferreira PA (2005). Limited proteolysis differentially modulates the stability and subcellular localization of domains of RPGRIP1 that are distinctly affected by mutations in Leber's congenital amaurosis. Hum Mol Genet 14(10): 1327-1340.

Lu Y and Xu X (2012). [The latest advance of the relationship between autophagy and diabetic retinopathy]. Zhonghua Yan Ke Za Zhi 48(7): 649-652.

Luzio JP, Pryor PR and Bright NA (2007). Lysosomes: fusion and function. Nat Rev Mol Cell Biol 8(8): 622-632.

M'Hamdi O, Ouertani I, Maazoul F and Chaabouni-Bouhamed H (2011). Prevalence of Bardet-Biedl syndrome in Tunisia. J Community Genet 2(2): 97-99.

M'Hamdi O, Ouertani I and Chaabouni-Bouhamed H (2014). Update on the Genetics of Bardet-Biedl Syndrome. Mol Syndromol 5(2): 51-56.

Ma X, Guan L, Wu W, Zhang Y, Zheng W, Gao YT, Long J, Wu N, Wu L, Xiang Y, Xu B, Shen M, Chen Y, Wang Y, Yin Y, Li Y, Xu H, Xu X and Li Y (2015). Whole-exome sequencing identifies OR2W3 mutation as a cause of autosomal dominant retinitis pigmentosa. Sci Rep 5: 9236.

Macaulay IC and Voet T (2014). Single Cell Genomics: Advances and Future Perspectives. PLoS Genet 10(1): e1004126.

Mack HI, Zheng B, Asara JM and Thomas SM (2012). AMPK-dependent phosphorylation of ULK1 regulates ATG9 localization. Autophagy 8(8): 1197-1214.

Mackay DS, Dev Borman A, Moradi P, Henderson RH, Li Z, Wright GA, Waseem N, Gandra M, Thompson DA, Bhattacharya SS, Holder GE, Webster AR and Moore AT (2011a). RDH12 retinopathy: novel mutations and phenotypic description. Mol Vis 17: 2706-2716.

Mackay DS, Ocaka LA, Borman AD, Sergouniotis PI, Henderson RH, Moradi P, Robson AG, Thompson DA, Webster AR and Moore AT (2011b). Screening of SPATA7 in patients with Leber congenital amaurosis and severe childhood-onset retinal dystrophy reveals disease-causing mutations. Invest Ophthalmol Vis Sci 52(6): 3032-3038.

Maeda A, Maeda T, Imanishi Y, Sun W, Jastrzebska B, Hatala DA, Winkens HJ, Hofmann KP, Janssen JJ, Baehr W, Driessen CA and Palczewski K (2006). Retinol Dehydrogenase (RDH12) Protects Photoreceptors from Light-induced Degeneration in Mice(). J Biol Chem 281(49): 37697-37704.

Maerker T, van Wijk E, Overlack N, Kersten FF, McGee J, Goldmann T, Sehn E, Roepman R, Walsh EJ, Kremer H and Wolfrum U (2008). A novel Usher protein network at the periciliary reloading point between molecular transport machineries in vertebrate photoreceptor cells. Hum Mol Genet 17(1): 71-86.

Magierowski S, Huang Y, Wang C and Ghafar-Zadeh E (2016). Nanopore-CMOS Interfaces for DNA Sequencing. Biosensors (Basel) 6(3).

Maiuri MC, Tasdemir E, Criollo A, Morselli E, Vicencio JM, Carnuccio R and Kroemer G (2009). Control of autophagy by oncogenes and tumor suppressor genes. Cell Death Differ 16(1): 87-93.

Mali P, Yang L, Esvelt KM, Aach J, Guell M, DiCarlo JE, Norville JE and Church GM (2013). RNA-guided human genome engineering via Cas9. Science 339(6121): 823-826.

Mansergh FC, Millington-Ward S, Kennan A, Kiang AS, Humphries M, Farrar GJ, Humphries P and Kenna PF (1999). Retinitis pigmentosa and progressive sensorineural hearing loss caused by a C12258A mutation in the mitochondrial MTTS2 gene. Am J Hum Genet 64(4): 971-985.

Marigo V (2007). Programmed cell death in retinal degeneration: targeting apoptosis in photoreceptors as potential therapy for retinal degeneration. Cell Cycle 6(6): 652-655.

Marlhens F, Bareil C, Griffoin JM, Zrenner E, Amalric P, Eliaou C, Liu SY, Harris E, Redmond TM, Arnaud B, Claustres M and Hamel CP (1997). Mutations in RPE65 cause Leber's congenital amaurosis. Nat Genet 17(2): 139-141.

Marmor MF and Melles RB (2015). Hydroxychloroquine and the retina. Jama 313(8): 847-848.

Martinez-Mir A, Paloma E, Allikmets R, Ayuso C, del Rio T, Dean M, Vilageliu L, Gonzalez-Duarte R and Balcells S (1998). Retinitis pigmentosa caused by a homozygous mutation in the Stargardt disease gene ABCR. Nat Genet 18(1): 11-12.

Martinez-Morales JR, Dolez V, Rodrigo I, Zaccarini R, Leconte L, Bovolenta P and Saule S (2003). OTX2 activates the molecular network underlying retina pigment epithelium differentiation. J Biol Chem 278(24): 21721-21731.

Mase Y, Yokogawa M, Osawa M and Shimada I (2012). Backbone resonance assignments for G protein alpha(i3) subunit in the GTP-bound state. Biomol NMR Assign 6(2): 217-220.

Massey AC, Zhang C and Cuervo AM (2006). Chaperone-mediated autophagy in aging and disease. Curr Top Dev Biol 73: 205-235.

Matet A, Amar N, Mohand-Said S, Sahel JA and Barale PO (2016). Argus II retinal prosthesis implantation with scleral flap and autogenous temporalis fascia as alternative patch graft material: a 4-year follow-up. Clin Ophthalmol 10: 1565-1571.

Mathijssen IB, Florijn RJ, van den Born LI, Zekveld-Vroon RC, Ten Brink JB, Plomp AS, Baas F, Meijers-Heijboer H, Bergen AA and van Schooneveld MJ (2016). LONG-TERM FOLLOW-UP OF PATIENTS WITH RETINITIS PIGMENTOSA TYPE 12 CAUSED BY CRB1 MUTATIONS: A Severe Phenotype With Considerable Interindividual Variability. Retina.

Mathur P and Yang J (2015). Usher syndrome: Hearing loss, retinal degeneration and associated abnormalities. BBA-Mol Basis 1852(3): 406-420.

Matsui R, McGuigan Iii DB, Gruzensky ML, Aleman TS, Schwartz SB, Sumaroka A, Koenekoop RK, Cideciyan AV and Jacobson SG (2016). SPATA7: Evolving phenotype from cone-rod dystrophy to retinitis pigmentosa. Ophthalmic Genet 37(3): 333-338.

Matsuo I, Kuratani S, Kimura C, Takeda N and Aizawa S (1995). Mouse Otx2 functions in the formation and patterning of rostral head. Genes Dev 9(21): 2646-2658.

Maugeri A, Klevering BJ, Rohrschneider K, Blankenagel A, Brunner HG, Deutman AF, Hoyng CB and Cremers FP (2000). Mutations in the ABCA4 (ABCR) gene are the major cause of autosomal recessive cone-rod dystrophy. Am J Hum Genet 67(4): 960-966.

Mavlyutov TA, Zhao H and Ferreira PA (2002). Species-specific subcellular localization of RPGR and RPGRIP isoforms: implications for the phenotypic variability of congenital retinopathies among species. Hum Mol Genet 11(16): 1899-1907.

Maw MA, Corbeil D, Koch J, Hellwig A, Wilson-Wheeler JC, Bridges RJ, Kumaramanickavel G, John S, Nancarrow D, Roper K, Weigmann A, Huttner WB and Denton MJ (2000). A

frameshift mutation in prominin (mouse)-like 1 causes human retinal degeneration. Hum Mol Genet 9(1): 27-34.

Maxam AM and Gilbert W (1977). A new method for sequencing DNA. Proc Natl Acad Sci U S A 74(2): 560-564.

McBee JK, Palczewski K, Baehr W and Pepperberg DR (2001). Confronting Complexity: the Interlink of Phototransduction and Retinoid Metabolism in the Vertebrate Retina. Prog Retin Eye Res 20(4): 469-529.

McGee TL, Seyedahmadi BJ, Sweeney MO, Dryja TP and Berson EL (2010). Novel mutations in the long isoform of the USH2A gene in patients with Usher syndrome type II or non-syndromic retinitis pigmentosa. J Med Genet 47(7): 499-506.

McKenzie TL, Jiang G, Straubhaar JR, Conrad DG and Shechter I (1992). Molecular cloning, expression, and characterization of the cDNA for the rat hepatic squalene synthase. J Biol Chem 267(30): 21368-21374.

Mead B, Berry M, Logan A, Scott RAH, Leadbeater W and Scheven BA (2015). Stem cell treatment of degenerative eye disease. Stem Cell Research 14(3): 243-257.

Mehalow AK, Kameya S, Smith RS, Hawes NL, Denegre JM, Young JA, Bechtold L, Haider NB, Tepass U, Heckenlively JR, Chang B, Naggert JK and Nishina PM (2003). CRB1 is essential for external limiting membrane integrity and photoreceptor morphogenesis in the mammalian retina. Hum Mol Genet 12(17): 2179-2189.

Meilleur KG, Zukosky K, Medne L, Fequiere P, Powell-Hamilton N, Winder TL, Alsaman A, El-Hattab AW, Dastgir J, Hu Y, Donkervoort S, Golden JA, Eagle R, Finkel R, Scavina M, Hood IC, Rorke-Adams LB and Bonnemann CG (2014). Clinical, pathologic, and mutational spectrum of dystroglycanopathy caused by LARGE mutations. J Neuropathol Exp Neurol 73(5): 425-441.

Meindl A, Dry K, Herrmann K, Manson F, Ciccodicola A, Edgar A, Carvalho MR, Achatz H, Hellebrand H, Lennon A, Migliaccio C, Porter K, Zrenner E, Bird A, Jay M, Lorenz B, Wittwer B, D'Urso M, Meitinger T and Wright A (1996). A gene (RPGR) with homology to the RCC1 guanine nucleotide exchange factor is mutated in X-linked retinitis pigmentosa (RP3). Nat Genet 13(1): 35-42.

Mellen MA, de la Rosa EJ and Boya P (2008). The autophagic machinery is necessary for removal of cell corpses from the developing retinal neuroepithelium. Cell Death Differ 15(8): 1279-1290.

Mellough CB, Collin J, Sernagor E, Wride NK, Steel DHW and Lako M (2014). Lab generated retina: Realizing the dream. Vis. Neurosci 31(4-5): 317-332.

Menon ST, Han M and Sakmar TP (2001). Rhodopsin: structural basis of molecular physiology. Physiol Rev 81(4): 1659-1688.

Mercuri E, Messina S, Bruno C, Mora M, Pegoraro E, Comi GP, D'Amico A, Aiello C, Biancheri R, Berardinelli A, Boffi P, Cassandrini D, Laverda A, Moggio M, Morandi L, Moroni I, Pane M, Pezzani R, Pichiecchio A, Pini A, Minetti C, Mongini T, Mottarelli E, Ricci E, Ruggieri A, Saredi S, Scuderi C, Tessa A, Toscano A, Tortorella G, Trevisan CP, Uggetti C, Vasco G, Santorelli FM and Bertini E (2009). Congenital muscular dystrophies with defective glycosylation of dystroglycan: a population study. Neurology 72(21): 1802-1809.

Metcalfe KA, Dennis C-L, Poll A, Armel S, Demsky R, Carlsson L, Nanda S, Kiss A and Narod SA (2016). Effect of decision aid for breast cancer prevention on decisional conflict in women with a BRCA1 or BRCA2 mutation: a multisite, randomized, controlled trial. Genet Med.

Metrailler S, Schorderet DF and Cottet S (2012). Early apoptosis of rod photoreceptors in Rpe65(-/-) mice is associated with the upregulated expression of lysosomal-mediated autophagic genes. Exp Eye Res 96(1): 70-81.

Metzker ML (2010). Sequencing technologies [mdash] the next generation. Nat Rev Genet 11(1): 31-46.

Meynert AM, Ansari M, FitzPatrick DR and Taylor MS (2014). Variant detection sensitivity and biases in whole genome and exome sequencing. BMC Bioinformatics 15: 247.

Michaelides M, Johnson S, Poulson A, Bradshaw K, Bellmann C, Hunt DM and Moore AT (2003). An autosomal dominant bull's-eye macular dystrophy (MCDR2) that maps to the short arm of chromosome 4. Invest Ophthalmol Vis Sci 44(4): 1657-1662.

Michaelides M, Hunt DM and Moore AT (2004). The cone dysfunction syndromes. Br J Ophthalmol 88(2): 291-297.

Michaelides M, Hardcastle AJ, Hunt DM and Moore AT (2006). Progressive cone and cone-rod dystrophies: phenotypes and underlying molecular genetic basis. Surv Ophthalmol 51(3): 232-258.

Michaelides M, Gaillard MC, Escher P, Tiab L, Bedell M, Borruat FX, Barthelmes D, Carmona R, Zhang K, White E, McClements M, Robson AG, Holder GE, Bradshaw K, Hunt DM, Webster AR, Moore AT, Schorderet DF and Munier FL (2010). The PROM1 mutation p.R373C causes an autosomal dominant bull's eye maculopathy associated with rod, rod-cone, and macular dystrophy. Invest Ophthalmol Vis Sci 51(9): 4771-4780.

Michele DE, Barresi R, Kanagawa M, Saito F, Cohn RD, Satz JS, Dollar J, Nishino I, Kelley RI, Somer H, Straub V, Mathews KD, Moore SA and Campbell KP (2002). Post-translational disruption of dystroglycan-ligand interactions in congenital muscular dystrophies. Nature 418(6896): 417-422.

Milam AH, Barakat MR, Gupta N, Rose L, Aleman TS, Pianta MJ, Cideciyan AV, Sheffield VC, Stone EM and Jacobson SG (2003). Clinicopathologic effects of mutant GUCY2D in Leber congenital amaurosis. Ophthalmol
110(3): 549-558.

Millan JM, Aller E, Jaijo T, Blanco-Kelly F, Gimenez-Pardo A and Ayuso C (2011). An update on the genetics of usher syndrome. J Ophthalmol 2011: 417217.

Miller S, Tavshanjian B, Oleksy A, Perisic O, Houseman BT, Shokat KM and Williams RL (2010). Shaping development of autophagy inhibitors with the structure of the lipid kinase Vps34. Science 327(5973): 1638-1642.

Misky D, Guillaumie T, Baudoin C, Bocquet B, Beltran M, Kaplan J, Dhaenens CM, Bonnefont JP, Meunier I and Hamel CP (2016). Pattern dystrophy in a female carrier of RP2 mutation. Ophthalmic Genet: 1-3.

Mitamura Y, Mitamura-Aizawa S, Nagasawa T, Katome T, Eguchi H and Naito T (2012). Diagnostic imaging in patients with retinitis pigmentosa. J Med Invest 59(1-2): 1-11.

Mitter SK, Rao HV, Qi X, Cai J, Sugrue A, Dunn WA, Grant MB and Boulton ME (2012). Autophagy in the Retina: A Potential Role in Age-Related Macular Degeneration. Adv Exp Med Biol 723: 83-90.

Mitter SK, Song C, Qi X, Mao H, Rao H, Akin D, Lewin A, Grant M, Dunn W, Jr., Ding J, Bowes Rickman C and Boulton M (2014). Dysregulated autophagy in the RPE is associated with increased susceptibility to oxidative stress and AMD. Autophagy 10(11): 1989-2005.

Mitton KP, Swain PK, Chen S, Xu S, Zack DJ and Swaroop A (2000). The leucine zipper of NRL interacts with the CRX homeodomain. A possible mechanism of transcriptional synergy in rhodopsin regulation. J Biol Chem 275(38): 29794-29799.

Mizushima N, Noda T, Yoshimori T, Tanaka Y, Ishii T, George MD, Klionsky DJ, Ohsumi M and Ohsumi Y (1998). A protein conjugation system essential for autophagy. Nature 395(6700): 395-398.

Mizushima N and Komatsu M (2011). Autophagy: Renovation of Cells and Tissues. Cell 147(4): 728-741.

Mizushima N, Yoshimori T and Ohsumi Y (2011). The role of Atg proteins in autophagosome formation. Annu Rev Cell Dev Biol 27: 107-132.

Modell B and Darr A (2002). Genetic counselling and customary consanguineous marriage. Nat Rev Genet 3(3): 225-229.

Moiseyev G, Chen Y, Takahashi Y, Wu BX and Ma J (2005). RPE65 is the isomerohydrolase in the retinoid visual cycle. Proc Natl Acad Sci U S A 102(35): 12413-12418.

Molday LL, Rabin AR and Molday RS (2000). ABCR expression in foveal cone photoreceptors and its role in Stargardt macular dystrophy. Nat Genet 25(3): 257-258.

Molday RS (2015). Insights into the Molecular Properties of ABCA4 and Its Role in the Visual Cycle and Stargardt Disease. Prog Mol Biol Transl Sci 134: 415-431.

Mole SE, Williams RE and Goebel HH (2005). Correlations between genotype, ultrastructural morphology and clinical phenotype in the neuronal ceroid lipofuscinoses. Neurogenetics 6(3): 107-126.

Montanaro F, Carbonetto S, Campbell KP and Lindenbaum M (1995). Dystroglycan expression in the wild type and mdx mouse neural retina: synaptic colocalization with dystrophin, dystrophin-related protein but not laminin. J Neurosci Res 42(4): 528-538.

Moore A, Escudier E, Roger G, Tamalet A, Pelosse B, Marlin S, Clement A, Geremek M, Delaisi B, Bridoux AM, Coste A, Witt M, Duriez B and Amselem S (2006). RPGR is mutated in patients with a complex X linked phenotype combining primary ciliary dyskinesia and retinitis pigmentosa. J Med Genet 43(4): 326-333.

Moore SJ, Green JS, Fan Y, Bhogal AK, Dicks E, Fernandez BA, Stefanelli M, Murphy C, Cramer BC, Dean JC, Beales PL, Katsanis N, Bassett AS, Davidson WS and Parfrey PS (2005). Clinical and genetic epidemiology of Bardet-Biedl syndrome in Newfoundland: a 22-year prospective, population-based, cohort study. Am J Med Genet A 132a(4): 352-360.

Morimura H, Fishman GA, Grover SA, Fulton AB, Berson EL and Dryja TP (1998). Mutations in the RPE65 gene in patients with autosomal recessive retinitis pigmentosa or leber congenital amaurosis. Proc Natl Acad Sci U S A 95(6): 3088-3093.

Morishita H and Mizushima N (2016). Autophagy in the lens. Exp Eye Res 144: 22-28.

Morrow EM, Furukawa T, Raviola E and Cepko CL (2005). Synaptogenesis and outer segment formation are perturbed in the neural retina of Crx mutant mice. BMC Neurosci 6: 5.

Mueller RF and Bishop DT (1993). Autozygosity mapping, complex consanguinity, and autosomal recessive disorders. J Med Genet 30(9): 798-799.

Muller J, Stoetzel C, Vincent MC, Leitch CC, Laurier V, Danse JM, Helle S, Marion V, Bennouna-Greene V, Vicaire S, Megarbane A, Kaplan J, Drouin-Garraud V, Hamdani M, Sigaudy S, Francannet C, Roume J, Bitoun P, Goldenberg A, Philip N, Odent S, Green J, Cossee M, Davis EE, Katsanis N, Bonneau D, Verloes A, Poch O, Mandel JL and Dollfus H (2010). Identification of 28 novel mutations in the Bardet-Biedl syndrome genes: the burden of private mutations in an extensively heterogeneous disease. Hum Genet 127(5): 583-593.

Muntoni F, Brockington M, Godfrey C, Ackroyd M, Robb S, Manzur A, Kinali M, Mercuri E, Kaluarachchi M, Feng L, Jimenez-Mallebrera C, Clement E, Torelli S, Sewry CA and Brown SC (2007). Muscular dystrophies due to defective glycosylation of dystroglycan. Acta Myol 26(3): 129-135.

Mustafi D, Engel AH and Palczewski K (2009). Structure of cone photoreceptors. Prog Retin Eye Res 28(4): 289-302.

Mustafi D, Kevany BM, Genoud C, Okano K, Cideciyan AV, Sumaroka A, Roman AJ, Jacobson SG, Engel A, Adams MD and Palczewski K (2011). Defective photoreceptor phagocytosis in a mouse model of enhanced S-cone syndrome causes progressive retinal degeneration. The FASEB Journal 25(9): 3157-3176.

Mykytyn K, Braun T, Carmi R, Haider NB, Searby CC, Shastri M, Beck G, Wright AF, Iannaccone A, Elbedour K, Riise R, Baldi A, Raas-Rothschild A, Gorman SW, Duhl DM, Jacobson SG, Casavant T, Stone EM and Sheffield VC (2001). Identification of the gene that, when mutated, causes the human obesity syndrome BBS4. Nat Genet 28(2): 188-191.

Myllykangas S, Buenrostro J and Ji HP (2012). Overview of Sequencing Technology Platforms. Bioinformatics for High Throughput Sequencing. N Rodríguez-Ezpeleta, M Hackenberg and M A Aransay. New York, NY, Springer New York**:** 11-25.

Na'amnih W, Romano-Zelekha O, Kabaha A, Rubin LP, Bilenko N, Jaber L, Honovich M and Shohat T (2014). Prevalence of consanguineous marriages and associated factors among Israeli Bedouins. J Community Genet 5(4): 395-398.

Nachury MV, Loktev AV, Zhang Q, Westlake CJ, Peranen J, Merdes A, Slusarski DC, Scheller RH, Bazan JF, Sheffield VC and Jackson PK (2007). A core complex of BBS proteins cooperates with the GTPase Rab8 to promote ciliary membrane biogenesis. Cell 129(6): 1201-1213.

Nagaya M, Ueno S, Kominami T, Nakanishi A, Koyasu T, Kondo M, Furukawa T and Terasaki H (2015). Pikachurin Protein Required for Increase of Cone Electroretinogram B-Wave during Light Adaptation. PLoS One 10(6): e0128921.

Nagel-Wolfrum K, Baasov T and Wolfrum U (2014). Therapy strategies for Usher syndrome Type 1C in the retina. Adv Exp Med Biol 801: 741-747.

Nakazawa M, Kikawa E, Chida Y and Tamai M (1994). Asn244His mutation of the peripherin/RDS gene causing autosomal dominant cone-rod degeneration. Hum Mol Genet 3(7): 1195-1196.

Nakazawa M, Wada Y and Tamai M (1998). Arrestin gene mutations in autosomal recessive retinitis pigmentosa. Arch Ophthalmol 116(4): 498-501.

Narasimhan VM, Hunt KA, Mason D, Baker CL, Karczewski KJ, Barnes MR, Barnett AH, Bates C, Bellary S, Bockett NA, Giorda K, Griffiths CJ, Hemingway H, Jia Z, Kelly MA, Khawaja HA, Lek M, McCarthy S, McEachan R, O'Donnell-Luria A, Paigen K, Parisinos CA, Sheridan E, Southgate L, Tee L, Thomas M, Xue Y, Schnall-Levin M, Petkov PM, Tyler-Smith C, Maher ER, Trembath RC, MacArthur DG, Wright J, Durbin R and van Heel DA (2016). Health and population effects of rare gene knockouts in adult humans with related parents. Science 352(6284): 474-477.

Nash BM, Wright DC, Grigg JR, Bennetts B and Jamieson RV (2015). Retinal dystrophies, genomic applications in diagnosis and prospects for therapy. Transl Pediatr 4(2): 139-163.

Neveling K, Collin RW, Gilissen C, van Huet RA, Visser L, Kwint MP, Gijsen SJ, Zonneveld MN, Wieskamp N, de Ligt J, Siemiatkowska AM, Hoefsloot LH, Buckley MF, Kellner U, Branham KE, den Hollander AI, Hoischen A, Hoyng C, Klevering BJ, van den Born LI, Veltman JA, Cremers FP and Scheffer H (2012). Next-generation genetic testing for retinitis pigmentosa. Hum Mutat 33(6): 963-972.

Ng PC and Henikoff S (2003). SIFT: Predicting amino acid changes that affect protein function. Nucleic Acids Res 31(13): 3812-3814.

Nguyen-Legros J and Hicks D (2000). Renewal of photoreceptor outer segments and their phagocytosis by the retinal pigment epithelium. Int Rev Cytol 196: 245-313.

Nichols LL, 2nd, Alur RP, Boobalan E, Sergeev YV, Caruso RC, Stone EM, Swaroop A, Johnson MA and Brooks BP (2010). Two novel CRX mutant proteins causing autosomal dominant Leber congenital amaurosis interact differently with NRL. Hum Mutat 31(6): E1472-1483.

Nishiguchi KM, Sandberg MA, Gorji N, Berson EL and Dryja TP (2005). Cone cGMP-gated channel mutations and clinical findings in patients with achromatopsia, macular degeneration, and other hereditary cone diseases. Hum Mutat 25(3): 248-258.

Nishimura DY, Searby CC, Carmi R, Elbedour K, Van Maldergem L, Fulton AB, Lam BL, Powell BR, Swiderski RE, Bugge KE, Haider NB, Kwitek-Black AE, Ying L, Duhl DM, Gorman SW, Heon E, Iannaccone A, Bonneau D, Biesecker LG, Jacobson SG, Stone EM and Sheffield VC (2001). Positional cloning of a novel gene on chromosome 16q causing Bardet-Biedl syndrome (BBS2). Hum Mol Genet 10(8): 865-874.

Nishimura DY, Swiderski RE, Searby CC, Berg EM, Ferguson AL, Hennekam R, Merin S, Weleber RG, Biesecker LG, Stone EM and Sheffield VC (2005). Comparative genomics and gene expression analysis identifies BBS9, a new Bardet-Biedl syndrome gene. Am J Hum Genet 77(6): 1021-1033.

Nyrén P and Lundin A (1985). Enzymatic method for continuous monitoring of inorganic pyrophosphate synthesis. Anal. Biochem. 151(2): 504-509.

O'Prey J, Skommer J, Wilkinson S and Ryan KM (2009). Analysis of DRAM-related proteins reveals evolutionarily conserved and divergent roles in the control of autophagy. Cell Cycle 8(14): 2260-2265.

O'Sullivan J, Mullaney BG, Bhaskar SS, Dickerson JE, Hall G, O'Grady A, Webster A, Ramsden SC and Black GC (2012). A paradigm shift in the delivery of services for diagnosis of inherited retinal disease. J Med Genet 49(5): 322-326.

Oishi M, Oishi A, Gotoh N, Ogino K, Higasa K, Iida K, Makiyama Y, Morooka S, Matsuda F and Yoshimura N (2016). Next-generation sequencing-based comprehensive molecular analysis of 43 Japanese patients with cone and cone-rod dystrophies. Mol Vis 22: 150-160.

Okano T, Kojima D, Fukada Y, Shichida Y and Yoshizawa T (1992). Primary structures of chicken cone visual pigments: vertebrate rhodopsins have evolved out of cone visual pigments. Proc Natl Acad Sci U S A 89(13): 5932-5936.

Okazaki H, Tazoe F, Okazaki S, Isoo N, Tsukamoto K, Sekiya M, Yahagi N, Iizuka Y, Ohashi K, Kitamine T, Tozawa R, Inaba T, Yagyu H, Okazaki M, Shimano H, Shibata N, Arai H, Nagai RZ, Kadowaki T, Osuga J and Ishibashi S (2006). Increased cholesterol biosynthesis and hypercholesterolemia in mice overexpressing squalene synthase in the liver. J Lipid Res 47(9): 1950-1958.

Omasits U, Ahrens CH, Muller S and Wollscheid B (2014). Protter: interactive protein feature visualization and integration with experimental proteomic data. Bioinformatics 30(6): 884-886.

Orchard S, Ammari M, Aranda B, Breuza L, Briganti L, Broackes-Carter F, Campbell NH, Chavali G, Chen C, del-Toro N, Duesbury M, Dumousseau M, Galeota E, Hinz U, Iannuccelli M, Jagannathan S, Jimenez R, Khadake J, Lagreid A, Licata L, Lovering RC, Meldal B, Melidoni AN, Milagros M, Peluso D, Perfetto L, Porras P, Raghunath A, Ricard-Blum S, Roechert B, Stutz A, Tognolli M, van Roey K, Cesareni G and Hermjakob H (2014). The MIntAct project--IntAct as a common curation platform for 11 molecular interaction databases. Nucleic Acids Res 42(Database issue): D358-363.

Ouechtati F, Merdassi A, Bouyacoub Y, Largueche L, Derouiche K, Ouragini H, Nouira S, Tiab L, Baklouti K, Rebai A, Schorderet DF, Munier FL, Zografos L, Abdelhak S and El Matri L (2011). Clinical and genetic investigation of a large Tunisian family with complete achromatopsia: identification of a new nonsense mutation in GNAT2 gene. J Hum Genet 56(1): 22-28.

Palczewski K (2010). Retinoids for Treatment of Retinal Diseases. Trends Pharmacol Sci 31(6): 284-295.

Pampliega O, Orhon I, Patel B, Sridhar S, Diaz-Carretero A, Beau I, Codogno P, Satir BH, Satir P and Cuervo AM (2013). Functional interaction between autophagy and ciliogenesis. Nature 502(7470): 194-200.

Pang JJ, Chang B, Kumar A, Nusinowitz S, Noorwez SM, Li J, Rani A, Foster TC, Chiodo VA, Doyle T, Li H, Malhotra R, Teusner JT, McDowell JH, Min SH, Li Q, Kaushal S and Hauswirth WW (2006). Gene therapy restores vision-dependent behavior as well as retinal structure and function in a mouse model of RPE65 Leber congenital amaurosis. Mol Ther 13(3): 565-572.

Pang JJ, Deng WT, Dai X, Lei B, Everhart D, Umino Y, Li J, Zhang K, Mao S, Boye SL, Liu L, Chiodo VA, Liu X, Shi W, Tao Y, Chang B and Hauswirth WW (2012). AAV-mediated cone rescue in a naturally occurring mouse model of CNGA3-achromatopsia. PLoS One 7(4): e35250.

Pareek CS, Smoczynski R and Tretyn A (2011). Sequencing technologies and genome sequencing. J Appl Genet 52(4): 413-435.

Park D-S, Kim J-H, Kim H-S, Park J-H, Shin J-K and Lee M (2003). A foveated-structure CMOS retina chip for edge detection with local light adaptation. Sensor Actuat A-Phys 108(1–3): 75-80.

Park SM, Kim K, Lee EJ, Kim BK, Lee TJ, Seo T, Jang IS, Lee SH, Kim S, Lee JH and Park J (2009). Reduced expression of DRAM2/TMEM77 in tumor cells interferes with cell death. Biochem Biophys Res Commun 390(4): 1340-1344.

Partanen S, Haapanen A, Kielar C, Pontikis C, Alexander N, Inkinen T, Saftig P, Gillingwater TH, Cooper JD and Tyynela J (2008). Synaptic changes in the thalamocortical system of cathepsin D-deficient mice: a model of human congenital neuronal ceroid-lipofuscinosis. J Neuropathol Exp Neurol 67(1): 16-29.

Patil SB, Hurd TW, Ghosh AK, Murga-Zamalloa CA and Khanna H (2011). Functional analysis of retinitis pigmentosa 2 (RP2) protein reveals variable pathogenic potential of disease-associated missense variants. PLoS One 6(6): e21379.

Patnaik SR, Raghupathy RK, Zhang X, Mansfield D and Shu X (2015). The Role of RPGR and Its Interacting Proteins in Ciliopathies. J Ophthalmol 2015: 414781.

Pattingre S, Tassa A, Qu X, Garuti R, Liang XH, Mizushima N, Packer M, Schneider MD and Levine B (2005). Bcl-2 antiapoptotic proteins inhibit Beclin 1-dependent autophagy. Cell 122(6): 927-939.

Paun CC, Ersoy L, Schick T, Groenewoud JM, Lechanteur YT, Fauser S, Hoyng CB, de Jong EK and den Hollander AI (2015). Genetic Variants and Systemic Complement Activation Levels Are Associated With Serum Lipoprotein Levels in Age-Related Macular Degeneration. Invest Ophthalmol Vis Sci 56(13): 7766-7773.

Paunescu K, Preising MN, Janke B, Wissinger B and Lorenz B (2007). Genotype-phenotype correlation in a German family with a novel complex CRX mutation extending the open reading frame. Ophthalmol 114(7): 1348-1357.e1341.

Pawlik B, Mir A, Iqbal H, Li Y, Nurnberg G, Becker C, Qamar R, Nurnberg P and Wollnik B (2010). A Novel Familial BBS12 Mutation Associated with a Mild Phenotype: Implications for Clinical and Molecular Diagnostic Strategies. Mol Syndromol 1(1): 27-34.

Payne A, Vithana E, Khaliq S, Hameed A, Deller J, Abu-Safieh L, Kermani S, Leroy BP, Mehdi SQ, Moore AT, Bird AC and Bhattacharya SS (2000). RP1 protein truncating mutations predominate at the RP1 adRP locus. Invest Ophthalmol Vis Sci 41(13): 4069-4073.

Payne AM, Morris AG, Downes SM, Johnson S, Bird AC, Moore AT, Bhattacharya SS and Hunt DM (2001). Clustering and frequency of mutations in the retinal guanylate cyclase

(GUCY2D) gene in patients with dominant cone-rod dystrophies. J Med Genet 38(9): 611-614.

Pelletier V, Jambou M, Delphin N, Zinovieva E, Stum M, Gigarel N, Dollfus H, Hamel C, Toutain A, Dufier JL, Roche O, Munnich A, Bonnefont JP, Kaplan J and Rozet JM (2007). Comprehensive survey of mutations in RP2 and RPGR in patients affected with distinct retinal dystrophies: genotype-phenotype correlations and impact on genetic counseling. Hum Mutat 28(1): 81-91.

Pellissier LP, Quinn PM, Alves CH, Vos RM, Klooster J, Flannery JG, Heimel JA and Wijnholds J (2015). Gene therapy into photoreceptors and Muller glial cells restores retinal structure and function in CRB1 retinitis pigmentosa mouse models. Hum Mol Genet 24(11): 3104-3118.

Pemberton TJ, Sandefur CI, Jakobsson M and Rosenberg NA (2009). Sequence determinants of human microsatellite variability. BMC Genomics 10(1): 1-19.

Peng GH, Ahmad O, Ahmad F, Liu J and Chen S (2005). The photoreceptor-specific nuclear receptor Nr2e3 interacts with Crx and exerts opposing effects on the transcription of rod versus cone genes. Hum Mol Genet 14(6): 747-764.

Peracchio C, Alabiso O, Valente G and Isidoro C (2012). Involvement of autophagy in ovarian cancer: a working hypothesis. J Ovarian Res 5(1): 22.

Perez-Carro R, Corton M, Sanchez-Navarro I, Zurita O, Sanchez-Bolivar N, Sanchez-Alcudia R, Lelieveld SH, Aller E, Lopez-Martinez MA, Lopez-Molina MI, Fernandez-San Jose P, Blanco-Kelly F, Riveiro-Alvarez R, Gilissen C, Millan JM, Avila-Fernandez A and Ayuso C (2016). Panel-based NGS Reveals Novel Pathogenic Mutations in Autosomal Recessive Retinitis Pigmentosa. Sci Rep 6: 19531.

Perrault I, Rozet J-M, Gerber S, Kelsell RE, Souied E, Cabot A, Hunt DM, Munnich A and Kaplan J (1998). A retGC-1 Mutation in Autosomal Dominant Cone-Rod Dystrophy. Am J Hum Genet 63(2): 651-654.

Perrault I, Rozet JM, Gerber S, Ghazi I, Leowski C, Ducroq D, Souied E, Dufier JL, Munnich A and Kaplan J (1999). Leber congenital amaurosis. Mol Genet Metab 68(2): 200-208.

Perrault I, Rozet JM, Gerber S, Ghazi I, Ducroq D, Souied E, Leowski C, Bonnemaison M, Dufier JL, Munnich A and Kaplan J (2000). Spectrum of retGC1 mutations in Leber's congenital amaurosis. Eur J Hum Genet 8(8): 578-582.

Perrault I, Hanein S, Gerber S, Barbet F, Ducroq D, Dollfus H, Hamel C, Dufier JL, Munnich A, Kaplan J and Rozet JM (2004). Retinal dehydrogenase 12 (RDH12) mutations in leber congenital amaurosis. Am J Hum Genet 75(4): 639-646.

Perrault I, Delphin N, Hanein S, Gerber S, Dufier JL, Roche O, Defoort-Dhellemmes S, Dollfus H, Fazzi E, Munnich A, Kaplan J and Rozet JM (2007). Spectrum of NPHP6/CEP290

mutations in Leber congenital amaurosis and delineation of the associated phenotype. Hum Mutat 28(4): 416.

Perrault I, Hanein S, Gerard X, Delphin N, Fares-Taie L, Gerber S, Pelletier V, Merce E, Dollfus H, Puech B, Defoort-Dhellemmes S, Petersen MD, Zafeiriou D, Munnich A, Kaplan J, Roche O and Rozet JM (2010). Spectrum of SPATA7 mutations in Leber congenital amaurosis and delineation of the associated phenotype. Hum Mutat 31(3): E1241-1250.

Peter I, Huggins GS, Ordovas JM, Haan M and Seddon JM (2011). Evaluation of New and Established Age-Related Macular Degeneration Susceptibility Genes in the Women's Health Initiative Sight Exam (WHI-SE) Study. Am J Ophthalmol 152(6): 1005-1013.e1001.

Petrou PA, Cunningham D, Shimel K, Harrington M, Hammel K, Cukras CA, Ferris FL, Chew EY and Wong WT (2015). Intravitreal sirolimus for the treatment of geographic atrophy: results of a phase I/II clinical trial. Invest Ophthalmol Vis Sci 56(1): 330-338.

Pikuleva IA and Curcio CA (2014). Cholesterol in the retina: the best is yet to come. Prog Retin Eye Res 41: 64-89.

Piri N, Gao YQ, Danciger M, Mendoza E, Fishman GA and Farber DB (2005). A substitution of G to C in the cone cGMP-phosphodiesterase gamma subunit gene found in a distinctive form of cone dystrophy. Ophthalmol 112(1): 159-166.

Plagnol V, Curtis J, Epstein M, Mok KY, Stebbings E, Grigoriadou S, Wood NW, Hambleton S, Burns SO, Thrasher AJ, Kumararatne D, Doffinger R and Nejentsev S (2012). A robust model for read count data in exome sequencing experiments and implications for copy number variant calling. Bioinformatics 28(21): 2747-2754.

Proud CG (2007). Cell signaling. mTOR, unleashed. Science 318(5852): 926-927.

Puffenberger EG, Jinks RN, Sougnez C, Cibulskis K, Willert RA, Achilly NP, Cassidy RP, Fiorentini CJ, Heiken KF, Lawrence JJ, Mahoney MH, Miller CJ, Nair DT, Politi KA, Worcester KN, Setton RA, DiPiazza R, Sherman EA, Eastman JT, Francklyn C, Robey-Bond S, Rider NL, Gabriel S, Morton DH and Strauss KA (2012). Genetic Mapping and Exome Sequencing Identify Variants Associated with Five Novel Diseases. PLoS One 7(1): e28936.

Purves D, Augustine G, Fitzpatrick D, Katz L, LaMantia A, McNamara J and Williams M (2001). Neuroscience, 2nd edition. Sunderland (MA), Sinauer Associates.

Pusch CM, Broghammer M, Jurklies B, Besch D and Jacobi FK (2002). Ten novel ORF15 mutations confirm mutational hot spot in the RPGR gene in European patients with X-linked retinitis pigmentosa. Hum Mutat 20(5): 405.

Pyle JL, Kavalali ET, Piedras-Renteria ES and Tsien RW (2000). Rapid reuse of readily releasable pool vesicles at hippocampal synapses. Neuron 28(1): 221-231.

Qidwai W, Syed IA and Khan FM (2003). Prevalence and perceptions about consanguineous marriages among patients presenting to family physicians, in 2001 at a Teaching Hospital in Karachi, Pakistan. Asia Pac Fam Med 2(1): 27-31.

Qin H, Diener DR, Geimer S, Cole DG and Rosenbaum JL (2004). Intraflagellar transport (IFT) cargo: IFT transports flagellar precursors to the tip and turnover products to the cell body. J Cell Biol 164(2): 255-266.

Raca G, Jackson C, Warman B, Bair T and Schimmenti LA (2010). Next generation sequencing in research and diagnostics of ocular birth defects. Mol Genet Metab 100(2): 184-192.

Rahner N, Nuernberg G, Finis D, Nuernberg P and Royer-Pokora B (2016). A novel C8orf37 splice mutation and genotype-phenotype correlation for cone-rod dystrophy. Ophthalmic Genet: 1-7.

Rajala A, Wang Y, Zhu Y, Ranjo-Bishop M, Ma JX, Mao C and Rajala RV (2014). Nanoparticle-assisted targeted delivery of eye-specific genes to eyes significantly improves the vision of blind mice in vivo. Nano Lett 14(9): 5257-5263.

Ramsden CM, Powner MB, Carr AJ, Smart MJ, da Cruz L and Coffey PJ (2013). Stem cells in retinal regeneration: past, present and future. Development 140(12): 2576-2585.

Ran FA, Hsu PD, Lin CY, Gootenberg JS, Konermann S, Trevino AE, Scott DA, Inoue A, Matoba S, Zhang Y and Zhang F (2013). Double nicking by RNA-guided CRISPR Cas9 for enhanced genome editing specificity. Cell 154(6): 1380-1389.

Rath MF, Morin F, Shi Q, Klein DC and Moller M (2007). Ontogenetic expression of the Otx2 and Crx homeobox genes in the retina of the rat. Exp Eye Res 85(1): 65-73.

Ravesh Z, El Asrag ME, Weisschuh N, McKibbin M, Reuter P, Watson CM, Baumann B, Poulter JA, Sajid S, Panagiotou ES, O'Sullivan J, Abdelhamed Z, Bonin M, Soltanifar M, Black GC, Amin-ud Din M, Toomes C, Ansar M, Inglehearn CF, Wissinger B and Ali M (2015). Novel C8orf37 mutations cause retinitis pigmentosa in consanguineous families of Pakistani origin. Mol Vis 21: 236-243.

Ravikumar B, Vacher C, Berger Z, Davies JE, Luo S, Oroz LG, Scaravilli F, Easton DF, Duden R, O'Kane CJ and Rubinsztein DC (2004). Inhibition of mTOR induces autophagy and reduces toxicity of polyglutamine expansions in fly and mouse models of Huntington disease. Nat Genet 36(6): 585-595.

Ravikumar B, Moreau K, Jahreiss L, Puri C and Rubinsztein DC (2010). Plasma membrane contributes to the formation of pre-autophagosomal structures. Nat Cell Biol 12(8): 747-757.

Rea R, Li J, Dharia A, Levitan ES, Sterling P and Kramer RH (2004). Streamlined synaptic vesicle cycle in cone photoreceptor terminals. Neuron 41(5): 755-766.

Redin C, Le Gras S, Mhamdi O, Geoffroy V, Stoetzel C, Vincent MC, Chiurazzi P, Lacombe D, Ouertani I, Petit F, Till M, Verloes A, Jost B, Chaabouni HB, Dollfus H, Mandel JL and

Muller J (2012). Targeted high-throughput sequencing for diagnosis of genetically heterogeneous diseases: efficient mutation detection in Bardet-Biedl and Alstrom syndromes. J Med Genet 49(8): 502-512.

Redmond TM, Yu S, Lee E, Bok D, Hamasaki D, Chen N, Goletz P, Ma JX, Crouch RK and Pfeifer K (1998). Rpe65 is necessary for production of 11-cis-vitamin A in the retinal visual cycle. Nat Genet 20(4): 344-351.

Reese MG, Eeckman FH, Kulp D and Haussler D (1997). Improved splice site detection in Genie. J Comput Biol 4(3): 311-323.

Regalado ES, Guo DC, Prakash S, Bensend TA, Flynn K, Estrera A, Safi H, Liang D, Hyland J, Child A, Arno G, Boileau C, Jondeau G, Braverman A, Moran R, Morisaki T, Morisaki H, Pyeritz R, Coselli J, LeMaire S and Milewicz DM (2015). Aortic Disease Presentation and Outcome Associated With ACTA2 Mutations. Circ Cardiovasc Genet 8(3): 457-464.

Reiners J, Nagel-Wolfrum K, Jurgens K, Marker T and Wolfrum U (2006). Molecular basis of human Usher syndrome: deciphering the meshes of the Usher protein network provides insights into the pathomechanisms of the Usher disease. Exp Eye Res 83(1): 97-119.

Riazuddin SA, Iqbal M, Wang Y, Masuda T, Chen Y, Bowne S, Sullivan LS, Waseem NH, Bhattacharya S, Daiger SP, Zhang K, Khan SN, Riazuddin S, Hejtmancik JF, Sieving PA, Zack DJ and Katsanis N (2010). A splice-site mutation in a retina-specific exon of BBS8 causes nonsyndromic retinitis pigmentosa. Am J Hum Genet 86(5): 805-812.

Richards DA, Guatimosim C, Rizzoli SO and Betz WJ (2003). Synaptic vesicle pools at the frog neuromuscular junction. Neuron 39(3): 529-541.

Riveiro-Alvarez R, Lopez-Martinez MA, Zernant J, Aguirre-Lamban J, Cantalapiedra D, Avila-Fernandez A, Gimenez A, Lopez-Molina MI, Garcia-Sandoval B, Blanco-Kelly F, Corton M, Tatu S, Jose PFS, Trujillo-Tiebas MJ, Ramos C, Allikmets R and Ayuso C (2013). Outcome of ABCA4 disease-associated alleles in autosomal recessive Retinal Dystrophies: Retrospective analysis in 420 Spanish families. Ophthalmol 120(11).

Rivolta C, Sweklo EA, Berson EL and Dryja TP (2000). Missense mutation in the USH2A gene: association with recessive retinitis pigmentosa without hearing loss. Am J Hum Genet 66(6): 1975-1978.

Rivolta C, Berson EL and Dryja TP (2001). Dominant Leber congenital amaurosis, cone-rod degeneration, and retinitis pigmentosa caused by mutant versions of the transcription factor CRX. Hum Mutat 18(6): 488-498.

Rizzo S, Belting C, Cinelli L, Allegrini L, Genovesi-Ebert F, Barca F and di Bartolo E (2014). The Argus II Retinal Prosthesis: 12-month outcomes from a single-study center. Am J Ophthalmol 157(6): 1282-1290.

Rizzolo LJ, Peng S, Luo Y and Xiao W (2011). Integration of tight junctions and claudins with the barrier functions of the retinal pigment epithelium. Prog Retin Eye Res 30(5): 296-323.

Robinson JT, Thorvaldsdottir H, Winckler W, Guttman M, Lander ES, Getz G and Mesirov JP (2011). Integrative genomics viewer. Nat Biotechnol 29(1): 24-26.

Rodieck RW and Rushton WA (1976). Cancellation of rod signals by cones, and cone signals by rods in the cat retina. J Physiol 254(3): 775-785.

Rodieck RW (1998). The First Steps in Seeing. Sunderland, MA, Sinauer Associates.

Rodriguez-Muela N, Koga H, Garcia-Ledo L, de la Villa P, de la Rosa EJ, Cuervo AM and Boya P (2013). Balance between autophagic pathways preserves retinal homeostasis. Aging Cell 12(3): 478-488.

Roduit R, Escher P and Schorderet DF (2009). Mutations in the DNA-binding domain of NR2E3 affect in vivo dimerization and interaction with CRX. PLoS One 4(10): e7379.

Roepman R, Bernoud-Hubac N, Schick DE, Maugeri A, Berger W, Ropers H-H, Cremers FPM and Ferreira PA (2000). The retinitis pigmentosa GTPase regulator (RPGR) interacts with novel transport-like proteins in the outer segments of rod photoreceptors. Hum Mol Genet 9(14): 2095-2105.

Roepman R, Letteboer SJF, Arts HH, van Beersum SEC, Lu X, Krieger E, Ferreira PA and Cremers FPM (2005). Interaction of nephrocystin-4 and RPGRIP1 is disrupted by nephronophthisis or Leber congenital amaurosis-associated mutations. Proc Natl Acad Sci U S A 102(51): 18520-18525.

Ronaghi M, Uhlén M and Nyrén P (1998). A sequencing method based on real-time pyrophosphate. Science 281(5375): 363-365.

Roosing S, Rohrschneider K, Beryozkin A, Sharon D, Weisschuh N, Staller J, Kohl S, Zelinger L, Peters Theo A, Neveling K, Strom Tim M, van den Born LI, Hoyng Carel B, Klaver Caroline CW, Roepman R, Wissinger B, Banin E, Cremers Frans PM and den Hollander Anneke I (2013). Mutations in RAB28, Encoding a Farnesylated Small GTPase, Are Associated with Autosomal-Recessive Cone-Rod Dystrophy. Am J Hum Genet 93(1): 110-117.

Roosing S, Thiadens AAHJ, Hoyng CB, Klaver CCW, den Hollander AI and Cremers FPM (2014). Causes and consequences of inherited cone disorders. Prog Retin Eye Res 42: 1-26.

Roosing S, van den Born LI, Sangermano R, Banfi S, Koenekoop RK, Zonneveld-Vrieling MN, Klaver CCW, van Lith-Verhoeven JJC, Cremers FPM, den Hollander AI and Hoyng CB (2015). Mutations in MFSD8, Encoding a Lysosomal Membrane Protein, Are Associated with Nonsyndromic Autosomal Recessive Macular Dystrophy. Ophthalmol 122(1): 170-179.

Rosenfeld PJ, Cowley GS, McGee TL, Sandberg MA, Berson EL and Dryja TP (1992). A null mutation in the rhodopsin gene causes rod photoreceptor dysfunction and autosomal recessive retinitis pigmentosa. Nat Genet 1(3): 209-213.

Rozet JM, Gerber S, Souied E, Perrault I, Chatelin S, Ghazi I, Leowski C, Dufier JL, Munnich A and Kaplan J (1998). Spectrum of ABCR gene mutations in autosomal recessive macular dystrophies. Eur J Hum Genet 6(3): 291-295.

Rozet JM, Perrault I, Gerber S, Hanein S, Barbet F, Ducroq D, Souied E, Munnich A and Kaplan J (2001). Complete abolition of the retinal-specific guanylyl cyclase (retGC-1) catalytic ability consistently leads to leber congenital amaurosis (LCA). Invest Ophthalmol Vis Sci 42(6): 1190-1192.

Rubinsztein DC, Codogno P and Levine B (2012). Autophagy modulation as a potential therapeutic target for diverse diseases. Nat Rev Drug Discov 11(9): 709-730.

Ruiz-Martinez MC, Berka J, Belenkii A, Foret F, Miller AW and Karger BL (1993). DNA sequencing by capillary electrophoresis with replaceable linear polyacrylamide and laser-induced fluorescence detection. Anal Chem 65(20): 2851-2858.

Ruiz A, Borrego S, Marcos I and Antinolo G (1998). A major locus for autosomal recessive retinitis pigmentosa on 6q, determined by homozygosity mapping of chromosomal regions that contain gamma-aminobutyric acid-receptor clusters. Am J Hum Genet 62(6): 1452-1459.

Ruiz A, Kuehn MH, Andorf JL, Stone E, Hageman GS and Bok D (2001). Genomic organization and mutation analysis of the gene encoding lecithin retinol acyltransferase in human retinal pigment epithelium. Invest Ophthalmol Vis Sci 42(1): 31-37.

Saari JC and Bredberg DL (1989). Lecithin:retinol acyltransferase in retinal pigment epithelial microsomes. J Biol Chem 264(15): 8636-8640.

Saari JC, Bredberg DL and Farrell DF (1993). Retinol esterification in bovine retinal pigment epithelium: reversibility of lecithin:retinol acyltransferase. Biochem J 291 (Pt 3): 697-700.

Sachidanandam R, Weissman D, Schmidt SC, Kakol JM, Stein LD, Marth G, Sherry S, Mullikin JC, Mortimore BJ, Willey DL, Hunt SE, Cole CG, Coggill PC, Rice CM, Ning Z, Rogers J, Bentley DR, Kwok PY, Mardis ER, Yeh RT, Schultz B, Cook L, Davenport R, Dante M, Fulton L, Hillier L, Waterston RH, McPherson JD, Gilman B, Schaffner S, Van Etten WJ, Reich D, Higgins J, Daly MJ, Blumenstiel B, Baldwin J, Stange-Thomann N, Zody MC, Linton L, Lander ES and Altshuler D (2001). A map of human genome sequence variation containing 1.42 million single nucleotide polymorphisms. Nature 409(6822): 928-933.

Sahu R, Kaushik S, Clement CC, Cannizzo ES, Scharf B, Follenzi A, Potolicchio I, Nieves E, Cuervo AM and Santambrogio L (2011). MICROAUTOPHAGY OF CYTOSOLIC PROTEINS BY LATE ENDOSOMES. Dev Cell 20(1): 131-139.

Saiki RK, Scharf S, Faloona F, Mullis KB, Horn GT, Erlich HA and Arnheim N (1985). Enzymatic amplification of β-globin genomic sequences and restriction site analysis for diagnosis of sickle cell anemia. Science 230(4732): 1350-1354.

Saiki RK, Gelfand DH, Stoffel S, Scharf SJ, Higuchi R, Horn GT, Mullis KB and Erlich HA (1988). Primer-directed enzymatic amplification of DNA with a thermostable DNA polymerase. Science 239(4839): 487-491.

Salway S, Ali P, Ratcliffe G, Such E, Khan N, Kingston H and Quarrell O (2016). Responding to the increased genetic risk associated with customary consanguineous marriage among minority ethnic populations: lessons from local innovations in England. J Community Genet 7(3): 215-228.

Sanger F and Coulson AR (1975). A rapid method for determining sequences in DNA by primed synthesis with DNA polymerase. J. Mol. Biol. 94(3): 441-448.

Sanger F, Nicklen S and Coulson AR (1977). DNA sequencing with chain-terminating inhibitors. Proc Natl Acad Sci U S A 74(12): 5463-5467.

Santos-Ferreira T, Volkner M, Borsch O, Haas J, Cimalla P, Vasudevan P, Carmeliet P, Corbeil D, Michalakis S, Koch E, Karl MO and Ader M (2016). Stem Cell-Derived Photoreceptor Transplants Differentially Integrate Into Mouse Models of Cone-Rod Dystrophy. Invest Ophthalmol Vis Sci 57(7): 3509-3520.

Sanyal S and Jansen HG (1981). Absence of receptor outer segments in the retina of rds mutant mice. Neurosci Lett 21(1): 23-26.

Saqib MAN, Nikopoulos K, Ullah E, Sher Khan F, Iqbal J, Bibi R, Jarral A, Sajid S, Nishiguchi KM, Venturini G, Ansar M and Rivolta C (2015). Homozygosity mapping reveals novel and known mutations in Pakistani families with inherited retinal dystrophies. Sci Rep 5: 9965.

Sarthy V and Ripps H (2001). Structural organization of retinal glia. New York, Kluwer Academic/Plenum Press.

Sato M, Nakazawa M, Usui T, Tanimoto N, Abe H and Ohguro H (2005). Mutations in the gene coding for guanylate cyclase-activating protein 2 (GUCA1B gene) in patients with autosomal dominant retinal dystrophies. Graefes Arch Clin Exp Ophthalmol 243(3): 235-242.

Sato S, Omori Y, Katoh K, Kondo M, Kanagawa M, Miyata K, Funabiki K, Koyasu T, Kajimura N, Miyoshi T, Sawai H, Kobayashi K, Tani A, Toda T, Usukura J, Tano Y, Fujikado T and Furukawa T (2008). Pikachurin, a dystroglycan ligand, is essential for photoreceptor ribbon synapse formation. Nat Neurosci 11(8): 923-931.

Sayer JA, Otto EA, O'Toole JF, Nurnberg G, Kennedy MA, Becker C, Hennies HC, Helou J, Attanasio M, Fausett BV, Utsch B, Khanna H, Liu Y, Drummond I, Kawakami I, Kusakabe T, Tsuda M, Ma L, Lee H, Larson RG, Allen SJ, Wilkinson CJ, Nigg EA, Shou C, Lillo C, Williams DS, Hoppe B, Kemper MJ, Neuhaus T, Parisi MA, Glass IA, Petry M, Kispert A, Gloy J, Ganner A, Walz G, Zhu X, Goldman D, Nurnberg P, Swaroop A, Leroux MR and

Hildebrandt F (2006). The centrosomal protein nephrocystin-6 is mutated in Joubert syndrome and activates transcription factor ATF4. Nat Genet 38(6): 674-681.

Schaefer E, Lauer J, Durand M, Pelletier V, Obringer C, Claussmann A, Braun JJ, Redin C, Mathis C, Muller J, Schmidt-Mutter C, Flori E, Marion V, Stoetzel C and Dollfus H (2014). Mesoaxial polydactyly is a major feature in Bardet-Biedl syndrome patients with LZTFL1 (BBS17) mutations. Clin Genet 85(5): 476-481.

Schaefer E, Stoetzel C, Scheidecker S, Geoffroy V, Prasad MK, Redin C, Missotte I, Lacombe D, Mandel JL, Muller J and Dollfus H (2016). Identification of a novel mutation confirms the implication of IFT172 (BBS20) in Bardet-Biedl syndrome. J Hum Genet 61(5): 447-450.

Scheidecker S, Etard C, Pierce NW, Geoffroy V, Schaefer E, Muller J, Chennen K, Flori E, Pelletier V, Poch O, Marion V, Stoetzel C, Strahle U, Nachury MV and Dollfus H (2014). Exome sequencing of Bardet-Biedl syndrome patient identifies a null mutation in the BBSome subunit BBIP1 (BBS18). J Med Genet 51(2): 132-136.

Schlichtenbrede FC, da Cruz L, Stephens C, Smith AJ, Georgiadis A, Thrasher AJ, Bainbridge JW, Seeliger MW and Ali RR (2003). Long-term evaluation of retinal function in Prph2Rd2/Rd2 mice following AAV-mediated gene replacement therapy. J Gene Med 5(9): 757-764.

Schmelzle T and Hall MN (2000). TOR, a Central Controller of Cell Growth. Cell 103(2): 253-262.

Scholl HPN and Kremers J (2003). Alterations of L- and M-cone driven ERGs in cone and cone–rod dystrophies. Vision Res 43(22): 2333-2344.

Schuster A, Janecke AR, Wilke R, Schmid E, Thompson DA, Utermann G, Wissinger B, Zrenner E and Gal A (2007). The phenotype of early-onset retinal degeneration in persons with RDH12 mutations. Invest Ophthalmol Vis Sci 48(4): 1824-1831.

Schwahn U, Lenzner S, Dong J, Feil S, Hinzmann B, van Duijnhoven G, Kirschner R, Hemberger M, Bergen AA, Rosenberg T, Pinckers AJ, Fundele R, Rosenthal A, Cremers FP, Ropers HH and Berger W (1998). Positional cloning of the gene for X-linked retinitis pigmentosa 2. Nat Genet 19(4): 327-332.

Schwartz SD, Regillo CD, Lam BL, Eliott D, Rosenfeld PJ, Gregori NZ, Hubschman JP, Davis JL, Heilwell G, Spirn M, Maguire J, Gay R, Bateman J, Ostrick RM, Morris D, Vincent M, Anglade E, Del Priore LV and Lanza R (2015). Human embryonic stem cell-derived retinal pigment epithelium in patients with age-related macular degeneration and Stargardt's macular dystrophy: follow-up of two open-label phase 1/2 studies. Lancet 385(9967): 509-516.

Schwarz JM, Cooper DN, Schuelke M and Seelow D (2014). MutationTaster2: mutation prediction for the deep-sequencing age. Nat Methods 11(4): 361-362.

Schwarz N, Hardcastle AJ and Cheetham ME (2012). Arl3 and RP2 mediated assembly and traffic of membrane associated cilia proteins. Vision Res 75: 2-4.

Scott JD and Pawson T (2009). Cell signaling in space and time: where proteins come together and when they're apart. Science 326(5957): 1220-1224.

Senda M and Natsumeda Y (1994). Tissue-differential expression of two distinct genes for human IMP dehydrogenase (E.C.1.1.1.205). Life Sci 54(24): 1917-1926.

Sergouniotis PI, Chakarova C, Murphy C, Becker M, Lenassi E, Arno G, Lek M, MacArthur DG, Bhattacharya SS, Moore AT, Holder GE, Robson AG, Wolfrum U, Webster AR and Plagnol V (2014). Biallelic variants in TTLL5, encoding a tubulin glutamylase, cause retinal dystrophy. Am J Hum Genet 94(5): 760-769.

Sergouniotis PI, McKibbin M, Robson AG, Bolz HJ, De Baere E, Muller PL, Heller R, El-Asrag ME, Van Schil K, Plagnol V, Toomes C, Ali M, Holder GE, Charbel Issa P, Leroy BP, Inglehearn CF and Webster AR (2015). Disease Expression in Autosomal Recessive Retinal Dystrophy Associated With Mutations in the DRAM2 Gene. Invest Ophthalmol Vis Sci 56(13): 8083-8090.

Shang L, Chen S, Du F, Li S, Zhao L and Wang X (2011). Nutrient starvation elicits an acute autophagic response mediated by Ulk1 dephosphorylation and its subsequent dissociation from AMPK. Proc Natl Acad Sci U S A 108(12): 4788-4793.

Shanks ME, Downes SM, Copley RR, Lise S, Broxholme J, Hudspith KA, Kwasniewska A, Davies WI, Hankins MW, Packham ER, Clouston P, Seller A, Wilkie AO, Taylor JC, Ragoussis J and Nemeth AH (2013). Next-generation sequencing (NGS) as a diagnostic tool for retinal degeneration reveals a much higher detection rate in early-onset disease. Eur J Hum Genet 21(3): 274-280.

Sharon D, Sandberg MA, Rabe VW, Stillberger M, Dryja TP and Berson EL (2003). RP2 and RPGR mutations and clinical correlations in patients with X-linked retinitis pigmentosa. Am J Hum Genet 73(5): 1131-1146.

Shaw RJ and Cantley LC (2006). Ras, PI(3)K and mTOR signalling controls tumour cell growth. Nature 441(7092): 424-430.

Shawky RM, Elsayed SM, Zaki ME, Nour El-Din SM and Kamal FM (2013). Consanguinity and its relevance to clinical genetics. Egyptian Journal of Medical Human Genetics 14(2): 157-164.

Shen B, Zhang W, Zhang J, Zhou J, Wang J, Chen L, Wang L, Hodgkins A, Iyer V, Huang X and Skarnes WC (2014a). Efficient genome modification by CRISPR-Cas9 nickase with minimal off-target effects. Nat Meth 11(4): 399-402.

Shen S, Sujirakul T and Tsang SH (2014b). Next-generation sequencing revealed a novel mutation in the gene encoding the beta subunit of rod phosphodiesterase. Ophthalmic Genet 35(3): 142-150.

Shendure J and Ji H (2008). Next-generation DNA sequencing. Nature Biotechnol 26(10): 1135-1145.

Sherwin JC, Hewitt AW, Ruddle JB and Mackey DA (2008). Genetic isolates in ophthalmic diseases. Ophthalmic Genet 29(4): 149-161.

Shevach E, Ali M, Mizrahi-Meissonnier L, McKibbin M, El-Asrag M, Watson CM, Inglehearn CF, Ben-Yosef T, Blumenfeld A, Jalas C, Banin E and Sharon D (2015). Association between missense mutations in the BBS2 gene and nonsyndromic retinitis pigmentosa. JAMA Ophthalmol 133(3): 312-318.

Shi Y and Majewski J (2013). FishingCNV: a graphical software package for detecting rare copy number variations in exome-sequencing data. Bioinformatics 29(11): 1461-1462.

Shintani K, Shechtman DL and Gurwood AS (2009). Review and update: Current treatment trends for patients with retinitis pigmentosa. Optometry 80(7): 384-401.

Shoji-Kawata S, Sumpter R, Leveno M, Campbell GR, Zou Z, Kinch L, Wilkins AD, Sun Q, Pallauf K, MacDuff D, Huerta C, Virgin HW, Helms JB, Eerland R, Tooze SA, Xavier R, Lenschow DJ, Yamamoto A, King D, Lichtarge O, Grishin NV, Spector SA, Kaloyanova DV and Levine B (2013). Identification of a candidate therapeutic autophagy-inducing peptide. Nature 494(7436): 201-206.

Shu X, Fry AM, Tulloch B, Manson FDC, Crabb JW, Khanna H, Faragher AJ, Lennon A, He S, Trojan P, Giessl A, Wolfrum U, Vervoort R, Swaroop A and Wright AF (2005). RPGR ORF15 isoform co-localizes with RPGRIP1 at centrioles and basal bodies and interacts with nucleophosmin. Hum Mol Genet 14(9): 1183-1197.

Shu X, Black GC, Rice JM, Hart-Holden N, Jones A, O'Grady A, Ramsden S and Wright AF (2007). RPGR mutation analysis and disease: an update. Hum Mutat 28(4): 322-328.

Shu X, McDowall E, Brown AF and Wright AF (2008). The human retinitis pigmentosa GTPase regulator gene variant database. Hum Mutat 29(5): 605-608.

Siintola E, Topcu M, Aula N, Lohi H, Minassian BA, Paterson AD, Liu XQ, Wilson C, Lahtinen U, Anttonen AK and Lehesjoki AE (2007). The novel neuronal ceroid lipofuscinosis gene MFSD8 encodes a putative lysosomal transporter. Am J Hum Genet 81(1): 136-146.

Silberstein M, Tzemach A, Dovgolevsky N, Fishelson M, Schuster A and Geiger D (2006). Online system for faster multipoint linkage analysis via parallel execution on thousands of personal computers. Am J Hum Genet 78(6): 922-935.

Simeone A, Acampora D, Mallamaci A, Stornaiuolo A, D'Apice MR, Nigro V and Boncinelli E (1993). A vertebrate gene related to orthodenticle contains a homeodomain of the bicoid class and demarcates anterior neuroectoderm in the gastrulating mouse embryo. EMBO J 12(7): 2735-2747.

Simons DL, Boye SL, Hauswirth WW and Wu SM (2011). Gene therapy prevents photoreceptor death and preserves retinal function in a Bardet-Biedl syndrome mouse model. Proc Natl Acad Sci U S A 108(15): 6276-6281.

Simonsen A and Tooze SA (2009). Coordination of membrane events during autophagy by multiple class III PI3-kinase complexes. J Cell Biol 186(6): 773-782.

Simpson DA, Clark GR, Alexander S, Silvestri G and Willoughby CE (2011). Molecular diagnosis for heterogeneous genetic diseases with targeted high-throughput DNA sequencing applied to retinitis pigmentosa. J Med Genet 48(3): 145-151.

Singh HP, Jalali S, Hejtmancik JF and Kannabiran C (2006). Homozygous null mutations in the ABCA4 gene in two families with autosomal recessive retinal dystrophy. Am J Ophthalmol 141(5): 906-913.

Slate J, Gratten J, Beraldi D, Stapley J, Hale M and Pemberton JM (2009). Gene mapping in the wild with SNPs: guidelines and future directions. Genetica 136(1): 97-107.

Slavotinek AM, Stone EM, Mykytyn K, Heckenlively JR, Green JS, Heon E, Musarella MA, Parfrey PS, Sheffield VC and Biesecker LG (2000). Mutations in MKKS cause Bardet-Biedl syndrome. Nat Genet 26(1): 15-16.

Smerdon D (2000). Anatomy of the eye and orbit. Curr Anaesth Crit Care 11(6): 286-292.

Smith LM, Sanders JZ, Kaiser RJ, Hughes P, Dodd C, Connell CR, Heiner C, Kent SB and Hood LE (1986). Fluorescence detection in automated DNA sequence analysis. Nature 321(6071): 674-679.

Smith M, Whittock N, Searle A, Croft M, Brewer C and Cole M (2007). Phenotype of autosomal dominant cone-rod dystrophy due to the R838C mutation of the GUCY2D gene encoding retinal guanylate cyclase-1. Eye (Lond) 21(9): 1220-1225.

Sohocki MM, Sullivan LS, Mintz-Hittner HA, Birch D, Heckenlively JR, Freund CL, McInnes RR and Daiger SP (1998). A range of clinical phenotypes associated with mutations in CRX, a photoreceptor transcription-factor gene. Am J Hum Genet 63(5): 1307-1315.

Sohocki MM, Bowne SJ, Sullivan LS, Blackshaw S, Cepko CL, Payne AM, Bhattacharya SS, Khaliq S, Qasim Mehdi S, Birch DG, Harrison WR, Elder FF, Heckenlively JR and Daiger SP (2000). Mutations in a new photoreceptor-pineal gene on 17p cause Leber congenital amaurosis. Nat Genet 24(1): 79-83.

Song W, Gardner SA, Hovhannisyan H, Natalizio A, Weymouth KS, Chen W, Thibodeau I, Bogdanova E, Letovsky S, Willis A and Nagan N (2016). Exploring the landscape of pathogenic genetic variation in the ExAC population database: insights of relevance to variant classification. Genet Med 18(8): 850-854.

Song WK, Park KM, Kim HJ, Lee JH, Choi J, Chong SY, Shim SH, Del Priore LV and Lanza R (2015). Treatment of macular degeneration using embryonic stem cell-derived retinal

pigment epithelium: preliminary results in Asian patients. Stem Cell Reports 4(5): 860-872.

Sparrow JR, Hicks D and Hamel CP (2010a). The retinal pigment epithelium in health and disease. Curr Mol Med 10(9): 802-823.

Sparrow JR, Wu Y, Kim CY and Zhou J (2010b). Phospholipid meets all-trans-retinal: the making of RPE bisretinoids. J Lipid Res 51(2): 247-261.

Srilekha S, Arokiasamy T, Srikrupa NN, Umashankar V, Meenakshi S, Sen P, Kapur S and Soumittra N (2015). Homozygosity Mapping in Leber Congenital Amaurosis and Autosomal Recessive Retinitis Pigmentosa in South Indian Families. PLoS One 10(7): e0131679.

Stamellos KD, Shackelford JE, Shechter I, Jiang G, Conrad D, Keller GA and Krisans SK (1993). Subcellular localization of squalene synthase in rat hepatic cells. Biochemical and immunochemical evidence. J Biol Chem 268(17): 12825-12836.

Sterling P and Matthews G (2005). Structure and function of ribbon synapses. Trends Neurosci 28(1): 20-29.

Stockman A, Sharpe LT, Tufail A, Kell PD, Ripamonti C and Jeffery G (2007). The effect of sildenafil citrate (Viagra) on visual sensitivity. J Vis 7(8): 4.

Stoetzel C, Laurier V, Davis EE, Muller J, Rix S, Badano JL, Leitch CC, Salem N, Chouery E, Corbani S, Jalk N, Vicaire S, Sarda P, Hamel C, Lacombe D, Holder M, Odent S, Holder S, Brooks AS, Elcioglu NH, Silva ED, Rossillion B, Sigaudy S, de Ravel TJ, Lewis RA, Leheup B, Verloes A, Amati-Bonneau P, Megarbane A, Poch O, Bonneau D, Beales PL, Mandel JL, Katsanis N and Dollfus H (2006). BBS10 encodes a vertebrate-specific chaperonin-like protein and is a major BBS locus. Nat Genet 38(5): 521-524.

Stoetzel C, Muller J, Laurier V, Davis EE, Zaghloul NA, Vicaire S, Jacquelin C, Plewniak F, Leitch CC, Sarda P, Hamel C, de Ravel TJ, Lewis RA, Friederich E, Thibault C, Danse JM, Verloes A, Bonneau D, Katsanis N, Poch O, Mandel JL and Dollfus H (2007). Identification of a novel BBS gene (BBS12) highlights the major role of a vertebrate-specific branch of chaperonin-related proteins in Bardet-Biedl syndrome. Am J Hum Genet 80(1): 1-11.

Stone EA and Sidow A (2005). Physicochemical constraint violation by missense substitutions mediates impairment of protein function and disease severity. Genome Res 15(7): 978-986.

Stone EM (2007). Leber congenital amaurosis - a model for efficient genetic testing of heterogeneous disorders: LXIV Edward Jackson Memorial Lecture. Am J Ophthalmol 144(6): 791-811.

Strauss O (2005). The retinal pigment epithelium in visual function. Physiol Rev 85(3): 845-881.

Strettoi E and Pignatelli V (2000). Modifications of retinal neurons in a mouse model of. Proc Natl Acad Sci U S A 97(20): 11020-11025.

Stuck MW, Conley SM and Naash MI (2016). PRPH2/RDS and ROM-1: Historical context, current views and future considerations. Prog Retin Eye Res 52: 47-63.

Sturm RA and Larsson M (2009). Genetics of human iris colour and patterns. Pigment Cell Melanoma Res 22(5): 544-562.

Sturtevant AH (1913). The linear arrangement of six sex-linked factors in Drosophila, as shown by their mode of association. J. Exp. Zool. 14(1): 43-59.

Sugita Y and Tasaki K (1988). The activation of cones in scotopic and rods in photopic vision. Tohoku J Exp Med 156(4): 311-317.

Sugita Y, Araki F, Chaya T, Kawano K, Furukawa T and Miura K (2015). Role of the mouse retinal photoreceptor ribbon synapse in visual motion processing for optokinetic responses. PLoS One 10(5): e0124132.

Sullivan LS, Bowne SJ, Birch DG, Hughbanks-Wheaton D, Heckenlively JR, Lewis RA, Garcia CA, Ruiz RS, Blanton SH, Northrup H, Gire AI, Seaman R, Duzkale H, Spellicy CJ, Zhu J, Shankar SP and Daiger SP (2006a). Prevalence of disease-causing mutations in families with autosomal dominant retinitis pigmentosa: a screen of known genes in 200 families. Invest Ophthalmol Vis Sci 47(7): 3052-3064.

Sullivan LS, Bowne SJ, Seaman CR, Blanton SH, Lewis RA, Heckenlively JR, Birch DG, Hughbanks-Wheaton D and Daiger SP (2006b). Genomic rearrangements of the PRPF31 gene account for 2.5% of autosomal dominant retinitis pigmentosa. Invest Ophthalmol Vis Sci 47(10): 4579-4588.

Sun LW, Johnson RD, Langlo CS, Cooper RF, Razeen MM, Russillo MC, Dubra A, Connor TB, Jr., Han DP, Pennesi ME, Kay CN, Weinberg DV, Stepien KE and Carroll J (2016). Assessing Photoreceptor Structure in Retinitis Pigmentosa and Usher Syndrome. Invest Ophthalmol Vis Sci 57(6): 2428-2442.

Sun W, Gerth C, Maeda A, Lodowski DT, Van Der Kraak L, Saperstein DA, Héon E and Palczewski K (2007). Novel RDH12 mutations associated with Leber congenital amaurosis and cone-rod dystrophy: Biochemical and clinical evaluations. Vision Res 47(15): 2055-2066.

Sun X, Pawlyk B, Xu X, Liu X, Bulgakov OV, Adamian M, Sandberg MA, Khani SC, Tan MH, Smith AJ, Ali RR and Li T (2010). Gene therapy with a promoter targeting both rods and cones rescues retinal degeneration caused by AIPL1 mutations. Gene Ther 17(1): 117-131.

Sundin OH, Yang JM, Li Y, Zhu D, Hurd JN, Mitchell TN, Silva ED and Maumenee IH (2000). Genetic basis of total colourblindness among the Pingelapese islanders. Nat Genet 25(3): 289-293.

Suspitsin EN and Imyanitov EN (2016). Bardet-Biedl Syndrome. Mol Syndromol 7(2): 62-71.

Swaroop A, Wang QL, Wu W, Cook J, Coats C, Xu S, Chen S, Zack DJ and Sieving PA (1999). Leber congenital amaurosis caused by a homozygous mutation (R90W) in the homeodomain of the retinal transcription factor CRX: direct evidence for the involvement of CRX in the development of photoreceptor function. Hum Mol Genet 8(2): 299-305.

Swaroop A, Kim D and Forrest D (2010). Transcriptional regulation of photoreceptor development and homeostasis in the mammalian retina. Nat Rev Neurosci 11(8): 563-576.

Tanackovic G, Ransijn A, Ayuso C, Harper S, Berson EL and Rivolta C (2011). A missense mutation in PRPF6 causes impairment of pre-mRNA splicing and autosomal-dominant retinitis pigmentosa. Am J Hum Genet 88(5): 643-649.

Tang Z, Lin MG, Stowe TR, Chen S, Zhu M, Stearns T, Franco B and Zhong Q (2013). Autophagy promotes primary ciliogenesis by removing OFD1 from centriolar satellites. Nature 502(7470): 254-257.

Tasdemir E, Maiuri MC, Galluzzi L, Vitale I, Djavaheri-Mergny M, D'Amelio M, Criollo A, Morselli E, Zhu C, Harper F, Nannmark U, Samara C, Pinton P, Vicencio JM, Carnuccio R, Moll UM, Madeo F, Paterlini-Brechot P, Rizzuto R, Szabadkai G, Pierron G, Blomgren K, Tavernarakis N, Codogno P, Cecconi F and Kroemer G (2008). Regulation of autophagy by cytoplasmic p53. Nat Cell Biol 10(6): 676-687.

Tavtigian SV, Deffenbaugh AM, Yin L, Judkins T, Scholl T, Samollow PB, de Silva D, Zharkikh A and Thomas A (2006). Comprehensive statistical study of 452 BRCA1 missense substitutions with classification of eight recurrent substitutions as neutral. J Med Genet 43(4): 295-305.

Tee JJ, Smith AJ, Hardcastle AJ and Michaelides M (2016). RPGR-associated retinopathy: clinical features, molecular genetics, animal models and therapeutic options. Br J Ophthalmol 100(8): 1022-1027.

Tepass U and Knust E (1990). Phenotypic and developmental analysis of mutations at therms locus, a gene required for the development of epithelia wiNdrows melanomas. Roux Arch Dev Biol 199(4): 189-206.

Tepass U, Tanentzapf G, Ward R and Fehon R (2001). Epithelial cell polarity and cell junctions in Drosophila. Annu Rev Genet 35: 747-784.

Thauvin-Robinet C, Cossee M, Cormier-Daire V, Van Maldergem L, Toutain A, Alembik Y, Bieth E, Layet V, Parent P, David A, Goldenberg A, Mortier G, Heron D, Sagot P, Bouvier AM, Huet F, Cusin V, Donzel A, Devys D, Teyssier JR and Faivre L (2006). Clinical, molecular, and genotype-phenotype correlation studies from 25 cases of oral-facial-digital syndrome type 1: a French and Belgian collaborative study. J Med Genet 43(1): 54-61.

Thiadens AA, den Hollander AI, Roosing S, Nabuurs SB, Zekveld-Vroon RC, Collin RW, De Baere E, Koenekoop RK, van Schooneveld MJ, Strom TM, van Lith-Verhoeven JJ, Lotery AJ, van Moll-Ramirez N, Leroy BP, van den Born LI, Hoyng CB, Cremers FP and Klaver

CC (2009a). Homozygosity mapping reveals PDE6C mutations in patients with early-onset cone photoreceptor disorders. Am J Hum Genet 85(2): 240-247.

Thiadens AA, Slingerland NW, Roosing S, van Schooneveld MJ, van Lith-Verhoeven JJ, van Moll-Ramirez N, van den Born LI, Hoyng CB, Cremers FP and Klaver CC (2009b). Genetic etiology and clinical consequences of complete and incomplete achromatopsia. Ophthalmol 116(10): 1984-1989.e1981.

Thiadens AAHJ, den Hollander AI, Roosing S, Nabuurs SB, Zekveld-Vroon RC, Collin RWJ, De Baere E, Koenekoop RK, van Schooneveld MJ, Strom TM, van Lith-Verhoeven JJC, Lotery AJ, van Moll-Ramirez N, Leroy BP, van den Born LI, Hoyng CB, Cremers FPM and Klaver CCW (2009c). Homozygosity Mapping Reveals PDE6C Mutations in Patients with Early-Onset Cone Photoreceptor Disorders. Am J Hum Genet 85(2): 240-247.

Thiadens AAHJ, Somervuo V, van den Born LI, Roosing S, van Schooneveld MJ, Kuijpers RWAM, van Moll-Ramirez N, Cremers FPM, Hoyng CB and Klaver CCW (2010). Progressive Loss of Cones in Achromatopsia: An Imaging Study Using Spectral-Domain Optical Coherence Tomography. Invest Ophthalmol Vis Sci 51(11): 5952-5957.

Thiadens AAHJ, Phan TML, Zekveld-Vroon RC, Leroy BP, Van Den Born LI, Hoyng CB, Klaver CCW, Roosing S, Pott JWR, Van Schooneveld MJ, Van Moll-Ramirez N, Van Genderen MM, Boon CJF, Den Hollander AI, Bergen AAB, De Baere E, Cremers FPM and Lotery AJ (2012). Clinical course, genetic etiology, and visual outcome in cone and cone-rod dystrophy. Ophthalmol 119(4): 819-826.

Thompson DA, Gyürüs Pt, Fleischer LL, Bingham EL, McHenry CL, Apfelstedt–Sylla E, Zrenner E, Lorenz B, Richards JE, Jacobson SG, Sieving PA and Gal A (2000). Genetics and Phenotypes of RPE65 Mutations in Inherited Retinal Degeneration. Invest Ophthalmol Vis Sci 41(13): 4293-4299.

Thompson DA, Li Y, McHenry CL, Carlson TJ, Ding X, Sieving PA, Apfelstedt-Sylla E and Gal A (2001). Mutations in the gene encoding lecithin retinol acyltransferase are associated with early-onset severe retinal dystrophy. Nat Genet 28(2): 123-124.

Thompson DA and Gal A (2003). Genetic defects in vitamin A metabolism of the retinal pigment epithelium. Dev Ophthalmol 37: 141-154.

Thompson DA, Janecke AR, Lange J, Feathers KL, Hubner CA, McHenry CL, Stockton DW, Rammesmayer G, Lupski JR, Antinolo G, Ayuso C, Baiget M, Gouras P, Heckenlively JR, den Hollander A, Jacobson SG, Lewis RA, Sieving PA, Wissinger B, Yzer S, Zrenner E, Utermann G and Gal A (2005). Retinal degeneration associated with RDH12 mutations results from decreased 11-cis retinal synthesis due to disruption of the visual cycle. Hum Mol Genet 14(24): 3865-3875.

Thoreen CC, Kang SA, Chang JW, Liu Q, Zhang J, Gao Y, Reichling LJ, Sim T, Sabatini DM and Gray NS (2009). An ATP-competitive mammalian target of rapamycin inhibitor reveals rapamycin-resistant functions of mTORC1. J Biol Chem 284(12): 8023-8032.

Tian F, Sun D and Zhang Y (2008). Establishment of paternity testing system using microsatellite markers in Chinese Holstein. J Genet Genomics 35(5): 279-284.

Tiwari A, Bahr A, Bähr L, Fleischhauer J, Zinkernagel MS, Winkler N, Barthelmes D, Berger L, Gerth-Kahlert C, Neidhardt J and Berger W (2016). Next generation sequencing based identification of disease-associated mutations in Swiss patients with retinal dystrophies. Sci Rep 6.

tom Dieck S and Brandstatter JH (2006). Ribbon synapses of the retina. Cell Tissue Res 326(2): 339-346.

Tooze SA and Yoshimori T (2010). The origin of the autophagosomal membrane. Nat Cell Biol 12(9): 831-835.

Torre V, Matthews HR and Lamb TD (1986). Role of calcium in regulating the cyclic GMP cascade of phototransduction in retinal rods. Proc Natl Acad Sci U S A 83(18): 7109-7113.

Tory K, Lacoste T, Burglen L, Moriniere V, Boddaert N, Macher MA, Llanas B, Nivet H, Bensman A, Niaudet P, Antignac C, Salomon R and Saunier S (2007). High NPHP1 and NPHP6 mutation rate in patients with Joubert syndrome and nephronophthisis: potential epistatic effect of NPHP6 and AHI1 mutations in patients with NPHP1 mutations. J Am Soc Nephrol 18(5): 1566-1575.

Tosi J, Tsui I, Lima LH, Wang NK and Tsang SH (2009). Case report: autofluorescence imaging and phenotypic variance in a sibling pair with early-onset retinal dystrophy due to defective CRB1 function. Curr Eye Res 34(5): 395-400.

Tozawa R, Ishibashi S, Osuga J, Yagyu H, Oka T, Chen Z, Ohashi K, Perrey S, Shionoiri F, Yahagi N, Harada K, Gotoda T, Yazaki Y and Yamada N (1999). Embryonic lethality and defective neural tube closure in mice lacking squalene synthase. J Biol Chem 274(43): 30843-30848.

Tsang SH, Burns ME, Calvert PD, Gouras P, Baylor DA, Goff SP and Arshavsky VY (1998). Role for the target enzyme in deactivation of photoreceptor G protein in vivo. Science 282(5386): 117-121.

Tsang SH, Tsui I, Chou CL, Zernant J, Haamer E, Iranmanesh R, Tosi J and Allikmets R (2008). A novel mutation and phenotypes in phosphodiesterase 6 deficiency. Am J Ophthalmol 146(5): 780-788.

Tsurusaki Y, Kosho T, Hatasaki K, Narumi Y, Wakui K, Fukushima Y, Doi H, Saitsu H, Miyake N and Matsumoto N (2013). Exome sequencing in a family with an X-linked lethal malformation syndrome: clinical consequences of hemizygous truncating OFD1 mutations in male patients. Clin Genet 83(2): 135-144.

Tsybovsky Y, Molday RS and Palczewski K (2010). The ATP-Binding Cassette Transporter ABCA4: Structural and Functional Properties and Role in Retinal Disease. Adv Exp Med Biol 703: 105-125.

Tucker BA, Park IH, Qi SD, Klassen HJ, Jiang C, Yao J, Redenti S, Daley GQ and Young MJ (2011). Transplantation of adult mouse iPS cell-derived photoreceptor precursors restores retinal structure and function in degenerative mice. PLoS One 6(4): e18992.

Tucker CL, Ramamurthy V, Pina AL, Loyer M, Dharmaraj S, Li Y, Maumenee IH, Hurley JB and Koenekoop RK (2004). Functional analyses of mutant recessive GUCY2D alleles identified in Leber congenital amaurosis patients: protein domain comparisons and dominant negative effects. Mol Vis 10: 297-303.

Tuson M, Marfany G and Gonzalez-Duarte R (2004). Mutation of CERKL, a novel human ceramide kinase gene, causes autosomal recessive retinitis pigmentosa (RP26). Am J Hum Genet 74(1): 128-138.

Udar N, Yelchits S, Chalukya M, Yellore V, Nusinowitz S, Silva-Garcia R, Vrabec T, Hussles Maumenee I, Donoso L and Small KW (2003). Identification of GUCY2D gene mutations in CORD5 families and evidence of incomplete penetrance. Hum Mutat 21(2): 170-171.

Ugur Iseri SA, Durlu YK and Tolun A (2010). A novel recessive GUCY2D mutation causing cone-rod dystrophy and not Leber's congenital amaurosis. Eur J Hum Genet 18(10): 1121-1126.

Valente EM, Silhavy JL, Brancati F, Barrano G, Krishnaswami SR, Castori M, Lancaster MA, Boltshauser E, Boccone L, Al-Gazali L, Fazzi E, Signorini S, Louie CM, Bellacchio E, Bertini E, Dallapiccola B and Gleeson JG (2006). Mutations in CEP290, which encodes a centrosomal protein, cause pleiotropic forms of Joubert syndrome. Nat Genet 38(6): 623-625.

Vallespin E, Cantalapiedra D, Riveiro-Alvarez R, Wilke R, Aguirre-Lamban J, Avila-Fernandez A, Lopez-Martinez MA, Gimenez A, Trujillo-Tiebas MJ, Ramos C and Ayuso C (2007a). Mutation screening of 299 Spanish families with retinal dystrophies by Leber congenital amaurosis genotyping microarray. Invest Ophthalmol Vis Sci 48(12): 5653-5661.

Vallespin E, Lopez-Martinez MA, Cantalapiedra D, Riveiro-Alvarez R, Aguirre-Lamban J, Avila-Fernandez A, Villaverde C, Trujillo-Tiebas MJ and Ayuso C (2007b). Frequency of CEP290 c.2991_1655A>G mutation in 175 Spanish families affected with Leber congenital amaurosis and early-onset retinitis pigmentosa. Mol Vis 13: 2160-2162.

Valverde D, Riveiro-Alvarez R, Aguirre-Lamban J, Baiget M, Carballo M, Antiñolo G, Millán JM, Sandoval BG and Ayuso C (2007). Spectrum of the ABCA4 Gene Mutations Implicated in Severe Retinopathies in Spanish Patients. Invest Ophthalmol Vis Sci 48(3): 985-990.

Valverde D, Pereiro I, Vallespin E, Ayuso C, Borrego S and Baiget M (2009). Complexity of phenotype-genotype correlations in Spanish patients with RDH12 mutations. Invest Ophthalmol Vis Sci 50(3): 1065-1068.

van de Pavert SA, Sanz AS, Aartsen WM, Vos RM, Versteeg I, Beck SC, Klooster J, Seeliger MW and Wijnholds J (2007). Crb1 is a determinant of retinal apical Muller glia cell features. Glia 55(14): 1486-1497.

van Dijk EL, Auger H, Jaszczyszyn Y and Thermes C (2014). Ten years of next-generation sequencing technology. Trends Genet 30(9): 418-426.

van Dijk J, Rogowski K, Miro J, Lacroix B, Edde B and Janke C (2007). A targeted multienzyme mechanism for selective microtubule polyglutamylation. Mol Cell 26(3): 437-448.

van Dijk J, Miro J, Strub JM, Lacroix B, van Dorsselaer A, Edde B and Janke C (2008). Polyglutamylation is a post-translational modification with a broad range of substrates. J Biol Chem 283(7): 3915-3922.

Van Ghelue M, Eriksen HL, Ponjavic V, Fagerheim T, Andreasson S, Forsman-Semb K, Sandgren O, Holmgren G and Tranebjaerg L (2000). Autosomal dominant cone-rod dystrophy due to a missense mutation (R838C) in the guanylate cyclase 2D gene (GUCY2D) with preserved rod function in one branch of the family. Ophthalmic Genet 21(4): 197-209.

van Huet RA, Estrada-Cuzcano A, Banin E, Rotenstreich Y, Hipp S, Kohl S, Hoyng CB, den Hollander AI, Collin RW and Klevering BJ (2013). Clinical characteristics of rod and cone photoreceptor dystrophies in patients with mutations in the C8orf37 gene. Invest Ophthalmol Vis Sci 54(7): 4683-4690.

van Reeuwijk J, Grewal PK, Salih MA, Beltran-Valero de Bernabe D, McLaughlan JM, Michielse CB, Herrmann R, Hewitt JE, Steinbrecher A, Seidahmed MZ, Shaheed MM, Abomelha A, Brunner HG, van Bokhoven H and Voit T (2007). Intragenic deletion in the LARGE gene causes Walker-Warburg syndrome. Hum Genet 121(6): 685-690.

van Wijk E, Pennings RJ, te Brinke H, Claassen A, Yntema HG, Hoefsloot LH, Cremers FP, Cremers CW and Kremer H (2004). Identification of 51 novel exons of the Usher syndrome type 2A (USH2A) gene that encode multiple conserved functional domains and that are mutated in patients with Usher syndrome type II. Am J Hum Genet 74(4): 738-744.

Vecino E, Rodriguez FD, Ruzafa N, Pereiro X and Sharma SC (2016). Glia–neuron interactions in the mammalian retina. Prog Retin Eye Res 51: 1-40.

Vervoort R, Lennon A, Bird AC, Tulloch B, Axton R, Miano MG, Meindl A, Meitinger T, Ciccodicola A and Wright AF (2000). Mutational hot spot within a new RPGR exon in X-linked retinitis pigmentosa. Nat Genet 25(4): 462-466.

Villanueva A (2014). Whole Exome Sequencing of a Dominant Retinitis Pigmentosa Family Identifies a Novel Deletion in PRPF31. 55(4): 2121-2129.

Vincent A, Forster N, Maynes JT, Paton TA, Billingsley G, Roslin NM, Ali A, Sutherland J, Wright T, Westall CA, Paterson AD, Marshall CR and Heon E (2014). OTX2 mutations cause autosomal dominant pattern dystrophy of the retinal pigment epithelium. J Med Genet 51(12): 797-805.

Vincent A, Ng J, Gerth-Kahlert C, Tavares E, Maynes JT, Wright T, Tiwari A, Tumber A, Li S, Hanson JV, Bahr A, MacDonald H, Bahr L, Westall C, Berger W, Cremers FP, den Hollander AI and Heon E (2016). Biallelic Mutations in CRB1 Underlie Autosomal Recessive Familial Foveal Retinoschisis. Invest Ophthalmol Vis Sci 57(6): 2637-2646.

Vuillaumier-Barrot S, Bouchet-Seraphin C, Chelbi M, Eude-Caye A, Charluteau E, Besson C, Quentin S, Devisme L, Le Bizec C, Landrieu P, Goldenberg A, Maincent K, Loget P, Boute O, Gilbert-Dussardier B, Encha-Razavi F, Gonzales M, Grandchamp B and Seta N (2011). Intragenic rearrangements in LARGE and POMGNT1 genes in severe dystroglycanopathies. Neuromuscul Disord 21(11): 782-790.

Walia S, Fishman GA, Jacobson SG, Aleman TS, Koenekoop RK, Traboulsi EI, Weleber RG, Pennesi ME, Heon E, Drack A, Lam BL, Allikmets R and Stone EM (2010). Visual acuity in patients with Leber's congenital amaurosis and early childhood-onset retinitis pigmentosa. Ophthalmology 117(6): 1190-1198.

Wang AL, Lukas TJ, Yuan M, Du N, Tso MO and Neufeld AH (2009a). Autophagy, exosomes and drusen formation in age-related macular degeneration. Autophagy 5(4): 563-564.

Wang DY, Chan WM, Tam POS, Baum L, Lam DSC, Chong KKL, Fan BJ and Pang CP (2005). Gene mutations in retinitis pigmentosa and their clinical implications. Clinica Chimica Acta 351(1–2): 5-16.

Wang H, den Hollander AI, Moayedi Y, Abulimiti A, Li Y, Collin RW, Hoyng CB, Lopez I, Abboud EB, Al-Rajhi AA, Bray M, Lewis RA, Lupski JR, Mardon G, Koenekoop RK and Chen R (2009b). Mutations in SPATA7 cause Leber congenital amaurosis and juvenile retinitis pigmentosa. Am J Hum Genet 84(3): 380-387.

Wang J, Whiteman MW, Lian H, Wang G, Singh A, Huang D and Denmark T (2009c). A non-canonical MEK/ERK signaling pathway regulates autophagy via regulating Beclin 1. J Biol Chem 284(32): 21412-21424.

Wang J, Chen X, Wang F, Zhang J, Li P, Li Z, Xu J, Gao F, Jin C, Tian H, Zhang J, Li W, Lu L and Xu GT (2016a). OFD1, as a Ciliary Protein, Exhibits Neuroprotective Function in Photoreceptor Degeneration Models. PLoS One 11(5).

Wang JS and Kefalov VJ (2011). The cone-specific visual cycle. Prog Retin Eye Res 30(2): 115-128.

Wang M, Gan D, Huang X and Xu G (2016b). Novel compound heterozygous mutations in CNGA1in a Chinese family affected with autosomal recessive retinitis pigmentosa by targeted sequencing. BMC Ophthalmol 16.

Wang P, Guo X and Zhang Q (2007). Further evidence of autosomal-dominant Leber congenital amaurosis caused by heterozygous CRX mutation. Graefes Arch Clin Exp Ophthalmol 245(9): 1401-1402.

Wang Y, Huang C, Zhang H and Wu R (2015). Autophagy in glaucoma: Crosstalk with apoptosis and its implications. Brain Res Bull 117: 1-9.

Warr A, Robert C, Hume D, Archibald A, Deeb N and Watson M (2015). Exome Sequencing: Current and Future Perspectives. G3: Genes|Genomes|Genetics 5(8): 1543-1550.

Wassle H (2004). Parallel processing in the mammalian retina. Nat Rev Neurosci 5(10): 747-757.

Watson CM, El-Asrag M, Parry DA, Morgan JE, Logan CV, Carr IM, Sheridan E, Charlton R, Johnson CA, Taylor G, Toomes C, McKibbin M, Inglehearn CF and Ali M (2014). Mutation screening of retinal dystrophy patients by targeted capture from tagged pooled DNAs and next generation sequencing. PLoS One 9(8): e104281.

Watson J and Crick F (1953). Molecular structure of nucleic acids. Nature(171): 709-756

Watson M (2014). Illuminating the future of DNA sequencing. Genome Biol 15(2): 108-108.

Weaver M and Hogan B (2001). Powerful ideas driven by simple tools: lessons from experimental embryology. Nat Cell Biol 3(7): E165-E167.

Webb TR, Parfitt DA, Gardner JC, Martinez A, Bevilacqua D, Davidson AE, Zito I, Thiselton DL, Ressa JHC, Apergi M, Schwarz N, Kanuga N, Michaelides M, Cheetham ME, Gorin MB and Hardcastle AJ (2012). Deep intronic mutation in OFD1, identified by targeted genomic next-generation sequencing, causes a severe form of X-linked retinitis pigmentosa (RP23). Hum Mol Genet 21(16): 3647-3654.

Weidberg H, Shvets E and Elazar Z (2011). Biogenesis and cargo selectivity of autophagosomes. Annu Rev Biochem 80: 125-156.

Weigell-Weber M, Fokstuen S, Torok B, Niemeyer G, Schinzel A and Hergersberg M (2000). Codons 837 and 838 in the retinal guanylate cyclase gene on chromosome 17p: hot spots for mutations in autosomal dominant cone-rod dystrophy? Arch Ophthalmol 118(2): 300.

Weisschuh N, Mayer AK, Strom TM, Kohl S, Glockle N, Schubach M, Andreasson S, Bernd A, Birch DG, Hamel CP, Heckenlively JR, Jacobson SG, Kamme C, Kellner U, Kunstmann E, Maffei P, Reiff CM, Rohrschneider K, Rosenberg T, Rudolph G, Vamos R, Varsanyi B, Weleber RG and Wissinger B (2016). Mutation Detection in Patients with Retinal Dystrophies Using Targeted Next Generation Sequencing. PLoS One 11(1): e0145951.

Weleber R, Francis P, Trzupek K and al. e (2013). Leber Congenital Amaurosis. GeneReviews® [Internet]. Seattle (WA): 1993-2016. R Pagon, M Adam, H Ardinger and e al. University of Washington, Seattle; .

Weleber RG, Michaelides M, Trzupek KM, Stover NB and Stone EM (2011). The Phenotype of Severe Early Childhood Onset Retinal Dystrophy (SECORD) from Mutation of RPE65 and Differentiation from Leber Congenital Amaurosis. Invest Ophthalmol Vis Sci 52(1): 292-302.

Wentzensen IM, Johnston JJ, Patton JH, Graham JM, Sapp JC and Biesecker LG (2016). Exome sequencing identifies a mutation in OFD1 in a male with Joubert syndrome, orofaciodigital spectrum anomalies and complex polydactyly. Hum Genome Var 3: 15069.

Wilkie SE, Newbold RJ, Deery E, Walker CE, Stinton I, Ramamurthy V, Hurley JB, Bhattacharya SS, Warren MJ and Hunt DM (2000). Functional characterization of missense mutations at codon 838 in retinal guanylate cyclase correlates with disease severity in patients with autosomal dominant cone-rod dystrophy. Hum Mol Genet 9(20): 3065-3073.

Willis TA, Potrata B, Ahmed M, Hewison J, Gale R, Downey L and McKibbin M (2013). Understanding of and attitudes to genetic testing for inherited retinal disease: a patient perspective. Br J Ophthalmol 97(9): 1148-1154.

Wright AF, Chakarova CF, Abd El-Aziz MM and Bhattacharya SS (2010). Photoreceptor degeneration: genetic and mechanistic dissection of a complex trait. Nat Rev Genet 11(4): 273-284.

Xiao X, Guo X, Jia X, Li S, Wang P and Zhang Q (2011). A recurrent mutation in GUCY2D associated with autosomal dominant cone dystrophy in a Chinese family. Mol Vis 17: 3271-3278.

Xilouri M, Brekk OR, Polissidis A, Chrysanthou-Piterou M, Kloukina I and Stefanis L (2016). Impairment of chaperone-mediated autophagy induces dopaminergic neurodegeneration in rats. Autophagy: 0.

Xu F, Dong F, Li H, Li X, Jiang R and Sui R (2013). Phenotypic characterization of a Chinese family with autosomal dominant cone-rod dystrophy related to GUCY2D. Doc Ophthalmol 126(3): 233-240.

Xu W, Dai H, Lu T, Zhang X, Dong B and Li Y (2011). Seven novel mutations in the long isoform of the USH2A gene in Chinese families with nonsyndromic retinitis pigmentosa and Usher syndrome Type II. Mol Vis 17: 1537-1552.

Yamashita T, Liu J, Gao J, LeNoue S, Wang C, Kaminoh J, Bowne SJ, Sullivan LS, Daiger SP, Zhang K, Fitzgerald ME, Kefalov VJ and Zuo J (2009). Essential and synergistic roles of RP1 and RP1L1 in rod photoreceptor axoneme and retinitis pigmentosa. J Neurosci 29(31): 9748-9760.

Yang RB, Robinson SW, Xiong WH, Yau KW, Birch DG and Garbers DL (1999). Disruption of a retinal guanylyl cyclase gene leads to cone-specific dystrophy and paradoxical rod behavior. J Neurosci 19(14): 5889-5897.

Yang Z, Peachey NS, Moshfeghi DM, Thirumalaichary S, Chorich L, Shugart YY, Fan K and Zhang K (2002). Mutations in the RPGR gene cause X-linked cone dystrophy. Hum Mol Genet 11(5): 605-611.

Yang Z, Chen Y, Lillo C, Chien J, Yu Z, Michaelides M, Klein M, Howes KA, Li Y, Kaminoh Y, Chen H, Zhao C, Chen Y, Al-Sheikh YT, Karan G, Corbeil D, Escher P, Kamaya S, Li C, Johnson S, Frederick JM, Zhao Y, Wang C, Cameron DJ, Huttner WB, Schorderet DF, Munier FL, Moore AT, Birch DG, Baehr W, Hunt DM, Williams DS and Zhang K (2008). Mutant prominin 1 found in patients with macular degeneration disrupts photoreceptor disk morphogenesis in mice. J Clin Invest 118(8): 2908-2916.

Yao J, Jia L, Shelby SJ, Ganios AM, Feathers K, Thompson DA and Zacks DN (2014). Circadian and noncircadian modulation of autophagy in photoreceptors and retinal pigment epithelium. Invest Ophthalmol Vis Sci 55(5): 3237-3246.

Yates JR, Sepp T, Matharu BK, Khan JC, Thurlby DA, Shahid H, Clayton DG, Hayward C, Morgan J, Wright AF, Armbrecht AM, Dhillon B, Deary IJ, Redmond E, Bird AC and Moore AT (2007). Complement C3 variant and the risk of age-related macular degeneration. N Engl J Med 357(6): 553-561.

Yau K-W and Hardie RC (2009). Phototransduction Motifs and Variations. Cell 139(2): 246-264.

Yokochi M, Li D, Horiguchi M and Kishi S (2012). Inverse pattern of photoreceptor abnormalities in retinitis pigmentosa and cone-rod dystrophy. Doc Ophthalmol 125(3): 211-218.

Yoon JH, Her S, Kim M, Jang IS and Park J (2012). The expression of damage-regulated autophagy modulator 2 (DRAM2) contributes to autophagy induction. Mol Biol Rep 39(2): 1087-1093.

Yorimitsu T and Klionsky DJ (2005). Autophagy: molecular machinery for self-eating. Cell Death Differ 12 Suppl 2: 1542-1552.

Yoshida S, Yamaji Y, Yoshida A, Kuwahara R, Yamamoto K, Kubata T and Ishibashi T (2006). Novel triple missense mutations of GUCY2D gene in Japanese family with cone-rod dystrophy: possible use of genotyping microarray. Mol Vis 12: 1558-1564.

Yoshimori T (2004). Autophagy: a regulated bulk degradation process inside cells. Biochem Biophys Res Commun 313(2): 453-458.

Young RW and Bok D (1969). Participation of the retinal pigment epithelium in the rod outer segment renewal process. J Cell Biol 42(2): 392-403.

Yu Y, Reynolds R, Fagerness J, Rosner B, Daly MJ and Seddon JM (2011). Association of Variants in the LIPC and ABCA1 Genes with Intermediate and Large Drusen and Advanced Age-Related Macular Degeneration. Invest Ophthalmol Vis Sci 52(7): 4663-4670.

Yucel-Yilmaz D, Tarlan B, Kiratli H and Ozgul RK (2014). Genome-wide homozygosity mapping in families with leber congenital amaurosis identifies mutations in AIPL1 and RDH12 genes. DNA Cell Biol 33(12): 876-883.

Yvon C, Ramsden CM, Lane A, Powner MB, da Cruz L, Coffey PJ and Carr A-JF (2015). Using Stem Cells to Model Diseases of the Outer Retina. Comput. Struct. Biotechnol. J. 13: 382-389.

Yzer S, Fishman GA, Racine J, Al-Zuhaibi S, Chakor H, Dorfman A, Szlyk J, Lachapelle P, van den Born LI, Allikmets R, Lopez I, Cremers FP and Koenekoop RK (2006). CRB1 heterozygotes with regional retinal dysfunction: implications for genetic testing of leber congenital amaurosis. Invest Ophthalmol Vis Sci 47(9): 3736-3744.

Zahn JR (1978). Incidence and characteristics of voluntary nystagmus. J Neurol Neurosurg Psychiatry 41(7): 617-623.

Zareparsi S, Branham KE, Li M, Shah S, Klein RJ, Ott J, Hoh J, Abecasis GR and Swaroop A (2005). Strong association of the Y402H variant in complement factor H at 1q32 with susceptibility to age-related macular degeneration. Am J Hum Genet 77(1): 149-153.

Zelhof AC, Hardy RW, Becker A and Zuker CS (2006). Transforming the architecture of compound eyes. Nature 443(7112): 696-699.

Zelinger L, Cideciyan AV, Kohl S, Schwartz SB, Rosenmann A, Eli D, Sumaroka A, Roman AJ, Luo X, Brown C, Rosin B, Blumenfeld A, Wissinger B, Jacobson SG, Banin E and Sharon D (2015). Genetics and Disease Expression in the CNGA3 Form of Achromatopsia: Steps on the Path to Gene Therapy. Ophthalmol 122(5): 997-1007.

Zhang N, Tsybovsky Y, Kolesnikov AV, Rozanowska M, Swider M, Schwartz SB, Stone EM, Palczewska G, Maeda A, Kefalov VJ, Jacobson SG, Cideciyan AV and Palczewski K (2015a). Protein misfolding and the pathogenesis of ABCA4-associated retinal degenerations. Hum Mol Genet 24(11): 3220-3237.

Zhang Q, Zulfiqar F, Xiao X, Riazuddin SA, Ahmad Z, Caruso R, MacDonald I, Sieving P, Riazuddin S and Hejtmancik JF (2007). Severe retinitis pigmentosa mapped to 4p15 and associated with a novel mutation in the PROM1 gene. Hum Genet 122(3-4): 293-299.

Zhang X, Liu H, Zhang Y, Qiao Y, Miao S, Wang L, Zhang J, Zong S and Koide SS (2003). A novel gene, RSD-3/HSD-3.1, encodes a meiotic-related protein expressed in rat and human testis. J Mol Med (Berl) 81(6): 380-387.

Zhang Y, Yu Z, Ban R, Zhang H, Iqbal F, Zhao A, Li A and Shi Q (2015b). DeAnnCNV: a tool for online detection and annotation of copy number variations from whole-exome sequencing data. Nucleic Acids Res 43(W1): W289-W294.

Zhao M, Wang Q, Wang Q, Jia P and Zhao Z (2013a). Computational tools for copy number variation (CNV) detection using next-generation sequencing data: features and perspectives. BMC Bioinformatics 14(Suppl 11): S1.

Zhao X, Ren Y, Zhang X, Chen C, Dong B and Li Y (2013b). A novel GUCY2D mutation in a Chinese family with dominant cone dystrophy. Mol Vis 19: 1039-1046.

Zhao Y, Hong DH, Pawlyk B, Yue G, Adamian M, Grynberg M, Godzik A and Li T (2003). The retinitis pigmentosa GTPase regulator (RPGR)-interacting protein: Subserving RPGR function and participating in disk morphogenesis. Proc Natl Acad Sci U S A 100(7): 3965-3970.

Zhao Y, Hosono K, Suto K, Ishigami C, Arai Y, Hikoya A, Hirami Y, Ohtsubo M, Ueno S, Terasaki H, Sato M, Nakanishi H, Endo S, Mizuta K, Mineta H, Kondo M, Takahashi M, Minoshima S and Hotta Y (2014). The first USH2A mutation analysis of Japanese autosomal recessive retinitis pigmentosa patients: a totally different mutation profile with the lack of frequent mutations found in Caucasian patients. J Hum Genet 59(9): 521-528.

Zito I, Downes SM, Patel RJ, Cheetham ME, Ebenezer ND, Jenkins SA, Bhattacharya SS, Webster AR, Holder GE, Bird AC, Bamiou DE and Hardcastle AJ (2003). RPGR mutation associated with retinitis pigmentosa, impaired hearing, and sinorespiratory infections. J Med Genet 40(8): 609-615.

Appendix

Appendix 1- List of UNIX commands used in targeted NGS and WES analysis

1.1 Alignment (Novoalign/Bowtie2)

$ novoalign -c 12 -d <path> b37/human_g1k_v37.nix -f sample_R1_001.fastq.gz sample_R2_001.fastq .gz -o SAM $'@RG\tID:sample_novoID\tSM:sample\tPL: ILLUMINA\tLB: sample_ exome' -k –K mismatches_sample_novoID.txt 2> novostats_sample_novoID.txt > sample_novoID.sam

$ <path> /bowtie2- version no /bowtie2 -x <path> /ucsc.hg19.idx -p 6 -q -1 <path> Sample_R1.fastq -2 <path> Sample_R2.fastq -S <path> Sample.sam --sam-rg ID: IN--sam-rg SM:IN --sam-rg PL:Illumina --sam-rg PU:HiSeq

1.2 Remove reads which don't map uniquely

$ sed '/XS:/d' <path> Sample.sam > <path> Sample_uniqueAlignment.sam

1.3 Sorting and idexing alignment sam file (Samtools or Picard)

$ <path> /samtools-version no/samtools view -bt <path> /DataFiles/ucsc.hg19.fasta.fai <path> Sample_ uniqueAlignment.sam > Sample_uniqueAlignment.bam

$ <path> /samtools-version no/samtools sort <path> Sample_uniqueAlignment.bam <path> Sample_ uniqueAlignment_sort

$ <path> /samtools-version no/samtools index <path> Sample_uniqueAlignment_sort.bam

$ java –Xmx8g -jar <path> /picard/picard-tools- version no/SortSam.jar I= Sample_uniqueAlignment .sam O= Sample_uniqueAlignment_sort.bam SO=coordinate CREATE_INDEX=TRUE

1.4 Remove duplicates (Picard)

$ java –Xmx8g -jar <path> /picard/picard-tools- version no/MarkDuplicates.jar I= <path> Sample_unique Alignment_sort.bam O= <path> Sample_uniqueAlignment_sort.rmdups.bam M=Sample. rmdups. metrics CREATE_INDEX=TRUE

Alternative

$ java -Xmx8g -jar <path> /picard/picard-tools- version no/MarkDuplicates.jar INPUT= <path> Sample_ uniqueAlignment_sort.bam REMOVE_DUPLICATES=true VALIDATION_STRINGENCY =LENIENT AS=true METRICS_FILE= Sample_uniqueAlignment_sort_metrics_file.dups OUTPUT= <path> Sample _uniqueAlignment_sort.rmdups.bam

1.5 Create indel realigner targets (GATK)

$ java -Xmx8g -jar <path>/GenomeAnalysisTK- version no /GenomeAnalysisTK.jar -T Realigner TargetCreator -R <path> /human_g1k_ v37.fasta –known <path> /b37/1000G_phase1. indels.b37.vcf -known <path> /Mills_and_1000G_gold_standard.indels.b37.sites.vcf -I <path> Sample_uniqueAlignment _sort.rmdups.bam -o <path> Sample_uniqueAlignment_sort.rmdups. indelrealign.intervals

Alternative

$ java -Xmx8g -jar <path>/GenomeAnalysisTK- version no /GenomeAnalysisTK.jar -T RealignerTargetCreator -R <path> /ucsc.hg19.fasta -I <path> Sample_uniqueAlignment_sort. rmdups.bam -known <path> /1000G_biallelic.indels.hg19.vcf -log <path> Sample_uniqueAlignment _sort.rmdups. indelrealign.intervals.log -o <path> Sample_uniqueAlignment_sort.rmdups.indelrealign.intervals

1.6 Perform indel realignment

$ java –Xmx8g -jar <path>/GenomeAnalysisTK- version no /GenomeAnalysisTK.jar -T IndelRealigner –R <path> / human_g1k_v37.fasta –known <path> /1000G_phase1.indels.b37.vcf –known <path> /Mills_and_1000G_ gold_standard.indels.b37.sites.vcf –I <path> Sample_uniqueAlignment_sort. Rmdups.bam -targetIntervals <path> Sample_uniqueAlignment_sort.rmdups.indelrealign.intervals –o <path> Sample_uniqueAlignment_sort.rmdups.indelrealign.bam

Alternative

$ java -Xmx8g -jar <path>/GenomeAnalysisTK- version no /GenomeAnalysisTK.jar -T IndelRealigner -R <path> /ucsc.hg19.fasta -I <path> Sample_uniqueAlignment_sort. rmdups.bam -targetIntervals path> Sample_uniqueAlignment_sort.rmdups.indelrealign.intervals -log <path> Sample_uniqueAlignment _sort .rmdups. indelrealign.intervals.log –o <path> Sample_uniqueAlignment_sort.rmdups.indelrealign .bam

1.7. Recalibrate base quality scores (GATK)

1.7.1 Get the recalibration model

$ java -Xmx8g -jar <path>/GenomeAnalysisTK- version no /GenomeAnalysisTK.jar -T BaseRecalibrator –I <path> Sample_uniqueAlignment_sort.rmdups.indelrealign.bam -R <path> /human_g1k_v37.fasta –o <path> Sample_uniqueAlignment_sort.rmdups.indelrealign.recal.grp –knownSites <path> /dbSnp version no.b37.vcf.gz –knownSites <path> /1000G_phase1.indels.b37.vcf –knownSites <path> /Mills_and_1000G _gold_standard.indels.b37.sites.vcf -nct [no.threads (8)]

1.7.2 Check the recalibration model

$ java –Xmx8g -jar <path>/GenomeAnalysisTK- version no /GenomeAnalysisTK.jar -T BaseRecalibrator –I <path> Sample_uniqueAlignment_sort.rmdups.indelrealign.bam -R <path> /human_g1k_v37.fasta –BQSR <path> Sample_uniqueAlignment_sort.rmdups.indelrealign.recal.grp -o <path> Sample_unique Alignment_sort.rmdups.indelrealign.postrecal.grp -knownSites <path> /dbSnp version no.b37.vcf.gz –knownSites <path> /1000G_phase1.indels.b37.vcf –knownSites <path> /Mills_and_1000G_gold_ standard.indels .b37.sites.vcf –nct 8

$ java –Xmx8g -jar <path>/GenomeAnalysisTK- version no /GenomeAnalysisTK.jar -T Analyze Covariates–R <path> /human_g1k_v37. fasta -before <path> Sample_uniqueAlignment_sort. rmdups. indelrealign.recal.grp –after <path> Sample_uniqueAlignment_sort.rmdups.indelrealign.postrecal.grp–plots <path> Sample_uniqueAlignment_sort.rmdups.indelrealign.postrecal.plots.pdf

1.7.3 Apply the recalibration

$ java –Xmx8g -jar <path> /GenomeAnalysisTK- version no /GenomeAnalysisTK.jar -T PrintReads –R <path> /human_g1k_v37.fasta -o <path> Sample_uniqueAlignment_sort.rmdups.indelrealign.recal.bam –

I <path> Sample_uniqueAlignment_sort.rmdups.indelrealign.bam –BQSR <path> Sample_unique Alignment_sort.rmdups.indelrealign.recal.grp –nct 8

1.8 Variant Calling (SNVs and indels) (UnifiedGenotyper/HaplotypeCaller)

$ java -Xmx4g -jar <path> /GenomeAnalysisTK- version no /GenomeAnalysisTK.jar -T HaplotypeCaller –R <path> /human_g1k_v37.fasta -D <path> /dbSnp version no.b37.vcf.gz -stand_call_conf 30 -stand_ emit_conf 10 –I <path> Sample_uniqueAlignment_ sort.rmdups.indelrealign.recal –o <path> Sample_ uniqueAlignment_sort.rmdups.indelrealign.recal.raw.vcf

$ java -Xmx8g -jar <path> /GenomeAnalysisTK- version no/GenomeAnalysisTK.jar –T UnifiedGenotyper -R <path> /ucsc.hg19.fasta –I <path> Sample_uniqueAlignment_ sort.rmdups. indelrealign.recal –D <path> /dbsnp_version no.hg19.vcf -L <path> /hg19_exome.interval_list -nt 8 -stand_call_conf 50.0 -stand_emit_conf 10.0 -dcov 200 -l INFO -A AlleleBalance -A FisherStrand –log <path> Sample_uniqueAlignment_sort. rmdups.indelrealign.recal.SNP.log –o <path> Sample_unique Alignment_ sort.rmdups.indelrealign.recal.variants.SNP.vcf

$ java -Xmx8g -jar <path> /GenomeAnalysisTK- version no/GenomeAnalysisTK.jar –T UnifiedGenotyper -R <path> /ucsc.hg19.fasta –I <path> Sample_uniqueAlignment_ sort.rmdups. indelrealign.recal –D <path> /dbsnp_version no.hg19.vcf -L <path> /hg19_exome.interval_list -nt 8 -stand_call_conf 50.0 -stand_emit_conf 10.0 -dcov 200 -l INFO -A AlleleBalance -A FisherStrand –log <path> Sample_uniqueAlignment_sort. rmdups.indelrealign.recal.Indel.log –o <path> Sample_unique Alignment_ sort.rmdups.indelrealign.recal.variants.Indel.vcf -glm INDEL

1.9 Variant recalibration/ Hard filtering (GATK)

$ java -Xmx8g -jar <path> /GenomeAnalysisTK- version no /GenomeAnalysisTK.jar -T VariantRecalibrator -R <path> /ucsc.hg19.fasta -input Sample_uniqueAlignment_sort.rmdups. indelrealign. SNP.vcf resource:hapmap,VCF,known=false,training=true,truth=true,prior=15.0 <path> hapmap_3.3.hg19.vcf -resource:omni,VCF,known=false,training=true,truth=false,prior=12.0 <path> /1000G_omni2.5.hg19.vcf -resource:dbsnp,VCF,known=true,training=false,truth=false,prior=8.0 <path> DataFiles/dbsnp_version no.hg19.vcf -an QD -an HaplotypeScore -an MQRankSum -an ReadPosRankSum -an FS -an MQ --maxGaussians 6 -nt 8 -log <path> Sample_uniqueAlignment_sort. rmdups.indelrealign.recal.log -recalFile <path> Sample_uniqueAlignment_sort.rmdups.indelrealign. recal.recal -tranchesFile <path> Sample_uniqueAlignment_sort.rmdups.indelrealign.recal.tranches -rscriptFile <path> Sample_uniqueAlignment_sort.rmdups.indelrealign.recal.plot.R

$ java -Xmx8g -jar <path> /GenomeAnalysisTK- version no /GenomeAnalysisTK.jar -T ApplyRecalibration -R <path> /ucsc.hg19.fasta -input Sample_uniqueAlignment_sort.rmdups. indelrealign.SNP -recalFile <path> Sample_uniqueAlignment_sort.rmdups.indelrealign. recal.recal -tranchesFile <path> Sample_uniqueAlignment_sort.rmdups.indelrealign.recal.tranches -ts_filter_level 99.0 -log Sample_uniqueAlignment_sort. rmdups.indelrealign.recal.log -o Sample_uniqueAlignment_ sort.rmdups.indelrealign.recal.vcf

$ java –Xmx8g - jar <path> /GenomeAnalysisTK- version no /GenomeAnalysisTK.jar -T Variant Filtration -R <path> /human_g1k_v37.fasta -V <path> Sample_uniqueAlignment_sort.rmdups .indelrealign

.recal.variants.SNP.vcf --filterExpression “QD < 2.0 || FS > 60.0 || MQ < 40.0 || HaplotypeScore > 13.0 || MappingQualityRankSum < -12.5 || ReadPosRankSum < -8.0” --filterName “snp_hard_filter” -o <path> Sample_uniqueAlignment_sort.rmdups .indelrealign .recal.variants.filtered. SNP.vcf

$ java –Xmx8g - jar <path> /GenomeAnalysisTK- version no /GenomeAnalysisTK.jar -T VariantFiltration -R <path> /human_g1k_v37.fasta -V <path> Sample_uniqueAlignment_sort.rmdups .indelrealign .recal.variants.Indel.vcf --filterExpression “QD < 2.0 || FS > 200.0 || ReadPosRankSum < -20.0” --filterName “indel_hard_filter” -o <path> Sample_uniqueAlignment_sort.rmdups .indelrealign .recal.variants.filtered.Indel.vcf

1.10 Combine variant lists (SNP and Indel) (GATK)

$ java –Xmx8g - jar <path> /GenomeAnalysisTK- version no /GenomeAnalysisTK.jar –T Combine Variants -R <path> /ucsc.hg19.fasta (<path> /human_g1k_v37.fasta) --variant <path> Sample_unique Alignment_ sort.rmdups.indelrealign.recal.variants.SNP.vcf --variant <path> Sample_ unique Alignment_ sort.rmdups.indelrealign.recal.variants.Indel.vcf -o <path> Sample_unique Alignment_ sort.rmdups.indelrealign.recal.variants. combined.vcf.

1.11 Variant filtering

1.11.1 dbSNP

$ perl <path> /vcfhacks/annotateSnps.pl -d <path> /dbSnp version no.b37.vcf.gz <path>/ clinvar_ 20150330.vcf.gz -b 129 -f 1 -pathogenic –i <path> Sample_unique Alignment_ sort.rmdups.indelrealign .recal.variants. combined.vcf -o <path> Sample_unique Alignment_ sort.rmdups.indelrealign.recal. variants. Combined_1pc.vcf

1.11.2 EVS

$ perl <path> /vcfhacks/filterOnEvsMaf.pl -d <path> /evs/ -f 1 --progress –I <path> Sample_unique Alignment_ sort.rmdups.indelrealign.recal.variants.combined.vcf_notindbSNP version no or 1pc –o <path> Sample_uniqueAlignment_sort.rmdups.indelrealign.recal.variants.combined_1pc_evs.vcf

1.11.3 ExAC

$ perl <path> /vcfhacks/filterVcfOnVcf.pl -f <path> /ExAC.Version no /sites.vep.vcf.gz -w -y 0.01 -i <path> Sample_uniqueAlignment_sort.rmdups.indelrealign.recal.variants.combined.vcf_1pc_evs –o <path> Sample_uniqueAlignment_sort.rmdups.indelrealign.recal.variants.combined_1pc_evs_ExAC.vcf

1.11.4 Control samples (3222 exomes of British Pakistani adults)

$ perl <path> /vcfhacks/filterVcfOnSample.pl -i <path> Sample_uniqueAlignment_sort.rmdups. indelrealign.recal.variants.combined.vcf_1pc_evs_ExAC -r <path> /bib/BUILD-2014-19-05/8.BB.anno .vcf. gz -o <path> Sample_uniqueAlignment_sort.rmdups. indelrealign.recal.variants.combined_1pc_ evs_ExAC_CF.vcf

1.12 Variant annotation (ANNOVAR)

$ perl <path> annovar/convert2annovar.pl <path> Sample_uniqueAlignment_sort.rmdups. indelrealign. recal.variants.combined.vcf_1pc_evs_ExAC_CF –outfile <path> Sample_uniqueAlignment_sort.rmdups. indelrealign. recal.variants.combined_1pc_evs_ExAC_CF.annovar.vcf

$ perl <path> annovar/table_annovar.pl <path> Sample_uniqueAlignment_sort.rmdups. indelrealign. recal.variants.combined_1pc_evs_ExAC_CF.annovar.vcf <path> /annovar/humandb -buildver hg19 -protocolrefGene,phastConsElements46way,genomicSuperDups,esp6500si_all,1000gVersion no apr_all ,snpversion no,ljb2_all -operation g,r,r,f,f,f,f -outfile <path> Sample_uniqueAlignment_sort.rmdups. indelrealign. recal.variants.combined_1pc_evs_ExAC_CF.annovar.vcf

Appendix 2- List of UNIX and R commands used in Fishing CNV and Exome depth analysis

2.1 Fishing CNV

2.1.1 Depth of Coverage (GATK)

$ java –Xmx8g –jar <path> /GenomeAnalysisTK- version no /GenomeAnalysisTK.jar –T DepthOf Coverage –R <path> /human_g1k_v37.fasta –I <path> Sample_uniqueAlignment_sort.bam –o <path> Sample_uniqueAlignment_sort.coveragedepth.txt –L <path> SSV4/5_regions_b37.bed -ct 4 -ct 9 -ct 14 -ct 19 -ct 24 -ct 29

2.1.2 Convert coverage file to PRKM

$ java –Xmx8g -jar <path> /FishingCNV_ version no_pipeline.jar -cc -c <path> Sample_unique Alignment_sort_summary –b <path> /FishingCNV_ version no_pipeline /S04380110_Regions_b37.bed -o <path> Sample_uniqueAlignment_sort _summary.rpkm

2.1.3 Pooling Multiple RPKM files

$ java –Xmx8g -jar <path> /FishingCNV_ version no_pipeline.jar -p –rpkm <path> ControlSamples. indelrealign.recal_interval_summary.rpkm -o ControlSamples.indelrealign.recal.pooled.controlrpkm.ctr

2.1.4 Apply Fishing CNV

$ Rscript <path> /FishingCNV_ version no_pipeline /FishingCNV.R -c <path> ControlSamples. indelrealign.recal.pooled.controlrpkm.ctr -v -s <path> Sample_uniqueAlignment_sort _summary.rpkm -o Sample_uniqueAlignment_sort _summaryResult –pca

2.2 Exome depth analysis

$ R

> library(ExomeDepth)

> data(exons.hg19)

> print(head(exons.hg19))

> Mohammed_bam_files <- c (“Sample_indelrealign_recal(File1).bam”, “File2.bam”,”File3.bam”, etc.)

> Mohammed_counts<-getBamCounts(bed.frame=exons.hg19, bam.files=Mohammed_bams, include.chr=FALSE, referenceFasta=" <path> /human_g1k_v37.fasta")

> ExomeCount.dafr <- as(my.counts[, colnames(my.counts)], 'data.frame')

> print(head(ExomeCount.dafr))

> Moh_counts.dafr<-as(Mohammed_counts[, colnames(Mohammed_counts)], 'data.frame')

> print(head(Moh_counts.dafr))

> Sample.test <- Moh.counts$ Sample_indelrealign_recal(File1).bam

> Moh.ref.samples <-c(File2.bam',File3.bam', etc.)

> Moh.reference.set<-as.matrix(Moh_Count.dafr[,Moh.ref.samples])

```
> Moh.choice<-select.reference.set
(test.counts=Sample.test,reference.counts=Moh.reference.set,bin.length=(Moh_Count.dafr$end
Moh_Count.dafr$start)/1000,n.bins.reduced=10000)
> print(Sample_choice[[1]])
> Moh.matrix <-as.matrix( Moh_Count.dafr[, Moh.choice$reference.choice, drop = FALSE])
> Moh.reference.selected<-apply(X=Moh.matrix,MAR=1,FUN=sum)
> Sample.all.exons <-new('ExomeDepth',test=Sample.test, reference=Moh.reference.selected,formula
='cbind(test, reference)~1')
> Sample.all.exons<-CallCNVs(x=sample_all.exons,transition.probability=10^-4, chromosome =Moh_
Count.dafr$space,start=Moh_Count.dafr$start,end=Moh_Count.dafr$end,name=moh_Count.dafr$names)
> head(Sample.all.exons@CNV.calls)
> data(Conrad.hg19)
> head(Conrad.hg19.common.CNVs)
> Sample.all.exons<-AnnotateExtra(x=Sample.all.exons, reference.annotation=Conrad.hg19.common.
CNVs, min.overlap=0.5, column.name='Conrad.hg19')
> print(head(Sample.all.exons@CNV.calls))
> exons.hg19.GRanges <- GenomicRanges::GRanges(seqnames=exons.hg19$chromosome,IRanges::I
Ranges(start=exons.hg19$start,end=exons.hg19$end),names=exons.hg19$name)
> Sample.all.exons <- AnnotateExtra(x=Sample.all.exons, reference.annotation=exons.hg19.GRanges,
min.overlap =0.0001, column.name='exons.hg19')
> Sample.all.exons@CNV.calls[3:6,]
> output.file <- 'Sample_calls_File1CNVs.csv'
> write.csv(file=output.file,x=Sample.all.exons@CNV.calls,row.names=FALSE)
```

Appendix 3- Genes targeted in the Retinome project

ABCA4	*CERKL*	*GNAT2*	*NPHP1*	*PROM1*	*RPGRIP1L*
ABCC6	*CFB*	*GPR98*	*NPHP3*	*PRPF3*	*RS1*
ADAM9	*CFH*	*GRK1*	*NPHP4*	*PRPF6*	*SAG*
AHI1	*CHM*	*GRM6*	*NR2E3*	*PRPF8*	*SDCCAG8*
AIPL1	*CLN3*	*GUCA1A*	*NRL*	*PRPF31*	*SEMA4A*
ALMS1	*CLRN1*	*GUCA1B*	*NYX*	*PRPH2*	*SNRNP200*
ARL6	*CNGA1*	*GUCY2D*	*OAT*	*PXMP3*	*SPATA7*
ARMS2	*CNGA3*	*HMCN1*	*OFD1*	*RAX2*	*TEAD1*
ATXN7	*CNGB1*	*HTRA1*	*OPA1*	*RB1*	*TIMM8A*
BBS1	*CNGB3*	*IDH3B*	*OPA3*	*RBP3*	*TIMP3*
BBS2	*CNNM4*	*IMPDH1*	*OPN1LW*	*RBP4*	*TLR3*
BBS4	*COL2A1*	*INPP5E*	*OPN1MW*	*RD3*	*TLR4*
BBS5	*COL9A1*	*INVS*	*OPN1SW*	*RDH12*	*TMEM126A*
BBS7	*COL11A1*	*IQCB1*	*OTX2*	*RDH5*	*TOPORS*
BBS9	*CRB1*	*JAG1*	*PANK2*	*RGR*	*TREX1*
BBS10	*CRX*	*KCNJ13*	*PAX2*	*RGS9*	*TRIM32*
BBS12	*CYP4V2*	*KCNV2*	*PCDH15*	*RGS9BP*	*TRPM1*
BEST1	*DFNB31*	*KLHL7*	*PDE6A*	*RHO*	*TSPAN12*
C2	*DMD*	*LCA5*	*PDE6B*	*RIMS1*	*TTC8*
C3	*EFEMP1*	*LRAT*	*PDE6C*	*RLBP1*	*TTPA*
CA4	*ELOVL4*	*LRP5*	*PDZD7*	*ROM1*	*TULP1*
CABP4	*ERCC6*	*MERTK*	*PEX1*	*RP1*	*UNC119*
CACNA1F	*EYS*	*MFRP*	*PEX7*	*RP2*	*USH1C*
CACNA2D4	*FBLN5*	*MKKS*	*PGK1*	*RP9*	*USH1G*
CC2D2A	*FSCN2*	*MTTP*	*PHYH*	*RPE65*	*USH2A*
CDH23	*FZD4*	*MYO7A*	*PITPNM3*	*RPGR*	*VCAN*
CEP290	*GNAT1*	*NDP*	*PRCD*	*RPGRIP1*	*WFS1*

Table S1. List of 162 genes used to generate the targeted reagent of the Retinome project.

Appendix 4- Exons not covered by the targeted reagent of the Retinome project

LOCATION (hg19)	EXON
Chr1:196670427-196670481	*CFH* terminal exon of NM_001014975.2 / ENST00000359637
Chr4:16004948-16004992	*PROM1* 4bp terminal exon in one UCSC transcript only (non CCDS, refseq or Ensembl)
Chr4:47972892-47973137	*CNGA1* first exon of CCDS47050.1
Chr6:66042196-66042330	*EYS* terminal exon of CCDS47446.1
Chr10:102777320-102777392	*PDZD7* terminal exon of CCDS31269.1
Chr14:88881544-88881630	*SPATA7* 3rd exon of uc001xws.2 (non-ccds refseq or Ensembl)
Chr16:53656110-53656288	*RPGRIP1L* exon 19 of CCDS32447.1
ChrX:38144793-38146598	*RPGR* terminal exon of one UCSC transcript only (ORF15)
ChrX:85226551-85226610	*CHM* terminal exon of CCDS48139.1

Table S2. List of nine exons that were not covered by the targeted reagent used in the Retinome project.

Appendix 5- Validating the Retinome capture reagent and establishing a pipeline for variant detection

To test the feasibility of identifying the pathogenic mutation in genomic DNA from patients with retinal degeneration, using the Retinome reagent a pilot study was performed. Four patients in whom the mutation had previously been identified and confirmed by Sanger sequencing were selected for analysis using the customised reagent. The preparation of libraries for targeted next generation sequencing was carried out by Clare Logan and the analysis of the data was conducted by David A. Parry, who had no prior knowledge of the mutations in the samples. Briefly, each patient's sonicated DNA was ligated to a different 6bp sequence tag. The tagged aliquots were pooled prior to hybridisation against the target enrichment reagent and the sample ran on a single lane of the Illumina GAIIx DNA Sequencer. The sequence data for each sample was sorted by the corresponding sequence tag and aligned against the human reference sequence for analysis of coverage and read depth (Table S3A). Pooling of four samples gave a range of coverage with at least 20 good quality reads following duplicate removal of 95.6 to 96.9%; 1 to 2% had less than 5X read depth. A list of variants was generated for each sample and these were filtered without knowledge of family history according to the criteria highlighted in Table S3B, to produce a list of candidate variants for each sample (Table S4)

Prioritisation of the variants was based on whether the genotype was consistent with disease symptoms, variant type and pathogenicity scores. For sample A with a diagnosis of RP, heterozygous mutations in *RP9*, *RP1* and *FSCN2* were deemed consistent with disease symptoms, and of these a high pathogenicity profile suggested that the strongest candidate for causation in sample A was the *RP9* variant. For sample B, though a number of changes were observed, only compound heterozygosity for a premature stop codon and a high pathogenicity missense mutation in *CRB1* fitted with the LCA diagnosis in this patient. For sample C, heterozygous variants in *RP1* and a homozygous variant in *USH2A* were considered possible candidates for causing RP in this patient. However based on pathogenicity scores and variant type, the strongest candidates for disease causation in sample C were the *RP1* variants. For sample D, only a heterozygous null mutation in *PRPF31* was identified as consistent with the diagnosis of RP. The variants that had previously been deemed causative in each sample are shown in Table S3C. As these variants had indeed been implicated as candidates for pathogenicity following filtering and prioritisation as highlighted above, this confirmed that the pipeline used to identify the pathogenic mutations was robust.

A

Sample	Tag	Aligned Reads	Reads on target	% Reads on target	Mean coverage	% ≥ 5	% ≥ 10	% ≥ 15	% ≥ 20	% ≥ 30	% ≥ 50
Patient A tag1	CAACCT	6,296,720	1,310,107	20.8%	133	98.5	97.7	96.8	95.7	93.3	86.5
Patient B tag2	AACCAT	5,788,340	1,359,182	23.5%	137	98.4	97.5	96.6	95.6	93.4	87.9
Patient C tag3	AAGGAT	8,539,613	2,174,816	25.5%	220	98.7	98.2	97.6	96.9	95.9	93.1
Patient D tag4	AATTAT	4,314,207	1,609,443	37.3%	164	98.5	97.6	96.7	95.8	93.9	88.8
Patient tag1 to 4, AVERAGE						98.5	97.8	96.9	96.0	94.1	89.1

B

Filtering process	Patient A	Patient B	Patient C	Patient D
Total variants identified	614	564	595	580
Exclude outside exon / splice junction	278	282	269	260
Exclude synonymous variants	134	142	131	124
Exclude if MAF ≥ 0.01	7	12	10	3

C

Patient	Diagnosis	Inheritance Pattern	Chr	Position	Gene	Coding Effect	cDNA change	Protein change	BLOSUM62	AGVGD class	SIFT prediction	MAPP prediction	Zygosity
A	RP	Dom.	7	33136162	*RP9*	missense	NM_203288.1:c.410A>T	p.His137Leu	-3	C15	Deleterious	bad	Het
B	LCA	Rec.	1	197390534	*CRB1*	nonsense	NM_201253.2:c.1576C>T	p.Arg526*	NA	NA	NA	NA	Het
			1	197404300	*CRB1*	missense	NM_201253.2:c.3307G>A	p.Gly1103Arg	-2	C25	Deleterious	bad	Het
C	RP	Dom.	8	55538727	*RP1*	frameshift	NM_006269.1:c.2285_2289 delTAAAT	p.Leu762Tyrfs*17	NA	NA	NA	NA	Het
D	RP	Dom.	19	54621976	*PRPF31*	frameshift	NM_015629.3:c.201delT	p.Ile67Metfs*14	NA	NA	NA	NA	Het

Table S3. Targeted capture and NGS for four-patient verification study of the Retinome project. (A) Coverage and read depth. The tagging, aligned reads, reads on target, % reads on target, mean coverage and % coverage with a particular minimum read depth are shown for each patient's DNA. (B) Filtering the variant lists. Exonic constitutes coding variants only. Splicing constitutes +/- 5bp around an exon. Full list of variants is shown in Table S4. (C) The previously identified pathogenic mutations in the four-patient study. The chromosome and position of the mutation is depicted according to the human genome assembly, hg19. NA = not annotated and Het = heterozygous.

Patient A

Chr	Position	Gene	Coding Effect	cDNA change	Protein change	BLOSUM62	AGVGD class	SIFT prediction	MAPP prediction	Zygosity
1	216219858	*USH2A*	missense	NM_206933.2:c.6240G>T	p.Lys2080Asn	0	C0	Tolerated	good	Het
4	47954624	*CNGA1*	missense	NM_001142564.1:c.302G>A	p.Arg101Gln	1	C0	Tolerated	good	Het
7	33136162	*RP9*	missense	NM_203288.1:c.410A>T	p.His137Leu	-3	C15	Deleterious	bad	Het
8	55541086	*RP1*	missense	NM_006269.1:c.4644T>G	p.Ser1548Arg	-1	C0	Tolerated	bad	Het
9	2718127	*KCNV2*	missense	NM_133497.3:c.388A>C	p.Thr130Pro	-1	C0	Deleterious	bad	Het
9	120470884	*TLR4*	missense	NM_138554.3:c.137A>G	p.Tyr46Cys	-2	C15	Tolerated	bad	Het
17	79502218	*FSCN2*	missense	NM_001077182.2:c.967G>A	p.Ala323Thr	0	C0	Tolerated	good	Het

Patient B

Chr	Position	Gene	Coding Effect	cDNA change	Protein change	BLOSUM62	AGVGD class	SIFT prediction	MAPP prediction	Zygosity
6	11374	*C2*	splicing	NM_000063.4:c.617-5C>A	p.?	NA	NA	NA	NA	Het
1	186045644	*HMCN1*	missense	NM_031935.2:c.8375A>G	p.Asn2792Ser	1	C45	Deleterious	Bad	Het
1	197390534	*CRB1*	nonsense	NM_201253.2:c.1576C>T	p.Arg526*	NA	NA	NA	NA	Het
1	197404300	*CRB1*	missense	NM_201253.2:c.3307G>A	p.Gly1103Arg	-2	C25	Deleterious	bad	Het
1	215953246	*USH2A*	missense	NM_206933.2:c.10878G>T	p.Arg3626Ser	-1	C0	Tolerated	good	Het
4	619426	*PDE6B*	missense	NM_000283.3:c.11G>T	p.Ser4Ile	-2	C0	Deleterious	good	Het
6	135811814	*AHI1*	missense	NM_017651.4:c.82C>T	p.Arg28Cys	-3	C0	Tolerated	unknown	Het
9	117266891	*DFNB31*	missense	NM_015404.3:c.191C>A	p.Ala64Asp	-2	C0	Deleterious	bad	Het
10	102782113	*PDZD7*	missense	NM_001195263.1:c.572T>A	p.Val191Glu	-2	C65	Deleterious	bad	Het
12	88472996	*CEP290*	missense	NM_025114.3:c.5237G>A	p.Arg1746Gln	1	C0	Tolerated	good	Het
X	31676133	*DMD*	missense	NM_004006.2:c.8001T>A	p.Asn2667Lys	0	C65	Deleterious	bad	Homo
X	38147286	*RPGR*	in-frame	NM_001034853.1:c.1579_1581delTTG	p.Gln527del	NA	NA	NA	NA	Het

Continue Table S4

Patient C

Chr	Position	Gene	Coding Effect	cDNA change	Protein change	BLOSUM62	AGVGD class	SIFT prediction	MAPP prediction	Zygosity
1	186158843	*HMCN1*	missense	NM_031935.2:c.16741G>A	p.Ala5581Thr	0	C0	Deleterious	bad	Het
1	216052344	*USH2A*	missense	NM_206933.2:c.8320G>A	p.Ala2774Thr	0	C0	Tolerated	good	Homo
2	110962496	*NPHP1*	missense	NM_000272.3:c.50A>G	p.Asn17Ser	1	C0	Tolerated	good	Het
8	55533891	*RP1*	missense	NM_006269.1:c.365G>C	p.Arg122Pro	-2	C15	Deleterious	bad	Het
8	55538727	*RP1*	frameshift	NM_006269.1:c.2285_2289 delTAAAT	p.Leu762Tyrfs*17	NA	NA	NA	NA	Het
10	50732202	*ERCC6*	missense	NM_000124.2:c.1274A>C	p.Asp425Ala	-2	C65	Deleterious	bad	Het
10	73270907	*CDH23*	missense	NM_022124.5:c.367G>C	p.Gly123Arg	-2	C15	Deleterious	bad	Het
11	76891457	*MYO7A*	missense	NM_000260.3:c.2624C>G	p.Ala875Gly	0	C0	Tolerated	bad	Het
16	57950041	*CNGB1*	missense	NM_001297.4:c.2209C>T	p.Arg737Cys	-3	C0	Tolerated	good	Het
X	38156584	*RPGR*	missense	NM_001034853.1:c.1367A>G	p.Gln456Arg	1	C0	Tolerated	bad	Het

Patient D

Chr	Position	Gene	Coding Effect	cDNA change	Protein change	BLOSUM62	AGVGD class	SIFT prediction	MAPP prediction	Zygosity
3	121500697	*IQCB1*	missense	NM_001023570.2:c.1303C>T	p.Arg435Cys	-3	C0	Deleterious	bad	Het
7	128415833	*OPN1SW*	missense	NM_001708.2:c.12G>A	p.Met4Ile	1	C0	Deleterious	bad	Het
19	54621976	*PRPF31*	frameshift	NM_015629.3:c.201delT	p.Ile67Metfs*14	NA	NA	NA	NA	Het

Table S4. List of candidate variants in the four-patient verification study of the Retinome project. The diagnosis of the patients was either RP (for A, C and D) or LCA (for B). The chromosome and position of the variants are depicted according to the human genome assembly, hg19. NA = not annotated. Homo = homozygous. Het = heterozygous.

Appendix 6- List of primers used in the work described in this thesis

Oligo name	Forward primer (5'-3')	Reverse primer (5'-3')	Product size (bp)	Annealing temperature (°C)	Purpose
ABCA4-I-MA18	CTCTTCCTCACCCTCCACAG	CATTGTGGTTCCTGTACTCAGC	298	57	S-PCR
ABCA4-II-MA18	CCTTGCTCTCACCCTGTCTC	TGTGACTTGCATTATGGCATT	232	57	S-PCR
ABCA4-MA2	GCTCTATGGTCATCCCTCCA	GCACGCTTCAGTTTCTCATCT	299	57	S-PCR
ABCC6-MA5	GGTGCAGGGAAGAGTTCTCA	CAGGGACCCAGAGAGAACAG	412	57	S-PCR
BBS12-I-MA14	CCGTGCTCACTAACCCAGTT	GTGGCATTTTGCAGATGATG	376	60	HS-PCR
BBS12-II-MA14	CAGAATTTGAAGCCAGCACA	CTTGGCAATAGCTGGCATTT	408	60	S-PCR
BBS2-MA11	TAAGCGAACAGGGGAAAGAA	CCCTGCACCTGTACTAACCA	263	56	S-PCR
BCAR3-MA14	GATTAGTGAAGCAGGCGGTC	TGACCTCAGCTCTTCCCAAG	399	57	S-PCR
C8ORF37-EXON6-MA13	CTGCAGTGAGCCATGATTGT	TTTTCCCACAGGGAATGGTA	424	57	S-PCR
CACNA1F-MA11	TACTCGCTCCACACACTCCA	GTGTCGTAAAGGGCAGAAGG	371	55	HS-PCR
CC2D2A-I-MA19	TTAATTGTGCAGAGCGCATT	GCAGGGACATCAGCTTTTTC	310	57	S-PCR
CC2D2A-II-MA19	CTCAACAGAGGGCCAAGAAG	ATGTCGTGCATGTGTGTGTG	331	57	S-PCR
CDH23-I-MA12	AAATGCTGTCAAGGCTGTCA	ACTGTCTGGATGGGGTTGAG	408	57	S-PCR
CDH23-II-MA12	AGGCCAGGAGTAGAGGGAAG	CCACTCTTCTAGGCCACAGC	349	57	S-PCR
CEP290-I-MA17	TTTGTGAAATATGTTCCATTAAACTCA	TGTCTAGCCACCAACAGTGC	408	60	HS-PCR
CEP290-II-MA17	AAAAGGCATACTTGTACCCACA	GAAAATGCATCCATCATTTACAA	447	60	HS-PCR
COL11A1-MA8	TCCAAAGGAGTGCAGAAGTG	CCCCACAAAATTGACTGGTT	255	60	S-PCR
CRB1-MA1	TGTGGTTTCACCGTCAACAT	AGGCAAGAGGCCAGTCAGTA	400	60	HS-PCR
DMD-MA19	GTGGATCGAATTCTGCCAGT	CGCTGTGTAACTACGCCAAA	408	57	S-PCR
DRAM2-EXON1(NC)	TCCGGGGGCTACCTTATG	CACCAGGGATCGTAATTTCA	450	57	S-PCR
DRAM2-EXON2(NC)	AGCCTAGTATTCTGCCCATGA	CCTAACAGATTGCTGGTGCAT	343	57	S-PCR

Oligo name	Forward primer (5'-3')	Reverse primer (5'-3')	Product size (bp)	Annealing temperature (°C)	Purpose
DRAM2-EXON3	GAAACAGCTTGGGGTGGTAA	CACAAAGAAAAAGCCAAATTCA	414	55	S-PCR
DRAM2-EXON4	GGTGAAGTAGGCAGATATTTGTGA	TTCCCATAAGTCCGCATTTC	442	57	S-PCR
DRAM2-EXON5	TCCAGCCTGTGCAACATAGA	GAATGCTTCAGGTTTCCCTTT	429	57	S-PCR
DRAM2-EXON6	TTGTAGAATTGGCCGAGCTT	AAAGGCTTCTTATACTGCACCAA	400	60	HS-PCR
DRAM2-EXON7	ACCCTCTGAGCAGCACATTT	GGTGACAGGAGAATATGGAAGG	442	57	S-PCR
DRAM2-EXON8	GCCTGGTAAGTCAAGGGTTG	TAGCCCCATTTTCAAGGCTA	447	56	S-PCR
DRAM2-EXON9A	TGAGAAGCTTGGTTTTTCCAG	TGGCTTCTTTCATGTTTCCTG	450	55	S-PCR
DRAM2-EXON9B (NC)	GACACTGCACCTTGCCCTAT	AAAAGTGCTCCTAACAAAACATGA	650	57	S-PCR
DRAM2-EXON9C (NC)	GCACCAATCAGTCTGCACAT	ACAGGTGCCTCTCTCCTTCA	422	57	S-PCR
DRAM2-EXOND (NC)	CTGGATTCATGTGGGCTCTT	TTGGATTGCCAATTTTGTTC	441	56	S-PCR
DRAM2-Gateway-*attb*	GGGGACAAGTTTGTACAAAAAAGCAGGCT TCATGTGGTGGTTTCAGCAAGG	GGG GAC CAC TTT GTA CAA GAA AGC TGG GTCAATATCTCTGGAAAGTAGCCGT	-	51	C-PCR
DRAM2-RT-PCR	EX6-GGAGCTGTGCTTACCTTTGG	EX7-GGGGTTCCAATGGAGTTTCT	222 /778	57	RT-PCR
DST-MA14	TTGACATACAACCATCAGACCT	TGCTATGCACGAGAGACAGG	423	57	S-PCR
EYS-I-MA4	TGATGGGAATTCATAACATTTTT	CCATGAAACAGTTCGATGACT	290	57	S-PCR
EYS-II-MA4	AAGCTGACGGAACTCCTGAA	TTGTGGAAGTGACGAAGGAA	260	57	S-PCR
EYS-TERM-MA4	GGCAAATCTATGTTTTCAATCC	TCAGATTGTGGAAGTTCCCTTT	445	60	HS-PCR
FDFT1-EXON1	CGGGGTCTTCCTAGTGTGAG	GGGAAGGCTCGAGGAAAG	504	57	S-PCR
FDFT1-EXON2	ACTCCCACTCCTGCTCCTC	CCGGGCTATGTTCTGGATAA	288	57	S-PCR
FDFT1-EXON3	GTGGCCAGGCACAAGTTATT	TATGGAGGCTACCGGACAAC	341	57	S-PCR
FDFT1-EXON4	TGTGATCTTTGGTGCCATGT	ATGAGGACTGCCAGCTCTGT	254	57	S-PCR
FDFT1-EXON5	CCATTCTCTTTTGAACCTGCTT	TTTTCCACATCCCCTTATGC	425	57	S-PCR

Oligo name	Forward primer (5'-3')	Reverse primer (5'-3')	Product size (bp)	Annealing temperature (°C)	Purpose
FDFT1-EXON6	CGCCCAGCCTGTATCATAGT	CCTCAAGGCTGAGCTGAGTT	471	60	HS-PCR
FDFT1-EXON7	ATTGCCCATTCAACAGAAGG	TCCAACCTACAGCCTTGCTC	488	57	S-PCR
FDFT1-EXON8	GCCAGTGGAGGGTTGTTGTA	ATGAGGCACCCTTTCCTTTC	492	60	HS-PCR
FDFT1-M-MA17	TGCCCATTCAACAGAAGGTT	GCTCGGCTCCTGTGAATAGA	421	57	S-PCR
FILIP1-MA14	AGCTCTTAGGCCCAGTGTGA	ATCTCCAAAGTCGCAGTGCT	429	57	S-PCR
FSCN2-MA14	TTCGGCTTCAAGGTCAATGC	CTCCGGAAGATGAGGGTGAG	458	57	S-PCR
GP6-MA14	TGTGTTCGGAGTAGGCACAG	TGCTGCCTCGTTATCTGATG	401	57	S-PCR
GPR98-I-MA13	CTTGGGCAACAGAGTGTGAC	GCTCACTTCTGCACCTCCTC	437	56	S-PCR
GPR98-II-MA13	CTGCTTCTGGGTTTGTTGTG	CCAAGTGTGCCTGCTAAAGA	450	56	S-PCR
GUCY2D-MA9	AGTGAACAGCCCCATGAGAG	TCAAAGTACTCGGGCTCCAC	408	57	S-PCR
HMCN1-MA9	TCCAAAAGTATGATTTCTCTGGAA	ACTTGTTGACGGCAAACTGA	252	55	S-PCR
HR-MA14	CCTTCTCTCTGCGAACTGCT	CAGTGCTCCTGGAAGAGGTG	438	57	S-PCR
LARGE-EXON10	ATGGCTTCCTACAGGTGTGA	ATGGGGGAGGTCCTTGAT	299	55	S-PCR
LARGE-EXON11	AATAAACTCAGGGGAGGGCA	ATGTGCCATCTCTTCCTGCT	394	57	S-PCR
LARGE-EXON12	CAAGTGTCACTGGAGGCAGA	CTGGAAAAGAAACCTGTTGGA	484	57	S-PCR
LARGE-EXON13	CCTCATGGGGGAAAGACCT	TAGCTTTGGCATCTGGGTTT	293	57	S-PCR
LARGE-EXON14	ACAGTTCAACTCACCCGAGG	TCCAAGGATCCCTTAAGCTC	391	60	HS-PCR
LARGE-EXON15	GTCCTTTGCCATCTGCTTGT	CTGTAGTGAGGGCAGCTTGG	481	57	S-PCR
LARGE-EXON2	CAGTTGAACCCCTTTCAGGA	TGACTGCTGCCAACTACCTG	450	57	S-PCR
LARGE-EXON3	AGGAGCCTCGCCATGTAGTA	TACACACCCGGGCTAGAATC	529	57	S-PCR
LARGE-EXON4	CAGGGCAATTTTTCTTTCTAGTGT	AACCCTTCCCCAAGGAAATA	248	57	S-PCR
LARGE-EXON5	TGAAGAGTGTGTTTTTGCAGC	GAGCTGAGATTTCTGGCATTG	300	57	S-PCR

Oligo name	Forward primer (5’-3’)	Reverse primer (5’-3’)	Product size (bp)	Annealing temperature (°C)	Purpose
LARGE-EXON6	TGGATACTTTTTGTGTGCTAGGC	GTCAACCCCTATTCTTGGCA	349	55	S-PCR
LARGE-EXON7	TGTGATGATTTGCCATTACCC	CCTCCTCCTGAGCTTTTGC	299	57	S-PCR
LARGE-EXON8	ATCATCCCCGAGAGACTGTG	ACTGGCAAGAATAAGGCAGC	360	57	S-PCR
LARGE-EXON9	CAGTGCCTTGAGAGCCAAA	TAAATCTCCCAGCCATCCAT	286	57	S-PCR
LARGE-M-MA14	TCCAAAGCTGTTGTGCTGTC	TTCCCCTACAGCATGTCTCC	391	57	S-PCR
LDB1-MA14	TCCCAAGTAGCTGGAACCAC	CTACTCCCTCCCCTTTCCAG	385	57	S-PCR
LILRB5-MA14	GGTCTCAGCTCAGAGCAAGG	TGGACAGCAGGTAGGGGTAG	325	57	S-PCR
METTL24-MA14	CAAGGATGGGGAAGCAATAA	AGTGCCTCTGACCAAGGAGA	425	55	S-PCR
MFSD8-EX11-MA5	TCAGCCATTTTTCAGAGGAG	TTGGAGACTTCCAAAGACCAA	440	56	S-PCR
MFSD8-EX13-MA5	CAGGGCTTCAGCAGACAGTA	TATTCCACACACCAGGCTGA	352	56	S-PCR
MUC4-MA14	AGCGAGAAGCACCCTAGATG	GGCAGAGGCCTGACATTAAG	437	57	S-PCR
MYO7A-I-MA13	AAAGTCATGCCCAGTTCCAG	ACCGGGTGACAGATGAGAAG	303	57	S-PCR
MYO7A-II-MA13	CAGGCCAGCTCTGACTTAGC	CATAAATCTCCCAGCCTCCA	492	57	S-PCR
NR2E3-MA8	TTGGGCAAAAATGTCCAAGC	AGGAAGGGTCAGGACGACAC	256	57	S-PCR
OFD1-MA17	GAGAGAGAACTTGTTCCTGTTTTT	CCAACCTACTAATAGCTGCAGGA	300	57	S-PCR
P53-RT-PCR	GTACTCCCCTGCCCTCAACA	CTGGAGTCTTCCAGTGTGAT	408/1057	57	RT-PCR
PCDH15-I-MA19	GGGCCCAAGAGAAAAGATTC	TTCCAAGGAACACTCAGCAG	406	57	S-PCR
PCDH15-II-MA19	TGATCTGGCTACATTTCAGCTC	TGCTGTCATCTGTTAAGCCAAA	373	57	S-PCR
PCM1-MA14	AGCTTCCACTTGGAATGAAGT	GGAAAGAGCACACATGAACG	224	57	S-PCR
PHYH-MA5	TCAAGTCTGCAACCCTTTCC	CGGGTTTTACAGGCAGACAT	322	57	S-PCR
PROM1-MA6	CAGCCTTAGTCCAGCAGCTT	GTCCCATCACAGCAGGATCT	387	55	S-PCR
PROM1-MA7	CTGAGTTGCAAAATGAGTGACTA	CGAATGACACAATTGTAAAGCTC	300	55	S-PCR

Oligo name	Forward primer (5'-3')	Reverse primer (5'-3')	Product size (bp)	Annealing temperature (°C)	Purpose
RDH12-MA6	TGGGCTGTCATTCCACTTTC	GGTCTGAGGACCATTTTTGC	300	57	S-PCR
RP2-MA8	GGAAGAAGCAGCTGAGGTGA	ACACACCCCAAAAATTCCAA	368	56	S-PCR
RPGR-MA8	TGCTTTGTGGTGACCTCATCT	TCAAGCAAATGTCAGAAAATAAAGA	284	60	HS-PCR
RPGR-RET	CAGAGGTCCAAAATGCCAGT	CACAGCTGCATCAGTTGCTT	251	60	HS-PCR
RPGRIP1-MA10	TCCAGGCAAGGAGTCTAATCTT	TTCAGCATCAGCACAAAACC	290	56	S-PCR
RPGRIP1L-MA5	CCATTGGCCTTCGTGTTTTA	GCCTGGCCCAACTTTATTTT	478	56	S-PCR
RS1-MA8	GCAAAGCAGATGGGTTTGTT	TTCCCAGGTTCAAGCAATTC	421	58	S-PCR
SNRNP200-MA5	GGAGGTAAAATTAGTAGCTCTTTGC	ATTATGCTGTGCCCAACAGG	286	57	S-PCR
SPATA7-MA15	TTGAAAGATTTGTTTTCCCTTTT	CAGGAAAAATTTGCTGACCCTA	265	56	S-PCR
TBC1D9B-MA14	TAGCGTCACCATCCTGTCTG	CTCCCAAAGTGCTGGGATTA	431	57	S-PCR
TNFRSF21-MA14	CCCTGGATGATTGTGCTTTT	CAGGGGAAAAGGAGGAAGAG	406	57	S-PCR
TTLL5-EXON19-MA19	GGGAAGCTTAGCCTTGGAAT	CTGGCAGGATCCAGATAAGG	278	57	S-PCR
USH2A-MA3	ATTGCAAGCACCTCCAGAAG	CCAGAGTTGTGATGCTGGTG	284	58	S-PCR
USH2A-MA5	CATGCATGGGATTTCAGGTT	CCTGGATATCGAGAGCCAACT	352	60	HS-PCR
VCAN-RET	TTACATACAATGCACAAAAAGCA	TTCCAGTGATTCCACATTGC	251	57	S-PCR
WFS1-MA19	CAACATGCTCCCGTTCTTCAT	AGGATGGTGCTGAACTCGATG	327	57	S-PCR
ZNF613-MA14	AAAGGTCCAGGCTCACTGAA	TGTGAGCAGGATTTTCCACA	421	57	S-PCR

Table S5. List of primers used in this study. Oligo name, forward and reverse primer sequences, product size, annealing temperature and purpose of using are shown. NC = non-coding, PCR = polymerase chain reaction, S-PCR = standard PCR, HS-PCR = Hot-Shot master mix PCR, C-PCR = cloning PCR and RT-PCR = reverse transcriptase PCR.

Appendix 7- Representative bioanalyser analysis for WES library preparation

A. The sheared DNA samples were analysed on the Bioanalyzer™ using DNA1000 assay kit (Agilent Technologies) to assess the distribution of DNA fragment sizes between 150-200 bp.

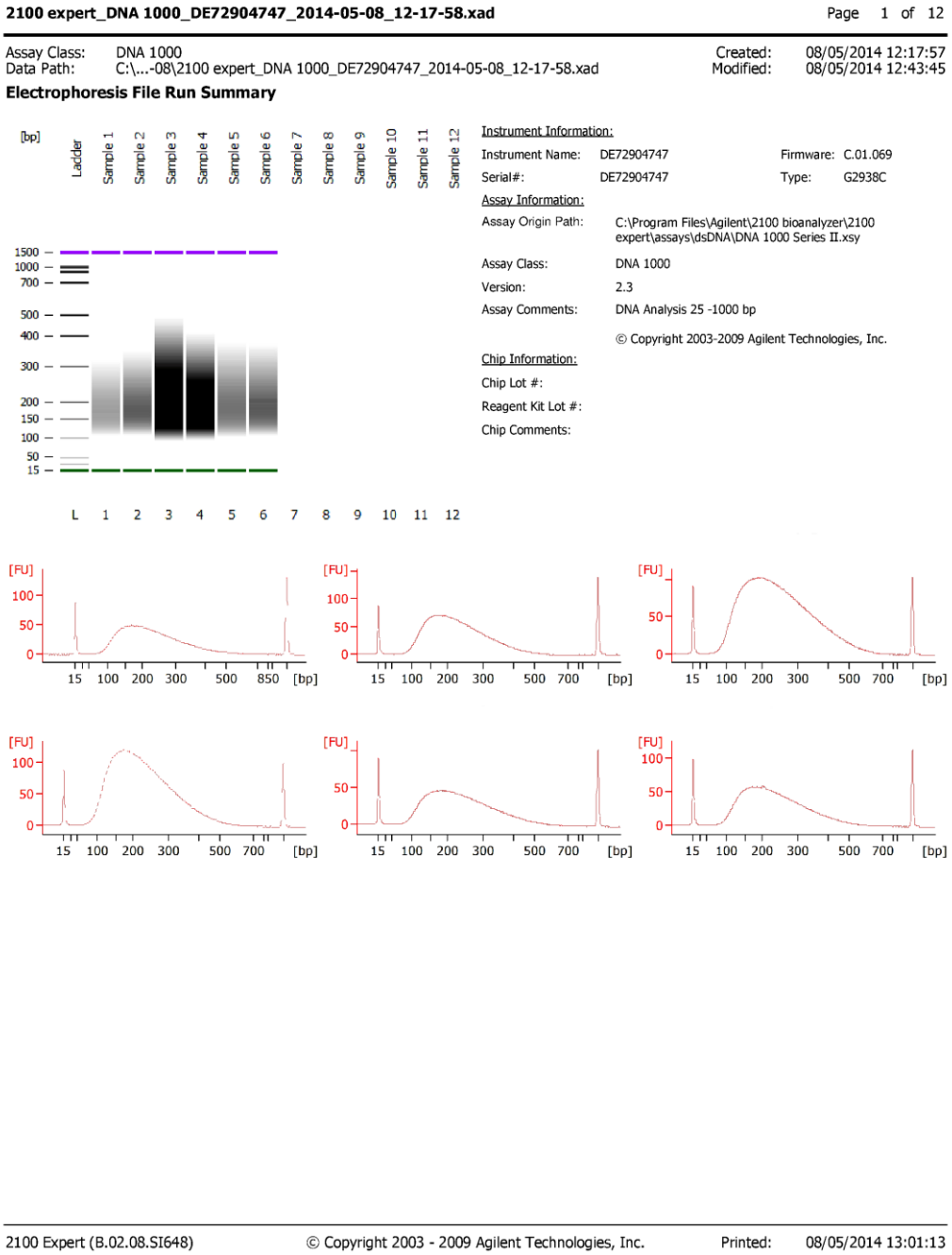

B. The amplified libraries were analysed on the Bioanalyzer™ using DNA1000 assay kit (Agilent Technologies) and only samples with an electropherogram reading showing a single peak around 250 to 275 bp were taken through to the hybridisation steps.

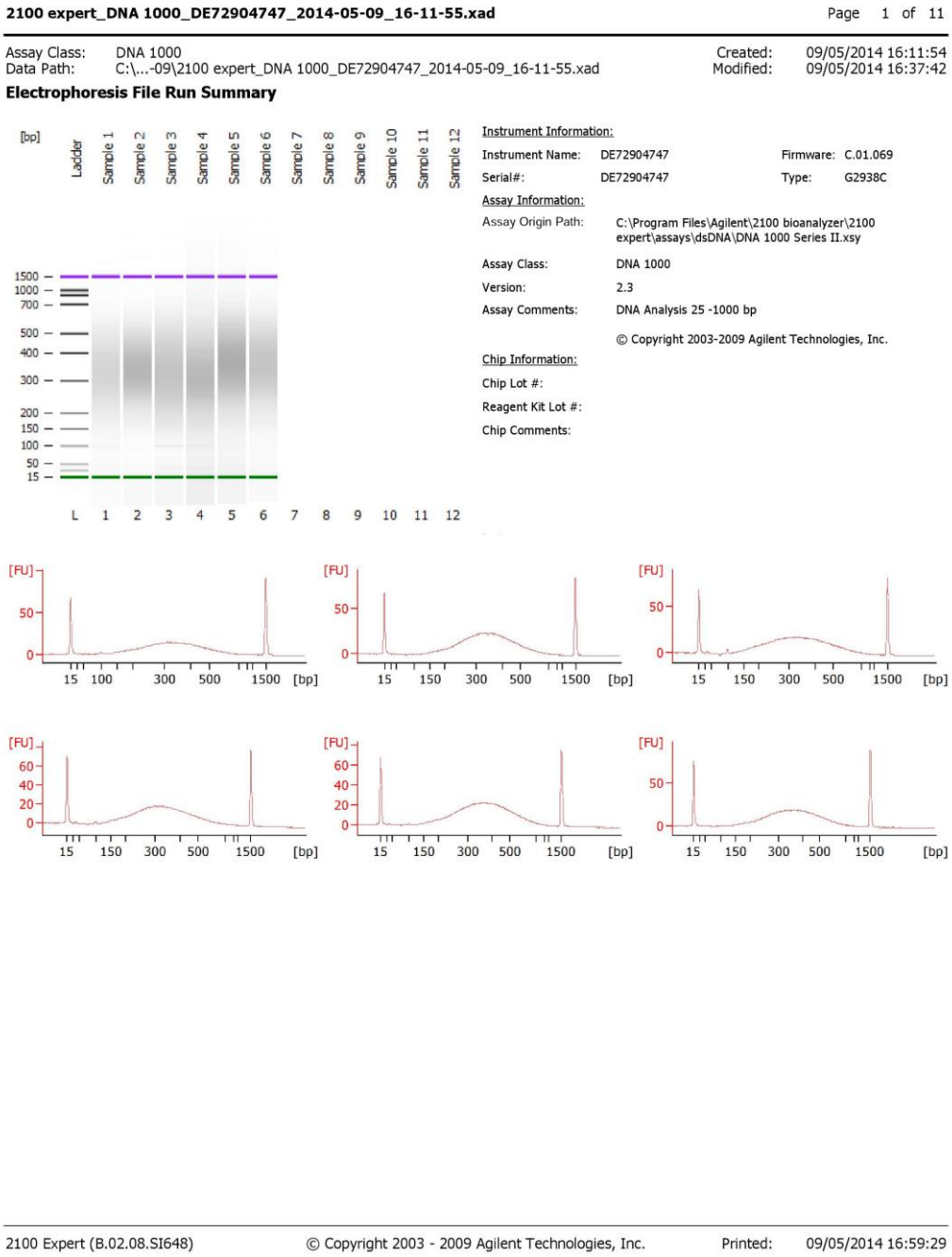

2100 expert_DNA 1000_DE72904747_2014-05-09_16-11-55.xad Page 1 of 11

Assay Class: DNA 1000 Created: 09/05/2014 16:11:54
Data Path: C:\...-09\2100 expert_DNA 1000_DE72904747_2014-05-09_16-11-55.xad Modified: 09/05/2014 16:37:42

Electrophoresis File Run Summary

Instrument Information:
Instrument Name: DE72904747 Firmware: C.01.069
Serial#: DE72904747 Type: G2938C

Assay Information:
Assay Origin Path: C:\Program Files\Agilent\2100 bioanalyzer\2100 expert\assays\dsDNA\DNA 1000 Series II.xsy
Assay Class: DNA 1000
Version: 2.3
Assay Comments: DNA Analysis 25 -1000 bp

Chip Information:
Chip Lot #:
Reagent Kit Lot #:
Chip Comments:

2100 Expert (B.02.08.SI648) Printed: 09/05/2014 16:59:29

C. The captured libraries after hybridisation were analysed on the Bioanalyzer™ using DNA high sensitivity assay kit (Agilent Technologies) to achieve a normal distribution around a peak ranging from approximately 300 to 400 bp before the pooling step of the samples.

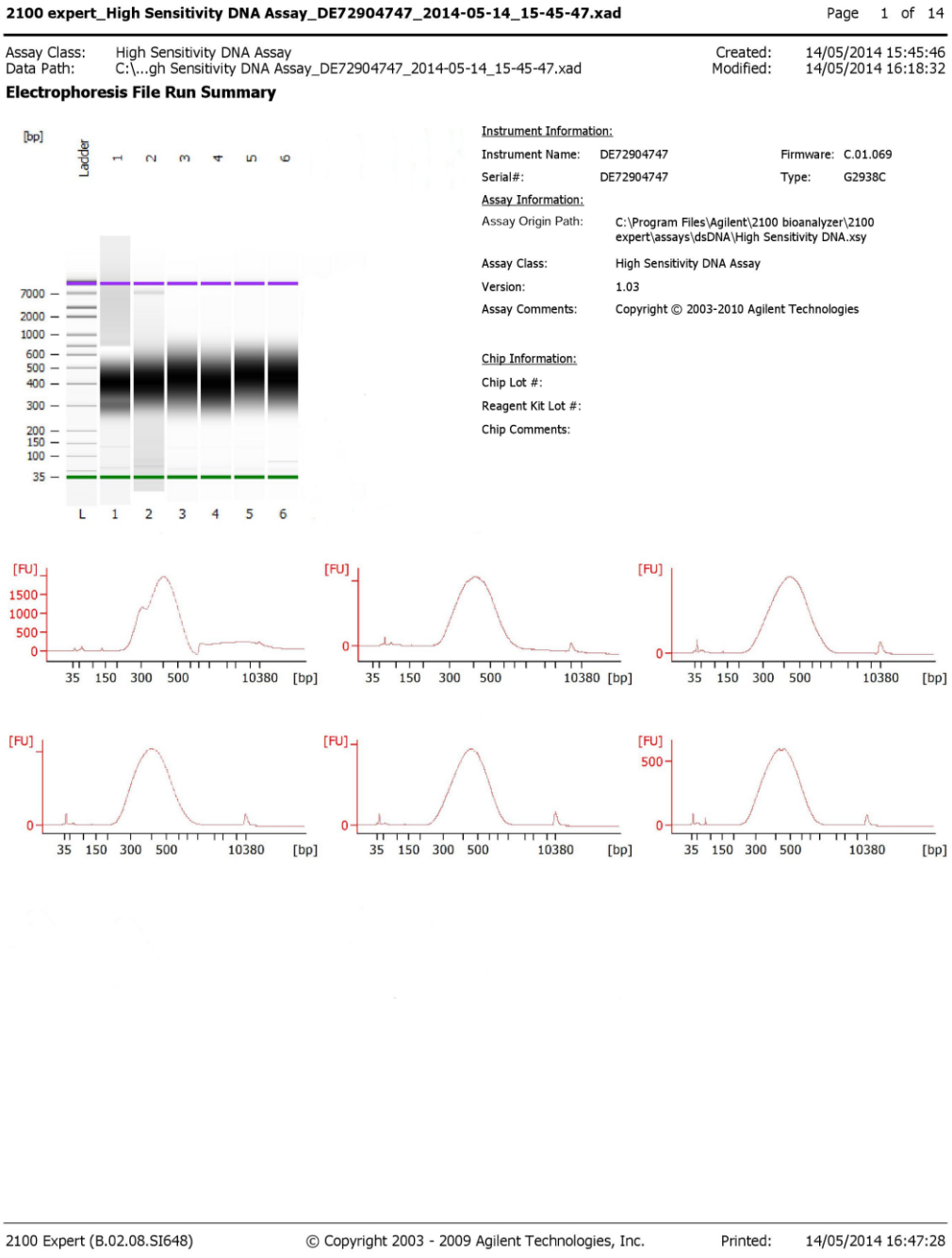

2100 expert_High Sensitivity DNA Assay_DE72904747_2014-05-14_15-45-47.xad Page 1 of 14

Assay Class: High Sensitivity DNA Assay
Data Path: C:\...gh Sensitivity DNA Assay_DE72904747_2014-05-14_15-45-47.xad

Created: 14/05/2014 15:45:46
Modified: 14/05/2014 16:18:32

Electrophoresis File Run Summary

Instrument Information:
Instrument Name: DE72904747 Firmware: C.01.069
Serial#: DE72904747 Type: G2938C

Assay Information:
Assay Origin Path: C:\Program Files\Agilent\2100 bioanalyzer\2100 expert\assays\dsDNA\High Sensitivity DNA.xsy
Assay Class: High Sensitivity DNA Assay
Version: 1.03
Assay Comments: Copyright © 2003-2010 Agilent Technologies

Chip Information:
Chip Lot #:
Reagent Kit Lot #:
Chip Comments:

2100 Expert (B.02.08.SI648) © Copyright 2003 - 2009 Agilent Technologies, Inc. Printed: 14/05/2014 16:47:28

Appendix 8- Immuno-localisation of DRAM2 to the eye cross sections of the mouse embryo

IHC staining on paraffin fixed cross eye sections of mouse embryo (P0/E21) stained for DRAM2 (brown) (B, C and E) and counterstained with haematoxylin (blue) comparing to control sections (A and D). The results showed nonspecific staining of DRAM2 to the eye layers. RPE = retinal pigment epithelium, NR= neural retina, HVP= hyaloid vascular plexus, C= cornea, L= lens and OFL= optic fibre layer.